WOODHEAD PUBLISHING SERIES IN COMPOSITES SCIENCE AND ENGINEERING

Lightweight Composite Structures in Transport

Design, Manufacturing, Analysis and Performance

Edited by James Njuguna

WP
WOODHEAD PUBLISHING

Lightweight Composite Structures in Transport

Related titles

Residual Stresses in Composite Materials
(ISBN 978-0-85709-270-0)

Fatigue and Fracture of Adhesively-bonded Composite Joints
(ISBN 978-0-85709-806-1)

Polymer Composites in the Aerospace Industry
(ISBN 978-0-85709-523-7)

Woodhead Publishing Series in Composites Science and Engineering: Number 67

Lightweight Composite Structures in Transport

Design, Manufacturing, Analysis and Performance

Edited by

J. Njuguna

AMSTERDAM • BOSTON • CAMBRIDGE • HEIDELBERG
LONDON • NEW YORK • OXFORD • PARIS • SAN DIEGO
SAN FRANCISCO • SINGAPORE • SYDNEY • TOKYO
Woodhead Publishing is an imprint of Elsevier

Woodhead Publishing is an imprint of Elsevier
The Officers' Mess Business Centre, Royston Road, Duxford, CB22 4QH, UK
50 Hampshire Street, 5th Floor, Cambridge, MA 02139, USA
Langford Lane, Kidlington, OX5 1GB, UK

Notices
Knowledge and best practice in this field are constantly changing. As new research and experience broaden our understanding, changes in research methods, professional practices, or medical treatment may become necessary.

Practitioners and researchers must always rely on their own experience and knowledge in evaluating and using any information, methods, compounds, or experiments described herein. In using such information or methods they should be mindful of their own safety and the safety of others, including parties for whom they have a professional responsibility.

To the fullest extent of the law, neither the Publisher nor the authors, contributors, or editors, assume any liability for any injury and/or damage to persons or property as a matter of products liability, negligence or otherwise, or from any use or operation of any methods, products, instructions, or ideas contained in the material herein.

ISBN: 978-1-78242-325-6 (print)
ISBN: 978-1-78242-343-0 (online)

British Library Cataloguing-in-Publication Data
A catalogue record for this book is available from the British Library

Library of Congress Cataloging-in-Publication Data
A catalog record for this book is available from the Library of Congress

Contents

This page intentionally left blank

List of contributors

A.I. Al-Mosawi Free Consultation, Babylon, Iraq

D.M. Baskin Materials and Structural Optimization Consultant, Dover, MA, United States

S. Boria University of Camerino – School of Science and Technology, Camerino, Italy

A. Daliri RMIT University, Melbourne, VIC, Australia; Defence Materials Technology Centre (DMTC Ltd), Hawthorn, VIC, Australia

J. Fan SKF Engineering & Research Center, Nieuwegein, Netherlands

M.V. Hosur Tuskegee University, Tuskegee, AL, United States

S. Jeelani Tuskegee University, Tuskegee, AL, United States

L.A. Khan CESAT, Islamabad, Pakistan

A.T. Mayyas University of California-Berkeley, Berkeley, CA, United States

A.R. Mayyas Arizona State University, Mesa, AZ, United States

A.H. Mehmood NED University of Engineering & Technology, Karachi, Pakistan

A. Misra NASA Glenn Research Center, Cleveland, OH, United States

A.A. Mohammed Tuskegee University, Tuskegee, AL, United States

Z. Mouti Eaton Automotive Group, West Midlands, United Kingdom

J. Njuguna Robert Gordon University, Aberdeen, United Kingdom

F. Ohlsson Oxeon AB, Borås, Sweden

M. Omar Masdar Institute of Science & Technology, Abu Dhabi, United Arab Emirates

G. Oncul TAI Turkish Aerospace Industry, Kazan, Ankara, Turkey

J.C. Quagliano Amado Institute of Scientific and Technical Research for the Defense (Citedef), Buenos Aires, Argentina

N. Saad Composite Materials Iraq, University of Babylon, College of Materials Engineering, Babylon, Iraq

J.F. Sanchez Cranfield University, Bedfordshire, United Kingdom

E.M. Smith Tuskegee University, Tuskegee, AL, United States

C.H. Wang RMIT University, Melbourne, VIC, Australia

K. Westwood Eaton Automotive Group, West Midlands, United Kingdom

Y. Xu Cranfield University, Bedfordshire, United Kingdom

R.N. Yancey VP Aerospace and Composites, Altair Engineering, Troy, MI, United States

S. Yousef Akhbar Elyom Academy, Giza, Egypt

S. Zainuddin Tuskegee University, Tuskegee, AL, United States

J. Zhang Deakin University, VIC, Australia

Woodhead Publishing Series in Composites Science and Engineering

1 **Thermoplastic aromatic polymer composites**
F. N. Cogswell
2 **Design and manufacture of composite structures**
G. C. Eckold
3 **Handbook of polymer composites for engineers**
Edited by L. C. Hollaway
4 **Optimisation of composite structures design**
A. Miravete
5 **Short-fibre polymer composites**
Edited by S. K. De and J. R. White
6 **Flow-induced alignment in composite materials**
Edited by T. D. Papthanasiou and D. C. Guell
7 **Thermoset resins for composites**
Compiled by Technolex
8 **Microstructural characterisation of fibre-reinforced composites**
Edited by J. Summerscales
9 **Composite materials**
F. L. Matthews and R. D. Rawlings
10 **3-D textile reinforcements in composite materials**
Edited by A. Miravete
11 **Pultrusion for engineers**
Edited by T. Starr
12 **Impact behaviour of fibre-reinforced composite materials and structures**
Edited by S. R. Reid and G. Zhou
13 **Finite element modelling of composite materials and structures**
F. L. Matthews, G. A. O. Davies, D. Hitchings and C. Soutis
14 **Mechanical testing of advanced fibre composites**
Edited by G. M. Hodgkinson
15 **Integrated design and manufacture using fibre-reinforced polymeric composites**
Edited by M. J. Owen and I. A. Jones
16 **Fatigue in composites**
Edited by B. Harris
17 **Green composites**
Edited by C. Baillie
18 **Multi-scale modelling of composite material systems**
Edited by C. Soutis and P. W. R. Beaumont
19 **Lightweight ballistic composites**
Edited by A. Bhatnagar

20 **Polymer nanocomposites**
Y.-W. Mai and Z.-Z. Yu
21 **Properties and performance of natural-fibre composite**
Edited by K. Pickering
22 **Ageing of composites**
Edited by R. Martin
23 **Tribology of natural fiber polymer composites**
N. Chand and M. Fahim
24 **Wood-polymer composites**
Edited by K. O. Niska and M. Sain
25 **Delamination behaviour of composites**
Edited by S. Sridharan
26 **Science and engineering of short fibre reinforced polymer composites**
S.-Y. Fu, B. Lauke and Y.-M. Mai
27 **Failure analysis and fractography of polymer composites**
E. S. Greenhalgh
28 **Management, recycling and reuse of waste composites**
Edited by V. Goodship
29 **Materials, design and manufacturing for lightweight vehicles**
Edited by P. K. Mallick
30 **Fatigue life prediction of composites and composite structures**
Edited by A. P. Vassilopoulos
31 **Physical properties and applications of polymer nanocomposites**
Edited by S. C. Tjong and Y.-W. Mai
32 **Creep and fatigue in polymer matrix composites**
Edited by R. M. Guedes
33 **Interface engineering of natural fibre composites for maximum performance**
Edited by N. E. Zafeiropoulos
34 **Polymer-carbon nanotube composites**
Edited by T. McNally and P. Pötschke
35 **Non-crimp fabric composites: Manufacturing, properties and applications**
Edited by S. V. Lomov
36 **Composite reinforcements for optimum performance**
Edited by P. Boisse
37 **Polymer matrix composites and technology**
R. Wang, S. Zeng and Y. Zeng
38 **Composite joints and connections**
Edited by P. Camanho and L. Tong
39 **Machining technology for composite materials**
Edited by H. Hocheng
40 **Failure mechanisms in polymer matrix composites**
Edited by P. Robinson, E. S. Greenhalgh and S. Pinho
41 **Advances in polymer nanocomposites: Types and applications**
Edited by F. Gao
42 **Manufacturing techniques for polymer matrix composites (PMCs)**
Edited by S. Advani and K.-T. Hsiao
43 **Non-destructive evaluation (NDE) of polymer matrix composites: Techniques and applications**
Edited by V. M. Karbhari

44 **Environmentally friendly polymer nanocomposites: Types, processing and properties**
S. S. Ray
45 **Advances in ceramic matrix composites**
Edited by I. M. Low
46 **Ceramic nanocomposites**
Edited by R. Banerjee and I. Manna
47 **Natural fibre composites: Materials, processes and properties**
Edited by A. Hodzic and R. Shanks
48 **Residual stresses in composite materials**
Edited by M. Shokrieh
49 **Health and environmental safety of nanomaterials: Polymer nanocomposites and other materials containing nanoparticles**
Edited by J. Njuguna, K. Pielichowski and H. Zhu
50 **Polymer composites in the aerospace industry**
Edited by P. E. Irving and C. Soutis
51 **Biofiber reinforcement in composite materials**
Edited by O. Faruk and M. Sain
52 **Fatigue and fracture of adhesively-bonded composite joints: Behaviour, simulation and modelling**
Edited by A. P. Vassilopoulos
53 **Fatigue of textile composites**
Edited by V. Carvelli and S. V. Lomov
54 **Wood composites**
Edited by M. P. Ansell
55 **Toughening mechanisms in composite materials**
Edited by Q. Qin and J. Ye
56 **Advances in composites manufacturing and process design**
Edited by P. Boisse
57 **Structural integrity and durability of advanced composites: Innovative modelling methods and intelligent design**
Edited by P.W.R. Beaumont, C. Soutis and A. Hodzic
58 **Recent advances in smart self-healing polymers and composites**
Edited by G. Li and H. Meng
59 **Manufacturing of nanocomposites with engineering plastics**
Edited by V. Mittal
60 **Fillers and reinforcements for advanced nanocomposites**
Edited by Y. Dong, R. Umer and A. Kin-Tak Lau
61 **Biocomposites: Design and mechanical performance**
Edited by M. Misra, J. K. Pandey and A. K. Mohanty
62 **Numerical modelling of failure in advanced composite materials**
Edited by P.P. Camanho and S. R. Hallett
63 **Marine applications of advanced fibre-reinforced composites**
Edited by J. Graham-Jones and J. Summerscales
64 **Smart composite coatings and membranes: Transport, structural, environmental and energy applications**
Edited by M. F. Montemor
65 **Modelling damage, fatigue and failure of composite materials**
Edited by R. Talreja and J. Varna

66 **Advanced fibrous composite materials for ballistic protection**
Edited by X. Chen
67 **Lightweight composite structures in transport: Design, manufacturing, analysis and performance**
Edited by J. Njuguna
68 **Structural health monitoring (SHM) in aerospace structures**
Edited by F.-G. Yuan

Preface

The use of lightweight composite structures has several predictable impacts on the design of transport vehicles, primarily by providing safer, faster, and eventually cheaper transportation in the future. This book therefore explores the recent developments on the use of lightweight composite structures in transport with a special focus on design, manufacturing, analysis, and performance of transport vehicles. It follows that the use of lightweight materials has become more prevalent as transport vehicle manufacturers strive to reduce vehicle weight to improve performance, to lower fuel and oil consumption, and to reduce emissions.

The book is divided in five distinctive parts. Part one covers the lightweighting philosophy and starts with an introduction to lightweight composite materials and their use in transport vehicles in chapter "An introduction to lightweight composite materials and their use in transport structures". This chapter provides an overall introduction into lightweight composite materials and their use in transport structures, mainly thermoplastic, thermosets, elastomers, and core materials. Chapter "Challenges, opportunities, and perspectives on lightweight composite structures: aerospace versus automotive" compares the manufacturing, use, performance, design, analysis, market and supply needs of each industry, and what each industry can learn from the other. The chapter also reviews the challenges and opportunities for the overall composites industry with the use of more composites in automotive applications. Weight as a design parameter is covered in chapter "Opportunities in the design stage of composite components to reduce weight during assembly operations" where the focus is on the lighweighting opportunities at the design stage of composite components to reduce weight during assembly operations. Chapter "The automotive body lightweighting design philosophy" reviews an experience-led philosophy on structural optimization and automobile structural development and yields a series of conclusions. These conclusions combine to form a design philosophy that is very different from that currently employed at both high volume and niche automobile manufacturers.

The second part of the book looks into current developments in manufacturing techniques for lightweight composite structures in the transport industry. In chapter "Cost-effective composites manufacturing processes for automotive applications", an overview is provided on the cost-effective processing techniques employed for manufacturing of automotive parts, primarily using carbon fiber-based thermoset composites. The techniques discussed are resin transfer molding, vacuum-assisted resin infusion process, Quickstep processing with particular emphasis on resin spray technology, pultrusin, filament winding, and compression molding, with emphasis on

recycled carbon fiber-reinforced composites. This is followed by chapter "Hybrid polymer composites for high strain rate applications" on hybrid polymer composites for high strain rate applications and chapter "Thermoset resin sandwich structures" on thermoset resin sandwich structures.

Spread tow carbon reinforcements are a new kind of composite reinforcement, suitable for saving weight. This interesting subject is covered in Part three of the book. The spread tow structure makes it possible to achieve thinner laminates. Straighter fibers with reduced crimp optimize and strengthen the composite. Fewer crimps reduce the amount of excess plastic, thereby minimizing weight. Hence, chapter "Weight reduction by optimized reinforcement structures" looks into some of the existing customer cases from both Formula 1 and aerospace sectors where this new technology has contributed to substantial weight savings.

Part four of the book has four chapters that focus on durability, damage tolerance, and structural integrity of lightweight composite structures in transport. Chapter "Influence of temperature on mechanical properties of short glass fibre-reinforced polyamide 6 and 66 composites for automotive oil pan application" looks into the influence of temperature on mechanical properties of short glass fiber-reinforced Polyamide 6 and 66 composites for automotive oil pan applications. The fatigue behavior of composite materials for high-temperature applications is covered in chapter "The fatigue behavior of composite materials for high-temperature applications" while chapter "Sustainable lightweight vehicle design: a case study in eco-material selection for body-in-white" concentrates on the flammability of composites. A special insight is also provided on composite materials for aerospace propulsion related to air and space transportation in chapter "Composite materials for aerospace propulsion related to air and space transportation".

The readers will also benefit from a set of case studies of lightweight composite design for transport structures. In chapter "Sustainable lightweight vehicle design: a case study in eco-material selection for body-in-white" a case study on ecomaterial selection for body-in-white is provided to demonstrate the sustainable lightweight vehicle design and its motivations. Another case study looks into lightweight design and crash analysis of composites in chapter "Flammability of composites". Next is remanufacturing and whole-life costing of lightweight components, a case study that serves as an inspiration on remanufacturing of composite structures and components. Chapter "Polymer nanocomposite components: a case study on gears" is a case study on gears manufacturing. The final case study covers the manufacture and testing of lightweight tubes for rocketry and centrifuges. Special attention is devoted to resins and fibers utilized in filament winding and damage assessment and prevention of failure, considering the high pressures involved in operation of tubes for rocketry and centrifuges.

This book covering such vital issues and topics definitely should be attractive to the scientific community. It will be a useful tool for scientists, academicians, research scholars, polymer engineers, and industries as it has a unique set of valuable contributions from renowned experts in the transport sector. This book is also supportive for undergraduate and postgraduate students and hopefully an inspiration to many young scientists to devote their efforts in research and development on lightweight designs

and constructions as well as composite materials. The editor is thankful to his postgraduate students, research students, and research fellows who have in one form or another contributed to this book directly or indirectly.

The editor is very thankful to the many contributors who devoted and contributed to this book, more so for their willingness to share their knowledge, expertise, and experience. The editor is also grateful to a great team at Woodhead Publishing and Elsevier for brilliant editorial support throughout this project. Special thanks to Gwen Jones, Kate Hardcastle, Lucy Beg, and Charlotte Cockle who were very helpful in this book project.

J. Njuguna

This page intentionally left blank

Part One

The lightweight philosophy: materials selection, principles and design solutions

This page intentionally left blank

An introduction to lightweight composite materials and their use in transport structures

1

J. Fan
SKF Engineering & Research Center, Nieuwegein, Netherlands

J. Njuguna
Robert Gordon University, Aberdeen, United Kingdom

1.1 Background

The aim of lightweight construction is to preserve or even expand a product's functionality while the overall weight of the product decreases. Existing approaches for reducing mass include the use of less dense materials, eg, metal foams and composite materials, or a decrease in the material volume by reducing wall thicknesses in key structural components. In both cases, less energy is needed for transportation of the ready-made product, so that the ecologically friendly aspect of lightweight construction is supported. For example, reducing a car mass by 100 kg saves about 0.7l fuel each 100 km (directly and indirectly).

Technologies based on fiber-reinforced thermoplastic materials can be integrated into the manufacturing process for lightweight composite structures. The main motivators for the lightweight materials applications are weight savings and possible cost savings. Significant weight reductions with improved performance will mean less fuel consumption and CO_2 emissions. The transport industry is customer sensitive and currently the customers are pushing for cost-effectiveness and more environmental friendly transport systems. By using low cost, ecofriendly, and reliable materials the economic burden would be reduced for both the customer and the automotive industry.

In addition to the reduction of mass, composite materials offer consistent potential advantages in terms of noise and vibration reduction, impact resistance, and energy absorption capability. They also offer advantages in the manufacturing process, such as cost reduction for producing low volume pieces and the possibility of integration, ie, structures which can be made with fewer subcomponents. Composites also possess a unique capability: to be tailored to meet design requirements which are ill-matched for conventional materials, by properly choosing the constituent materials and the orientation of the reinforcement fibers. This is of primary importance for performance optimization, the target objective being a minimization of the mass and/or of stress concentrations, guaranteeing the required performance.

Lightweight Composite Structures in Transport. http://dx.doi.org/10.1016/B978-1-78242-325-6.00001-3

1.1.1 Lightweighting benefits—automotive example

The need for high performance and the capability of designing material characteristics to meet specific requirements has made polymeric materials a first choice for many aerospace applications. Such materials can be tailored to give high strength coupled with relatively low weight and corrosion resistance to most chemicals and offer long-term durability under most environmentally severe conditions. Polymer materials have key advantages over other conventional metallic materials due to their specific strength properties with weight saving of 20–40%, potential for rapid process cycles, ability to meet stringent dimensional stability, lower thermal expansion properties, and excellent fatigue and fracture resistance. On application of polymer composite materials, for instance, 30% weight savings have been achieved on military fighter aircraft.

In the automotive industry, for example, there is a constant need to upgrade cheap, easily available, and easy to process materials such as polypropylenes, polyethylene, polyamides, etc. to engineering polymers. Vehicle appearance will be an added advantage. In this case, material recyclability is improved with a high percentage of return-to-use products. There is also a need for processing optimization for specific structural and semistructural applications. Use of lightweight materials also aligns with most recent energy conservation regulations and policies, eg, the European Commission with the End of Life Vehicles (ELV) European Union directive requiring vehicles to be constructed of 95% recyclable materials, with 85% recoverable through reuse or mechanical recycling and 10% through energy recovery or thermal recycling.

Unfortunately, vehicle weights have increased over the years especially in the automotive industry. For instance, while a Volkswagen Golf MK1 in 1974 weighed just ~780 kg its relative Volkswagen Golf MK5 (2004) weighed 1300 kg. This trend in increase in vehicle weight can be seen in many car types and models. This is mainly due to added electronics systems, front impact, and general crash requirements among other modern car utilities. It is possible to achieve a 10% further weight savings from a typical compact car (eg, Volkswagen Golf) with total vehicle mass of 1160 kg and whose car body weight (body in white, BIW) is 296 kg. In particular, a 30% mass reduction on its BIW structure is feasible. For a lifetime road performance of 150,000 km, fuel consumption reduction in this lifetime is around ~398 L (~998 kg CO_2 savings) or approximately 0.3 L/100 km fuel savings for each car. In the United Kingdom, for instance, with about 2.3 million/year new vehicles cars entering the UK roads, the total CO_2 savings for the 150,000 km amounts to 2.3 million tons or at least 915 million liters fuel savings and the total CO_2 savings is significant.

Further, reduction in the mass of engines is a key factor for improving the fuel efficiency. Currently, most manufacturers in automotive sector, for example, have replaced cast iron (density = 7.8 g/cm^3) engine blocks with lightweight and low cost aluminum–silicon (density = 2.79 g/cm^3) crankcases. Several Al-based alloys and metal–matrix composites, such as A319Al, A356Al, A390Al, and A360Al, are in use. To continue using Al alloy engine blocks (due to lighter weight) and to improve wear resistance of the engine bore surface several techniques for forming new composite and/or monolithic protective layers on the bore surface must be explored. By

obviating the need for liners on automotive engines, the engine dimension can be significantly reduced. It is estimated that a direct weight savings of about 1 kg per engine can be easily achieved. Every kilogram reduction of payload is important for improvement in fuel efficiency. Reduction of about 110 kg in a typical automobile of weight 1100 kg will improve fuel economy by 7%. In the lifetime of a car this reduction of engine weight is significant.

Weight reduction, manufacturing process, and recycling are paramount in the transport sector for CO_2 reduction especially for aircraft, marine vessels, cars, trucks, and vans. The importance of weight reduction is demonstrated by the fact that almost 85% of the total life-cycle energy consumption occurs during functional operations. This is due to the fact that fuel is burned to produce force. The lighter the mass, the better the acceleration, thanks to Newton's second law of motion. The weight reduction is an effective way of reducing CO_2 for any source of energy whether oil (petrol, diesel, etc.), electric, biofuels, or fuel cells.

1.1.2 Historical overview on composites

Composites can be defined as materials that consist of two or more chemically and physically different phases separated by a distinct interface. The different systems are combined judiciously to achieve a system with more useful structural or functional properties not attainable by any of the constituents alone. Composites, the wonder materials, are becoming an essential part of today's materials due to the advantages such as low weight, corrosion resistance, high fatigue strength, and faster assembly. They are extensively used as materials in making aircraft structures, electronic packaging to medical equipment, and space vehicles to home building. The basic difference between blends and composites is that the two main constituents in the composites remain recognizable while these may not be recognizable in blends. The predominant useful materials used in our day-to-day life are wood, concrete, ceramics, and so on. Surprisingly, the most important polymeric composites are found in nature and these are known as natural composites. The connective tissues in mammals belong to the most advanced polymer composites known to mankind where the fibrous protein, collagen, is the reinforcement. It functions both as a soft and a hard connective tissue.

Composites are combinations of materials differing in composition, where the individual constituents retain their separate identities. These separate constituents act together to give the necessary mechanical strength or stiffness to the composite part. Composite material is a material composed of two or more distinct phases (matrix phase and dispersed phase) and having bulk properties significantly different from those of any of the constituents. Matrix phase is the primary phase having a continuous character. Matrix is usually a more ductile and less hard phase. It holds the dispersed phase and shares a load with it. Dispersed (reinforcing) phase is embedded in the matrix in a discontinuous form. This secondary phase is called the dispersed phase. Dispersed phase is usually stronger than the matrix; therefore, it is sometimes called reinforcing phase.

Composites in structural applications have the following characteristics:

- They generally consist of two or more physically distinct and mechanically separable materials.
- They are made by mixing the separate materials in such a way as to achieve controlled and uniform dispersion of the constituents.
- They have superior mechanical properties and in some cases uniquely different from the properties of their constituents.[1]

Most advanced examples perform routinely on spacecrafts in demanding environments. Advanced composites have high-performance fiber reinforcements in a polymer matrix material such as epoxy. Examples are graphite/epoxy, Kevlar/epoxy, and boron/epoxy composites. Advanced composites are traditionally used in the aerospace industries, but these materials have now found applications in commercial industries as well.

On the basis of the matrix phase, composites can be classified into metal matrix composites (MMCs), ceramic matrix composites (CMCs), and polymer matrix composites (PMCs).[2] The classifications according to types of reinforcement are particulate composites (composed of particles), fibrous composites (composed of fibers), and laminate composites (composed of laminates) as shown in Fig. 1.1.

Fibrous composites can be further subdivided on the basis of natural/biofiber or synthetic fiber. Biofiber-encompassing composites are referred to as biofiber composites. They can be again divided on the basis of matrix, that is, nonbiodegradable matrix and biodegradable matrix.[3] Bio-based composites made from natural/biofiber and biodegradable polymers are referred to as green composites.[4] These can be further subdivided as hybrid composites and textile composites. Hybrid composites comprise a combination of two or more types of fibers.

Polymer composite materials have been a part of the aerospace and automotive industry for several decades, with early notable application in the jet fighter and also in the 1953 Corvette, respectively. These materials have been used for applications with low production volumes, because of their shortened lead times and lower investment costs relative to conventional steel fabrication. Important drivers of the growth of polymer composites have been the reduced weight and parts consolidation opportunities the material offers, as well as design flexibility, corrosion resistance, material

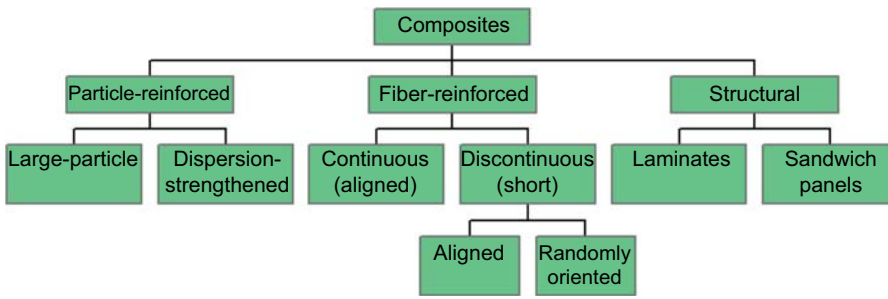

Figure 1.1 Classification of composites.

anisotropy, and mechanical properties. Although these advantages are well known to the industry, polymer composite use has been impeded by high material costs, slow production rates, and to a lesser extent concerns about recyclability. Several factors have hindered large-scale mass automotive applications of polymer composites, although the PMCs have excelled in the high-performance aerospace industry. Among these are concerns about crash energy absorption/management, recycling challenges, competitive and cost pressures, and the industry's general lack of experience and comfort with the material.

The cost of composite materials is usually much higher (up to 10 times higher when using carbon fibers) than those of conventional metals. Therefore, the main targets for future development must be the use of hybrid composites (low-cost fibers to be used where possible and aramid and carbon fibers to be used only where they are required for damage tolerance or stiffness reasons), the evaluation of highly automated and rapid manufacturing processes including the application of intelligent preforms or half-finished goods, and the full use of the potential of composites for parts integration, either glass or carbon, reinforced in the matrix of thermoset or thermoplastic polymer materials. The glass-reinforced thermoplastic composites are the most commonly used composite in automotive applications today while thermosets dominate the aerospace industry.

Most commercially produced composites use a polymer matrix material often called a resin solution. There are many different polymers available depending on the starting raw ingredients. There are several broad categories, each with numerous variations. The most common are polyester, vinyl ester, epoxy, phenolic, polyimide, polyamide, polypropylene, polyether ether ketone, and others. The reinforcement materials are often fibers but can also be common ground minerals.[5] The various methods described below have been developed to reduce the resin content of the final product. As a rule of thumb, hand layup results in a product containing 60 wt% resin and 40 wt% fiber, whereas vacuum infusion gives a final product with 40 wt% resin and 60 wt% fiber content. The strength of the product is greatly dependent on this ratio. PMCs are very popular due to their low cost and simple fabrication methods. The use of nonreinforced polymers as structure materials is limited by the low level of their mechanical properties, namely strength, modulus, and impact resistance. Reinforcement of polymers by a strong fibrous network permits fabrication of PMCs, which is characterized by the following:

- High specific strength
- High specific stiffness
- High fracture resistance
- Good abrasion resistance
- Good impact resistance
- Good corrosion resistance
- Good fatigue resistance
- Low cost.

The main disadvantages of PMCs are:

- Low thermal resistance and
- High coefficient of thermal expansion.

The polymer composites constitute up to 80% of modern launch vehicles meant for satellites and used in several vital satellite components such as the honeycomb structures, equipment panels, cylinder support structures, solar array substrates, and antennas. The rocket motor cases of the space shuttle's solid booster comprise 30 tons of graphite-reinforced epoxy composites, for example. Current development of micrometer thickness films may eventually become enabling for certain types of spacecrafts such as solar sails. There is currently a demand for flexible and compliant materials for Gossamer spacecraft applications such as antennas, solar sails, sunshields, radar, rovers, reflect arrays, and solar concentrators. Such Gossamer structures can be folded or packaged into small volumes in conjunction with those available on convectional launch vehicles. Once in space, they can then be deployed by mechanical, inflation, or other means into a large ultralightweight functioning spacecraft. As a prerequisite, Gossamer structures must maintain and possess specific and unique combinations of properties over a long period of time in a relatively harsh environment mainly exposed to atomic oxygen, ultraviolet, and vacuum ultraviolet radiation.

1.2 Polymers—general introduction

Polymers (or macromolecules) are very large molecules made up of smaller units, called monomers or repeating units, covalently bonded together. This specific molecular structure (chainlike structure) of polymeric materials is responsible for their intriguing mechanical properties. Polymer architecture can vary. In Fig. 1.2 three possible molecule architectures are depicted.

A linear polymer consists of a long chain of monomers. A branched polymer has branches covalently attached to the main chain. Cross-linked polymers have monomers of one chain covalently bonded with monomers of another chain. Cross-linking results in a three-dimensional network; the whole polymer is a giant macromolecule. Elastomers are loosely cross-linked networks while thermosets are densely cross-linked networks.

Another classification of polymers is based on the chemical type of the monomers (Fig. 1.3): Homopolymers consist of monomers of the same type; copolymers have different repeating units. Furthermore, depending on the arrangement of the types of monomers in the polymer chain, we have the following classification:

- In random copolymers two or more different repeating units are distributed randomly.
- Alternating copolymers are made of alternating sequences of the different monomers.
- In block copolymers long sequences of a monomer are followed by long sequences of another monomer.
- Graft copolymers consist of a chain made from one type of monomers with branches of another type.

Many properties of polymeric materials depend on the microscopic arrangement of their molecules. Polymers can have an amorphous or semicrystalline (partially crystalline) structure (Fig. 1.4). Amorphous polymers lack order and are arranged in a random

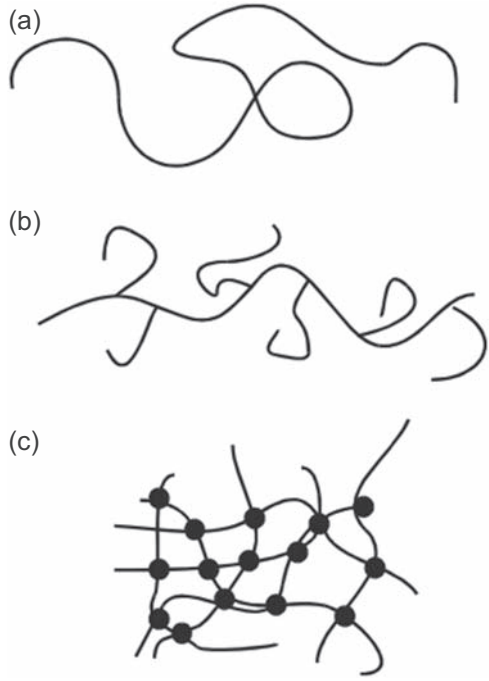

Figure 1.2 Types of molecular configurations: (a) linear chain, (b) branched molecule, (c) cross-linked network. Molecules are linked through covalent bonds. The network extends over the whole sample which is a giant macromolecule.

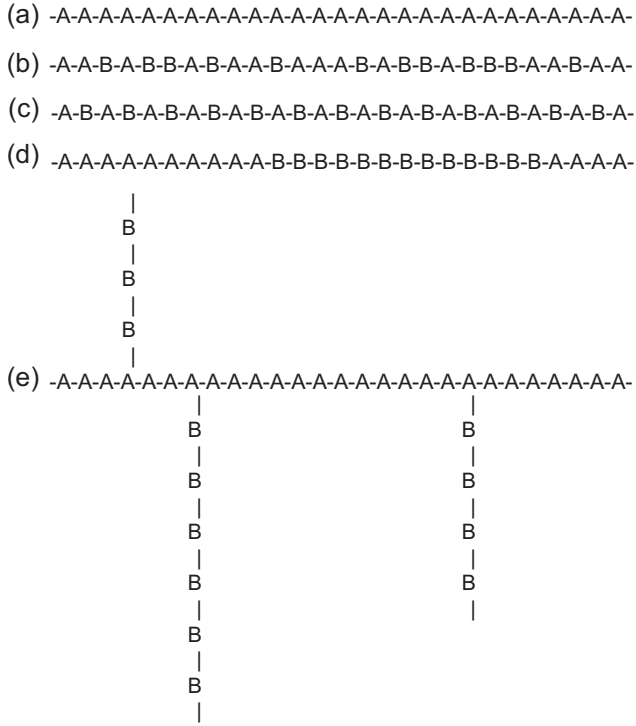

Figure 1.3 (a) Homopolymer, (b) Random copolymer, (c) Alternating copolymer, (d) Block copolymer, (e) Graft copolymer.

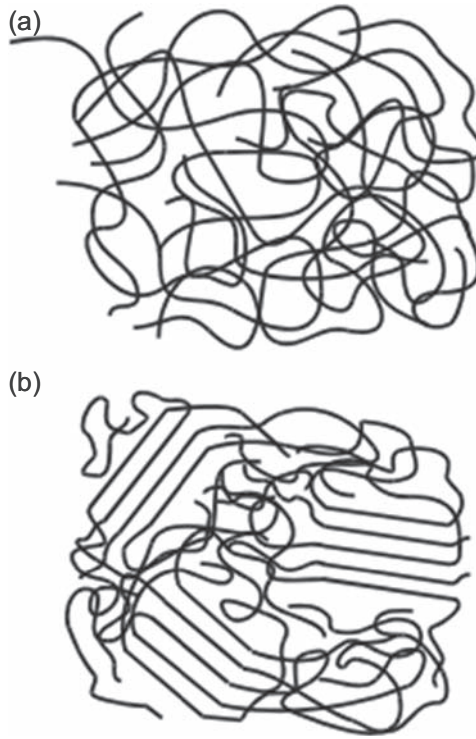

Figure 1.4 (a) Amorphous polymer (observe the entanglements among the polymer chains) and (b) semicrystalline polymer.

manner, while semicrystalline polymers are partially organized in orderly crystalline structures.

In addition to the different arrangements that the polymer chains may take to give different properties, different polymers are also used to gain the desired properties. Table 1.1 describes some common polymers along with their corresponding names, abbreviations and uses.

Table 1.1 Common polymers

Name	Abbreviation	Common uses	Properties
Poly(ethylene terapthalate)	PET	Soda (pop) bottles	Amorphous, rigid
High density polyethylene	HDPE	Food containers	Crystalline, rigid
Polystyrene	PS	Styrofoam cups	Brittle
Polyvinyl chloride	PVC	Piping	Hard
Poly(methyl methacrylate)	PMMA	Plexiglass	Rigid, transparent

Table 1.1 Continued

Name	Abbreviation	Common uses	Properties
Polybutadiene	PB	Automobile tires	Flexible, soft
Low-density polyethylene	LDPE	Garbage bags	Noncrystalline, rigid
Poly(tetrafluoroethylene)	Teflon	Coating in frying pans	Nonstick
Polypropylene	PP	Plastic Drinking straws	Flexible, tough
Kevlar	Kevlar	Bullet-proof vests	Stronger than steel

1.3 Engineering polymers—selected examples

1.3.1 Thermosets

As the name implies, thermosetting plastics or thermosets are set, cured, or hardened into a permanent shape. The curing process generally occurs rapidly under room temperature conditions, heat or ultraviolet (UV) light, and leads to an irreversible cross-linking of the polymer.

Thermoset polymers have covalent bonds linking the polymer chains in three dimensions. These links prevent the chains from sliding past one another resulting in a higher modulus and improved creep resistance. Usually thermosets are more brittle than thermoplastics. Note that thermosets are similar to elastomers. The polymer chains in thermosets are below their glass transition at room temperature, making them glassy. In contrast, the polymer chains in elastomers are above their glass transition at room temperature, making them rubbery. Thermosets are formed from thermoplastic polymer chains which are then covalently bonded to each other in a process known as cross-linking. The thermoplastic polymer flows easily and can be molded into the desired shape.

Once the precursor is cast into the desired shape the polymer is cross-linked, creating the thermoset material. Cross-linking is initiated by heat, light, or the addition of other chemicals. It is not a reversible process, resulting in materials which cannot be recycled. Once shaped into a permanent form, usually with heat and pressure, a thermosetting plastic cannot be remelted or reshaped because the basic polymeric component has undergone an irreversible chemical change. The operation by which the raw material is converted to a hard, insoluble, and infusible product is referred to as cure (or curing) and corresponds to the final step of the polymerization reaction.

A thermosetting material may be cured by the use of heat, radiation, catalysts, or a combination of these. The polymer component consists of molecules with permanent cross-links between linear chains that form a rigid three-dimensional network structure which cannot flow. The tightly cross-linked structure of thermosetting polymers

immobilizes the molecules, providing hardness, strength at relatively high temperature, insolubility, good heat and chemical resistance, and resistance to creep.

Thermosetting materials are usually preferred for structural applications because their strength is generally higher than that of thermoplastics and they do not have a tendency to cold flow (creep) at room temperature. The major families are epoxies, unsaturated polyesters, phenolics, amino resins (urea− and melamine−formaldehyde) and alkyds. Typical properties for some of the main resins are represented in Table 1.2.

Thermosets have cross-linked or network structures with covalent bonds with all molecules. They do not soften but decompose on heating. Once solidified by a cross-linking process they cannot be reshaped. Common examples are epoxies, polyesters, phenolics, ureas, melamine, silicone, and polyimides.

Thermosetting resins are used in molded and laminated plastics.[6] They are first polymerized into a low-molecular-weight linear or slightly branched polymer or oligomer, which is still soluble, fusible, and highly reactive during final processing. Thermoset resins are generally highly filled with mineral fillers and glass fibers. Thermosets are generally catalyzed and/or heated to finish the polymerization reaction, cross-linking them to almost infinite molecular weight. This step is often referred to as cure. Such cured polymers cannot be reprocessed or reshaped. The high filler loading and the high cross-link density of thermoset resins results in very high densities and very low ductility, but very high rigidity and good chemical resistance.

1.3.1.1 Phenolic resins

Phenolic resins combine the high reactivity of phenol and formaldehyde to form prepolymers and oligomers called resoles and novolacs. These materials are combined with fibrous fillers to give a phenolic resin, which when heated provides rapid, complete cross-linking into highly cured structures. The high cross-linked aromatic structure has high hardness, rigidity, strength, heat resistance, chemical resistance,

Table 1.2 Typical properties of selected thermoset resins

Properties	Epoxy	Phenolic	Toughned bismaleimide	Cyanate ester
Density (kg/m^3) $\times 10^{-3}$	1.2−1.25	1.24−1.32	1.2−1.3	1.1−1.35
Use temperature (°C)	RT-180	200−250	∼200	∼200
Tensile modulus (MPa) $\times 10^{-3}$	31−3.8	3−5	3.4−4.1	3.1−3.4
Dielectric constant (1 MHz)	3.8−4.5	4.3−5.4	3.4−4.7	2.7−3.2
Cure temperature (°C)	RT-180	150−190	220−300	180−250
Mold shrinkage (mm)	0.0006	0.002	0.007	0.004
TGA onset (°C)	260−340	360−400	360−400	400−420

and good electrical properties. Phenolic applications include automotive uses (distributor caps, rotors, brake linings), appliance parts (pot handles, knobs, bases, electrical/electronic components (connectors, circuit breakers, switches)), and as an adhesive in laminated materials (eg, plywood).

1.3.1.2 Epoxy resins

The most common epoxy resins are prepared from the reaction of bisphenol A and epichlorohydrin to yield low-molecular-weight resins that are liquid either at room temperature or on warming. Each polymer chain usually contains two or more epoxide groups. The high reactivity of the epoxide groups with amines, anhydrides, and other curing agents provides facile conversion into highly cross-linked materials. Cured epoxy resins exhibit hardness, strength, heat resistance, electrical resistance, and broad chemical resistance. Epoxy resins are used in glass-reinforced, high-strength composites in aerospace, pipes, tanks, and pressure vessels; encapsulation or casting of various electrical and electronic components (printed wiring boards, etc.); adhesives; protective coatings in appliances, flooring, and industrial equipment; and sealants.

1.3.1.3 Unsaturated polyesters

Unsaturated polyesters are prepared by the condensation polymerization of various diols and maleic anhydride to give a very viscous liquid that is dissolved in styrene monomer. The addition of styrene lowers the viscosity to a level suitable for impregnation and lamination of glass fibers. The low-molecular-weight polyester has numerous fumarate ester units that provide easy reactivity with styrene monomer. Properly formulated glass-reinforced unsaturated polyesters are commonly referred to as sheet molding compound (SMC), or reinforced plastics. In combination with reinforcing materials such as glass fiber, cured resins offer outstanding strength, high rigidity, impact resistance, high strength-to-weight ratio, and chemical resistance. SMC typically is formulated with 50% calcium carbonate filler, 25% long glass fiber, and 25% unsaturated polyester. The highly filled nature of SMC results in high density and brittle easily pitted surfaces. Bulk molding compound (BMC) is formulated similar to SMC except that in one to four chopped glass is used. The shorter glass length provides easier processing but lower strength and impact.

The prime use of unsaturated polyesters is in combination with glass fibers in high-strength composites and in SMC and BMC materials. The applications include transportation markets (large body parts for automobiles, trucks, trailers, buses, and aircraft), marine markets (small- to medium-sized boat hulls and associated marine equipment), building panels, housing and bathroom components (bathtub and shower stalls), appliances, and electrical/electronic components.

1.3.1.4 Alkyd resins

Alkyd resins are based on branched prepolymers from glycerol, phthalic anhydride, and glyceryl esters of fatty acids. Alkyds have excellent heat resistance, are dimensionally stable at high temperatures, and have excellent dielectric strength ($\sim$14 MV/m),

high resistance to electrical leakage, and excellent arc resistance. Alkyd resin applications include drying oils in enamel paints, lacquers for automobiles and appliances; and molding compounds when formulated with reinforcing fillers for electrical applications (circuit breaker insulation, encapsulation of capacitors and resistors, and coil forms).

1.3.1.5 Diallyl phthalate

Diallyl phthalate (DAP) is the most widely used compound in the allylic family. The neat resin is a medium-viscosity liquid. These low-molecular-weight prepolymers can be reinforced and compression molded into highly cross-linked, completely cured products. The most outstanding properties of DAP are excellent dimensional stability and high insulation resistance. In addition, DAP has high dielectric strength, excellent arc resistance, and chemical resistance. DAP applications include electronic parts, electrical connectors, bases, and housings. DAP is also used as a coating and impregnating material.

1.3.1.6 Amino resins

The two main members of the amino family of thermosets are the melamine and urea resins. They are prepared from the reaction of melamine and urea with formaldehyde. In general, these materials exhibit extreme hardness, scratch resistance, electrical resistance, and chemical resistance. Melamine resins find use in colorful, rugged dinnerware, decorative laminates (countertops, tabletops, and furniture surfacing), electrical applications (switchboard panels, circuit breaker parts, arc barriers, and armature and slot wedges), and adhesives and coatings. Urea resins are used in particleboard binders, decorative housings, closures, electrical parts, coatings, and paper and textile treatment.

1.3.2 Thermoplastics

Thermoplastics consist of linear or branched chain molecules having strong intramolecular bonds but weak intermolecular bonds. They can be reshaped by application of heat and pressure and are either semicrystalline or amorphous in structure. Examples include polyethylene, polypropylene, polystyrene, nylons, polycarbonate, polyacetals, polyamideimides, polyether ether ketone, polysulfone, polyphenylene sulfide, polyether imide, and so on.

Thermoplastics differ from thermosetting materials in that they do not set or cure under heat.[7] When heated, thermoplastics merely soften to a mobile, flowable state where they can be shaped into useful objects. On cooling, thermoplastics harden and hold their shape. Thermoplastics can be repeatedly softened by heat and shaped.

Thermoplastics can be classified as amorphous or semicrystalline plastics.[8] Most polymers are either completely amorphous or have an amorphous component even if they are crystalline. Amorphous polymers are hard, rigid glasses below a sharply defined temperature, which is known as the glass transition temperature. Above the

glass transition temperature the amorphous polymer becomes soft and flexible and can be shaped. Mechanical properties show profound changes near the glass transition temperature. Many polymers are not completely amorphous but are semicrystalline. Crystalline polymers have melting points that are above their glass transition temperature. The degree of crystallinity and the morphology of the crystalline phase have an important effect on mechanical properties. Crystalline plastics will become less rigid above their glass transition temperature but will not flow until the temperature is above the crystalline melting point. At ambient temperatures crystalline/semicrystalline plastics have greater rigidity, hardness, density, lubricity, creep resistance, and solvent resistance than amorphous plastics.

Engineering thermoplastics comprise a special high-performance segment of synthetic plastic materials that offer premium properties.[9] When properly formulated, they may be shaped into mechanically functional, semiprecision parts or structural components. Mechanically functional implies that the parts may be subjected to mechanical stress, impact, flexure, vibration, sliding friction, temperature extremes, hostile environments, etc., and continue to function. As substitutes for metal in the construction of a mechanical apparatus, engineering plastics offer advantages such as transparency, lightweight, self-lubrication, and economy in fabrication and decorating. Replacement of metals by plastic is favored as the physical properties and operating temperature ranges of plastics improve and the cost of metals and their fabrication increases.

1.3.2.1 Polyesters (thermoplastic)

Poly(butylene terephthalate), PBT, is prepared from the condensation polymerization of butanediol with dimethyl terephthalate.[10] PBT is a crystalline polymer that has a fast rate of crystallization that facilitates rapid molding cycles. It seems to have a unique and favorable balance of properties between polyamides and polyacetals. PBT has low moisture absorption, extremely good self-lubricity, fatigue resistance, good solvent resistance, and good maintenance of mechanical properties at elevated temperatures. PBT resins are often used with reinforcing materials such as glass fiber to enhance strength, modulus, and heat deflection temperature. Applications of PBT include gears, rollers, bearings, housings for pumps and appliances, impellers, pulleys, switch parts, automotive components, and electrical/electronic components. A high-density PBT is also used in countertops and sinks.

1.3.2.2 Polyamides (nylon)

The two major types of polyamides are nylon 6 and nylon 66.[11] Nylon 6, or polycaprolactam, is prepared by the polymerization of caprolactam. Poly(hexamethylene adipamide), or nylon 66, is derived from the condensation polymerization of hexamethylene diamine with adipic acid. Polyamides are crystalline polymers. Their key features include a high degree of solvent resistance, toughness, and fatigue resistance. Nylons do exhibit a tendency to creep under applied load. Glass fibers or mineral fillers are

often used to enhance the properties of polyamides. In addition the properties of nylon are greatly affected by moisture.

The largest application of nylons is in fibers. Molded applications include automotive components, related machine parts (gears, cams, pulleys, rollers, boat propellers, etc.), appliance parts, and electrical insulation.

1.3.2.3 Polyacetals

Polyacetals are prepared via the polymerization of formaldehyde or the copolymerization of formaldehyde with ethylene oxide.[12] Polyacetals are crystalline polymers that exhibit rigidity, high strength, solvent resistance, fatigue resistance, toughness, self-lubricity, and cold-flow resistance. They also exhibit a tendency to thermally depolymerize and, hence, are difficult to flame retard. Properties are enhanced by the addition of glass fiber or mineral fillers. Applications of polyacetals include moving parts in appliances and machines (gears, bearings, bushings, etc.), in automobiles (door handles, etc.), plumbing and irrigation (valves, pumps, faucets, shower heads, etc.), industrial or mechanical products (rollers, bearings, gears, conveyer chains, and housings), and consumer products (cams, zippers, pen barrels, disposable lighters, and combs).

1.3.2.4 Polyphenylene sulfide

The condensation polymerization of dichlorobenzene and sodium sulfide yields a crystalline polymer, polyphenylene sulfide (PPS).[13] It is characterized by high heat resistance, rigidity, excellent chemical resistance, low friction coefficient, good abrasion resistance, and electrical properties. PPS is somewhat difficult to process due to the very high melting temperature, relatively poor flow characteristics, and some tendency for slight cross-linking during processing. PPS resins normally contain glass fibers for mineral fillers.

The reinforced materials are used in aerospace applications, chemical pump components, electrical/electronic components, and appliance parts, and in automotive applications (electrical connectors, under-the-hood applications).

1.3.2.5 Polycarbonates

Most commercial polycarbonates are derived from the reaction of bisphenol A and phosgene.[14] Polycarbonates (PC) are transparent amorphous polymers. PCs are among the stronger, tougher, and more rigid thermoplastics. Polycarbonates also show resistance to creep and excellent electrical insulating characteristics.

Applications of PC include safety glazing, safety shields, nonbreakable windows, automotive taillights, electrical relay covers, various appliance parts and housings, power tool housings, automotive exterior parts, and blow-molded bottles.

1.3.2.6 Polysulfone

Polysulfone is prepared from the condensation polymerization of bisphenol A and dichlorodiphenyl sulfone.[15] The transparent, amorphous resin is characterized by excellent thermooxidative stability, high heat resistance, hydrolytic stability, outstanding chemical resistance (acids, bases, and alcohols), and creep resistance.

Typical applications of polysulfones include microwave cookware, medical and laboratory equipment where repeated sterilization by steam is required, coffee makers, and electrical/electronic components, and chemical processing equipment.

1.3.2.7 Modified polyphenylene ether

Blends of poly(2,6-dimethyl phenylene ether), PPE, with styrenics (ie, HIPS, ABS, etc.) form a family of modified PPE-based resins.[16] These amorphous blends cover a wide range of heat deflection temperatures, which is dependent on the PPE-to-HIPS ratio. They are characterized by outstanding dimensional stability at elevated temperatures, outstanding hydrolytic stability, long-term stability under load, and excellent dielectric properties over a wide range of frequencies and temperatures.

Applications include automotive (instrument panels, trim, etc.), TV cabinets, electrical connectors, pumps, plumbing fixtures, business machines, medical, telecommunication equipment, microwavable food packaging, and appliances.

1.3.2.8 Polyimides

Polyimides are a class of polymers prepared from the condensation reaction of a carboxylic acid anhydride with a diamine.[17] Thermoplastic and thermoset grades of polyimides are available. The thermoset polyimides are among the most heat-resistant polymers; for example, they can withstand temperatures up to 250°C. Thermoplastic polyimides, which can be processed by standard techniques, fall into two main categories—polyetherimides (PEI) and polyamideimides (PAI).[18] In general, polyimides have high heat resistance, high deflection temperatures, very good electrical properties, very good wear resistance, superior dimensional stability, outstanding flame resistance, and very high strength and rigidity.

Polyimide applications include gears, bushings, bearings, seals, insulators, electrical/electronic components (printed wiring boards, connectors, etc.). PEI is used in transportation (under-the-hood temperature sensors, fuel system components, high-strength transmission, and jet engine parts), medical (autoclaveable parts), electrical/electronics, packaging, appliances, industrial (heat and corrosion resistance, air and fluid handling components), cooking utensils, microwave oven components, and structural components. PAI is used in automobile transmissions (thrust washers and seal rings), parts for gas turbine engines, business machines, hot glass-handling equipment, and plasma-cutting torches. Polyimide foam is used for thermal and sound-dampening insulation and seat cushions in aerospace, marine, and industrial applications.

1.3.3 Elastomers

Elastomeric materials are rubberlike polymers with glass transition temperatures below room temperatures. Below that glass transition temperature an elastomer will become rigid and lose its rubbery characteristics. Elastomers are long polymer chains above their glass transition temperature. Elastomers are usually lightly cross-linked and are easily deformed. Common elastomers include polybutadiene (used in shoe soles), polyisobutylene (used in automobile tires), and polyisoprene (natural rubber).

Elastomeric polymer chains can be cross-linked, or connected by covalent bonds. This process is sometimes called vulcanization. Cross-linking is initiated by heat, light, or the addition of chemicals. Cross-linking makes elastomers reversibly stretchable for small deformations. When stretched, the polymer chains become elongated and ordered along the deformation direction. This is entropically unfavorable. When no longer stretched, the chains randomize again. The cross-links guide the elastomer back to its original shape.

An elastomer is a polymer with the property of viscoelasticity, generally having a notably low Young's modulus (E) and high yield strain compared with other materials. The term, which is derived from elastic polymer, is often used interchangeably with the term rubber, although the latter is preferred when referring to vulcanizates. Each of the monomers that link to form the polymer is usually made of carbon, hydrogen, oxygen, and silicon. Elastomers are amorphous polymers existing above their glass transition temperature, so that considerable segmental motion is possible. At ambient temperatures, rubbers are relatively soft ($E = 3$ MPa) and deformable. Their primary uses are for seals, adhesives, and molded flexible parts. Natural rubber, synthetic polyisoprene, polybutadiene, chloroprene rubber, butyl rubber, ethylene propylene rubber, epichlorohydrin rubber, silicone rubber, fluoroelastomers, thermoplastic elastomers, polysulfide rubber, and so on are some of the examples of elastomers.

Elastomers are polymers that can be stretched substantially beyond their original length and can retract rapidly and forcibly to essentially their original dimensions (on release of the force).[19]

The optimum properties and/or economics of many rubbers are obtained through formulating with reinforcing agents, fillers, extending oils, vulcanizing agents, antioxidants, pigments, etc. End-use markets for formulated rubbers include automotive tire products (including tubes, retread applications, valve stems, and inner liners), adhesives, cements, caulks, sealants, latex foam products, hoses (automotive, industrial, and consumer applications), belting (V conveyor and trimming), footwear (heels, soles, slab stock, boots, and canvas), molded, extruded, and calendered products (athletic goods, flooring, gaskets, household products, O-rings, blown sponge, thread, and rubber sundries).

1.3.4 Foams

Many natural materials are cellular: wood and bone, for example; cork and coral, for instance. There are good reasons for this: cellular materials permit an optimization of stiffness, or strength, or of energy absorption, for a given weight of material. These

natural foams are widely used by people (wood for structures, cork for thermal insulation), and synthetic foams are common too: cushions, padding, packaging, insulation, are all functions filled by cellular polymers. Foams provide a way of making solids which are very light and, if combined with stiff skins to make sandwich panels, they give structures which are exceptionally stiff and light. The engineering potential of foams is considerable, and, at present, incompletely realized.

Most polymers can be foamed easily. It can be done by simple mechanical stirring or by blowing a gas under pressure into the molten polymer. But by far the most useful method is to mix a chemical blowing agent with the granules of polymer before processing: it releases CO_2 during the heating cycle, generating gas bubbles in the final molding. Similar agents can be blended into thermosets so that gas is released during curing, expanding the polymer into a foam; if it is contained in a closed mold it takes up the mold shape accurately and with a smooth, dense surface.

The properties of a foam are determined by the properties of the polymer, and by the relative density, ρ/ρ_s: the density of the foam (ρ) divided by that of the solid (ρ_s) of which it is made. This plays the role of the volume fraction V_f of fibers in a composite, and all the equations for foam properties contain ρ/ρ_s. It can vary widely, from 0.5 for dense foam to 0.005 for a particularly light one.

The cells in foams are polyhedral, like grains in a metal (Fig. 1.5). The cell walls, where the solid is concentrated, can be open (like a sponge) or closed (like a flotation foam), and they can be equiaxed (like the polymer foam in the figure) or elongated (like cells in wood). But the aspect of structures which is most important in determining properties is none of these; it is the relative density and direction of growth.

1.3.5 Ceramic–matrix composites

A number of ceramic composites systems have reached the commercial stage of development in which process and properties are defined and available in commercial quantities and geometries. The different systems are described in terms of their fabrication technology—chemical vapor infiltration, directed metal oxidation, polymer-derived ceramics, oxide systems by sintering and hot pressing, and carbon–carbon composites by pyrolysis or chemical vapor deposition.

For ceramic composites, a number of historical and developmental fabrication technologies have not yet advanced to commercial availability. These methods are important to the market in terms of background and historical information and also for the potential of future commercialization, depending on technical and economic success. The specific fabrication systems are: sol–gel processing, reaction processing, and fibrous monoliths.

Polymer-derived ceramics offer a unique solution to fabricating ceramic matrix composites. By tailoring polymer molecular structure and molecular weight, materials can be produced that allow fabrication using polymer composite processes such as lay-up–autoclave consolidation, resin transfer molding, filament winding, and fiber placement. Using polymers with high char yields, the resulting parts can be heat treated (pyrolyzed) in inert or reactive atmospheres to yield fiber-reinforced ceramic matrix composites. This approach has been used to fabricate a variety of

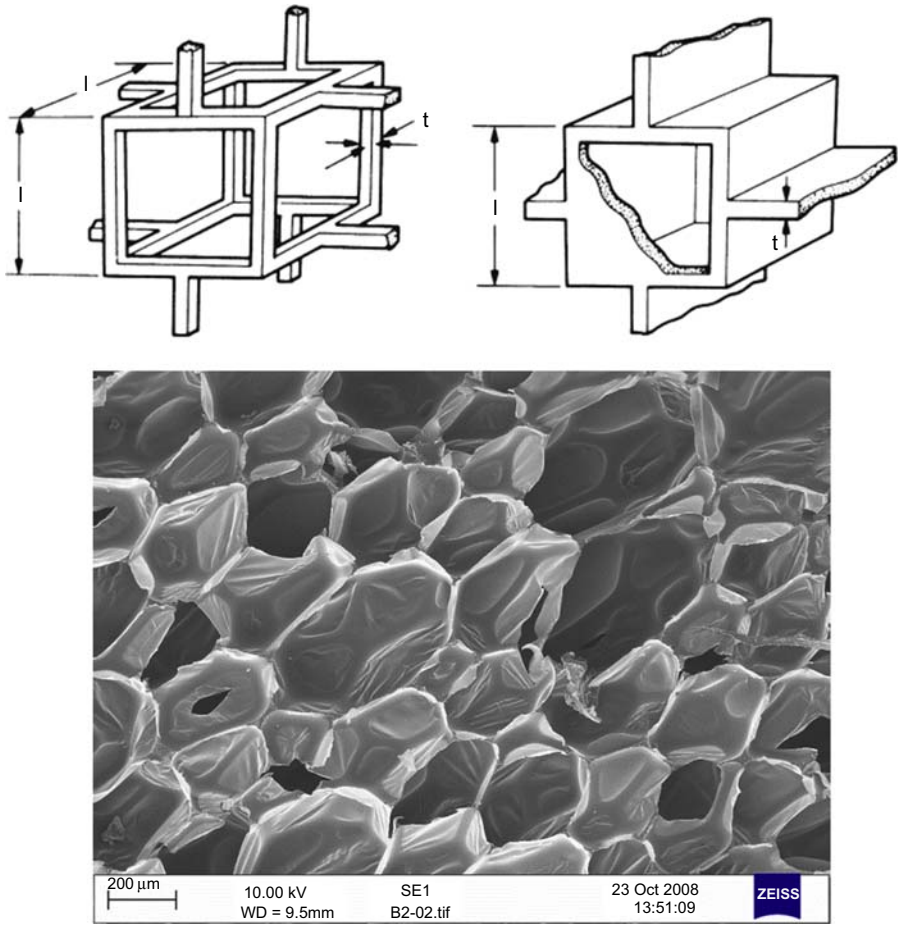

Figure 1.5 Polymeric foams, showing the polyhedral cells. Some foams have closed cells, others have cells which are open.

ceramic matrix composite compositions, including the commonly available matrices of Si−C, Si−C−O, Si−N, and Si−N−C.

As is the case with other ceramic matrix composites being discussed, coated continuous fibers are introduced into the polymer-derived ceramic matrix to provide the desired strength, toughness, and "graceful failure." The coating is designed to properly tailor the fiber−matrix interface to achieve the desired material properties and is similar, both in composition and in method of application, to those used with other ceramic matrix composites. Similar fibers are also used with the added ability to incorporate lower temperature capable fibers (Astroquartz, Nextel 312) into a polymer-derived ceramic matrix when fabricated at low processing temperatures (<1832°F (<1000°C)).

Particulate ceramics and ceramic whiskers and platelets can be used to supplement the matrix provided by the pyrolyzed polymer. Fillers can improve matrix properties by reducing and disrupting the regularity of matrix cracks that form during the shrinkage of the polymer precursor. In addition, the fillers can enhance the ceramic yield during initial pyrolysis by their mass or by reacting with pyrolysis by-products or the pyrolysis atmosphere and can be used to strengthen and toughen the matrix. Well-chosen fillers can slightly raise composite modulus and improve interlamina properties.

1.3.6 Metal–matrix composites

A metal matrix composite system is generally designated simply by the metal alloy designation of the matrix and the material type, volume fraction, and form of the ceramic reinforcement. For example, 6061Al/30v/o SiCp designates a discontinuously reinforced 6061 aluminum alloy with 30 volume percent silicon carbide particulate reinforcement.

MMCs differ from other composite materials in several ways. Some of these general distinctions are as follows:

1. The matrix phase of an MMC is either a pure or alloy metal as opposed to a polymer or ceramic.
2. MMCs evidence higher ductility and toughness than ceramics or CMCs, although they have lower ductility and toughness than their respective unreinforced metal matrix alloys.
3. The role of the reinforcement in MMCs is to increase strength and modulus as is the case with PMCs. Reinforcement in CMCs is generally to provide improved damage tolerance.
4. MMCs have a temperature capability generally higher than polymers and PMCs but less than ceramics and CMCs.
5. Low to moderately reinforced MMCs are formable by processes normally associated with unreinforced metals.

Metals are extremely versatile engineering materials. A metallic material can exhibit a wide range of readily controllable properties through appropriate selection of alloy composition and thermomechanical processing method. The extensive use of metallic alloys in engineering reflects not only their strength and toughness but also the relative ease and low cost of fabrication of engineering components by a wide range of manufacturing processes. The development of MMCs has reflected the need to achieve property combinations beyond those attainable in monolithic metals alone. Thus, tailored composites resulting from the addition of reinforcements to a metal may provide enhanced specific stiffness coupled with improved fatigue and wear resistance, or perhaps increased specific strength combined with desired thermal characteristics (eg, reduced thermal expansion coefficient and conductivity) in the resulting MMC. However, the cost of achieving property improvements remains a challenge in many potential MMC applications.

MMCs involve distinctly different property combinations and processing procedures as compared to either PMCs or CMCs. This is largely due to the inherent differences among metals, polymers, and ceramics as matrix materials and less so to the nature of the reinforcements employed. Pure metals are opaque, lustrous chemical elements and are generally good conductors of heat and electricity. When polished, they tend to reflect light well. Also, most metals are ductile but are relatively high in density. These characteristics reflect the nature of atom bonding in metals, in which the atoms tend to lose electrons; the resulting free electron "gas" then holds the positive metal ions in place. In contrast, ceramic and polymeric materials are chemical compounds of elements. Bonding in ceramics and intramolecular bonding in polymers are characterized by either the sharing of electrons between atoms or the transfer of electrons from one atom to another. The absence of free electrons in ceramics and polymers (no free electrons are formed in polymers due to intermolecular van der Waals bonding) results in poor conductivity of heat and electricity, and lower deformability and toughness in comparison to metallic materials.

1.4 Reinforced composites

1.4.1 Synthetic fiber reinforcement

A fiber-reinforced polymer (FRP) is a composite material consisting of a polymer matrix imbedded with high-strength fibers, such as glass, aramid, and carbon.[20] Generally, polymer can be classified into two classes, thermoplastics and thermosettings. Thermoplastic materials currently dominate, as matrices for biofibers; the most commonly used thermoplastics for this purpose are polypropylene, polyethylene, and polyvinyl chloride; while phenolic, epoxy, and polyester resins are the most commonly used thermosetting matrices.[21] In the recent decades, natural fibers as an alternative reinforcement in polymer composites have attracted the attention of many researchers and scientists due to their advantages over conventional glass and carbon fibers.[22] These natural fibers include flax, hemp, jute, sisal, kenaf, coir, kapok, banana, henequen, and many others.[23] The various advantages of natural fibers over man-made glass and carbon fibers are low cost, low density, comparable specific tensile properties, nonabrasive to the equipment, nonirritation to the skin, reduced energy consumption, less health risk, renewability, recyclability, and biodegradability. These composites materials are suitably applicable for aerospace, leisure, construction, sport, packaging, and automotive industries, especially for the last noted application.[24] However, the certain drawback of natural fibers/polymers composites is the incompatibility between the hydrophilic natural fibers and the hydrophobic thermoplastic matrices. This leads to undesirable properties of the composites. It is therefore necessary to modify the fiber surface by employing chemical modifications to improve the adhesion between fiber and matrix.

1.4.2 Particle reinforcement

Particle reinforcement is the cheapest and most widely used. This fall into two categories depending on the size of the particles:

- Large-particle composites: a type of particle-reinforced composite wherein particle−matrix interactions cannot be treated on an atomic or molecular level; the particle reinforced the matrix phase.
- Dispersion-strengthened composites, containing 10- to 100-nm particles, similar that discussed under precipitation hardening. The matrix bears the major portion of the applied load and the small particles hinder dislocation motion, limiting plastic deformation.

Some polymeric materials to which fillers have been added are really large- particle composites. The fillers modify or improve the properties of the material. An example of a large-particle composite is concrete, which is composed of cement (the matrix) and sand and gravel (the particulates).

Particles can have quite a variety of geometries, but they should be of approximately the same dimension in all direction (equiaxed). For effective reinforcement, the particles should be small and evenly distributed throughout the matrix. The volume fraction of the two phases influences the behavior; mechanical properties are enhanced with increasing particulate content.

Rule of mixture: equation to predict that the elastic modulus should fall between an upper and a lower bound as shown:

$$E_c(u) = E_m V_m + E_p V_p$$

$$E_c(l) = \frac{E_m E_p}{V_m E_p + V_p E_m}$$

where E_c is elastic modulus of composite; E_p is elastic modulus of particle; E_m is elastic modulus of matrix; V_m is volume fraction of matrix; V_p is volume fraction of particle.

1.4.3 Green composites

One of the major growing concerns in all the industries including automotive is an increased awareness for the environment. Technical issues such as the "protection of resources," "reduction of CO_2 emissions," and "recycling" are increasing the topics of consideration.

European Union legislation implemented in 2006 dictates that a significant percentage of the vehicle should be reused or recycled. The ELV directive from the environment agency aims to reduce the amount of waste produced from vehicles when they are scrapped. Around two million vehicles reach the end of their life in the United Kingdom each year. These vehicles are classed as hazardous waste until they have

been fully treated. The directive requires ELV treatment sites to meet stricter environmental standards. This would mean that the last owner of a vehicle must be issued with a Certificate of Destruction for their vehicle and they must be able to dispose of their vehicle free of charge. Vehicle manufacturers and importers must cover all or most of the cost of the free take-back system. It also sets higher reuse, recycling, and recovery targets and limits the use of hazardous substances in both new vehicles and replacement vehicle parts.

As a result of the new legislations, no discussion of new materials in the automotive industry should conclude without a consideration of recycling. Considerable R&D efforts are now focused on developing materials with greater potential of recycling and reuse or developing ways of recycling and reuse of the current materials. This includes both metal and composite materials. The composition and forming processes of the metal materials are changing to accommodate this recycle and reuse demand. This also justifies the great attention toward natural fiber-based composites and new high temperature-resistant thermoplastic resins.

The lightweight, low cost natural fibers offer the possibility of replacing a large portion of the glass and mineral fillers in several automotive interior and exterior parts. From 2005 to 2015, natural fiber composites with thermoplastic and thermoset matrices have been embraced by European car manufacturers and suppliers for door panels, seat backs, headliners, package trays, dashboards, and interior parts. Fig. 1.6 lists several vegetable and cellulose fiber classifications. Natural fibers such as kenaf, hemp, flax, jute, and sisal are providing automobile part reinforcement due to such drivers as reductions in weight, cost, and CO_2, less reliance on foreign oil sources, recyclability, and the added benefit that these fiber sources are "green" or ecofriendly. As a result, today most automakers are evaluating the environmental impact of a vehicle's entire life cycle, from raw materials to manufacturing to disposal.[25] At this time, glass fiber-reinforced plastics have proven to meet the structural and durability demands of automobile interior and exterior parts. Good mechanical properties and a well-developed, installed manufacturing base have aided in the insertion of fiberglass-reinforced plastics within the automotive industry. However, glass-reinforced plastics show shortcomings such as relatively high fiber density

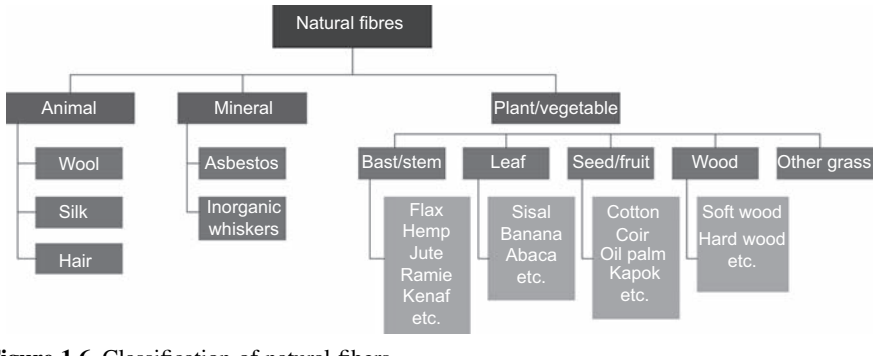

Figure 1.6 Classification of natural fibers.

(approximately 40% higher than natural fibers), difficulty to machine, and poor recycling properties, not to mention the potential health hazards posed by glass-fiber particulates.

An ecological evaluation, or ecobalance, of natural fiber mats as compared to glass-fiber mats offers another perspective. The energy consumption to produce a flax-fiber mat (9.55 MJ/kg), including cultivation, harvesting, and fiber separation, amounts to approximately 17% of the energy to produce a glass-fiber mat (54.7 MJ/kg).[26] Though natural fiber-reinforced plastic parts offer many benefits as compared to fiberglass, several major technical considerations must be addressed before the engineering, scientific, and commercial communities gain the confidence to enable wide-scale acceptance, particularly in exterior parts where a Class A surface finish is required. Challenges include the homogenization of the fiber's properties, and a full understanding of the degree of polymerization and crystallization, adhesion between the fiber and the matrix, moisture repellence, and flame-retardant properties, to name but a few. Technology for implementing natural fiber composites into interior trim continues to be developed by Tier I and Tier II automotive suppliers, typically in partnership with producers of natural fiber-based processing capabilities for mat or other material forms. Compression molding, injection molding, thermoforming, and structural reaction injection molding are all processes utilized to process natural fiber composites.

Some recent developments are pushed by the fact that, unfortunately, even these "green" composites are not fully ecocompatible, since their recyclability has some limitations and their biodegradability regards only the filler but not, of course, traditional (petroleum-based) polymer matrices.[27]

For this reason, research efforts are progressing in developing a new class of fully biodegradable green composites by combining fibers with biodegradable resins. The major attractions about green composites are that they are ecofriendly fully degradable and sustainable; that is, they are truly green in every way. The design and life cycle assessment of green composites have been exclusively dealt with by Baillie. Green composites may be used effectively in many applications such as mass-produced consumer products with short life cycles or products intended for one time or short time use before disposal. The important biodegradable matrices are polyamides, polyvinyl alcohol, polyvinyl acetate, polyglycolic acid, and polylactic acid, which are synthetic as well as polysaccharides, starch, chitin, cellulose, proteins, collagens/gelatin, lignin, and so on, which are natural.[28] In the majority of cases, they degrade through enzymatic reactions in suitable environments (typically, humid).[29]

As a general rule, biodegradable polymers can be classified according to their origin, ie, into agropolymers (eg, starch), microbial-derived (eg, PHA) and chemically synthesized from agro-based monomers (eg, PLA) or conventional monomers (eg, synthetic polyesters).[30]

Bio-based composites with their constituents developed from renewable resources are being developed and their applications have extended to almost all fields. Natural fiber composites can be used as a substitute for timber and for a number of other applications. It can be molded into sheets, boards, gratings, pallets, frames, structural sections, and many other shapes. They can be used as a substitute for wood, metal, or

masonry for partitions, false ceilings, facades, barricades, fences, railings, flooring, roofing, wall tiles, and so on.[31] It can also be used in prefabricated housing, cubicles, kiosks, awnings, and sheds/shelters.

1.5 Sandwich composites

Sandwich-structured composites are a special class of composite materials which have become very popular due to high specific strength and bending stiffness. Low density of these materials makes them especially suitable for use in aeronautical, space, and marine applications.

The concept of sandwich-structured composite materials can be traced back to as early as the year AD 1849[32] but the potential of this construction could be realized only during the Second World War.

Developments in aviation posed requirement of lightweight, high strength, and highly damage-tolerant materials. Sandwich-structured composites fulfilling these requirements became the first choice for many applications including structural components. Now their structural applications spread even to ground transport and marine vessels.

1.5.1 Definition

Sandwich composites comprise two thin but stiff face sheets attached on either side of a lightweight, thick slab known as the core. Many variations of this definition are available but the key factor in making this type of material remains the lightweight core, which reduces the overall density of the material and stiff skins providing strength. The structure of sandwich composites is shown in Fig. 1.7.

Integral bonding between skins and core prevents the interfacial failure under the applied load enhancing the flexural properties of sandwich composites. There is no general rule about the relationship between the thickness of skin and core. It depends on the application and required properties. A major advantage of sandwich-structured composites is the possibility of tailoring properties by choosing appropriate constituting materials and their volume fractions.

1.5.2 Components in sandwich composites

Sandwich composites primarily have two components, namely skin and core as shown in Fig. 1.7. If an adhesive is used to bind skins with the core, the adhesive layer can also be considered as an additional component in the structure. The thickness of the adhesive layer is generally neglected because it is much smaller than the thickness of skins or the core. The properties of sandwich composites depend on properties of the core and skins, their relative thickness, and the bonding characteristics between them.

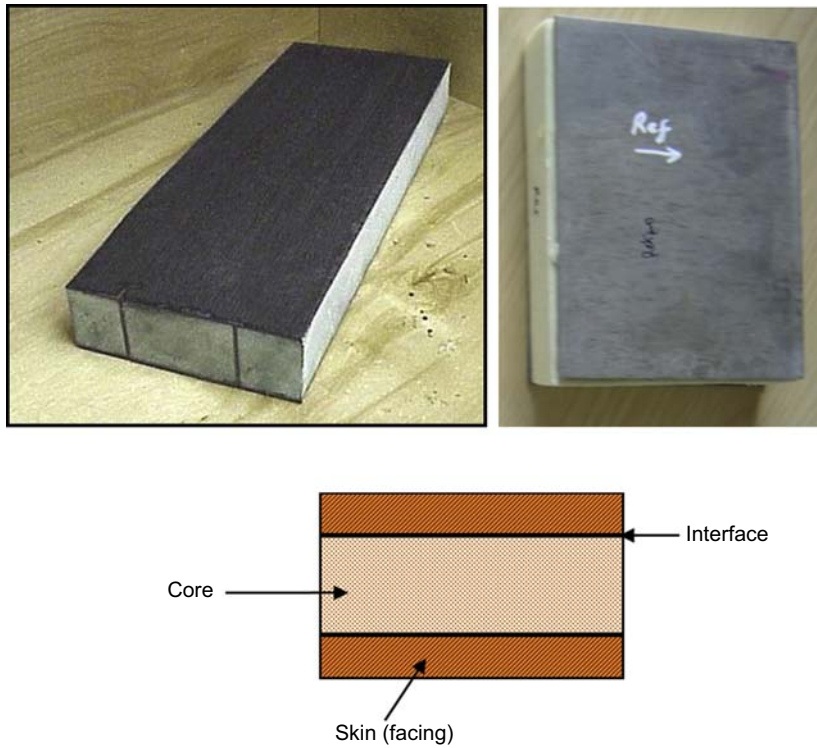

Figure 1.7 The structure of a sandwich composite.

1.5.2.1 Core

Based on the performance requirements, large numbers of materials are used as core.[33] Popular core materials can be divided into three classes as described below.

1. Low-density solid materials: open and closed cell structured foams, balsa, and other types of wood.
2. Expanded high-density materials in cellular form: honeycomb, web core.
3. Expanded high-density materials in corrugated form: truss, corrugated sheets.

High-density materials used for the purpose of making expanded core include aluminum, titanium, and various polymers. The structure of the core material affects the interfacial contact area between the skin and the core. Expanded high-density materials normally provide much smaller contact area compared to the solid low-density materials. The choice of appropriate structure for core provides additional parameters for designing a sandwich composite as per given specifications or service conditions.

The use of cores like closed cell structured foam gives some distinct advantages over open cell structured foams and cores. The specific compressive strength of close cell structured foams is much higher. They also absorb less moisture than open cell structured foam.

1.5.2.2 Skins

A wide variety of materials are available for use as skins. Sheets of metals such as aluminum, titanium, and steel and fiber-reinforced plastics are some of the common examples of skin materials. In the case of fiber-reinforced skins, the material properties can be controlled directionally to tailor the properties of the sandwich composite. Fiber-reinforced polymers are used widely as skins due to their low density and high specific strength. Another advantage offered by the use of polymer composites in skins is that the same polymer can be used to make the skin and the core. Cross-linking of polymer between core and skin would provide adhesion strength level equal to the strength of the polymer. This provides the possibility of making the skin an integral part of the structure, eliminating the requirement of the adhesive.

When an adhesive is used to bond the skin and the core together, selection of adhesives becomes very important, as they should be compatible with both the skin and the core materials. The adhesion must have the desired strength level and should remain unaffected by the working environment.

In the case of metallic components, welding or brazing is used as a means of binding the core and skins together. Use of adhesives is also possible but is limited to such cases where one or more of the components cannot withstand heat.

Choice of skins is important from the point of view of the work environment as this part of the structure comes in direct contact with the environment. Corrosion, heat transfer characteristics, thermal expansion characteristics, moisture absorption, and other properties of the whole sandwich composite can be controlled by proper choice of skin material. In most cases both skins of the sandwich are of the same type, but could be of different type depending on specific requirements. Difference may be in terms of materials, thickness, fiber orientation, and fiber volume fraction or in any other possible form.

1.5.2.3 Properties of sandwich composites

The main advantage of any type of composite material is the possibility of tailoring their properties according to the application. The same advantage also applies to sandwich composites. Proper choice of core and skins makes sandwich composites adaptive to a large number of applications and environmental conditions. Some general characteristics of sandwich composites are described below:

1. Low density: choice of lightweight core or expanded structures of high-density materials decrease the overall density of the sandwich composite. Volume of core is considerably higher in the sandwich composite compared to the volume of skins so any decrease in the density of the core material has a significant effect on the overall sandwich density.
2. Bending stiffness: this property comes from the skin part of the sandwich. Due to a higher specific stiffness sandwich composites result in lower lateral deformation, higher buckling resistance, and higher natural frequencies compared to other structures.
3. Tensile and compressive strength: the z direction (Fig. 1.8) properties are controlled by the properties of core and x and y directions (Fig. 1.8) properties are controlled by the properties of the skins.

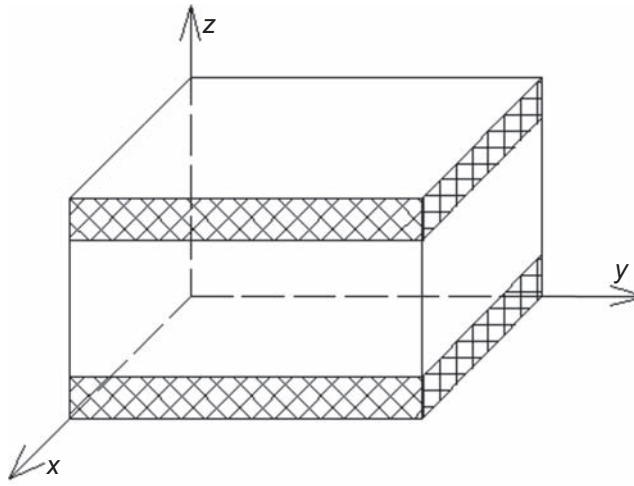

Figure 1.8 Illustration of geometrical properties of sandwich composite.

4. Damage tolerance: use of flexible foam or crushable material as core makes sandwich material a highly damage-tolerant structure. For this reason foam core or corrugated core sandwich-structured materials are popular materials in packaging applications.

Some of the advantages of sandwich composites are:

- Tailoring of properties according to requirements;
- Large available choice of constituents for core and skins;
- Low density leading to saving of weight;
- High bending stiffness;
- Higher damage tolerance;
- In situ fabrication;
- Good vibration damping capacity.

Despite all these advantages, sandwich composites suffer sensitivity to impact-loading damage, and thus are limited in their function. Current limitations that can be overcome through the development of new materials and manufacturing methods include the higher thickness of the sandwich composites, higher cost of sandwich composites compared to conventional materials, processing is expensive, and difficult to join and difficult to repair, if damaged.

Further, low energy impact can cause structural damage to the core material, while the face sheet remains undamaged. If the damage to the core material remains undetected, a potential risk for the application arises. This is imaginable for real-life scenarios, such as tool dropping, runway debris, bird strikes, hailstorms, and ballistic loading. Therefore, it is crucial that the damage resistance characteristics of sandwich structures are improved. The damage initiation thresholds and damage size in sandwich structures primarily depend on the properties of the core materials and face sheets and the relationship between them. Honeycombs or foams have been classified as traditional core materials, for which thin face sheets are bound for sandwich

constructions. However, to decrease the damage, traditional core materials have been reinforced with nano-sized fillers[34–37] such as solid nanoparticles, nanoclays, and nanofibers. Innovativeness is essential in finding new combinations of core and skin materials and new ways to use them in various applications where conventional materials have already reached their performance limits.

There are several applications that require materials of low density, high strength, and high damage tolerance. Due to their light weight, sandwich composites are widely used in various kinds of vehicles used for air, ground, or sea transportation. Some of the main areas of applications of sandwich composites are listed below.

1. Structural applications: aircraft, spacecraft, submarine, ships and boats, surface transport vehicles, building materials, etc.
2. Packaging materials
3. Thermal and electrical insulation
4. Storage tanks

1.6 Outlook

Development of polymer materials from the mid-1990s to 2015 has been vigorous and promising, and the potentials are enormous. As a result, specific polymer materials fulfilling specific needs in and out of transport vehicles have been developed for vast applications. Polymer materials have therefore sprung up as a prominent material, amalgamating and greatly benefiting other industries, such as lithography, communication, leisure, electronic, civil engineering, and the transportation industry and for applications tenable to aerospace. Such materials have thus found their way into other industries, extending the horizons for more advancements, and back into transport applications, thereby completing the "utilization cycle."

Composites are able to meet diverse design requirements with significant weight savings as well as high strength-to-weight ratios as compared to conventional materials. Some advantages of composite materials over conventional ones are listed below:

- Tensile strength of composites is four to six times greater than that of steel or aluminum;
- Improved torsional stiffness and impact properties;
- Higher fatigue endurance limit (up to 60% of the ultimate tensile strength);
- 30–45% lighter than aluminum structures designed to the same functional requirements;
- Lower embedded energy compared to other structural materials such as steel and aluminum;
- Composites are less noisy while in operation and provide lower vibration transmission than metals;
- Composites are more versatile than metals and can be tailored to meet performance needs and complex design requirements;
- Long life offers excellent fatigue, impact, environmental resistance, and reduced maintenance;
- Composites enjoy reduced life-cycle cost compared to metals;
- Composites exhibit excellent corrosion resistance and fire retardancy;

- Improved appearance with smooth surfaces and readily incorporable integral decorative melamine are other characteristics of composites;
- Composite parts can eliminate joints/fasteners, providing part simplification and integrated design compared to conventional metallic parts.

Examples of future composites applications in the transportation sector can be expected as follows.

1.6.1 Automobiles

Despite the potential benefits of lighter weight and durability resulting from corrosion resistance, advanced composites are not recognized as a material of choice in the near term for automotive applications. Significant changes on a broad spectrum would be required to make advanced composites attractive for widespread commercial use in cars and trucks. The principal barrier is the high cost of the raw and fabricated materials when compared to existing options.

However there are opportunities for advanced composites in specific components in the commercial automotive sector. In specialty vehicles of several types, produced in small numbers, advanced composite materials have an opportunity to demonstrate their performance benefits, apart from the requirements of the competitive marketplace.

The composite industry worldwide is investing in process improvements for the molding of polymer composites using forms of conventional E-glass in mid-level performance resins, both thermoplastic and thermoset. Automobile's segment of composites accounts for about 50% of the thermoplastic and 24% of the thermoset composite market in the world.

Glass-reinforced thermoplastic polymer is a promising material for weight reduction because of the relatively low cost of the fiber, its fast cycle time, and its ability to facilitate parts integration. Carbon fiber-reinforced polymer is another candidate but will require breakthroughs in cost and manufacturing techniques to be cost-effective for high volume production.

Pressure for reductions in energy use and lower emissions levels makes advanced composites a favorable option for the automotive sector. The likely future business opportunities in automotive sector are as follows.

- Pultruded driveshafts
- RTM panel
- Fiberglass/epoxy springs for heavy trucks and trailers
- Rocker arm covers, suspension arms, wheels and engine shrouds
- Filament-wound fuel tanks
- Electrical vehicle body components and assembly units
- Valve guides
- Automotive racing brakes and train brakes
- Clutch plates

1.6.2 Marine

With composites exhibiting excellent resistance to the marine environment, their applications have made good inroads in the marine sector worldwide. Complex

configurations and the advantages of seamless hulls were the main driving factors in the development of FRP boats.

Racing powerboats employ advanced and hybrid composites for a higher performance craft and driver safety. Major structural elements, viz. deckhouses, hatch covers, king posts, and bow modules, appear to be very well suited for FRP construction.

Advanced composites materials on vessels have a potential to reduce fabrication and maintenance cost, enhance styling, reduce outfit weight, and increase reliability. Potential ship applications for composite materials are:

- Shafting overwraps,
- Life rails, handrails,
- Masts, stacks, and foundations
- Stanchions
- Propellers vanes, fans, and blowers
- Gear cases
- Valves and strainers
- Condenser shells.

1.6.3 Bicycles

Composite bicycle frames have been a largely American phenomenon, as a spin-off technology from the aircraft and boating industries. Manufacturing of composites requires greater technical expertise and investment for product development. A carbon composite bike frame is a complex structure with performance characteristics that include lightness, rigidity, durability, shock absorption, etc.

As composites fabrication offers variation over the length of the tube providing different fiber angles, different plies, different ply thickness, and different combinations of materials. So the properties of the end product made from composites can be tailored to specifications. Hybrid fiber (carbon and aramid), carbon/kevlar epoxy materials are ideal composite materials for bicycle components. The composites are finding application in bicycle components, such as

- Forks
- Handle bars and connecting bar ends
- Seat posts.

References

1. Mayer C, Wang X, Neitzel M. *Compos Part A* 1998;**29**:783−93.
2. Avila AF, Paulo CM, Santos DB, Fari CA. *Mater Charact* 2003;**50**:281−91.
3. Nicoleta I, Hickel H. *Dent Mater* 2009;**25**:810−9.
4. Bunsell AR, Harris B. *Composites* 1974;**5**:157.
5. Mkaddem A, Demirci I, Mansori ME. *Compos Sci Technol* 2008;**68**:3123−7.
6. Goodman SH, editor. *Handbook of thermoset plastics*. 2nd ed. Brookfield, CT: Plastics Design Library; 1999.

7. Peters EN. In: Brady Jr RF, editor. *Desk reference of polymer characterization and analysis*. Washington, DC: American Chemical Society; 2002.
8. Olabisi O, editor. *Handbook of thermoplastics*. New York: Marcel Dekker; 1998.
9. Peters EN, Arisman RK. In: Craver CD, Carraher CE, editors. *Applied polymer science—21st century*. New York: Elsevier; 2000.
10. Jaquiss DBG, Borman WFH, Campbell RW. *Kirk-othmer encyclopedia of chemical technology*. 3rd ed., vol. 18. New York: Interscience; 1982.
11. Kohan MI, editor. *Nylon plastics handbook SPE monograph*. Cincinnati, OH: Hanser Gardner; 1995.
12. Bottenbruch L, editor. *Engineering thermoplastics: polycarbonates-polyacetals—polyesters—cellulose esters*. Cincinnati, OH: Hanser Gardner; 1996.
13. Short JM, Hill HW. *Chemtech* 1972;**2**:481.
14. LeGrand DG, Bendler JT, editors. *Polycarbonates: science and technology*. New York: Marcel Dekker; 1999.
15. Johnson RN, Farnham AG, Clendinning RA, Hale WF, Merriam CN. *J Polym Sci Part A-1* 1967;**5**:2375.
16. Hay AS. *J Polym Sci* 1962;**58**:581.
17. Sroog CE. *J Polym Sci Macromol Rev* 1976;**11**:161.
18. Floryan DE, Serfaty IW. *Mod Plast* 1982;**59**:146.
19. Morton M, editor. *Rubber technology*. New York: Van Norstrand Reinhold; 1973.
20. Groover MP. *Fundamental of modern manufacturing*. 2nd, ed. 111 River Street, Hoboken, NJ: John Wiley & Sons, Inc; 2004.
21. Malkapuram R, Kumar V, Yuvraj SN. Recent development in natural fibre reinforced polypropylene composites. *J Reinf Plastics Compos* 2008;**28**:1169—89.
22. Nabi Saheb D, Jog JP. Natural fiber polymer composites: a review. *Adv Polym Technol* 1999;**18**:351—63.
23. Li X, Tabil LG, Panigrahi S, Crerar WJ. The influence of fiber content on properties of injection molded flax fiber-HDPE biocomposites. *Can Biosyst Eng* 2009;**08-148**:1—10.
24. Wambua P, Ivens J, Verpoest I. Natural fibres: can they replace glass in fibre reinforced plastics. *Compos Sci Technol* 2003;**63**:1259—64.
25. Holbery J, Houston D. Natural-fiber-reinforced polymer composites in automotive applications. *JOM* 2006;**11**:80—6.
26. Wötzel K, Wirth R, Flake R. Life cycle studies on hemp fibre reinforced components and ABS for automotive parts. Braunschweig University and Seeber. *Angew Makromol Chem* 1999;**272**(4763):121—7.
27. Marsh G. Next steps for automotive materials. *Mater Today* 2003;**6**:36—43.
28. Jayanarayanan K, Jose T, Thomas T, Joseph K. *Eur Polym J* 2009;**45**:1738—47.
29. Netravali AN, Chabba S. Composites get greener. *Mater Today* 2003;**6**:22—6.
30. Satyanarayana KG, Arizaga GC, Wypych F. Biodegradable composites based on lignocellulosic fibers—an overview. *Prog Polym Sci* 2009;**34**:982—1021.
31. Paul SA, Joseph K, Mathew JDG, Pothen LA, Thomas S. *Part A* 2010;**41**:1380—7.
32. Noor AK, Burton WS, Bert CW. Computational models for sandwich panels and shells. *Appl Mech Rev* 1996;**49**(3):155—98.
33. Vinson JR. *The behavior of sandwich structures of isotropic and composite materials*. Lancaster: Technomic; 1999.
34. Sachse S, Poruri M, Silva F, Michalowski S, Pielichowski K, Njuguna J. Effect of nanofillers on low energy impact performance of sandwich structures with nanoreinforced polyurethane foam cores. *J Sandwich Struct Mater* 2014;**16**(2):173—94.

35. Njuguna J, Pielichowski K. Polymer nanocomposites. *Struct Mater Process Transp* 2013: 339−69.
36. Njuguna J, Michałowski S, Pielichowski K, Kayvantash K, Walton AC. Fabrication, characterization and low-velocity impact testing of hybrid sandwich composites with polyurethane/layered silicate foam cores. *Polym Compos* 2011;**32**(1):6−13.
37. Njuguna J, Sachse S, Silva F. Energy absorption and low-velocity impact performance of nanocomposites: cones and Sandwich structures. In: *Structural nanocomposites*. Springer Berlin Heidelberg; 2013. p. 187−205.

2 Challenges, opportunities, and perspectives on lightweight composite structures: aerospace versus automotive

R.N. Yancey
VP Aerospace and Composites, Altair Engineering, Troy, MI, United States

2.1 Introduction

Composite usage continues to grow and all forecasts show that the composite materials industry will grow at a faster rate than most industries from 2015 to 2025 [1–3]. Two forecast graphs are shown in Figs. 2.1 and 2.2. While aerospace and wind energy dominate the usage today, many forecasts show a large growth potential in automotives. Given the volumes of material used by the automotive industry, any significant usage in mainstream automobiles will lead to a large increase in the composite materials market. In fact, the market in automotives could easily outstrip the aerospace and energy markets in a very short time.

The aerospace industry has driven much of the composites usage from 1995 to 2015 with significant acceleration in their use in primary structures. The automotive industry is now taking a serious look at composites and how they can help the industry meet the demanding fuel efficiency requirements in the near future. Both the aerospace and the automotive industries have needs for strong and lightweight materials that can perform in harsh environments, which composites offer. Both industries can also benefit from the corrosion and fatigue resistance of advanced composites and both industries must

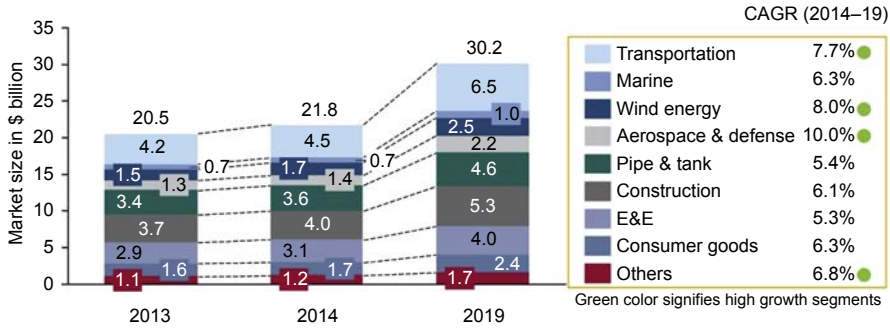

Figure 2.1 Global composites materials market forecast. Lucintel.

Lightweight Composite Structures in Transport. http://dx.doi.org/10.1016/B978-1-78242-325-6.00002-5

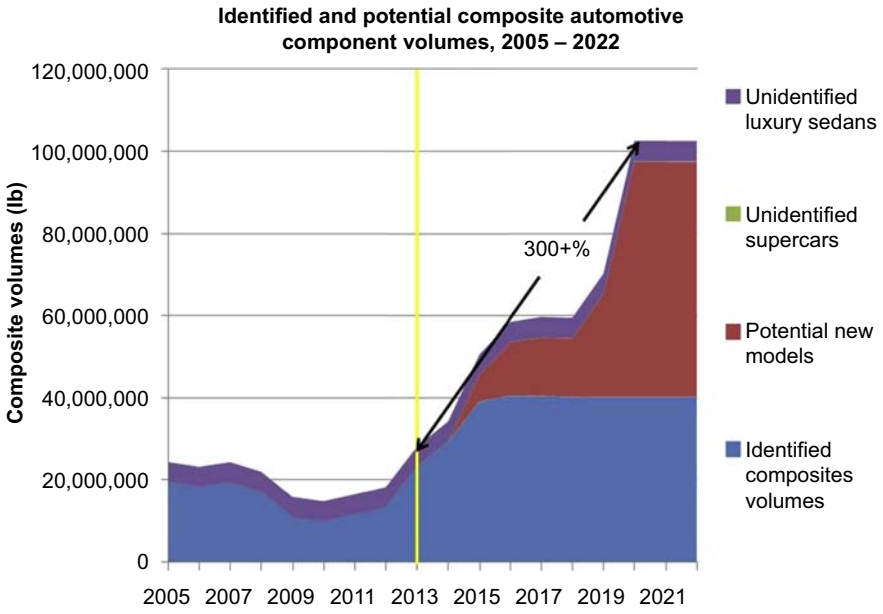

Figure 2.2 Automotive composites usage forecast.
Composites Forecasts and Consulting, LLC.

address recycling and repair issues with these materials. The aerospace industry has some requirements that are not pertinent to the automotive industry such as requirements for structural certification and buckling stability. The automotive industry has a number of other requirements unique from aerospace requirements that are the main limiting factors currently in the wider usage of these materials. These include requirements for cost, surface finish, impact performance, manufacturing cycle time, joining, manufacturing infrastructure, and volume. The automotive industry will take the extensive knowledge and experience that the aerospace industry has gained from 1995 to 2015 and use that as it moves forward with composites. Likewise, there are many areas of knowledge and expertise that the automotive industry will gain in addressing its unique challenges and requirements that will make it back to the aerospace industry to improve manufacturing and design methods for these materials. It truly is a symbiotic relationship between these two industries and in the end, the consumer will benefit from the advances made in the use of composite materials.

A key question to ask is if the use of composites in the aerospace industry is secure and if the potential use of composites in automotive is a reality or just wishful thinking. For the aerospace industry, composites have been used successfully for decades. Even though their use in primary structures in commercial aviation is relatively new, we have had lots of experience in their use on military aircrafts for some time. For commercial aviation, switching materials is a very expensive undertaking since material allowables are what drives design allowables and generating these allowables requires a lot of physical testing. Since airplanes such as the Boeing 787 and Airbus A350 have

committed to carbon fiber composites for major portions of the airplanes, barring a catastrophic series of failures traced back to these materials, they are here to stay and will likely be used in even greater percentages on future airplane designs.

For the automotive industry, the use of composites to date has been limited to race cars, high-end performance vehicles, and some high-end luxury vehicles. The higher cost of these materials is more easily justified for the high-end consumer market vehicles and the higher performance of composites justifies their use in race cars. What is driving their potential use for mainstream automotive is the increasing fuel economy standards being put in place in the United States and Europe. There are a number of design modifications that can lead to better fuel economy, but reducing the weight of the structure is one way of accomplishing this goal. The lower weight of the structure leads to a lower power generation requirement that has a multiplying effect on fuel economy. For example, if you now can achieve acceptable performance with a 4-cylinder engine versus a 6-cylinder engine by reducing weight of the automobile structure, you reduce the weight of the engine as well as the structure, which leads to even greater fuel economy.

One industry trend that points to the increasing interest of the automotive industry in the use of composites in the partnerships that have been formed over the last few years. BMW and SGL have partnered to build a carbon fiber production plant in Washington state in the United States to supply material for the BMW i3 and i8 vehicles, General Motors and Teijin have teamed up, Toyota, Toray, and FHI have created a partnership, Ford and Dow are working together, and Aston Martin, Delta Motorsport, Pentangle Engineering Services, and Umeco are cooperating.

These partnerships are promising but they do not confirm that composites will be used in mainstream passenger vehicles in the near future. All it means is that an increased usage of composites is one of the areas the automotive companies are investigating for meeting the evolving fuel economy standards. There are a number of roadblocks that could potentially derail these efforts and keep composites limited to performance or luxury vehicles. One roadblock that has always been discussed is the higher cost of composites versus metals. In relative terms, the cost of composites has come down but cost reduction is not likely to progress much further, even with increasing production volumes that the automotive industry would trigger. This is mainly due to the high capital costs associated with constructing a carbon fiber line and this is not likely to change unless someone develops a radically cheaper method of producing carbon fiber. The high capital costs of producing fiber also affects supply since fiber producers are not willing to make the capital investments without firm data on future demand. The aerospace industry is more willing to make long-term commitments for fiber supply since their order backlogs are measured in years whereas the automotive industry does not have that luxury. Another limiting factor is that many automotive structural applications do not really require the attractive material properties of composites so the motivation for using composites is often simply weight reduction. There are multiple ways of reducing the weight of nonstructural parts that may be less expensive. The traditional material suppliers to the automotive industry are aggressively working to preserve their market and are developing lower weight and higher performing materials. In summary, the use of composites in mainstream

automotive applications shows promise but there a number of factors that will affect this. The remainder of this chapter will discuss the similarities and differences between aerospace and automotive applications and present a realistic review of the advantages and disadvantages of these materials for these applications.

2.2 Manufacturing, use, and performance requirements

The aerospace and automotive markets share some common material requirements. Both desire lower weight materials since their customers achieve operational cost efficiencies from lower weight vehicles. Both have needs for corrosion-resistant materials since they operate under similar environmental conditions. Both also desire materials that are fatigue resistant since both operate with lots of vibrational and cyclic loading which can generate fatigue damage. Composites offer advantages in all of these areas and these are all high priority for the aerospace industry and a main reason, aside from weight reduction, why composites are the material of choice for aerospace applications.

The automotive industry has a number of other material needs that are not so important in aerospace. These material requirements either are not high priority needs in aerospace or are such that the advantages of weight and corrosion/fatigue resistance far outweigh other downsides. Each one of these material needs for automotives that are not so important for aerospace will be discussed below.

2.2.1 Look and feel

For the automotive industry, surface finish requirements are very important but not of high importance in aerospace. Automotive customers expect an ultrasmooth, glossy surface finish for the outside of the vehicle. The process for achieving such a surface finish for metal stamped parts is well established but not well established for composites. For some of the current model high-end vehicles, great progress has been made in producing composite parts with a Class A surface finish. An example of this is shown in Fig. 2.3 with the Dodge Viper carbon fiber hood with a highly contoured Class A

Figure 2.3 Dodge Viper carbon fiber hood with a Class A surface.
SPE Automotive.

surface. It requires some novel manufacturing and finishing methods but these parts can now be produced. A key question moving forward is can these methods developed for luxury vehicle parts apply economically to higher volume production runs.

Another related topic for composite parts is methods for painting these parts. Currently, metal automotive components are painted using a high-temperature process that essentially bakes the coating onto the material. If all of the exterior body panels are made from similar metals, matching the color between adjacent panels can be achieved. For composites, the high-temperature baking process will not work as it would degrade material properties during the process. If you have to use a different painting process for metal parts versus composite parts, can you match the color between the parts? For plastic parts, such as bumper and tailgate covers, processes are well established for obtaining a similar color and surface finish on these parts to match the metal body panels on the vehicle, so likely similar processes can be used for composites. If you choose a low-temperature process for painting the parts, similar to the process used to paint an aircraft, how does this compare to current automotive painting methods with regard to quality, cost, and uniformity? Some manufacturers of consumer products made with carbon composites have gotten around this by exposing the material with a transparent coating. This can enhance the "cool" factor of the product and may offer a solution to this issue for automobiles. One option being pursued is to not paint the composite section directly but to bond or adhere a colored plastic face sheet on the composite. This provides a wide selection of colors for the consumer and makes repairs of scratches relatively easy and inexpensive.

Aside from the look of the parts made from composites, another important aspect of the product from the customer perception point of view is the feel of the product. Some early consumer testing of automotive exterior components made from composites have revealed that when customers slam a trunk lid or hood, a lightweight composite trunk or lid feels "cheap" to the consumer. The light weight and the higher pitched sound on impact conjure up the image of an inexpensive plastic part to the consumer so even though the part is more expensive and stiffer than a metal component, the consumer perceives that the lid or hood is inferior and of lower quality. Over time, this perception may change but for now, it is a key factor in buying decisions from the public and it will take significant efforts from manufacturers to overcome this. We have seen over the years the use of more plastics for body panels but this has proceeded slowly due to perception issues.

2.2.2 Environment, recycling, and repair

For any consumer product today, people want to know the impact on the environment from any change in materials. There are a number of issues with carbon fiber that need to be addressed by both the aerospace and the automotive industries. From a public perception point of view, direct and indirect effects on the environment are important distinctions to consider. Direct effects get much more attention from the public because they can easily see and relate to direct effects. Indirect effects, even when they are more pronounced, are not as easy for the public to understand so they consequently get less attention.

With carbon fiber, direct effects are such things as recyclability and repair [4]. Automobiles deteriorate over time and people get in accidents where they are damaged beyond repair. We have an extensive infrastructure for the disposal of automobile components. Metals from automobiles can be recycled and turned into other products or raw materials. Carbon fiber can also be recycled but in different ways. The most promising recycling method for carbon fiber composites is to burn off the matrix material and then chop up the carbon fiber for use in other products. The fibers will have degraded properties from the original fibers but can still provide value in their degraded state. The aerospace industry is developing recycling methods for efficiently extracting the carbon fiber from discarded composites and identifying products that can use this fiber. The challenge for the automotive industry is that the potential volume of carbon fiber can be much higher than aerospace and the lifetime of an airplane is also much longer than that of an automobile. One potential being considered is that recycled or scrapped automotive carbon fibers from body panels could be used for other structural applications in the automobile. This can further reduce the weight of the automobile while providing a downstream use of the recycled carbon fiber.

Repair is another direct effect that will be seen by the buying public. We have an excellent infrastructure for repairing metal body panels. Virtually no infrastructure exists to repair composite body panels. If the automotive industry moves to composite body panels, this infrastructure will need to be developed. For BMW's i3 and i8 largely composite vehicles, they have set up specialized repair shops for this since they realize that the traditional repair shop will not have the equipment nor expertise to do repairs on these vehicles. This is a major inhibitor to vehicle manufacturers with regard to the successful introduction of composites in mainstream vehicles. One trend that may help with this is that many automotive repairs now just simply replace the damaged panel rather than repair it. We see this especially with plastic panels such as bumpers that are now common. This approach will allow more traditional repair shops to simply bolt on a new panel rather than learning how to repair an existing damaged panel.

For automotives, one advantage they have over aerospace is that there is less repair risk associated with automotive repairs versus aerospace repairs. To repair an aerospace primary structure, the repair must be conducted to ensure that it is as structurally sound as the original item. More precise repair methods, more inspections, and more testing are required because of this. For automotive, many of the repairs required are for nonstructural parts where the biggest concern is the look of the part to appear like the original and to make sure the part still functions as intended (eg, trunk lid closing properly).

The biggest indirect effect of carbon fiber composites is the energy required to manufacture the fiber. The raw materials for carbon fiber are readily available but it requires lots of energy to produce the carbon fiber, which is a primary driver of the cost of the fiber. The public will not see this effect as much and a good example of this is what we see in the electric car industry. The buying public perceives that an electric vehicle is "cleaner" for the environment since they do not directly see exhaust from the vehicle. The electricity used to charge the batteries may be produced with exhaust and the real effect on the environment may not be much different. Therefore, the public will generally just see price and performance of the vehicle. The manufacturer will see

the energy costs associated with the production of carbon fiber and this will be factored into the cost of the vehicle.

2.2.3 Manufacturing and joining

The biggest difference in manufacturing for aerospace versus automotive is the sheer volume of units that are produced annually. An aerospace manufacturer is producing tens or possibly hundreds of airplanes a year whereas an automotive manufacturer is producing tens of thousands and hundreds of thousands of vehicles a year. Consequently, the manufacturing methods must be suitable for mass production in automotive where that requirement does not exist in aerospace. For example, automotive body panels are stamped from metal with press times of seconds. Even the fastest composite manufacturing methods available today have cycle times in minutes. In automotives, all manufacturing methods must be suitable to an assembly line process. There are assembly lines in aerospace as well but in aerospace the process is measured in terms of days per station where in automotives, the process is measured in terms of minutes or seconds per station. The manufacturing process in aerospace needs adequate space since airplanes are large. The manufacturing process in automotives needs adequate equipment since the process is highly automated. Manufacturing adjustments are made continually in automotives. In aerospace, there is a period of time in R&D to adjust the process but then it is set and variations are not made once the process is defined and accepted. In fact, the manufacturing process is part of the certification documentation in aerospace so changes to the process are not made easily or quickly.

One advantage composite materials could yield in the automotive industry is the fact that often multiple parts can be made as a one piece structure where a traditional metal structure would be made in several pieces and then welded, bonded, or attached together. For example, the Boeing 787 is made with large integrated fuselage sections that are cured as one piece. With a metal airplane, this structure would contain many rivets to join the different sections of the metal fuselage. In automotives, they would be willing to live with longer manufacturing cycle times if they could save time and equipment downstream for welding and joining operations.

Joining in the automotive industry is dominated by spot and laser welding processes. These joining methods can be highly automated, they are fast, and they do not need a “clean room” environment. Joining methods in aerospace are heavily dominated by rivets and adhesives. These are more difficult to automate and the environment must to be more tightly controlled. The automotive manufacturing infrastructure is set up with welding and stamping equipment which is very expensive but very fast. If composite manufacturing can be set up to take advantage of this infrastructure, it will be an easier transition for the automotive industry. For example, stamping presses could potentially be converted to make formed composite panels, or metal—composite hybrid materials could be used to provide the stiffness and weight advantages of composites while still being weldable. Any joining method will need to be evaluated in terms of the crash performance of the joint. The joint performance during crash is an important consideration in designing the vehicle so that the energy absorption during crash can be controlled [5].

The automotive industry is used to using the best material in terms of cost and performance for each part of the automobile and we do not see that changing. Composites do offer advantages for some applications but not for all applications on the automobile. Hence, we expect composites to be used where it most makes sense and as a result, robust and economical joining methods between composites and other materials will be important in moving forward. In aerospace, joining between composites and metals is generally done with mechanical fasteners or adhesive. These methods may work for some automotive applications but neither are good for high volume production environments so this will need to be addressed.

2.3 Design and analysis

The design of composite structures is much different compared to designing with metals or plastics. For metals or plastics, the material properties are isotropic so the designer only has to worry about size, shape, and material properties. As the design develops, the designer can change shape, size, thickness, or materials to achieve acceptable performance and meet design requirements.

For composites, the material properties are nonisotropic and the designer must worry about many other design variables in the process. The directionality of the fibers, the stacking sequence, different materials at different layers (eg, a honeycomb or foam core), and transition regions are some of the design options that must be considered. Because of the large number of variables, the laminate configuration is often specified as quasiisotropic, which eliminates many of the variables from the design but it also eliminates some of the inherent advantages of composite materials.

2.3.1 Stiffness versus crash requirements

For aerospace designs, structural components are designed primarily for stiffness and durability. In general, the designs keep materials in the linear behavior range and no permanent deformation is allowed under normal operation. Impact loads are seen as an infrequent condition and components damaged by impact loads (hail, bird strike, etc.) will be repaired immediately. Aerospace designs usually have redundancy so that the structure can still perform its mission (safe operation and landing) if a particular component or system fails.

For automotive designs, there is a balance between components that are designed for stiffness and durability and components that are designed for crash performance [6,7]. The stiffness and durability dominant designed parts generally are the frame and support structure. The design intent is to provide a smooth and quiet ride for the passenger along with good ride handling. The crash performance dominant designs include body panels and key support beams such as the B pillar in a 4-door passenger vehicle and the front and rear bumpers. Crumple zones are designed in areas that are likely impact zones to absorb the energy of the crash and protect the occupant. Crumple zones are made from metal since the deformation and energy absorption can be

more easily controlled. Composites also offer good energy absorption but the process for absorbing energy results in catastrophic disintegration rather than controlled deformation. Composites are good for stiffness dominant designs but these requirements are generally in the frame and more bulky type parts which are not as easy to manufacture with composites. Because of the less controlled energy absorption characteristics of composites, they have limitations in the crash performance critical areas of the structure. These challenges are not insurmountable but they do require a different thinking toward design of the composite structure versus the traditional design requirements for aerospace structures.

2.3.2 Fatigue and failure

The fatigue performance of carbon composites is seen as an advantage in the aerospace industry since composites generally perform better in fatigue than metals [8,9]. Composites also have better damage tolerance than metals since their dual material nature can help to arrest cracks and stop their further growth. Thermoset resins are better in fatigue than thermoplastic resins, which is part of the reason thermosets are used in most primary structure applications. Any fatigue degradation potential for composites are addressed with material allowables and factors of safety in the design phase.

Fatigue of composites is more a result of the manufacturing process than a material property. The aerospace industry generally uses an autoclave manufacturing process which drives almost all air from the material so the final structure has few voids which can become initiation sites for cracks. An autoclave process is not practical for automotive applications so manufacturing processes for automotives will inherently generate materials with more voids and hence will be worse in fatigue. More common failure modes in composites are delaminations and disbonding, or stress concentrations coming from wrinkles or fiber waviness resulting from the manufacturing process. These types of failure modes are not familiar to the automotive design engineer and so this inserts more risk in the design since there is not a history for the use and performance of these materials and how failure develops over time. In contrast, the commercial aviation industry can refer to the decades of composites used in the defense aerospace industry. In general the fatigue performance of composites is not seen as an advantage in the automotive industry and the different types of failure modes for composites are seen as a design risk.

2.3.3 Certification requirements

In the aerospace industry, planes are certified by agencies such as the US Federal Aviation Administration (FAA), the European Aviation Safety Agency (EASA), or their counterparts in other jurisdictions. In general, the certification requirements are put in place to ensure safe operation of the airplane under all expected flying conditions. From a structural standpoint, the certifications ensure that the structure will carry the expected loads of operation. As part of this, extensive material testing is carried out on any material used in the structure and for composites, the testing also must be carried out on the different laminate configurations to be used. The range of material

properties derived from the testing results in the creation of material allowables, ensuring that the material will perform its function for the range of material properties that are possible. These allowables are further enhanced by applying factors of safety to the design. giving further assurance of their safe operation. As noted previously, aerospace designs have redundancy so one can ensure safe operation even if a part or system fails. Buckling is a major driver of design in aerospace. Design requirements are set to prevent a buckled condition but certification requirements must account for safe operation in a postbuckled state. In general, material selection in aerospace is driven by the certification requirements and as a result, material changes are not commonly made without a large benefit since the expense of qualifying a new material can be significant.

Automotive design requirements are much different than those in aerospace. There are no federal agencies that certify the vehicle design but there are agencies, both government and commercial, that rate the vehicle performance in crash. It is an important marketing message if your vehicle performs well in these crash performance ratings so there is plenty of motivation for the manufacturers to do well on this scale. The other ratings of the vehicle are really done in the public marketplace where vehicles are rated in terms of ride and comfort, value, depreciation, repair costs, and performance. The automotive industry relies on material suppliers to provide the material property data and the industry is much faster at switching to new materials if it can provide even a slightly better value to the manufacturer and consumer. A major issue in the automotive industry is to be diligent in creating designs free of defects in design or manufacturing. Great care is taken to ensure that the design and the manufacturing processes are robust and that the range of expected performance is managed appropriately. A defective part can result in a recall and lawsuits that can be very expensive for the manufacturer. In general, material selection in automotives is driven by cost and performance issues.

2.3.4 Numerical simulation

Numerical structural simulation is used extensively in both aerospace and automotives but the techniques, methods, and general use are quite different. In automotives, simulation is used extensively to virtually test crash performance, vibrational characteristics, durability, aerodynamics, and thermodynamics of the engine. Given the speed of the design development cycle and the competitive marketplace, automotive companies have automated common modeling processes and methods to achieve quick results and ensure consistency of the modeling process. An automotive company may look at 50 design iterations in a few weeks to optimize performance or cost and they need simulation methods that can do this very quickly. Much time and effort have been spent in developing modeling practices that achieve accurate results and physical testing is often done just as a final confirmation of the design performance.

The aerospace industry has used numerical simulation methods for decades and pioneered much of the development of the mathematics and tools that the automotive industry uses today for simulation. In contrast, numerical simulation is used primarily in aerospace to determine loads in the structure from the different conditions under which

the airplane will operate. These loads models are developed very precisely and utilize a lot of test data, experience, and specialized methods to construct. Whereas the automotive industry wants to evaluate tens of iterations in a few weeks, the aerospace industry may only utilize a few iterations of the global loads model in the entire airplane development cycle. The global loads model is then used to feed loads to the design teams who develop detailed designs of individual components. These detailed designs then provide revised stiffness information back to the global loads team which they use in the next iteration of the global loads model.

In aerospace, the detailed design teams may or may not use numerical simulation methods for their designs. Due to certification requirements, numerical simulation, such as finite element analysis (FEA), can only be used as part of the design analysis. FEA methods must be coupled with test data and analytical formulations as backup. In automotives, the confidence of well-developed FEA methods is such that the predictions from simulation are relied on heavily and sometimes solely to make design decisions. Every part of the automobile is analyzed with FEA or computational fluid dynamics (CFD) codes and it is a standard part of the design process. This is not the case in aerospace, although the use and reliance on FEA in aerospace are growing.

2.3.5 Simulation of composites

Simulation of composite structures presents challenges to both industries. There are a number of differences between metals and composites with regard to simulation. For metals, the main design variables are geometry and material properties, which are usually isotropic in nature. The visualization of stress results, for example, is best shown on the geometry itself, especially for thin-walled structures such as body panels and rails. The failure modes for metals are generally based on stress invariants that are easy to calculate from the FEA results and are well-established methods. For composites, geometry is still a variable but the material properties are anisotropic and there is an endless variation of the properties based on how the fibers or plies are aligned and stacked. For a laminate structure, the results must be visualized at each ply layer where a single finite shell element may be used to simulate the entire laminate stack at that location. An example of a finite element model of a composite is shown in Fig. 2.4 where you need to visualize the ply orientation on each layer. Visualizing the information results is also critical and the manner of presenting data is varied. Fig. 2.5 shows an example of having the colors represent the ply layer which has the highest principal stress and allowing the user to interrogate this information easily.

The failure modes for composites are more diverse and less understood and can require complicated postprocessing of the data. Since the aerospace industry has been using composites for decades, the methods for numerically analyzing composite structures has been developed but there still is little consensus on which method is best. The aerospace industry primarily uses laminated composites which provide the stiffest structure but the manufacturing process for laminated composites is slow. Since this process is not economical or feasible in the automotive industry, other manufacturing methods for composites are being developed and most are not laminated structures but use short or chopped fibers that can be more easily formed quickly in an automated process. Due to

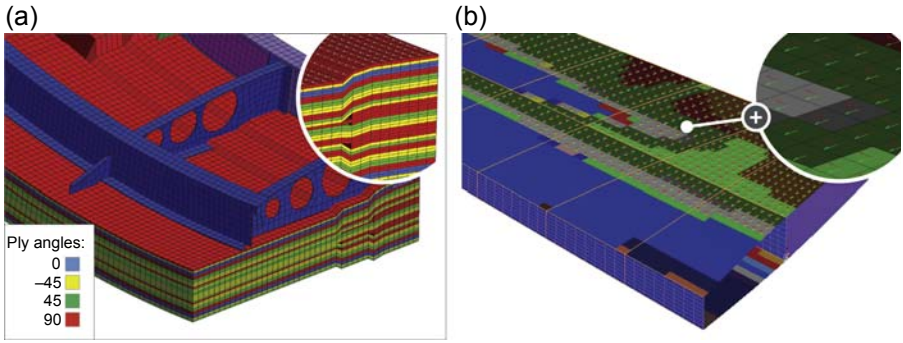

Figure 2.4 Finite element model of a composite structure showing ply orientations on the model and on the results. (a) Ply representation with ply angles represented by colors. (b) Ply representation with ply angles represented by colors and ply angle direction shown as vector on each element.
Altair Engineering, Inc.

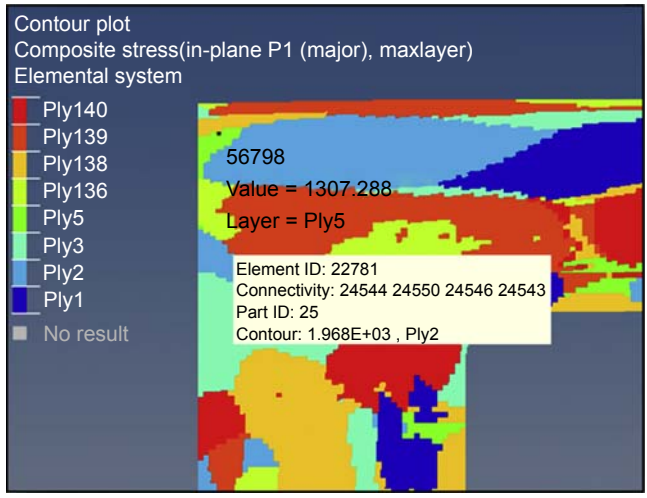

Figure 2.5 Visualizing maximum stress results by ply layer.
Altair Engineering, Inc.

this, the simulation methods that have been developed in aerospace are not likely applicable in automotives. The automotive industry will need to develop their own methods for analyzing composite parts. Fortunately, the automotive industry can still draw on the extensive knowledge the aerospace industry has gained in terms of a basic understanding of common failure modes and material behavior under a variety of conditions.

The challenge in analyzing composite structures has led to the common design process in the industry referred to as "black aluminum" design. This process refers to creating a laminate that has isotropic material properties in the plane of the laminate and is often referred to as a quasiisotropic design. The vast majority of the laminate test data available are on quasiisotropic test articles. A quasiisotropic design eliminates the

design variable of material orientation and allows the designer to just worry about shape, thickness, and materials as their design variables, which is more in line with the design process for metal structures. Composites are attractive because they have a high stiffness-to-weight ratio but they can also provide directional material properties which can provide significant advantages. If we look at the composites in nature such as bone structure or trees, they are not designed as quasiisotropic structures but they have highly directional stiffness that give the item stiffness and strength only where it is needed.

2.3.6 Design optimization

Given the large number of variables available to the designer of a composite structure, numerical optimization methods are required to really design efficient composite structures that have the stiffness and strength where required. Fortunately, numerical optimization methods are available now that can help designers sort through all of the variables and obtain an optimized design in terms of weight and performance [10–13]. An example of this is shown in Fig. 2.6 which shows design optimization applied to an open hole tensile coupon. The process shows composite free-size optimization to determine the optimal ply shapes, composite size optimization to

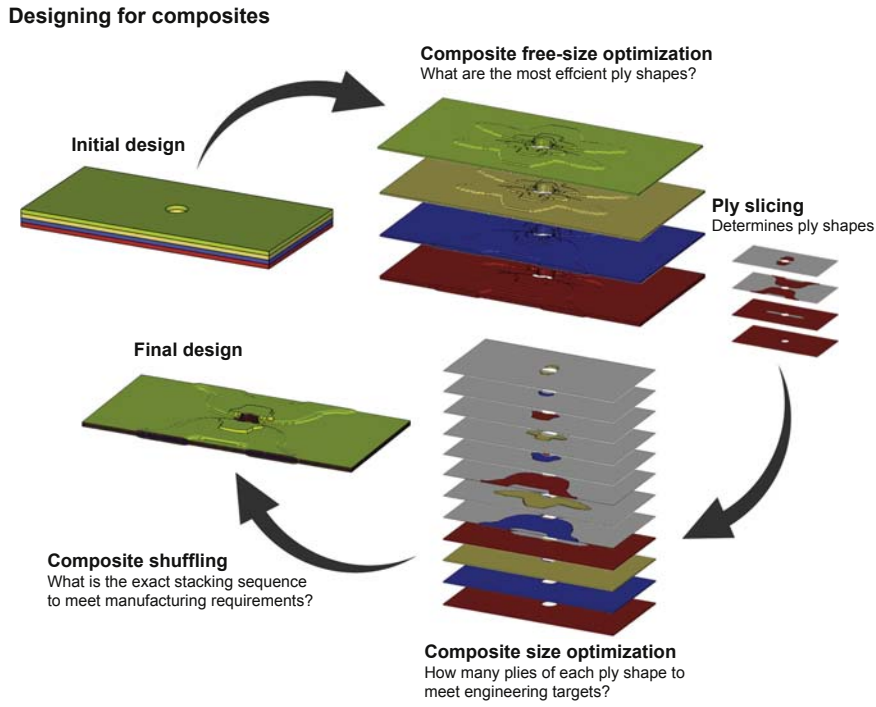

Figure 2.6 Composite design optimization applied to an open hole tensile coupon. Altair Engineering, Inc.

determine how many plies of each shape are required to meet engineering targets, and composite shuffling optimization to determine the optimal stacking sequence of the plies that meets manufacturing requirements. As more experience is gained in using these methods, the weight of airplanes and automobiles can be further reduced. In addition, the results can produce geometry that is difficult to manufacture using traditional methods but with the advent of additive layered manufacturing or 3D printing methods, the future holds the prospect of making components that are truly optimized, much like we see in nature.

2.4 Market and supply issues

There are some important differences between the markets for the automotive and aerospace industries. Buying decisions, sensitivity to costs, and value (perceived and real) are different and important to understand. The supply chains are also quite different for the two industries, which affects how the vehicles are designed and produced.

2.4.1 Costs

For many years, it was commonly stated that the cost of carbon fiber was the main deterrent from their wider use in automotive applications. As discussed in this chapter, there are many other reasons beyond costs that present difficulties in the wider adoption of automotive composites. That being said, costs are a factor in the use of composites in automobiles.

The airplane industry is willing to pay a lot of money to reduce weight. Although numbers vary by program, in general, the airplane manufacturers are willing to spend $1000−$2000 to save 1 pound of weight. The airlines are also willing to spend that kind of money to save a pound of weight. This is largely driven by the fuel savings over the lifetime of the airplane, which can be 20−30 years.

For the automotive industry, the amount of money the automotive manufacturers are willing to spend to save a pound of weight is on the order of $1−$4. This varies depending on where the weight savings occur with higher value in saving a pound above the center of gravity of the vehicle. This is largely driven by how much a consumer would be willing to pay for a more efficient vehicle. This is changing due to the tighter fuel economy standards that are being required in the United States and Europe so the decision to save weight is driven more by requirements than consumer preference. Also, the automotive industry is pushing the limits on powertrain efficiency so weight reduction may be the only way to further improve the fuel efficiency of the vehicle.

For the composites industry, they have a lot of competition with regard to lighter weight materials. New high-strength steels, aluminum, and magnesium are all competing to reduce the weight of the vehicle. These materials all have the advantage of conforming better with current automotive manufacturing methods and they are generally lower cost. Composites do have some unique advantages so to be successful,

the industry will need to demonstrate how these advantages can outweigh their disadvantages and help the industry understand how to best use these materials from both a design and a manufacturing standpoint.

2.4.2 Providing value to the customer

For any business to succeed, it must provide value to the customer. This is true in both the aerospace and the automotive industries but the customers for each industry are quite different and they have different needs and requirements. For the aerospace industry, the ultimate customer is the passenger but the customer for the airplane is actually the airline and then the passenger is the customer of the airline. Most passengers book their airline tickets based on cost, convenience, and customer loyalty programs. In most cases, they do not consider what model airplane they will fly. The airline has the goal of making a profit so their interest is to operate their fleet efficiently. The efficiency of the airplane is one factor but not the only factor in fleet efficiency. Route network and customer service are just as important to their bottom line. The airlines do make demands of the airplane's original equipment manufacturer (OEM) for efficient vehicles but they also want airplanes that can provide a good passenger experience in terms of comfort and security. For the new composite aircraft such as the Boeing 787 and Airbus A350, the customer experience is as much a selling point to the airlines as fuel efficiency from the use of composites. For example, the 787 touts the higher cabin pressure and large windows as key advantages which are both the result of having a composite fuselage. Therefore, the airplane OEMs are really meeting the needs of their airline customers, who take a long-term view to their purchase decisions and put great value on passenger mile costs. The airlines then use this value to provide a good economic value to the customer while using the interior design and comfort, customer service, route network, and customer loyalty programs to attract and retain passenger customers.

The automotive industry is much different in this regard. The customer of the automobile is the passenger so there is a more direct relationship between the passenger needs and desires and the automotive OEMs. Automotive customers usually base their buying decisions on emotion, perceived value, and safety. The customer is usually focused on short-term value and does not often look at the long-term costs of the purchase. Hence, the automotive industry focuses on providing exciting vehicles in terms of styling or performance that have solid safety ratings. A poor rating on styling, performance, or safety will doom a vehicle so they are all important. Overall value is also important in the buying decision but it is at most a 5-year value window being considered. If there is only a slight difference in value, the customer will make the decision on emotion and perception. It is also important to note that the perceived value can be quite different than actual value. For example, the US automotive industry still suffers on the perceived value scale because at one time, the US automobiles were generally inferior in quality to Japanese or European models. In most cases, this quality gap has been closed but the perceived value gap lingers. Fuel prices also heavily affect the perceived value argument as fuel-efficient vehicles have higher value when fuel costs are going up than when going down. It is a difficult game to play with the OEMs since

they cannot predict what fuel costs will be in the future and must provide a range of vehicle options that will hopefully meet the needs of the moment when the vehicle is produced. This makes it challenging to commit to composites in vehicles given the enormous costs associated with this change and the prospect that fuel-efficient vehicles will be "out of vogue" when the vehicle hits the market. The market demands of the automotive industry can change very quickly.

2.4.3 Engineering talent

Engineering with composites is much different than engineering with metals. Both the aerospace and the automotive industry suffer from a lack of broad expertise in designing and manufacturing structures with composite materials. The suppliers have the greatest difficulty attracting talent since the OEMs in both industries are often able to attract and retain the best engineering talent. The problem is that the suppliers end up manufacturing the parts and if they do not have sufficient and adequate engineering talent with composites experience, it will be difficult for them to be successful with these new materials. Because of this, many composite parts on current vehicles are actually designed and manufactured by the OEM.

The aerospace industry does have the advantage of relying on more long-term relationships and commitments with their suppliers. If an aerospace supplier has a 10-year contract to produce composite components for an airplane, it is easier for them to invest in the equipment, infrastructure, and talent to be successful. Automotive OEMs typically have a shorter term relationship with their suppliers and they are willing to switch suppliers more regularly. This makes it difficult for the automotive suppliers to invest in new capabilities and new skills to be successful with composite structures. What we see are small, entrepreneurial composite companies being established that try to capture the automotive composites market and if they are successful, they will threaten the more established automotive suppliers that specialize in metal processes.

2.4.4 Production needs

A key difference between the automotive and the aerospace industries is in the production logistics of the operation. The aerospace industry sells globally and they source globally. A good example of this is the Boeing 787 program with key suppliers in Japan, Korea, Italy, France, United Kingdom, and India. There is generally one manufacturing site for each key component or section of the airplane and the suppliers have long-term contracts with the OEM. In exchange for the long-term contracts, the suppliers invest significantly in people, equipment, and facilities to meet the contract with the OEM. The only real customization of the airplane occurs with the interior where the airlines have a large choice of suppliers and can customize the interior per their specifications, desires, and needs. The interior supply base looks much more like an automotive supply base.

For the automotive industry, they utilize a platform engineering approach which designs the basic parameters of the vehicle such as the frame, chassis, and powertrain.

The vehicle is then customized with regard to body design, interior, suspension, controls, and amenities. There is often a custom vehicle for each country where the vehicle is sold. Where possible, local suppliers and materials are contracted by the OEMs to supply material and components for a local manufacturing line. Contracts with suppliers are short-term since the vehicle production lifetime may only be a few years and OEMs are willing to switch suppliers mid-program if they can get a better price or better response from a new supplier. As a result, suppliers are not as willing to invest in new equipment or experience to win a new program. This presents a problem for the use of composites in automotives since suppliers do not have the facilities nor expertise to supply the demand. To solve this issue, the OEMs will likely need to either do the manufacturing of composite components themselves or change the types of relationships they have with suppliers.

2.5 Conclusions

As discussed, there are a few similarities and many differences between the aerospace and the automotive industries with regard to their use of composite materials. It is often perceived that the automotive industry will learn from the aerospace industry as to how to use more composites in their vehicles but the needs can be so different that the automotive industry will have to learn on their own in many cases. This in turn, however, can provide value back to the aerospace industry and they will learn from the automotive industry.

Today, what can the automotive industry learn from the aerospace industry in the use of composites? The aerospace industry has many decades of experience in the use of carbon fiber composites so there are many lessons that the automotive industry can take with regard to material behavior and performance in many types of environments. The aerospace industry has compiled significant material testing data that can also be used but not all of these data will be relevant for automotive applications. The aerospace industry also has a lot of experience with the maintenance and repair of composite structures that can be helpful. Another key area of aerospace experience is in the area of modeling and analyzing composite structures. Many of these modeling methods and the associated material and failure models of composites will be relevant in automotive applications.

As the automotive industry advances in their use of composites, what can they provide back to the aerospace industry of value? Given the high volume production needs of the automotive industry, the manufacturing methods developed will help the aerospace industry lower costs of production on future airplanes. Having a larger supply of carbon fiber will bring more price and volume stability to this market. Since crash performance is a key design parameter in the automotive industry, the behavior of carbon fiber composites under impact loading will be better understood and characterized by the automotive industry which can help the aerospace industry design structures that can better withstand impact loads from a bird strike, turbulence, or a hard landing. Automotive engineers must better understand the nonlinear behavior of materials

which will lead to a better understanding of the nonlinear behavior of aerospace composite structures. In the area of modeling and simulation, the automotive industry is much better at developing automated modeling methods and procedures which can improve design efficiency for the aerospace industry.

The greater use of composites in vehicles should continue to increase going forward. There are a number of factors, as explained here, that will influence how fast this market increases. The aerospace and automotive industries both have a need to increase vehicle efficiency, improve safety, and provide value to their customers. Composites meet current needs in the aerospace industry and we expect composites to increasingly meet needs in the automotive industry as well.

References

[1] Growth opportunities in the global carbon fiber market 2014−2019. Irving, TX USA: Lucintel; March 2014. www.lucintel.com.
[2] 2014−2023 global composite aerostructures market outlook. Mesa, AZ USA: Composites Forecasts Consulting; 2014. www.compositesforecasts.com.
[3] The emergence of CFRP in mass production automobiles: 2013−2022. Mesa, AZ USA: Composites Forecasts Consulting; 2013. www.compositesforecasts.com.
[4] Pimenta S, Pinho ST. Recycling carbon fibre reinforced polymers for structural applications: technology review and market outlook. Waste Manag 2011;31:378.
[5] Bauraltar E, Chevalier J, Bonnet F, Kaplan D, Claeys J. Impact tensile test: a new type of crash test for welded joints in automotive applications. In: DYMAT 2009. EDP Sciences; 2009. p. 235−41.
[6] Monnet S. PSA's views on compatibility: a potential two-step approach to improve compatibility among the vehicle fleet. France, PSA Peugeot Citroen, Paper Number 343; 2000.
[7] Stiffness relevance and strength relevance in crash of car body components. European Aluminum Association; May 2010. Official Report 83440 by ika.
[8] Salkind MJ. Fatigue of composites. In: Composite materials: testing and design (2nd conference) by H.T. Corton. ASTM; 1972.
[9] Harris B. Fatigue in composites. Woodhead Publishing; 2003.
[10] Wollschlager JA, Yancey RN. The integration of composite constituent-level failure models during composite size optimization. In: SAMPE Tech; 2012. Charleston, SC.
[11] Yancey RN, Mestres E, Mouillet J-B, Asaker R, Jeunechamps P-P, Boisot G, et al. Simulating impact performance of composites. In: SAMPE; 2011. Long Beach, CA.
[12] Stefanovic M, Yancey RN, Gies J, Hill D. Simulation driven weight optimization of a composite UAV spar using multiscale analysis. In: SAMPE; 2010. Seattle, WA.
[13] Pignacca L. Simulation: the connection between speed and safety in racing. In: Concept to Reality. Penton Media, Inc.; Summer/Fall 2012. c2r.altair.com.

3 Opportunities in the design stage of composite components to reduce weight during assembly operations

G. Oncul
TAI Turkish Aerospace Industry, Kazan, Ankara, Turkey

3.1 Benefits of composite parts

Increased performance requirements bring the necessity of the full application of carbon fibres in the primary structures of newly designed aircraft. Switching from metal to composite materials decreases the structural weight of the aircraft.

The excellent strength-to-weight and stiffness-to-weight properties of composite materials are the main drivers of increasing the composite parts ratio in aircraft. Different stack-ups and orientations give high strength-to-weight ratios to composites. Less weight on aircraft means less fuel consumption. It is a more economical and environmentally friendly condition, which gives the product value and competitiveness with other companies; longer range, higher speed and more efficient flight are reached for the airliners.

More integrated, single one-shot, complexly shaped parts manufacturing can be possible with composite materials and processes. Integrated large part maintenance and inspection costs are comparatively less, and corrosion and fatigue resistance of the composite parts is higher, which have a positive total impact on the life cycle and costs of the parts.

Compared to metallic parts, composite parts have less weight for the same dimensions and they have optimization possibilities in the x, y and z directions according to the design requirements.

Composites are corrosion resistant. They do not rust or corrode. They have long-term resistance to almost all chemicals and environmental conditions. They have long service life and minimum maintenance requirements.

Composites have high dielectric strength and they have very good electrical insulation according to the design requirement.

Composites have good fatigue endurance and residual fatigue strength properties throughout the life of the material.

Lightweight Composite Structures in Transport. http://dx.doi.org/10.1016/B978-1-78242-325-6.00003-7

3.2 Shortcomings of composite parts

Composites cannot always be the cheapest solution. Cost-effective design strategies need to be applied in which cost, weight and desired laminate quality will be considered [1].

One strategy is to reduce the non-recurring cost of the composite parts, in which tooling and material costs have a high percentage.

Assembly and interface management are not easy owing to spring-back of impact on cured composite parts, in which the shape and/or geometrical variation changes from 4% to 7% and causes obvious tolerance accumulation on interfaces. This requires shimming and needs to be managed carefully.

For composite parts the repair concept is not mature enough and needs more trials and special methods based on aircraft service life experience. Composite manufacturing processes are not so stable for defects occurring during manufacturing, and increasing the size of parts has a risk of scrapping owing to unacceptable manufacturing defects.

Impact damage is the main concern for composite components because composites are brittle and impact damage can occur suddenly, and to prevent catastrophic failure many research studies have been performed, and from these a damage-tolerant structure design principle has been accepted.

Composites are famous for "hidden damage" issues. Even barely visible damage can be harmful to the interior and not be detected. This is known as matrix crack and fibre breakage below the surface. The damaged area increases conically towards the inside, starting from the impact point, and delamination can occur very rapidly through the back side of the laminate.

Composites are poor in electrical and thermal conductivity and damage tolerance. There is not enough collected design data to secure the design and certify whether it needs structural validation with coupons and full-scale tests for composite components.

The quality of the manufactured composites depends upon the processing and, if the automation is not sufficient, workmanship skills. Each manufactured composite part needs to be subjected to ultrasonic testing such as nondestructive testing (NDT). NDT currently has key importance for catching manufacturing defects such as voids, porosity, fibre misalignment, wrinkling, resin-rich or resin-poor regions and delamination inside the composites [1]. There have been many studies on NDTs; they are still an expensive and time-consuming process.

3.3 Weight opportunities in assembly

3.3.1 Tolerance analysis

Tolerance analysis is used to predict the effects of manufacturing variations on finished products from the aircraft (A/C) level to the component, assembly and part levels. Tolerance analysis is a complex study and variations are considered in aerodynamic, assembly, manufacturing and tooling tolerances.

Newly designed A/C need their design and assembly times reduced as much as possible to increase business opportunities and profit rates. Tolerance deviation issues cause matching problems for different subassemblies coming from different manufacturing centres or subcontractors seen frequently on the final assembly line. Time limitations on the assembly phase force engineers to find robust and efficient solutions during the design phase of the A/C.

Tolerance analysis strongly leads the manufacturer during the design phase not only to eliminate excessive shimming, which structurally has no added value, but also to decrease the necessity of tooling revisions, which is extremely time and cost consuming.

Efficient tolerance analysis should start at the top level of the A/C. It starts with the definition of the key characteristics, which include the final customer requirements of the A/C and also include aerodynamic tolerances and in-flight tolerances. Key characteristics are a product's geometric features and material properties that are highly constrained or that deviate from the nominal specifications (regardless of manufacturing capability) and have a significant impact on the product's performance and form-fit functions. They flow down in a systematic manner from the A/C level to the assembly and part levels. A schematic representation of tolerance analysis is shown in Fig. 3.1.

Defined key characteristic values cascade from the top to the component and detail parts levels. This process is necessary to set the final requirements, including those from the customer.

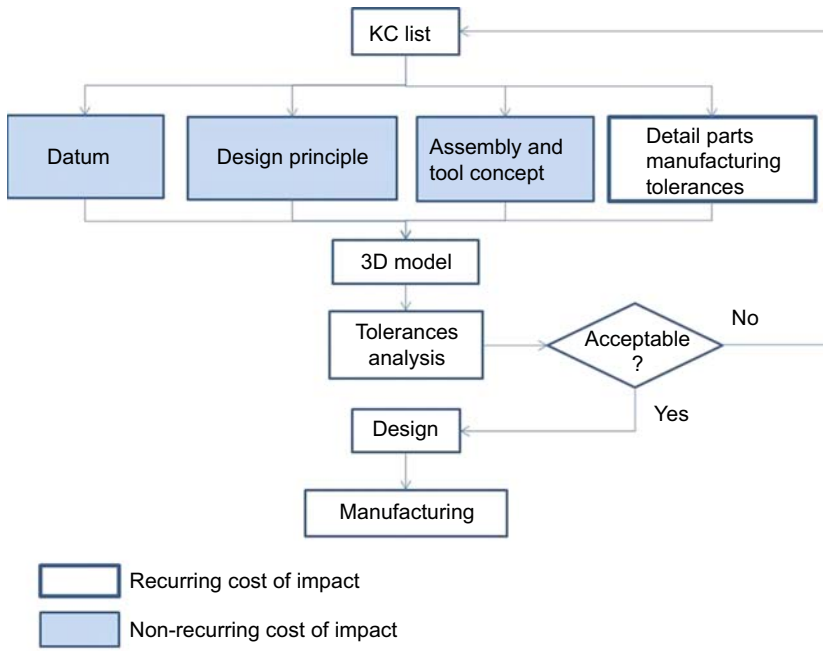

Figure 3.1 3D tolerance analysis flow chart. *KC*, key characteristics.

The second step of the tolerance analysis needs datum definitions from the A/C level to the detail part level. Data are the reference points in tolerance analysis.

Design principles are the perfect studies to understand the tolerance deviations and tolerance distribution on the detail part level in the very early phase of the design, which will be the input of the one-dimensional (1D) and 3D tolerance analysis. This is a very complex and specific effort and a special computer-aided tolerances tool is required to perform correct tolerance analysis.

The long processing time of tool design and manufacturing forces the designer to give priority to tool input even before the design is mature. This is a serious risk that needs mitigation and new studies are being developed to minimize the risk. Design principle studies concentrate on junctions and put all the risks on 2D demonstrations.

Assembly and tool concepts are the major drivers of the tolerance analysis. The assembly sequence and tool concepts bring special tolerance requirements to mating surfaces and the tolerance requirements including manufacturing and tooling tolerances need to be analysed with those of the manufacturer.

Correct and efficient tolerance analyses can be possible only when the manufacturing capability and manufacturing tolerances are well known. Otherwise the calculated values will never reach the realistic values in analysis [2].

A 3D assembly model in a computer-aided design environment will be used to create a tolerance analysis 3D model. Kinematic analysis of the detail parts is performed by using a 3D model and degrees of freedom are decided for each connection.

The degrees of freedom coming from kinematic analysis, assembly sequence and tooling tolerances are the inputs to the 3D tolerance analysis software. As an example, the degrees of freedom of an aileron hinge fitting are shown in Fig. 3.2.

The 3D tolerance analysis is performed by using dedicated tools and directly calculates gaps or mismatches in the connecting surfaces. If the results are not satisfactory when compared to the requested key characteristic values, a new loop needs to be started by challenging the data, design principles, tooling sequence or concept. Even the detail manufacturing capability may need to be improved [2].

Tolerance accumulation, shown in Fig. 3.3, brings problems such as gaps and mismatches in mating surfaces. Both are very critical with regard to time and cost at the final assembly line. Computer-aided tolerance analyses with advanced tools are useful in calculating correct shimming during the design phase. Shimming is not a structural material and increases the total structural weight by 2−4%.

3.3.2 Shimming on assembly

Shimming is often used to level the gaps and steps created by geometrical variation in the parts. Although this is a common practice in assembly, liquid shim preparation and application, waiting for curing and trimming cause time loss. In addition, factors like additional weight and excessive use of materials with different mechanical properties cause some deficiencies.

Laminated shim (peelable), shown in Fig. 3.4, is another type of shim frequently used in industry. Laminated shims are more appropriate to reduce assembly time. Their

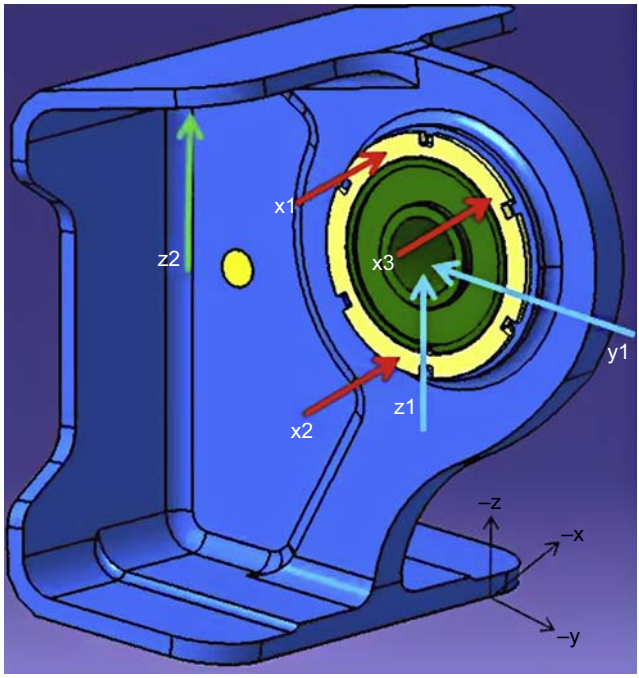

Figure 3.2 Three-dimensional computer-aided design model with degrees of freedom.

Figure 3.3 Tolerance accumulation brings gaps, and shimming is necessary to fill them during assembly.

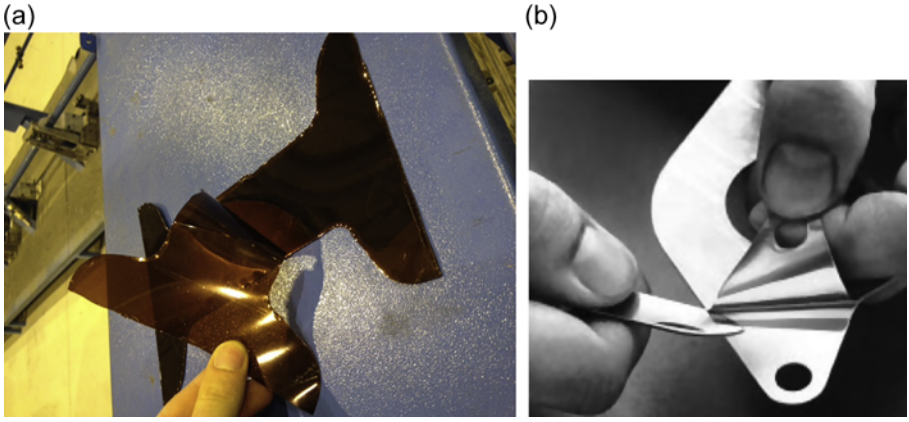

Figure 3.4 (a) Composite laminated shim. (b) Metal laminated shim.

dimensional accuracy is better and there is no need for expensive machining of components. It is possible to make quick production line adjustments and field repairs. The weight impact is comparatively less than that of liquid shim application.

Laminated shim material is produced by surface bonding, with resin, individual layers of precision metal foil (0.002 or 0.003 in.) or composite film (0.002 or 0.003 in.) into sheets whose total thickness can range from 0.006 to 0.250 in. The bond is made by heat and pressure. An optimal hardening of the resin is obtained and the bonding agent is reduced to such proportions that it can no longer be measured [3].

In industrial shimming applications, shown in Fig. 3.5, up to 2.5 mm of liquid and solid shimming on interfaces is allowed; however, after 1 mm shimming degradation of the joint needs to be analysed.

Shimming weight should not exceed 2−4% of the total weight of the components.

Figure 3.5 Shimming application on actuator fittings.

To reduce the shimming operation and shimming amount, the following may be instrumental:

- Single one-shot large composite parts will reduce interfaces and shim requirement.
- Advanced 3D tolerance analysis will reduce the shimming value of the interfaces.
- Manufacturing and assembly trials provide the opportunity to see deviations and actual gap values before the real assembly begins. This will make it possible to modify tools for reducing gaps and shimming. To see the real gap values and make reverse tool modifications accordingly will reduce the shimming requirement.

3.3.3 Assembly loads

Assembly load is considered when the components are mounted with hinges. Ailerons to wing rudder to vertical stabilizer and elevator to horizontal stabilizer are examples of hinge-type connections.

In a perfect assembly, hinges should be aligned and the corresponding interfaces should be aligned as well, which means that installation will not bring excessive loads.

Only the tolerances on the radial position of hinge interfaces, shown in Fig. 3.6, generate assembly loads.

Axial gaps coming from manufacturing and assembly tolerances need to be managed carefully especially on actuator fittings.

Assembly loads are generated when structures are deformed during the assembly. As rotations are free at all interfaces, the connection of the first two interfaces does not cause assembly loads. When there are more than two interfaces at a hinge connection misalignment should be considered. The effect of assembly loads is taken into account through a down factor and increases the applied loads on hinges.

Assembly loads need to be calculated to cope with the loads coming from hinge line misalignment during component assembly. Improvements in manufacturing techniques tend to reduce assembly loads and consequently reduce bearing and fitting structure weights. An alternative way to solve the misalignment at hinges is to bore the hinges and bring the line concentricity into the required tolerances band with a special tooling attachment on the assembly jig [4].

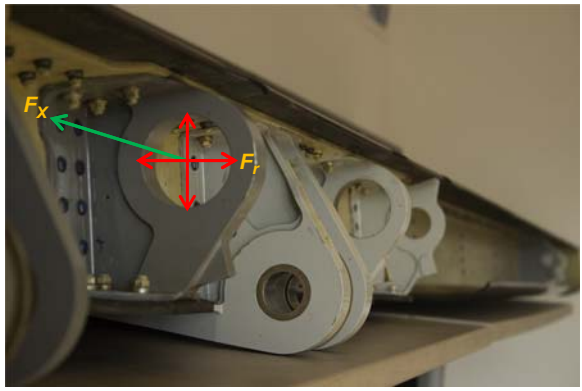

Figure 3.6 Assembly load directions on hinge fittings.

High loads on bearings need a special design and this brings extra weight. The load increase can be around 5%.

3.3.4 Reducing the quantity of fasteners on assembly

Composite materials are increasingly being used for large and complex primary structures in the aeronautics industry, because of their advantages over traditional materials. Large parts decrease the fastener requirement and this is the main weight advantage on newly designed A/C. Assembling numerous small parts can be substituted by a single one-shot large part. However, this technology route must be economically sustainable.

Fasteners in large quantities are still required in today's composite structures. The bonding design approach mostly brings chicken fasteners (dummy fasteners which are used as secondary connections for the primary surfaces) as a requirement of damage-tolerant design for certification. Chicken fasteners are one means to fulfil this requirement in specific bonded areas where theoretical methods are at their limit or where excessive testing would be necessary to justify a rivetless design. They are used as an additional safety means and for risk mitigation.

This is another challenge, to decrease the quantity of fasteners; it is not necessary from the structural point of view but sometimes is needed for certification.

Decreasing the quantity of fasteners and selecting a suitable fastener according to the application area always brings extra weight reduction opportunity. When steel nuts, for example, ASNA2536 seen on Fig. 3.7, are replaced with ABS1738K titanium nuts the weight reduction will be between 4.85 and 11.34 kg according to the diameter size per 1000 fasteners. However, the price of the ABS1738K is six times greater than that of ASNA2536.

3.3.5 Automatic fibre placement process

Automatic fibre placement (AFP) machines enable the designer to think of more complex and compact parts to be manufactured in one shot. However, their well-known manufacturing weaknesses drive many companies to develop new methods to obtain

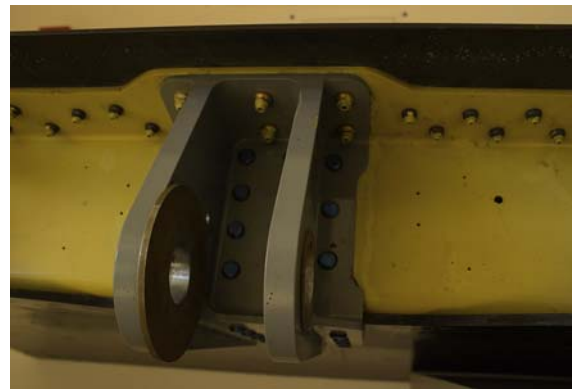

Figure 3.7 ASNA2536 steel nuts as used in fittings.

better part quality. The introduction of aeroplanes with parts made by the AFP process has increased the demand for this method. An AFP machine consists of a computer-controlled robotic arm with a placement head and an end effector that lays rolls of prepreg strips onto the layup tool to construct the part. 8 to 32 prepreg strips, called tows, which are aligned side by side by the placement head, constitute the rolls. For each ply, the machine accurately places the tows on the layup tool by respecting the proper ply angles and the covering technique.

The part is then placed in an autoclave to polymerize the resin material and consolidate the plies. Another advantage of this process is the possibility of making variable-stiffness laminates with a curvilinear fibre path for the purpose of optimizing the composite structure. This technique has been proven to be effective to enhance the buckling load and reduce the effect of stress concentration, reduce the notch sensitivity and maximize the fundamental frequency. However, to manufacture complex shapes or variable-stiffness parts, misalignments are induced on the band edges, which introduce gaps and/or overlaps. This is the real manufacturing problem and to overcome this situation, very special software is provided [5].

Repairing defects that may occur during the service life needs to be considered during the design and manufacturing of the composite parts. Most of the time the remove-and-replace solution is selected, and it is not feasible cost-wise.

Figs 3.8 and 3.9 show traditional and composite fuselage assemblies.

3.3.6 Lightning strike

The lightning strike is a well-known hazardous phenomenon for A/Cs. Design precautions have to be taken for the components as part of an A/C-wide lightning strike discharge system to avoid any damage to the A/C structure. Whereas a metallic A/C

Figure 3.8 Traditional metallic fuselage assembly sections.

Figure 3.9 Composite fuselage assembly section; the skin panels are manufactured by the AFP process [6].

fuselage designed with enough material thickness exhibits very good performance against lightning, composite structures need additional protection measures to withstand the adverse effects of lightning.

A/C are struck by lightning on average every 10,000 flight hours for commercial airlines, the equivalent of one strike per A/C per year, and the probability of having a lightning strike in flight is on the order of 10^{-4} per flight hour [7]. The direct effect of a lightning strike on the exterior can be burning or melting at the lightning strike point that results in damage especially to the carbon fibre-reinforced plastic (CFRP) structures, since they have low electrical conductivity [8].

Like the thunderstorm's impact on the sharp conductive ends of the landscape, the lightning is likely to impact the edges of the A/C, like the trailing edge of the wing parts. If a composite part is concerned, the huge electrical energy strongly damages the composite at the point at which it hits. To solve this issue, generally, conductive metallic strips are positioned along the trailing edges and/or additional conductive meshes inside the whole skin laminate are added.

The effects of lightning can be electrical sparks at fasteners or joints, melt-through of metallic skins and puncturing of non-metallic skins. Increasing the skin thickness can reduce the risk of melt-through for metallic and non-metallic skins. Moreover, the electrical conductivity of non-metallic skins can be improved by applying a metallic coating such as copper foil or bronze mesh. To prevent sparking due to lightning currents, the electrical continuity needs to be satisfied by proper bonding of the structure components to the metallic A/C fuselage. These all have weight penalties, as well as corrosion problems and problems with obtaining good joints. A poor bonding mechanism causes voltage differences among the fasteners or joints, which may lead to increased damage in the case of a lightning strike [9].

Aluminium has been the principal material used in A/C and aerospace construction since 1950. Today composite material usage has increased to up to 53% of the total weight. However, composites are poor conductors of electrical current.

The physical damage at the point of lightning strike appears as holes burned in metallic skins, puncturing of composite structures, hot spot formations and welding

Table 3.1 Lightning current components

Lightening zone	Current components
1A: First return stroke zone	A + B + C*
1B: First return stroke zone with long hang on	A + B + C + D
1C: Transition zone for first return stroke	A_h + B + C + D
2A: Swept stroke zone	D + B + C*
2B: Swept stroke zone with long hang on	D + B + C
3: Any attachment of the lightening channel is unlikely	A/5 + B + C*

or roughening of moveable hinges and bearings. To realize the extent of this damage, it is required to characterize the lightning strike with several current components and their associated effects on A/C structure. For this purpose, the Society of Automotive Engineers (SAE) Committee AE-2 (lightning) has defined six lightning current components, described in Table 3.1 [10].

During the interception of an A/C by a lightning strike, not all of the A/C regions experience the same level of lightning flash current because of the movement of the A/C. The SAE Committee has published a lightning zoning document, which defines a set of lightning strike zones, and their associated current components are given in Table 3.2 [11].

Table 3.2 Lightning zones

Current component	Current level	Action integral or change level	Effects on aircraft structures
A: First return stroke	200 kA	200 MJ/Ω	Shock wave, overpressure and magnetic force effects
A_h: Transition zone for first return stroke	150 kA	0.8 MJ/Ω	Shock wave, overpressure and magnetic force effects
B: Intermediate current	2 kA	10 C	Melting, hole burning, hot spots
C: Continuous current	200−800 A	200 C	Melting, hole burning
C*: Modified component C	400 A	18 C	Melting, hole burning
D: Restrike	100 kA	0.25 MJ/Ω	Shock wave, overpressure and magnetic force effects

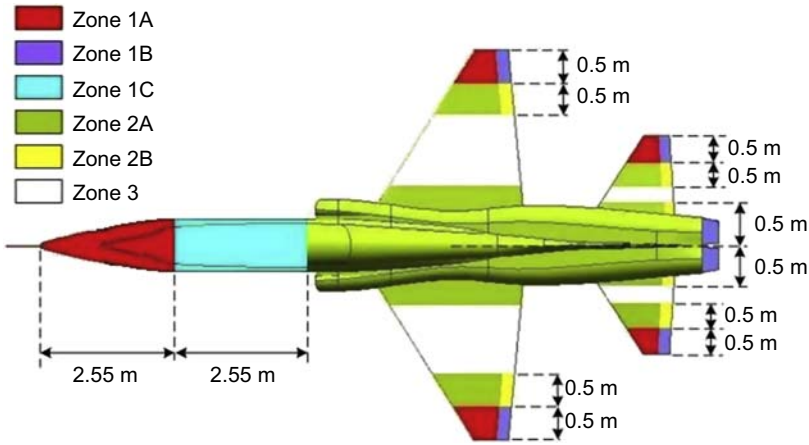

Figure 3.10 A typical zoning example of TIHA Aircraft.

Improving the ability of the composite skins to withstand lightning is usually accomplished by applying a conductive layer on the outside surface. Materials that have performed especially well include flame- or arc-sprayed metals, metal foils, or woven wire meshes. These all have weight penalties, as well as corrosion problems, and do not always make good joints.

The lightning zone definitions, which represent the regions likely to experience the various types of lightning currents, are a fundamental step in determining appropriate lightning protection for A/C. A typical zoning example is shown in Fig. 3.10 for Turkish Unmanned Aircraft (TIHA).

Lightning strike precautions on components can increase the total weight by 1.5−5% depending on the zoning requirements. The new challenge is in using conductive composite materials and thereby eliminating excessive weight due to lightning strike protection measures.

Sometimes smart design solutions can help to reduce the weight on trailing edges for flying control surfaces. The trailing edge of a control box is very prone to lightning strike damage. The solution is to scarify the external trailing edges (ETEs) after the lightning strike instead of replacing all components. See Fig. 3.11.

Using the ETE solution, it is possible to achieve a minimum 5% weight reduction on skin panels [12].

Compliance with lightning strike protection is required by Certification Items CS 25.581 and CS 25.899 [13], in which the protection of the control box panels is demonstrated by coupon-level tests. Fig. 3.12 shows damage after three lightning impacts on a full composite panel with a metallic strip, which was removed after the impact. The damage is seen as black burnt plies at the top of the laminate. Inside the laminate, delamination occurred and the epoxy matrix was burnt. The first important observation is that the damage is localized at the trailing edge zone where the metallic strip was hit by the current. Although the electricity was transmitted over the metallic strip, it may have damaged the CFRP structure below. Second is that the damage could be so severe that the whole part must be replaced.

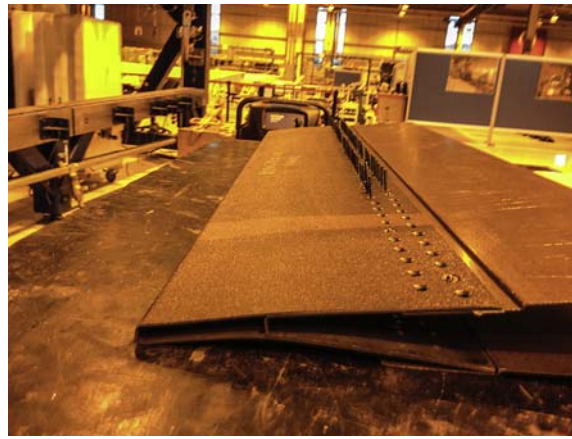

Figure 3.11 External trailing edge manufacturing.
Adapted from: Gozluklu B, Oncul G, Koseoglu U. Design concept of a CFRP external trailing edge for Ailerons. In: Proceedings of the ASME 2013 International Mechanical Engineering Congress & Exposition, IMECE2013-66066; 2013.

The damage would be located at the ETE, especially at the outer part of the component. Therefore, the trailing edge of the control surface can be replaced easily instead of the whole component, which is going to be much cheaper (Fig. 3.13).

3.3.7 Final paint

The function of the external paint system is to ensure the aesthetical appearance (colour, glossiness, general appearance) and the substrate protection against aggressive

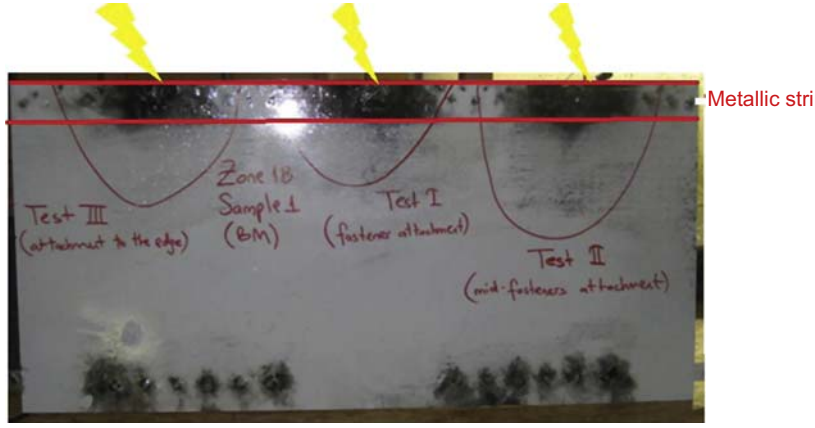

Figure 3.12 Damage after three lightning impacts at the trailing edge zone of a full composite panel with metallic strips located in between the two red lines.
Adapted from: Gozluklu B, Oncul G, Koseoglu U. Design concept of a CFRP external trailing edge for Ailerons. In: Proceedings of the ASME 2013 International Mechanical Engineering Congress & Exposition, IMECE2013-66066; 2013.

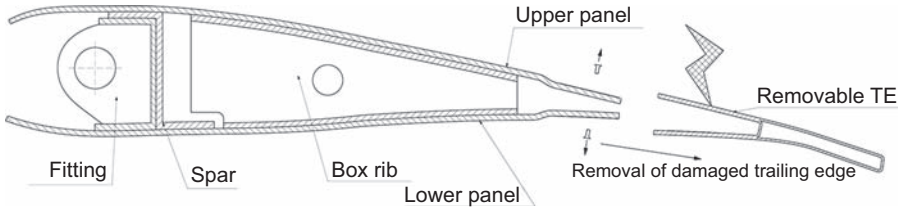

Figure 3.13 After the lightning strike the damaged external trailing edge is removed and replaced with a new one [13]. *TE*, trailing edge.

media and ultraviolet radiation. There are generally four specific areas where external painting is required:

1. the external surfaces of the A/C (see Fig. 3.14(a))
2. specific external areas or aerodynamic surfaces, including flight control, that require special protection such as antierosion paints, abrasion-resistant coating, wear-resistant coating, antistatic coating and high-temperature coating

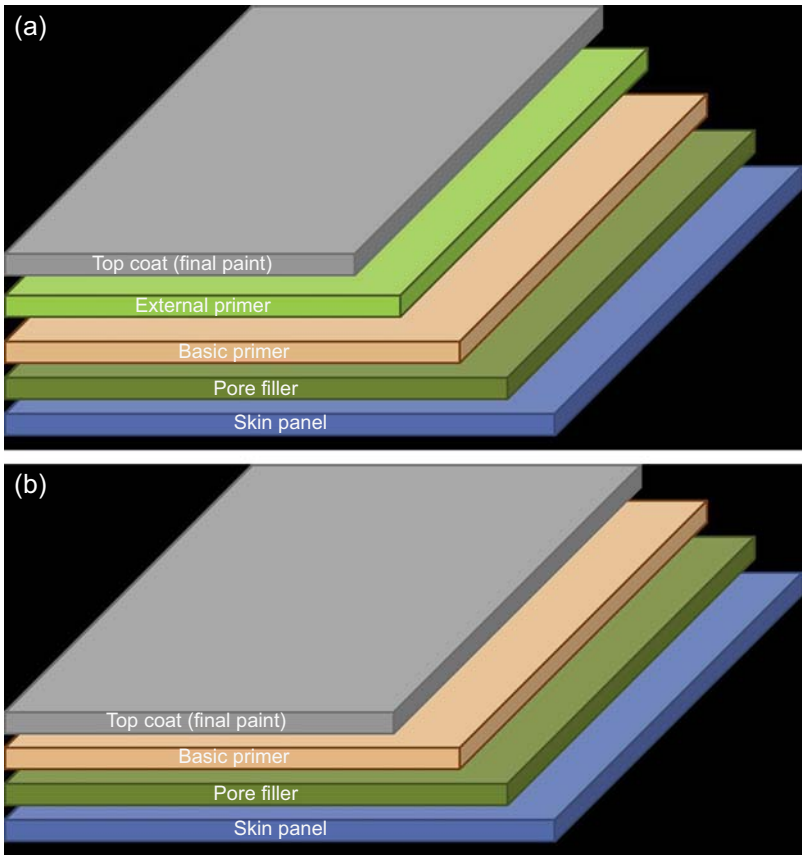

Figure 3.14 (a) External area paint scheme. (b) Hidden area paint scheme.

3. the hidden areas that are not visible during flight or are visible for a short time that are protected against corrosion (see Fig. 3.14(b))
4. unpainted external areas

Each area needs a specific paint scheme, which defines the primer and topcoat combination. The paint thickness can be changed to obtain weight reduction depending on the external paint requirement.

Surface quality needs to satisfy the A/C appearance after final painting and meet the customer's requirements. Surface defects coming from manufacturing or small scratches that occurred during storage and transportation need to be filled with pore filler after cleaning and prior to the painting operation.

Producing high-quality surface composite panels and selecting the correct paint according to the external paint requirements are opportunities to decrease the paint weight.

The utilization of advanced external paint schemes can provide savings of up to 30%. This approach can save more the 100 kg for a large A/C.

3.3.8 Unfolding

One of the widely used geometrically complex parts in advanced commercial A/C is the L-shaped composite. Owing to the sharp curved geometry, interlaminar opening stresses are induced and delamination occurs under considerable mode-mixities in L-shaped beams. An important contribution to civil A/C is the use of L-flanges to reinforce ribs in boxed structures such as wings and control surfaces; however, the use of laminated composites in this geometry leads to an unexpected failure mode not seen in metals, which is delamination at the curvature (bend) under interlaminar tensile ('opening') stresses due to the severe curvature of the bend (Fig. 3.15(c)) [15]. These stresses are in addition to the interlaminar shear stresses that are widely studied in the composites literature, making delamination at the bend of the L-shaped laminate a mixed-mode problem for a typical L-shaped part as shown in Fig. 3.15(a). The acting forces are the axial force parallel to the arm, P; the transverse load, V; and the moment, M, as shown in Fig. 3.15(b) [14]. Failure mode is generally called unfolding.

Unfolding is the one of the main design criteria for L-shaped composites and, owing to the delamination at the radius area (see Figs 3.15(d) and (e)), is the bottleneck of design, requiring a larger radius and more thickness. The weight increase due to unfolding criteria is around 5% [4].

Designers need to consider unfolding effects on radius area and manufacturing capabilities must be improved to meet the unfolding requirements for critical radius. The designer needs to know the safe radius for unfolding before the design is approved and manufacturing starts, otherwise the weight impact will be obvious, as well as the time and effort being lost.

3.3.9 Aluminium–lithium alloys

Aluminium–lithium (Al–Li) alloys are being used more frequently in the A/C industry on all metallic parts such as actuator and hinge fittings, for which the fatigue and damage tolerance criteria are important.

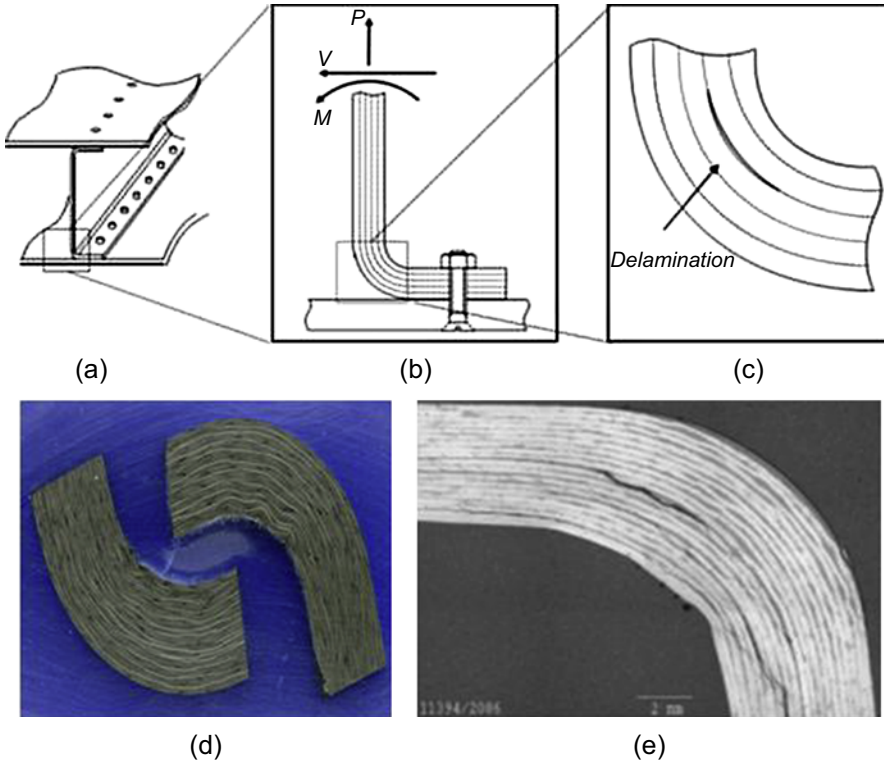

Figure 3.15 Unfolding in L-shaped composites.
Adapted from: Report 91-B-009; 1991. Gozluklu B, Coker D. Modelling of dynamic delamination in L-shaped unidirectional laminated composites. Compos Struct 2012;94:1430–42.

Al–Li alloys are lighter and have high tensile and yield strength compared to the conventional high-strength aluminium alloys. They are resistant to fatigue crack propagation; however, their corrosion resistance still needs to be improved.

The current availability of Al–Li is not sufficient and current lead times do not support high production rates. Stock sizes can be another difficulty for the designer.

Al–Li alloys are relatively expensive compared to other aluminium alloys. Special attention to safety considerations associated with the fabrication, segregation, recycling and disposal of Al–Li alloys is required.

A 20% weight reduction is expected by using Al–Li alloys on metallic parts.

3.3.10 Safety health monitoring

Structural health monitoring (SHM) is based on advanced sensor technology to meet operational requirements in a very effective cost manner and to reduce maintenance costs.

SHM is very widely used in the A/C industry. Flight tests are very effective, and also continuous life sensors are very commonly used throughout the A/C service life to provide continuous observation.

Through the use of SHM technologies it is possible to continuously monitor the structure and detect damage at its onset and track its evolution.

In the A/C industry SHM is considered to comprise two main subjects, load monitoring and damage detection. Strain gauges, accelerometers and fibre-optic sensors are very widely used on load monitoring, and ultrasonic and acoustic sensors based on piezoelectric materials are used for damage detection.

SHM is based on sensing to monitor the behaviour of a structure, assess its performance and identify damage at an early stage. The use of SHM can contribute to reducing structural weight by changing design principles.

The use of SHM technologies makes it possible to monitor the presence of damage in the form of barely visible impact damage (BVID) or other defects and follow its status during the operational life of the structure. Certification imposes no growth of BVID for the entire service life of the structure. This, in turn, limits the level of strain/stress at which the structure can be designed.

Certification requirements for the composite parts impose very conservative design approaches with application of high additional safety factors on damage tolerance analysis.

There is much research on SHM to use in optimal manufacturing of lightweight aeronautical composite structures. With the help of sensors, the curing process can be monitored and porosity detection can be detected with real-time monitoring. The purpose is to develop a complete integrated quality control platform for an optimal and reliable manufacturing process that can control the variable manufacturing parameters, especially for liquid composite moulding processes (eg, resin transfer moulding, pultrusion, infusion). The benefits are shortened process time and decreased scrap rate.

With a robust and controlled manufacturing process there is no need to consider manufacturing defects during the design phase and no need to put safety factors. Lighter weight designs can be possible.

SHM technologies will be the key to A/C structure in the future. Even so, there are now too many research studies and available products; the maturity level and economic benefits of SHM technologies need to be improved.

3.3.11 Automation in assembly

Automated technologies in the assembly line allow for more predictable and reliable quality of assembly with improved inspection processes. This is very recent but absolutely will be one of the important concepts in the aviation industry. Accelerated A/C delivery rates in the future plans of A/C manufacturers are forcing a ramping up of industrial activities to meet the strong demand for qualified and time-efficient assembly lines.

Assembly fixtures as part of the assembly line are designed by considering design principles and tolerance requirements, and design studies are started with the manufacturing plans at very early stages of the design. Resizing and positioning of

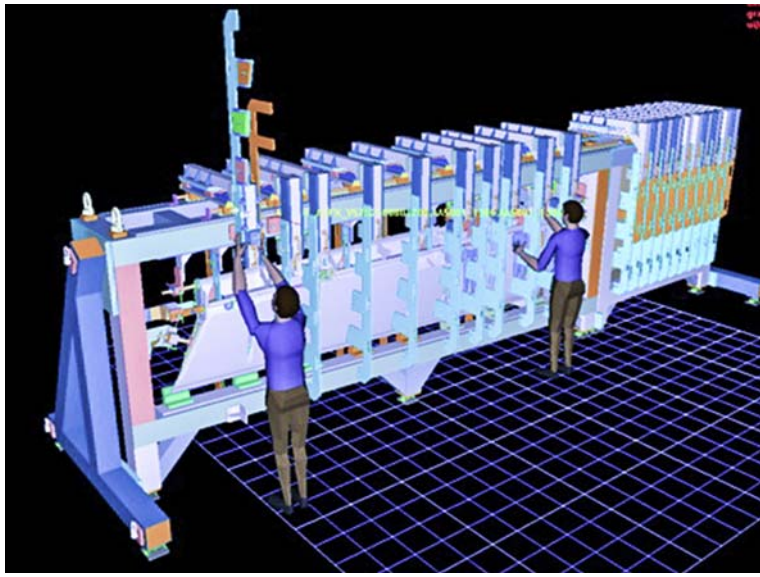

Figure 3.16 Digital mock-up unit on assembly fixture.

the assembly fixture is the starting point in the virtual environment. After the trials between the design and the manufacturing teams are final, the best data, tooling holes, positioning and reference points details are decided for accurate installation. Whenever a digital mock-up unit (DMU) of the product is 3D modelled, then the assembly simulation can start on the assembly fixture (see Fig. 3.16), which is the real demonstration of gap and mismatch problems in the virtual environment at very early stages of the design.

The DMU is the starting point of the high-precision reference points in the design phase; however, it should be supported by laser tracker during the assembly stage.

The automated assembly fixture is equipped with measurement systems and axis systems with suitable software, which allows the best-fit location of parts on assembly. Holes, surfaces and slots are positioned to enable self-locating of parts. This minimizes the need for part-locating tools. This will allow no, or less, shimming for assemblies, especially huge components like fuselages and wings; weight savings are increased and assembly time is reduced.

The automated assembly line is integrated with a flexible robotic drilling (Fig. 3.17)/trimming system and/or automated drill countersink and riveting machines. Integration can be required with auxiliary tooling to support the automated machines (Fig. 3.18) that facilitates the mechanic's ability to position, hold, drill, countersink and fasten the airframe assembly together [16]. Automated machines either are attached to the assembly tool or stand independent of the assembly tool, with the machine supported by its own structure.

Most of the assembly-line hand tools are used for the drilling operation. Most of the hand tools, the drilling feed and the rotational speed (rpm) of the drilling process are

Figure 3.17 Robotic drilling machine.

not adjustable according the material type and thickness to be drilled. On composite structures resin burns the holes inside owing to the high rpm and excessive heat during the drilling operation [16], and drill quality of holes and flaking problems, as shown in Fig. 3.19, are always risks with hand tools. Automated machines completely solve such kinds of problems and during the design stage there is no need to put any load factor for manufacturing defects such as delamination on holes, chip damage to the skin, burrs and end-hole disturbance. These design factors increase the structural weight of the components.

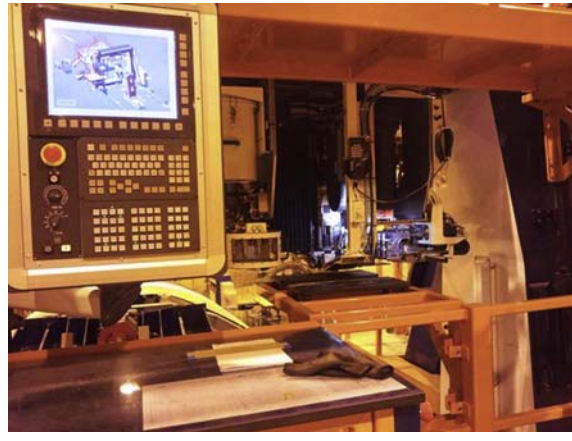

Figure 3.18 Automatic riveting machine.

Figure 3.19 Hole flaking after drilling operation on composite parts.

3.3.12 Titanium alloy parts manufacturing

Titanium is a very important material that has an advantageous weight-to-strength ratio.

Titanium is starting to replace aluminium parts in A/C design and manufacturing, not only for weight also for its ability to resist heat and corrosion when it comes in contact with carbon material. Titanium is now widely used as a fastening element on composite components [17].

It can be possible to obtain up to 20% weight savings by smart design and selecting titanium instead of aluminium materials. However, to work with titanium, especially drilling on the assembly line, is very difficult and needs special drilling equipment, and the process and procurement times are very long, necessitating special attention to the time scale of delivery.

If titanium is selected in the design phase, an automated or semi-automated drilling machine provides a more accurate and efficient drilling operation in the manufacturing phase.

Titanium raw material is not easy to supply in the required lead times and prices can be high compared to aluminium.

Forged titanium can be a good opportunity for weight savings and in fatigue-critical high-loaded areas; however, the material supply can be difficult because of the A/C manufacturer reserve policy on titanium.

3.3.13 Laser beam welding in assembly

Laser beam welding (LBW) is a technique to join multiple metallic and composite (composite-reinforced thermoplastic) pieces by welding through the use of a laser.

Welding of detail parts instead of fastening permits one to obtain assembly with weight reduction and cost savings. Currently, joining composite materials is a matter of intense research because traditional joining technologies are not directly transferable to composite structures [18].

LBW is a new process for composites. It is an accurate and high-speed process and brings many advantages; however, it is difficult to achieve because there are too many variables that make the process complex, such as the joint type and structure, the

process type and parameters, as well as the fixtures. All these aspects have a great influence on the successful achievement of welding.

Automated LBW has been used on stringers on A380 lower-shell skin panels and brought a process time reduction of up to about 90% compared to conventional riveting methods. A 75% weight savings can be possible using welding technology compared with traditional riveted splices [19].

3.4 Conclusions

Lightweight A/C components are possible by increasing the composite percentage in structure design, but are more challenging. Design achievement is linked to the easy and fast manufacturing and assembly of a product with approved but minimal quality checks.

Design solutions need to support simple assembly concepts with minimum assembly time and minimum tolerance accumulation on mating surfaces. Minimum shimming and minimum weight impact and no technical problems are the major expectations for a component during delivery ramp-up periods.

Importantly, this study shares the experience of applicable weight opportunities on assembly, which were considered mainly during the design phase.

- Three-dimensional tolerance studies are essential to see the gap and mismatch values on assembly after the tooling concept, data, design principles and assembly sequences are agreed upon at the very early phase of the program.
- Laminated shims are more practical and accurate in the assembly operation compared to liquid and solid shims.
- Increasing the detail part geometry and decreasing the part numbers on assembly give weight benefits. AFP machines are very effective at manufacturing complex shapes or variable-stiffness parts.
- Reducing fastener numbers and increasing bonding type connections will reduce the weight.
- Lightning strike precautions on components can increase the total weight by 1.5−5% depending on the zoning requirements. Weight impact can be minimized by considering smart design and new technology solutions.
- The paint scheme should be carefully studied. The utilization of advanced external paint schemes can provide savings of up to 30%. This approach can save more the 100 kg for a large A/C.
- Unfolding needs to be checked before the design is approved and manufacturing started. Otherwise the weight impact will be obvious, as well as the time and effort being lost.
- A 20% weight reduction can be possible on metallic parts of the assembly just by using Al−Li.
- SHM technologies continuously monitor the structure, detect damage at its onset and track its evolution. This is the good opportunity to get rid of design conservatism and unnecessary weight.
- An automated assembly fixture allows the best-fit location of parts and reduced shimming on assembly.
- It can be possible to gain up to 15% weight savings by smart design and selecting titanium instead of aluminium.
- Weight savings can be possible using welding technology compared with traditional riveted splices.

References

[1] Kaufmann M, Zenkert D, Mattei C. Cost optimization of composite aircraft structures including variable laminate qualities. Compos Sci Technol 2010;68(13):2748.
[2] Oncul G, Atak B. Üç Boyutlu Tolerans Analiz Modeli ile Yapılan Tasarım Çalışmasının Montaj İşlemine Kattığı Kazançlar. In: USMOS Konferansı. Ankara: ODTU; 2013.
[3] Shim laminated features and benefits. January 3, 2014. https://www.spirol.com/library/sub_catalogs/shim-Laminated_Features_and_Benefits_us.pdf.
[4] Oncul G. Design solutions to reduce weight during assembly operations. In: Transport weight loss diet conference; 2013. Stuttgart, Germany.
[5] Croft K, Lessard L, Pasini D, Hojjati M, Chen J, Yousefpour A. Experimental study of the effect of automated fiber placement induced defects on performance of composite laminates. Compos Part A 2011;42:484−91.
[6] Boeing 787 Dreamliner and Airbus A350 comparison. January 21, 2014. http://www.examiner.com/article/boeing-787-dreamliner-and-airbus-a350-compared.
[7] O'Loughlin JB, Skinner SR. General aviation lightning strike report and protection level study. U.S. Department of Transportation; 2004. FAA. DOT/FAA/AR-04/13.
[8] Jones RM. Mechanics of composite materials. Taylor & Francis Group; 1999.
[9] Onal T, Akyuz S, Oncul G. Lightning strike protection in composite flight control surfaces. In: AIAC conferences METU; 2011. Ankara.
[10] Aircraft lightning environment and related test waveforms. February 2005. Rep. of SAE Committee AE-2.
[11] Aircraft lightning zoning standard. February 2005. Rep. of SAE Committee AE-2.
[12] Gozluklu B, Oncul G, Koseoglu U. Design concept of a CFRP external trailing edge for Ailerons. In: Proceedings of the ASME 2013 International mechanical engineering Congress & Exposition; 2013. IMECE2013−66066.
[13] European Aviation Safety Agency. EASA certification specifications for large aeroplanes−CS 25; 2007.
[14] Martin RH, Jackson WC. Damage prediction in cross-plied curved composite laminates. NASA Technical Memorandum 104089, USAAVSCOM Technical.
[15] Report 91-B-009; 1991 Gozluklu B, Coker D. Modelling of dynamic delamination in L-shaped unidirectional laminated composites. Compos Struct 2012;94:1430−42.
[16] Bullen GN. Automated/mechanized drilling and countersinking of airframes [Chapter 5], eISBN: 978-0-7680-7995-1.
[17] Titanium and the aerospace industry. February 1, 2014. http://titaniummetalsupply.com/blog/titanium-and-the-aerospace-industry/.
[18] da Costa AP, Botelho EC, Costa ML, Narita NE, Tarpani JR. A review of welding technologies for thermoplastic composites in aerospace applications. J Aerosp July−September, 2012;4(3):255−65.
[19] Airbus's automated future features robotics. May 2013. http://www.aviationweek.com/Article.aspx?id=/article-xml/AW_05_06_2013_p47-570060.xml&p=3. Aviation week.

The automotive body lightweighting design philosophy

4

D.M. Baskin
Materials and Structural Optimization Consultant, Dover, MA, United States

4.1 Introduction

Contemporary efforts to reduce the weight of automobiles have resulted in a number of production vehicles utilizing carbon-reinforced plastic composites as the primary structure. These efforts predominately fall into one of two categories: (1) Carbon fiber is substituted for steel to form components that resemble stamped metal parts and are glued together at flanges to form a unitized construction (aka the black metal approach). (2) An approach similar to Grand Prix racing cars is employed in which metallic suspension bearing assemblies are bolted to a central carbon fiber "tub" or monocoque structure. In reality these efforts have translated into incremental rather than revolutionary weight reductions roughly on the order of 0−20% compared to similar vehicles made from high strength steels (Fig. 4.1) or aluminum.[1−7]

Considering that even low-cost commercial grade carbon fibers have greater than 10 times the specific (normalized by density) strength and 5 times the specific stiffness than even the highest grades of aerospace steel alloys,[8] greater weight savings should be achievable. Granted, about one-third to one-half of these capabilities are lost when the fibers are consolidated in a polymer matrix. Nonetheless, there should still be higher weight savings. As proof, consider high-end road racing bicycles. For 1975 to 2015, these bicycles, which similarly benefit from weight reduction and high stiffness as automobile structures, have undergone the transition from primarily high strength steel construction to nearly full carbon fiber composite construction. In this example, weight reductions resulting from this transition have been round about 45% and continue to increase as better and better manufacturing processes and structural optimization techniques are explored. For example, in the early 1980s the author owned high-end alloy steel road racing bicycles that weighed ca. 21 pounds. By the late 2000s, carbon fiber road racing bicycles made by a variety of manufactures were available in the range of 12−14 pounds.[9−11] Similar reductions should be possible in automobiles; however a somewhat different approach is required than those described previously. Discussed herein will be a revised body-in-white lightweighting design philosophy.

Lightweight Composite Structures in Transport. http://dx.doi.org/10.1016/B978-1-78242-325-6.00004-9

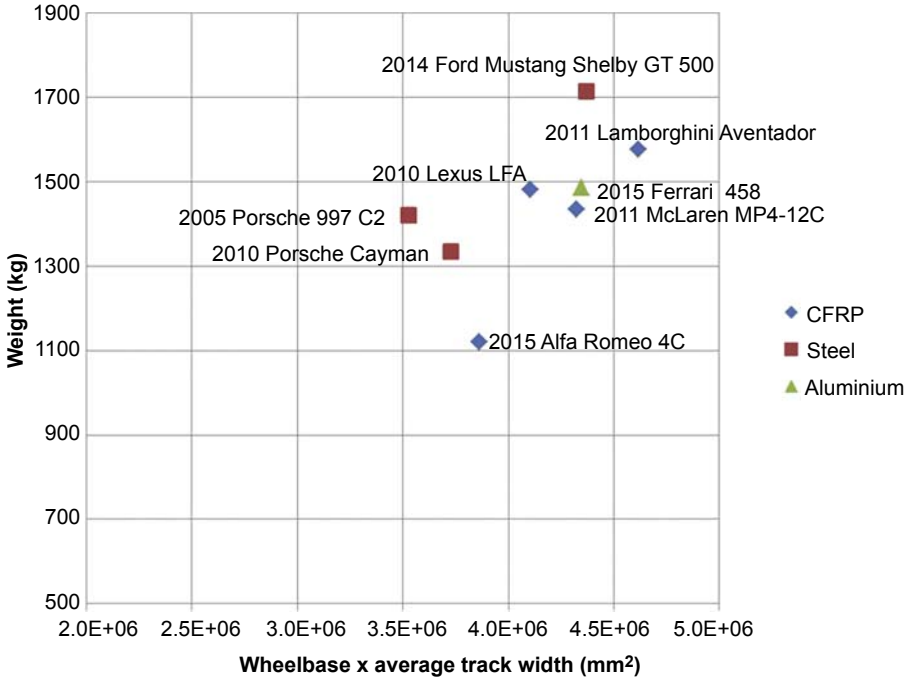

Figure 4.1 Graph of curb weight versus plan area as defined as wheelbase times the average of the tracks. The graph shows that the weight reductions associated with switching to a carbon fiber primary structure are evolutionary and not revolutionary.

4.2 The automotive lightweighting design philosophy

The central concepts of the automotive lightweighting design philosophy are listed below for clarity and then expanded on in subsequent paragraphs. The list is as follows:

1. Structural efficiency and exterior design are inseparable.
2. Pursue suspension-mount centric design.
3. The most structurally efficient design lies somewhere between a space frame construction and a monocoque. Herein, I introduce the term "mid-spectrum" design to denote this type of structure.
4. Maximizing structural efficiency requires employing modern structural optimization tools to optimize topology, wall thicknesses, cross-sectional geometry, fiber ply orientation (assuming a composite material will be used), etc. Intuition alone will not yield the optimum design.
5. Close out panels that are primarily used to keep out wind and water should not be made from materials with high mechanical capabilities, even carbon fiber composites.
6. Joint efficiency is critical.

To explain these six concepts, the first step is to realize that the automobile body is in reality a bridge of four suspension mounts containing shock towers and control arm attachment points for four wheels. Automobile bodies primarily experience bending

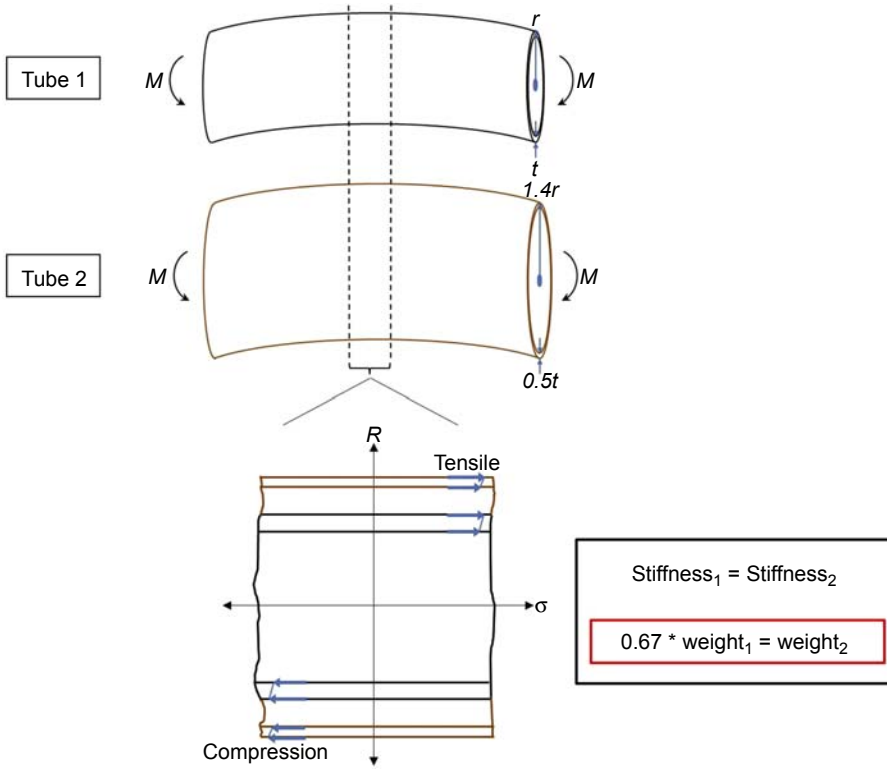

Figure 4.2 A tube in bending can be made lighter without reducing stiffness by increasing the diameter and reducing the wall thickness.

and torsion loads (assuming that the vehicle has not been involved in an impact). Minimizing the displacement of this structure subject to these loading conditions is critical for promoting the best handling characteristics and comfort of the vehicle. This is achieved through first considering the laws of solid mechanics, materials selection, and joint design. Solid mechanics dictates that when a tube of symmetric and constant cross-section (whether round, square, rectangular, etc.) is subject to a bending load, the stresses at the outer diameter of the tube perpendicular to the plane of bending are higher than the stresses at the inner diameter (Fig. 4.2).[12] Assuming constant loading, if the diameter of the tube is increased, the stresses at the surface of the tube will decrease with the fourth power of the outer radius. It then follows that if the wall thickness is decreased as the diameter is increased, a tube with the same stiffness can be produced at a lower weight. Therefore, to use the minimum possible material to support a given bending load it makes sense to engineer sections with thin walls and large dimensions parallel to the plane of bending. A tube in torsion behaves similarly, but the dimension (radius for a round tube) 360 degrees around the axis of torsion must be maximized. (It should be noted that there is an optimum extent to which this principle can be carried out because at some point when the wall thickness is low enough,

buckling takes over as the primary failure mode.) Applying this concept to engineering automobile bodies highlights an important point: to achieve the minimum weight at the maximum stiffness the auto body as a whole should be designed to use the maximum envelope possible, wherein the height is limited mainly by aesthetics produced by the designer or stylist, occupant packaging, and aerodynamics constraints.

The topology of the auto body, or how loads and stress are directed throughout the volume available for structure, is dependent on the exterior aesthetics. Direct, smooth, and continuous load paths are always preferable with regard to promoting the maximum stiffness or strength at the minimum weight (these ratios we can loosely define as "structural efficiency"). Minimum weight will require a smooth and continuous load path between the four suspension mounting point areas (one for each wheel) as these are the primary areas of load input. This is especially true at the areas where the shocks and springs mount to the primary structure, as normally these are the areas with the highest load inputs. Therefore, the bases of the body's A- and C-pillars should be stretched to line up directly with the front and rear shock mounts. Moreover, a smooth arch between these pillars, allowing for occupant packaging requirements, should be created. To maximum the outer dimensions of the body structure (ie, its bending section), the bottom end of the suspension mounting areas should gently transition to the lowest area on the body structure—the sill or rocker longitudinal members. Cross-members between the suspension mount areas are necessary as well and should be given similar consideration for structural efficiency. The arrangement of the members and how they direct stress from one load input area (the suspension mounts) to the other are the topology of the body structure. Moreover, the topology described defines a major portion of the vehicle's aesthetics, and hence the inseparable relationship between exterior design and structural efficiency.

Engineering topology to smoothly and efficiently flow stress exclusively between suspension mounts is extremely intuitive. However, when taking into account the needs for impact safety, noise abatement, and packaging requirements for engines, dynamic tire envelopes (aka "bee hives"), gas tanks, exhaust systems, transmission, etc., engineering topology becomes too complex and challenging for mere intuition. Modern structural optimization software, such as Genesis from Vanderplaats R&D and Optistruct from Altair, provides a means to extend intuition. Using algorithms that can iterate through literally millions of design possibilities in hours, structural optimization software can calculate the optimum topology given nearly any group of loading conditions and packaging requirements. An example of a topology optimization result is shown in Fig. 4.3. Although a proper explanation of the methods used in these topology optimization tools can be found in Refs. 13–27, in summary, the process begins with a CAD (computer-aided drafting) model of an outer design surface for the vehicle being developed. (Catia and Solidworks, both from Dassault Systems, have been used in this regard previously.) In CAD space, this outer surface is filled completely with solids. Piece by piece, solids are removed to define areas where structure cannot exist. For example, solids are removed in places where occupants sit or areas reserved for payload, powertrain, electronics, etc., to prevent the optimizer from placing structural members in these areas. This "packaging volume" is then discretized in CAE space with a mesh of finite elements and nodes. After loading the

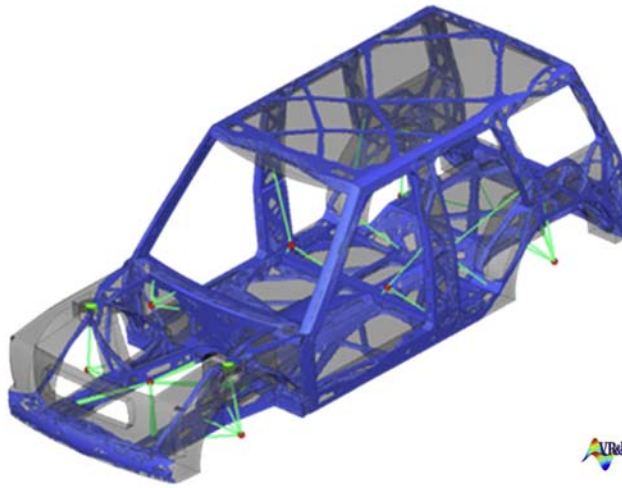

Figure 4.3 Topology optimization result for a sport utility vehicle body structure. Vanderplaats R&D.

meshed packaging volume into appropriate structural optimization software, boundary conditions that simulate various scenarios, such as torsion, bending, front impact, and roof loading, are applied to the packaging volume. The user then constrains the number of elements (which is the same as constraining the amount of material in the model) to some value lower than the number in the original discretization. Next, the optimization software seeks to distribute the remaining material throughout the packing volume such that, given the boundary conditions, the aggregate strain energy of the system is minimized. What results is a distribution of material that will provide the stiffest structure given the boundary conditions, and more importantly for the design engineer, a map of the most efficient topology (ie, the best load paths) and therefore the best places to apply structure within the packaging volume.

The initial geometry, especially the exterior form, of the packaging volume will dictate the potential to achieve high structural efficiency in the final product. A packaging volume that demands vertical pillars demands awkward tortuous discontinuous load paths or functions counter to the mechanics of a beam in bending by constraining the beam height in critical locations will drive weight into the final primary structure.

4.3 The mid-spectrum concept

Automobile body structures have been built using many structural approaches. If these approaches could be placed on a spectrum, on one end of the spectrum would be the ladder frame, in the middle would be the space frame, and on the other end would be the monocoque. Ladder frames derive from the days of horse-drawn carriages and are currently used on most pickup trucks. They are best at providing absolute strength, but not necessarily the stiffest solution. The space frame construction employs a truss structure of small

Figure 4.4 Late 1950s Maserati Tipo 61 (aka Birdcage Maserati). Extreme example of an automotive space frame body structure.
Image courtesy of John Chapman, available at: http://en.wikipedia.org/wiki/File:Maserati_T61_engine_bay_Donington.jpg.

diameter tubes that are typically welded together and then covered with a lightweight body. Good examples of historic vehicles produced using this construction include the Mercedes 300SL and the Maserati Tipo 61 (aka the "Birdcage") (Fig. 4.4). More contemporary examples of production vehicles utilizing a space frame primary structure include the Pontiac Fiero, the SRT Viper, and the Chevrolet Lumina APV. In monocoque construction, the outer "stressed skin" is the primary structure of the vehicle. There are no tubes or trusses. There are only large continuous surfaces used to support the vehicle and react road inputs through the suspension mounting points. Modern passenger airplanes are true monocoques. Although a pure monocoque construction has never been achieved in a passenger car, perhaps the beautiful Lotus Type 14 Elite (Fig. 4.5) most closely achieves the ideal. This vehicle employs several large, concentric shells made of fiberglass to form the body structure. (Ferdinand Porsche applied for a US patent for a similar construction in the same year that the Type 14 was launched, 1958. However, Porsche never built any vehicles as described in his patent.) Nearly all vehicles on the road today use a unitized sheet construction where metal sheets, usually steel, are stamped into appropriate shapes and welded together at flanges using spot welds. These types of structures are often mistakenly referred to as monocoques, but they are not. The reason they are not is because quasiladder frame structures are stamped from sheet metal and used to support the underside of the vehicle. Additionally, the lower suspension inputs are almost always supported by space frame-like subframes. Today's ubiquitous unitized sheet steel construction lies, in reality, somewhere between a space frame and a monocoque on the spectrum, although closer to a monocoque.

But which type of construction produces the most structurally efficient automobile body? Years of experience analyzing topology optimization results from full body

Figure 4.5 Late 1950s Lotus Elite—perhaps the most successful effort to produce an automobile body structure that most closely approaches a true monocoque.

packaging volumes confirm that the most structurally efficient automobile body solution lies somewhere between a space frame and a monocoque, but somewhat closer to a space frame than most production vehicles today. The explanation for this can be found in the raw output from topology optimization results. "Density plots," which are available as output from most structural optimization software, use various coloring strategies to indicate the positions at which the optimizer has distributed material within the packaging volume. Just to emphasize, the results are not binary (e.g., material or no material), rather they indicate a spectrum of material density ranging continuously from zero to full density (typically chosen as 1). Shown in Fig. 4.6 are several cross-sections through a density plot for a packaging volume model that was loaded simultaneously in torsion, bending, front impact, rear impact, and side impact (on the B-pillar).

These particular cross-sections are cut through the floor pan underneath the dash panel and through the bottoms of the hinge pillars. The areas shown in red represent locations where the optimizer has placed full-density material (density equal to one in this example) and areas shown in blue are areas void of material. Areas shown in colors not red or blue have densities somewhere between one and zero. The areas in red should become the structural members shown in the final structural design. Of particular interest in these plots is that the optimizer has seldom distributed material on the very outer perimeter of the surface of the vehicle. For example, looking at the bottom of the vehicle, there are portions of the floor pan void of material. Similarly, from looking at topology optimization results for a large sports utility vehicle in Fig. 4.3, which only shows volumes where the density of the material is close to one, it is clear that most areas on the surface of the vehicle are void of material. Also note the "K" and "V" members shown in the roof of the SUV defined by void areas in between. As discussed in Ref. 13, such members are extremely effective at adding

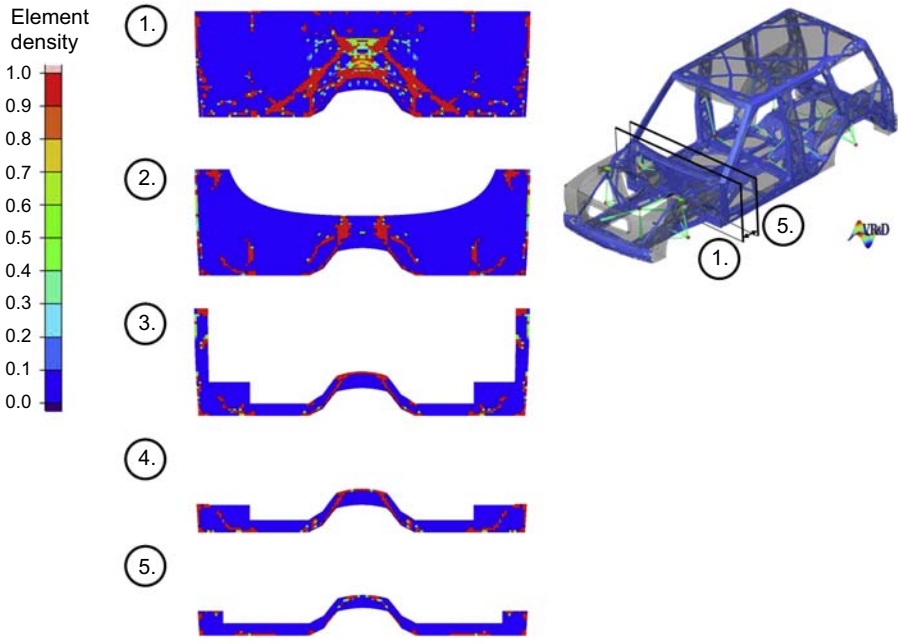

Figure 4.6 Density plot for a topology optimization result for a sports utility vehicle body structure.
Vanderplaats R&D.

stiffness to a body structure but are rarely seen in current production vehicles. An important implication of these results: if a true monocoque were the most structurally efficient construction method, then the preceding would not be the case. Instead, all the material would be distributed at the surface of the packaging volume. But this was not the case. Therefore, true monocoque structures are not optimum. Inevitably, pursuing a monocoque construction will lead to understressed and superfluous material and therefore useless mass.

Topology optimization results do not imply a space frame construction either. Looking again at Figs. 4.3 and 4.6, the high-density areas are rarely round or have a constant cross-section. Rather they are flat and mostly broad with large fluid radii at the junctions between structural elements. This is uncharacteristic of space frames. Most often, space frame structures are made of struts with nearly homogeneous equiaxed cross-sections. Moreover, space frames are characterized by discrete joints or "nodes" where the struts intersect. Again, this is quite different than the large joining radii between joining structural members seen in the topology optimization results. Finally, by definition the struts found in space frames are subject to only tensile and compressive forces. However, the large radii joining structural elements implied by topology results would certainly lead to bending, shear, and torsion loads in addition to tensile and compression.

All of this clearly indicates that the most structurally efficient automotive primary structure would lie somewhere between a space frame and a monocoque. This

Figure 4.7 High-end carbon fiber racing bicycle frame. From a structural efficiency perspective, bicycle frames such as these are perhaps the most structurally optimized of any consumer product. Every tube at every cross-section has been optimized for shape, wall thickness, and fiber orientation.

mid-spectrum structure would be composed of a relatively few (compared to a space frame) large structural members with cross-sections mainly having high aspect ratios (ie, small height to large width). The joints between the members would be highly distributed with large flowing radii; one member would flow gently into another. Interestingly, the modern carbon fiber road racing bicycle frame comes very close to this ideal. Fig. 4.7 shows a typical example in this category.

Note the large cross sectional, high aspect "tubes" that intersect with large flowing radii. As previously noted, these structures are marvels of structural efficiency. For example, they are able to support riders over 120 kg, as well as the significantly higher forces applied at the pedals by strong riders. In fact, according to Ref. 28 the thrust forces at the pedals can be as high as hundreds of newtons. Yet, these frames weigh a mere 2 kg or less.[9–11] Such bicycle frames are made in the hundreds of thousands per year. The majority of these frames are produced by a few factories in Asia. They are made using a method known as bladder or mandrel molding where carbon fiber prepreg is wrapped around either inflatable bladders or silicone mandrels. Typically, these bladders and mandrels are shaped in roughly the same shape desired for the final product. These wraps are then placed inside a metallic female mold and the assembly is placed in a large oven. Pressure needed to consolidate the carbon fiber and polymer matrix making up the prepreg is supplied either by inflating the bladders or by taking advantage of the high thermal expansion behavior (relative to steel) of the silicone mandrels to compress the composite material against the walls of the female mold. The orientation of the fibers throughout the component is very critical to the structural efficiency of the frame. The same optimization software used to optimize topology is often used to optimize fiber orientations throughout the lay-up.[27] Also of interest is that the geometry of each cross-section of each member varies continuously from one end to the other. In fact, no two cross-sections along any given tube are

the same. Another capability of most structural optimization packages is shape (cross-section) optimization. This is achieved through using a perturbation approach where mesh nodes are displaced in various directions (toward and away from the centroids of the tubes) at various distances until the stiffest solution at the lowest mass of the entire structure is determined. Given the sum of all these efforts to maximize structural efficiency: carbon fiber construction, gauge thickness optimization, fiber orientation, shape optimization, etc., it may be that from a structural efficiency perspective, the modern road racing bicycle frame may be the most highly optimized and engineered structure of any consumer product.

There is an important difference between engineering bicycles and automobile primary structure. Namely, automobiles must be designed to absorb energy in front and rear impacts. Bicycle frames currently do not have this requirement. However, material absorption research has shown that thermoplastics reinforced with braided, continuous reinforced carbon fiber have a higher specific energy absorption (energy absorption per unit density) than steels and aluminum.[29–31] Therefore, it should still be possible to produce vehicles with full composites that meet crash energy absorption requirements and are substantially lighter. However, whereas metals absorb energy through plastic deformation and dislocation activity, composites absorb energy through functional sliding between fiber and matrix and through splintering. The result is that composite vehicles involved in accidents may leave more debris on the ground than metallic ones. At least in the United States, this failure mode may pose certain legal and product liability issues that would need to be addressed before all-composite vehicles can be released fully into the stream of commerce.

A potential use challenge associated with using composites such as carbon fiber epoxy is recyclability. Separation of the fiber material from the polymer matrix is perhaps one of the biggest challenges to recycling this material. However, this is an area of ongoing research at many automotive original equipment manufacturers. In addition, the company Materials Innovations Technologies—Reclaiming Carbon Fiber LLC (MIT-RCF LLC) in Lake City, South Carolina, USA has made progress toward reclaiming and reusing end-of-life components. MIT is able to reduce these streams of material into various forms of chopped, short-strand material and pellets that can be made into new carbon fiber products. However, there does exist the caveat that the mechanical properties of the new material are always reduced compared to the original material. For more information, see Ref. 32.

Developing a strategy to panel the spaces between structural members in the mid-spectrum concept will be critical to implementation. Such panels will be necessary to keep wind, water, and debris out of the engine compartment, passenger compartment, trunk, etc. But this will be their only requirement if the primary structure is designed properly. Consequently, the mechanical requirements of these close-out panels are modest. Undoubtedly, using steel in these applications would result in underutilized mechanical ability and superfluous mass. Using carbon fiber composite material in these applications is similarly wasteful. Utilizing low-cost, polymeric materials reinforced with low-cost fillers, such as millimeter length glass fibers or microspheres, in these close-out panel applications will be more appropriate as well as key to realizing lightweight automotive structures. Such polymer panel products currently

exist. For example, the polymer blend used to make the exterior body panels on Daimler's Smart Fortwo is promising. The blend consisted of polycarbonate and polybutylene terephthalate and was originally sold by GE Plastics (now Sabic Innovation Plastics) and marketed under the name Xenoy.[33] Many challenges exist in developing polymer materials for body close-out panels. For example, to keep the gaps between body panels acceptably small, the material must have a low thermal expansion coefficient. Additionally, degradation by ultraviolet light can also be an issue as can be long production cycle times that result in higher production costs. Providing color and a good durable "Class A" surface finish to the final part can be a great challenge as well. Regardless, automotive suppliers such as Ticona (now Celanese),[34] BASF,[35] and Bayer[36] continue to make advances in these areas.

4.4 High-performance composite materials and realizing the mid-spectrum concept in automotive primary structure

From a lightweighting perspective, today's unitized steel construction automotive body structures lie far away from the level of optimization found in modern racing bicycle frames. Load paths are often discontinuous and tortuous and even contain large dislocations. For example, loads from the front shock towers are often directed first through the upper rail structure (the stampings that support the front fenders), through the cowl, and then finally into the A-pillars (Fig. 4.8). Additionally, heavy steel panels are used for the sole purpose of keeping wind and water out of the passenger compartment. Achieving truly dramatic weight savings will require a level of optimization

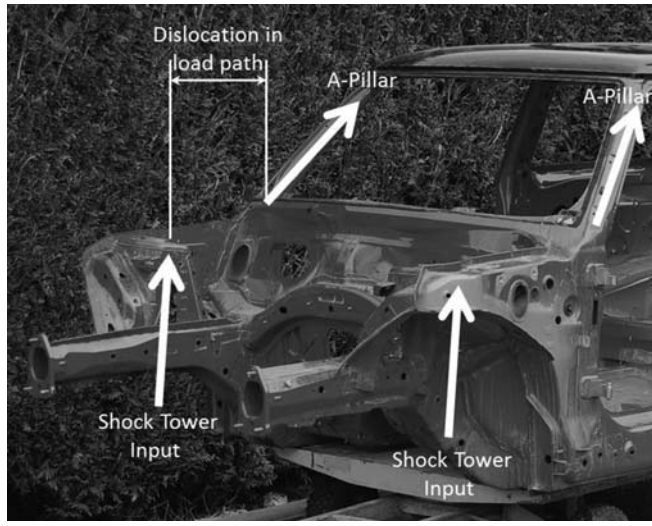

Figure 4.8 Suboptimization typical of modern automotive steel body structures. The load path from the shock input to the A-pillar has a significant dislocation.

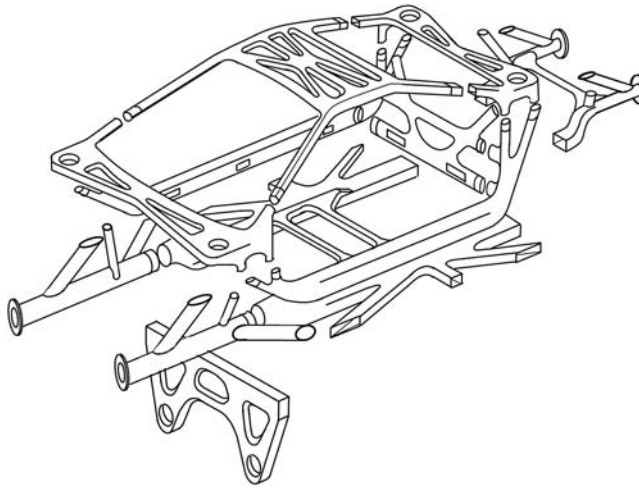

Figure 4.9 Artist's conception of what a "mid-spectrum" body structure may look like. Note that the same optimization and production methods used to make high-end carbon fiber bicycle structures could potential be used to produce the various "chunks" shown in the concept.

similar to that used in bicycle frames. This includes the use of more efficient topologies (the mid-spectrum concept), better optimized cross-sections, improved joint efficiency, and the use of materials with higher specific strength, stiffness, and specific energy absorption. Choosing materials and processing routes that can translate topology optimization results into real physical structures is perhaps the most important requirement. In this regard, continuous fiber-reinforced composite materials, such as carbon fiber epoxy composites, perhaps offer the best geometrical freedom and therefore the best chance of translating topology results. Also as discussed earlier in this chapter, carbon fiber composites can exhibit specific (normalized for density) mechanical properties that are many times higher than even advanced aerospace alloys of steel.[8,37] In fact, the geometrical freedom, the ability to create three-dimensional matrixes of structural elements that come together with large sweeping radii, and the ability to create thin-walled members with varying, complicated cross-sectional geometries are perhaps the best reasons to use carbon fiber composites. Aluminum castings can be used to meet the external geometrical requirements, but will never be made with submillimeter wall thicknesses. Metal stampings can meet the wall thickness requirements, but not the external geometrical designs. Additionally, stampings typically come with heavy flanges. Random chopped fiber-reinforced composites may allow thin walls and sufficient geometrical freedom but likely will not have the needed mechanical properties. Continuously reinforced, high fiber volume fraction, carbon fiber/polymer matrix composites, molded via bladder or silicone mandrel routes, offer the best ability to translate topology optimization results.

A mid-spectrum concept automotive body structure is proposed in Fig. 4.9. The concept is produced by bonding together several sections that are roughly the size and complexity of a bicycle frame and can likely be made in one piece. The concept

is broken up as follows: the greenhouse structure is a single three-dimensional matrix of structural members comprised of the right and left A-pillars, roof rails, and C-pillars connected by a representative series of "K" and "V" members. Moving further down the vehicle, the front right and left shock towers, cowl plenum, and lower portions of the A-pillars are combined into one piece. A similar structure is made up of the right and left rear shock towers, and lower portions of the right and left C-pillars. Next, right and left sill structures would be combined with the hinge pillar and diagonal members running from the shock towers to the sills. Then, a molding made up of "X" and "K" members could be made to form the front separation bulkhead wall between the engine bay and the passenger compartment. A similar bulkhead structure could be molded to form the rear separation structure between the trunk and the passenger compartment. In both front and rear bulkhead structures, members would be included that triangulate to the shock towers. Front, right, and left rails and rear right and left rail structures would all be made separately, but would include various diagonal members to further stabilize the shock tower structures as well as direct impact energy into the roof rail pillar structures. The final section is the floor, which contains various "K" and "V" members to provide global torsional rigidity and to absorb side impact energy.

Costs will be higher than current unitized steel construction, but perhaps not entirely unreasonable. This may sound surprising. However, consider a few items. First, the bicycle industry has developed processing methods for producing hundreds of thousands of carbon fiber bicycle frames per year. Some estimate that Far East manufacturers only spend 2–5% of the retail selling price of an average frame on direct materials and labor.[38] In time, and with continued development efforts, perhaps such efficiencies could be reached with automotive mid-spectrum designs. It is also worth noting that carbon fiber tennis racquets have been produced using similar processing methods, but in even higher volumes. The point is that there is the ability to produce highly optimized carbon fiber structures in high volumes that many can afford.

4.5 Future trends: how autonomous vehicles will enable mass reduction

Development of future autonomous vehicles may surprisingly enable significant weight reductions. A recent study sponsored by the Michigan Economic Development Corporation in the United States explored the implications of passenger vehicles becoming fully autonomous.[39,40] In one scenario, vehicle-to-vehicle communications complemented by a matrix of range proximity sensors are projected to drastically reduce or nearly eliminate vehicle-to-vehicle and vehicle-to-stationary object impacts. Consequently, it may only be necessary for the primary structure of the vehicle to be strong and stiff enough to meet its own durability and stiffness requirements for longevity, handling, and NVH (noise vibration and harshness) without as many measures in place for occupant protection. Some structures in automotive bodies, such as side intrusion beams and bumper beams, are designed purely for absolute strength. They tend to be heavier than other similarly sized structures on the vehicle whose designs are, for example, purely driven by stiffness. Under this scenario, these

inherently heavier structures could be mostly eliminated. This would significantly reduce the amount of material going into the vehicle, thus further reducing weight and potentially making up for some of the extra costs associated with the paradigm shift to carbon fiber construction. But autonomous vehicles may enable even further weight reductions through the elimination of steering wheels, gear shifters, pedals, etc. Without these control items, completely new seating configurations are possible which open up new styling possibilities, potentially even more structurally efficient primary structure topologies, less material use, and more weight reduction. However, this scenario is indeed far off in the future. It will require that all vehicles are autonomous and would have been for several generations of vehicles to evolve out all potential failure points. Such a scenario is likely many years out and it would be necessary to reduce the cost of all carbon fiber mid-spectrum designs through more conventional routes, lower raw material costs, improved processing, accelerated cycle times, etc., in the mid-term.

4.6 Summary

The concepts presented herein were developed from a myriad of topology optimization studies, direct involvement in many automotive lightweighting studies, and three decades witnessing the evolution of high-end racing bicycle frames. These experiences teach the following. There are very structurally efficient topologies for automobile body structures and there are ones that are not. Considering that the topology of the structure is the majority component of the vehicle's styling leads to the axiom that exterior styling and structural efficiency are inseparable. In addition, topology optimizers tend to not distribute material continuously along the outer envelope of the available packaging space. Rather, they tend to distribute mass along discrete load paths, implying that a monocoque construction is not the lightest solution for the automotive body structure. The fact that the topology optimizers tend to imply few, large structural members joined by large sweeping radii connecting members indicates that pure space frame construction does not offer the highest structural efficiency either. The optimum structural efficiency will be obtained from a structure that is mid-spectrum between these two concepts. Translation of topology optimization results for a full automotive body requires a material and processing route that can offer an extremely high degree of geometrical freedom. Bladder or mandrel molding of composite material prepregs, as used on high-end racing bicycle frames, offers this freedom and offers thin-walled construction as well. Carbon fibers are astoundingly strong and stiff. Although consolidation of carbon fibers into a polymer matrix results in the degradation to some extent of these properties, the composite as a whole offers specific strength and stiffness higher than any competitor materials. Finally, the mid-spectrum design concept leaves open many spaces where wind and water can unwantedly enter interior spaces of the vehicle. The openings should not be plugged using materials with high structural capability such as steel or carbon fiber. Rather, low-cost, low-density, lightly reinforced polymer panels are available today to serve these purposes.

References

1. www.conceptcarz.com.
2. www.porscheusa.com.
3. www.ferrari.com.
4. www.mclaren.com.
5. www.4c.alfaromeo.com.
6. www.ford.com.
7. www.wikipedia.com.
8. Baskin DB, Dinda S, Moore TS. *A simple approach to selecting automotive body-in-white primary-structural materials*. 2002. SAE Paper# 2002-01-2050.
9. www.scott-sports.com.
10. www.specialized.com.
11. www.giant-bicycles.com.
12. Beer FP, Johnston Jr ER. *Mechanics of materials*. 2nd ed. New York: McGraw Hills, Inc.; 1992.
13. Baskin DM, Reed DB, Seel TN, et al. *A case study in structural optimization of an automotive body-in-white design*. 2008. SAE Paper# 2008-01-0880.
14. Schmit LA. Structural synthesis—its genesis and development. *AIAA J* 1981;**19**(10): 1249−63.
15. Schmit LA, Farshi B. Some approximation concepts for structural synthesis. *AIAA J* 1974; **12**(5):692−9.
16. Vanderplaats GN, Miura H. *Trends in structural optimization: some considerations in using standard finite element software*. 1986. SAE Paper# 860801.
17. Vanderplaats GN. *Automated design using numerical optimization*. 1979. SAE Paper# 791061.
18. Vanderplaats GN, Salajegheh E. An efficient approximation technique for frequency constraints in frame optimization. *Int J Numer Methods Eng* 1988;**26**:1057−69.
19. Bendsoe MP, Kikuchi N. Generating optimal topologies in structural design using homogenization method. *Comp Methods Appl Mech Eng* 1988;**71**:197−224.
20. Laxman S, Mohan R. *Structural optimization: achieving a robust and light-weight design of automotive components*. 2007. SAE Paper# 2007-01-0794.
21. Soto CA. Structural topology optimization: from minimizing compliance to maximizing energy absorption. *Int J Vehicle Des* 2001;**25**(1/2):142−63.
22. Fredricson HA. *Design for property based optimization of vehicle body structures*. 2003. SAE Paper# 2003-01-2755.
23. Nomura A, et al. *Improvements of BIW NVH characteristics using a concurrent design optimization approach*. 2003. SAE Paper# 03NVC-322.
24. Fukushima J, Suzuki K, Kikuchi N. *Shape topology optimization of a car with multiple loading conditions*. 1992. SAE Paper# 920777.
25. Reed C. *Application of optistruct optimization to body in white design*. Coventry England: Altair Engineering; 2002.
26. Powers JB, Laxman S, Farahani A, Sharifi H. *Future steel vehicle design methodology: detail design concept using 3G optimization*. 2012. SAE Paper# 2012-01-1345.
27. www.vrand.com.
28. Whitt F, Wilson D. *Bicycle science*. 2nd ed. Cambridge: The MIT Press; 1994.
29. Caliskan AG. *Design and analysis of composite impact structures for formula one using explicit FEA techniques*. 2002. SAE Paper# 2002-01-3326.

30. Caliskan AG. *Crashworthiness of composite materials and structures for vehicle applications*. 2000. SAE Paper# 2000-01-3536.
31. Fueller K-H. *Multimaterial lightweighting design—a challenge for development and production*. Internal Publication at Daimler AG; 2013.
32. www.emergingmit.com.
33. www.sabic-ip.com (See Case Studies, Smart ForFour).
34. www.celanese.com/engineered-materials/ (See Celanex PBT).
35. www.polyurethanes.basf.de/pu/solutions/ (See Elastolit).
36. www.materialscience.bayer.us/Products-and-Services/.
37. Ashby MF. *Materials selection in mechanical design*. Burlington, Massachusetts, USA: Butterworh-Heinemann; 1999.
38. McQuaid P. *Statement to the press by UCI president*. July 2011.
39. Francis N, et al. *Michigan automotive industry strategic plan*. Michigan Economic Development Corporation; 2014.
40. Mitchell WJ, Borroni-Bird CE, Burns LD. *Reinventing the automobile: personal urban mobility for the 21st century*. Cambridge, Massachusetts: The MIT Press; 2010.

Part Two

Current developments in manufacturing techniques for lightweight composite structures in the transport industry

This page intentionally left blank

Cost-effective composites manufacturing processes for automotive applications

5

L.A. Khan
CESAT, Islamabad, Pakistan

A.H. Mehmood
NED University of Engineering & Technology, Karachi, Pakistan

5.1 Introduction

> *Currently the whole of the motor industry has a major focus on weight and weight reduction. The main reasons for this are first, as car manufacturers, we have a concern for… the effect the motor vehicle has on the environment and second, there is legislation to 'encourage' us in this direction… To make a body shell as light as possible, low density, high specific property materials should be used, which could lead to the use of polymer matrix composites for the entire body structure.*
>
> *D.A. Jeanes (Senior Manager, Rover-BMW Group), in a paper "The Virtuous Weight Spiral" presented in IBCAM Vehicle Technology—1997; Tucker and Lindsey (2002).*

The desire in the above quote was not new, even in 1997. In the late 1930s, Henry Ford tried to develop wood-filled composite car bodies with phenolic resins, which he attempted to extract from soya oil (Tucker and Lindsey, 2002). So, what are "composites" and why are "polymer composites" important?

The word "composite" in composite materials signifies that two or more components with different properties are combined on a macroscopic scale to form a useful material. Modern structural composites are a blend of two major components: one has strong, stiff, and thin fibers (long, short, or woven) and the other is a matrix which holds the fiber in place. The fiber's strength and stiffness are usually several times greater than that of the matrix material (Jones, 1999). When the fibers and matrices are joined together, they retain their individual identities and directly affect the composites final characteristics (Jones, 1999).

The matrix material binds the reinforcing component together in the desired orientation, provides rigidity and shape to the structure, acts as a load transfer medium, helps to determine the physical properties of the end product, and protects it from hostile environmental conditions. As a continuous phase, the matrix also controls the transverse properties, interlaminar strength, and elevated temperature strength of composites (Miracle et al., 2001). The matrix material may be a polymer, a metal, or a ceramic. Several chemical compositions and microstructural arrangements are possible

Lightweight Composite Structures in Transport. http://dx.doi.org/10.1016/B978-1-78242-325-6.00005-0

in each category. Polymer matrix composites (PMCs) are comparatively mature in terms of raw materials and manufacturing technology and it is reported that the PMC market share is 75% of all composites (Tucker and Lindsey, 2002).

Fiber or reinforcement is the major component of composite materials providing strength and integrity to the structure by carrying the majority of any imposed structural loads. Reinforcements can be broadly categorized into four groups, namely particulates (rough spherical particles with diameters typically 1−100 μm), whiskers (length of fiber <10 mm), short or chopped fibers (length 10−200 mm), and continuous fibers. The principal fibers in commercial use are several types of glass, carbon, and Kevlar. Other fibers are also available such as boron, silicon carbide, and aluminum oxide, but their applications and usage quantities are limited (Mallick, 2008).

Glass fibers are the most widely used reinforcement (Dwight, 2000) due to a number of reasons. The principal advantages of glass fibers, however, are low cost, high tensile strength, high chemical resistance, and excellent insulating properties, although there are some disadvantages including low tensile modulus, high density (among the commercial fibers), relatively low fatigue resistance, and high hardness, which cause excessive wear on molding dies and cutting tools (Mallick, 2008).

Although glass fibers are considered as the most commonly used reinforcement, the higher strength/weight and stiffness/weight ratios and outstanding fatigue characteristics of carbon fibers made them the leading reinforcing material used in polymer matrix composites, where high performance is required (Shindo, 2000). Carbon fibers are available commercially in a variety of tensile moduli which range from high strength, low modulus (190 GPa), to ultrahigh modulus (1050 GPa).

Carbon fibers are manufactured from two types of precursors: (1) textile precursors such as poly acrylonitrile (PAN) and rayon; (2) pitch precursors, such as poly(vinyl chloride) (PVC), petroleum asphalt, and coal tar. It is reported that PAN fibers are used on a large scale and one of the most suitable and widely applied precursors for making high-performance carbon fibers at relatively affordable cost (Scuccimarra, 2012).

According to new US regulations, from 2017, all new cars must consume less than 6.5 L per 100 km. Along with fuel consumption, the automotive sector is also under constant pressure to reduce carbon emissions with enhanced safety requirements. One possible route for accomplishing these goals is through significant weight reduction with the use of "carbon fiber composites," which are usually termed as "lighter than aluminum and stronger than steel."

Carbon fiber is a leading constituent of composite materials, in all high-performance applications. The annual demand of carbon fibers was 43,000 ton/annum in 2011 and is expected to increase to 340,000 ton/annum by 2020 and 1.5M ton/annum by 2023, mainly driven by the aerospace, automotive, and wind energy sectors (Quickstep, 2011).

However, there are challenges which need to be addressed for effective utilization of carbon fiber reinforced composite materials in automotive applications, ie, high material cost, high-speed, and low-cost parts manufacturing with improved exterior finish, repairability, and recyclability.

Thermoset composites have been widely used in the fabrication of racing and luxury cars for many years; however, low volume and labor-intensive processing of thermoset composites result in high cost, which is affordable by these industries. The time

required to fabricate a component, in larger volume production (in most cases), however, may not be more than 1 min, so other avenues of materials or processing routes or approaches have been investigated (Tencate, 2014). One approach is that the metallic structure has hundreds of parts and thousands of fasteners for the assembling of components. Drilling holes and installing fasteners are labor- and time-intensive tasks. Routes for developing integrated composite automotive structures may be sought to accommodate the rapid production requirements (Khan et al., 2014a).

This chapter discusses the recent developments in manufacturing techniques of carbon fiber reinforced composites for high-volume production in the automotive sector, and comprises five sections. Section "Resin transfer molding" gives an overview of resin transfer molding (RTM) with emphasis on recent success stories in automotives. Section "Vacuum-assisted resin infusion process" describes another vacuum-based technique, VARI (vacuum-assisted resin infusion), capable of producing integrated structures. Two success stories related to VARI of monolithic and sandwich structures for automotive applications are explained in detail. Section "Quickstep processing" explains Quickstep processing, an emerging approach for leading applications ranging from aerospace, automotive, to sports goods. A few academic studies are provided, depicting the suitability of the approach for automotive applications. Resin spray transfer (RST) technology, developed in conjunction with Quickstep processing for high-volume production of automobile parts, is explained in detail.

Section "Review of other processes" gives an overview of different processes such as pultrusion, filament winding, compression molding, and programmable powdered preforming process (P4) for automotive applications and lastly, references along with an additional reading section are provided for interested readers.

5.2 Resin transfer molding

5.2.1 Process brief

Resin transfer molding has emerged as the most appropriate route to mass production for small- to medium-sized composite components of complex shapes. A schematic diagram of the RTM process is shown in Fig. 5.1. In this process, a release agent is applied to the mold for easy removal of the part, sometimes a gel coat is also applied to the mold for better surface finish. Preforms are then placed inside the mold which is then clamped and heated to a specified temperature. Thermoset resin and a catalyst which were placed in two tanks of the dispensing equipment are then injected through inlet ports, until the mold is completely filled. Sometimes a vacuum is created inside the mold to assist the resin flow and reduce the porosity. The pressure inside the mold is then increased to ensure that the remaining porosity is collapsed. After curing the part is removed from the mold (Mazumdar, 2001).

Some of the major advantages of RTM are low capital and operating costs, better dimensional accuracy, ease in manufacturing complex parts, good surface finish on both sides, relatively high-fiber volume fraction, and "low volatile emissions" due to closed mold technology. Though, some major limitations are that the tooling design

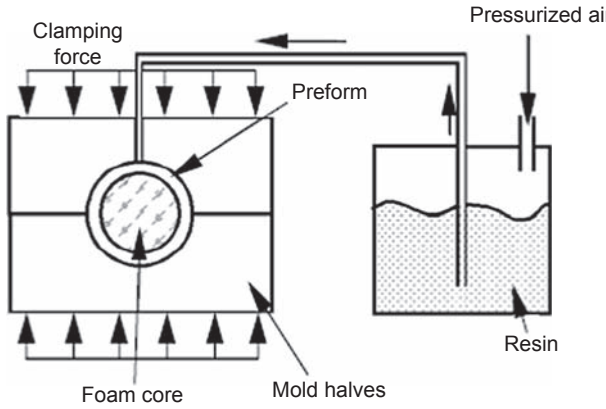

Figure 5.1 Schematic diagram of a typical RTM process.
Adapted from: Mazumdar, S., 2001. Composites Manufacturing: Materials, Product, and Process Engineering. Taylor & Francis, Florida, USA.

is complex and the manufacture of complex parts requires substantial hit and miss experiments or flow modeling (Mazumdar, 2001).

5.2.2 Recent developments and success stories

McLaren used RTM for the production of carbon fiber components for the Mercedes SLR and observed high production rates using this technology. Similarly, the nonwoven fabric preforms and the RTM technique were utilized by BMW to manufacture carbon fiber reinforced plastic (CFRP) roofs for their M3 and M6 models and bumper backing for the M6 (Jacob, 2010). RTM-based solutions for CFRP components, developed by Toray Industries (a leading supplier of advanced composites), have reduced molding cycle times from 80 to 10 min (Stewart, 2009). Toray Industries along with Mercedes-Benz also targeted production series figures of between 20,000 and 40,000 parts per annum (Europe, 2011).

Han et al. proposed a new high-speed RTM process, with multiple vacuum gates. The objective was to reduce the impregnation time, because the conventional RTM processes have limitations in producing larger structures due to significantly increasing impregnation times in proportion to the surface area of the products (Han et al., 2015). The important aspect of that study was to change the resin flow direction from in plane to through the thickness, for the preform. It was observed that the trends from the experimental results matched well with the CFD simulation results in terms of degassing time and the time taken to complete impregnation of the preform. It was also found that the impregnation velocity of through-thickness RTM increased by over 10 times that of the velocity of in-plane RTM (Han et al., 2015).

A convertible roof module was developed by Edag and BASF jointly, with a fiber-reinforced composite sandwich design that represents high potential for weight savings, compared to metallic assembly. They used continuous fiber reinforcement in the sandwich roof module and utilized RTM for high-volume production (Claus

et al., 2012). It was reported that this process is beneficial in producing large and complex composite components by using very-low-viscosity and fast-curing resins in a multilayer fiber, or fabric-reinforced structure. A one-shot method was selected to impregnate sandwich preforms containing carbon fiber face sheets, and PU foam as core material. High compressive strength and heat resistance at a low density were observed for the sandwich structure fabricated by the RTM process (Claus et al., 2012).

Zoltek together with partners (KraussMaffei, Henkel, Chomarat, and Ruhl) introduced a surface RTM process for producing fiber/polyurethane (PU) autobody panels with Class A surfaces. The Zoltek's Panex 35 carbon fiber and a PU resin system were utilized by a surface RTM process followed by overmolding with a PU paint coating, which resulted in a premium and paintable surface quality composite part, directly out of the mold (Compositesworld, 2013). The studies revealed that the process starts with a fabric of carbon fiber developed by Chomarat and injection of a PU resin in it. After curing the mold is opened slightly to inject PU overmolding material provided by Ruhl and the part is again allowed to cure. It was reported that a time of less than 6 min was spent from tool closure to tool open. Finally the part was removed from the tool, washed, and supplied to the painter for application of a top and clear coat. It was claimed that Chomarat's C-Ply fabrics developed by Zoltek's low-cost, large-tow carbon fiber is a step ahead in reducing cost and will set a new standard for price and quality of carbon fiber panels. Moreover, the use of primer and sand processes to hide print-through will also eliminate using surface RTM, which also contribute toward reducing the cost of finished parts (Compositesworld, 2013).

Mubea Carbo Tech developed carbon fiber-based monocoque structures for McLaren by using a patented system to produce hollow structures through an RTM process with a molding cycle time of about 4 h (Gardiner, 2014). The system utilizes two sets of tools, which can produce 10 tubs per day. They compared this fast production rate to a standard autoclaved prepreg process, where one monocoque is produced every week. Hence, though the design is delivered by McLaren, the effort is made by Carbo Tech to achieve a structure with very high quality, while reducing the production times. The tubs they developed use epoxy resin and a 12K carbon fiber noncrimp fabric with a very high fiber volume content, which, according to them, cannot be achieved with any other RTM process. Moreover, Mubea Carbo Tech not only developed monocoque structures for McLaren they also produce carbon fiber tubs for the Porsche 918 Spyder (as shown in Fig. 5.2), which includes an integrated windshield frame (windscreen) and twin rollover hoops (Gardiner, 2014).

Carbo Tech also worked as a partner of Volkswagen in developing the one-piece CF center monocoque/safety cell for the XL1 diesel hybrid vehicle using "advanced RTM," which is shown in Fig. 5.3.

5.3 Vacuum-assisted resin infusion process

Although the RTM technique is appropriate for relatively small components, the mold closure forces sometimes become excessive as component size increases

Figure 5.2 Mubea Carbo Tech developed carbon fiber monocoque for the Porsche 918 Spyder.
Gardiner, G., 2014. More from JEC: High-Quality Carbon Fiber Monocoques in Two Hours. (Online) Available: http://www.compositesworld.com/blog/post/more-from-jec-high-quality-carbon-fiber-monocoques-in-two-hours.

Figure 5.3 Mubea Carbo Tech developed Volkswagen's new XL1 hybrid diesel featuring a carbon fiber monocoque.
Gardiner, G., 2014. More from JEC: High-Quality Carbon Fiber Monocoques in Two Hours. (Online) Available: http://www.compositesworld.com/blog/post/more-from-jec-high-quality-carbon-fiber-monocoques-in-two-hours.

(Summerscales, 2009). One solution to this problem is to use only vacuum to drive resin flow and to enclose the laminate in a bag rather than in a matched pair of molds. This technique is commonly known as "resin infusion." It is believed that the fiber volume fraction achieved using a vacuum infusion process is almost equal to that obtained from autoclave-cured prepregs.

5.3.1 Process brief

In the most basic form, resin infusion is similar to RTM except that the second mold face is replaced by a flexible skin (bagging film) (Summerscales, 2009). The dry fabric

is placed in the mold tool and enclosed in a vacuum bag. One set of pipework delivers the resin while a second set of pipework allows the vacuum to be drawn in the cavity. The resin then flows through the mold and impregnates the reinforcement. The flow front in the reinforcement also pushes any residual air toward the vacuum port. As the resin infusion process sucks the resin to soak the reinforcement only, only the required quantity of resin is introduced, which results in a higher fiber to resin ratio and specific strength. The resin is then allowed to be cured. The mold is then opened and the product is demolded (Khan et al., 2014a). The major disadvantage of resin infusion techniques, however, is the sensitivity to leakage, which can result in void-rich areas in the component.

5.3.2 Recent developments and success stories

Recently, a few reports have been published indicating that the resin infusion process is a cost-effective technique for developing automotive structural bodies and their components from carbon fiber reinforced composites. It is shown that the resin-infused structures are promising due to their overall weight saving, uniform consolidation, functional integration, and significantly lower tooling cost.

Zhang et al. fabricated unidirectional carbon fiber reinforced composite laminates through VARI. The intention was to reduce curing time as it is critical for improving the processing efficiency of automotive composite parts (Zhang et al., 2014). Three different processes were employed, namely quick, quick-post, and preheating, and a rapid curing epoxy resin was used. The filling time was reduced by preheating of mold and fiber as compared with the filling time of the quick process. A postcure stage was investigated for the quick-post process to verify the composite properties fabricated by the quick process. It was observed that the preheating process is a suitable method for improving the processing efficiency of VARI when the rapid curing epoxy resin system was utilized. The processing quality and mechanical properties of composite fabricated by the preheating process were also not affected. Moreover, the preheating temperature decreases the viscosity of resin which eventually improves the infiltration of resin and results in lower void content, shorter filling time, and good interfacial bonding (Zhang et al., 2014).

Khan et al. (2014a) demonstrated the cost-effective development and manufacturing of an automotive (car) body of dimensions $2.6 \times 0.8 \times 0.8$ m from carbon fiber reinforced epoxy composite materials, using a one-shot vacuum infusion process. The automotive was to take part in the Shell Eco-Marathon race. The design for manufacturing approach was adopted, for which three different designs were nominated. An optimum design based on aerodynamic requirements, structural performance, cost-effectiveness, and crash worthiness was then selected (Fig. 5.4).

The car body could be manufactured using VARTM and vacuum infusion processes, so a judicious selection of the appropriate manufacturing process was required. For this purpose, samples were manufactured using ASTM standards from both techniques and their physical and mechanical properties were evaluated. It was observed that specimens manufactured from the vacuum infusion process showed a better structural response due to the high-fiber volume fraction than their counterpart.

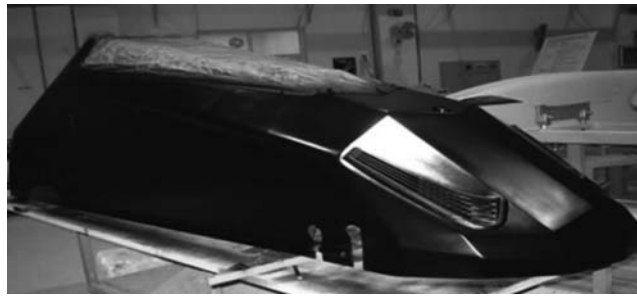

Figure 5.4 The all-composite car body manufactured from the resin infusion process.

Since most of the current composite designs in racing car industries are based on the monocoque stretched skin approach, a new design is proposed based on shell structure to accommodate different cutout regions for easy accessibility, potential to sustain local loads, and ease of manufacturing. The commercial CAD and analysis packages were used for drafting and finite element analysis, respectively, and three assumptions were taken into account as per directions given by the Shell Eco Marathon organizers; ie, the maximum speed will be 50 km/h, the impact crumbled zone will be the front of car, and the car body will be constrained by the front axle and top of the roll bar. Design and analysis were carried out using different combinations of fiber materials and orientations and an optimal solution was provided, fulfilling the above-noted requirements. A factor of safety of 3.5 was chosen and a design for manufacturing aspects was taken into consideration in these activities.

The first step in the manufacturing of structural components is the development of pattern and molds. There are different approaches used for tooling development, which includes rapid prototyping, CNC, and conventional machining. However, these approaches are not cost-effective. In this study, a cost-effective method was used, in which the slices of different sections of the actual product are marked, drawn, cut, and pasted into suitable pattern material. These slices are then joined to develop the pattern and subsequently the mold.

Although different software packages are available for predicting the anomalies raised during the vacuum infusion process, in this study, the infusion activity solely relied on the operator's skills and experiences. Judicious selections of resin inlet and exit locations and placement of flow media, omega flow line, and other accessories on this complex geometry were very challenging tasks, because once infusion starts, corrective actions may not be undertaken. A detailed description of this issue has been provided by the corresponding authors (Khan et al., 2014a).

The windscreen on the automotive was developed in house by a plug-assisted thermoforming process (a technique which ensures uniform wall thickness). To accommodate different coefficients of thermal expansion of mold and product materials, the plug mold was calibrated against the cavity mold. The thermoforming process was carried out under vacuum at 168°C. The crashworthy crumble zone was developed using a sandwich scheme, in which a 12-mm-thick phenolic-coated honeycomb was bonded with PVC foam. To enhance the bond surface area, a

nonstructural glass fabric was sandwiched between honeycomb and PVC foam. The panel was then machined to fit under the hood. All these components along with canopy, access doors, engines, and other accessories were then assembled and took part in the Shell Eco Marathon race.

To reduce the mass of the commercial vehicle (urban buses and delivery trucks), the rear of a hybrid bus is redesigned and manufactured using a composite sandwich structure, as a part of a European collaborative project, HCV (Hybrid Commercial Vehicle) (Neves et al., 2014). This part of the project was a joint venture of Volvo Bus Co. (Sweden) and IDMEC, Portugal. The overall objective of this project was to develop lightweight structures, which will operate using second generation hybrid electric technology. For this purpose, an 18 ton passenger bus and a 6 ton distribution vehicle will be developed, with a lightweight body and advanced hybrid technology. It is reported that the "benefit" of weight reduction in terms of fuel consumption is higher for buses than any other medium of transportation (Neves et al., 2014).

First, numerical and modal analyses of a benchmark model, with proprietary load cases (both provided by Volvo), were carried out for subsequent comparative study of replacing aluminum alloy superstructures with composites sandwich structures, which were to be produced by the vacuum infusion process. While designing the largest sandwich panel, several challenges were faced: (1) vibration of plates may come out in the resonance frequency range, due to excitation imposed by engine, exhaust, and rear axle; (2) to obtain access to the engine from the interior for maintenance, a cutout patch had to be provided at critical locations of the panel, resulting in a significant reduction of mechanical properties; (3) the placement of the rear door imposed serious difficulties. An optimum design consisting of four independent sandwich panels is provided to accommodate all these challenges.

Composite material properties required in the design phase were evaluated by coupon testing. For this purpose, a plate of dimension 522×142 mm was produced, the lay-up was validated by microscopy, and average cured ply thickness was determined. The lay-up sequence of the sandwich panel is provided in the paper.

Instead of using barrier film and infusing the upper and lower skins separately, another method was used. The holes were drilled in a regular pattern in the perforated foam to provide a vertical channel for the resin, to flow from upper skin to lower skin during infusion. Although the drilled holes account for only 0.8% of the total core volume, this resulted in enhanced core stiffness in the transverse direction. Since the resin flowed from upper skin to lower skin, this accounted for variable ply thicknesses due to varying fiber volume fractions.

The composites sandwich panels as an alternative of metallic frames for the rear side of the bus were successfully modeled, fabricated, and validated. Although the weights of fabricated panels were not provided, the modeled data suggested that the weight of the main rear panel is 62.3 kg and the floor panel together with two seat bases is 25.8 kg (Neves et al., 2014). This resulted in an effective weight reduction of 308 kg in the rear part of the bus structure. It is also reported that the development of the prototype bus has been completed and ready for the production phase. With a

completely finished structure, a trial run of 10 km has already been made. Although this trial run was not intended for structural testing or other necessary assessments, nothing was detected, validating the success of the project. The overall reduction of weight was observed to be 900 kg, 80% higher than the initial assessment made for this project, again indicating a successful incorporation of an advanced thermoset carbon fiber-based foam-cored sandwich structure, using the vacuum infusion process in automotive industries.

5.3.3 Variations of the resin infusion process

The resin infusion technique has several names; some of them are listed in Table 5.1. Summerscales has categorized them into four types based on flow ability and direction of flow of resin. A pictorial representation and name of each type are provided in Fig. 5.5.

Table 5.1 Abbreviation and acronym of resin infusion

Abbreviation	Full name/description	Originator
CIRTM	Coinjection RTM	
VI	Vacuum infusion	Scott bader
DRDF	Double RIFT diaphragm forming	Warwick Uni
LRI	Liquid resin infusion	
MVI	Modified vacuum infusion	Airbus
RFI	Resin film infusion	
RIFT	Resin infusion under flexible tooling	ACMC, Plymouth
RIRM	Resin injection recirculation molding	
SCRIMP	Seemann composites resin infusion molding	TPI
VAIM	Vacuum-assisted injection molding	
VAP	Vacuum-assisted processing	EADS patent
VARI	Vacuum-assisted resin injection system	Lotus cars
VARIM	Vacuum-assisted resin injection molding	
V(A)RTM	Vacuum-assisted resin transfer molding	
VIM	Vacuum infusion molding	
VIMP	Vacuum infusion molding process	
VM/RTM	A Hybrid RIFT/RTM	Magnum venus
VIP	Vacuum infusion process	

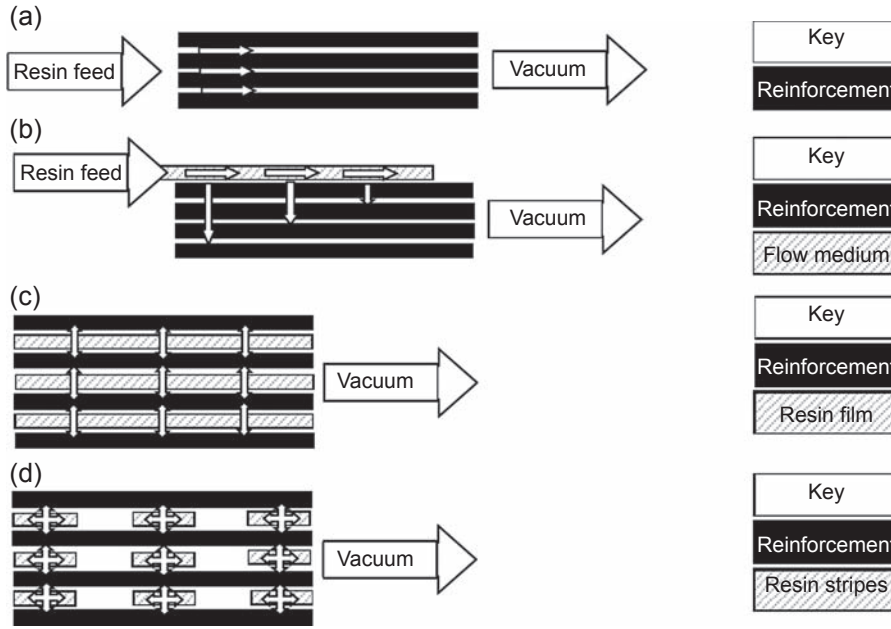

Figure 5.5 Schematic representations of categories of the resin infusion process. (a) Resin infusion in-plane flow process. (b) Through-plane flow from a flow medium. (c) Resin film infusion. (d) Semipreg infusion process.
Summerscales, J., 2009. A Taxonomy for Resin Infusion Processes. ICMAC, Belfast, Ireland.

5.4 Quickstep processing

Autoclave cure of thermoset/thermoplastic prepregs and sandwich schemes are still considered as a reliable technique for manufacturing critical aerostructures. This technique requires high processing temperature, pressure, heavy tooling, and a cure cycle time of several hours. These attributes along with high capital expenditure, infrastructure requirements, and time to commission have made autoclave processing increasingly undesirable. As the aerospace timescale requirements are shortening, an increase in production rates is required and this is difficult to achieve with traditional autoclave manufacturing. Thus, the development of cost-effective processing techniques that can produce autoclave-cured quality parts at significantly lower cost and time is needed (Ryder, 2009).

Quickstep is a relatively new technique for manufacturing composites. The technique is developed by Quickstep Technologies Pty Ltd in Perth, Western Australia, and was patented in 1996 (Graham, 1997). Fig. 5.6 highlights the principles involved in the Quickstep process.

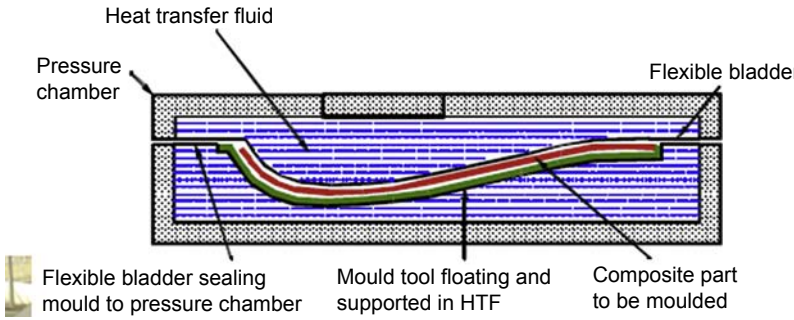

Figure 5.6 Schematic of the Quickstep process.
Quickstep, 2013. Quickstep RST process targets auto industry. Reinforced Plastics.

5.4.1 Process brief

The Quickstep functions by quickly applying heat to the composite laminate, placed between two balanced and floating rigid or semirigid molds, by passing a heat transfer fluid (HTF) at high velocity over the part. The curing part and the mold are separated from HTF by flexible special membranes. Quickstep provides a much faster cure cycle than the autoclave process due to the fact that increased heat capacity and thermal conductivity of the heat transfer fluid allow faster and more efficient cure than nitrogen or air-filled autoclaves.

Typical heating and cooling rates of 10−12 K/min have been made possible with the Quickstep setup. Due to high heating and cooling rates during the processing of composites, the reaction exotherms are not manifested as a significant temperature rise within the lay-up, because the circulating fluid removed any excess heat generated during the process.

In contrast to the autoclave processing, the Quickstep process is a low-pressure process, where approximately 10 kPa pressure is applied during processing as compared to 700 kPa external pressure typically applied during autoclave processing. As the external pressure of the autoclave is used to collapse high pressure voids that may arise from volatile solvents, other avenues of void removal are utilized in Quickstep processing (Khan, 2010; Khan et al., 2010, 2013a,b,c,d).

Several advantages of Quickstep over autoclave processing have been reported since the invention of Quickstep technology. The parts manufactured from Quickstep have been found to be comparable or sometimes superior to autoclave-cured parts in terms of strength, stiffness, surface finish, and appearance while achieving an aerospace grade void content of less than 2%. The other important parameter is low pressure employed for Quickstep processing, which results in better safety, light molds, and hence in cost savings. The rapid processing reduces the production cost and hence these features enable Quickstep technology for mass production.

5.4.2 Quickstep for the automotive industry

Initially, the technique was intended for aerospace applications and considered as an "out of autoclave" approach. However, with successful entry into the aerospace

industry, the automotive industry is the next important target of Quickstep. In the year 2007, Quickstep teamed up with Victorian center for advanced materials manufacturing for an R&D program which focused on two emerging industries of composites, ie, aerospace and automotive. This resulted in an important outcome of the capability of Quickstep technology for automotive applications.

Silcock et al. used Quickstep for the manufacturing of tubes which could potentially be used in the automotive industry for crash structures. The tubes were tested by DMA and crush testing. The Quickstep curing time was 7 min, which was 95% less than the time required for the autoclaved with little preparation time as well (Silcock et al., 2007). The degree of cure for the Quickstep manufactured tubes was found to be higher than the autoclaved and also produced highly repeatable energy-absorption characteristics under crush conditions. However, the Quickstep part exhibited a higher void content (Silcock et al., 2007).

Herring and Fox (2011) and Herring et al. (2010) analyzed the environmentally exposed painted surfaces of composites manufactured from Quickstep and autoclave processes. These automotive quality, painted carbon fiber samples manufactured from both processes were exposed to different environments including combinations of temperatures (70, 120, and 170°C), UV-B, humidity (95% RH), and immersion in water. It was found that Quickstep-manufactured surfaces were less susceptible to damage in the aging environment than the surface of the autoclaved samples. Also, the surface roughnesses of the autoclaved samples were up to three times ($R_a = 0.72$ μm) the roughness of the Quickstep samples ($R_a = 0.23$ μm) (Herring and Fox, 2011; Herring et al., 2010).

In 2012; Quickstep participated in a joint development project by the German Government and car manufacturer Audi to develop new processing techniques for mass production of automotive parts and in the subsequent year, Quickstep announced that its RST along with Quickstep processing is targeting automotive industries around the globe (Quickstep, 2013).

5.4.3 Resin spray transfer technology

RST technology is being considered now as a paradigm shift in cost- and time-effective composite manufacturing, especially for automotive applications. It provides a complete manufacturing solution, through an automated system. A complete manufacturing solution means that it covers the whole cycle of manufacturing, which includes lay-up, impregnation, consolidation, and cure.

5.4.3.1 Resin spray transfer technology—step by step

The RST process is slightly similar to that of resin film infusion (RFI). The film of resin is created by spraying molten resin into mold directly, with a robotic arm. Due to the novel chemical composition of the resin system, the rheology of resin is controlled in a way that the resin freezes, when coming into contact with the mold surface. The dry fibers are preformed in a separate production process and placed again by robot over the cooled and solid resin film. The resin film made intimate contact with the

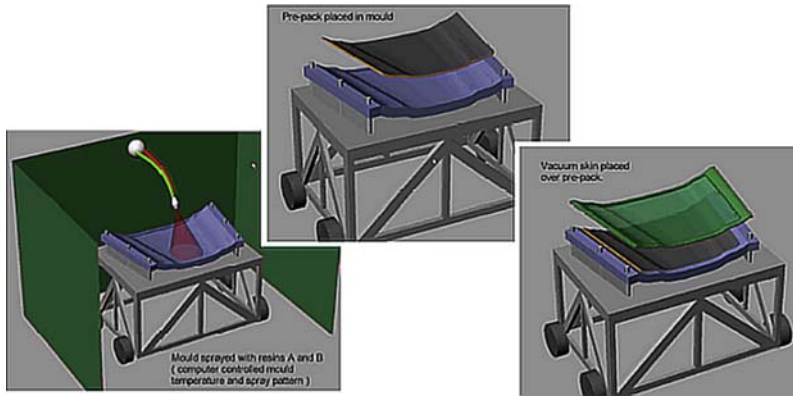

Figure 5.7 Schematic of the RST process.
Quickstep, 2013. Quickstep RST process targets auto industry. Reinforced Plastics.

mold surface and preform, but since it is in the solid state, it provides adequate space for degassing before the part is heated and cured. The subassembly consisting of mold, resin film, and preform is placed under vacuum and the whole assembly is then moved to the Quickstep curing chamber for subsequent heating and curing (Fig. 5.7). The principle of Quickstep has already been explained above.

5.4.3.2 Resin spray transfer attributes

The RST works on the novel composition of the resin system. It is reported that several companies involved in the development, manufacture, and production of commercial resin systems have shown interest and are formulating the appropriate system(s) for RST. The two most important attributes for the RST matrix system are "very fast-curing time" and "low cost." Exotherms evolved during polymerization may have localized thermal effects and even burn the part. The commercial resin manufacturers are using different retardants to control the exotherms, which subsequently increases the cost. As the Quickstep inherently controls the exotherms evolved during the process, the cost of the matrix system may be reduced as the exotherm retardants may not be required in the composition used for RST/Quickstep process.

RST technology is highly automated, which reduces significantly the labor cost. Since prepregs are not used in this process, the requirements of costly freezers and clean rooms are eliminated. Usage of automotive grade carbon fibers and the resin system (noted above) also significantly reduces the cost. Since a high-quality surface finish is achievable from the mold, the requirement of postprocessing such as bogging and sanding is eliminated, thus reducing the cost. Finally, inexpensive molds, reusable vacuum bags, and potential to spray the primer directly to the mold also played a vital role in cost reduction.

5.4.3.3 Recent developments and success stories

In September 2013, Quickstep announced that RST has passed one of the toughest environmental conditioning tests for carbon fiber body panels, developed for a

prestigious European luxury car maker. It is reported that attaining a top-quality paint finish and maintaining that for a long period of time are much harder with carbon fiber composites than with metals. It is also reported that only few composite technologies have achieved this benchmark and RST technology may deliver this quality at a much lower expense.

As noted above, in 2012, Quickstep participated in a joint development project by the German Government and car manufacturer Audi to develop new processing techniques for mass production of automotive parts and in the subsequent year, Quickstep announced that its RST along with Quickstep processing is targeting automotive industries around the globe (Quickstep, 2013). The targets set by OEM (Audi) was to develop a QS/RST demonstrator having highly complex geometry, Class A exterior surface finish, and production capability of 2000 shipsets/year.

Although it is noted that QS/RST may develop highly complex geometry parts with Class A exterior finishes, further details related to production requirement are not available to date.

5.5 Review of other processes

5.5.1 Pultrusion

Pultrusion is a low-cost and a high-volume manufacturing process and therefore the major reasons for the growth of the pultrusion market. A typical pultrusion process is illustrated in Fig. 5.8. In this process, several fiber yarns are taken from creels, which first pass through a "guide" and then pass through the resin bath containing mixed resin

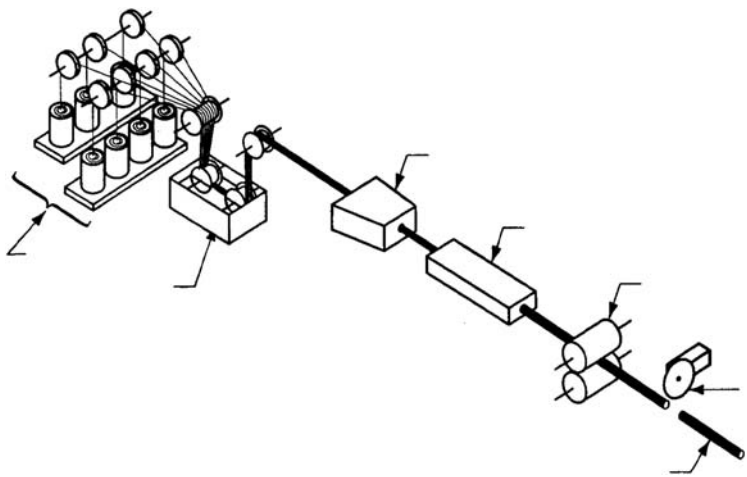

Figure 5.8 Schematic of a typical pultrusion process.
Mazumdar, S., 2001. Composites Manufacturing: Materials, Product, and Process Engineering. Taylor & Francis, Florida, USA.

and hardener. The impregnated fibers then pass through a heated die, which is heated to a specified temperature for the cure of resin. The partially or fully cured composites are then pulled at constant speed from the die using a pulling unit. The pultruded part is then cut to the desired length. The surface is then prepared for painting. Surface preparation is an important step for performing the finishing operation as the mold-releasing agent forms a film on the outer surface of the part. This film can be removed by solvent wiping, sanding, or sandblasting, and among them the solvent swiping using acetone or toluene is the most commonly used method for this purpose (Mazumdar, 2001).

One of the major advantages of pultrusion is the possibility of high-volume production of low-cost commercial products (Mazumdar, 2001); however, the major limitations are: (1) the technique is confined to constant or slightly variable cross-sections along the length and complex shapes cannot be produced; (2) difficulties in producing very-high-tolerance parts; (3) properties are limited to the axial direction only.

Since the demand for CFRP is increasing rapidly, the availability of efficient composite fabrication processes will be of increasing importance. Among the techniques including direct conversion routes, pultrusion is quite common along with filament winding, mandrel wrapping, and other techniques for the production of high-strength, lightweight profiles. Improved surface finishes are also developed to increase the fiber/resin translation properties (Friedrich and Almajid, 2013; Roberts, 2007).

Bruckmeier and Wellnitz (2012) investigated an innovative pultrusion process for designing the body of a car with PU composites with superior mechanical properties compared to most traditional lightweight materials. The innovative technique provides up to 72% fiber volume fraction and hence the composite exhibits improved strength, stiffness, and impact resistances. The study explored the novel application of pultruded composites as a structural part in a racing car powered by hydrogen. It was claimed that the new pultruded composite proved to be an attractive automotive design material which eventually reduces weight and cuts emissions and environmental damage. Moreover, it can be a promising step toward increased sustainability (Bruckmeier and Wellnitz, 2012).

Yang et al. (2013) proposed a new design of fiber-reinforced polymers impact beam energy absorption member in vehicles having combinations of conventional thin-wall tubes with square cross-sections and embedded short tubes with circular cross-sections made through pultrusion processes. It was claimed that the new design concept provides not only convenient assembly owing to the square cross-section of the outer tube but also had the high-energy absorption of the inner circular tubes toward the external impact force which results in improved impact energy absorption for automobile safety (Fig. 5.9).

The new design was tested in lateral compression and it was observed that it had much better energy absorption capability and enough strength compared with the conventional design (only square tube without having circular tubes inside). Moreover, a range of composite combinations from glass and carbon fiber reinforcement for the circular and square tube components and with different taper angles was investigated. It was observed experimentally that the glass fiber reinforced plastic (GFRP) square

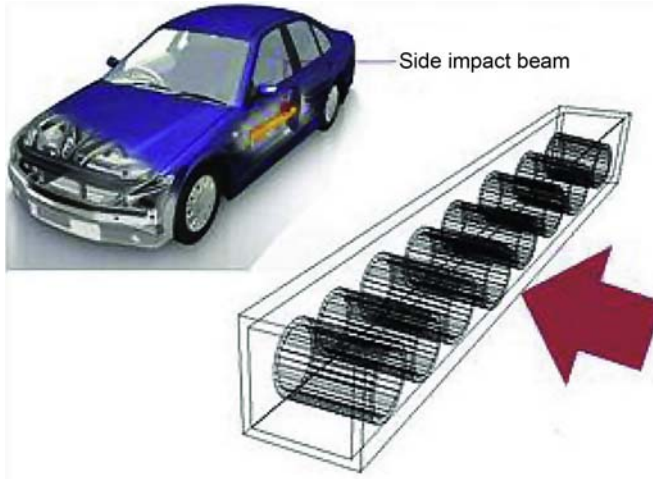

Figure 5.9 Schematic illustration of impact beam within the door of an automobile.
Yang, Y., Wu, X., Hamada, H., 2013. Application of fibre-reinforced composites beam as energy absorption member in vehicle. International Journal of Crashworthiness 18, 103−109.

cross-sectional tube with embedded CFRP circular cross-sectional tubes and the 45 degree taper on the circular tubes had the highest energy absorption capability (Yang et al., 2013).

It is believed that replacement of steel parts with high-performance thermoset composites may result in weight reduction of up to 40%. It is reported that although the transport industries are currently using around 350,000 tons/year of GFRP, their usage in structural parts is still minimal and confined in prototype cars. The extensive utilization of advanced thermoset composites in automotives may ensure lighter and stronger vehicles in the future (Miazza, 2014). The author, however, believes that a major hindrance in widespread application of advanced composites in automotives is the lack of automation in processing composites, which not only increases the cost but also are not suitable for high-volume production, again an essential requirement of automotive manufacturers. Pultrusion is considered as the most automated, efficient, and competitive process, among all composite manufacturing techniques, to fabricate constant cross-sectional composites parts. However, for automotive applications, two major drawbacks of the pultrusion process are: "secondary operation for class A exterior surface finish" and "time required for polymerization, resulting in slow processing speed." A collaborative EU-funded project, named COALINE, was initiated in 2013 to resolve these issues.

The objective of this project is to develop a methodology for in-line coating of pultruded parts, while simultaneously reducing the polymerization time with novel microwave heating and specially formulated thermoset resin systems (Miazza, 2014). The COALINE process in comparison with a traditional pultrusion process is shown in Fig. 5.10 (Miazza, 2014).

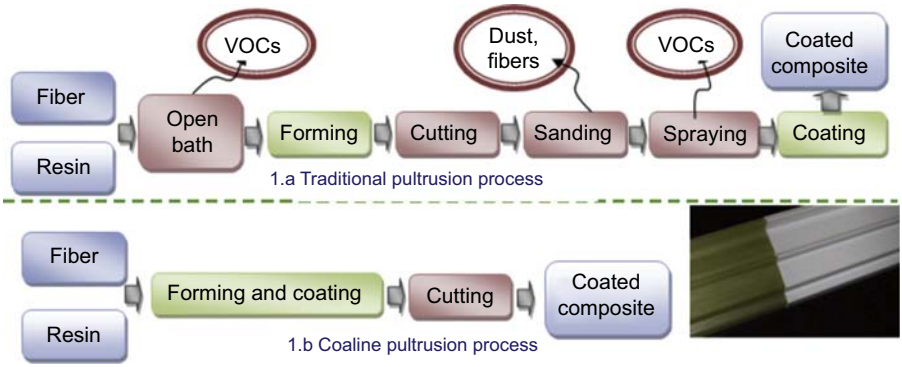

Figure 5.10 Comparison of traditional pultrusion process with the COALINE technique. Miazza, N.L., 2014. Automotive: pultrusion for high volume manufacturing. Reinforced Plastics 58, 40–41.

5.5.2 Filament winding

The filament winding process is used for making tubular parts and specialized structures such as pressure vessels. The process involves winding the resin-impregnated fibers at the desired angle over a rotating mandrel. Fig. 5.11 shows the fibers' passage moving through the resin bath. After impregnation, they move back and forth by means of the guide, while the mandrel rotates at a specified speed. The desired angle is achieved by controlling the motion of the guide and the mandrel. The process can be automated for making high-volume parts in a cost-effective manner.

In all above-noted applications of composites in automotives, the interior and body components of an automobile are considered. However, in the broader sense of

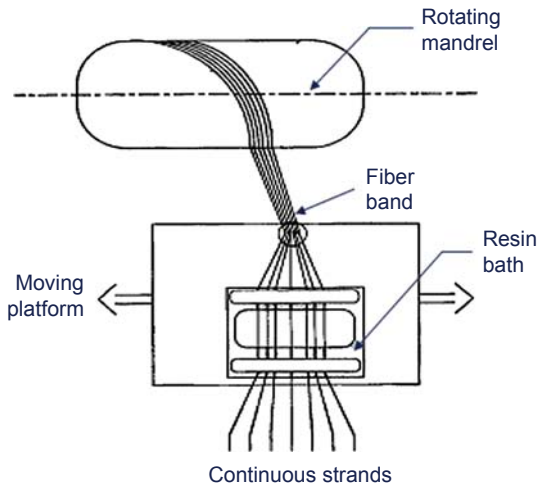

Figure 5.11 Schematic diagram of the filament winding process.

transportation, there is another impressive application in the area of large transporting cylinders for compressed gas. It is reported that the associated advantage of using composite gas cylinders is enhanced safety, due to high-impact strength, anticorrosion, and antiexplosion attributes (Meyer et al., 2014). Composite cylindrical storage tanks are mainly manufactured using carbon fiber reinforced epoxy composites and the filament winding process. These storage cylinders can be typically categorized in five ways, four of which use filament winding as part of the manufacturing process. These categories are schematically shown in Fig. 5.12.

Category I pressure vessel includes all metal body, with no composites reinforcements. Category II depicts the pressure vessel with mostly metallic body and some fiber wrapping in the hoop direction. Category III pressure vessels are manufactured using complete composite wrapping with metallic liners, while category IV depicts a pressure vessel with polymer liner and all composite wrapping. Category V pressure vessel does not include any liner and all composite constructions are carried out using filament winding (Meyer et al., 2014). It is reported that category I pressure vessels account for roughly 90% of the total commercial market, but the major limitation is heavy weight and higher cost of transportation, when compared to their type III and IV filament-wound composite counterparts. The composite pressure vessels also provide the added advantage of high operating pressure for higher energy storage density (Meyer et al., 2014). The authors also discussed the success stories of enhanced toughness (in fact, double) of the VORA-Force system, developed by Dow Chemical, with

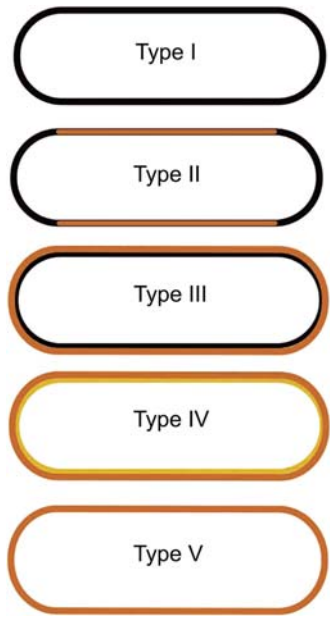

Figure 5.12 Five categories of pressure vessels based on materials configurations.
Meyer, K., Pignagnoli, F., Potts, D., Hunter, G., 2014. Lightweighting matters in energy storage. Reinforced Plastics 58, 20−23.

minimal change of processing and other mechanical properties. The enhanced fracture toughness of thermosets ensures the high-impact resistance of filament-wound pressure vessels. The authors also discussed the need for speeding up the production cycle to meet the larger market demands (Meyer et al., 2014). An optimized design of a type 4 hydrogen tank using carbon fiber composites is also provided in the literature with an operating pressure of 700 kPa. A technical assessment is also provided for the use of filament-wound carbon fiber composite hydrogen storage tanks, for automotive applications (Roh et al., 2013; Hua et al., 2011).

Power transmitted composite drive shafts have also been designed and recommended recently for automotive applications (Montagnier and Hochard, 2013; Badie et al., 2006, 2011; Abu Talib et al., 2010). It is reported that metallic drive shafts account for higher weight, low critical speed, and vibration, while composite counterparts have proven that they can provide a solution for all the problems imposed by metallic shafts.

5.5.3 Compression molding

Compression molding is a closed mold process which is used for the processing of both thermosetting and thermoplastic materials. The molding compound is placed in an open and heated mold and a matched metal mold cavity is used to close the mold. Metallic molds are used in this process and pressure is applied through a variety of methods including the tightening of screws, through pressure and other means to obtain a high-volume fraction of composites. Heat is also applied during the curing stage in some applications. The part size that can be obtained ranges from 1 mm thickness to over 50 mm thickness.

5.5.3.1 Recycled carbon fibers—an evolution

Palmer et al. (2010) reported the first ever attempt at recycled and original carbon fiber-based molding compounds, which is expected to replace traditional glass fiber-based materials. A newly designed processing route allows the incorporation of recycled carbon fibers in existing sheet molding compound (SMC) production lines, providing a viable solution with careful control of original and recycled fiber distribution against the standardized and mature glass fiber-based SMCs (Palmer et al., 2010).

A similar study was conducted by Turner et al. (2010) in which a route for recovery and reuse of carbon fiber is provided and the technical aspects are discussed with regard to future directions. Several material demonstrators have been developed and used to fabricate automotive parts, which showed promising mechanical properties as compared to commercial glass fiber-based molding compounds (Turner et al., 2010).

Pimenta and Pinho (2011) noted "the sustainability and recycling" as major goals of the UK governmental policy for the composites industry. Several facts and figures are provided regarding carbon fiber composite wastes and their resources are identified. It is reported that approximately 8500 commercial aircrafts will be retired by 2025 and on average each aircraft contains more than 20 tons of carbon fiber composites. It also showed that within this time frame, the wind industry would also be the major source

of CFRP wastes (Pimenta and Pinho, 2011). SMC and bulk molding compounds molded using compression molding are the most promising manufacturing techniques for these waste materials. In this article, the major challenges of carbon fiber recycling and potential future applications of these materials are discussed in detail, confirming the widespread application of compression molding processes in the near future specially in automotive industries (Pimenta and Pinho, 2011). Several studies are now focusing on potential applications of recycled carbon fiber-based sheet molding compounds in automotives (for example, Jones, 2011) and a list of some other references is provided in the additional reading section.

5.5.4 The programmable powdered preforming process technique

Owens Corning Composite Solutions LLC along with Aplicator System AB developed the P4, where the automated glass roving chopper gun was developed by Aplicator System. In that process, a robotic arm was used to chop and spray the glass fibers onto a screen, having the shape of the part to be manufactured and a partial vacuum was drawn through the screen. A powdered binder was applied at the same time, usually at 3% to 5% by weight. Later, the heated air passed through the screen, after compaction of the preform to melt the binder (Palmer et al., 2010). The binder was cooled once the preform was fully compacted and solidified with the passage of cold air through the screen. It also helps in removing the preform from the screen tool (Black, 2008; Brandt and Reeve, 2001).

P4 is popular because of following advantages:

- Higher degree of automations;
- Very low requirement for touch labor;
- Wide range of preforms can be developed with complex geometries to near-net shapes;
- The potential for parts integration including typical separately molded and secondarily bonded rib stiffeners and other elements;
- The ability to integrate core materials and openings into the preform.

P4 is an early example of automated directed fiber preforming which uses glass reinforcement; later the process was adapted for use with carbon fibers by the derivatives. A low-cost raw material (glass fiber rovings/tows) is utilized by P4, providing a 40% reduction in raw material costs over preforms developed with continuous strand mat (Chavka and Dahl, 1999).

F3P is a derivative of P4 featured with offline robotic programming and advanced chopper gun technology along with other machines. Improvement in the process was also observed as a robotic track adding a seventh axis. It was also reported that the deposition rates are higher (4 kg/min) with scrap rates of range less than 1% (Dahl et al., 2003; Devries et al., 2001).

Das (2011) investigated the life-cycle assessment of carbon fiber reinforced polymer composites. He worked on two precursor types, conventional textile-type acrylic fibers and renewable-based lignin, and determined their relative life-cycle benefits. According to his studies, the lignin-based part developed by using P4 technology offered

the greatest life-cycle energy and CO_2 emissions benefits. The production of carbon fiber is estimated to be around 14 times more energy intensive than conventional steel production.

5.6 Summary

Cost-effective ways of manufacturing automobile parts using thermoset composites are presented. Resin transfer molding with several proprietary (from a geometry viewpoint) modifications is by far the most commonly used technique for fabricating integrated automotive body structures. The integrated approach thus resulted in reduction of assembly time and cost. However, the limitations of high tooling and accessories costs of RTM led to the development of integrated automobile body structures using the cost-effective VARI process. Two success stories are provided, which portray the efficacy of the process over the traditional RTM process. However, automation of the VARI process is required for mass production of automotive parts. A success story from Volvo (Sweden) has depicted the future of this process in the automobile sector.

Quickstep processing of advanced thermoset composites is an emerging field. Relatively more popular in the aerospace sector, Quickstep Pty Ltd., an Australian-based company, developed a proprietary RST to meet high-volume production requirements of the automotive industries. An automated system with a complete assembly line is suggested and the corresponding author believes that the technology will revolutionize the effective utilization of composite materials in the automobile industry in the near future.

A collaborative EU-funded project, named COALINE, initiated in 2013, is addressing the efficient manufacturing of automotive pultruded parts for high-volume production. The project is underway and is expected to be another revolutionary step of advanced thermoset composites in automotives. Development of large transportation tanks using filament winding is another promising area where utilization of composites is heading in the transportation industries, and the use of recycled carbon fibers in sheet and bulk molding compounds will be an important step in cost reduction of automotive parts, manufactured from polymeric composites.

Additional reading

The author suggests that interested readers review all the references noted above, related to different processing techniques for automotive applications. In addition, the following books and articles are also recommended. (Boland, 2014; Chaudhari et al., 2012; Crowley et al., 2013; Deléglise et al., 2011; Feraboli et al., 2012; Fleischer and Schaedel, 2013; Hillermeier et al., 2013; Khan et al., 2013e, 2014b; Khoun et al., 2012; Macarrão and Kaminski, 2006; Maffezzoli et al., 2012; Mahmood et al., 2014; Maier et al., 2014; Manson, 2012; McConnell, 2011; Mohamed et al., 2014; Morey, 2011; Ornaghi et al., 2010; Patel and Mahajan, 2014, Poorzeinolabedin et al., 2014;

Roh et al., 2013; Sapiai et al., 2014; Song et al., 2009; Sopher and Sasaki, 2012; Stewart, 2011; Sukmaji et al., 2013; Swolfs et al., 2014; Wolf et al., 2011; Wood, 2014; Zhang et al., 2012a,b)

References

Abu Talib, A., Ali, A., Badie, M.A., Azida Che Lah, N., Golestaneh, A., 2010. Developing a hybrid, carbon/glass fiber-reinforced, epoxy composite automotive drive shaft. Materials & Design 31, 514−521.

Badie, M., Mahdi, A., Abutalib, A., Abdullah, E., Yonus, R., 2006. Automotive composite driveshafts: investigation of the design variables effects. International Journal of Engineering and Technology 3, 227−237.

Badie, M.A., Mahdi, E., Hamouda, A.M.S., 2011. An investigation into hybrid carbon/glass fiber reinforced epoxy composite automotive drive shaft. Materials & Design 32, 1485−1500.

Black, S., 2008. High-volume preforming for automotive application. Composites Technology 14 (5), 43 (USA).

Boland, C., 2014. Life Cycle Energy and Greenhouse Gas Emissions of Natural Fiber Composites for Automotive Applications: Impacts of Renewable Material Content and Lightweighting. University of Michigan, Ann Arbor.

Brandt, M., Reeve, S., 2001. Directed fibre preform case studies. Composites 1−10.

Bruckmeier, S.C., Wellnitz, J., 2012. Car body design with polyurethane composites produced by an innovative pultrusion process. In: Subic, A., Wellnitz, J., Leary, M., Koopmans, L. (Eds.), Sustainable Automotive Technologies 2012. Springer, Berlin Heidelberg.

Chaudhari, R., Viehban, F., Karcher, M., Elsner, P., Henning, F., 2012. Characterization of high performance composites manufactured by using high-pressure RTM process variants. In: Internationale AVK-Tagung—ccd Congress Center Düsseldorf. Düsseldorf, Germany.

Chavka, N., Dahl, J., 1999. P4: glass fiber preforming technology for automotive applications. In: Resin Transfer Molding. SAMPE Monograph, pp. 165−174.

Claus, D., Sandler, J., Hillebrecht, M., Reul, W., 2012. Fibre-reinforced composite concept for a convertible roof module. ATZ Online 5 (3), 28−33 (Germany).

Compositesworld, 2013. Zoltek Demonstrates Surface RTM for Automotive Body Panels (Online). Available: http://www.compositesworld.com/news/zoltek-demonstrates-surface-rtm-for-automotive-body-panels (accessed 24.08.14.).

Crowley, D.M., Ward, C., Potter, K., 2013. A Status of Acceptance Criteria and Process Requirements in Advanced Composites Manufacturing, and Whether They Are Fit for Purpose (SAE Technical Paper).

Dahl, J., Debolt, M., Steenkamer, D., 2003. Processing and performance of chopped glass fiber reinforced RTM composites. In: Proceedings of 14th International Conference on Composite Materials (ICCM-14) (San-diego, USA).

Das, S., 2011. Life cycle assessment of carbon fiber-reinforced polymer composites. The International Journal of Life Cycle Assessment 16, 268−282.

Deléglise, M., Le Grognec, P., Binetruy, C., Krawczak, P., Claude, B., 2011. Modeling of high speed RTM injection with highly reactive resin with on-line mixing. Composites Part A: Applied Science and Manufacturing 42, 1390−1397.

Devries, J., Chavka, N., Dahl, J., 2001. Recent advances in glass fiber preforming: implementation of the Ford Programmable Preform Process (F3P). In: International Conference for Manufacturing of Advanced Composites.

Dwight, D.W., 2000. 1.08-Glass fiber reinforcements. In: Kelly, A., Zweben, C. (Eds.), Comprehensive Composite Materials. Oxford, Pergamon.

Europe, C., 2011. Composites Europe highlights solutions for mass production of automotive composites. Reinforced Plastics 55, 45−46.

Feraboli, P., Kawakami, H., Wade, B., Gasco, F., Deoto, L., Masini, A., 2012. Recyclability and reutilization of carbon fiber fabric/epoxy composites. Journal of Composite Materials 46, 1459−1473.

Fleischer, J., Schaedel, J., 2013. Joining automotive space frame structures by filament winding. CIRP Journal of Manufacturing Science and Technology 6, 98−101.

Friedrich, K., Almajid, A.A., 2013. Manufacturing aspects of advanced polymer composites for automotive applications. Applied Composite Materials 20, 107−128.

Gardiner, G., 2014. More from JEC: High-Quality Carbon Fiber Monocoques in Two Hours (Online). Available: http://www.compositesworld.com/blog/post/more-from-jec-high-quality-carbon-fiber-monocoques-in-two-hours.

Graham, N., 1997. Improved Method of Manufacturing Composites. Munich, Germany patent application PCT/AU1995/000593.

Han, S.H., Cho, E.J., Lee, H.C., Jeong, K., Kim, S.S., 2015. Study on high-speed RTM to reduce the impregnation time of carbon/epoxy composites. Composite Structures 119, 50−58.

Herring, M., Fox, B., 2011. The effect of a rapid curing process on the surface finish of a carbon fibre epoxy composite. Composites Part B: Engineering 42, 1035−1043.

Herring, M., Mardel, J., Fox, B., 2010. The effect of material selection and manufacturing process on the surface finish of carbon fibre composites. Journal of Materials Processing Technology 210, 926−940.

Hillermeier, R., Hasson, T., Friedrich, L., Ball, C., 2013. Advanced Thermosetting Resin Matrix Technology for Next Generation High Volume Manufacture of Automotive Composite Structures (SAE Technical Paper).

Hua, T., Ahluwalia, R., Peng, J.-K., Kromer, M., Lasher, S., Mckenney, K., Law, K., Sinha, J., 2011. Technical assessment of compressed hydrogen storage tank systems for automotive applications. International Journal of Hydrogen Energy 36, 3037−3049.

Jacob, A., 2010. BMW counts on carbon fibre for its megacity vehicle. Reinforced Plastics 54, 38−41.

Jones, B.A., 2011. Investigating the Mechanical Properties of Compression Molded Carbon Fiber Reinforced Sheet Molding Compound.

Jones, R.M., 1999. Mechanics of Composite Material. Taylor & Francis, New York.

Khan, L., Mahmood, A.H., Hassan, B., Sharif, T., Khushnod, S., Khan, Z.M., 2014a. Cost-effective manufacturing process for the development of automotive from energy efficient composite materials and sandwich structures. Polymer Composites 35, 97−104.

Khan, L.A., 2010. Cure Optimization of 977-2A Carbon/Epoxy Composites for Quickstep Processing (Ph.D. thesis). The University of Manchester.

Khan, L.A., Iqbal, Z., Hussain, S.T., Kausar, A., Day, R.J., 2013a. Determination of optimum cure parameters of 977-2A carbon/epoxy composites for quickstep processing. Journal of Applied Polymer Science 129, 2638−2652.

Khan, L.A., Kausar, A., Hussain, S.T., Iqbal, Z., Day, R.J., Ahmad, S., Khan, Z., 2013b. Cure characterization of Cycom 977-2A carbon/epoxy composites for quickstep processing. Polymer Engineering & Science 54, 887−898.

Khan, L.A., Mahmood, A.H., Ahmad, S., Khan, Z., Day, R.J., 2013c. Effect of hygrothermal conditioning on the fracture toughness of carbon/epoxy composites cured in autoclave/Quickstep. Journal of Reinforced Plastics and Composites 32, 1165−1176.

Khan, L.A., Mahmood, A.H., Ahmed, S., Day, R.J., 2013d. Effect of double vacuum bagging (DVB) in quickstep processing on the properties of 977-2A carbon/epoxy composites. Polymer Composites 34, 942−952.

Khan, L.A., Mahmood, A.H., Khan, Z., 2013e. Post curing effect of poly epoxy on visco-elastic and mechanical properties of different sandwich structures. Polymer Composites 34, 477−481.

Khan, L.A., Nesbitt, A., Day, R.J., 2010. Hygrothermal degradation of 977-2A carbon/epoxy composite laminates cured in autoclave and Quickstep. Composites Part A: Applied Science and Manufacturing 41, 942−953.

Khan, Z.M., Mahmood, A.H., Mills, B., Khan, L.A., 2014b. The drilling-induced failure mechanisms in T800/924C toughened carbon-epoxy composite materials. Journal of Reinforced Plastics and Composites 33, 202−211.

Khoun, L., Maillard, D., Bureau, M.N., 2012. Effect of process variables on the performance of glass fibre reinforced composites made by high pressure resin transfer moulding. In: Proceedings of the 12th Annual Automotive Composites Conference & Exhibition (ACCE 2012), p. 380.

Macarrão, L., Kaminski, P.C., 2006. Vacuum Bagging: Fiberglass Parts Fabrication With Quality (SAE Technical Paper).

Maffezzoli, A., Gennaro, R., Greco, A., 2012. Thermoplastic Composite Manufacturing Cost Analysis. Wiley Encyclopedia of Composites.

Mahmood, A., Khan, L., Zahid, B., 2014. Mechanical properties of composites made from locally manufactured carbon fabrics and the composites produced from air-textured glass yarns. Fibers and Polymers 15, 1004−1009.

Maier, A., Schmidt, R., Oswald-Tranta, B., Schledjewski, R., 2014. Non-destructive thermography analysis of impact damage on large-scale CFRP automotive parts. Materials 7, 413−429.

Mallick, P.K., 2008. Fiber-Reinforced Composites: Materials, Manufacturing, and Design. CRC Press.

Manson, J.-A., 2012. HIVOCOMP: large-scale use of carbon composites in the automotive industry. Reinforced Plastics 56, 44−46.

Mazumdar, S., 2001. Composites Manufacturing: Materials, Product, and Process Engineering. Taylor & Francis, Florida, USA.

Mcconnell, V.P., 2011. Not just another road trip. Reinforced Plastics 55, 18−23.

Meyer, K., Pignagnoli, F., Potts, D., Hunter, G., 2014. Lightweighting matters in energy storage. Reinforced Plastics 58, 20−23.

Miazza, N.L., 2014. Automotive: pultrusion for high volume manufacturing. Reinforced Plastics 58, 40−41.

Miracle, D.B., Donaldson, S.L., Vander Voort, G.F., 2001. ASM Handbook. ASM International Materials Park, OH, USA.

Mohamed, M., Vuppalapati, R., Bheemreddy, V., Chandrashekhara, K., Schuman, T., 2014. Characterization of polyurethane composites manufactured using vacuum assisted resin transfer molding. Advanced Composite Materials 1−19.

Montagnier, O., Hochard, C., 2013. Optimisation of hybrid high-modulus/high-strength carbon fibre reinforced plastic composite drive shafts. Materials & Design 46, 88−100.

Morey, B., 2011. Carbon fiber on its way? Manufacturing Engineering 147, 81−91.

Neves, P., Fernandes, A., Lantz, D., Carldén, L., Andersson, K., 2014. Bus BiW weight optimization using composite Sandwich panels. In: Transport Research Arena (TRA) 5th Conference: Transport Solutions from Research to Deployment.

Ornaghi, H.L., Bolner, A.S., Fiorio, R., Zattera, A.J., Amico, S.C., 2010. Mechanical and dynamic mechanical analysis of hybrid composites molded by resin transfer molding. Journal of Applied Polymer Science 118, 887–896.

Palmer, J., Savage, L., Ghita, O.R., Evans, K.E., 2010. Sheet moulding compound (SMC) from carbon fibre recyclate. Composites Part A: Applied Science and Manufacturing 41, 1232–1237.

Patel, V., Mahajan, Y., 2014. Polymer nanocomposites: emerging growth driver for the global automotive industry. In: Handbook of Polymernanocomposites. Processing, Performance and Application. Springer.

Pimenta, S., Pinho, S.T., 2011. Recycling carbon fibre reinforced polymers for structural applications: technology review and market outlook. Waste Management 31, 378–392.

Poorzeinolabedin, M., Parnas, L., Dashatan, S.H., 2014. Resin infusion under flexible tooling process and structural design optimization of the complex composite part. Materials & Design 64, 450–455.

Quickstep, 2007. Quickstep and VCAMM develop R&D programme. Reinforced Plastics 51, 9.

Quickstep, 2011. Quickstep. JEC Asia Automotive (Singapore).

Quickstep, 2012. Quickstep and Audi join automotive project. Reinforced Plastics 56, 15.

Quickstep, 2013. Quickstep RST process targets auto industry. Reinforced Plastics 57, 16.

Roberts, T., 2007. Rapid growth forecast for carbon fibre market. Reinforced Plastics 51, 10–13.

Roh, H., Hua, T.Q., Ahluwalia, R.K., 2013. Optimization of carbon fiber usage in Type 4 hydrogen storage tanks for fuel cell automobiles. International Journal of Hydrogen Energy 38, 12795–12802.

Ryder, A., 2009. The design and manufacturing of primary aircraft structures via out-of-autoclave techniques. In: ICMAC Conference. Belfast Waterfront, UK.

Sapiai, N., Jumahat, A., Hakim, R., 2014. Tensile and compressive properties of hybrid carbon fiber/kenaf polymer composite. Advances in Environmental Biology 8, 2655–2661.

Scuccimarra, D., 2012. Vehicle Lightening With Composite Materials: Objective Performance Comparison of Material-systems for Structural Applications.

Shindo, A., 2000. 1.01-Polyacrylonitrile (PAN)-based carbon fibers. In: Kelly, A., Zweben, C. (Eds.), Comprehensive Composite Materials. Oxford, Pergamon.

Silcock, M.D., Garschke, C., Hall, W., Fox, B.L., 2007. Rapid composite tube manufacture utilizing the quickstepTM process. Journal of Composite Materials 41, 965–978.

Song, Y.S., Youn, J.R., Gutowski, T.G., 2009. Life cycle energy analysis of fiber-reinforced composites. Composites Part A: Applied Science and Manufacturing 40, 1257–1265.

Sopher, S.R., Sasaki, H., 2012. Lightweight Door Panel Made With Bio-Based Composite Material (SAE Technical Paper).

Stewart, R., 2009. Carbon fibre composites poised for dramatic growth. Reinforced Plastics 53, 16–21.

Stewart, R., 2011. Rebounding automotive industry welcome news for FRP. Reinforced Plastics 55, 38–44.

Sukmaji, I., Anwar, M., Wijang, W., Danardono, D., 2013. Hybrid carbon-glass fiber composite for the door electric car application. In: 2013 Joint International Conference on Rural Information & Communication Technology and Electric-Vehicle Technology (rICT & ICeV-T). IEEE, pp. 1–3.

Summerscales, J., 2009. A Taxonomy for Resin Infusion Processes. ICMAC, Belfast, Ireland.

Swolfs, Y., Gorbatikh, L., Hine, P., Ward, I., Verpoest, I., 2014. Tough carbon fiber composites by hybridization with self-reinforced composites. In: SEICO 14 SAMPE Europe, 35th International Technical Conference & Forum, pp. 397–404.

Tencate, 2014. DRIVING THE CHANGE − Thermoplastic and Thermoset Composites for Automotive Applications (Online). Available: http://www.tencate.com/emea/industrial-composites/applications/automotive/default.aspx (accessed 21.07.14.).

Tucker, N., Lindsey, K., 2002. An Introduction to Automotive Composites. Rapra Technology, Shawbury, Shrewsbury, Shropshire, SY4 4NR, United Kingdom.

Turner, T., Warrior, N., Pickering, S., 2010. Development of high value moulding compounds from recycled carbon fibres. Plastics, Rubber and Composites 39, 151−156.

Wolf, D., DEIßER, O., Chaudhari, R., Ahlborn, H., 2011. Glass fibre composite system for chassis concepts. ATZ Worldwide eMagazine 113, 16−21.

Wood, K., 2014. Composite leaf springs: saving weight in production suspension systems. Composites Technology 19.

Yang, Y., Wu, X., Hamada, H., 2013. Application of fibre-reinforced composites beam as energy absorption member in vehicle. International Journal of Crashworthiness 18, 103−109.

Zhang, J., Chaisombat, K., He, S., Wang, C.H., 2012a. Hybrid composite laminates reinforced with glass/carbon woven fabrics for lightweight load bearing structures. Materials & Design 36, 75−80.

Zhang, K.-M., Li, M., Gu, Y.-Z., Zhang, Z.-G., 2012b. Advanced composite materials and key technology for automotive. Fiber Reinforced Plastics S1.

Zhang, K., Gu, Y., Li, M., Zhang, Z., 2014. Effect of rapid curing process on the properties of carbon fiber/epoxy composite fabricated using vacuum assisted resin infusion molding. Materials & Design 54, 624−631.

This page intentionally left blank

Hybrid polymer composites for high strain rate applications

6

A. Daliri
RMIT University, Melbourne, VIC, Australia; Defence Materials Technology Centre (DMTC Ltd), Hawthorn, VIC, Australia

J. Zhang
Deakin University, VIC, Australia

C.H. Wang
RMIT University, Melbourne, VIC, Australia

6.1 Introduction

Performance requirements and recent environmental regulations place new demands on the aerospace and automotive industries to develop and utilise advanced lightweight structural technologies. Vehicle weight reduction without excessive cost increase calls for the development of new advanced structural materials (Yang et al., 2013). Such novel materials could be developed in the form of completely new materials or through hybridisation of existent materials with the aid of recent developments in areas such as nanotechnology.

Nonhybrid composite materials (eg, carbon fibre-reinforced polymer matrix (CFRP) composites) exhibit high specific strength and stiffness which makes them suitable for weight reduction in aerospace, maritime and land vehicles. However, there is now a greater demand to lower cost and increase energy absorption under blast and ballistic impact conditions and vibration damping. Hybridisation provides an effective method for meeting these new requirements. Hybrid materials comprise various constituents from a broad range of materials. The focus of this chapter is hybrid fibre-reinforced polymer composites, which are already employed in a wide range of industries to reduce the weight of safety-critical structures.

Hybrid composites, composed of more than one type of reinforcement, can be in the form of continuous fibre-reinforced composites, short fibre-reinforced composites, particulate-reinforced composites, fibre metal laminates (FMLs), or a combination of these materials. In this chapter we present a critical review of recent developments towards the use of hybrid composites for improving impact resistance, energy absorption and vibration damping characteristics. This review focuses on recent advances in fibre-reinforced hybrid composites, nanoparticle-reinforced hybrid composites, and FMLs.

Lightweight Composite Structures in Transport. http://dx.doi.org/10.1016/B978-1-78242-325-6.00006-2

6.2 Continuous fibre reinforcements

Hybrids manufactured from two or more types of fibre reinforcements are the most common type of polymer-based hybrid composites. This type of hybrid composite has been studied extensively at a quasi-static (QS) range of strain rates (ie, $10^{-6}\ s^{-1} <$ strain rate $< 10^{-3}\ s^{-1}$) to obtain the synergistic effect. The term 'synergistic effect' refers to the additional increase in properties exhibited by a hybrid composite above that expected from a linear combination of the property improvement by each individual constituent.

Recent studies demonstrate the existence of a synergistic effect in the woven-carbon/woven-glass/epoxy hybrid composites, where the optimum flexural properties and compressive strength are achieved with equal amounts of carbon and glass fibres (Zhang et al., 2012). The flexural strength of the $[C_2G_2]_s$ stacking sequence is equal to 89% of the flexural strength of the $[C]_8$ carbon fibre composite, showing a synergistic effect. Likewise, the flexural modulus is enhanced significantly by placing two carbon layers at the exterior of the hybrid composite (Zhang et al., 2012).

The tensile and compressive stress–strain curves for five types of hybrid and non-hybrid composite laminates are shown in Fig. 6.1. At the same glass/carbon fibre ratio, the effect of stacking sequence on the tensile strength of the hybrid composite is negligible; however, the compressive strength of the $[CGCG]_s$ stacking sequence is higher compared with the $[C_2G_2]_s$ and other hybrid configurations. This enhancement in the compressive strength has been attributed to the bridging effect of the carbon fibres between the failed glass fibre layers, though not enough to show a synergistic effect (Zhang et al., 2012).

The Young modulus of a hybrid composite consisting of carbon fibre and glass fibre reinforcements can be predicted using the simple rule of mixtures (ROM) as (Zhang et al., 2012):

$$E_H = \alpha E_C + (1 - \alpha) E_G \qquad [6.1]$$

where E_H, E_C and E_G are the moduli of the hybrid composite, carbon fibre composite and glass fibre composite, respectively, and α is the ratio of carbon fibres to the total of carbon and glass fibres. By assuming that α is the percentage of the thickness of carbon layers (t_C) in the whole laminate ($t_C + t_G$) and the composite fails when the strain of laminates reaches the critical failure strain of carbon fibres (ε_C), the strength of the hybrid composite (σ_H) can be expressed as (Zhang et al., 2012):

$$\sigma_H = (E_C t_C + E_G t_G)\varepsilon_C / (t_C + t_G) \qquad [6.2]$$

However, in practice, glass fibres carry the load until the ultimate strain of glass fibre composite is reached; therefore, we have (Zhang et al., 2012):

$$\sigma_{H,max} = \max[(E_C t_C + E_G t_G)\varepsilon_C / (t_C + t_G), E_G t_G \varepsilon_G / (t_C + t_G)] \qquad [6.3]$$

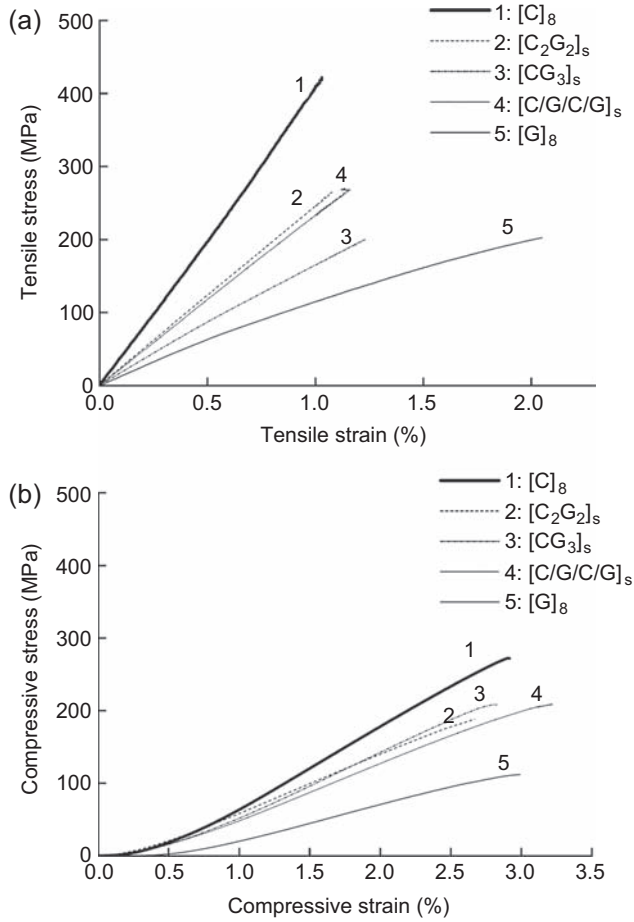

Figure 6.1 (a) Tensile and (b) compressive stress−strain curves for five types of hybrid and nonhybrid carbon/glass epoxy composites.
Reproduced from: Zhang, J., Chaisombat, K., He, S., Wang, C.H., 2012. Hybrid composite laminates reinforced with glass/carbon woven fabrics for lightweight load bearing structures. Materials & Design 36, 75−80.

Fig. 6.2 shows that ROM predicts the tensile strength of the hybrid composite very well; however, it overpredicts the compressive strength of the hybrid composite. In addition, ROM does not include the effect of hybrid stacking sequence and therefore is unable to distinguish between the compressive strength of $[C_2G_2]_s$ and $[CGCG]_s$ composites (Zhang et al., 2012).

The search for the synergistic effect has not been limited to the low strain rate range. Table 6.1 and Fig. 6.3 show the hybrid effect for satin weave carbon/plain weave E-glass/epoxy hybrid composites compared to their nonhybrid constituents at high

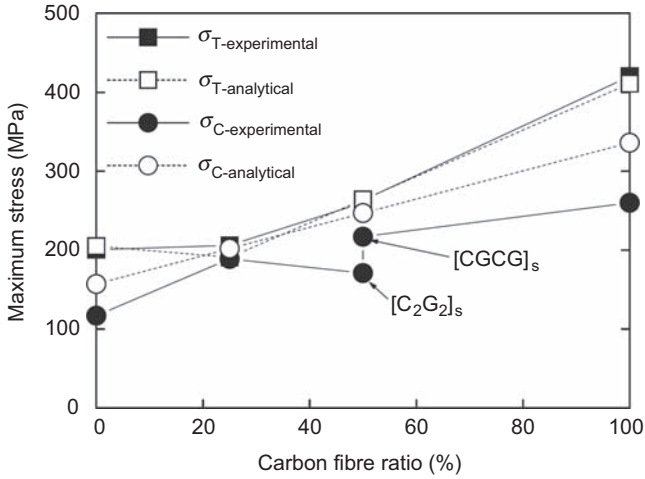

Figure 6.2 Tensile and compressive strength of composite laminates affected by the carbon fibre ratios in the reinforcement (both experimental and analytical results). σ_T is the tensile strength and σ_C is the compressive strength.
Reproduced from: Zhang, J., Chaisombat, K., He, S., Wang, C.H., 2012. Hybrid composite laminates reinforced with glass/carbon woven fabrics for lightweight load bearing structures. Materials & Design 36, 75−80.

Table 6.1 Compressive properties of hybrid and nonhybrid woven carbon/glass composite materials at high strain rates

Direction	Material	Strain rate (s^{-1})	Strength (MPa)	Ultimate strain (%)	Modulus, *E* (GPa)
Warp	Carbon plain weave	1000	301	1.45	22.4
	Carbon satin weave	1000	317	1.57	23.2
	Hybrid	1000	325	1.80	22.0
	E-glass plain weave	1000	279	1.72	21.4
Weft	Carbon plain weave	1000	313	1.56	23.3
	Carbon satin weave	1000	339	1.49	25.6
	Hybrid	1000	347	1.51	23.0
	E-glass plain weave	1000	278	1.61	19.8
Thickness	Carbon plain weave	1503	532	4.71	12.0
	Carbon satin weave	1503	621	2.71	11.3
	Hybrid	1503	680	2.06	13.6
	E-glass plain weave	1503	593	4.9	8.9

Adapted from: Naik, N.K., Ch, V., Kavala, V.R., 2008. Hybrid composites under high strain rate compressive loading. Materials Science and Engineering: A 498, 87−99.

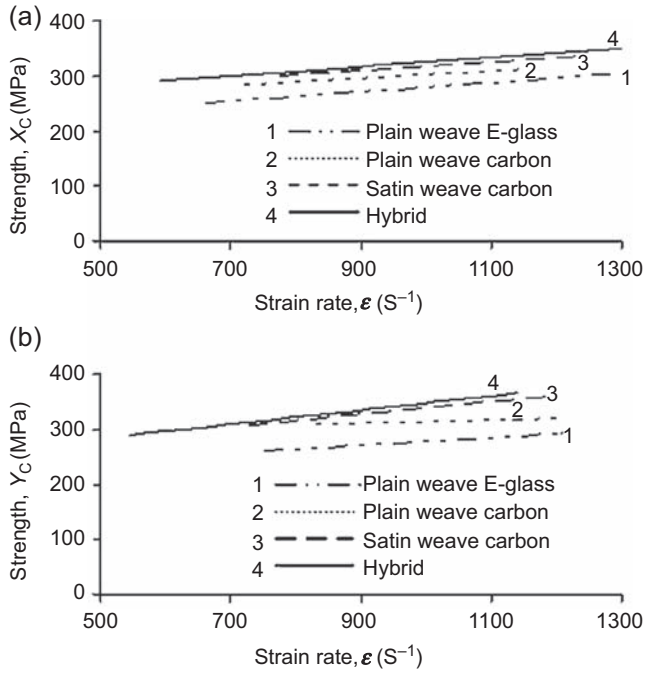

Figure 6.3 Comparison of hybrid and nonhybrid woven carbon/glass epoxy composite strength along (a) warp (X_C) and (b) weft (Y_C) directions at various strain rates.
Reproduced from: Naik, N.K., Ch, V., Kavala, V.R., 2008. Hybrid composites under high strain rate compressive loading. Materials Science and Engineering: A 498, 87–99.

strain rates (HSRs). The compressive strength under HSR loading is higher for satin weave carbon/plain weave E-glass/epoxy hybrid composite compared with satin weave carbon/epoxy. For the hybrid composite, the ultimate strain increases considerably compared with that for satin weave carbon/epoxy. The order of HSR compressive strength for the studied composites is (Naik et al., 2008):

(satin weave carbon/plain weave E-glass/epoxy hybrid) > (satin weave carbon/epoxy) > (plain weave carbon/epoxy) > (plain weave E-glass/epoxy).

The properties of carbon/Kevlar™/epoxy woven hybrid composites have also been investigated at HSRs (Sung-Choong et al., 2013). The strength increases by as much as 80% with increasing strain rate over the range of 1008 to 1922 s^{-1}, while the failure strain decreases by approximately 16%. When strain rate is in the vicinity of 1007 s^{-1}, the average peak strength is 415 MPa. The peak strength increases to 613 and 746 MPa at strain rates of 1476 and 1922 s^{-1}, respectively. The average failure strain at a strain rate of 1007 s^{-1} is 0.0182, but it decreases to 0.0173 and 0.0154 at strain rates of 1476 and 1922 s^{-1}, respectively (Sung-Choong et al., 2013).

The toughness (evaluated by calculating the area under the stress–strain curve) increases from 4.99 MPa at a strain rate of 1007 s^{-1} to 5.42 and 5.75 MPa at strain rates of 1476 and 1922 s^{-1}, respectively. Although the strength increases and failure

strain decreases with increasing strain rate, the combination of these two factors causes the toughness to marginally increase when the strain rate increases. Overall, carbon/Kevlar™/epoxy woven hybrid composites show strain rate-dependent behaviour; however, there is no comparison available between the properties of the hybrid composite and its nonhybrid constituents to show a synergistic effect (Sung-Choong et al., 2013).

Three-dimensional (3D) orthogonal woven hybrid composites are a new generation of hybrids which allow modification of material properties individually in three principal directions. 3D orthogonal woven hybrids fabricated from glass and Twaron™ fibres utilise both the advantages of high strength of Twaron™ tows at HSRs and the relatively cheap price of glass tows (Sun and Gu, 2006; Lv et al., 2006). These hybrid textile composites exhibit HSR sensitivity during shear loading, including shear failure stress, shear failure strain, stiffness, and specific energy absorbed (SEA) both in weft and in warp directions (Sun and Gu, 2006; Lv et al., 2006).

The shear failure strain decreases with the increase of strain rate in both directions (Fig. 6.4) while the shear stiffness increases with the increase of strain rate in both directions (Fig. 6.5) (Sun and Gu, 2006). The shear failure stress increases with increasing shear strain rate, and the shear failure strain decreases with increasing shear strain rate in the weft direction (Fig. 6.6) (Sun and Gu, 2006). In the warp direction, however, the shear strength is nearly invariable with the increasing shear strain rate while the failure strain decreases with the increasing shear strain rate.

The energy absorption of 3D orthogonal woven hybrid composites increases with the increase of the impact velocity in both warp and weft directions. However, the failure load and the energy absorption in the warp direction are slightly lower than

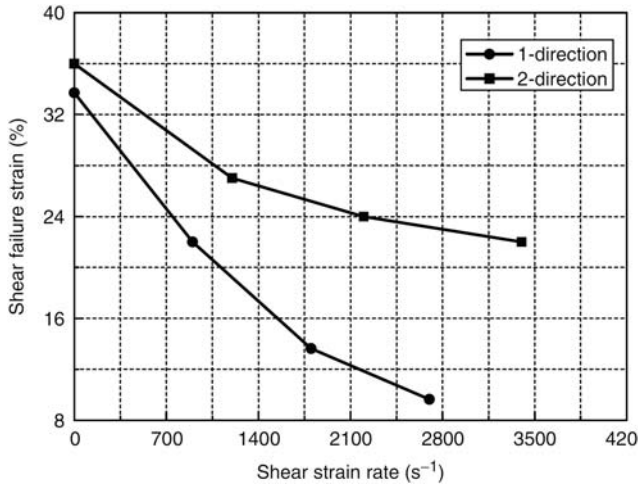

Figure 6.4 Shear failure strain of 3D orthogonal woven hybrid composites in the warp (1-direction) and weft (2-direction) directions at various strain rates.
Reproduced from: Sun, B., Gu, B., 2006. Shear behavior of 3D orthogonal woven fabric composites under high strain rates. Journal of Reinforced Plastics and Composites 25, 1833−1845.

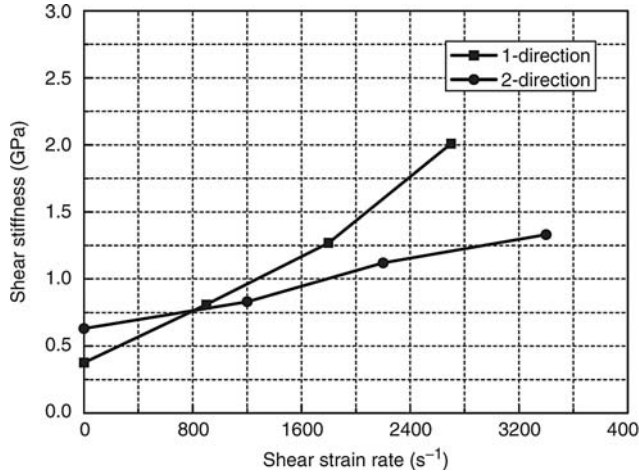

Figure 6.5 Shear stiffness of 3D orthogonal woven hybrid composites in the warp (1-direction) and weft (2-direction) directions at various strain rates.
Reproduced from: Sun, B., Gu, B., 2006. Shear behavior of 3D orthogonal woven fabric composites under high strain rates. Journal of Reinforced Plastics and Composites 25, 1833−1845.

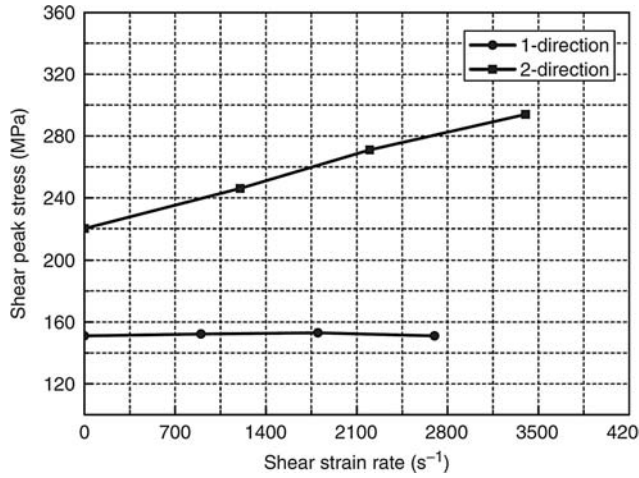

Figure 6.6 Shear failure stress of 3D orthogonal woven hybrid composites in the warp (1-direction) and weft (2-direction) directions at various strain rates.
Reproduced from: Sun, B., Gu, B., 2006. Shear behavior of 3D orthogonal woven fabric composites under high strain rates. Journal of Reinforced Plastics and Composites 25, 1833−1845.

those of the weft direction at the same impact velocity because of the lower linear density of warp (Twaron™) yarns (Fig. 6.7) (Lv et al., 2006). The variations of the impact resistance in different directions are due to the different rate sensitivities of Twaron™ yarns and glass yarns as well as the 3D structure of the hybrids.

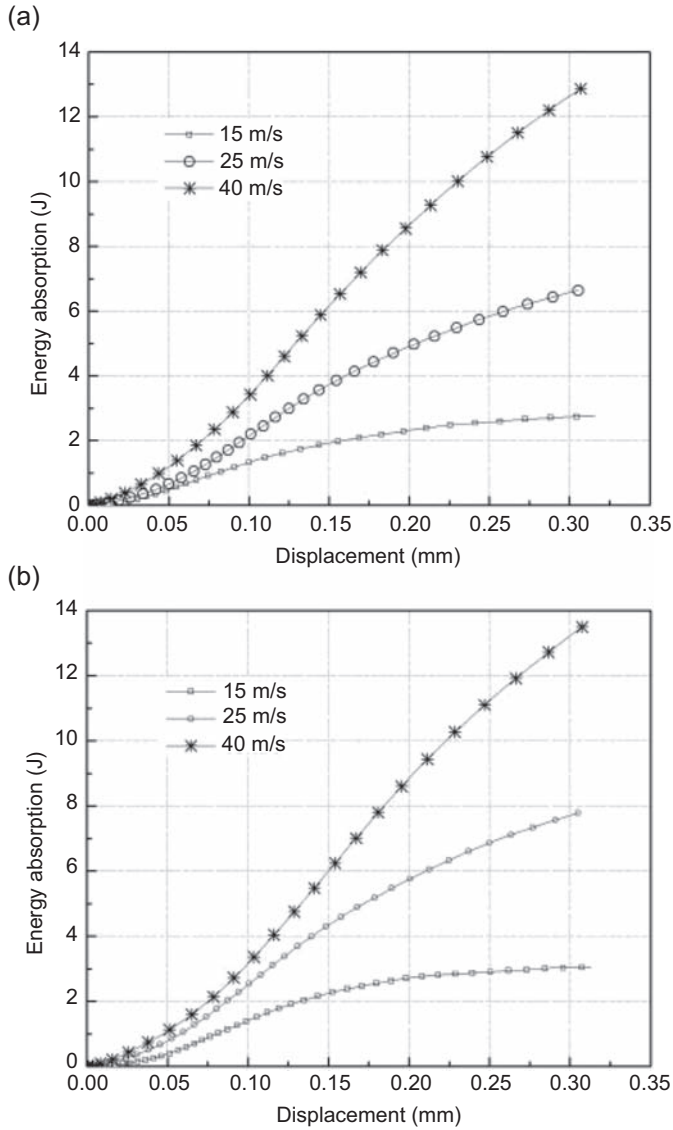

Figure 6.7 Energy absorption−displacement curves for 3D orthogonal woven hybrid Twaron™/glass composites in (a) warp and (b) weft directions at various impact velocities. Reproduced from: Lv, L., Sun, B., Qiu, Y., Gu, B., 2006. Energy absorptions and failure modes of 3D orthogonal hybrid woven composite struck by flat-ended rod. Polymer Composites 27, 410−416.

As a result, engineers have more flexibility in tailoring the properties of such hybrid composites for various design criteria.

In aerospace and defence industries both low and HSR properties of materials and the ballistic performance of structures are critical in determining the material to be used for protective structures. Factors such as the fibre and matrix characteristics, the layup

sequence, and the weave type affect both the HSR properties and the ballistic performance of composite materials (Pandya et al., 2013). For example, glass/polyester shows poor resistance to impact damage due to the lack of plastic deformation mechanisms for absorbing impact energy in both fibres and matrix (Muhi et al., 2009) while glass/epoxy shows superior impact resistance.

Similarly, for the same target thickness and projectile mass, the ballistic impact velocity (V_{50}) is higher for plain weave E-glass/epoxy than for 8H satin weave T300 carbon/epoxy (Pandya et al., 2013). As a result, techniques used for enhancing mechanical properties of composites at HSRs such as hybridisation may also be used to improve the ballistic protection capability of composites. However only limited studies on the ballistic impact behaviour of hybrid composites have been reported (Pandya et al., 2013).

The V_{50} is higher for the E-glass/T300 carbon hybrids compared with the carbon fibre composites with the same thickness (Pandya et al., 2013, 2012). For structures of identical thickness the V_{50} is in the following order (Pandya et al., 2013, 2012):

Plain weave E-glass/epoxy > hybrid composite $[G_2C_2]_s$ > hybrid composite $[C_2G_2]_s$ > 8H satin weave T300 carbon/epoxy.

These results suggest that the ballistic performance of carbon fibre composites could be improved through hybridisation. The ranking of performance is associated with stress wave attenuation in composite materials, which leads to reduction in peak strains as the stress wave propagates away from the point of impact (Pandya et al., 2012). The stress wave attenuation has the same hierarchy as the V_{50} for these materials (Pandya et al., 2012). Based on the comparison between the $[G_2C_2]_s$ and the $[C_2G_2]_s$ or $[G_3C_2]_s$ and $[C_2G_3]_s$ (Pandya et al., 2013, 2012), placing E-glass layers in the exterior and carbon layers in the interior provides a higher ballistic velocity limit than placing carbon layers in the exterior and E-glass layers in the interior. However, the difference in V_{50} for two hybrids, $[G_2C_2]_s$ and $[C_2G_2]_s$, is within a marginal value of 3.6% (Pandya et al., 2013); hence the improvement is very moderate.

Although the hybrid composites can provide higher impact resistance than the carbon composites with the same thickness, projectile mass and projectile diameter, the areal density is different for the laminates considered. The order of the V_{50} normalised to the areal density is (Pandya et al., 2013):

8H satin weave T300 carbon/epoxy > plain weave E-glass/epoxy > hybrid composite $[G_2C_2]_s$ > hybrid composite $[C_2G_2]_s$.

The above ranking shows that the hybridisation has no advantage in terms of the 'specific' ballistic performance. Improvement in the ballistic performance has also been reported in the hybrid glass/graphite/glass composite compared with the nonhybrid graphite composite (Sevkat, 2012). Similarly, the hybrid composite has an added weight compared to the nonhybrid graphite constituent. Replacing some of the graphite fabrics by glass fabrics at outer layers increases the weight of the composite by approximately 10% (Sevkat, 2012). For lightweight applications where weight reduction is the main goal, specific properties need to be considered in designing hybrid composite components. In the case of ballistic performance the 'specific V_{50}'

(ie, V_{50}/density) must be used in assessing the synergistic effect or improvement in the hybrids compared to their nonhybrid counterparts.

Studies on the ballistic performance of carbon/Kevlar™ composite panels indicate that at a fixed thickness, both the stacking sequence and the number of carbon/Kevlar™ lamina substantially affect the ballistic performance of the composite (Grujicic et al., 2006). This is illustrated in Fig. 6.8 where [K/C] and [K/C/K/C] hybrid composites are capable of stopping the projectile while none of the nonhybrid carbon or Kevlar™ composites (with the same thickness) can stop the projectile.

Similar to carbon/glass hybrids the armour consisting of one layer of Kevlar™ and one layer of carbon, with Kevlar™ being at the outer surface of the hybrid composite, exhibits the maximum ballistic performance (see Fig. 6.8) (Grujicic et al., 2006). In addition, hybrid glass/Kevlar™ composites with the addition of one Kevlar™ layer show improved toughness compared to the glass composite constituent, leading to enhanced ballistic performance (Muhi et al., 2009). Fig. 6.9 shows that the maximum absorbed energy of the hybrid composite is achieved when the Kevlar™ layer is away from the impacted surface (regardless of the projectile geometry) due to the higher stiffness and strength of Kevlar™ than glass. Therefore, there is a general agreement that the tougher material should be at the outside of the hybrid composite panel and preferably only at the nonimpact side of the panel (Vaidya and Hosur, 2003; Vaidya et al., 2001; Pandya et al., 2013, 2012; Sevkat, 2012; Muhi et al., 2009;

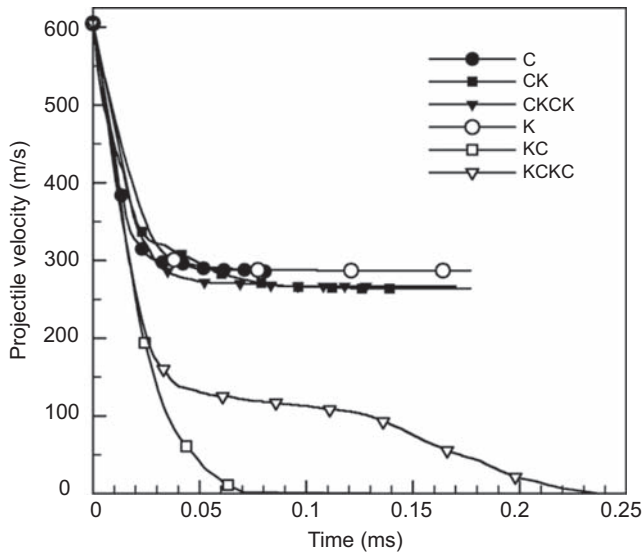

Figure 6.8 Temporal variation of the projectile velocity for different cases of the nonhybrid and hybrid carbon/Kevlar™ laminates.
Reproduced from: Grujicic, M., Pandurangan, B., Koudela, K.L., Cheeseman, B.A., 2006. A computational analysis of the ballistic performance of light-weight hybrid composite armors. Applied Surface Science 253, 730−745.

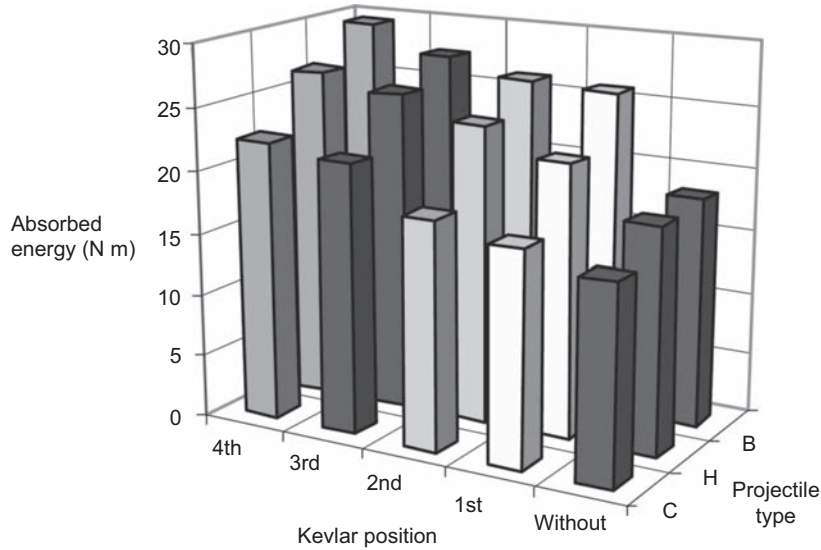

Figure 6.9 Energy absorbed by hybrid composites of glass/Kevlar™ for different positions of the Kevlar™ layer impacted by three different projectile geometries (*B*, blunt; *H*, hemispherical; *C*, conical).
Reproduced from: Muhi, R.J., Najim, F., De Moura, M.F.S.F., 2009. The effect of hybridization on the GFRP behavior under high velocity impact. Composites Part B: Engineering 40, 798−803.

Grujicic et al., 2006). However, it is still not clear whether intimate mixing of the constituents or placing all the similar layers at one location is a more effective approach (Aronhime et al., 1992; Saka and Harding, 1987; Grujicic et al., 2006; Muhi et al., 2009).

Vehicle weight reduction, especially in the automotive industry, can also be achieved with utilisation of natural fibre/synthetic fibre hybrid composites as a more environmental friendly and economical alternative to synthetic fibre/synthetic fibre hybrid composites. Natural plant fibres used for composite reinforcement are primarily bast fibres (such as hemp, flax, wheat straw, jute, kenaf and ramie) or leaf fibres (such as sisal and banana). Bast fibres are long, strong fibres that typically grow in the length of the plant stalk (Kim et al., 2012). Natural fibres are cost-effective, renewable, and environmentally friendly due to reduced CO_2 emissions in their production phase compared with the synthetic fibres (Kim et al., 2012; Mansor et al., 2013). However, due to their low mechanical strength and high level of variability their application has been limited to nonstructural components such as dashboard, floor pan and interior accessories (Mansor et al., 2013).

Natural fibres in thermoset composites dissipate energy at lower levels of stress and higher strain than glass-reinforced composites (Kim et al., 2012). In the case of thermoplastic matrices, the effect on energy dissipation from natural fibres compared with conventional glass reinforcement is highly dependent on resin properties (Kim et al., 2012). Natural fibres in polypropylene (PP) homopolymer show

improved reinforcement but have inferior energy dissipation compared to glass; whereas in PP copolymer, natural fibres result in improved energy dissipation compared to glass fibres (Kim et al., 2012).

Despite the aforementioned issues, hybrid natural fibre/synthetic fibre composites have found their way into the load bearing applications. For example, hybrid kenaf/glass/epoxy composites have been employed in the small-sized car bumper beam (Davoodi et al., 2011, 2010) or passenger vehicle centre lever parking brake component (Mansor et al., 2013). Recent developments indicate that hybrid composites made with kenaf/glass/unsaturated polyester resin are potential candidates for structural applications provided that the kenaf fibres have undergone proper surface treatment (Atiqah et al., 2014).

Natural fibre-reinforced composites and their hybrids have also been the subject of HSR studies. Fig. 6.10 compares the tensile strength for hemp and glass fibre reinforced vinyl ester composites at various strain rates. When the strain rate is between approximately 6×10^2 and $1.5 \times 10^3\ s^{-1}$, the strength of the hemp composite is slightly less than, but very close to, that of the glass composite. Up to $1376\ s^{-1}$, rate hardenings in the glass and hemp composites are essentially equal. At higher strain rates the hardening is seen to greatly decrease for hemp fibres. The low level of hardening can be beneficial if the material is used in impact safety applications, where energy must be dissipated at low stress levels (Kim et al., 2012). The hemp−glass/vinyl ester hybrid composites possess intermediate elastic modulus and stress−strain behaviour compared to the nonhybrid hemp and the glass composites (Kim et al., 2012). The research on HSR properties of natural fibre/synthetic fibre hybrid composites is still in its embryonic stage and requires further investigations.

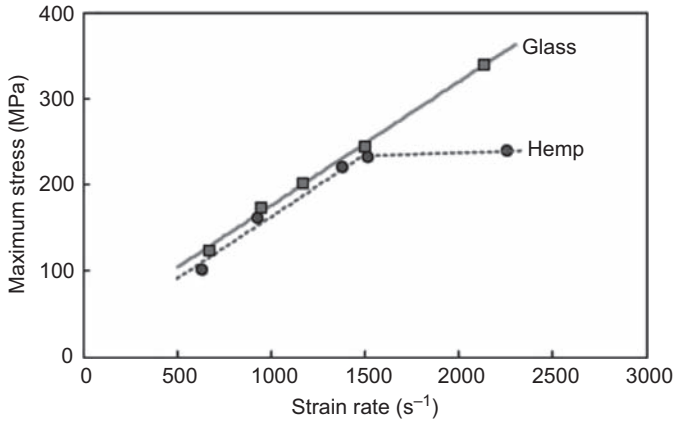

Figure 6.10 Maximum stresses of glass (*solid line*) and hemp (*dotted line*) fibre-reinforced vinyl ester composites at various strain rates.
Reproduced from: Kim, W., Argento, A., Lee, E., Flanigan, C., Houston, D., Harris, A., Mielewski, D.F., 2012. High strain-rate behavior of natural fiber-reinforced polymer composites. Journal of Composite Materials 46, 1051−1065.

6.3 Nanoparticle reinforcements

Particle reinforcements have been widely used to modify polymers to improve mechanical and electrical properties such as toughness and electrical conductivity. With the advent of nanotechnology research on hybrid composites fabricated from one or more types of nanoparticles added to polymers or their fibre-reinforced composites has gained momentum. Among several different nanoparticles used in modification of epoxy for structural applications, carbon nanotubes (CNTs) have attracted more attention due to their extraordinary properties including high aspect ratio, low weight, exceptional strength and stiffness, high flexibility and elongation at break, and high thermal and electrical conductivity (Ma et al., 2014; Gómez-del Río et al., 2014; Hu et al., 2013; Mujika et al., 2012). Factors such as bonding between the nanoparticle and the matrix, functionalization processes, alignment and dispersion of nanoparticles strongly influence the properties of CNT-modified polymers (Mujika et al., 2012), resulting in the study of other nanoparticles as potential reinforcements. Kandare et al. (Kandare et al., 2014) reported that mixing one-dimensional (carbon nanofibres) and two-dimensional (graphene nanoplatelets) nanostructures can yield substantial synergistic improvement in electrical conductivity and mechanical properties.

Recent studies on polymers filled with one type of nanoparticle show noticeable enhancement of mechanical properties at HSRs. However, functionalization processes can influence the enhancement of mechanical properties. For example, the impact energy absorption of polycarbonate increases by 10−20% with the addition of 0.5, 1, and 2 wt% synthesized multiwall carbon nanotubes (MWCNTs) compared to the neat polycarbonate within the strain rate range of 2000−2600 s^{-1}. However, the use of functionalized MWCNTs instead of synthesized MWCNTs at 0.5 and 2 wt% reduces the impact energy absorption (Jindal et al., 2013; Jindal, 2013).

Enhancements in mechanical properties could be limited to one or two mechanical properties and consequent reduction in other properties. For instance, compressive strength of epoxy reinforced with 2 and 5 wt% alumina nanoparticles compared with the neat epoxy at the strain rate of 3000 s^{-1} is increased by about 5.5% and 8.6%, respectively (Fig. 6.11). However, the ultimate strain decreases with the addition of alumina nanoparticles by 1% and 4% for 2 and 5 wt% alumina nanoparticle concentrations, respectively, which results in a reduction of the SEA for the modified epoxies (Naik et al., 2014).

Likewise, the addition of MWCNTs into high-density polyethylene (HDPE) improves the impact strength of the HDPE at strain rates up to 10^4 s^{-1} but with a simultaneous reduction in the yield stress (Al-Lafi et al., 2010). Young's modulus and yield strength of HDPE are also improved by the addition of pristine or vinyltrimethoxysilane (VTMS)-treated alumina nanoparticles (Figs 6.12 and 6.13). However, the impact toughness of the alumina/HDPE nanocomposites is reduced by 14−25% compared with the neat HDPE as seen in Fig. 6.14 (Liao and Tjong, 2012).

The type of nanoparticle reinforcement is very important for the level of enhancement achieved in the mechanical properties of polymers at HSRs. For example, the

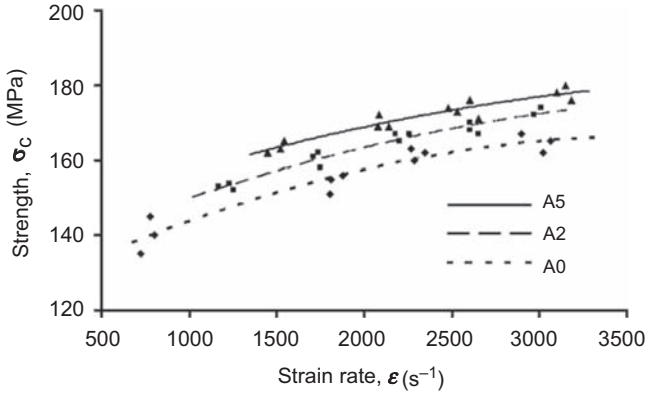

Figure 6.11 Compressive strength for neat epoxy (A0) at various strain rates compared with epoxy modified with 2 wt% (A2) and 5 wt% (A5) alumina nanoparticles.
Reproduced from: Naik, N.K., Pandya, K.S., Kavala, V.R., Zhang, W., Koratkar, N.A., 2014. Alumina nanoparticle filled epoxy resin: high strain rate compressive behavior. Polymer Engineering & Science 54 (12), 2890−2901.

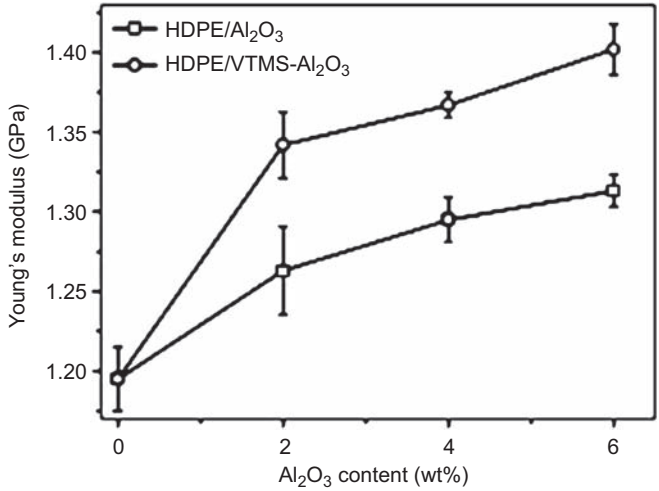

Figure 6.12 Variation of Young's modulus with filler content for HDPE-based nanocomposites.
Reproduced from: Liao, C.Z., Tjong, S.C., 2012. Mechanical and thermal performance of high-density polyethylene/alumina nanocomposites. Journal of Macromolecular Science, Part B 52, 812−825.

compressive strengths of HDPE filled with carbon nanofillers (CNFs) with various surface treatments and pristine graphite nanoplatelets (GNPs) are compared with the neat HDPE at the strain rates of 10^{-2}, 10^3, 4×10^3, and 7×10^3 s^{-1} in Fig. 6.15. CNFs improve the compressive strength of the HDPE while GNP nanoplatelets have very

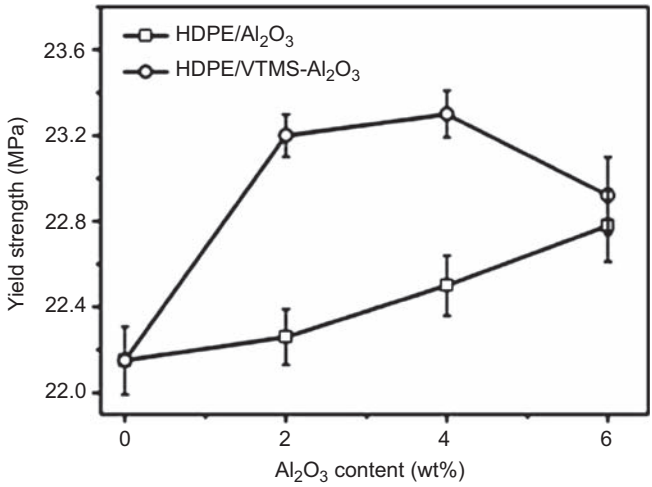

Figure 6.13 Variation of yield strength with filler content for HDPE-based nanocomposites. Reproduced from: Liao, C.Z., Tjong, S.C., 2012. Mechanical and thermal performance of high-density polyethylene/alumina nanocomposites. Journal of Macromolecular Science, Part B 52, 812−825.

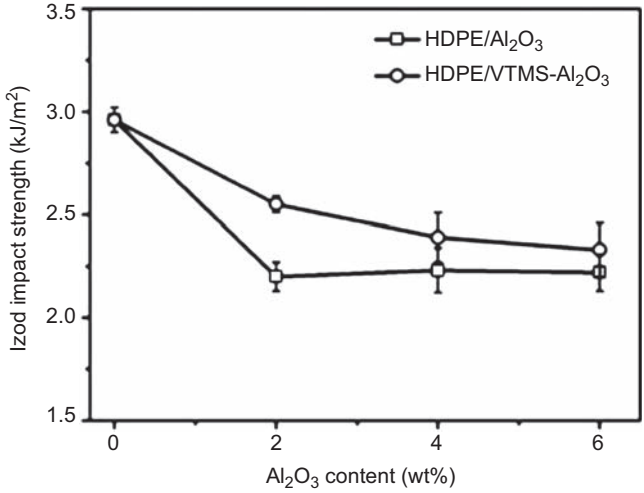

Figure 6.14 Variation of Izod impact strength with filler content for HDPE-based nanocomposites.
Reproduced from: Liao, C.Z., Tjong, S.C., 2012. Mechanical and thermal performance of high-density polyethylene/alumina nanocomposites. Journal of Macromolecular Science, Part B 52, 812−825.

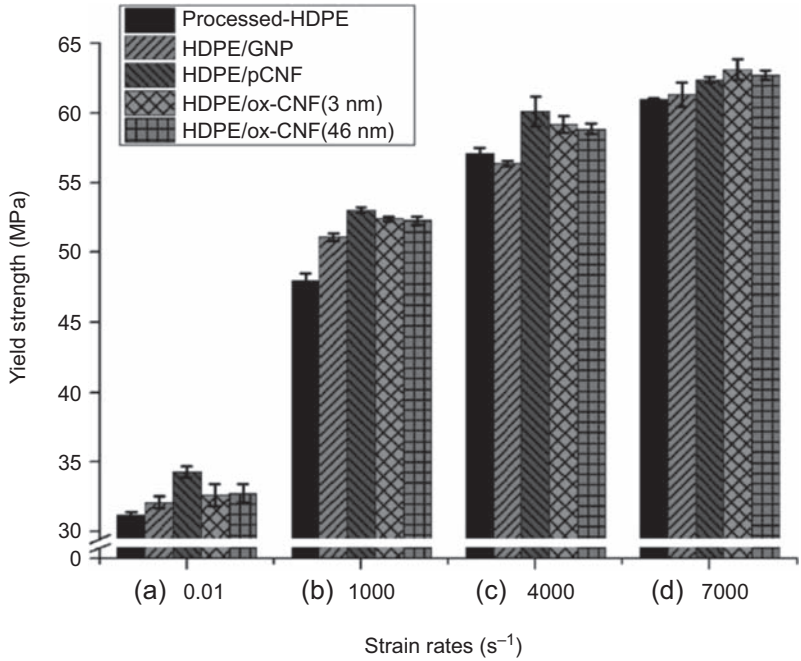

Figure 6.15 Comparison of yield strength for neat HDPE and its nanocomposites at various strain rates (a) 0.01 (S^{-1}); (b) 1000 (S^{-1}); (c) 4000 (S^{-1}) and (d) 7000 (S^{-1}).
Reproduced from: Hu, Y., Liu, T., Ding, J.L., Zhong, W.H., 2013. Behavior of high density polyethylene and its nanocomposites under static and dynamic compression loadings. Polymer Composites 34, 417–425.

limited effects in general and even degraded the compressive strength of HDPE at the strain rate of 4×10^3 s^{-1}. The effect of GNPs is likely due to the defect formation around the interface as a result of substantial incompatibility between HDPE and GNP. The surface treatment of CNFs reduces the compressive strength of HDPE in most cases (Hu et al., 2013).

The addition of pristine and VTMS-treated halloysite nanotube (HNT) particles up to 5 wt% into the unsaturated polyester (UP) increases the impact strength and energy absorption of the nanocomposite (Albdiry et al., 2013). Further addition of nanoparticles results in particle clustering and consequent reduction in the impact strength and energy absorption. However, the surface treatment of HNT nanoparticles using VTMS results in higher impact strength and energy absorption compared with the pristine HNT nanoparticles. The enhanced impact strength is a result of improved interfacial bonding between the UP matrix and the nanoparticles (Albdiry et al., 2013).

The impact strength and energy absorption of hybrid nanocomposites containing two types of nanoparticles at HSRs have been studied recently. For example, the addition of carboxyl terminated butadiene acrylonitrile rubber into epoxy improves the fracture toughness of the epoxy resin to a certain limit. The addition of silica

nanoparticles significantly enhances the toughness of the rubber/epoxy. However, the increase in the compressive moduli and yield stress is insignificant (Liang and Pearson, 2010). There is no improvement in the toughness when silica nanoparticles are not dispersed perfectly which causes particle clustering. Furthermore, the size of silica nanoparticles (compared for 20 and 80 nm particles) shows no effect on the fracture toughness improvement (Liang and Pearson, 2010).

The addition of silica nanoparticles and rubber nanoparticles/submicrometre particles into epoxy results in an enhancement of the elastic modulus but a reduction of the tensile strength, indicating a complex behaviour for the hybrid silica/rubber nanoparticles (Tang et al., 2012; Liu et al., 2011). The Mode I fracture toughness (G_{IC}) of silica/epoxy, rubber/epoxy and hybrid silica/rubber/epoxy nanocomposites is significantly higher than the neat epoxy due to nanosilica debonding and bridging before pull-out and nanorubber cavitation and matrix plastic shearing. Debonding of silica nanoparticles from matrix in the hybrid composite is less than the composite filled only with silica nanoparticles (Tang et al., 2012). However, no synergistic effect exists for G_{IC} in these hybrid nanocomposites (Tang et al., 2012; Liu et al., 2011).

The elastic modulus of hybrid particle-reinforced composites can be predicted within 10% of experimental results using a modified Halpin–Tsai model. The Halpin–Tsai model (Affdl and Kardos, 1976) predicts the elastic modulus of composites filled with one type of particle (Tang et al., 2012):

$$\frac{E_c}{E_m} = \frac{1 + A_1 B_1 V_1}{1 - B_1 V_1} \qquad [6.4]$$

where E_c and E_m are the modulus of the particle-filled composite and polymer matrix, respectively, V_1 is the volume fraction of the particles, A_1 is a shape factor which depends on the geometry of the particles (for spherical particles $A_1 = 2$), and the constant B_1 defines the relative modulus of the particles and the matrix (Tang et al., 2012):

$$B_1 = \frac{(E_1/E_m) - 1}{(E_1/E_m) + A_1} \qquad [6.5]$$

where E_1 is the modulus of the filled particles.

The composite filled with the first type of particle can be considered as a new matrix filled with the second type of particle. Therefore, the modulus of the hybrid composite can be expressed as (Tang et al., 2012):

$$\frac{E_c'}{E_c} = \frac{1 + A_2 B_2 V_2}{1 - B_2 V_2} \qquad [6.6]$$

where E_c' is the modulus of the hybrid composite, and V_2 is the volume fraction of the second type of particle. The relationship between the modulus of the hybrid

composite and the neat matrix is found by substituting Eq. [6.6] into Eq. [6.4] (Tang et al., 2012):

$$\frac{E_c'}{E_m} = \frac{1 + A_1B_1V_1 + A_2B_2V_2 + A_1B_1V_1A_2B_2V_2}{1 - B_1V_1 - B_2V_2 + B_1V_1B_2V_2} \quad [6.7]$$

The constant B_2 can be expressed as:

$$B_2 = \frac{(E_2/E_c) - 1}{(E_2/E_c) + A_2} = \frac{(1 - B_1V_1)E_2 - (1 + A_1B_1V_1)E_m}{(1 - B_1V_1)E_2 + (1 + A_1B_1V_1)E_mA_2} \quad [6.8]$$

where E_2 is the modulus of the second type of particle. Fig. 6.16 compares the experimental results and prediction of the tensile modulus for the silica nanoparticle/epoxy and silica nanoparticle/rubber/epoxy composites using Halpin−Tsai and modified Halpin−Tsai models (Tang et al., 2012). Fig. 6.17 shows the fracture toughness−elastic modulus chart for the particle-filled epoxy composites normalised to the neat epoxy properties from various studies. Hybrid composites with both rigid and soft additives can simultaneously improve the elastic modulus and fracture toughness and show superior advantages to composites modified with one type of particle (Tang et al., 2012).

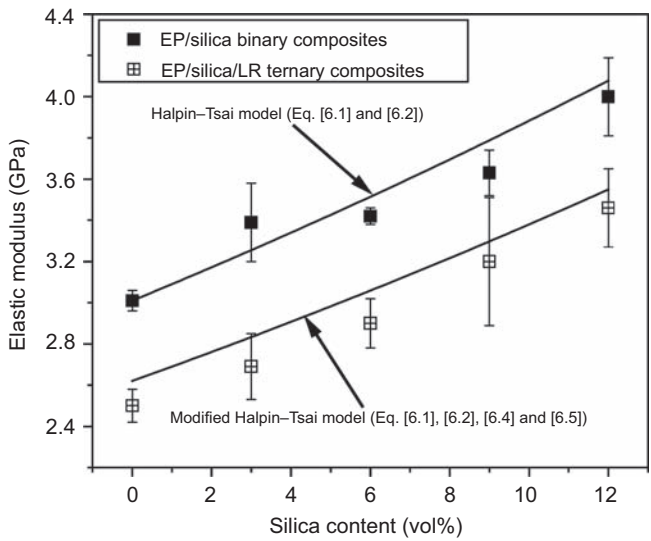

Figure 6.16 Comparison of experimental and predicted elastic modulus using Halpin−Tsai and modified Halpin−Tsai models.
Reproduced from: Tang, L.-C., Zhang, H., Sprenger, S., Ye, L., Zhang, Z., 2012. Fracture mechanisms of epoxy-based ternary composites filled with rigid-soft particles. Composites Science and Technology 72, 558−565.

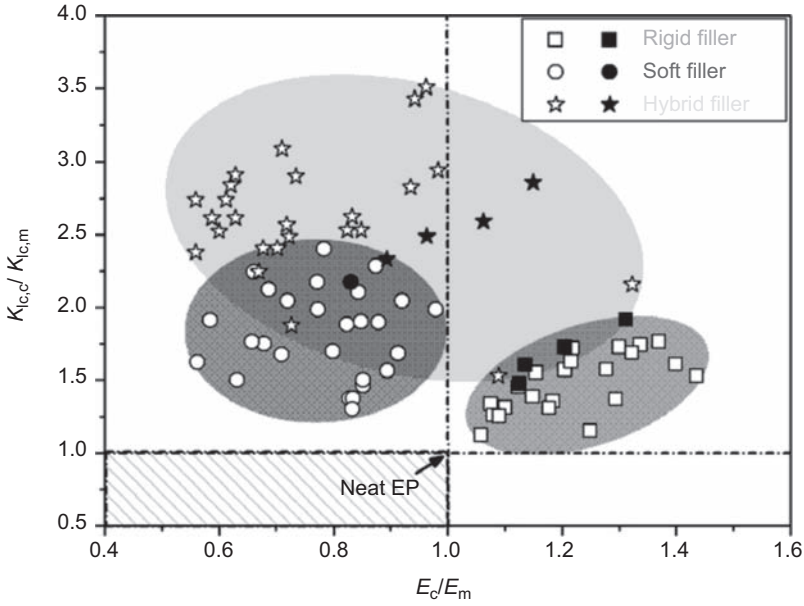

Figure 6.17 Comparison of elastic modulus and fracture toughness for epoxy resins filled with soft, rigid and rigid/soft hybrid particles.
Reproduced from: Tang, L.-C., Zhang, H., Sprenger, S., Ye, L., Zhang, Z., 2012. Fracture mechanisms of epoxy-based ternary composites filled with rigid-soft particles. Composites Science and Technology 72, 558−565.

An alternative hybrid nanocomposite can be fabricated with the addition of one type of hybrid nanoparticle instead of two types of separate nanoparticles. For example, the core−shell polymer (CSP) nanoparticles have a soft rubber core and a transparent shell of poly methyl methacrylate with an epoxy functional group to improve the interfacial bond of the nanoparticles with epoxy matrix (Ali and Joshi, 2013). The addition of 14 wt% CSP nanoparticles within the ply interfaces of glass/epoxy composites increases the impact energy absorption of the composite material. This is due to the deformation of the CSP nanoparticles and the crushing of their outer shells, which prevents the initiation of matrix cracks at lower impact energies. The crushed particles further impede crack propagation at higher impact energies, which increases the energy absorption of the composite (Ali and Joshi, 2013).

Introducing nanoparticles into the FRP composites can produce another type of hybrid nanocomposites for HSR applications. For example, the compressive strength of glass/epoxy nanocomposites within the strain rate range of 400−600 s^{-1} has been found to increases with the addition of spherical silica nanoparticles up to 30 wt% (Tsai and Cheng, 2009). The increase in the compressive strength is due to the enhanced interfacial bonding between fibres and epoxy resulting from the addition of silica nanoparticles (Tsai and Cheng, 2009). The damage area and energy absorption in sandwich composites fabricated from glass warp-knitted fabric/epoxy skins

and foam core increase with the addition of MWCNTs in the epoxy matrix. Increasing the carbon nanotube content up to 1.5 wt% increases the energy absorption by more than 250% and 150% at impact velocities of 10 and 20 m/s, respectively (Ma et al., 2014).

The addition of montmorillonite (MMT) nanoclay (Closite 30B) with various weight percentages into E-glass (plain weave)/epoxy composite at ballistic impact velocities improves the mechanical properties of the laminate including the energy absorption capability. The energy absorption is increased by nearly 5% with the addition of 5 wt% nanoclay. However, improvements in different mechanical properties can reach its maximum at different nanoclay weight percentages, showing different optimum weight percentage for each property. It should be noted that the improvement in mechanical properties depends on the impact velocity (Pol et al., 2013).

The SEA values of glass fibre-reinforced Polyamide-6 (PA-6) and glass fibre-reinforced PP thermoplastic composites modified with silica, MMT and glass sphere nanoparticles are compared in Fig 6.18. Glass sphere nanoparticles significantly increase the dynamic SEA of PA-6 while the increase in SEA due to the addition of silica nanoparticles is much less and the MMT nanoparticles reduce the SEA of PA-6. The addition of all three nanoparticles into the glass-reinforced PP reduces the dynamic SEA. This is because the strong bonding between PP and reinforcements and good dispersion of untreated nanoparticles in the PP matrix are hard to achieve, which result in nanoparticle clustering. The toughness of composites increases by increasing the dispersion of nanoparticles (Silva et al., 2013b).

Glass fibre-reinforced composites modified by tetra-needle-like ZnO nanowhiskers in the epoxy matrix show enhanced mechanical properties at HSRs due to the

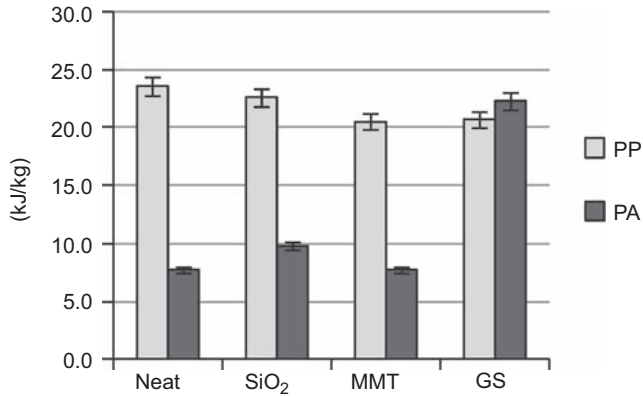

Figure 6.18 Comparison of dynamic SEA for PA-6 and PP modified with various nanoparticles.
Reproduced from: Silva, F., Njuguna, J., Sachse, S., Pielichowski, K., Leszczynska, A., Giacomelli, M., 2013b. The influence of multiscale fillers reinforcement into impact resistance and energy absorption properties of polyamide 6 and polypropylene nanocomposite structures. Materials & Design 50, 244−252.

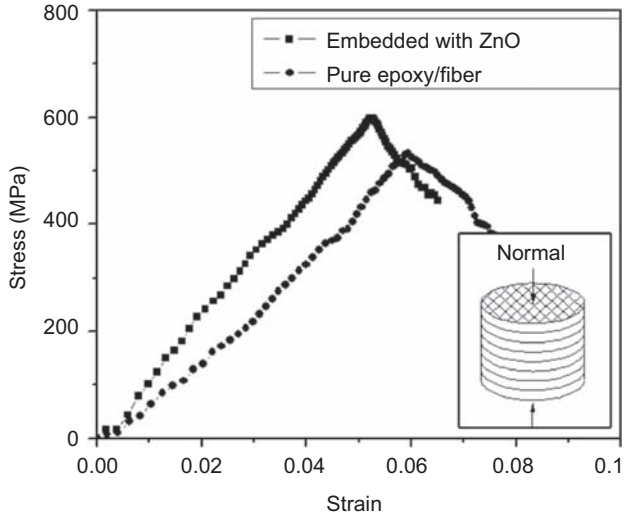

Figure 6.19 Effect of ZnO nanowhiskers on the mechanical properties in the normal direction of composites at 700 s^{-1}.
Reproduced from: Cao, M.S., Zhou, W., Shi, X.L., Chen, Y.J., 2007. Dynamic response and reinforcement mechanism of composites embedded with tetraneedlelike ZnO nanowhiskers. Applied Physics Letters 91.

three-dimensional structure of ZnO nanowhiskers (Cao et al., 2007). Figs 6.19 and 6.20 show the compressive stress−strain response of the hybrid nanocomposites compared with the glass fibre/epoxy composite at 700 s^{-1} for the through-the-thickness and in-plane directions, respectively. The modulus and the compressive strength of the nanocomposites are higher in both cases while the ultimate strain is reduced compared with the neat glass fibre/epoxy (Cao et al., 2007). The influence of ZnO nanowhiskers on the QS fracture toughness of glass fibre polymer composites is negligible; however, the dynamic fracture toughness decreases by 31% when increasing the ZnO nanowhiskers content up to 20 wt% (Rong et al., 2010).

Although most of the research has been focussing on the addition of nanoparticles to GFRP, CFRP has also been modified with nanoparticles. The initiation and propagation fracture toughness of carbon fibre (T300)/epoxy composites can be improved with the addition of functionalised MWCNTs by 22% and 14%, respectively. However, the addition of nonfunctionalized MWCNTs has no effect on the fracture toughness of carbon fibre/epoxy composites due to both the lack of adhesion between the nanotubes and the epoxy matrix and the insufficient dispersion of the CNTs. The functionalization of MWCNTs improves their dispersion in the solvent and enhances their adhesion to epoxy (Mujika et al., 2012).

Simultaneous addition of two types of nanoparticles into FRPs is a new hybridisation method for development of particle fibre reinforced nanocomposites, which have been rarely studied at HSRs. Simultaneous addition of CNTs and block copolymer styrene-b-butadiene-b-poly methyl methacrylate (SBM) nanoparticles into the epoxy

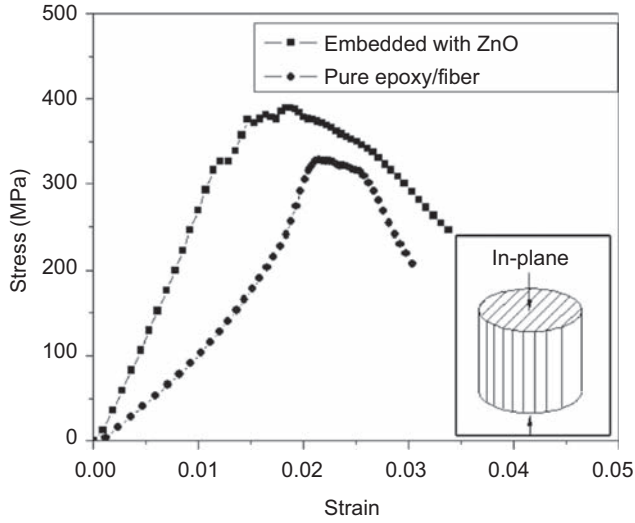

Figure 6.20 Effect of ZnO nanowhiskers on the mechanical properties in the in-plane direction of composites at 700 s^{-1}.
Reproduced from: Cao, M.S., Zhou, W., Shi, X.L., Chen, Y.J., 2007. Dynamic response and reinforcement mechanism of composites embedded with tetraneedlelike ZnO nanowhiskers. Applied Physics Letters 91.

resin is an example of hybrid particulate composites with enhancement in both strength and toughness of the neat epoxy at HSRs. In addition, the presence of CNT and SBM nanoparticles in the epoxy increases its strain rate sensitivity with SBM nanoparticles being more effective at low rates and CNTs being more effective at high rates (Gómez-del Río et al., 2014). Fig. 6.21 shows the effect of nanoparticle addition on the compressive yield strength of epoxy resin at a wide range of strain rates. This type of hybrid nanocomposite has the potential to improve several mechanical properties of FRPs simultaneously with synergistic effects.

Incorporation of nanoparticles into polymer matrix requires advanced processes due to their high surface area/aspect ratio, small size, and their tendency to agglomerate or clump (Henry, 2009). The main challenge in the manufacturing of nanoparticle-reinforced composites is the proper dispersion of nanoparticles in the matrix to avoid agglomerates. The particle-reinforced composites will not inherit the properties of nanoscale particles if agglomerates form within the mixture. The most popular methods for dispersion of nanoparticles in polymers include ultrasonication, high-shear mixing and three roll milling. Ultrasonication and high-shear mixing cannot be used effectively for nanoparticles with high aspect ratios (eg, carbon nanofibres) because the process will break the particles into smaller fragments. However, three roll mixing has been reported as an effective technique for mixing nanofibres into polymer matrix. Details on dispersion methods used for mixing nanoparticles with polymer composites are discussed in Henry (2009), Capek (2006) and Bittmann et al. (2009).

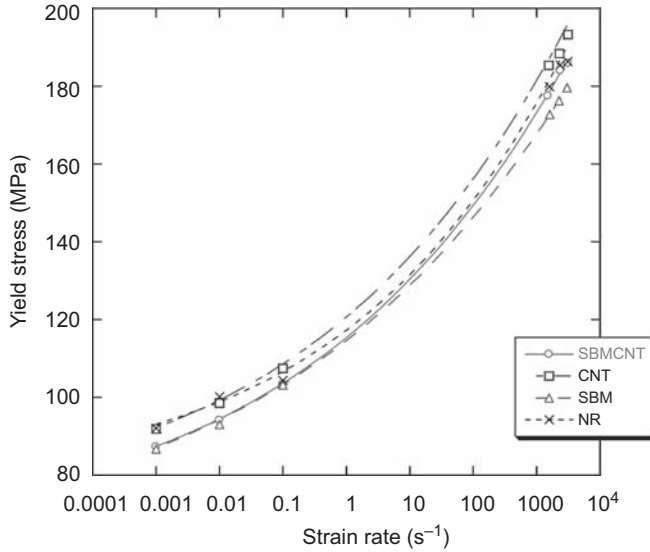

Figure 6.21 Compressive yield stress experimental values at various strain rates for pure epoxy (NR), SBM-modified epoxy (SBM), epoxy reinforced with CNTs (CNT) and hybrid composite with SBM triblock copolymer and CNTs (SBMCNT).
Reproduced from: Gómez-Del Río, T., Rodríguez, J., Pearson, R.A., 2014. Compressive properties of nanoparticle modified epoxy resin at different strain rates. Composites Part B: Engineering 57, 173−179.

6.4 Fibre metal laminates

Another type of hybrid composite commonly utilised in the aerospace industry is the FMLs. FMLs are hybrid composite materials fabricated by mechanically and/or adhesively bonding of thin metal layers and fibre-reinforced adhesives. ARALL (aramid-reinforced aluminum laminate) is the first developed FML which was introduced in 1978 at the Delft University of Technology (Sinmazçelik et al., 2011). Other common FMLs include GLARE (glass-reinforced aluminum laminate) and CARALL (carbon-reinforced aluminum laminate). Titanium−FMLs are called TiGr (titanium graphite) or HTCL (hybrid titanium composite laminate). The HTCLs are suitable for critical fatigue and high-temperature applications such as engines and supersonic structures. This is because HTCL has higher tensile strength and tensile modulus than GLARE and CARALL laminates even under hygrothermal and thermal shock conditions (Silva et al., 2013a).

ARALL was first used in the wing panels of Fokker 50 for 20% weight reduction. However, this first application of FMLs was not successful due to the low compressive strength of aramid fibre composites (Silva et al., 2013a). Due to its high membrane stiffness GLARE undergoes 33% more displacement than its aluminum counterpart in impact events and has found more applications than ARALL (Morinière et al., 2013a). The early applications of GLARE were in C5-A Galaxy

by the United States Air Force in 1995 and later in Boeing B 777 (Silva et al., 2013a). Airbus A380 is the first aircraft to use GLARE in the primary structure, resulting in a 25% reduction in weight (Silva et al., 2013a; Wu and Yang, 2005). GLARE is also used in cargo floors, engine cowlings, patch repair, stringers, cargo containers and seamless tubes (Morinière et al., 2013a).

FMLs exhibit superior mechanical properties compared to fibre-reinforced composites and aluminum alloys, including high specific strength in the fibre direction, high modulus of elasticity, improved toughness and impact resistance, higher residual compressive strength, fire resistance and slower fatigue crack growth (Sinmazçelik et al., 2011; Botelho et al., 2008; Seyed Yaghoubi et al., 2011; Zhu and Chai, 2012; Vlot, 1993). In addition, FMLs have excellent corrosion resistance because composite layers act as moisture barriers between metal layers and simultaneously the metal layers protect the composite layers from the environment (Wu and Yang, 2005).

The storage modulus of glass/epoxy composites degrades under hygrothermal conditions, while the storage modulus of GLARE laminates remains unchanged under similar conditions because aluminum layers protect glass/epoxy layers from moisture absorption (Botelho et al., 2005; Zhu and Chai, 2012). As shown in Fig. 6.22, glass/epoxy absorbs 1.5 wt% of moisture after the saturation point while GLARE absorbs less than 0.1 wt% of moisture after the saturation point. Moreover, unlike composite materials, aluminum-based FMLs can be repaired using conventional aluminum repair techniques (Morinière et al., 2012b).

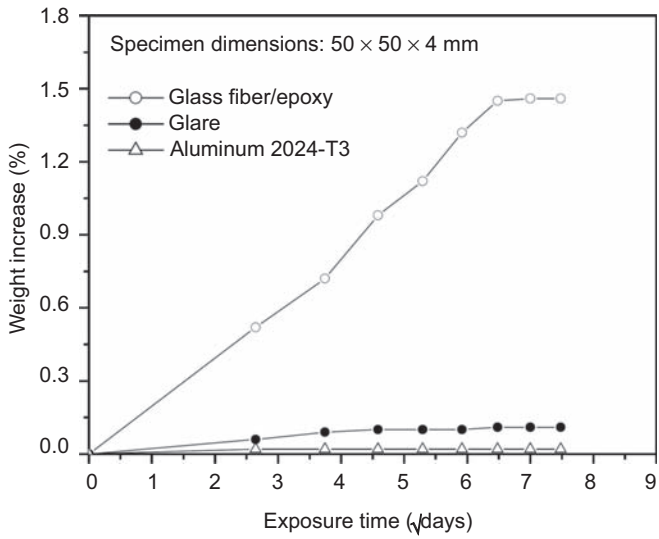

Figure 6.22 Weight increase of glass/epoxy composite, aluminum and GLARE specimens exposed at 80°C and 90% RH.
Reproduced from: Botelho, E.C., Pardini, L.C., Rezende, M.C., 2005. Hygrothermal effects on damping behavior of metal/glass fiber/epoxy hybrid composites. Materials Science and Engineering: A 399, 190−198.

In FMLs, delamination absorbs less than 10% of the low-velocity impact energy, which is limited to the vicinity of the impact location (Vlot, 1993; Morinière et al., 2013b; Hoo Fatt et al., 2003) and is always smaller than the size of the plastic deformation of the outer aluminum layers (Seyed Yaghoubi et al., 2011); consequently, aluminum absorbs more energy (Morinière et al., 2013a,b). As a result, the impact energy must increase by increasing the volume fraction (thickness) of aluminum layers (Morinière et al., 2013b). However, the increase of energy absorption by increasing the aluminum thickness is limited. In fact, composite layers induce a more global deformation to the aluminum layers, which results in more energy absorption in GLARE compared to monolithic aluminum (Morinière et al., 2013a; Vlot, 1993).

The global flexural deformation of the laminate, interfacial debonding, and bending and stretching of aluminum layers absorb most of the impact energy in FMLs (Morinière et al., 2012a; Seyed Yaghoubi and Liaw, 2012). The composite layers delay the crack initiation in the aluminum by modifying the flexural deformation profile of the aluminum. The front aluminum layer dampens the impact on the composite plies and the rear aluminum layer delays the delamination growth (Morinière et al., 2013b). At a large scale the energy distribution is balanced between the aluminum layers; however, the contribution of aluminum remains dominant (Morinière et al., 2013a). Aluminum cracking and petaling are more effective energy-absorbing mechanisms compared to the low-energy-absorbing delamination and fibre failure (Morinière et al., 2012a).

The impact damage area in FMLs increases with the increase of the GLARE thickness. This is due to the changes in the failure modes with changing thickness. For example, the major impact failure mechanisms in thin GLARE-5 are debonding in the nonimpacted side, fibre failure, and fracturing of the aluminum layers, while for thicker samples delamination occurs near the impacted side at relatively lower impact energies followed by fibre failure at higher impact energies (Seyed Yaghoubi et al., 2011). Impact damage progression in GLARE-5 based on repeated low-velocity studies has the following order (Morinière et al., 2012a):

- plasticity and cracking of matrix with delamination and yielding of aluminum;
- debonding at the interface between composite and aluminum;
- fracture of composite layers followed by aluminum cracking;
- penetration in the laminate and petaling of aluminum.

The role of the material constituents in impact performance of FMLs requires further investigation (Morinière et al., 2013a). The failure mechanisms of FMLs are rather complex due to their inhomogeneous structure, which is composed of constituents with significantly different properties that remain distinct in the final composition. However, metal volume fraction (MVF) defined as the ratio of the sum of each individual aluminum layer to the total thickness of FML can be used to predict the tensile strength and shear yield strength of FMLs by assuming a linear relationship between the basic material properties and the MVF; similar to the ROM in FRPs (Zhu and Chai, 2012):

$$\text{FML property} = [\text{MVF} \times \text{Metal property}] + [(1 - \text{MVF}) \times \text{Fibre property}] \quad [6.9]$$

Eq. [6.9] predicts the tensile yield strength of FMLs within the range of $0.45 < \text{MVF} < 0.85$, to within 5% accuracy of the experimental results (Zhu and Chai, 2012).

Because the mechanical response of FMLs is rather complex and is affected by many factors, simulating their failure behaviour with greater accuracy remains a primary challenge (Chen et al., 2014). A very recent review on the analytical studies involving empirical, structural and energy approaches shows that numerical techniques are not fully exploited to model impact in FMLs (Morinière et al., 2014). The classical laminate theory integrated into an energy-balance model appears to be a promising technique and may reveal the major impact mechanisms in FMLs (Morinière et al., 2014). Recently, a finite element model which includes interply and intraply damage effects was developed for progressive failure analyses of perforated aluminum/CFRP FMLs (Chen et al., 2014). However, by disregarding debonding between the composite and the metal layers, simulations resulted in overestimated bearing yield of the unidirectional and cross-ply GLARE. Therefore, both in-plane failure mechanisms and out-of-plane delamination failure should be incorporated in any numerical model to realistically represent the behaviour of FMLs (Chen et al., 2014).

Furthermore, the layup of the FRP layer and the type of reinforcements affect the properties of FMLs. The cross-ply stacking of fibres along the diagonals of aluminum plate and distribution of aluminum layers between glass layers results in up to 70% higher SEA in GLARE compared to a monolithic aluminum plate (Morinière et al., 2012b). However, the FMLs with unidirectional layups show higher tensile failure loads compared to cross-ply and quasi-isotropic (QI) layups (Chen et al., 2014). In addition, FMLs fabricated with woven fabric have lower SEA compared to those fabricated with UD fibres. This is because of the higher stiffness and strength of the UD fibres compared with woven fabrics, which affect the bending and stretching of aluminum layers (Zhu and Chai, 2012).

The energy to create the first crack in FMLs with aramid and carbon fibres is comparable to fibre-reinforced composite materials and is relatively low compared to aluminum and FML with glass fibres (GLARE) (Vlot, 1993, 1996). The damage size in FMLs is smaller than their composite counterparts and the dent depth is almost equal to the monolithic aluminum (Vlot, 1993, 1996). The strength and energy absorption of GLARE are strain rate sensitive due to the strain rate-dependent behaviour of the glass fibre layers (Vlot, 1993, 1996). However, in most cases, this strain rate dependency is usually not accounted for in analytical and computational analyses.

The energies required for creating a through crack for static, low-velocity and high-velocity impact loading for Al 2024-T3, GLARE-3, GLARE-3I, ARALL and carbon/epoxy with similar areal density are compared in Fig. 6.23. ARALL and carbon/epoxy have low failure energies. The failure energies of GLARE and monolithic aluminum are comparable while GLARE provides higher impact energy absorption. The energy absorption increases with strain rate for all the materials shown in Fig. 6.23.

The V_{50} of FMLs has been the subject of recent studies for defence-related applications. The V_{50} increases by increasing the thickness or the composite volume

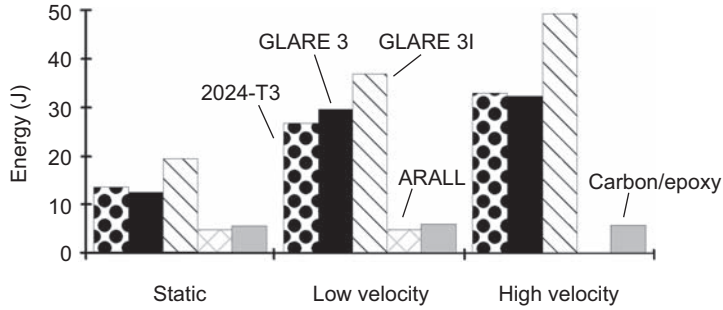

Figure 6.23 Comparison of puncture energy (through crack) for aluminum and various FMLs. Reproduced from: Vlot, A., 1996. Impact loading on fibre metal laminates. International Journal of Impact Engineering 18, 291−307.

fraction of the FML (Seyed Yaghoubi and Liaw, 2012). The V_{50} of GLARE-5 beams varies in a parabolic trend with respect to the MVF and specimen thickness as shown in Fig. 6.24. The V_{50} is generally insensitive to the stacking sequence of GLARE-5 beams with UD glass fibres except for the case when fibres are perpendicular to the beam direction, which has lower impact resistance (Seyed Yaghoubi and Liaw, 2013). In addition, V_{50} is slightly higher for the QI specimens. However, the cross-ply $[0/90 \text{ degree}]_s$ layup absorbs more energy compared with other cases. For the QI specimens, the damage shape on the nonimpacted side of the specimen is a mixture of the damage shape in both the unidirectional and the cross-ply specimens (Seyed Yaghoubi and Liaw, 2013).

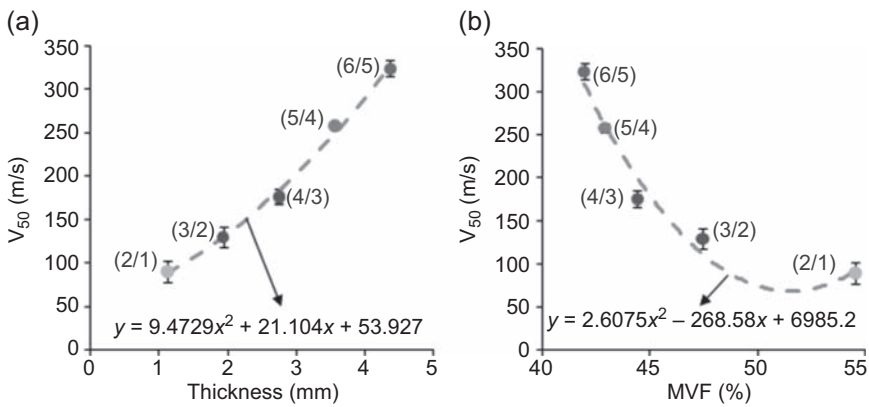

Figure 6.24 Variation of ballistic limit velocity as a function of (a) specimen thickness and (b) MVF. In figure (a) *x* stands for thickness and *y* for V_{50}. In figure (b) *x* stands for MVF and *y* for V_{50}.
Reproduced from: Seyed Yaghoubi, A., Liaw, B., 2012. Thickness influence on ballistic impact behaviors of GLARE 5 fiber-metal laminated beams: experimental and numerical studies. Composite Structures 94, 2585−2598.

Thermoplastic-based FMLs have several advantages including very short processing times, ease of forming, improved chemical resistance, and superior interlaminar fracture toughness properties compared to thermoset FMLs (Abdullah and Cantwell, 2012, 2006). Epoxy-based GLARE increases the ballistic limit of aluminum about 15% while PP-based GLARE increases the ballistic limit of aluminum by almost 50% (Hoo Fatt et al., 2003). PP is a thermoplastic with twice the fracture toughness of a thermoset such as epoxy that increases significantly with strain rate (Hoo Fatt et al., 2003).

Among the thermoplastic-based FMLs self-reinforced polypropylene (SRPP) shows higher potential for use in ballistic protection and impact-resistant components (Abdullah and Cantwell, 2012, 2006). Fig. 6.25 compares the specific perforation energy (SPE) of four different FMLs based on thermoplastic composites including SRPP, glass/polyethylenimine, glass/PA6-6, Kevlar/PA6-6 and a thermosetting woven glass/phenolic composite. The SPE of SRPP FML is more than 250% higher than that of a Kevlar/PA6-6 FML due to the high strain to failure of the PP fibres (Abdullah and Cantwell, 2012, 2006).

Recently, FMLs have been used in sandwich structures for improving the energy absorption capacity (Ghalami-Choobar and Sadighi, 2014; Reyes Villanueva and Cantwell, 2004). Study on the high-velocity impact response of sandwich specimens with FML skins and polyurethane foam core shows that FML skins absorb most of the impact energy while the SEA of sandwich panels decreases with the increase of the foam density (Ghalami-Choobar and Sadighi, 2014). Sandwich structures with glass/PP FML skins and aluminum foam core offer excellent energy absorbing

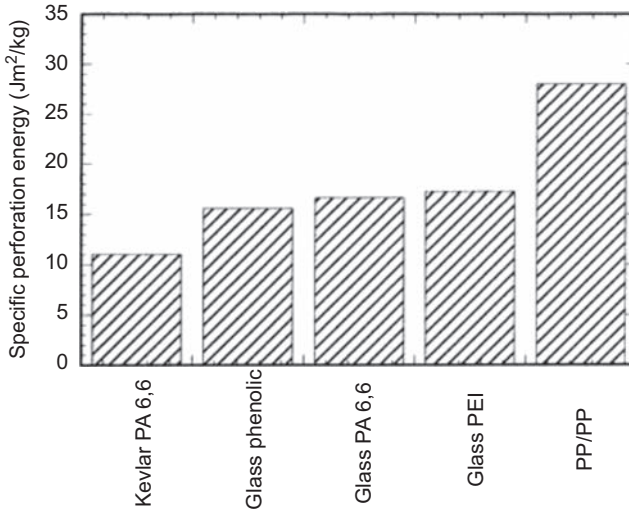

Figure 6.25 Comparison of the specific perforation energy of four thermoplastic-based FMLs. Reproduced from: Abdullah, M.R., Cantwell, W.J., 2012. The high velocity impact response of self-reinforced polypropylene fibre metal laminates. In: Tamin, M.N. (Ed.), Damage and Fracture of Composite Materials and Structures. Springer, Berlin, Heidelberg.

characteristics under high-velocity impact loading conditions, ie, 23% higher SPE than their plain composite counterparts (Reyes Villanueva and Cantwell, 2004). The SPE of the cross-ply laminates is approximately 10% greater than that of the woven samples. This is because unidirectional FML sandwich structures exhibit more energy-absorbing mechanisms under high-velocity impact conditions than the woven FML sandwich systems. For example, the delamination in the glass fibre layers is less noticeable when the woven glass fabric is used instead of the cross-ply UD glass laminate (Reyes Villanueva and Cantwell, 2004).

Apart from FMLs, other forms of metal/composite hybrids with applications in the automotive industry have recently been developed. Hybrid composite/metal technology has been used in the Ford Focus C-Max van to reduce the thickness of the metal walls and subsequently overall weight of the structure (1 kg reduction in the case of C-Max) without any reduction in the strength or the impact performance (LANXESS Deutschland GmbH, 2004).

Likewise, hybrid shafts consisting of an aluminum tube wound by glass and/or carbon fibres/epoxy composites exhibit higher torque transmission capability, higher fundamental natural bending frequency and less noise and vibration (Mutasher, 2009). The maximum static torsional capacity of the hybrid shaft can be achieved with $[+45/-45]_2$ composite layup for both carbon fibre and glass fibre-reinforced composites. However, regardless of the stacking sequence, the use of carbon fibre composites provides higher torsional capacity (Mutasher, 2009). Fig. 6.26 shows that hybridisation of carbon and glass composite provides enhanced torsional capacity compared with the glass fibre composite.

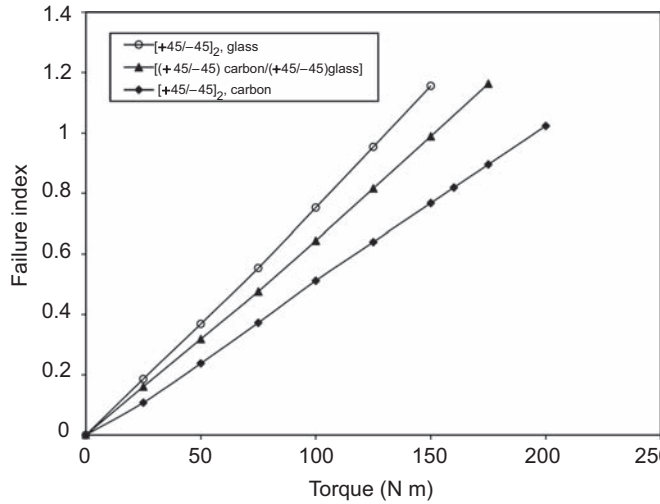

Figure 6.26 Effect of hybridization on the failure indices for aluminum tube wound externally by carbon, glass and hybrid carbon/glass composites.
Reproduced from: Mutasher, S.A., 2009. Prediction of the torsional strength of the hybrid aluminum/composite drive shaft. Materials & Design 30, 215–220.

Hybrid CFRP/titanium bolted joints (Fig. 6.27) have been developed very recently due to higher compressive strength, greater extent of impact damage and improved fatigue behaviour compared with CFRP composites (Kolks and Tserpes, 2014; Camanho et al., 2009; Kolesnikov et al., 2008). Titanium can be used in conjunction with carbon fibre composites in hybrid form due to its good specific mechanical properties, electrochemical compatibility with carbon and relatively low coefficient of thermal expansion. Replacing CFRP bolted joints with hybrid CFRP/titanium bolted joints with 50% titanium content increases the specific bearing strength and stiffness of the joint by 29% and 31%, respectively (Camanho et al., 2009). The transition region does not represent the weak point in the hybrid CFRP/titanium bolted joints. This prevents the premature failure of the material at the transition region and allows possible reduction in the number of bolts (Camanho et al., 2009; Kolesnikov et al., 2008). In addition, the hybrid CFRP/titanium bolted joints are less sensitive to the laminate configuration and environmental effects (Camanho et al., 2009).

The manufacturing process of FMLs is similar to the vacuum bagging method used in fabricating fibre-reinforced composites using prepreg material. The main difference is the presence of thin aluminum layers and adhesive layers in the laminate. One adhesive layer is placed at each interface of aluminum and prepreg material. The use of an adhesive is that the resin in the prepregs is typically too brittle to handle the high-stress concentrations at the interface between aluminum and composite ply near edges or cutouts. To ensure adequate bonding, the aluminum must be properly surface treated to increase the adhesion between the aluminum and the adhesive layer.

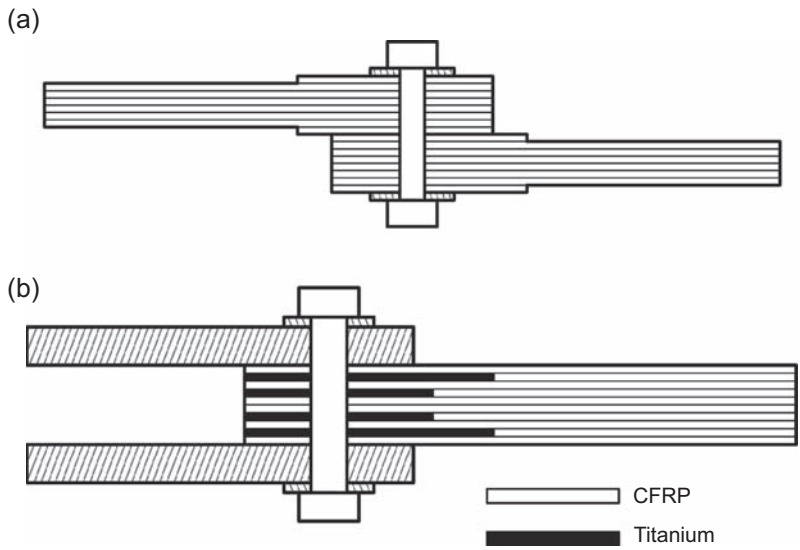

Figure 6.27 Schematic sectional view of: (a) single-lap bolted CFRP joint; (b) double-lap bolted hybrid composite joint with four composite layers locally substituted by titanium plies. Reproduced from: Kolks, G., Tserpes, K.I., 2014. Efficient progressive damage modeling of hybrid composite/titanium bolted joints. Composites Part A: Applied Science and Manufacturing 56, 51−63.

This includes (1) mechanical abrasion (eg, using aluminum oxide sand paper), (2) cleaning the surface using distilled water followed by a water break test to ensure that the bonding surface has achieved a low contact angle needed for wetting by the adhesive, (3) chemical treatment of the mechanically treated surface (eg, chemical etching, phosphoric acid anodizing, chromic acid anodizing, treatment using silane solution or AC-130 sol−gel). Details on manufacturing of FMLs and aluminum surface treatment can be found in Wegman and Van Twisk (2012).

6.5 Damping and vibration properties in hybrid composites

Damping systems (both active and passive) form an integral part of automobiles and aircrafts due to the importance of vibrational loads in the fatigue life of load-bearing structures. For instance, when exposed to high-frequency out-of-plane vibration, standard repairs on the fuselage of typical fighter aircrafts proved to be ineffective (Callinan et al., 2010). The amplitude of vibration is inversely proportional to the square root of the damping ratio; therefore, a highly damped repair can prevent any crack growth on the fuselage (Callinan et al., 2010). Undesirable vibrations in structures can be reduced by increasing the damping capacity (loss tangent, which describes the rate of decay of the vibration amplitude) and/or increasing the stiffness (storage modulus), ie, through passive vibration dumping. A figure of merit for the capability of a structure in vibration reduction is the loss modulus (which relates to the energy dissipation) and is the product of loss tangent and storage modulus (Chung, 2003; Han and Chung, 2012).

Although composites such as CFRP have low density, high modulus and high strength, they have low energy absorption and damping capabilities (Han and Chung, 2012). Lightweight structural composites can provide both high damping and high stiffness if they are properly used in the hybrid form. The loss modulus in a composite can be altered in several ways including the modification of the matrix by including additives such as nanoparticles, the modification of the fibre−matrix interface region through fibre surface treatment, the use of interlaminar additives such as metal or viscoelastic polymer particles, the optimisation of the stacking sequence, or by forming hybrid composites using materials such as viscoelastic interlayers (constrained-layer damping) (Chung, 2003). The vibration damping of CFRP composites can also be improved passively by utilising resistively shunted, surface-bonded piezoelectric ceramic ($PbZrO_3$−$PbTiO_3$) sheets (Rose and Wang, 2001). Vibration loads deform the CFRP beam in bending, which results in electric charge development in the attached PZTs. A resistor dissipates the produced energy in the form of heat, which appears as improvement in the mechanical damping of the beam (Tanimoto, 2007).

Hybrid composites with interleaved viscoelastic materials (VEMs) show higher damping characteristics compared with nonhybrid composites (Chung, 2003; Rao et al., 1997; Berthelot et al., 2008; Tanimoto, 2007; Restuccia and Lofaro, 2013).

For example, the use of VEMs can significantly enhance the loss tangent of CFRP albeit with some stiffness degradation (Chung, 2003). Simultaneous addition of three or more different types of VEM layers in a hybrid composite improves the damping of the composite more than when only one type of VEM is used, showing a synergistic effect (Rao et al., 1997).

The damping loss factor of hybrid CFRP/pyramidal truss sandwich panels increases by embedding VEMs into the CFRP face sheets. Increasing the thickness of the viscoelastic layer results in an increase in the damping loss factor by up to 6.75% (Yang et al., 2013). An interlayer made of a discontinuous nonwoven material that allows resin to flow through the interlayer could be used in lieu of traditional VEMs. The resulting hybrid composites exhibit superior strength compared to the hybrid composites fabricated with continuous or partially continuous damping interlayers (Restuccia and Lofaro, 2013). However, the utilisation of VEMs in hybrid composites results in considerable weight penalty, and therefore reduces weight efficiency (Restuccia and Lofaro, 2013), which is of critical importance to the transport industry.

The addition of nanoparticles such as exfoliated graphite (EG), single-walled carbon nanotubes (SWCNTs), MWNTs, HNTs, SiC nanowhiskers and nanoclay between the layers of CFRP composites is an alternative and emerging approach for increasing the vibration damping performance (Han and Chung, 2012; Khan et al., 2011; Rajoria and Jalili, 2005; Zhou et al., 2004). The loss modulus and loss tangent of the CFRP−MWCNT hybrid nanocomposites increase with the MWCNT content, due to the frictional effects (stick−slip mechanism) at the MWCNT−matrix interface (Khan et al., 2011; Rajoria and Jalili, 2005; Zhou et al., 2004). The stick−slip mechanism is the result of low MWCNT−epoxy adhesion and is explained in detail in Rajoria and Jalili (2005) and Zhou et al. (2004). Weak adhesion in the CNT−epoxy interface results in improved energy dissipation and damping ratio with negligible effect on the stiffness.

The addition of 5 wt% MWCNTs enhances the damping ratio of neat epoxy by up to 700% due to their very high specific surface area with aspect ratio of the order of 10^3. However, further increase of the MWCNTs content does not result in further enhancement in the damping ratio due to clustering of nanoparticles (Rajoria and Jalili, 2005). The size and surface area of the fillers are critical factors in the damping properties of particle-reinforced hybrid composites. For example, a higher loss factor can be achieved by using SWCNTs compared with carbon whiskers and carbon black with similar critical bonding stress (Zhou et al., 2004).

EG as a sole filler is more effective than SWCNTs, MWCNTs, HNTs or nanoclay in enhancing the loss tangent. In addition, the MWCNTs, SiC nanowhiskers and HNTs as sole fillers are effective for increasing the storage modulus. Hybrid nanocomposites simultaneously containing a storage modulus-enhancing filler (eg, MWCNTs, SiC nanowhiskers or HNTs) and a loss tangent-enhancing filler (eg, EG or nanoclay) have both enhanced storage modulus and loss tangent (Han and Chung, 2012). However, in hybrid nano- and/or microcomposites the loss tangent does not follow the rule of mixture and therefore the rule of mixture is considered inaccurate for the calculation of loss tangent (Han and Chung, 2012).

The effect of the nanoparticles on other mechanical properties such as flexural modulus should be considered before using them for damping improvement

(Han and Chung, 2012; Rajoria and Jalili, 2005). For instance, the addition of CNTs in epoxy and its composites results in greater enhancement in damping ratio than the stiffness of the composite (Rajoria and Jalili, 2005). Likewise, hybridisation using EG and HNT increases the loss modulus by 110% with a penalty of 14% reduction in the flexural strength. However, hybridisation using nanoclay and HNT increases the loss modulus by 96% without degrading the flexural strength (Han and Chung, 2012). It should also be noted that the layup of the fibre reinforcements directly influences the effect of nanoparticles. For example, hybridisation of FRPs using nanoparticles is more effective in cross-ply layup than UD layup (Han and Chung, 2012). In addition, the effect of MWCNTs on the damping ratio is more effective in CFRP composites than neat epoxy, although the initial damping ratio of neat epoxy is higher than that of CFRP (Khan et al., 2011).

Loss modulus and damping ratio of UD and QI glass/epoxy composite laminates increase significantly with the addition of 1.0 wt% MWCNTs as shown in Fig. 6.28 (Alnefaie et al., 2013). The damping ratio of the hybrid UD and QI composites is 70.4% and 100% higher compared to the nonhybrid composites, respectively. The enhancements in the damping ratio of hybrid UD and QI composites are about 10 and 14 times higher than the improvement in the hybrid MWCNT/epoxy nanocomposite. The high interfacial friction between microglass fibres−MWCNTs and epoxy−MWCNTs (stick−slip motion) is the reason for improvement in the damping ratio (Alnefaie et al., 2013).

The loss tangent of CFRP composites can also be increased by adding lead zirconate titanate (PZT) particles in the ply interfaces of the composite (Fig. 6.29) (Kim et al., 2011). The increase in the loss tangent is controlled by the joule heat of

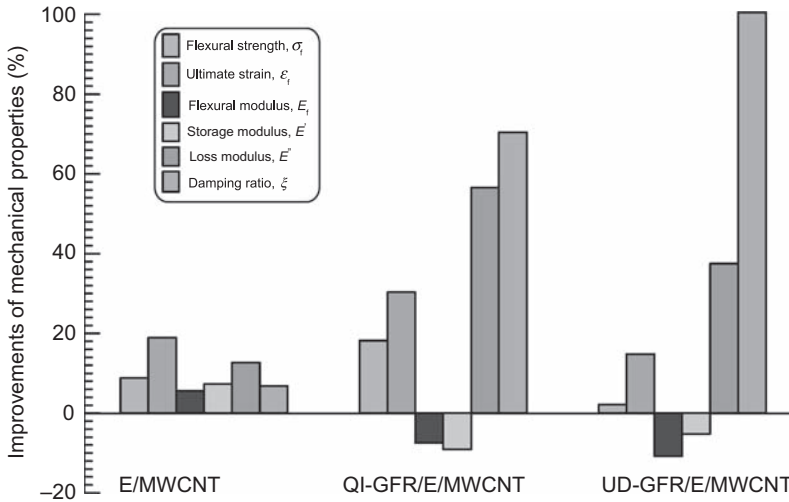

Figure 6.28 Improvements of the mechanical properties of various nanocomposites.
Reproduced from: Alnefaie, K.A., Aldousari, S.M., Khashaba, U.A., 2013. New development of self-damping MWCNT composites. Composites Part A: Applied Science and Manufacturing 52, 1−11.

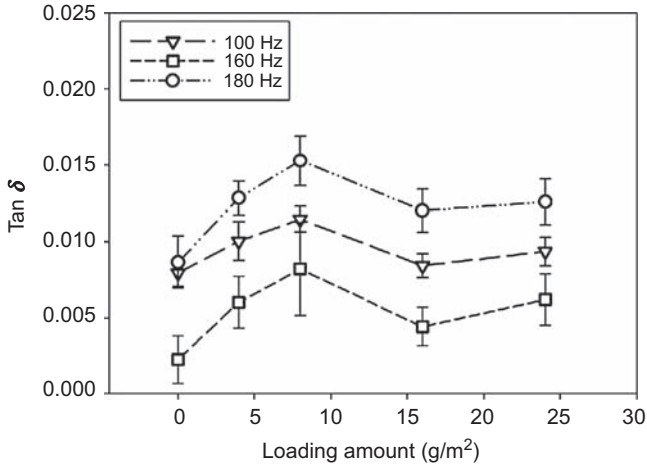

Figure 6.29 Variation in loss factor in CFRP composites with plain PZT particle-enhanced ply interfaces at different frequencies.
Reproduced from: Kim, S.Y., Tanimoto, T., Uchino, K., Nam, C.H., Nam, S., Lee, W.I., 2011. Effects of PZT particle-enhanced ply interfaces on the vibration damping behavior of CFRP composites. Composites Part A: Applied Science and Manufacturing 42, 1477−1482.

electric current between PZT particles and carbon fibres. At a high percentage of PZT particles the increase in loss tangent discontinues due to the incomplete connectivity resulting from particle clustering. When the PZT particle loading exceeds a certain amount, the particles themselves inhibit a connection to the adjacent carbon fibres as shown in Fig. 6.30. However, coating PZT particles with carbon black eliminates the incomplete connectivity by introducing sufficient electrical conductivity on the particle surfaces, which results in a continuous increase of the loss factors with PZT content (Fig. 6.31) (Kim et al., 2011).

A more recent approach for improving the damping performance of composites using nanoparticles is to grow nanoparticles on the surface of microfibres instead of dispersing them into the matrix composites to avoid the nanoparticle clustering during the dispersion process (Alipour Skandani et al., 2012; Tehrani et al., 2013; Tanimoto, 2007). For example, bilayered carbon fibre/ZnO−nanorod/epoxy hybrid composites can be fabricated by growing ZnO nanorods on top of carbon fibres (Fig. 6.32) (Alipour Skandani et al., 2012). The damping performance of such hybrid nanocomposites increases by 50% compared to nonhybrid composites, albeit with a slight decrease (7%) in the storage modulus. The enhanced damping of the hybrid composites is a result of the frictional mechanisms between the ZnO nanorod/epoxy and the nanorod/nanorod interfaces combined with the piezoelectric effect of ZnO (Alipour Skandani et al., 2012). The effect of PZT particles on the tensile modulus and interlaminar shear strength of the CFRP composites is negligible (Tanimoto, 2007).

Likewise, the loss tangent of hybrid nanocomposites fabricated by growing MWCNTs on carbon fibre surfaces is improved by 56% compared with the nonhybrid composites (Tehrani et al., 2013). The energy dissipation in the hybrid MWCNTs

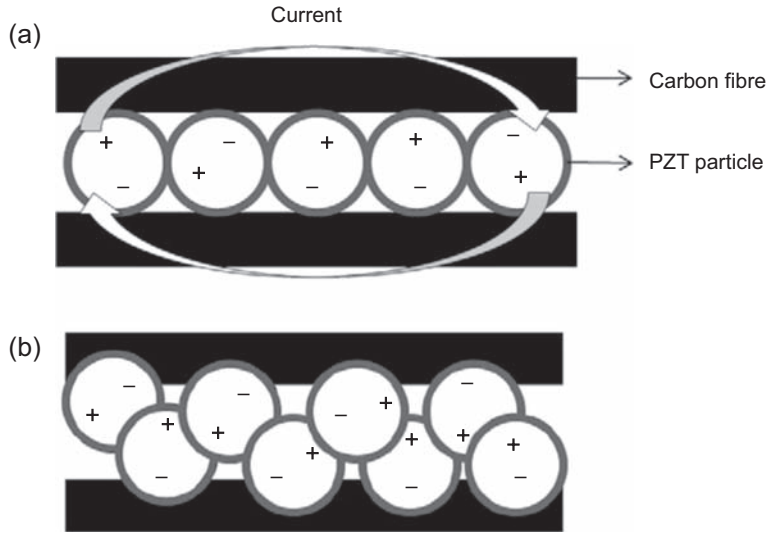

Figure 6.30 (a) At low particle contents the PZT particles are connected to both carbon fibre layers. (b) At high particle contents the PZT particles are connected to one carbon fibre layer. Reproduced from: Kim, S.Y., Tanimoto, T., Uchino, K., Nam, C.H., Nam, S., Lee, W.I., 2011. Effects of PZT particle-enhanced ply interfaces on the vibration damping behavior of CFRP composites. Composites Part A: Applied Science and Manufacturing 42, 1477−1482.

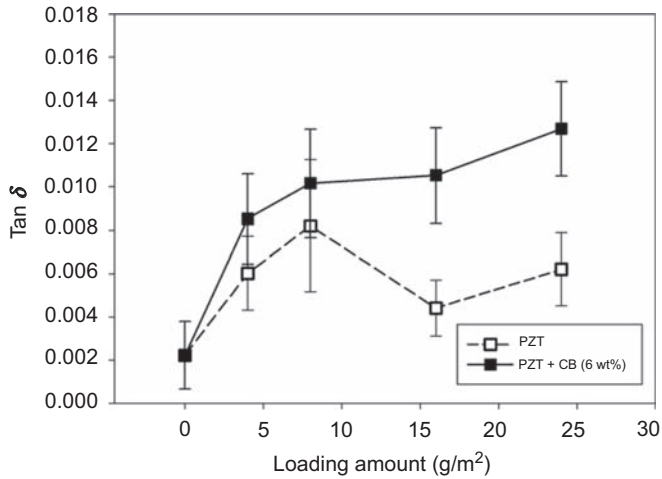

Figure 6.31 Comparison of loss factor for distributing the plain PZT and the carbon black-coated PZT in the ply interfaces of CFRP composites at 160 Hz.
Reproduced from: Kim, S.Y., Tanimoto, T., Uchino, K., Nam, C.H., Nam, S., Lee, W.I., 2011. Effects of PZT particle-enhanced ply interfaces on the vibration damping behavior of CFRP composites. Composites Part A: Applied Science and Manufacturing 42, 1477−1482.

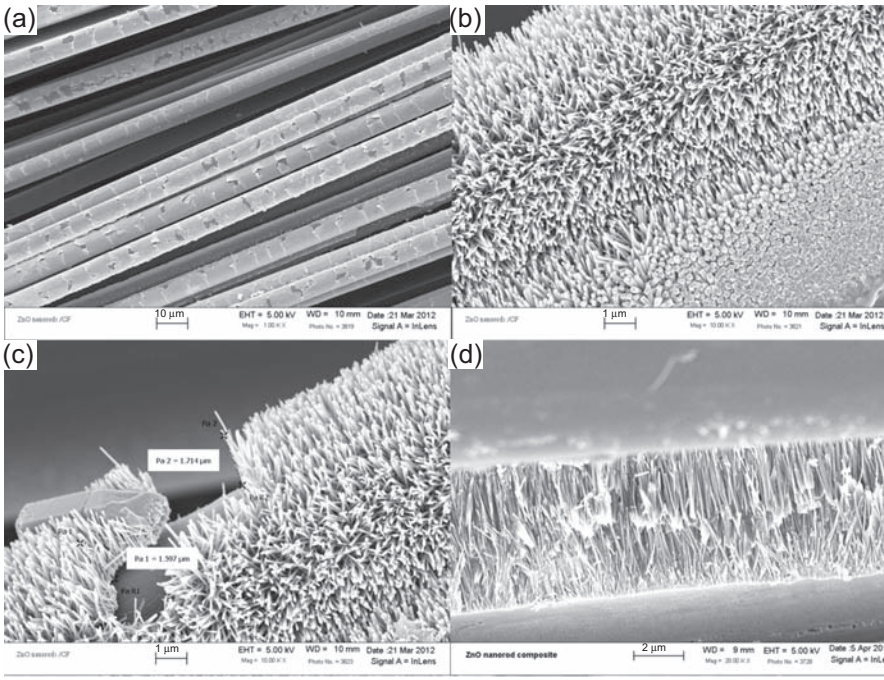

Figure 6.32 SEM micrograph of hydrothermally grown ZnO nanorods (a−c) before and (d) after hand layup process.
Reproduced from: Alipour Skandani, A., Masghouni, N., Case, S.W., Leo, D.J., Al-Haik, M., 2012. Enhanced vibration damping of carbon fibers-ZnO nanorods hybrid composites. Applied Physics Letters 101.

nanocomposites is primarily due to the frictional sliding at the MWCNTs/epoxy interface (Tehrani et al., 2013). Hybrid CFRP composites with a combination of the aforementioned damping techniques are potential candidates for transport applications (eg, automotive and spacecraft components) where high specific stiffness and improved vibration damping are required simultaneously.

6.6 Future research trends

Hybrid fibre-reinforced composites including two types of reinforcements are the most studied among various types of hybrid composites. Their QS properties are well understood; however, the understanding of their impact properties is not yet complete. In addition, despite the well-known advantages of hybrid composites compared to their constituents, their application in aerospace and automotive industries is very limited. Further research in this area should focus on hybridisation using more than two types of fibre reinforcements, which may result in possible synergistic effects or further cost

reduction in practical components. In addition, all possible hybrid configurations (eg, intraply hybrids and 3D woven composites) are not fully explored especially at HSRs. Another trending topic is the use of natural fibres in conjunction with synthetic fibres in hybrid form to further reduce the cost and environmental impact of composite materials especially in the automotive industry.

The current limited literature on HSR properties of nanocomposites shows a great potential for their application in enhancing the energy absorption capability of composite structures. However, the HSR properties of nanoparticle-modified polymers and their fibre-reinforced composites have not been studied comprehensively. In addition, most of the research is focused on the incorporation of carbon-based fillers, especially CNTs, in continuous fibre polymer matrix composites. Hybridisation with other nanoparticles can result in similar enhancements in the mechanical properties with great reduction in the product cost. Further research on the effect of noncarbon-based nanocomposites at impact rates of strain could pave the way towards the application of composite materials in the automotive industry. In addition, the research should focus on the simultaneous use of two or more types of nanoparticles which may result in synergistic enhancement in the material properties.

In the area of FMLs to achieve a comprehensive understanding of their mechanical behaviour, further attention to 3D progressive damage modelling covering HSR effects is necessary. In addition, further fundamental research in mechanical properties such as in-plane shear strength, bearing strength, fatigue behaviour and crack growth rates, notched sensitivity, impact behaviour, delamination and damage characterization are required. Most of the research available in the literature is limited to the commercial types of FMLs; however, innovative materials could be further developed using various metals and composite materials. FMLs with two or more types of composite materials and/or metals may exhibit synergistic effects. While FMLs have attracted a great amount of attention in the aerospace industry, their potential applications in the automotive industry have not yet been fully discovered.

The damping properties of composite materials have been studied in the literature which shows a great potential for application of nanocomposites in aerospace and automotive industries. However, the improvements achieved in damping characteristics of nanocomposites usually result in degradation of other mechanical properties such as strength. To utilise nanocomposites for practical applications hybrid nanocomposites with two or more types of nanoparticles should be further studied since they may provide enhanced damping capacity and unaffected, if not improved, mechanical properties.

Further reading

Readers are further encouraged to study the hybrid textile composites and their characteristics. Great information on different types of hybrid textile composites is provided in Alagirusamy (2010) and Sivasubramanian et al. (2012). To further increase their knowledge on nanoparticle-reinforced hybrid composites, the readers are referred

to a recent book on carbon nanotube-reinforced composites (Paipetis and Kostopoulos, 2013). This book provides a comprehensive knowledge source on this type of hybrid composite including dispersion and functionalization methods for CNTs, their physical properties and some of their important applications. A historical review on FMLs is provided in Vermeeren (2003) and more information on various types of FMLs and their properties can be found in Vlot and Gunnink (2001), Hoo Fatt et al. (2003), Sadighi et al. (2012), and Wu and Yang (2005). A recent review on modelling impact damage of FMLs in Morinière et al. (2014) is a good starting point for those who want to perform computational studies on FMLs.

Acknowledgements

This research was conducted within the Defence Materials Technology Centre, which was established and is supported by the Australian Government's Defence Future Capability Technology Centre (DFCTC) initiative.

References

Abdullah, M.R., Cantwell, W.J., 2006. The impact resistance of polypropylene-based fibre–metal laminates. Composites Science and Technology 66, 1682–1693.

Abdullah, M.R., Cantwell, W.J., 2012. The high velocity impact response of self-reinforced polypropylene fibre metal laminates. In: Tamin, M.N. (Ed.), Damage and Fracture of Composite Materials and Structures. Springer, Berlin, Heidelberg.

Affdl, J.C.H., Kardos, J.L., 1976. The Halpin-Tsai equations: a review. Polymer Engineering & Science 16, 344–352.

Al-Lafi, W., Jin, J., Xu, S., Song, M., 2010. Performance of MWCNT/HDPE nanocomposites at high strain rates. Macromolecular Materials and Engineering 295, 519–522.

Alagirusamy, R., 2010. 12-Hybrid yarns for thermoplastic composites. In: Alagirusamy, R., Das, A. (Eds.), Technical Textile Yarns. Woodhead Publishing.

Albdiry, M.T., Ku, H., Yousif, B.F., 2013. Impact fracture behaviour of silane-treated halloysite nanotubes-reinforced unsaturated polyester. Engineering Failure Analysis 35, 718–725.

Ali, M., Joshi, S., 2013. Damage evolution in glass/epoxy composites engineered using core–shell microparticles under impact loading. Journal of Materials Science 48, 8354–8367.

Alipour Skandani, A., Masghouni, N., Case, S.W., Leo, D.J., Al-Haik, M., 2012. Enhanced vibration damping of carbon fibers-ZnO nanorods hybrid composites. Applied Physics Letters 101.

Alnefaie, K.A., Aldousari, S.M., Khashaba, U.A., 2013. New development of self-damping MWCNT composites. Composites Part A: Applied Science and Manufacturing 52, 1–11.

Aronhime, J., Harel, H., Gilbert, A., Marom, G., 1992. The rate-dependence of flexural shear fatigue and uniaxial compression of carbon- and aramid-fibre composites and hybrids. Composites Science and Technology 43, 105–116.

Atiqah, A., Maleque, M.A., Jawaid, M., Iqbal, M., 2014. Development of kenaf-glass reinforced unsaturated polyester hybrid composite for structural applications. Composites Part B: Engineering 56, 68–73.

Berthelot, J.-M., Assarar, M., Sefrani, Y., Mahi, A.E., 2008. Damping analysis of composite materials and structures. Composite Structures 85, 189−204.

Bittmann, B., Haupert, F., Schlarb, A.K., 2009. Ultrasonic dispersion of inorganic nanoparticles in epoxy resin. Ultrasonics Sonochemistry 16, 622−628.

Botelho, E.C., Pardini, L.C., Rezende, M.C., 2005. Hygrothermal effects on damping behavior of metal/glass fiber/epoxy hybrid composites. Materials Science and Engineering: A 399, 190−198.

Botelho, E.C., Rezende, M.C., Pardini, L.C., 2008. Hygrotermal effects evaluation using the iosipescu shear test for glare laminates. Journal of the Brazilian Society of Mechanical Sciences and Engineering 30, 213−220.

Callinan, R., Wang, C., Galea, S., Sanderson, S., 2010. A generic design procedure for the repair of acoustically damaged panels. In: Ho, S.-Y. (Ed.), Structural Failure Analysis and Prediction Methods for Aerospace Vehicles and Structures. Bentham Science Publishers, United States.

Camanho, P.P., Fink, A., Obst, A., Pimenta, S., 2009. Hybrid titanium−CFRP laminates for high-performance bolted joints. Composites Part A: Applied Science and Manufacturing 40, 1826−1837.

Cao, M.S., Zhou, W., Shi, X.L., Chen, Y.J., 2007. Dynamic response and reinforcement mechanism of composites embedded with tetraneedlelike ZnO nanowhiskers. Applied Physics Letters 91.

Capek, I., 2006. Nanocomposite Structures and Dispersions. Elsevier.

Chen, J.-F., Morozov, E.V., Shankar, K., 2014. Progressive failure analysis of perforated aluminium/CFRP fibre metal laminates using a combined elastoplastic damage model and including delamination effects. Composite Structures 114, 64−79.

Chung, D.D.L., 2003. Structural composite materials tailored for damping. Journal of Alloys and Compounds 355, 216−223.

Davoodi, M.M., Sapuan, S.M., Ahmad, D., Aidy, A., Khalina, A., Jonoobi, M., 2011. Concept selection of car bumper beam with developed hybrid bio-composite material. Materials & Design 32, 4857−4865.

Davoodi, M.M., Sapuan, S.M., Ahmad, D., Ali, A., Khalina, A., Jonoobi, M., 2010. Mechanical properties of hybrid kenaf/glass reinforced epoxy composite for passenger car bumper beam. Materials & Design 31, 4927−4932.

Ghalami-Choobar, M., Sadighi, M., 2014. Investigation of high velocity impact of cylindrical projectile on sandwich panels with fiber−metal laminates skins and polyurethane core. Aerospace Science and Technology 32, 142−152.

Gómez-Del Río, T., Rodríguez, J., Pearson, R.A., 2014. Compressive properties of nanoparticle modified epoxy resin at different strain rates. Composites Part B: Engineering 57, 173−179.

Grujicic, M., Pandurangan, B., Koudela, K.L., Cheeseman, B.A., 2006. A computational analysis of the ballistic performance of light-weight hybrid composite armors. Applied Surface Science 253, 730−745.

Han, S., Chung, D.D.L., 2012. Mechanical energy dissipation using carbon fiber polymer−matrix structural composites with filler incorporation. Journal of Materials Science 47, 2434−2453.

Henry, C.A., 2009. The Incorporation of Nanomaterials into Polymer Media. Polymer Nanocomposites Handbook. CRC Press.

Hoo Fatt, M.S., Lin, C., Revilock Jr., D.M., Hopkins, D.A., 2003. Ballistic impact of GLARE™ fiber−metal laminates. Composite Structures 61, 73−88.

Hu, Y., Liu, T., Ding, J.L., Zhong, W.H., 2013. Behavior of high density polyethylene and its nanocomposites under static and dynamic compression loadings. Polymer Composites 34, 417−425.

Jindal, P., 2013. Compressive strain behaviour under different strain rates in multi-walled carbon nanotubes-polycarbonate composites. Journal of Material Science and Engineering 2, 2169−0022.1000.

Jindal, P., Pande, S., Sharma, P., Mangla, V., Chaudhury, A., Patel, D., Singh, B.P., Mathur, R.B., Goyal, M., 2013. High strain rate behavior of multi-walled carbon nanotubes−polycarbonate composites. Composites Part B: Engineering 45, 417−422.

Kandare, E., Khatibi, A.A., Yoo, S., Wang, R., Ma, J., Olivier, P., Gleizes, N., Wang, C.H., 2014. Improving the through-thickness thermal and electrical conductivity of carbon/epoxy laminates by exploiting synergy between graphene and silver nano-inclusions. Composites Part A 69, 72−82.

Khan, S.U., Li, C.Y., Siddiqui, N.A., Kim, J.-K., 2011. Vibration damping characteristics of carbon fiber-reinforced composites containing multi-walled carbon nanotubes. Composites Science and Technology 71, 1486−1494.

Kim, S.Y., Tanimoto, T., Uchino, K., Nam, C.H., Nam, S., Lee, W.I., 2011. Effects of PZT particle-enhanced ply interfaces on the vibration damping behavior of CFRP composites. Composites Part A: Applied Science and Manufacturing 42, 1477−1482.

Kim, W., Argento, A., Lee, E., Flanigan, C., Houston, D., Harris, A., Mielewski, D.F., 2012. High strain-rate behavior of natural fiber-reinforced polymer composites. Journal of Composite Materials 46, 1051−1065.

Kolesnikov, B., Herbeck, L., Fink, A., 2008. CFRP/titanium hybrid material for improving composite bolted joints. Composite Structures 83, 368−380.

Kolks, G., Tserpes, K.I., 2014. Efficient progressive damage modeling of hybrid composite/titanium bolted joints. Composites Part A: Applied Science and Manufacturing 56, 51−63.

LANXESS Deutschland GmbH, 2004. Ford Focus van features hybrid metal/composite front-end. Reinforced Plastics, September 2004, p. 4.

Liang, Y.L., Pearson, R.A., 2010. The toughening mechanism in hybrid epoxy-silica-rubber nanocomposites (HESRNs). Polymer 51, 4880−4890.

Liao, C.Z., Tjong, S.C., 2012. Mechanical and thermal performance of high-density polyethylene/alumina nanocomposites. Journal of Macromolecular Science, Part B 52, 812−825.

Liu, H.-Y., Wang, G.-T., Mai, Y.-W., Zeng, Y., 2011. On fracture toughness of nano-particle modified epoxy. Composites Part B: Engineering 42, 2170−2175.

Lv, L., Sun, B., Qiu, Y., Gu, B., 2006. Energy absorptions and failure modes of 3D orthogonal hybrid woven composite struck by flat-ended rod. Polymer Composites 27, 410−416.

Ma, P., Zhang, F., Gao, Z., Jiang, G., Zhu, Y., 2014. Transverse impact behaviors of glass warp-knitted fabric/foam sandwich composites through carbon nanotubes incorporation. Composites Part B: Engineering 56, 847−856.

Mansor, M.R., Sapuan, S.M., Zainudin, E.S., Nuraini, A.A., Hambali, A., 2013. Hybrid natural and glass fibers reinforced polymer composites material selection using analytical hierarchy process for automotive brake lever design. Materials & Design 51, 484−492.

Morinière, F., Alderliesten, R., Tooski, M., Benedictus, R., 2012a. Damage evolution in GLARE fibre-metal laminate under repeated low-velocity impact tests. Central European Journal of Engineering 2, 603−611.

Morinière, F.D., Alderliesten, R.C., Benedictus, R., 2012b. Development of fibre-metal laminates for improved impact performance. The European Physical Journal Special Topics 206, 79−88.

Morinière, F.D., Alderliesten, R.C., Benedictus, R., 2013a. Low-velocity impact energy partition in GLARE. Mechanics of Materials 66, 59−68.

Morinière, F.D., Alderliesten, R.C., Benedictus, R., 2014. Modelling of impact damage and dynamics in fibre-metal laminates − a review. International Journal of Impact Engineering 67, 27−38.

Morinière, F.D., Alderliesten, R.C., Sadighi, M., Benedictus, R., 2013b. An integrated study on the low-velocity impact response of the GLARE fibre-metal laminate. Composite Structures 100, 89−103.

Muhi, R.J., Najim, F., De Moura, M.F.S.F., 2009. The effect of hybridization on the GFRP behavior under high velocity impact. Composites Part B: Engineering 40, 798−803.

Mujika, F., Vargas, G., Ibarretxe, J., De Gracia, J., Arrese, A., 2012. Influence of the modification with MWCNT on the interlaminar fracture properties of long carbon fiber composites. Composites Part B: Engineering 43, 1336−1340.

Mutasher, S.A., 2009. Prediction of the torsional strength of the hybrid aluminum/composite drive shaft. Materials & Design 30, 215−220.

Naik, N.K., Ch, V., Kavala, V.R., 2008. Hybrid composites under high strain rate compressive loading. Materials Science and Engineering: A 498, 87−99.

Naik, N.K., Pandya, K.S., Kavala, V.R., Zhang, W., Koratkar, N.A., 2014. Alumina nanoparticle filled epoxy resin: high strain rate compressive behavior. Polymer Engineering & Science 54 (12), 2890−2901.

Paipetis, A., Kostopoulos, V., 2013. Carbon Nanotube Enhanced Aerospace Composite Materials. Springer.

Pandya, K.S., Dharmane, L., Pothnis, J.R., Ravikumar, G., Naik, N.K., 2012. Stress wave attenuation in composites during ballistic impact. Polymer Testing 31, 261−266.

Pandya, K.S., Pothnis, J.R., Ravikumar, G., Naik, N.K., 2013. Ballistic impact behavior of hybrid composites. Materials & Design 44, 128−135.

Pol, M.H., Liaghat, G.H., Hajiarazi, F., 2013. Effect of nanoclay on ballistic behavior of woven fabric composites: experimental investigation. Journal of Composite Materials 47, 1563−1573.

Rajoria, H., Jalili, N., 2005. Passive vibration damping enhancement using carbon nanotube-epoxy reinforced composites. Composites Science and Technology 65, 2079−2093.

Rao, M.D., Echempati, R., Nadella, S., 1997. Dynamic analysis and damping of composite structures embedded with viscoelastic layers. Composites Part B: Engineering 28, 547−554.

Restuccia, C.L., Lofaro, C., 2013. Structural Composite Material with Improved Acoustic and Vibrational Damping Properties. Google Patents.

Reyes Villanueva, G., Cantwell, W.J., 2004. The high velocity impact response of composite and FML-reinforced sandwich structures. Composites Science and Technology 64, 35−54.

Rong, J.-L., Wang, X., Cao, M.-S., Xu, T.-F., 2010. Dynamic fracture toughness and failure mechanisms of ZnO whiskers secondary reinforced composites. Chinese Physics Letters 27, 086201.

Rose, L., Wang, C., 2001. Modelling and optimisation of passive damping for bonded repair to acoustic fatigue cracking. In: IUTAM Symposium on Smart Structures and Structronic Systems, pp. 49−56.

Sadighi, M., Alderliesten, R.C., Benedictus, R., 2012. Impact resistance of fiber-metal laminates: a review. International Journal of Impact Engineering 49, 77−90.

Saka, K., Harding, J., 1987. The deformation and fracture of hybrid reinforced composites under tensile impact. In: Kawata, K., Shioiri, J. (Eds.), Macro- and Micro-mechanics of High Velocity Deformation and Fracture. Springer, Berlin Heidelberg.

Sevkat, E., 2012. Experimental and numerical approaches for estimating ballistic limit velocities of woven composite beams. International Journal of Impact Engineering 45, 16−27.

Seyed Yaghoubi, A., Liaw, B., 2012. Thickness influence on ballistic impact behaviors of GLARE 5 fiber-metal laminated beams: experimental and numerical studies. Composite Structures 94, 2585−2598.

Seyed Yaghoubi, A., Liaw, B., 2013. Effect of lay-up orientation on ballistic impact behaviors of GLARE 5 FML beams. International Journal of Impact Engineering 54, 138−148.

Seyed Yaghoubi, A., Liu, Y., Liaw, B., 2011. Low-velocity impact on GLARE 5 fiber-metal laminates: influences of specimen thickness and impactor mass. Journal of Aerospace Engineering 25, 409−420.

Silva, D., Botelho, E., Ancelotti, A., Damato, C., 2013a. Environmental conditioning effects on the mechanical properties of titanium fiber-metal laminates. In: Composite Materials, 19th International Conference on, July 28−August 2, 2013, pp. 7828−7836.

Silva, F., Njuguna, J., Sachse, S., Pielichowski, K., Leszczynska, A., Giacomelli, M., 2013b. The influence of multiscale fillers reinforcement into impact resistance and energy absorption properties of polyamide 6 and polypropylene nanocomposite structures. Materials & Design 50, 244−252.

Sinmazçelik, T., Avcu, E., Bora, M.Ö., Çoban, O., 2011. A review: fibre metal laminates, background, bonding types and applied test methods. Materials & Design 32, 3671−3685.

Sivasubramanian, P., Pothan, L.A., Thiruchitrambalam, M., Thomas, S., 2012. Hybrid Textile Polymer Composites. Polymer Composites. Wiley-VCH Verlag GmbH & Co. KGaA.

Sun, B., Gu, B., 2006. Shear behavior of 3D orthogonal woven fabric composites under high strain rates. Journal of Reinforced Plastics and Composites 25, 1833−1845.

Sung-Choong, W., Tae-Won, K., Jin-Young, K., 2013. Notice of Retraction Rate-dependent behavior and failure characteristics of carbon/Kevlar hybrid woven composites. In: Quality, Reliability, Risk, Maintenance, and Safety Engineering (QR2MSE), 2013 International Conference on, July 15−18, 2013, pp. 808−812.

Tang, L.-C., Zhang, H., Sprenger, S., Ye, L., Zhang, Z., 2012. Fracture mechanisms of epoxy-based ternary composites filled with rigid-soft particles. Composites Science and Technology 72, 558−565.

Tanimoto, T., 2007. A new vibration damping CFRP material with interlayers of dispersed piezoelectric ceramic particles. Composites Science and Technology 67, 213−221.

Tehrani, M., Safdari, M., Boroujeni, A.Y., Razavi, Z., Case, S.W., Dahmen, K., Garmestani, H., Al-Haik, M.S., 2013. Hybrid carbon fiber/carbon nanotube composites for structural damping applications. Nanotechnology 24, 155704.

Tsai, J.-L., Cheng, Y.-L., 2009. Investigating silica nanoparticle effect on dynamic and quasi-static compressive strengths of glass fiber/epoxy nanocomposites. Journal of Composite Materials 43, 3143−3155.

Vaidya, U.K., Hosur, M.V., 2003. High strain rate impact response of graphite/epoxy composites with polycarbonate facing. Journal of Thermoplastic Composite Materials 16, 75−95.

Vaidya, U.K., Kulkarni, M., Hosur, M.V., Mayer, A., Dutta, P., 2001. High strain rate response of S2-glass/epoxy composites with polycarbonate facing. Polymers & Polymer Composites 9, 67−80.

Vermeeren, C.A.J.R., 2003. An historic overview of the development of fibre metal laminates. Applied Composite Materials 10, 189−205.

Vlot, A., 1993. Impact properties of fibre metal laminates. Composites Engineering 3, 911−927.

Vlot, A., 1996. Impact loading on fibre metal laminates. International Journal of Impact Engineering 18, 291−307.

Vlot, A., Gunnink, J.W., 2001. Fibre Metal Laminates: An Introduction. Springer.
Wegman, R.F., Van Twisk, J., 2012. Surface Preparation Techniques for Adhesive Bonding. Elsevier Science.
Wu, G., Yang, J.M., 2005. The mechanical behavior of GLARE laminates for aircraft structures. JOM 57, 72−79.
Yang, J., Xiong, J., Ma, L., Wang, B., Zhang, G., Wu, L., 2013. Vibration and damping characteristics of hybrid carbon fiber composite pyramidal truss sandwich panels with viscoelastic layers. Composite Structures 106, 570−580.
Zhang, J., Chaisombat, K., He, S., Wang, C.H., 2012. Hybrid composite laminates reinforced with glass/carbon woven fabrics for lightweight load bearing structures. Materials & Design 36, 75−80.
Zhou, X., Shin, E., Wang, K.W., Bakis, C.E., 2004. Interfacial damping characteristics of carbon nanotube-based composites. Composites Science and Technology 64, 2425−2437.
Zhu, S., Chai, G.B., 2012. Low-velocity impact response of fibre−metal laminates − experimental and finite element analysis. Composites Science and Technology 72, 1793−1802.

This page intentionally left blank

Thermoset resin sandwich structures

7

S. Zainuddin, M.V. Hosur, A.A. Mohammed, E.M. Smith, S. Jeelani
Tuskegee University, Tuskegee, AL, United States

7.1 Introduction

Thermoset resin-based sandwich structures are increasingly used in aerospace, marine, automotive, transportation, and other high technology industries. A few examples of such applications are helicopter blades, optical benches for space applications, nonferrous ship hulls, Raytheon's Premier I, Lockheed-Martin's X-33, and future tilt rotors by Boeing Defense and Space Group, Helicopter Division are some of the applications [1]. Typically, sandwich composites in these applications use thin face sheets bonded to honeycomb or foam cores. The main advantage of sandwich structures is their ability to provide increased bending rigidity without significant increase in structural weight. Other benefits of sandwich structures include excellent thermal insulation, acoustic damping, fire retardation, ease of machining, ease of forming, etc.

A major concern that limits the usage of thermoset sandwich structures is their susceptibility to damage due to impact loading. There are practical situations such as tool drops, runway debris, bird strikes, hailstorms, and others. The impact of a foreign object on sandwich structures can induce damage to the facings, the core material, and the core−facing interface [2]. Damage initiation thresholds and damage size depend on the properties of the core materials, face sheets, and the relationship between the properties of the cores and those of the facings. Much of the earlier work involved in the study on sandwich composites under impact loading focused on the honeycomb core sandwich constructions [3−8]. Usually honeycomb cores are made out of aluminum or out of composite materials: Nomex, glass thermoplastic, or glass phenolic. One of the problems in the honeycomb sandwich constructions is the low surface area of core for bonding. For impacts, damage is confined to the top facing, the core−top facing interface, and the core. The other most commonly used core materials are expanded foams, which are often thermoset to achieve reasonably high thermal tolerance, though thermoplastic foams are also used. One of the advantages of foam cores is the increased support surface for bonding with the face sheets. The response of foam core sandwich constructions to impact loading is studied by many investigators [9−15]. The response of the foam core sandwich composites depends on the density and the modulus of the foam [12,13]. Shear fracture was found to occur in poly(vinyl chloride) (PVC)/polyurethane (PU) system-based brittle core materials. In contrast, buckling failures in the uppermost composite skin were observed in the intermediate modulus systems, whereas initial damage in the higher modulus PVC/PU systems took the form of delamination within the top surface skin.

Lightweight Composite Structures in Transport. http://dx.doi.org/10.1016/B978-1-78242-325-6.00007-4

In recent years, there has been a growing emphasis on improving the properties of thermoset polymers and foam materials through the inclusion of a small amount of nanoparticles such as carbon nanotubes and nanofibers, TiO_2, and nanoclays to improve the materials properties [16–25]. Nano-infused polymeric materials have gained interest due to their unique behavior in mechanical and thermal properties over their neat counterparts. A number of publications can be found on nanoparticle-infused polymers where the investigators have reported that nanophased polymer systems exhibit enhanced mechanical and thermal properties as compared with pure polymer systems. There have been a couple of studies reported in open literature on the effect of nanoclay on polymeric foams. Benedicte et al. [22] reported the study of poly (ε-caprolactone)/clay nanocomposites prepared by melt intercalation. In their study, they reported that stiffness and thermal stability were increased with clay loading up to 5%. Cao et al. [23] used the organoclay to modify the PU and found an increase in thermal and mechanical properties such as glass transition temperature, compressive strength, and moduli. They concluded that the presence of clay results in an increase in cell density and a reduction of cell size compared to pure PU foam. Uddin et al. [24] infused three different types of nanoparticles, namely TiO_2, carbon nanofibers, and carbon nanotube to modify rigid PU foams, and studied their static and high strain rate properties. They reported significant improvement in the failure strength and energy absorption in nanophased PU foams. However, the nanoparticles used by Uddin et al. [24] are very expensive. On the other hand, nanoclay is widely available and is very cheap. Mohammed et al. [25] fabricated PU foams with nanoclay and obtained significant improvement in their thermal, flexural, static, and high strain rate properties. Though there have been some studies in the processing and characterization of nanophased foams, their usage in sandwich construction has been very limited. Mahfuz et al. [17] used TiO_2 nanoparticles in fabricating nanophased PU foams for sandwich construction. They characterized the flexural response of the nanophased sandwich and obtained 53% increase in the load-carrying capacity over the neat foam sandwich. However, their study has been limited to the evaluation of static properties only.

It is clear from the literature review that there is a need for developing stronger sandwich composites especially for applications where they are subjected to impact loading. Hence, the current work is focused on developing stronger sandwich composites by utilizing the benefits of nanoclay through its addition in both foam core and face sheets. PU foams core were made using 0.5% and 1% by weight of Nanocor® I-28E nanoclay. Sandwich composites with these cores were fabricated with three-layered plain weave carbon/SC-15 epoxy laminate face sheets with 1% and 2% by weight nanoclay loading. In addition, sandwich composites with neat foam core and face sheets (without the addition of nanoclay) were also fabricated for baseline comparison. Samples were precisely cut from these composite panels and tested under impact loading at 15, 30, and 45 J, respectively. Impact damage was characterized through microscopic studies.

7.2 Experimental

7.2.1 Synthesis of nanophased foam

PU foam was prepared with two different weight percentages of nanoclay, namely 0.5% and 1%. Because of the low density of nanoclay, low weight percentages were selected for infusion to avoid the agglomeration of nanoparticles in PU foam. The fabrication of nanophased PU foam was carried out in two steps; the first was the doping of liquid PU with nanoparticles and the second, casting of the foam. The density of the liquid foam (Utah Foam Products) used in this investigation, as specified by the supplier, was 240 kg/m^3. It has two parts. Part A is diphenylmethane diisocyanate and part B is polyol. The mixing ratio of part A and B is 52:48 by weight. Part A was selected for infusion of nanoparticles since it is less reactive and has lower viscosity. Nanocor® I-28E, organically modified clay, was first carefully measured along with part A to have a specific percentage of loading by weight. The mixing was carried out by irradiation with a high-intensity ultrasonic horn (Ti-horn, 20 kHz, and 100 W/cm^2) in open air for 30 min at room temperature. To avoid temperature rise during sonication, external cooling was employed by submerging the mixing beaker in a cooling bath maintained at 5°C. After infusion, the modified part A was mixed with part B by using a mechanical stirrer at 2500 rpm. After mixing the part A and part B, the mixture was poured into a rectangular mold and sandwiched (clamped) in a hot press as illustrated in Fig. 7.1. Hot press temperature was maintained at 38°C and a load of 2.5 kN was applied. After 4−5 h, mold was taken out from the hot press and demolded to obtain a PU foam product, a sample of which is shown in Fig. 7.2.

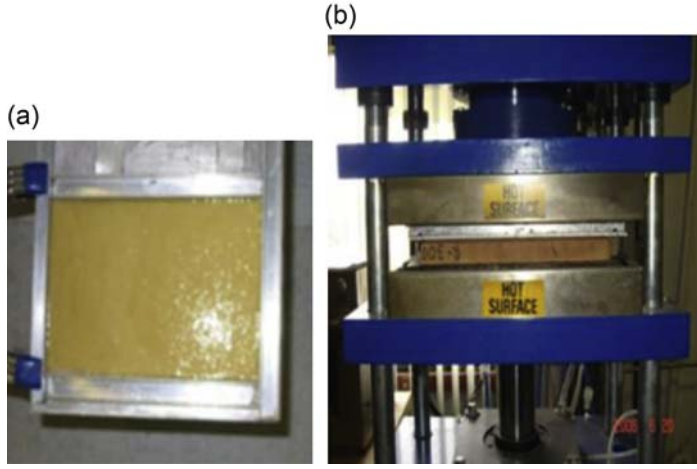

Figure 7.1 (a) Casting of the foam panel in a mold, and (b) placement of mold in the press.

Figure 7.2 Polyurethane foam core.

7.2.2 Fabrication of sandwich panels with nanophased face sheets

Plain weave carbon fabric was used as the fiber material and SC-15 epoxy resin was selected as the matrix. SC-15 was obtained from Applied Poleramic, Inc. It has two parts, part A (epoxy) and part B (hardener, alkyl polyamine). Part A itself is a mixture of three components, namely diglycidyl ether of bisphenol A, aliphatic diglycidyl ether, and epoxy toughener. Sandwich panels were manufactured using the coinjection resin transfer molding process to infuse the resin simultaneously into the fabrics for both the top and the bottom face sheets. For nanoclay face sheet sandwich structures, part A of SC-15 epoxy resin was doped with the desired weight percentage of nanoclay in it. The mixing was carried out by irradiation with a high-intensity ultrasonic horn (Ti-horn, 20 kHz, and 100 W/cm^2) in open air for 30 min at room temperature, as explained for doping of PU foam. To avoid temperature rise during sonication, external cooling was employed by submerging the mixing beaker in a cooling bath maintained at 5°C. This homogenized solution of resin was then mixed with part B (hardener) at a ratio of 10:3 by a high-speed mechanical stirrer for about 10 min just before the infusion.

For the sandwich fabrication, an aluminum plate was laid on a flat surface. A mold release agent was applied on the surface of the mold and a nonporous Teflon layer was placed over the mold to allow easy release of the panel. Then a layer of distribution mesh was laid on the nonporous Teflon layer. Three layers of plain weave carbon fabrics were then laid over the distribution mesh to form a bottom face sheet. The PU foam core was then placed on the top of the bottom face sheet fabrics. Three layers of woven carbon fabrics were then laid over the core to form the top face sheet. Another porous Teflon layer and a distribution mesh were laid on the top face sheet fabrics. After stacking, the complete assembly was covered with a heat-resistant vacuum bag, and two infusion lines (one for the top face sheet and the other for the bottom face sheet) and one suction line were installed. The entire assembly was subjected to vacuum to drive away any trapped air by opening the vacuum line while closing the resin infusion line. A premixed quantity of resin was then infused into the assembly

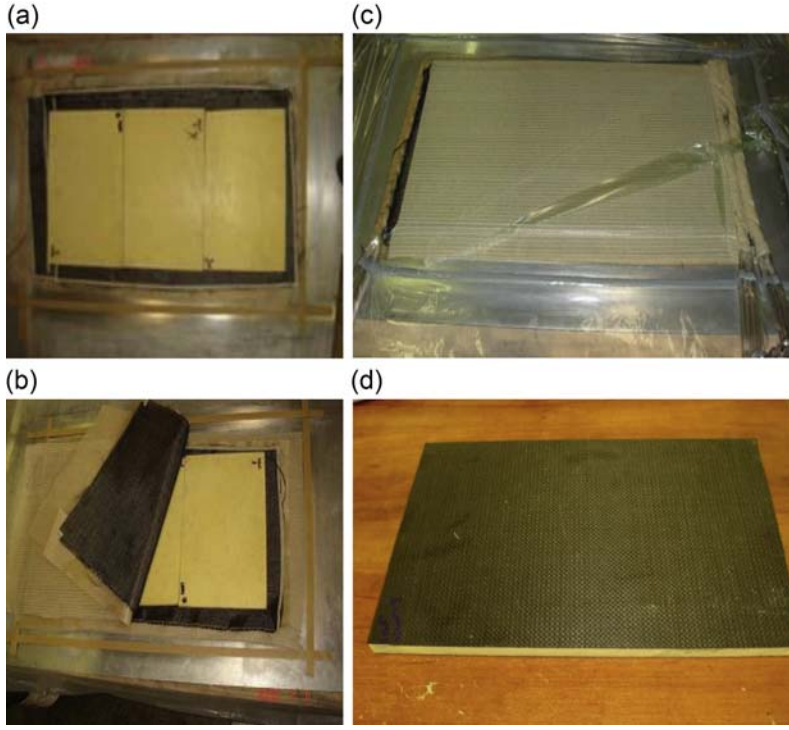

Figure 7.3 Fabrication of sandwich composites with nanophased core: (a) layup of core over the bottom face sheet fabrics; (b) placement of top face sheet fabric over the core; (c) vacuum bagging and resin infusion, and (d) finished sandwich panel.

by opening the infusion line. Resin was drawn into the assembly by the vacuum. After resin was completely infused, the infusion line was sealed and kept under vacuum for 24 h to obtain the sandwich panel. Details of the fabrication are depicted in Fig. 7.3.

7.2.3 Low-velocity impact testing

All the impact tests in this study were conducted using an instrumented impact drop tower device—DYNATUP Model 8210. DYNATUP is equipped with the Impulse data acquisition system, version 3. Impulse v.3 can acquire 8192 data points. Using this machine, impact energy and velocity can be varied by changing the mass and height of the dropping weight. During the testing, the specimen was held under clamped edge conditions in the fixture placed at the bottom of the drop tower which provided a clamped circular support span of 75 mm in diameter. The weight of the cross head was maintained at 6.62 kg and it was guided through two smooth guide columns. The impactor end of the drop mass was fitted with a 12.7 mm instrumented tup with hemispherical end having a capacity of 15.56 kN to record the transient response of the specimens. To carry out the impact tests, 100 × 100 mm composite samples

were placed between the pneumatic clamps. Heights were adjusted depending on the desired energy level. The height is the distance between the tip of the indenter and the top surface of the samples held between the pneumatic clamps. Once the height required to attain a particular energy level was known, the indenter was moved accordingly to that height before it was dropped on the specimen for the test. The machine is also fitted with a velocity detector that measures the velocity of the tup just before it strikes the specimen. It is also fitted with a pneumatic rebound brake, which prevents multiple impacts on the specimen.

Transient responses of the samples included velocity, deflection, load, and energy as function of time. From the transient response data, load and energy versus time response curves were plotted at different energies and superimposed for comparison. Impact parameters such as peak load, absorbed energy, time to peak load, and deflection at peak load were extracted from the curves and tabulated. For each type of laminate, at least three samples were subjected to impact at 15, 30, and 45 J. The data were analyzed in terms of peak load and absorbed energy. The absorbed energy is calculated as the difference of total energy (at the end of the event) and the energy at peak load. The impact energy is, in general, mainly absorbed in the form of elastic deformation, plastic deformation, and through various damage modes. As composite materials have no plastic deformation, all the energy is absorbed through elastic deformation and through different failure modes. Hence, in the current study, absorbed energy is attributed to the energy spent in creating damage.

7.2.4 Optical microscopy

One sample from each type at each energy level was cut into two halves and scanned using a scanner. Further, the impact region was studied under an optical micrograph to investigate the failure modes of the sample. The optical microscopy was performed using Unitron ZST (Zoom Stereo Trinocular) from Excel Technologies Inc. This microscope features a 6.5:1 ratio, continuously variable zoom objective system 0.7X to 4.5X at a constant long working distance of 86 mm, which enables investigation of the crack or fracture. The fractured surfaces were exposed to the optical microscope, using polarized light.

7.2.5 Scanning electron microscopy

Scanning electron microscopy (SEM) studies were carried out using a JEOL-JSM 5800. One sample from each set impacted at 30 J was observed under SEM to understand the deformation and failure behavior at various magnifications.

7.3 Results and discussion

The impact response of sandwich structures with and without nanoclay cores was evaluated. Three samples of each set were tested at energy levels of 15, 30, and 45 J.

Transient data were collected for each sample, which included time, load, energy, velocity, and deflection. Failure modes were studied through microscopic examination of the samples.

7.3.1 A 1% nanoclay face sheet sandwich

Load and energy versus time plots of representative samples with a 1% nanoclay face sheet with neat, 0.5%, and 1% nanoclay cores at 15, 30, and 45 J are shown in Figs. 7.4–7.6. Average values of the impact parameters of samples are given in Table 7.1. A qualitative indication of severe damage in the sample is given by a sharp load drop. A localized damage may not exhibit a sharp load drop. However, a qualitative indication of localized damage can be visualized through the change in the slope of the load–time curve. It is noticeable from Fig. 7.4 that all the three types of samples exhibited localized damage, which was evident from the change in the slope of load–time curves. This was noted at a load of around 1.2–1.5 kN, with the neat core sandwich having a lower value. This means that damage initiation occurred at much lower load for the neat core sandwich than the nanophased core sandwich samples. From Table 7.1, it is seen that the average peak load at 15 J for the neat core sandwich samples was 1.79 kN and it was 1.98 kN for the 0.5% and 1% nanophased core sandwich samples. The deflection at peak load is a qualitative indication of the stiffness of the material. It is seen from the table that the neat core sandwich samples had higher deflection at peak load. In addition, the total time and the time to peak load were also higher for the neat core sandwich samples. These two parameters are direct indications of the stiffness of the sample. Samples which are more compliant take more time to complete the impact event and also deflect more, which in the current case

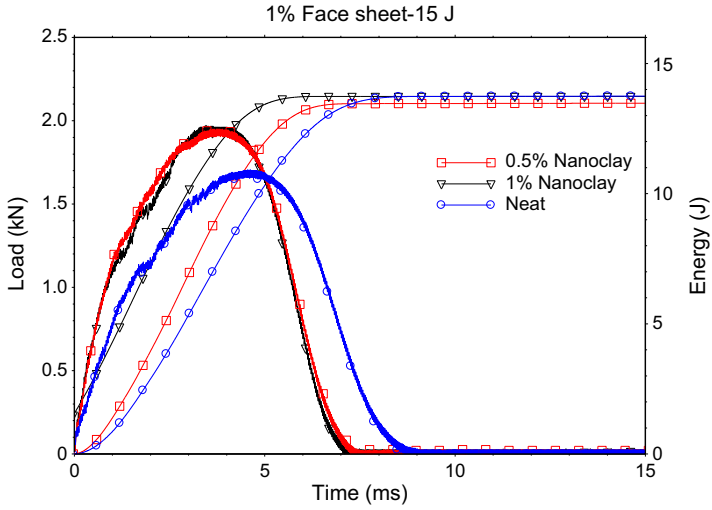

Figure 7.4 Load and energy versus time plot for 1% face sheet sandwiches with neat and nanoclay cores impacted at 15 J.

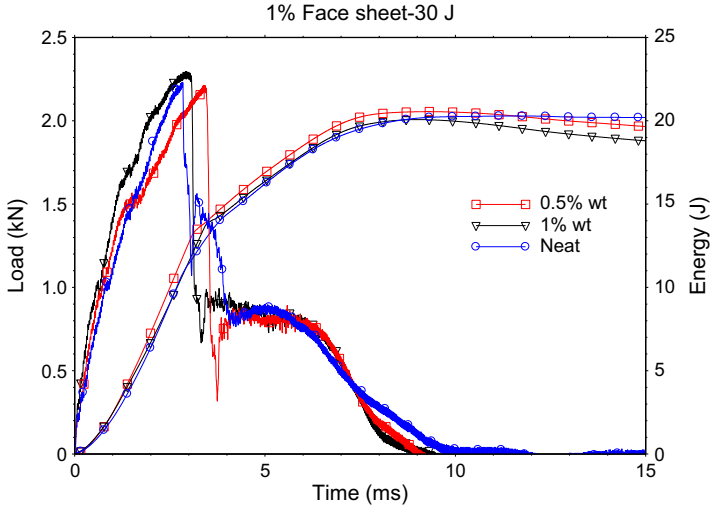

Figure 7.5 Load versus deflections plot for 1% face sheet sandwiches with neat and nanoclay cores impacted at 30 J.

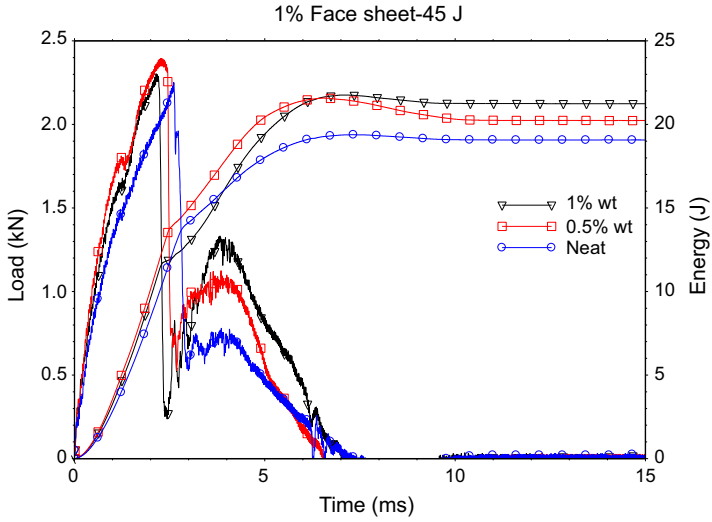

Figure 7.6 Load and energy versus time plot for 1% face sheet sandwiches with neat and nanoclay cores impacted at 45 J.

were neat foam core sandwich samples. Absorbed energy was, however, within a close range for all the samples. The energy absorption in any material under impact loading is mainly through the elastic deformation in the initial stage, with some energy absorbed through friction. Once the energy level is beyond the level required for maximum elastic deformation, the sample will absorb the excess energy in the form

Table 7.1 Average impact parameters for 1% face sheet sandwich with neat and nanoclay core samples impacted at 15, 30, and 45 J

Type of core	Impact energy (J)	Peak load (kN)	Deflection at peak load (mm)	Energy to max load (J)	Total energy (J)	Impact velocity (m/s)	Total time (ms)	Absorbed energy (J)	Time to max load (ms)
Neat	14.91	1.79	7.74	9.02	13.69	2.12	8.35	4.67	4.13
0.5%	14.97	1.98	6.85	9.02	13.69	2.126	7.22	4.66	3.68
1%	14.72	1.978	6.78	8.73	13.44	2.10	7.03	4.70	3.63
Neat	29.52	2.30	8.89	12.87	20.67	2.98	11.08	7.79	3.25
0.5%	29.46	2.22	8.81	12.45	19.62	2.98	8.80	7.17	3.21
1%	29.54	2.36	8.56	13.63	23.08	2.98	8.76	9.44	3.15
Neat	44.62	2.19	8.73	12.52	19.45	3.67	6.43	6.93	2.51
0.5%	44.57	2.26	7.02	10.09	19.07	3.66	6.53	8.97	1.99
1%	44.60	2.24	7.32	10.37	20.29	3.67	6.55	9.92	2.08

of plastic deformation in the case of ductile materials or through various damage mechanisms in the case of brittle materials. As the composite materials are inherently brittle in nature, this excess energy is spent in the creation of damages. In the case of sandwich samples, the damage is mainly initiated in the form of top face sheet indentation, failure of the core through collapsing and crushing of cells and shear fracture, failure of the interface between the top and the bottom face sheets and the core, and finally the failure of the bottom face sheet. In the current study, the difference of the total energy (which is the energy at the end of impact event) and the energy to peak load was considered as the absorbed energy. The load and energy versus time plots illustrated in Figs. 7.5 and 7.6 exhibit a drastic difference from those seen in Fig. 7.4. In these figures, it can be seen that there is a sharp drop in the load−time curves once the peak load is reached. At 30 J, the nanophased samples show a sudden drop after the peak load while the neat core sandwich sample illustrated an initial sharp drop and then a gradual drop. On the other hand, at 45 J all the samples exhibited a sharp drop in the load. These sharp drops are indications of clear penetration of the top face sheet. The samples again picked up the load. This was attributed to the load carried by partially damaged core. It is seen from Fig. 7.5 that this secondary peak load was highest for the 1% nanophased core, followed by the 0.5% nanophased core, while the neat foam core had the least value. As far as the impact parameters are concerned, it can be noted that the nanophased core sandwich samples, in general, had higher peak loads, lower deflection at peak load, higher energy to maximum load, lower time to peak load, and higher absorbed energy at 30 J, with the exception of 0.5% nanophased core sandwich which had lower absorbed energy and lower energy to peak load. On the other hand, at 45 J both nanophased core sandwich samples exhibited higher peak load, lower time to peak load, lower total time, lower deflection at peak load, lower energy to maximum load, and higher absorbed energy. When impacted at higher energies (30 and 45 J), the impact parameters are influenced by the state of damage rather than the elastic response of the samples. Higher peak loads for nanophased foam core sandwich samples compared to neat foam sandwich samples were attributed to the fact that nanoclay foams had thicker cell walls and more cells per unit volume [25].

To understand the impact response and the failure modes in a more quantitative manner, the samples were sectioned into two halves and scanned using an optical scanner, an optical microscope, and a scanning electron microscope. Figs. 7.7 and 7.9 illustrate the pictures of the top surface (left), scanned cross-sections obtained from an optical scanner (middle), and an optical microscope (right) for the samples impacted at 15 and 30 J, respectively. Similar information was obtained for the samples impacted at 45 J. Since there was not much of a difference in the behavior or failure pattern of the samples impacted at 30 and 45 J, only the information of samples impacted at 30 J is presented. It is seen in the images given in Fig. 7.7 that all the face sheets were dented and there was some crushing damage in the core material. However, nanophased cores had a distinct difference in behavior when compared with that of the neat core. From Fig. 7.7, it can be seen that the region of crushed core was much wider with a shallow depth in the case of neat core with a near elliptical shape, whereas it had less width and more depth of damage in the case of nanophased

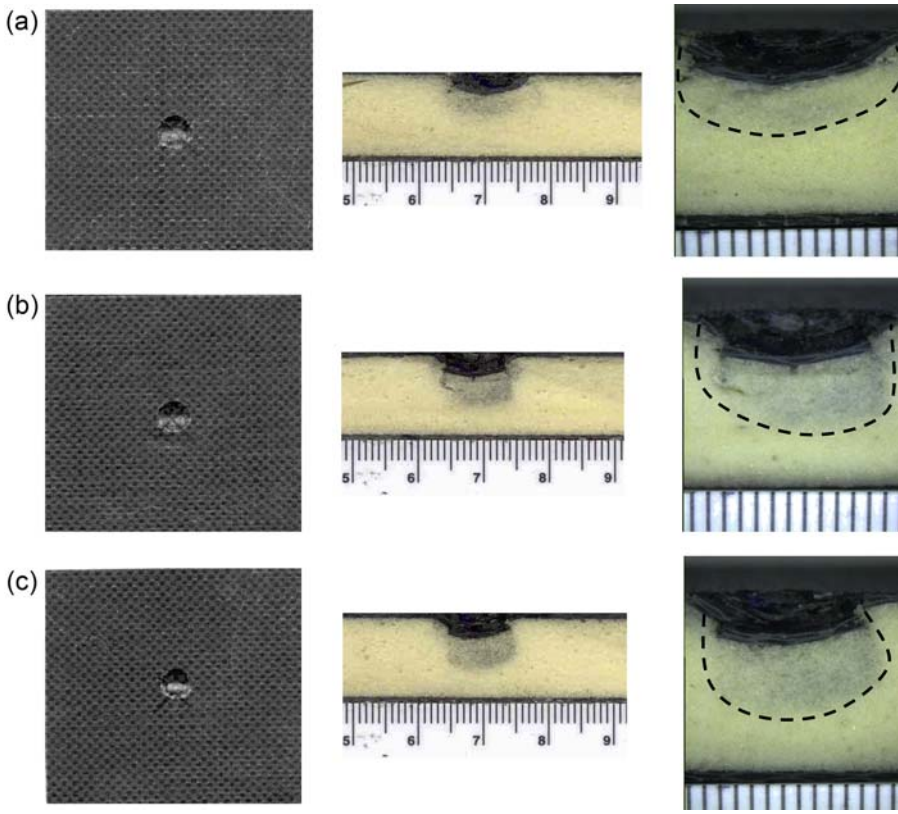

Figure 7.7 Impact surface, scanned and optical micrographs of cross-sectional views of 1% nanoclay face sheet sandwiches: (a) neat; (b) 0.5% nanoclay; and (c) 1% nanoclay core samples impacted at 15 J.

core with a cylindrical shape. From Fig. 7.8, it can be seen that the damage mechanisms are different in the case of neat and nanophased core sandwich samples. The depth of penetration of the sample was more in the case of nanophased core sandwich samples than the neat core sandwich samples. In the case of neat core sandwich samples, the core crushing was limited to a small region below the penetrated face sheet.

The shear crack in the core, which extended until the back face sheet, emanated from the edge of the penetrated face sheet. The width at the base of the core is large. On the other hand, for the 0.5% nanoclay core, there was a prominent region of crushed core below the penetrated face sheet. In addition, there was shear cracking on either side, up to the core bottom face sheet interface. However, the base width was much smaller than that seen in the neat core sandwich sample. For the 1% nanoclay core sandwich sample, the failure phenomenon was similar to that seen in the 0.5% nanoclay core sandwich sample.

However, the depth of crushed core was much more and the region of shear fracture was smaller. Similar modes of failure were observed in the case of samples impacted

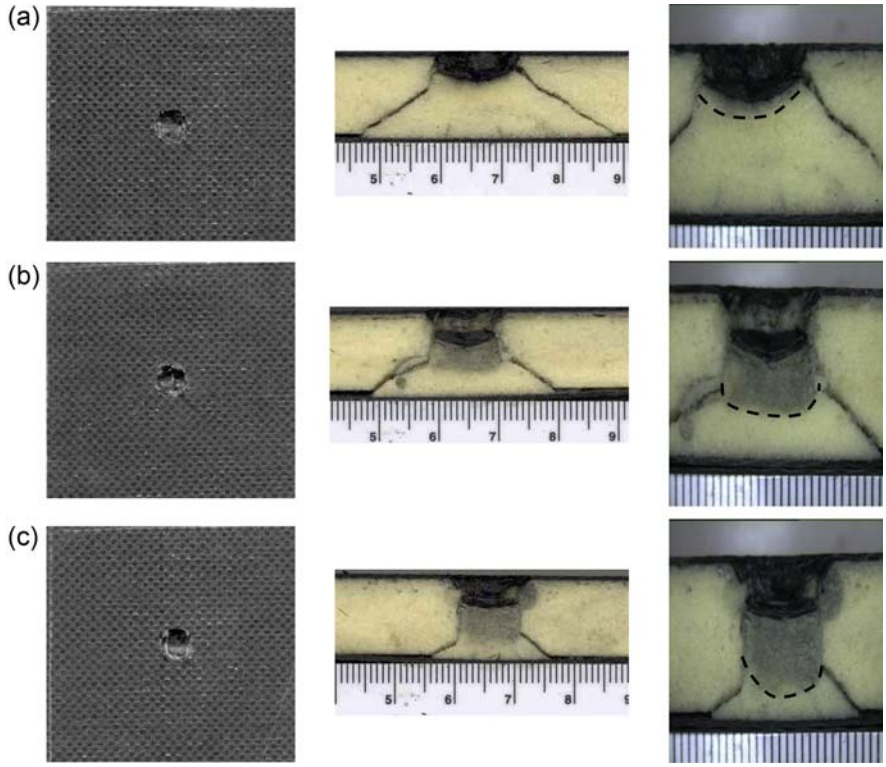

Figure 7.8 Impact surface, scanned and optical micrographs of cross-sectional views of 1% nanoclay face sheet sandwiches: (a) neat; (b) 0.5% nanoclay; and (c) 1% nanoclay core samples impacted at 30 J.

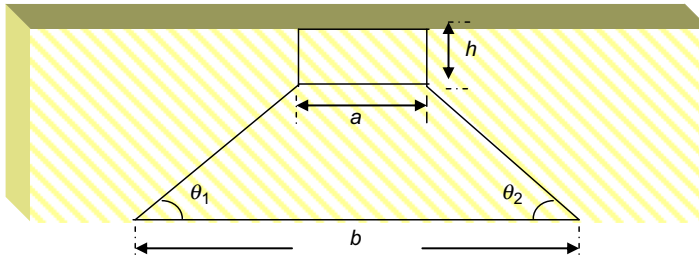

Figure 7.9 Schematic diagram of cross-sectional view of tested samples impacted at 30 and 45 J.

at 45 J. To quantify the damage, the total damaged area was divided into two zones: one rectangular region which measured the width and depth of penetration; the other a frustrum of cone which measured the shear fracture of the core as shown schematically in Fig. 7.9. Here, h is the penetration depth, a is the width of penetration as well as the top width of the cone, b is the base width of the cone, and θ_1 and θ_2 are

Table 7.2 Damage parameters for samples impacted at 30 and 45 J

Type of core	Left angle (θ_1)	Right angle (θ_2)	Top width (a) mm	Base width (b) mm	Indentation depth (h) mm
Impact energy 30 J					
1% Face sheet sandwich					
Neat	34	36	11.3	40.69	No dent
0.5% Clay	36	38	9.1	30.20	6.32
1% Clay	40.5	38	9.5	20.48	4.04
2% Face sheet sandwich					
Neat	31	26	9.9	21.52	3.98
0.5% Clay	31	20	9.9	20.06	5.42
1% Clay	45	40	8.9	15.39	3.61
Impact energy 45 J					
1% Face sheet sandwich					
Neat	38	29	11.64	35.22	3.52
0.5% Clay	45	35	11.54	31.75	4.04
1% Clay	37	44	11.66	27.47	4.35
2% Face sheet sandwich					
Neat	32	26	13.37	49.49	No dent
0.5% Clay	43	41	11.56	25.39	3.74
1% Clay	36	45	10.44	27.53	5.50

the base angles of the cone with horizontal line. These measures are listed in Table 7.2 for both 1% and 2% face sheet sandwich samples impacted at 30 and 45 J. From this table, it can be seen that the base width for the neat core sandwich samples was much more than that for the nanophased core sandwich samples, with 1% nanoclay core sandwich samples having the lowest value at both 30 and 45 J. On the other hand, the base angles for the neat core had lower values, indicating a gradual slope, as against nanophased core samples which had higher values of the base angles, indicating much steeper slopes. Scanning electron micrographs along with the optical micrographs of 1% nanoclay face sheets with different core materials are illustrated in Fig. 7.10(a)–(c). In this figure, SEM pictures taken from two different regions of the core are depicted. The top row shows the optical and scanning electron micrographs of the neat core sandwich sample. The SEM image just below the penetrated region of the face sheet shows a distinct elastic response, in that the cells exhibit a tendency to collapse on one another rather than break. The SEM image taken from the region which does not indicate damage in the optical micrograph depicts the deformed but still intact cells. From these micrographs it can be inferred that, in the case of neat core sandwich samples, the core exhibited an elastic response. On the other hand,

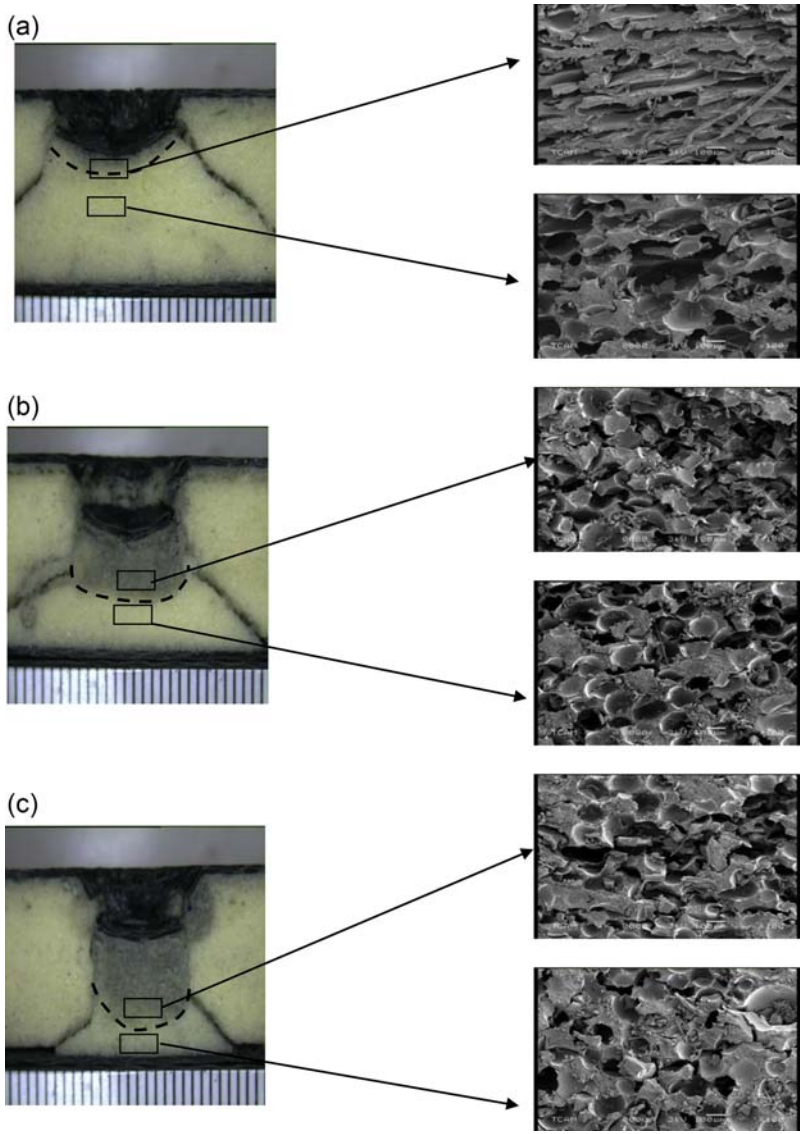

Figure 7.10 Scanning electron micrographs of 1% nanoclay face sheet sandwiches: (a) neat; (b) 0.5% nanoclay; and (c) 1% nanoclay cores tested at 30 J.

the SEM images of the 0.5% (middle row) and 1% (bottom row) nanoclay core sandwich samples illustrate cores whose cells had a tendency to exhibit brittle fracture. The SEM images obtained from the region that did not show damage in the optical micrograph show most of the cells intact with some broken cells, the number of which is more in the case of 1% nanoclay core.

7.3.2 A 2% nanoclay face sheet sandwich

In this section, the impact response of sandwich samples whose face sheets were infused with SC-15 epoxy with 2% nanoclay and which had neat, 0.5%, and 1% nanoclay-infused PU foam cores is described. Load and energy versus time plots for 2% nanoclay face sheet sandwiches with neat and nanophased cores impacted at 15, 30, and 45 J are shown in Figs. 7.11–7.13. Different impact parameters for neat, 0.5%, and 1% nanoclay foam samples are given in Table 7.3. In almost all cases nanoclay foam sandwiches exhibited improved peak values over neat foam sandwich structures.

As shown in Fig. 7.11, peak load was higher for 0.5% and 1% nanoclay foam sandwiches as compared with neat foam sandwich at all energy levels except at 15 J. The response of all three types of cores at 15 J was more or less the same. The load–time response of the sandwich samples was relatively smooth except at about 1.5 kN load where there is a change in the slope of the curve, indicating the damage to the face sheet. However, the energy level was not high enough to cause severe damage to the core. On the other hand, when impacted at 30 and 45 J, all the samples indicated a sudden drop in the load–time response. The load dropped by about one-third for the samples when impacted at 30 J and it was more severe in the case when the samples were impacted at 45 J. As seen in the case of 1% face sheet samples, the sudden load drop was the indictor of the complete penetration of the face sheet and severe damage to the core.

When compared with the 1% face sheet neat core sample, the 2% face sheet neat core sample exhibited a higher peak load, but other impact parameters such as

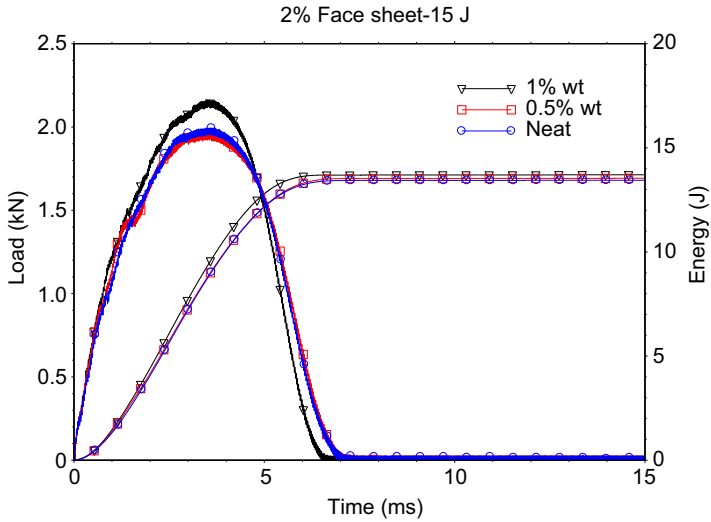

Figure 7.11 Load and energy versus time plots for 2% nanoclay face sheet sandwiches with neat and nanoclay cores impacted at 15 J.

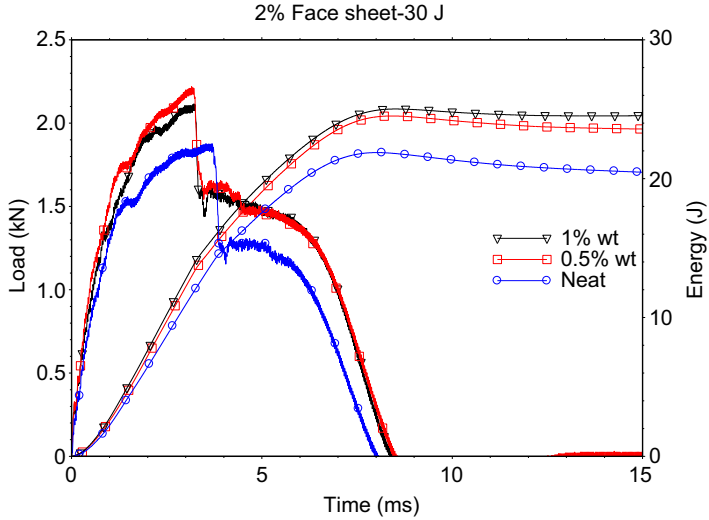

Figure 7.12 Load and energy versus time plots for 2% nanoclay face sheet sandwiches with neat and nanoclay cores impacted at 30 J.

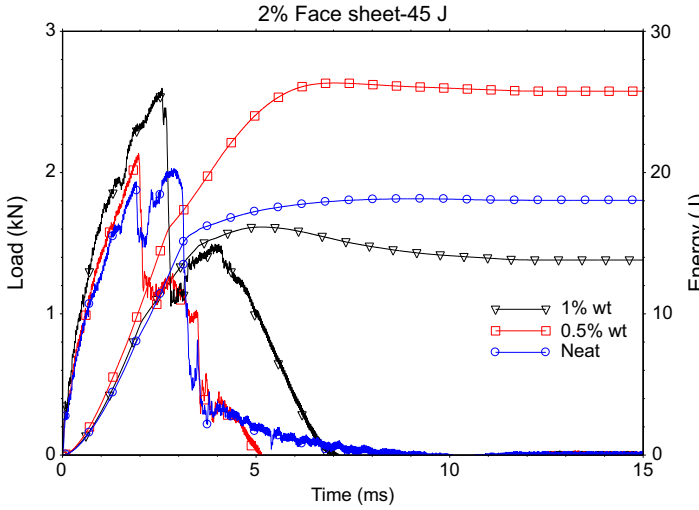

Figure 7.13 Load and energy versus time plots for 2% nanoclay face sheet sandwiches with neat and nanoclay cores impacted at 45 J.

deflection at peak load, time to maximum load, and energy to maximum load were lower for the 2% face sheet samples of all types of cores. When nanoclay is infused into the carbon fibers it makes them stiffer and at the same time brittle, reducing their strain to failure when they are subjected to bending [26]. This is also reflected when nanoclay-reinforced carbon fabric laminates are used as face sheets to make sandwich

Table 7.3 Average impact parameters for 2% face sheet sandwich with neat and nanoclay core samples impacted at 15, 30, and 45 J

Type of core	Impact energy (J)	Peak load (kN)	Deflection at peak load (mm)	Energy to max load (J)	Total energy (J)	Impact velocity (m/s)	Total time (ms)	Absorbed energy (J)	Time to max load (ms)
Neat	14.77	2.03	6.46	8.71	13.50	2.11	6.92	4.78	3.44
0.5%	14.79	1.92	6.59	8.78	13.50	2.11	6.97	4.71	3.53
1%	14.92	2.00	6.69	9.09	13.54	2.12	6.79	4.44	3.58
Neat	29.49	1.83	10.26	13.97	21.49	2.98	9.40	7.52	3.82
0.5%	29.44	2.18	8.47	13.29	24.82	2.98	8.35	11.52	3.13
1%	29.51	2.12	8.45	12.58	23.93	2.98	8.45	11.35	3.09
Neat	44.54	1.94	9.10	11.85	20.12	3.66	7.12	8.26	2.62
0.5%	44.59	2.60	8.89	14.98	24.11	3.67	6.85	9.13	2.59
1%	44.46	2.03	7.04	9.01	16.39	3.66	5.91	7.38	1.99

composites. It is noticeable that, in general, the peak load for the 2% nanoclay face sheet sandwich samples is lower than that for the 1% face sheet sandwich samples at 30 and 45 J. It is also true that at higher energy levels of 30 and 45 J, nanophased core sandwich samples with 2% nanoclay face sheets had higher peak loads. At 30 J, neat core sandwich samples had higher deflection at peak load, lower energy to peak load, lower total energy, higher total time, and time to peak load than the nanophased core sandwich samples. Higher deflection and durations are attributed to the relatively flexible core, while lower absorbed and total energy are attributed to the increased strength of the nanophased cores. The nanophased cores are also brittle. The higher the clay content, the more brittle the core. When the impact energy was increased from 30 to 45 J, these facts contributed to the response of the samples. The 0.5% nanoclay core sandwich samples exhibited the best impact properties. Even though the 1% nanoclay core sandwich samples had higher peak load than the neat core sandwich samples, they exhibited lower impact properties in terms of the energy to peak load and absorbed energy, as well as the time to peak load and total time. This is attributed to brittle face sheets and a relatively more brittle core than the other two types of cores.

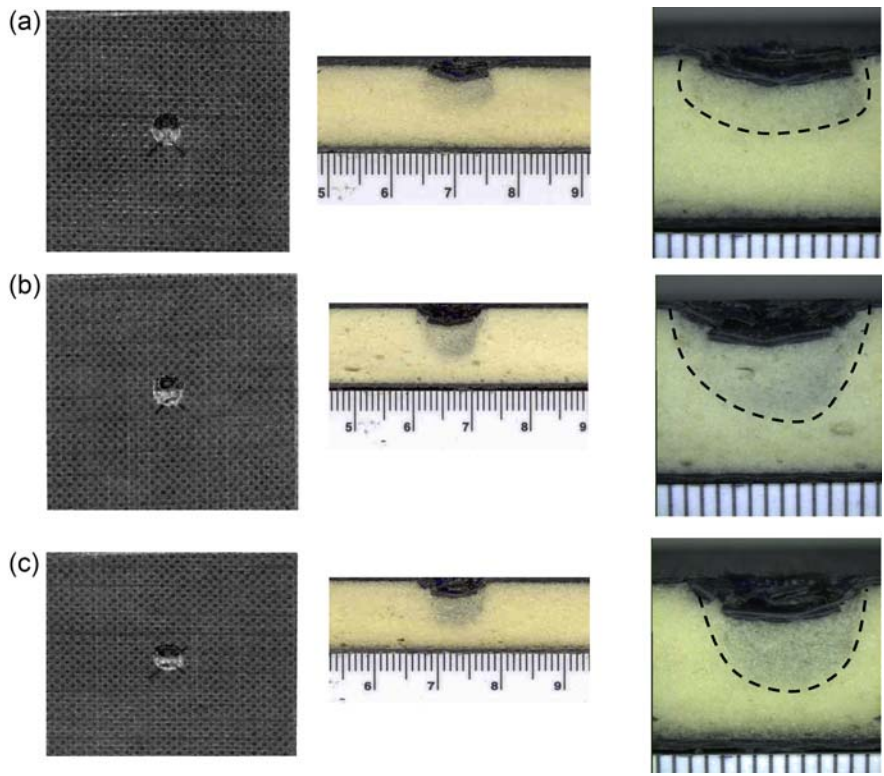

Figure 7.14 Impact surface, scanned and optical micrographs of cross-sectional views of 2% face sheet sandwiches: (a) neat; (b) 0.5% nanoclay; and (c) 1% nanoclay cores impacted at 15 J.

Fig. 7.14(a)–(c) illustrates impact surface, scanned pictures, and optical micrographs of the samples impacted at 15 J. It is seen clearly from these pictures that there was a penetration of the top face sheets. The core did suffer damage in the form of crushing as seen by the darkened region below the face sheet. While the damage to the core is shallow in the case of neat core sandwich samples, its depth increased with the increase in the nanoclay content in the core. However, as was qualitatively seen from the transient response curves of the samples, there is no catastrophic failure in the core. Fig. 7.15(a)–(c) illustrates impact surface, scanned pictures, and optical micrographs of the samples impacted at 30 J. In this case, all the samples had a complete penetration of the top face sheet and two different modes of failure in the core material, as was seen in the case of 1% nanoclay face sheet samples. The core exhibited crushing failure as well as the failure through a conical shear fracture. The depth of the cylindrical region of failure was more in the case of nanophased core sandwich samples, with the higher depth for the 1% nanoclay core samples. One noticeable difference in the behavior of neat core sandwich samples with 2% nanoclay face sheets when compared with the counterpart with the 1% nanoclay face sheet is the origin of the shear fracture zone when impacted at 30 J. In the case of the 1% nanoclay face sheet sandwich

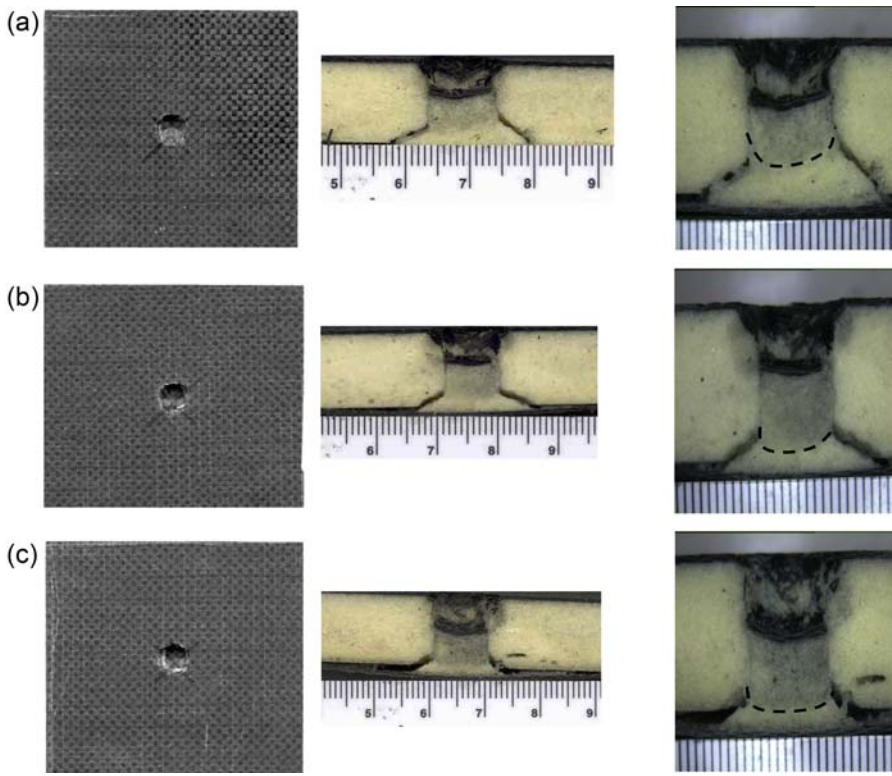

Figure 7.15 Impact surface, scanned and optical micrographs of cross-sectional views of 2% face sheet sandwiches: (a) neat; (b) 0.5% nanoclay; and (c) 1% nanoclay cores impacted at 30 J.

samples, the shear fracture emanated from the edge of the penetrated face sheet, whereas in the case of the 2% nanoclay face sheet it started from the middle of the core. Further, the width of the conical fracture zone is much less. On the other hand, at 45 J, there was not much penetration and hence the base width of the conical damage area was much wider. When the impact damage pattern of the nanophased core sandwich samples is compared for the two different nanoclay weight percentage face sheets,

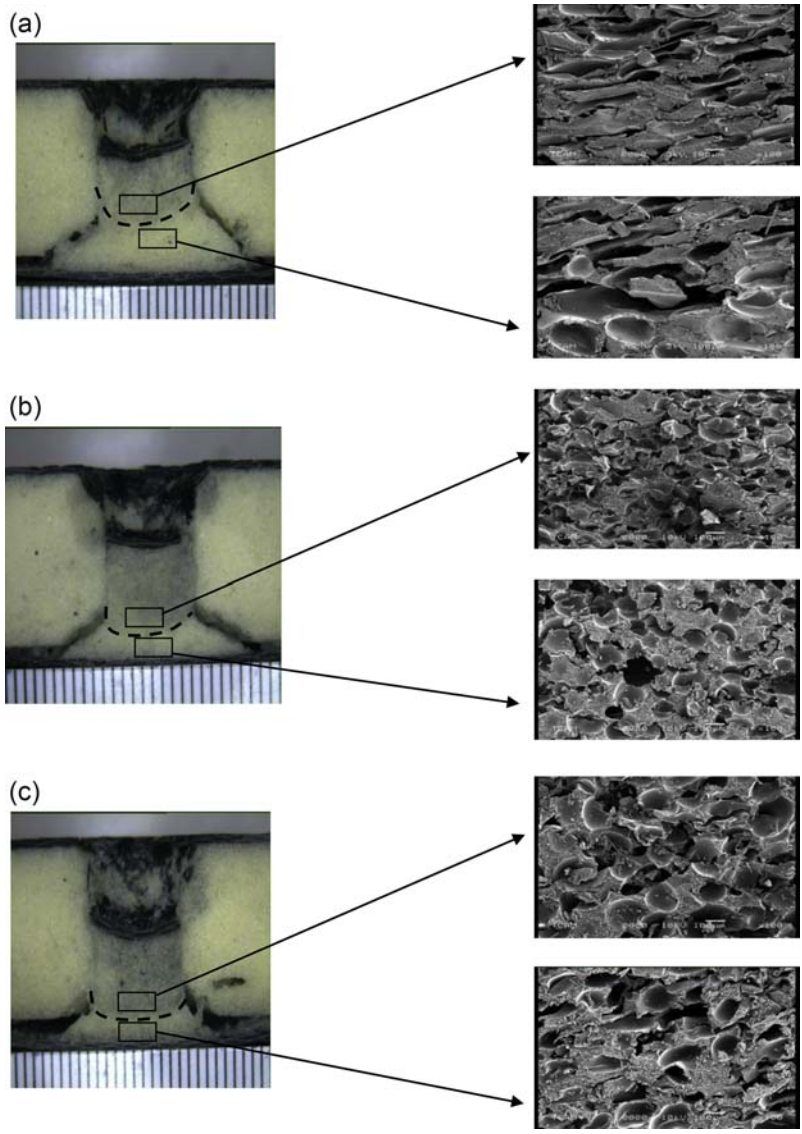

Figure 7.16 Scanning electron micrographs of 2% nanoclay face sheet sandwiches: (a) neat; (b) 0.5% nanoclay; and (c) 1% nanoclay cores tested at 30 J.

the 2% nanoclay face sheet had lower damage size. Damage patterns for the samples impacted at 45 J were similar and hence are not presented. Fig. 7.16(a)–(c) illustrates the optical and SEM images of the sandwich samples with the 2% nanoclay face sheet and different types of core impacted at 30 J. Here again, it can be seen that the behavior of neat core is completely in contrast to that of the nanophased cores. While the neat core exhibited collapsing of the cells under the penetrated face sheet, the nanophased cores exhibited brittle fracture of the cells.

Results of the investigation carried out in the current work have important implications in the composite industry. It is impossible to prevent sandwich structures from being subjected to impact loading. When such a situation occurs, there will be a damage to the structure and hence reduction in the mechanical properties. By using nanophased sandwich constructions, it is not only possible to carry higher loads but also to minimize the damage to the structure in the event of impact loading. When the damage size is smaller, the reduction in the mechanical properties is lower. Further, if a repair is warranted, then the cost of the repair is also lower as the repair volume is less.

7.4 Conclusion

The following conclusions were drawn from the study:

- Transient load–time plots gave qualitative indications of the state of damage in the sample. Nanoclay-infused foam sandwich structures exhibited higher peak loads compared with that of neat foam sandwich structures.
- Damage analyses showed that nanoclay-infused foams had smaller damage areas than their neat counterparts.
- SEM study revealed that neat foam samples absorb impact energy through the collapsing of cells as well as shear fracture, whereas nanoclay foam cores failed through brittle facture of the cells as well as through shear.
- By adopting nanophased sandwich constructions in structures, it is possible to sustain higher loads, reduce the damage size during impact-like events, lower the reduction in mechanical properties, and lower the cost of repairs, if warranted.

Acknowledgments

Authors would like to thank the support received by NSF-EPSCoR and NSF-REU for carrying out this work.

References

[1] Tromblin J, Lacy T, Smith B, Hooper S, Vizzini A, Lee S. Review of damage tolerance for composite sandwich airframe structures. U.S. Department of Transportation; 1999. Federal Aviation Administration Report No. DOT/FAA/AR-99/49.

[2] Abrate S. Localized impact on sandwich structures with laminated facings. ASME Appl Mech Rev 1997;50(2):69–82.

[3] Nettles AT, Hodge AJ. Impact testing of glass/phenolic honeycomb panels with graphite/epoxy face sheets. In: Proceedings of 35th int. SAMPE symp. and exhibition, Anaheim, CA, April 2−5 vol. 35; 1990. p. 1430−40.
[4] Kim CG, Jun EJ. Impact characteristics of composite laminated Sandwich structures. In: Proc. of 8th int. conf on composite mat. (ICCM/8), Honolulu, July 15−19 vol. 32; 1991. G1−8.
[5] Kim CG, Jun E. Impact resistance of composite laminated Sandwich plates. Compos Mat 1992;26(15):2247−61.
[6] Palm TE. Impact resistance and residual compression strength of composite sandwich panels. In: Proc. 8th int. conf on composite mat. (ICCM/8), Honolulu, July 15−19 vol. 3; 1991. G.1−13.
[7] Charles JP, Guedra-Degeorges D. Impact damage tolerance of helicopter sandwich structures. In: Proc. 23rd int. SAMPE conf., Kiamesha Lake, NY, October 21−24; 1991. p. 51−61.
[8] Herup EWJ, Palazotto AN. Low velocity impact damage initiation in graphite/epoxy/nomex honeycomb-sandwich plates. Compos Sci Technol 1997;57:1581−98.
[9] Weeks CA, Sun CT. Multi-core composite laminates. J Adv Mater April 1994:28−37.
[10] Wu CL, Sun CT. Low velocity impact damage in composite sandwich beams. Compos Struct 1996;34:21−7.
[11] Hazizan AM, Cantwell WJ. The low velocity impact response of foam based sandwich structures. Compos Part B Eng 2002;33:193−204.
[12] Caprino G, Teti R. Impact and post impact behavior of foam core sandwich structures. Compos Struct 1994;29:47−55.
[13] Abot JL, Daniel IM. Composite sandwich beams under low-velocity impact. In: CD proc. 42 AIAA/ASME/ASCE/AHS/ASC SD conf., Seattle, WA; April 2001. Paper No. 2001−1186.
[14] Anderson T, Madenci E. Experimental investigation of low velocity impact characteristics of sandwich composites. Compos Struct 2000;50:239−47.
[15] Mines RAW, Worrall CM, Gibson AG. Low velocity perforation behavior of polymer composite sandwich panels. Int J Impact Eng 1998;21(10):855−79.
[16] Mahfuz H, Rangari VK, Islam MS, Jeelani S. Fabrication, synthesis and mechanical characterization of nanoparticles infused polyurethane foams. Compos Part A Appl Sci Manuf 2004;35(4):453−60.
[17] Mahfuz H, Islam MS, Rangari VK, Saha MC, Jeelani S. Response of sandwich composites with nanophased cores under flexural loading. Compos Part B Eng 2004;35(6−8):543−50.
[18] Schubel PM, Luo J, Daniel IM. Low velocity impact behavior of composite sandwich panels. Compos Part A Appl Sci Manuf 2005;36:1389−96.
[19] Yu JL, Li JR, Hu SS. Strain-rate effect and micro-structural optimization of cellular metals. Mech Mater 2006;38(1−2):160−70.
[20] Lee Y, Yoon KB. Effect of composition of polyurethane foam template on the morphology of silicalite foam. Microporous Mesoporous Mater 2005;88(1−3):176−86.
[21] Song B, Chen WW, Dou S, Winfreeb NA, Kang JH. Strain-rate effects on elastic and early cell-collapse responses of a polystyrene foam. Int J Impact Eng 2005;31(5):509−21.
[22] Benedicte L, Myriam D, Nadege P, Michael A, Dana K, Cedric C, et al. Poly(1-caprolactone)/clay nanocomposites prepared by melt intercalation: mechanical, thermal and rheological properties. Polymer 2002;43(16):4017−23.

[23] Cao X, Lee LJ, Widya T, Macosko C. Polyurethane/clay nanocomposites foams: processing, structure and properties. Polymer 2005;46(3):775−83.
[24] Uddin MF, Mahfuz H, Zainuddin S, Jeelani S. Anisotropic behavior of rigid polyurethane foam with acicular nanoparticles infusion under high strain rate compression. In: CD proceedings of 20th technical conference of the American Society for Composites, Philadelphia, PA; 2005. p. 1−15. Paper 37.
[25] Mohammed AA, Hosur MV, Jeelani S. Processing and characterization of nanophased polyurethane foams. Cell Polym 2006;25(6):293−306.
[26] Chowdhury FH, Hosur MV, Jeelani S. Studies on the flexural and thermomechanical properties of woven carbon/nanoclay-epoxy laminates. Mater Sci Eng A 2006;421: 298−306.

This page intentionally left blank

Part Three

Structural optimization and structural analysis: modelling and simulation

This page intentionally left blank

Weight reduction by optimized reinforcement structures

8

F. Ohlsson
Oxeon AB, Borås, Sweden

8.1 Traditional reinforcement structures and their limitations

Continuous carbon fibre reinforcements are available in, among other forms, unidirectional (UD) tapes, non-crimp fabrics (NCFs) and woven fabrics. UD tapes are available in a wide variety of areal weights and constitute fibres highly oriented in only one direction. The UD orientation of fibres makes its draping in complex geometries difficult because the UD sheet tends to split, wrinkle and fold, creating uneven fibre distribution. Woven UD materials are often constructed with a glass fibre or polymer weft allowing for simpler draping but introducing fibre crimp.

NCFs provide either two-, three- or four-directional fibre orientations in one 'sheet' construction directly. The low areal weights achievable are dependent on the count of the tows (usually 3k to 24k) that are used to build up the layers of the NCF. However, NCF materials present difficulties in draping, particularly at sharp and tight bends, depending on stitch density and stitching pattern/style. This is because the stitches tend to lock the multi-directionally oriented fibres in their positions and thereby restrict the fibres from sliding past easily relative to one another to conform to the required draping geometry. Research done by Edgren [1] has also shown that the stitching threads introduce fibre kinks, which can reduce the composites' compression performances significantly.

In comparison to UD tapes and NCF materials, traditional woven fabrics present fibre orientations in two mutually perpendicular directions and with improved draping ability. However, such a woven material's mechanical properties are lowered because of the inherent crimp or waviness that is introduced into the fibres by the weave. To minimize the loss of mechanical properties arising from crimp, two things are considered. First, tows of low count, usually 1k to 6k, are used to keep the crimp angle as low as possible. Second, to reduce the frequency of the crimp, and also to enable gentler weaving of carbon fibres, the spacing between the constituent tows/yarns is increased. Different weave patterns such as twills and satins are also employed to achieve lower crimp frequency.

Crimp can be present both in the plane and out of the plane. For the forthcoming discussions, out of the plane crimp will be considered.

Crimp angle is defined as the angle inclination a warp or a weft element will be forced to form to allow a clear passage in the woven fabric.

Lightweight Composite Structures in Transport. http://dx.doi.org/10.1016/B978-1-78242-325-6.00008-6

Crimp frequency is defined as the number of angle inclinations a warp or a weft element will hold over a given length.

With 1k−6k tow counts, the typical areal weights of woven reinforcements achievable are in the range of about 90−300 gsm. However, the low-areal-weight woven fabrics have correspondingly reduced cover factor and uneven fibre distribution. The fabric construction tends to be loose and exhibits gaps/openings (which is undesirable because filling gaps with matrix increases the dead weight of the composite material). A typical such carbon fabric is the commonly available 95-gsm plain-weave fabric produced using 1k tow. Its low areal weight is due to its low cover factor and such a material is not relatively thin either. As a consequence, the composite material incorporating it would tend to be correspondingly heavier.

As the carbon fibres become abraded and damaged easily during the weaving process compared with commonly used fibres like cotton, polyester, glass, aramid, etc., there is a limit to how closely they can be packed in the fabric by the weaving process. Because low-areal-weight woven fabrics are somewhat open in construction, a number of fabrics have to be plied to close the gaps/openings. However, such plying causes the composite material to become relatively thicker and heavier than actually necessary.

8.2 Spread-tow fabric history

Various methods have been devised to spread a tow into tape. The principles of some methods are described briefly in Table 8.1. These methods illustrate the need and the attempts to convert tow to tape. A general outline of the process is illustrated in Fig. 8.1 to acquaint the reader with different stages of tow-to-tape production.

The technology for weaving warp and weft tapes that are 20−50 mm wide is rather new even if weaving has been in practice for over 5000 years and baskets have been hand woven with bamboo tapes. Khokar [12] has developed a technology which is not based on traditional yarn-handling looms. It is, however, pertinent to mention here that a conventional weaving machine has been modified to weave narrow-width tapes (up to 16 mm) as exemplified by Homma et al. [13]. Another tape-weaving machine development is attributed to Kawabe et al. [14]. However, these weaving systems follow traditional working lines.

8.3 Spread-tow products

Spread-tow products, not to be mixed up with flat-tow products, are defined by the width of the original tow being substantially widened, often three times or more, during a spreading process. Within the category of spread-tow products several types of reinforcements are available. Spread-tow tapes, spread-tow fabrics and spread-tow NCFs are some products in this relatively new category of reinforcement materials.

Spread-tow tapes are produced in various widths and areal weights just like traditional dry and prepregged UD materials. The main differences when comparing the

Table 8.1 Spreading technologies

Method	Principle
Air jet (Daniels [2])	A tow is pulled through a venturi tube in a direction opposite to the air jet flow and is spread
Vibration (Iyer and Drzal [3])	A tow, zigzagging between rods, is passed over a vibrating loudspeaker to separate the filaments
Vacuum (Baucom et al. [4])	Air is drawn through the filaments passing over a perforated plate connected to vacuum pressure to separate the filaments
Spreader bars (Calkins [5])	A tow is passed over and under a series of spreader bars under tension and sharp bends to obtain a flat array of separate fibres
Combinations (Muzzy and Varughese [6])	A tow passes over−under a first set of three rods, then an air jet 'comb' zone and finally over−under a second set of three rods to separate the filaments
Spreading rolls (Nakagawa and Ohsora [7])	The fibre separator comprises a plurality of fixed barrel-shaped rolls that revolve to contact the tow alternately to separate the fibres
Corona (Peritt et al. [8])	A tow is passed over a corona discharge region of an electrically connected sheet to separate the fibres
Expander (Lifke et al. [9])	A tow is fed at the closest point of mutually angled discs, which rotate about their axis, holding an expandable band such that the tow is expanded laterally as it moves towards the widest point of discs
Bending (Kawabe and Tomoda [10])	A tow moving over a cavity under vacuum pressure tends to bend in an arch and thereby spreads width-wise
Water jet (Hiroharu and Toshiyuki [11])	A tow is drawn in a water bath against water jets and ultrasonic waves are applied to separate the filaments

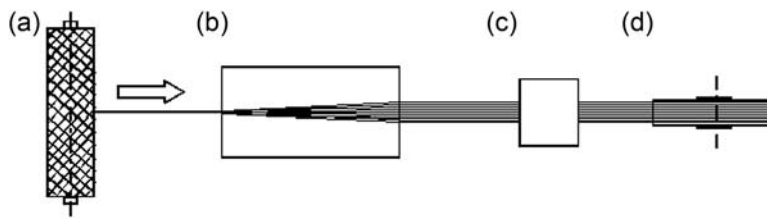

Figure 8.1 Schematic of tow-to-tape production. (a) Tow(s) from bobbin in creel is supplied to (b) the spreading unit from where the spread fibres proceed to (c) the optional stabilizing unit to obtain the tape that is next wound into spools at (d) the winding unit.

spread-tow tapes with the traditional products are the tow size being used to produce a certain areal weight or product thickness. Traditional prepregged UD products with an areal weight below 50 gsm will be constructed using tows, with a tow count below 6k, that are positioned parallel next to one another to close the gaps between each tow, and the prepreg resin will hold the product together, as can be seen in Fig. 8.2. A dry UD product will probably be constructed like a woven UD comprising a thin weft yarn from either glass or a polymer material. In both materials the filaments will not be highly aligned or tightly packed. There will be spacing between tows, which will generate resin pockets, and the thickness of each ply will present a high risk of generating transverse matrix cracks upon loading. More on this will be presented in a later section.

When spreading is applied to a carbon fibre tow the filaments will not only widen so that the tow transforms into a tape, but the filaments will align tightly next to one another, and with the proper technique combinations of several tows can create a wide tape material in the requested width and weight with almost no spacing between the tows as can be seen in Fig. 8.3.

Spread-tow tapes are preferably stabilized with a binder material to keep the spread tow from falling back into its narrow yarn shape upon handling. Such binder material can, among others, be thermoplastic-, thermoset- or fibrous-based materials.

Spread-tow fabrics, Fig. 8.4, are constructed of spread-tow tapes that are interlaced in a plain, twill or satin weave pattern. Just like traditional fabric reinforcement a set of warp tapes is combined with a set of weft tapes. The tapes in a spread-tow fabric can be of widths from $\sim$15 mm and upwards.

As mentioned in an earlier chapter, there are various production methods available to produce the spread-tow fabrics. Some are based on modified looms, while others are specially developed to handle spread-tow tapes.

Figure 8.2 Conventional carbon tapes.

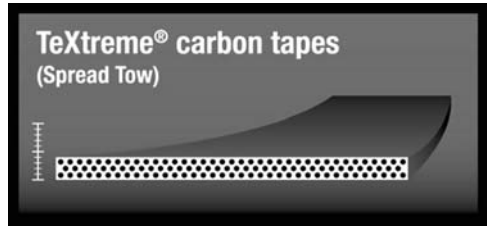

Figure 8.3 Spread tow tape.

Figure 8.4 Spread tow fabric.

Significant for spread-tow fabrics are the low crimp angle that comes from the interlacing of extremely thin tapes. The thinner the tapes, the lower the crimp angle and the straighter the fibres will be presented, and, quite naturally, the most use can be made of them.

Because the spread-tow fabrics are constructed from thin and wide tapes, the crimp frequency is also kept low, even when considering a plain-weave structure. With the crimp frequency low the interlacing points are few and hence, resulting risks such as possible pin-hole and resin shrinkage sections are reduced. The cover factor compared to traditional yarn-woven reinforcements is considerably higher in a spread-tow fabric.

Spread-tow fabrics with fibre orientations other than 0 and 90 degrees are available. Fabrics with fibre angles oriented in $+\alpha/-\beta$ degrees, for example $+45/-45$, as can be seen in Fig. 8.5, are constructed and present the same typical characteristics as a 0-/90-degree fabric except for its fibre orientations.

In Fig. 8.6 three different $+\alpha/-\beta$ constructions are shown. As can be inferred, they represent the constituent spread-tow tapes arranged in (Fig. 8.6(a)) an obtuse angle, (Fig. 8.6(b)) a right angle and (Fig. 8.6(c)) an acute angle. These constructions of course have the tapes oriented in equal but opposite angles. Should there be a need for having an $+\alpha/-\beta$ construction wherein the tapes are incorporated unequally, then such an $+\alpha/-\beta$ can also be produced as shown in Fig. 8.6(d).

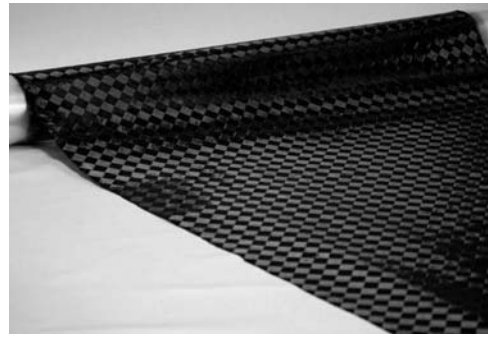

Figure 8.5 Spread-tow $+\alpha/-\beta$ fabric with $+45/-45$ fibres.

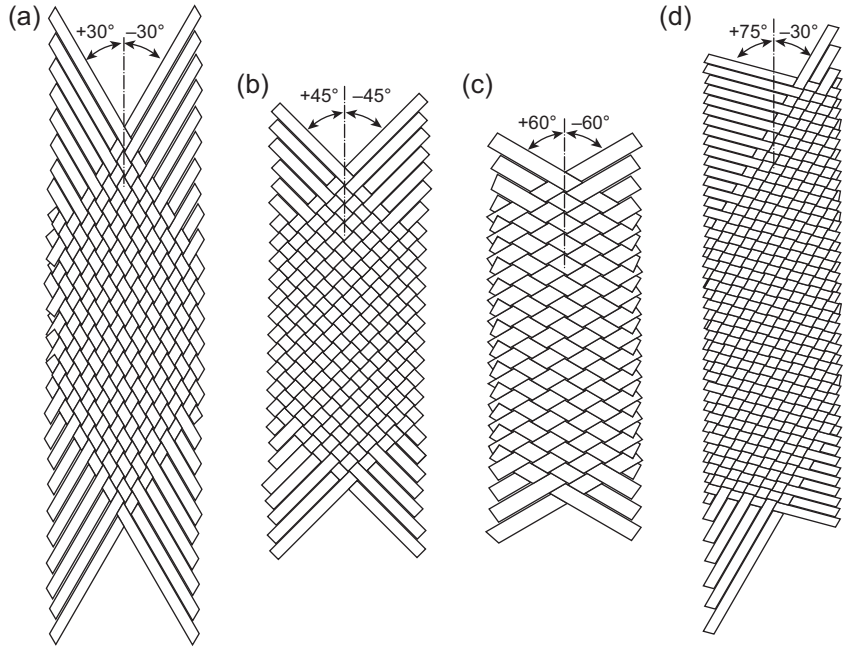

Figure 8.6 To be suitable for use as reinforcement in tubular applications, $+\alpha/-\beta$ spread-tow fabrics are producible in equal (a–c) and unequal (d) angular orientations of the constituent tapes.

The fibre angle flexibility in the material provides, for example, the possibility of tailor producing an $+\alpha/-\beta$ spread-tow fabric with about +55/−55 degrees to uniquely enable direct production of pressure vessels. Such a fabric could be wound over itself to as many layers as needed to meet the required performance demand.

As was explained earlier, spread-tow products can benefit from the binder material that prevents the spread-tow tape from contracting/bunching/deforming back to a narrow tow during its subsequent handling and processing. If such a binder material also can provide sufficient structural stability by adhering the respective $+\alpha$ and $-\beta$ tapes, together the fabric will display a unique handling ability as there will be no fibres running along the length of the fabric. Such cohesion is necessary in a $+\alpha/-\beta$ spread-tow fabric for it not to shear when handled and also to be able to be cut in a dry state, either manually or automatically, without the risk of unravelling or disintegration, as can be inferred from Fig. 8.7. The ease of cutting $+\alpha/-\beta$ spread-tow fabrics, without causing fraying/unravelling, can contribute to significant material waste reduction.

The positive impact of this aspect becomes immediately apparent when complex geometries are required to be directly cut, prepared and handled without providing for unnecessarily large margins/allowances for overlapping joints. The availability of continuous-length $+\alpha/-\beta$ spread-tow fabrics minimizes joints. The reduced fibre discontinuities in turn improve the mechanical reliability and performance of composite materials comprising $+\alpha/-\beta$ spread-tow fabrics. With the frequency of thick places

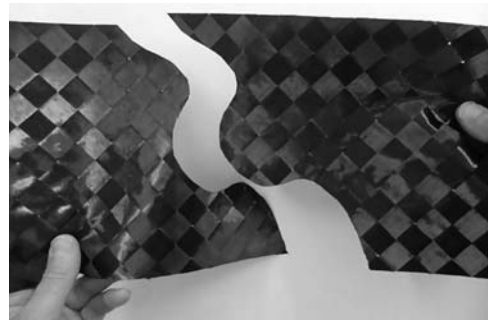

Figure 8.7 Cutting and handling of $+\alpha/-\beta$ spread-tow fabrics does not cause fraying/unravelling.

arising from overlapping joints either eliminated or substantially reduced, the final composite material naturally tends to be of even thickness and improved quality.

8.4 Reinforcement flexibility

It is to enable production of various areal weights of carbon reinforcements that the fibre producers are required to be flexible in producing various tow sizes. Table 8.2 shows available tow counts of some commonly used carbon fibre products to reflect the flexibility in supply. However, such flexibility comes with increased production cost owing to the setting changes involved.

Table 8.2 should not lead one to assume that low tow counts are produced for all carbon fibre types. There are many carbon fibre products which are available in only one tow count (eg, T1000G (12k), M30S (18k), HS40 (12k), IM6 (12k), IMS65 (24k), etc.) and some in only two tow counts (eg, M35J (6k and 12k), IM7 (6k and 12k), etc.). Obviously it is not possible for the converters (ie, producers of woven, NCF and UD materials) to process many of these higher tow counts into high-performance and low-areal-weight reinforcements.

To make available so many different tow counts of a fibre type presents a challenge to the fibre producers because, on one hand, the fibre producers have to meet the

Table 8.2 Tow count availability of various carbon fibre products

Fibre producer	Fibre product	Tow counts available
Tenax	HTA40/HTS40	1k, 3k, 6k, 12k, 24k
Toray	T300	1k, 3k, 6k, 12k
Hexcel	AS4	3k, 6k, 12k
Formosa	TC33	1.5k, 3k, 6k, 12k, 24k
Mitsubishi Rayon	TR50	6k, 12k, 15k, 18k

varying demands of the market and, on the other, they have to consider uninterrupted production. Changing settings for producing different counts of tows involves considerable time and effort and causes production loss, which at times could be up to 30% in reference to installed capacity. As a consequence, it becomes difficult to run the productions steadily and there is fluctuation in fibre quality (between lots) and a drop in output. The loss in production has to be made up with higher prices for low tow counts (1k−6k).

This situation can be improved if low-areal-weight reinforcements that are currently obtained using tow counts of 1k−6k are replaced by low-areal-weight reinforcements produced using higher tow counts such as 12k or 24k. The fibre manufacturers could then have the possibility of running their production lines more steadily. As a consequence, the market would be also assured of non-fluctuating availability of fibres and lightweight reinforcements.

From this it follows that production of spread-tow fabrics is relevant because a lightweight woven carbon fabric can be obtained using any fibre product that is available in a tow count of 12k or higher. The route of spread-tow fabric production is therefore outlined here. It comprises the steps of converting tows into spread-tow tapes and weaving such tapes into spread-tow fabric. Production of high-performance and lightweight woven carbon fabric using higher tow counts, like 12k and 24k, involves two steps. In the first step one or more tows of higher count are subjected to a spreading action whereby the constituent filaments are displaced laterally and a thin-and-wide spread-tow tape is produced. The spreading action can be controlled to obtain a set width of the spread-tow tapes, usually from 20 mm and above. Thus, the same tow can be spread to different widths, within certain practicable limits, and thereby correspondingly different areal weights of spread-tow tapes can be realized. To enable handling of the spread-tow tape, it is stabilized and wound into spools. The subsequent step involves production of spread-tow fabric by weaving spread-tow tapes as warp and weft.

When using homogeneous materials like steel or aluminium the construction of a product is designed to fit the material's structural properties. However, when using composites, the material is designed instead according to the engineering needs of the constructional design of the product. Through this, the structure will be more optimized and hence unnecessary weight can be eliminated. However, conventional fabric constructions and areal weights obtainable have until now been strictly connected and limited to the tow sizes being used and therefore complete optimization has not been possible. A simple overview of the strong link between carbon fibre tow counts and fabric areal weight produced in the conventional manner is shown in Table 8.3. Spread-tow fabrics do not follow these set rules. Instead, a few tow sizes are enough to create a large-areal-weight span; spread-tow fabrics of even lighter areal weight than conventional fabrics produced using 1k fibre are possible.

To explain Table 8.3 in relation to the flexibility in producing spread-tow fabrics with a wide range of areal weights, the following may be considered.

By spreading and stabilizing one or several Torayca T700SC 12k fibre tows to 20 mm width, four different tape areal weights could be achieved, 40, 80, 120, and 160 gsm, as shown in Fig. 8.8.

Table 8.3 Comparison of approximate areal weights

Fibre type and tow count	Traditional woven fabrics (gsm)	Spread-tow fabrics (gsm)
High Strength		
1k	90–120	—
3k	200–400	—
6k	300–500	—
12k	500–600	64–800
Intermediate Modulus		
6k	200–400	—
12k	300–400	—
18k	—	76–400
24k	—	82–400
High Modulus		
6k	200–500	—
12k	300–500	60–245

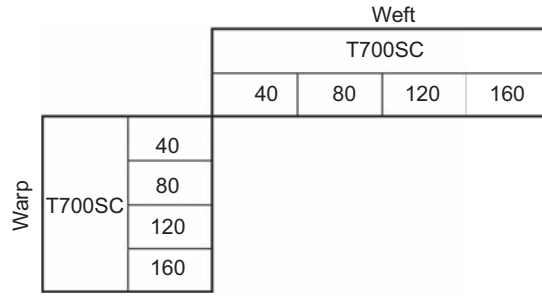

Figure 8.8 Areal weight variations on a 20-mm-wide tape from Torayca T700SC 12k fibre tow.

These different areal weight tape constructions can be used as warp and weft in 16 different fabric areal weight combinations, wherein four constructions will be balanced (the shaded ones in Fig. 8.9).

To meet the specific application and performance needs, either different carbon fibre types or other fibre types such as aramid, glass, polyethylene, polypropylene and polybenzobisoxazole could be used as well in spread-tow fabric construction. These fibres can themselves be spread to different areal weights and in this way the matrix of possible fabric constructions in reference to fibre types and areal weights can be directly enlarged as can be seen in Fig. 8.10.

Warp \ Weft	T700SC 40	T700SC 80	T700SC 120	T700SC 160
T700SC 40	80	120	160	200
T700SC 80	120	160	200	240
T700SC 120	160	200	240	280
T700SC 160	200	240	280	320

Figure 8.9 Sixteen variations of spread-tow fabrics from T700SC 12ks, four being balanced (shaded).

Warp		Weft: T700SC 40	T700SC 80	T700SC 120	T700SC 160	TR50S 50	TR50S 100	TR50S 150	Zylon HM 33	Zylon HM 49	Zylon HM 65	Zylon HM 81	Zylon HM 98	Zylon HM 114
T700SC	40	80	120	160	200	90	140	190	73	89	105	121	135	154
T700SC	80	120	160	200	240	130	180	230	113	129	145	161	177	193
T700SC	120	160	200	240	280	170	220	270	153	169	165	201	218	234
T700SC	160	200	240	280	320	210	260	310	193	209	225	241	258	274
TR50S	50	90	130	170	210	100	150	200	83	99	115	131	148	164
TR50S	100	140	180	220	260	150	200	250	133	149	165	181	195	214
TR50S	150	190	230	270	310	200	250	300	183	199	215	231	248	264
Zylon HM	33	73	113	153	193	83	133	183	66	82	98	114	131	147
Zylon HM	49	89	129	169	209	99	149	199	82	96	114	130	147	163
Zylon HM	65	105	145	185	225	115	165	215	98	114	130	146	163	179
Zylon HM	81	121	161	201	241	131	181	231	114	130	146	192	179	195
Zylon HM	98	138	177	218	258	148	198	248	131	147	163	179	196	212
Zylon HM	114	154	193	234	274	164	214	264	147	163	179	195	212	228

Figure 8.10 The spread-tow fabric flexibility matrix with three ingoing fibres.

Fig. 8.10 illustrates the flexibility in producing various areal weight spread-tow fabrics with only three fibre types. If the number of fibre types is increased to seven, as shown in Fig. 8.11, the possibilities of engineering various areal weights and fibre combinations increase enormously. The fabric areal weight−fibre type matrix can grow almost infinitely large if more fibres are considered and also if the tape width is not limited to 20 mm but varied.

The preceding section has already introduced hybrid variants of spread-tow fabrics, as the matrix suggested fabric constructions containing more than one fibre type; in these cases one fibre type will be present in the 0 degree direction and one in the 90 degree direction. Such hybrid fabric styles are not unique for spread-tow fabrics; instead they are readily available also from traditional yarn-woven fabrics. A commingled hybrid is a product in which two or more fibre types are mixed so that there is no clearly identified interface between the different fibres. Such fabric constructions are extra suitable for spread-tow constructions as the tows from the different materials

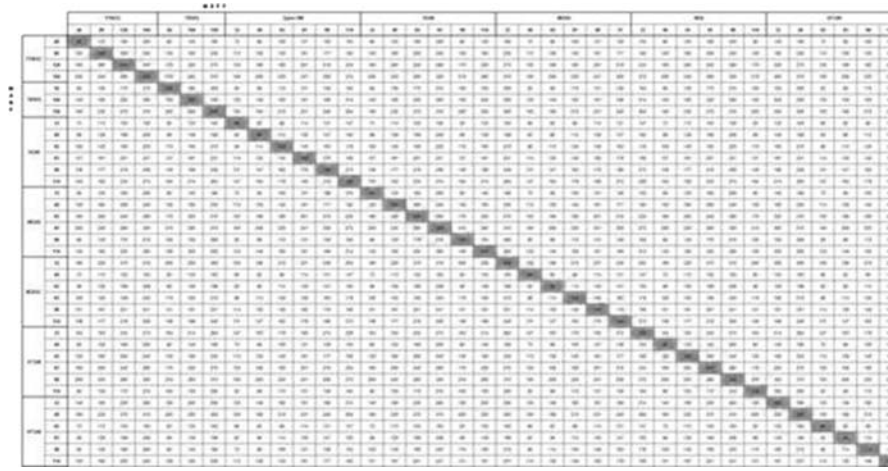

Figure 8.11 The number of spread-tow fabric possibilities could be almost infinitely large as the tape width can vary and many more fibres are available.

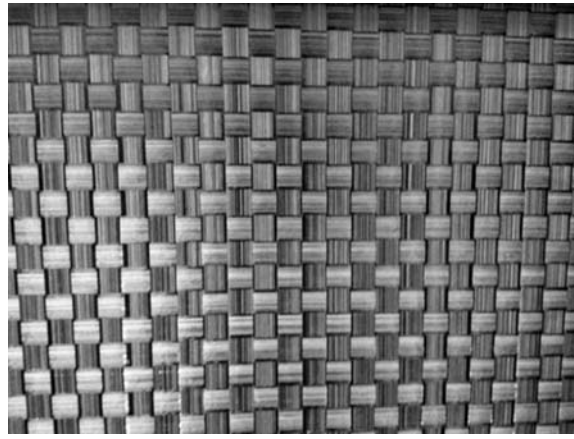

Figure 8.12 Commingled hybrid spread-tow fabric.

can achieve a high degree of mixture as the filaments are spread out over the width, see Fig. 8.12. Hybrid materials of commingled type are a relatively new spread-tow development but have already displayed increased impact toughness and residual strength and will undergo deeper research.

8.5 Mechanical performance

There are many guidelines and design rules connected to composite usage in, for example, the aeronautics industry, design rules that limit and reduce the full weight

saving possibilities connected with using composites rather than isotropic materials such as aluminium and other metallic materials.

For instance, for certain composite structures, four-ply angles (0, ±45 and 90 degrees) must be used at all times. Also, each of these fibre angles must display a minimum 10% presence. This phenomenon, often related to the expression "black aluminium," comes from the fact that the full usage of composites is not fully realized. Furthermore, the rules for achieving a full symmetry around the midplane to avoid thermal warpage, B matrix equal to 0 and balanced laminates to avoid anisotropy, A16 and A26 equal to 0 according to Fig. 8.13, are also limiting the opportunities associated with composite flexibility. Add to these rules ply drop rules to achieve specific tapering and design with a maximum strain level of 0.4% to minimize the risk for matrix cracks.

Many of the design limitations explained here are related to, and generated by, the traditional usage of UD prepregs. By implementing spread-tow reinforcements some of these rules can be challenged. Thin spread-tow fabrics display, even though symmetrically balanced because of the interlacing, almost no virtual crimp, and the knock-down factor in stiffness is almost negligible compared to UD prepregs in crossply. Therefore, quasi-isotropic layups can be achieved using virtually fewer fibre angles and plies when implementing spread-tow fabrics of 0/90 and ±45 constructions according to Table 8.4 and Fig. 8.14. This can lead to saved weight in the composite structure even though design rules are being followed.

$$\begin{bmatrix} N_x \\ N_y \\ N_{xy} \\ M_x \\ M_y \\ M_{xy} \end{bmatrix} = \left[\begin{array}{ccc:ccc} A_{11} & A_{12} & 0 & 0 & 0 & 0 \\ A_{12} & A_{22} & 0 & 0 & 0 & 0 \\ 0 & 0 & A_{66} & 0 & 0 & 0 \\ \hdashline 0 & 0 & 0 & D_{11} & D_{12} & D_{16} \\ 0 & 0 & 0 & D_{12} & D_{22} & D_{26} \\ 0 & 0 & 0 & D_{16} & D_{26} & D_{66} \end{array}\right] \begin{bmatrix} \varepsilon_x^o \\ \varepsilon_y^o \\ \varepsilon_{xy}^o \\ \kappa_x \\ \kappa_y \\ \kappa_{xy} \end{bmatrix}.$$

Figure 8.13 Symmetry and uncoupled laminas are requested from a design rule perspective.

Table 8.4 Symmetrical quasi-isotropic construction

Material	Ply sequence	No. of fibre layers required for symmetry
UD	[0/90/+45/−45/−45/+45/90/0]	8
NCF	[$NCF_{(0/90/+45/-45)}$/$NCF_{(-45/+45/90/0)}$]	8
Spread-tow fabrics	[Spread-tow $fabric_{(0/90)}$/spread-tow $fabric_{(+45/-45)}$/spread-tow $fabric_{(0/90)}$]	6

UD, unidirectional; *NCF*, non-crimp fabric.

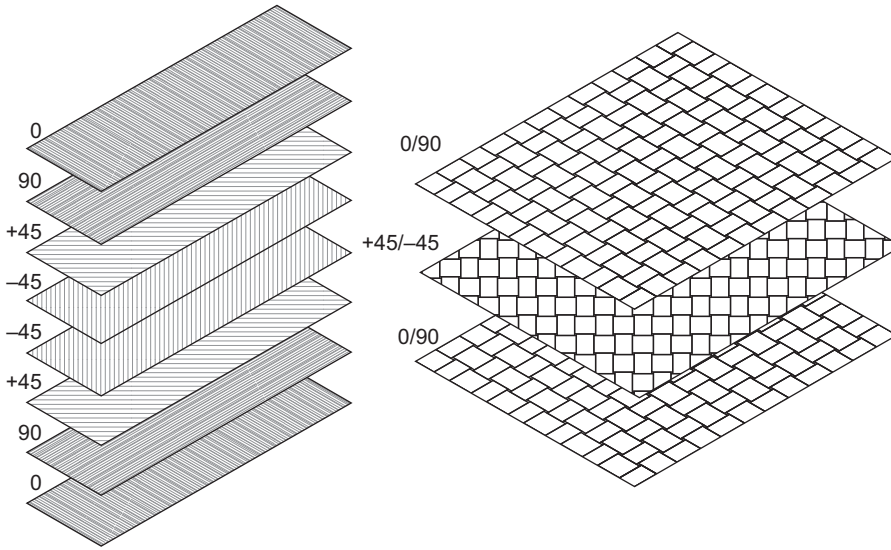

Figure 8.14 Symmetrical quasi-isotropic construction of unidirectional/non-crimp fabric (left) and $+\alpha/-\beta$ spread-tow fabric (right).

In a similar way, using spread-tow fabrics, bidirectional fibre angle layups can be achieved using fewer plies compared to when utilizing UD materials, even for ±45 degrees according to Table 8.5 and Fig. 8.15.

Furthermore, since spread-tow fabrics are available in ply thicknesses lower than those of standard UD prepreg materials, design rules related to minimum percentage covering in each fibre angle can be redesigned. The total laminate thickness can be reduced, as can be seen on the left in Fig. 8.16. Alternatively, the laminate thickness can be kept equally thick and the percentage in each fibre angle can be adjusted and optimized for the given load case. This can be seen on the right in Fig. 8.16.

Spread-tow fabrics demonstrate improved mechanical performance compared to traditional woven reinforcements owing to the unique weave structure created by interlacing tapes rather than yarns, but also to the fact that the corresponding tapes are

Table 8.5 Symmetrical bidirectional construction

Material	Ply sequence	No. of fibre layers required for symmetry
UD	[+45/−45/−45/+45]	4
NCF	[$NCF_{(+45/-45)}$/$NCF_{(-45/+45)}$]	4
Spread-tow fabrics	[Spread-tow $fabric_{(+45/-45)}$]	2

UD, unidirectional; *NCF*, non-crimp fabric.

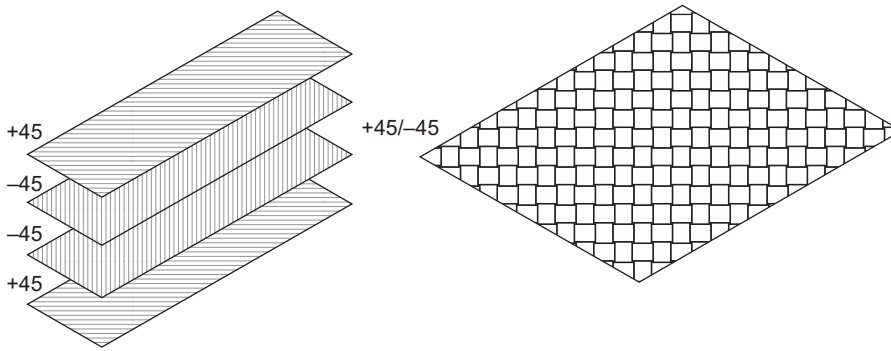

Figure 8.15 Symmetrical bidirectional construction of unidirectional/non-crimp fabric (left) and $+\alpha/-\beta$ spread-tow fabric (right).

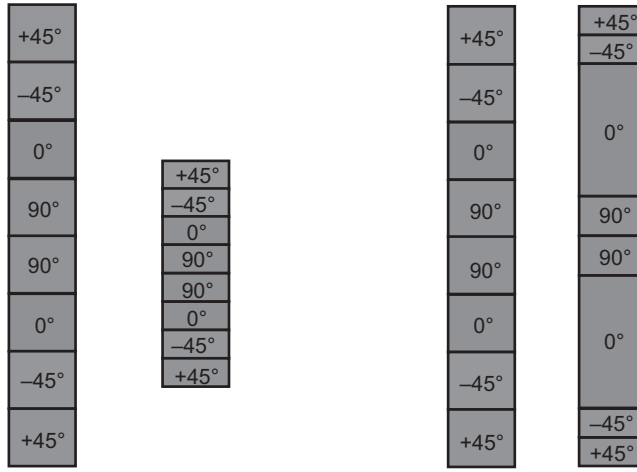

Figure 8.16 Flexibility to reduce laminate thickness (left) or optimize the fibre angle distribution (right).

relatively thin. Simple laminate theory and Fig. 8.17 show that with thin plies the interlaminar stresses are reduced significantly at bending.

In a study [15] conducted by the Swedish research institute Swerea SICOMP, mechanical properties for five different reinforcement structures were investigated. The test materials were spread-tow fabric, woven UD, NCF, 3k Plain Weave and 1k Plain Weave. All candidate materials were dry reinforcements, commonly available, produced from standard high-strength fibres and with an area weight as close to 100 gsm as possible. Further, all materials were plied in $[0/90]_s$ layup and vacuum infused with the same resin (LY556/HY917/DY070) under fixed process parameters and postcured under equivalent conditions to keep all external parameters fixed. The mechanical data were not normalized with respect to a theoretical fibre volume fraction, such as 60%. This was because the test was aimed at comparing real mechanical data that were possible to reach and not data that were available only in theory.

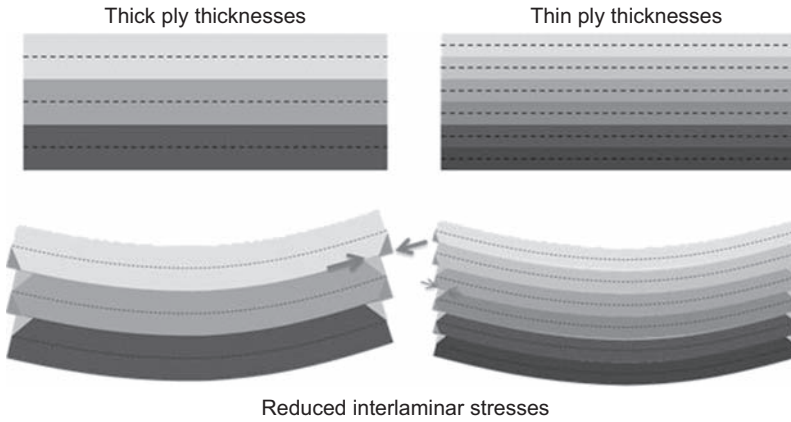

Figure 8.17 Thin plies reduce interlaminar stresses at bending.

Mechanical data for tensile, compression, in-plane shear and intralaminar shear stresses are presented in Table 8.6 and also in Fig. 8.18 in which all candidate material data have been normalized in comparison to the spread-tow fabric.

From the tests it can be seen that spread-tow fabrics show relatively higher mechanical performance compared to the other materials for tests that are fibre dominated. It can also be seen that spread-tow fabrics and also UD materials present a much smoother surface, reducing the amount of nesting between the layers, which affects the measurement of the performance between the layers.

Composite structures used within the aeronautics industry are by design rule limitations not allowed to be loaded to more than a 0.4% strain in a structure because of the risk of matrix cracks transverse to the fibres. This fracture mode is normally the initial damage type which grows and meets a neighbouring reinforcement layer or fibre

Table 8.6 Mechanical data from spread-tow, CP-UD, NCF, 3k and 1k fabric

	σ_{11}	E_{11}	ε_{f11}	ν_{12}	σ_{11}^{c}	E_{11}^{c}	τ_{12}	G_{12}	ILSS	V_f
	MPa	GPa	%		MPa	GPa	MPa	GPa	MPa	%
Spread tow	1259	69.1	1.48	0.033	656	56.9	102	5.5	44.4	59
CP-UD	1129	67.5	1.52	0.036	471	70.8	101	5	40.4	60
NCF	1151	55.5	1.38	0.04	584	53.8	120	5.4	67.5	49
3k	794	57.4	1.25	0.034	503	61.7	98	4.4	55.4	47
1k	724	55.6	1.27	0.039	544	52.4	122	5.4	65.1	52

CP-UD, cross ply unidirectional; *NCF*, non-crimp fabric; σ_{11}, Tensile strength; E_{11}, Tensile modulus; ε_{f11}, Tensile strain; ν_{12}, Poisson ration; σ_{11}^{c}, Compression strength; E_{11}^{c}, Compression modulus; τ_{12}, In plain shear strength; G_{12}, In plain shear modulus; ILSS, Inter laminar shear strength and V_f, Fiber volume fraction.

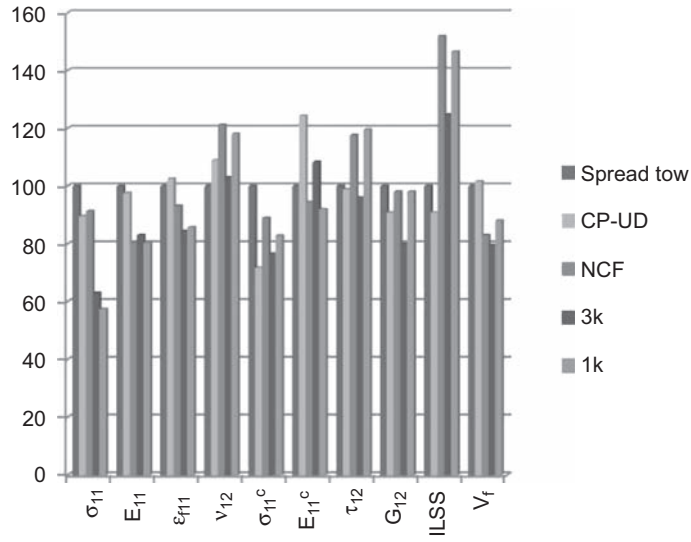

Figure 8.18 Mechanical data normalized against the spread-tow data. *CP-UD*, cross ply unidirectional; *NCF*, non-crimp fabric; σ_{11}, Tensile strength; E_{11}, Tensile modulus; ε_{f11}, Tensile strain; ν_{12}, Poisson ration; $\sigma_{11}{}^{c}$, Compression strength; $E_{11}{}^{c}$, Compression modulus; τ_{12}, In plain shear strength; G_{12}, In plain shear modulus; ILSS, Inter laminar shear strength and V_f, Fiber volume fraction.

direction and in this intersection develops severe delamination, which can lead to disastrous failure.

When it comes to matrix cracks under transverse loading ply thickness plays a major role. Various ply thicknesses will, through what has been referred to as in situ strength, determine whether a crack will appear or if the resistance to matrix cracks is pushed further up towards higher strain levels.

In situ strength is often explained as the thinner the fibrous plies being used in a composite, the higher the resistance towards transverse failure. This has been explained by Olsson [16] via the diagram in Fig. 8.19, in which the apparent strength or, as we can refer to it, the theoretical transverse strength, as it could be difficult to observe the small matrix cracks as they appear, is plotted versus the ply thickness of the material.

The diagram explains that the transverse strength of a UD material (dashed line) with fibres in only one direction is constant and not dependent on ply thickness. This strength is lower than that of a ply with supporting layers at other fibre angles. The diagram, however, explains that when the ply thickness gets thinner it approaches a certain thickness at which the in situ strength of thin plies will be greater than that of thick plies. The apparent strength will, at this ply thickness, vary with the thickness.

To study the possible formation of damage of thin-ply spread-tow fabric-reinforced composites during an experimental investigation on in situ strength made by Xu [17], not all specimens were loaded to catastrophic failure in tension. For two specimens the tests were deliberately ended approximately at strain levels 1.1% and 1.3%, to assess possible initial damage. The third specimen was loaded to catastrophic failure at 1.8%

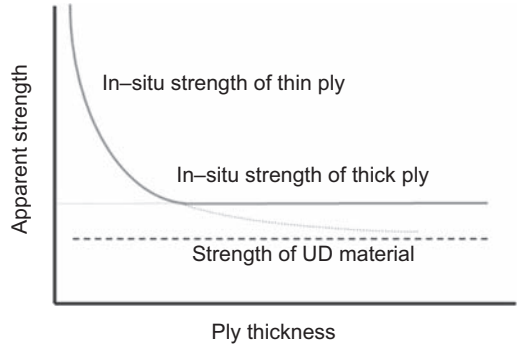

Figure 8.19 In situ strength diagram.

strain. After testing, the specimens were cut parallel to the loading direction and polished to allow study of the cracks in the specimens using an optical microscope. From the two specimens that were unloaded when the strain level reached 1.1% and 1.3%, respectively, two pieces were cut to study the cracks both in the centre of the specimen and on the surface of the specimen edge. It was expected that matrix cracks would be apparent at strain levels 1.1% and 1.3%. However, no matrix cracks were detected using the brightest light settings in the microscope for the specimen encased in fluorescent epoxy. There were a number of possible explanations for this; primarily it should be noted that this study was carried out after the specimens had been fully unloaded, because of this there is a possibility that there were microcracks formed during the tensile loading, but this did not become apparent since the cracks closed upon unloading. Second, it is uncertain whether the fluorescent epoxy was able to penetrate any cracks owing to its high viscosity. To eliminate this possible source of error, the specimens were also inspected with a low-viscosity penetrant fluid. The dye penetrant inspection was governed by capillary action, since the surface tension of the penetrant fluid was low; it penetrated into surface discontinuities of the specimen. Despite this additional investigation, matrix cracks still could not be observed. The only observed damage in the material was fibre breakage, and some very limited transverse matrix cracking in the specimen loaded to final failure at 1.8% strain, see Fig. 8.20.

So, by utilizing spread-tow reinforcements, which are naturally based on thin plies, the design rule of maximum loading to 0.4% strain can be challenged.

Impact is one of the most lethal threats to composites as it often damages the fibre/matrix structure, but not always leaving any indication visible to the naked eye. This leads to unnecessary over-dimensioned structure with high safety margins giving excessive weight or requirements for complex and expensive non-destructive testing to make sure a structure has not developed a weak zone.

Initial studies made by Hellström [18] on spread-tow fabrics that have undergone impact loading have shown an increased amount of broken fibres at the top and bottom surfaces, but somewhat fewer matrix cracks compared to traditional UD reinforcements. The fibre failures showed flexural characteristics and were somewhat more severe on the compression side rather than the tension side. This should be only logical

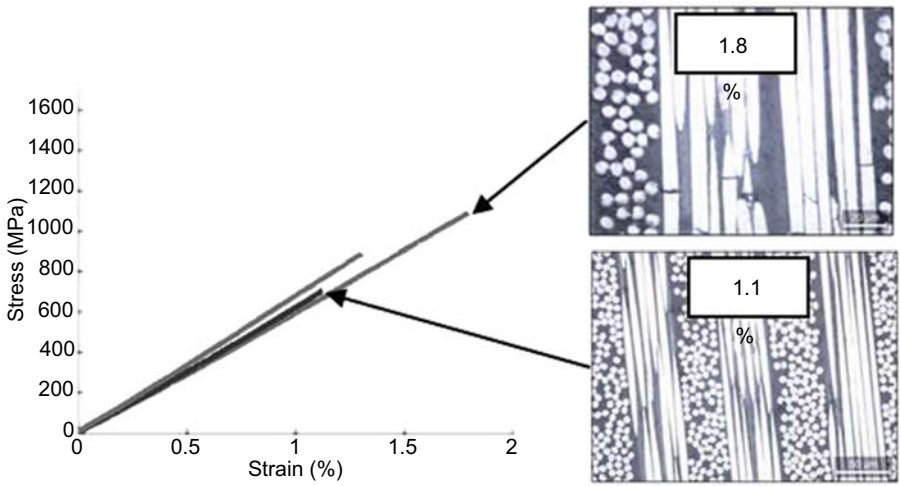

Figure 8.20 Stress versus strain curves for three 100-gsm TeXtreme® laminate specimens loaded in tension (with only limited visible damage accumulation).

as the composite compression strength traditionally is lower than that in tension. Traditionally the fibre fractures are more evenly distributed as the laminates tend to lose flexural stiffness along with increased delamination.

8.5.1 Surface smoothness

Most carbon fibres and epoxy resins have different coefficients of thermal expansion. This often leads to surface imperfections when a composite undergoes temperature cycles as the resin shrinks at the cross-section points in yarn-woven reinforcements. Spread-tow fabrics are constructed by interlacing wide and thin tapes. As an effect of this the crimp angle and crimp frequency are kept low and the areas of matrix accumulation are kept at a minimum number and size.

In an experimental investigation made on a boat hull construction with three different surface-reinforcement materials, glass fibre fabric, carbon fibre 3k fabric and spread-tow fabric, the last provided a relatively smoother surface compared to the traditional yarn-woven alternatives. All materials were temperature and humidity cycled equally before being measured. The measurement was conducted via an Opti-Topo surface topography unit on a 30 × 30-mm surface area. Figs 8.21–8.23 show the height differences between the various surface materials.

8.6 Challenges in testing large unit cell specimens

When conducting various testing of composite materials, procedures according to certain test standards are recommended so that results can be well compared. Spread-tow reinforcements, especially fabrics of various constructions, are unique in

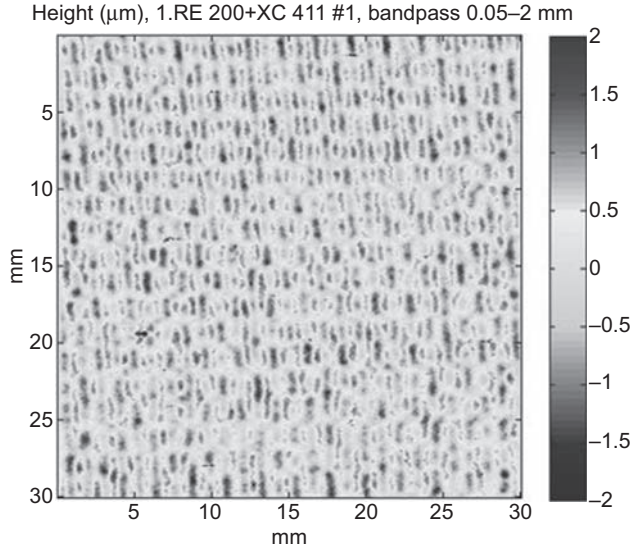

Figure 8.21 Surface smoothness for glass fibre fabric as surface material.

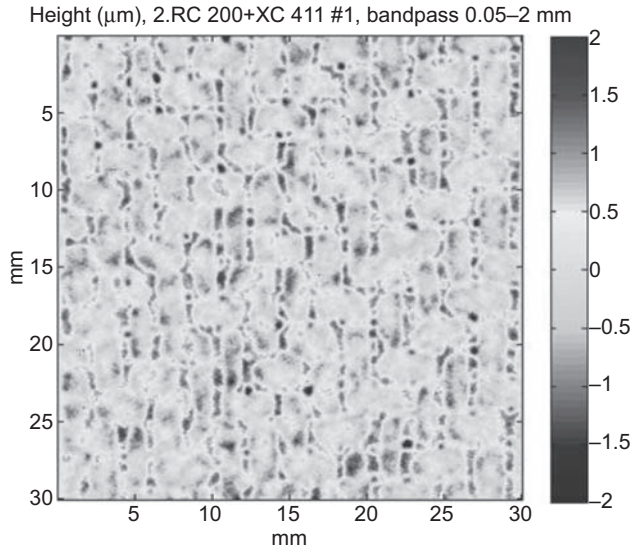

Figure 8.22 Surface smoothness for carbon fibre 3k fabric as surface material.

the sense that their unit cell size is substantially larger than those of traditional yarn-woven fabrics. The ASTM D6856-03 "Standard Guide for Testing Fabric-Reinforced Textile Composite Materials" [19] clarifies the size of a textile structure's unit cell as the smallest repeatable section in its pattern. For the simplest weave pattern, plain weave, that leads to two times the tape width, and for a spread-tow fabric

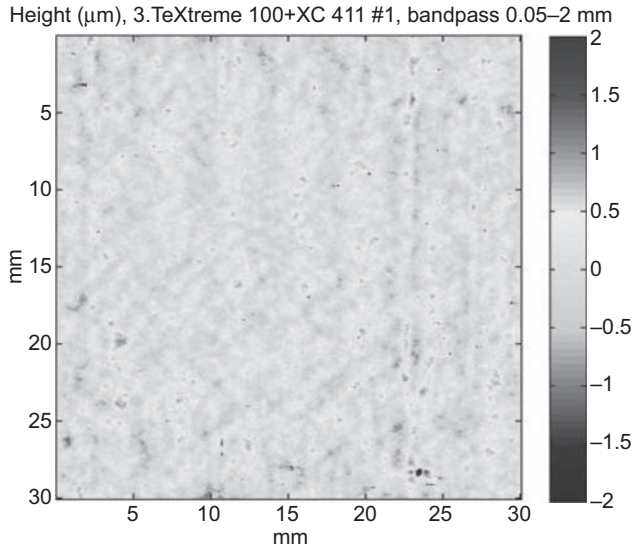

Figure 8.23 Surface smoothness for carbon fibre spread-tow fabric as surface material.

woven using 20-mm-wide tapes, the unit cell size will be 40 × 40 mm, meaning that for simple procedure testing such as tensile testing the specimens are recommended to be twice the unit cell, eg, 80 mm wide. This leads to challenges related to accuracy in strain gauges that record strain only at a limited part of the specimen. Further, with recommended specimen thicknesses greater than 2 mm, the cross section of the specimen tends to grow large, so large that more powerful load cells than normal are needed. Alternatively, if large enough load cells are not available, the specimen thickness must be reduced to allow the maximum load to occur during the test. When moving outside of the test standards like this, owing to the large unit cell size, the possible influence of testing a shell rather than a beam specimen must be considered.

8.7 Examples of customer cases

8.7.1 Formula 1

Back in 1983 when McLaren constructed their MP4/1C cars equipped with the first carbon fibre monocoque, most of the technology was borrowed from the aeronautics industry. The improvements in drivers' safety that the composites provided have been enormous and have saved the lives of many in racing accidents ever since.

The Formula 1 (F1) teams are constantly chasing weight savings in their cars to cut lap time around the circuits during the races. Even though an F1 car is restricted to holding a minimum weight during racing, saved weight can be redistributed as ballast at positions in the car to alter the balance and as close to the ground as possible so as not to affect the vertical point of gravity in a negative way.

Based on the technical regulations provided by the Fédération Internationale de l'Automobile (FIA) the challenge is to utilize available materials to their best. Various parts in F1 cars are constructed for stiffness or strength or a combination of both. The industry has traditionally used normal high-strength fibres where the absolute thinnest composite skins have been requested, mainly because low-areal-weight reinforcements have been based on low-tow-count yarns, eg, 1k, and these have been available only as high-strength fibres. Intermediate- and high-modulus fibres with minimum tow counts of 6k have limited the fabric areal weight to around 200 gsm at the minimum. The balance between fibre property and reinforcement areal weight has been inevitable.

Around the time of the 2008 season TeXtreme® spread-tow fabrics entered the series, offering a bidirectional reinforcement with a mechanical performance close to those of crossplied UD tapes, with the drapability of a traditional fabric and with intermediate- and high-modulus fibres in areal weights that were lighter than those available from 1k high-strength fibres.

The lightweight 1k fabrics that earlier were used displayed a relatively poor cover factor leading to excessive usage of padding and fillers to handle defects in the thin single or sandwich skins. Spread-tow fabrics have reduced a lot of this extra work and by this also removed the weight associated with the filler.

8.7.2 America's Cup, Oracle team USA

The America's Cup has always been a quest for lightweight solutions producing better and lighter structures and the 34th version of the competition was no exception. To meet these demands Oracle Team USA used TeXtreme® spread-tow carbon reinforcements manufactured by Oxeon, with which substantial weight savings were achieved. The Oracle Team USA AC72 was built by Core Builders Composites, a company based in New Zealand, see Fig. 8.24.

A majority of the laminates used in the AC72 have reinforcements in at least two directions, consequently an 80-gsm spread-tow fabric would have 20% reduced weight compared to two layers of 50-gsm UD tapes. Reduced labour cost was also a factor in using fabric rather than UD. It was possible to put down half the number of plies as opposed to the two layers of UD tape. Depending on the application spread-tow fabric was used at both +45/−45 and 0/90. Normally when placing UD fibres on the bias this is considered tedious as the UD fabric needs to be cut and placed manually at the exact degree desired. The tapes in the spread-tow fabric are well aligned, so laying down +45/−45 plies could be executed in a very efficient way.

Another time-saving aspect noted by Core Builders during the construction of the AC72 was the handling properties associated with binder-stabilized spread-tow fabrics, especially for the dry cloth. Conventional dry materials have nothing but a selvedge to hold them together, which means that as soon as one starts cutting them, they tend to fall apart unless handled in a very gentle manner. With the TeXtreme® cloths this was not a problem thanks to the binder that keeps the fabric together.

Figure 8.24 Oracle Team USA AC72.
Photo: Guilain Grenier.

An additional advantage was the increased toughness due to the interleaved spread tows of UD fibres. The 160-gsm cloth was used on exposed surfaces, where the increased skin thickness/toughness offset the weight penalty. The 100-gsm cloth was used widely on the construction of the wing elements and fairings. The 80-gsm cloth was used in the lightest weight fairings, typically on a foam sandwich rather than honeycomb. The most visible usage of TeXtreme® on the AC72 is on the flap noses and aft portions of the main element hard shell. The flap noses are primarily in torsion and are stiffness and strength critical. The angle of the flap laminate is optimized to provide the correct torsional stiffness profile along the length of the aerodynamic foil. Because the flaps are quite exposed, the durability of the honeycomb structure also had to be considered over reduced weight at all costs.

In contrast, the aft portion of the main element hard shell was designed to be as light as possible. Here the thin sandwich laminate of TeXtreme® and lightweight foam core form the extended hard shell of the wing main element and deliver increased aerodynamic performance. The only structural requirement was to be sufficiently rigid to maintain the aerodynamic shape.

8.7.3 e-Go and Shark ultralight aircrafts

Ultralight aircrafts or ULAs are a classification of aircraft with fewer certification requirements compared to classes above them. ULAs often hold only one or two seats and are regulated by weight. Therefore, to stay below the maximum weight limitations material choices are of great importance. For every kilogram saved in structural weight the aircraft can instead be equipped with navigation equipment and flight-tracking devices.

In the United Kingdom a special class of ULA exists, the SSDR class. To be approved for this class an aircraft must not weigh in at more than 115 kg. The company e-Go, Fig. 8.25, managed to stay below the strict weight limitation by utilizing spread-tow fabrics as an alternative to traditional yarn-woven reinforcements. From earlier prototypes a 200-gsm high-strength 3k 2 × 2 twill fabric was replaced by an 80-gsm TeXtreme® spread-tow fabric. This led to a total weight savings of 10% for the fibre-reinforced structure and as much as 53% weight savings on the specific TeXtreme®-made parts.

The Slovak Republic ULA manufacturer Shark Aero produces an aircraft, see Fig. 8.26, under the classification which is limited by maximum takeoff weight of 472.5 kg, or 300 kg when empty. Also Shark realized weight-saving potential by constructing its plane using spread-tow fabrics. They replaced a 200-gsm 3k fabric with 160-gsm TeXtreme® and a 90-gsm 1k with 80-gsm TeXtreme® and achieved a total weight savings of about 50 kg. Some specific parts, such as the rudder, displayed a weight savings of up to 60%.

Figure 8.25 e-Go SSDR ultralight aircraft.
© e-Go aeroplanes, with kind permission.

Figure 8.26 Shark Aero ultralight aircraft.
© Shark.Aero s.r.o., with kind permission.

8.8 Conclusions and future outlook

Spread-tow reinforcements have, during a relatively short period of time, shown great ability to provide weight savings and performance increases for applications within various transportation areas because of their unique fibre structure by which the fibre's performance is better utilized. A new type of construction flexibility based on thinner plies and new reinforcement variants is changing the way composite structures are designed and built. Spread-tow reinforcements provide possibilities of challenging traditional design rules that are based on the black aluminium approach, in which the full usage of composites is not realized.

Spread-tow reinforcements will see further developments related to finding their full potential. Investigations on how hybridization can improve fracture- and impact-related threats are requested. Additional research is needed to understand draping and process-related simulations as well as how the composite production step, using many thin plies, shall be done in a cost-effective way.

References

[1] Edgren, et al. Failure of NCF composites subjected to combined compression and shear loading. Compos Sci Technol 2006;66.
[2] Daniels CG. Pneumatic spreading of filaments. USA: Philco-Ford Corp.; 1974. USP 3795944.
[3] Iyer S, Drzal T. Method and system for spreading a tow of fibers. USA: Michigan State University; 1991. USP 5042122.
[4] Baucom RM, Snoha JJ, Marchello JM. Process for application of powder particles to filamentary materials. USA: NASA; 1991. USP 5057338.
[5] Calkins RW. Fiber impregnation process. USA: Garlock Inc.; 1991. USP 4994303.
[6] Muzzy JD, Varughese B. Flexible multiply towpreg and method of production thereof. USA: Georgia Tech Research Corp.; 1992. USP 5094883.
[7] Nakagawa N, Ohsora Y. Fiber separator for producing fiber reinforced metallic or resin body. Japan: Ube Industries; 1992. USP 5101542.
[8] Peritt JM, Everett R, Edelstein A. Electrostatic fiber spreader including a corona discharge device. USA: Secretary of the Navy; 1993. USP 5200620.
[9] Lifke JL, Busselle LD, Finley DJ, Gordon BW. Method and apparatus for spreading fiber bundles. USA: Adherent Technologies, Inc.; 2000. USP 6049956.
[10] Kawabe K, Tomoda S. Multi-filament split-yarn sheet and method and device for the manufacture thereof. Japan: Industrial Technology Centre of Fukui Prefecture; 2000. USP 6032342.
[11] Hiroharu O, Toshiyuki O. Apparatus and method for manufacturing opened sheet. Japan: OBS: KK; 2003. JP 3398133 and JP 3382603.
[12] Khokar N. A method for weaving tape-like warp and weft. J Text Inst 1999;90(3). Part 1.
[13] Homma K, Nishimura A, Horibe I. Carbon fiber woven fabric, its weaving method and weaving apparatus. Japan: Toray Industries; 1995. USP 5455107.
[14] Kawabe K, Tomota S, Shinkawato H. Production of open yarn fabric and apparatus therefor. Japan: Industrial Technology Centre of Fukui Prefecture; 2000. JP 2983531.

[15] Nilsson G. Comparison of mechanical properties between TeXtreme® and other textile based composites. 2012. Swerea SICOMP report CR12-081.
[16] Olsson R. Initial analysis of simplified tests for initiation of matrix cracking in fibre reinforced pipes. 2011. Swerea SICOMP report TR11-011.
[17] Xu J. Material models development of damage formation in thin ply carbon/epoxy textile composites. 2013. Swerea SICOMP report CR13-085.
[18] Peter H. Characterisation of impact damage generation in thin-ply carbon/epoxy textile composites. 2013. Swerea SICOMP report CR13-062.
[19] ASTM D. 6856-03 standard guide for testing fabric-reinforced textile composite materials. West Conshohocken. 2008. Annual Book of ASTM Standards.

This page intentionally left blank

Part Four

Durability, damage tolerance and structural integrity of lightweight composite structures in transport

This page intentionally left blank

9 Influence of temperature on mechanical properties of short glass fibre-reinforced polyamide 6 and 66 composites for automotive oil pan application

J. Njuguna
Robert Gordon University, Aberdeen, United Kingdom

Z. Mouti, K. Westwood
Eaton Automotive Group, West Midlands, United Kingdom

9.1 Introduction

Polyamides are a very attractive class of engineering polymers and have been used for numerous engineering applications because of their excellent tensile properties, chemical and abrasion resistance, high melting point and fatigue resistance. Polyamides are classified as crystalline polymers, but they are only mostly crystalline; some amorphous regions do exist. The crystalline regions form because the amide group of the polymer is polar. The electrons shared between some atoms are not shared equally, resulting in regions of slight positive and slight negative charges in the polymer chain. These charged regions are attracted to one another causing the polymer chain to fold over repeatedly. Of particular interest in this study are the polyamide 6 and 66 grades and the effects of their properties due to temperature changes.

To provide a background, the degradation of polyamides is a complex process and can lead to many different products. The principal degradation product from polyamide 6 (PA6) pyrolysis is generally agreed to be the cyclic monomer caprolactam, but the question of which additional products are detected seems to depend upon the sample size and the experimental conditions used [1].

Researchers agree, however, that the main route of thermal degradation of PA6 is the formation of caprolactam with yields as high as 85%—the presence of oligomeric products with nitrile and vinyl chain ends which are formed as a result of depolymerisation [1]. The increase in reaction order of the overall decomposition of PA6 above 420°C is correlated with the formation of by-products. Especially, the formation of the cyclic dimer seems to be a second-order reaction, which is responsible for the increase in the overall reaction order. The observed first-order reaction of ε-caprolactam formation is consistent with the mechanism of *cis*-elimination suggested whereby the *cis*-elimination proceeds via a six-membered intermediate (Fig. 9.1) [2].

Lightweight Composite Structures in Transport. http://dx.doi.org/10.1016/B978-1-78242-325-6.00009-8

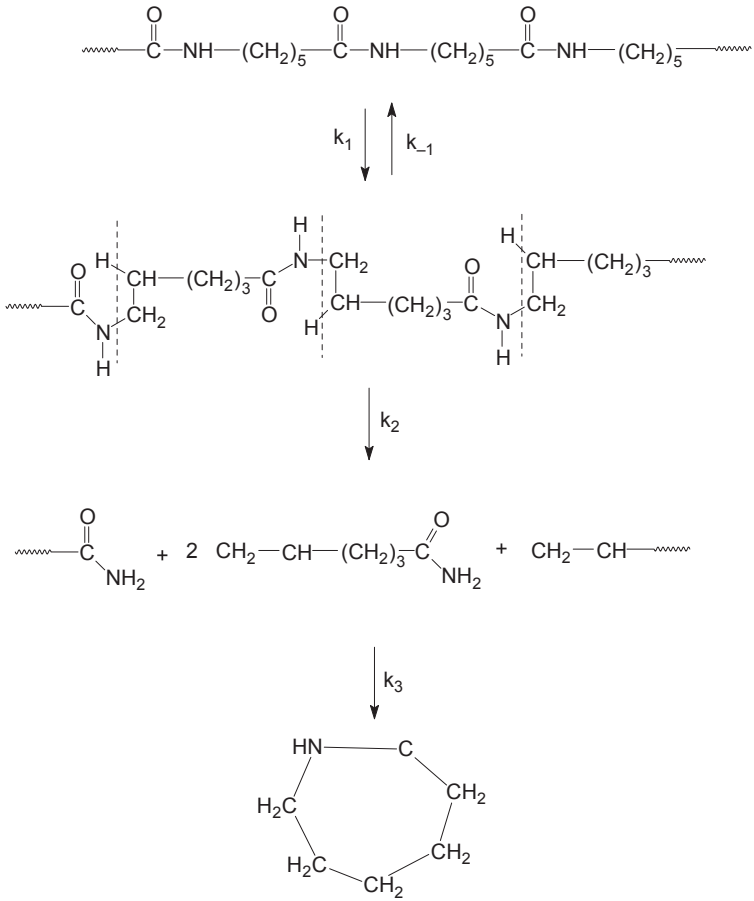

Figure 9.1 Degradation of PA6 via *cis*-elimination.

PA66 is also extensively used in engineering applications thanks to its excellent mechanical properties, and it has a good combination of high strength and ductility. However, it is acknowledged that when PA66 is loaded in the presence of a high-stress-concentration area, such as a notch, for instance, the resistance to failure of the material can be seriously reduced in relatively low fracture toughness. The use of thermoplastics reinforced with short glass fibres increases both stiffness and strength, but these improvements are accompanied by a reduction in the ultimate strain. Thermal degradation reactions of PAs, PA66, for example, produce mostly linear or cyclic oligomeric fragments and monomeric units. Primary PA chain scission (C(O)−NH or NH−CH_2 bonds), hydrolysis, homolytic scission, intramolecular C−H transfer and *cis*-elimination are all suggested from the product distribution as possible mechanisms.

PA66 eliminates as a main organic product cyclopentanone but also some hydrocarbons, nitriles and vinyl fragments. The main degradation product of PA66 is cyclopentanone, which is formed by a cyclic degradation mechanism in the adipic acid unit.

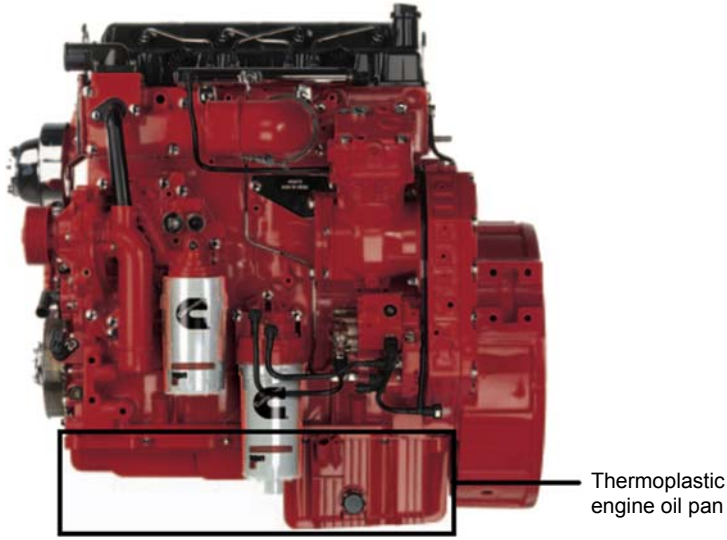

Figure 9.2 Thermoplastic engine oil pan fitted on an ISF 3.8 Cummins engine.

Initially a polymer chain with cyclopentanone end functionality is formed. In a subsequent equilibrium reaction an isocyanate is formed and cyclopentanone may split off. The resultant isocyanate reacts to form a carbodiamide and the cyclopentanone causing cross-link reactions. In PA66 these reactions lead to an increased tendency to cross-linking and non-soluble residue formation. The degradation of caprolactam mainly leads to oligomers with different end groups (−C−N amongst others) and the cyclic dimers of caprolactam. Degradation of mixtures of caprolactam with melamine, cyanuric acid and melamine did not lead to additional products. In these degradation experiments, caprolactam was found to be much less reactive than cyclopentanone. The formation of cyclopentanone during the degradation of PA66 was studied by pyrolysis−gas chromatography−mass spectrometry and it was reported that the degradation of PA66 at 400°C leads to various cyclopentane derivatives, cyclopentanone and ammonia condensation products [3].

Results from modelling of the thermal degradation of PA66 showed that the first bond that breaks leaves a free methylene radical and a free carbonyl radical and also that the carbonyl carbon is the part of the PA66 chain that is most susceptible to free radical attack [4]. When the methylene radical was allowed to fold back and attack this susceptible carbonyl carbon, then cyclopentanone was formed. Cyclopentanone was, indeed, reported as one of the major thermal breakdown products of PA66. In the absence of specific reactions, such as a retro-Diels−Alder, condensation or hydrolysis reaction, the initial step in any thermal decomposition is likely to be bond homolysis. It was assumed that the weakest bond will break first on heating, and that the weakest bond will also break first on stretching the chain. Thus, to identify the weakest bond, equivalent atoms at each end of the repeating unit are pulled until a bond breaks.

In automotive under-the-hood components (oil pan, see Fig. 9.2) subjected to loadings or impacts, this brittle behaviour is unwelcome.

In recent times, the toughening of thermoplastics with a rubbery phase has been promising to prevent such brittle failure, producing strong, tough and impact-resistant materials. However, such inclusions often reduce the modulus, stiffness and strength, which are important for material performance. The combination of reinforcement with a rubber toughening phase may be a solution to balance the end-use performance. In the literature, impact-modified PA6/elastomer blends were investigated in terms of the morphology−property relationship with maleated rubbers. It emerges that they are good impact modifiers for room-temperature toughening [5,6]. However, the understanding of such materials is a relatively unexplored area.

The properties of thermoplastics are temperature dependent owing to the fact that they are soft when heated and hard when cooled. The increase in temperature reduces the Young's modulus and tensile strength but increases the failure strain leading to a material more ductile and less stiff [7,8]. Thomason [9,10] found that additional energy dissipation mechanisms are activated thanks to the addition of fibres. Lhymn et al. [11] and Chevali et al. [12] mentioned that the moisture absorption can also be increased with the temperature [12]. On the other hand, the effect of thermal ageing on unreinforced and glass-reinforced PA66 was reported by Eriksson et al. [13] and Rudzinski et al. [14] to cause oxidative degradation on the surface region resulting in a decreased elongation at break and embrittlement of the material. Of particular concern are the under-the-hood thermoplastic parts that are required to be functional at elevated temperatures (around 80°C) encountered in and around the engine. The thermoplastic oil pan, for example (Fig. 9.3), is subjected to the heat created by the engine which is transferred via its connection by contact, the circulating oil and the surrounding air.

9.2 Experiments

9.2.1 Materials

Two commercial grades of PA66 with 35 wt% discontinuous glass fibre, Ultramid A3HG7 (short glass fibre-reinforced (SGFR) PA66) and Ultramid A3ZG7 (rubber-toughened SGFR PA66), were manufactured, ie, PA66-GF35 and PA66-i-GF35, respectively. The rubber modifier in the rubber-toughened material has been intimately melt-blended into the base material. The nature and amount of rubber information was not accessible from the material producer but previous studies have shown that one of the most promising types of elastomers used as a toughening agent for PAs is ethylene propylene rubber (EPR) copolymer added to about 20 wt% in the form of small particles. The PAs are copolymerised with the EPR chains on the terminal amine groups of the PA. The graft copolymers produced aid dispersion, creating separate phases in the solid enhancing interfacial adhesion.

The glass fibres had an average length (l) of 300 μm and diameter (d) of 13 μm, thus yielding an average aspect ratio (l/d) of 23. The materials were initially extrusion compounded into pellets by dry blending glass fibres with PA66 pellets and then injection moulded into test samples (tensile, flexural, and plate specimens). After injection moulding, the test samples were immediately sealed in antistatic and opaque polyethylene

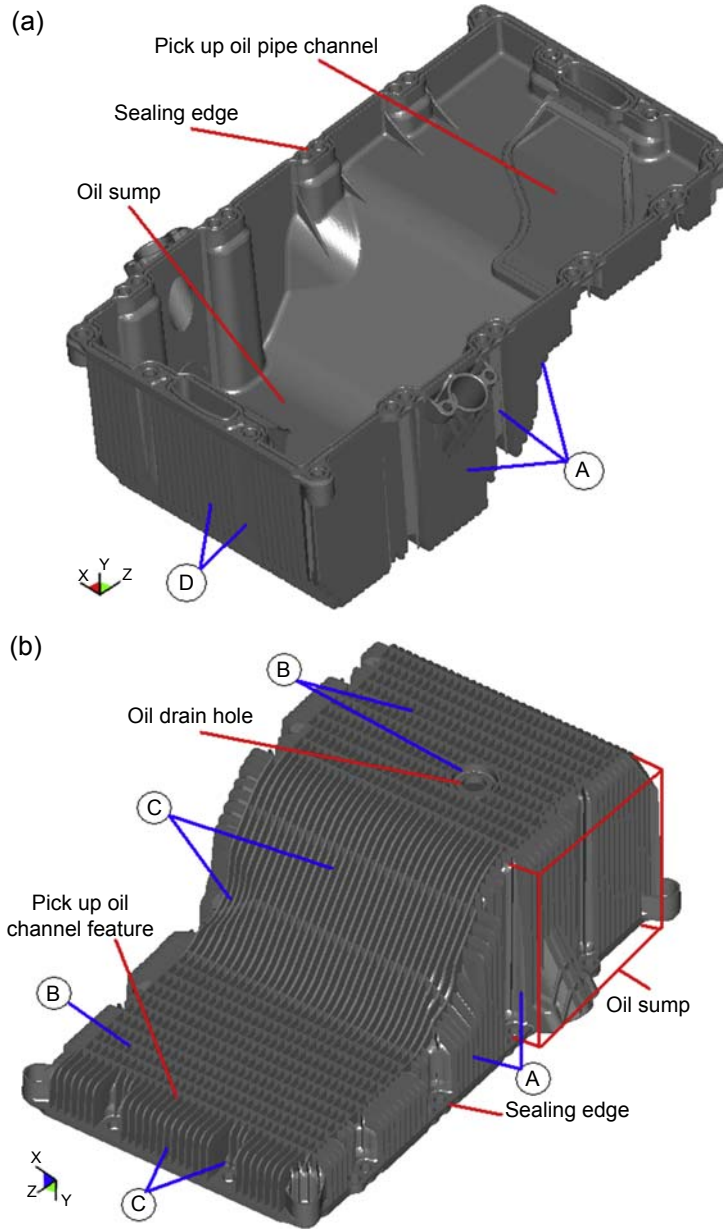

Figure 9.3 Improved version of the oil pan and key areas. (a) Inner view, (b) outer view.

bags to keep them dry as moulded and avoid any exposure to or contamination from the exterior. All test samples in this study came from the same batch of material and are henceforth named PA66-GF35 (A3HG7) and PA66-i-GF35 (A3ZG7) for the toughened material.

Ultramid B3ZG8 is a rubber-modified SGFR PA6 with 35 wt% fibre and is manufactured by BASF. This material is henceforth named PA6-i-GF35. PA6-i-GF35 was used in some experiments and compared against PA66-GF35 when PA66-i-GF35 was not yet available. PA66-GF35 and PA66-i-GF35 are based on the same polymer, PA66, but the latter is rubber toughened. PA6-i-GF35 is based on another PA, PA6, and is rubber toughened as well. Finally, pieces were cut off from the ribbing of each oil pan to make test samples.

9.2.2 Characterisation

Two thermal analysis techniques were conducted. Differential scanning calorimetry (DSC) measures heat exchange during physical transformation between a sample and a reference. The DSC instrument used was a DSC 200 from NETZSCH. The temperature was linearly increased at a rate of 10°C per minute in a range from ambient to 300°C. The reference used was air, which has a constant heat capacity in the range of temperature studied. Analyses were performed under argon, an inert gas, to avoid any reaction of the sample with the atmosphere of the furnace. This test also determines the maximum operating temperature for each material.

The thermogravimetric analysis (TGA) measures mass variation of a sample which is linked to phase transitions and thermal degradation during a thermal cycle of heating. This test was performed to assess the temperature of decomposition and the rate of degradation of each sample. The TGA instrument used was a TG 209 from NETZSCH. The temperature was set at 30°C and then linearly increased by 10°C per minute until reaching 610°C.

9.2.3 Ageing tests in oil and air

Ageing tests were conducted in collaboration with industrialists (BASF and Eaton Corporation) to assess the heat ageing effect in oil and air [15,16]. Tensile samples of PA66-i-GF35 and PA6-i-GF35 were aged in chambers at 150°C immersed in oil (Shell Helix Plus SAE 5W-40) or at 150°C in air for a period of up to 3000 h. Weekly, five tensile samples per condition were taken off from their chambers and tensile tests were performed and the evolution of tensile strength and tensile strain of each material was measured.

9.2.4 Mechanical testing

PA66-GF35 and PA66-i-GF35 samples were tested in dry as-moulded condition in quasi-static and dynamic loads. All of the test samples are ensured to be free of visible flaws, scratches, pits, sink marks or other imperfections. All the tests are conducted at a room temperature of 23°C. The damage assessment after a test was made by visual inspection on the external surfaces of the tested sample.

For the quasi-static tests, tensile tests at constant rate were carried out on an Instron 5500R 5/100 KN electromechanical testing machine. The specifications of tensile and flexural test specimens complied with their respective International Organization for Standardization (ISO) standards, ISO 527. Tensile test samples were flat dumbbell-type

1A with an overall length of 170 mm, a width at the ends of 20 mm, a width at the narrow portion of 10 mm and a thickness of 4 mm. The crosshead displacement was set to 1 mm/min. Flexural test samples were rectangular parallelepiped bars with an overall length of 80 mm, a width of 10 mm and a thickness of 4 mm. The crosshead displacement was set to 2 mm/min. In both cases, the injection moulding was made lengthwise. A minimum of 10 samples per tested material were performed.

9.3 Finite element analysis

The assessment of the material impact resistance in various configurations with varying parameters has driven the need to employ finite element simulations to approach, benchmark and predict strength and fracture behaviour of stressed parts. The finite element method is used as a tool for its predictive capabilities to solve numerically and represent analytically the behaviour of a physical system. This system is divided into elements linked together by nodes forming a mesh to which properties and relations of interactions are allocated. This method gives an approximate solution to a problem.

The simulations conducted in this work are based on the stress−strain relations obtained from the experimental work with fixed conditions to describe a specific situation. The representation of the material uses the elastoplastic material law [17,18]. The elastic Young's modulus defines the stress−strain relation up to the yield stress. Above yield stress, the plastic behaviour is described by the effective stress and effective plastic strain coordinates. The effective plastic strain is the unrecoverable portion of the true strain beyond the yield limit. When defining the effective stress versus effective plastic strain curve, the first plastic strain value would be zero and the first stress value would be the initial yield stress. The material failure is set using a strain failure criterion. If the calculated effective plastic strain for any element exceeds the predefined value, the element is removed from the model and the simulation continues with the eroded model. For simulating the behaviour of a rate-dependent material, the stress versus effective plastic strain curve implemented in the material card is adjusted in correlation with the strain rate applied to the model. Therefore, the failure criterion is updated in relation to the strain rate.

The test samples were directly designed and meshed within the computer using HyperMesh from Altair HyperWorks 9.0 with the LS-DYNA interface. Once the geometries are ready, the preprocessing begins assigning sections, materials properties and configuring behaviours, interactions and boundary conditions in the environment. The preprocessing was completed with LS-PrePost 2.4 whilst the simulations were processed with LS-DYNA Solver version 970, both from Livermore Software Technology Corporation. LS-DYNA was selected for its analysis capabilities (non-linear dynamics, failure analysis, crack propagation and more) and also its comprehensive library of materials models and contact algorithms. LS-PrePost 2.4 was also used to complete the postprocessing analyses.

Low-velocity impact tests were performed on a two-dimensional ribbed structure (11,286 shells elements, 1 mm per element) to assess the impact performance of PA66-GF35 and PA6-i-GF35 with the influence of the temperature. The ribbed

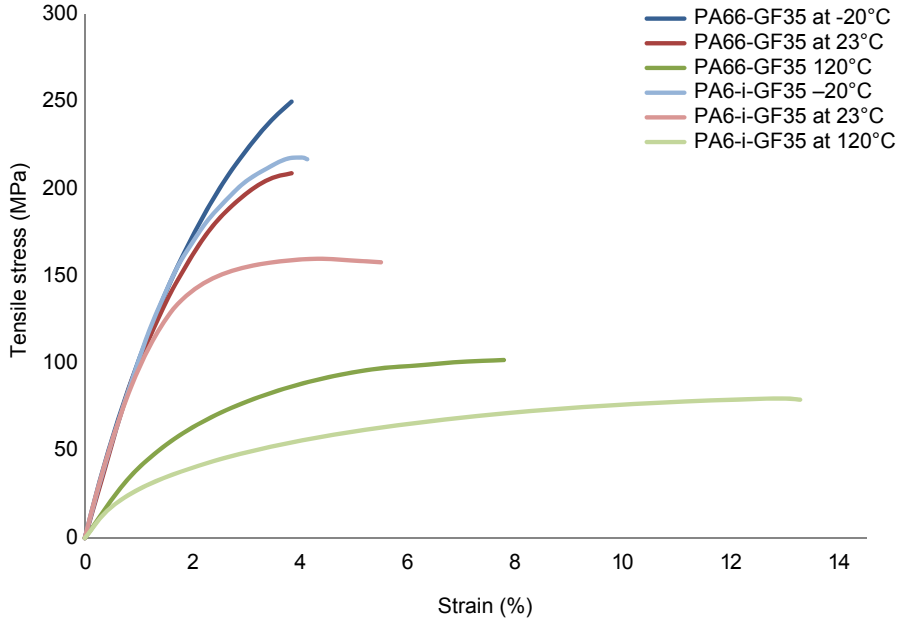

Figure 9.4 Temperature dependency of tensile stress−strain relations up to the breaking point of PA66-GF35 and PA6-i-GF35 [19].

Table 9.1 Strain to failure of PA66-GF35 and PA6-i-GF35 at −20, 23, 120°C [19]

Material	Temperature (°C)	Maximum strain at break (%)	Effective plastic strain at break (%)
PA66-GF35	−20	4.1 at 262 MPa	1.64
PA6-i-GF35	−20	3.98 at 217 MPa	2.04
PA66-GF35	23	3.8 at 213 MPa	1.90
PA6-i-GF35	23	5.3 at 158 MPa	3.64
PA66-GF35	120	7.4 at 104 MPa	5.18
PA6-i-GF35	120	12.8 at 79.3 MPa	11.06

structure was constrained on its edges. The impact locations were on the ribs and between the ribs. PA6-i-GF35 was used instead of PA66-i-GF35 because of the available data under different temperatures and similar impact response. Therefore, the purpose of this study was to investigate the influence of the rubber modifier on the impact performance. Single-impact tests were performed with a 10-mm diameter and 22-g projectile (defined as the rigid part) shot at 90 degrees to surface at 26 m/s so as to achieve the impact energy of 7.5 J. Fig. 9.4 and Table 9.1 illustrate the temperature dependency of PA66-GF35 and PA6-i-GF35 and the stress−strain relations at −20, 23 and 120°C implemented into the simulations.

9.4 Results and discussion

9.4.1 DSC results

Fig. 9.5 shows the DSC of PA66-GF35. The mass of the sample studied was 4.3 mg. The graph shows heat flow on the left and the variation of heat flow on the right versus the temperature. A negative peak related to an endothermic transition is observed at 260.9°C that corresponds to the temperature of fusion of the PA66-GF35 material. The peak begins at 234°C and finishes at 269°C. The integration of the area under the peak determines the enthalpy of this endothermic transition, $\Delta H_{\text{PA66-GF35}} = -45.16$ J/g. This refers to the consumption of heat needed for the sample to melt. At 234°C, the organised structure of the sample starts to dislocate and the chains of polymers move about. From this point, the temperature of the sample will not increase further until all the organised areas have melted. That is the reason that, at the same time, the variation of the heat flow fluctuates. Indeed, the DSC instrument has to keep up and maintain the temperature ramp set. A lot of heat is absorbed by the sample. After 269°C, less heat is required to increase the temperature of the sample and the variation of heat flow is back to null.

Fig. 9.6 shows the DSC of PA66-i-GF35. The mass of the sample studied was 4.4 mg. In this analysis, the endothermic transition is characterised by two peaks. The main peak is at 258.1°C, stretched from 230 to 264°C, followed by a small one at 268°C from 264 to 274°C. The possible explanation is that two different entities have reached their melting points. The first peak is the melting transition of the PA polymer but the second peak could result from the melting point of the rubber additives or its effects. The curve of the variation of the heat flow helps us to spot changes of phases when matched with the heat flow curve. The enthalpy of the first transition is $\Delta H_{\text{PA66-i-GF35}} = -36.8$ J/g.

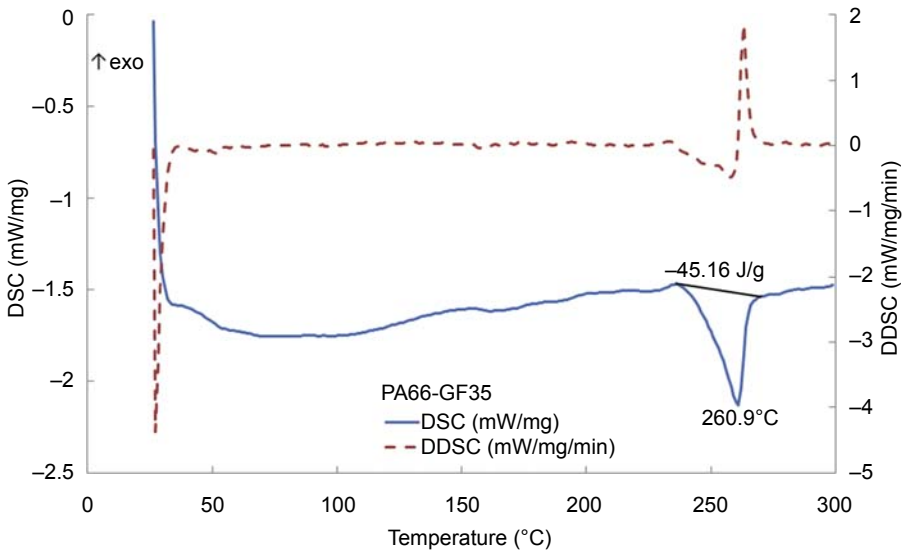

Figure 9.5 Differential scanning calorimetry (DSC) results for PA66-GF35.

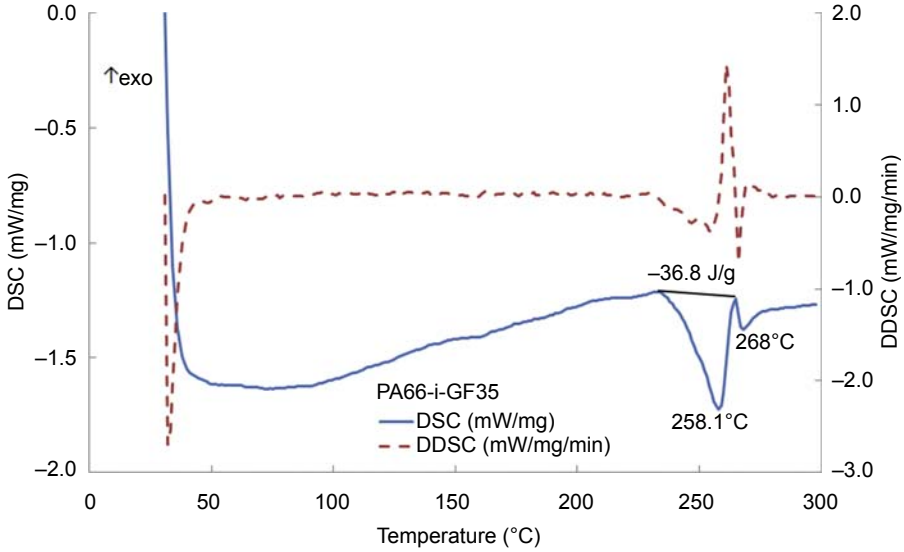

Figure 9.6 Differential scanning calorimetry (DSC) results for PA66-i-GF35.

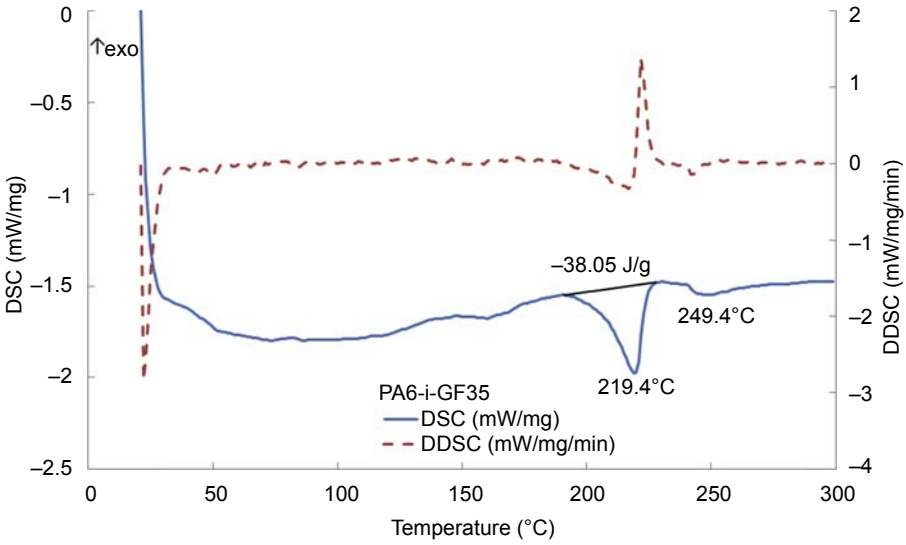

Figure 9.7 Differential scanning calorimetry (DSC) results for PA6-i-GF35.

Fig. 9.7 shows the DSC of PA6-i-GF35. The mass of the sample studied was 4.4 mg. PA6-i-GF35, like PA66-i-GF35, presents two peaks. The big peak from 191 to 227°C has its maximum at 219.4°C. The second peak is detached from the first one, it is small and weakens from 238 to 262°C and reaches its maximum at 249.4°C. A statement comparable to that previously given can explain each peak. The enthalpy of the first transition is $\Delta H_{\text{PA6-i-GF35}} = -38.05$ J/g and that is comparable to $\Delta H_{\text{PA66-i-GF35}}$.

Table 9.2 Material comparison of relevant differential scanning calorimetry data

Material	Literature value of melting point (°C) [19]	Recorded melting point (°C)	Enthalpy of fusion (J/g)	Glass transition (°C)
PA66-GF35	260	260.9	−45.16	155
PA66-i-GF35	260	258.1	−36.8	155
PA6-i-GF35	220	219.4	−38.05	155

Table 9.3 Specific heat capacities

Materials	Literature values of specific heat capacity (J)—endothermic [19]	Recorded data of specific heat capacity (J)—endothermic (solid state−melted state)
PA66-GF35	1500	1750−1470; average 1610
PA66-i-GF35	1500	1640−1220; average 1430
PA6-i-GF35	–	1790−1480; average 1635

The difference between PA66-GF35 and PA66-i-GF35 is the rubber-based additive. These thermoplastics have the same PA66 PA grade, which can be spotted by the similar peak at about 206°C. The PA66-i-GF35 and PA6-i-GF35 materials are respectively PA66 and PA6 polymers. Therefore their temperatures of fusion are different. However, the DSC graphs illustrate that they have practically the same enthalpy. Thus, the only correlation is the rubber content that levels this energy. The hypothesis is that the rubber additive spaces the polymer chains from one another by getting in between them. The consequence is that the energy linking the chains is lowered. Table 9.2 compares relevant DSC data findings.

These three materials exhibited a barely noticeable smooth glass transition at just about the same temperature of 155°C. However, there was no distinctive sign of crystallisation peaks. All materials faced a phase transition when heated, which changed their heat capacity (Table 9.3). The polymer in solid state had a lower heat capacity than when melted. That is to say, with a minor elevation of the temperature, the polymer in the melted state absorbs more heat.

9.4.2 Thermogravimetric results

Fig. 9.8 shows the thermogravimetric (TG) results for PA66-GF35. The mass of the sample at the start was 5.1 mg. The graph illustrates the variation in mass in percentage

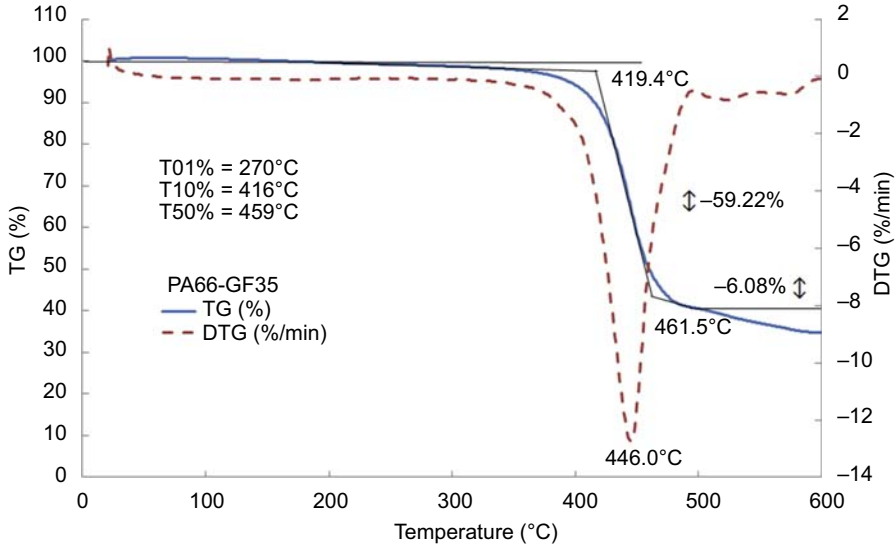

Figure 9.8 Thermogravimetric (TG) results for PA66-GF35.

on the left and its time derivative on the right. The increase in mass at the start may be a sign of oxidation that is translated as a gain of mass in the curve. The material at 270°C, which is over its melting point, has lost just 1% of its original mass. The temperature of degradation is reached at 446°C after having lost, since the beginning, 47% in mass and at 459°C it has lost 50% of its mass. Over 600°C, the mass seems to stabilise after 65.3% of mass lost.

Fig. 9.9 shows the TG of PA66-i-GF35. The mass of the sample at the start was 5.1 mg. The same comment can be used concerning the increase in mass at the beginning as a sign of oxidation. The material at 221°C has lost 1% of its original mass. The temperature of degradation is reached at 444.3°C after having lost, since the beginning, 33% in mass and at 467°C it has lost 50% of its mass. Over 600°C, the mass does not seem to stabilise but the rate of mass lost decreases after 68.3%.

Fig. 9.10 shows the TG of PA6-i-GF35. The mass of the sample at the start was 5.2 mg. The same comment can be used concerning the increase in mass at the beginning as a sign of oxidation. The material at 174°C has lost 1% of its original mass. The temperature of degradation is reached at 459.8°C after having lost, since the beginning, 34.2% in mass and at 464°C it has lost 50% of its mass. Over 600°C, the mass seems to stabilise with a very small slope after 68.2% of mass lost.

The temperatures of degradation of PA66-GF35 and PA66-i-GF35 are nearly identical within 1.7°C, since they are based on the same PA (PA66). PA66-i-GF35 and PA6-i-GF35 lost a very similar amount of weight of 2% before the degradation at respectively around 250 and 270°C. This correlates with the peaks suspected to be due to the additives in the DSC analysis, which are similar in each material.

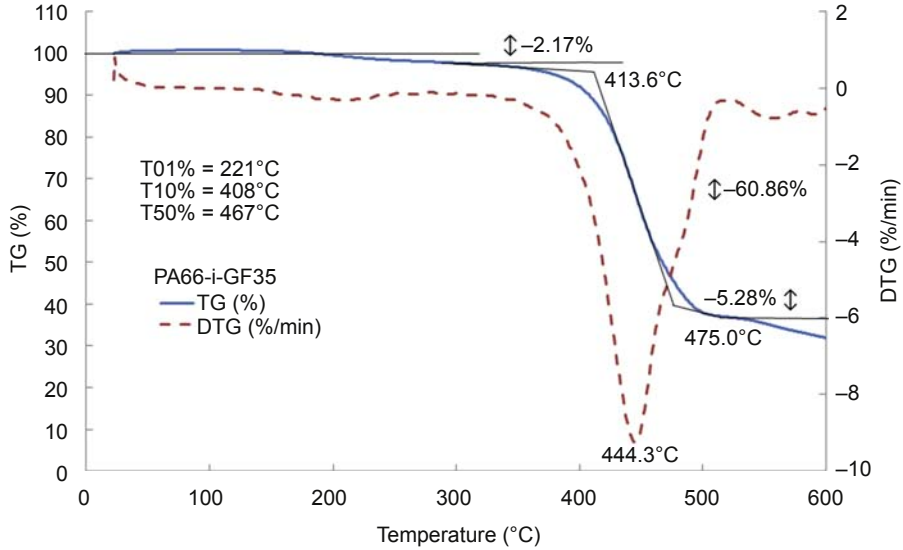

Figure 9.9 Thermogravimetric (TG) results for PA66-i-GF35.

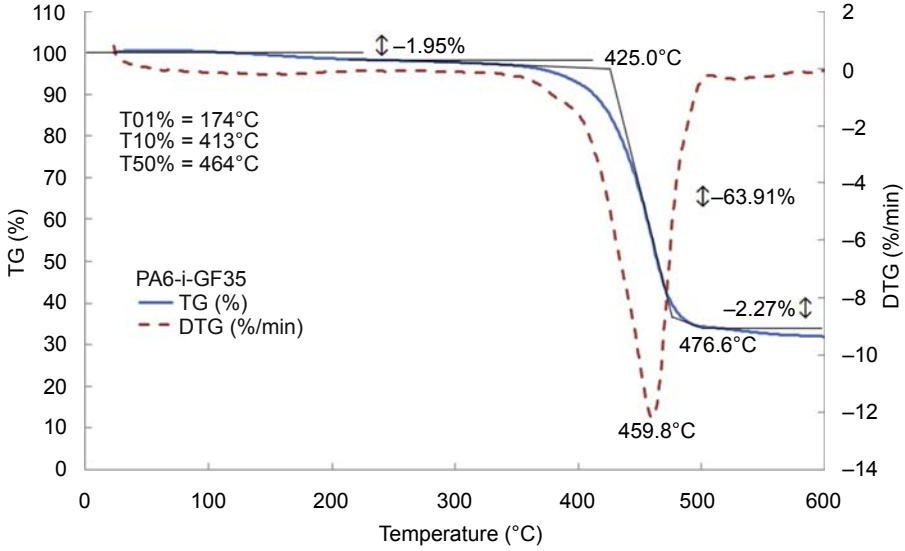

Figure 9.10 Thermogravimetric (TG) results for PA6-i-GF35.

The evaporation of these additives has for a consequence a loss of weight. The fact that it is not at the same temperature is explained by their divergent arrangements with the different PAs. Table 9.4 gathers temperatures of degradation and masses lost by each material.

Table 9.4 Temperature of degradation and mass loss

Material	Original mass (mg)	Temperature of degradation (°C) and mass loss (%)	Total mass loss (%)
PA66-GF35	5.1	446.0°C; 47%	65.3%
PA66-i-GF35	5.1	444.3°C; 33%	68.3%
PA6-i-GF35	5.2	459.8°C; 34.2%	68.2%

9.4.3 Ageing test results

Fig. 9.11 shows the consequence of heat ageing in oil (Shell Helix Plus SAE 5W-40) on the properties of two rubber-toughened PA grades, PA66-i-GF35 and PA6-i-GF35 (ASTM 105). The effect of oil on PAs may be slightly different depending on the composition of the oil. Some oils have a tendency to strengthen the material and some others to weaken it [16]. However, in this particular case, short-term tensile properties were increased up to 1000 h and then after 1000 h in a long-term assay were unchanged or stabilised. The exception was the tensile strain of PA6-i-GF35 that seemed affected and decreased during the first 1000 h of heat ageing.

Fig. 9.12 shows the consequences of heat ageing in the air on the properties of two rubber-toughened PA grades, PA66-i-GF35 and PA6-i-GF35. The oxidation appears to have more dramatic effects on the material mechanical properties in such a way that heat ageing in air is more problematic than that with different types of oil. Tensile strength and strain declined significantly whilst under heat ageing in air [4]. Even after 3000 h in hot air, which represents more than 4 months, this degradation of properties does not seem that it would end if the tests were continued.

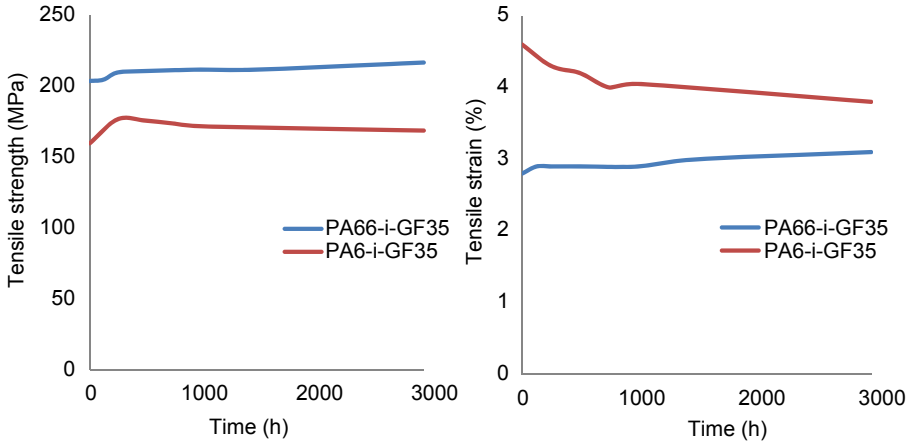

Figure 9.11 Heat ageing in oil at 150°C.

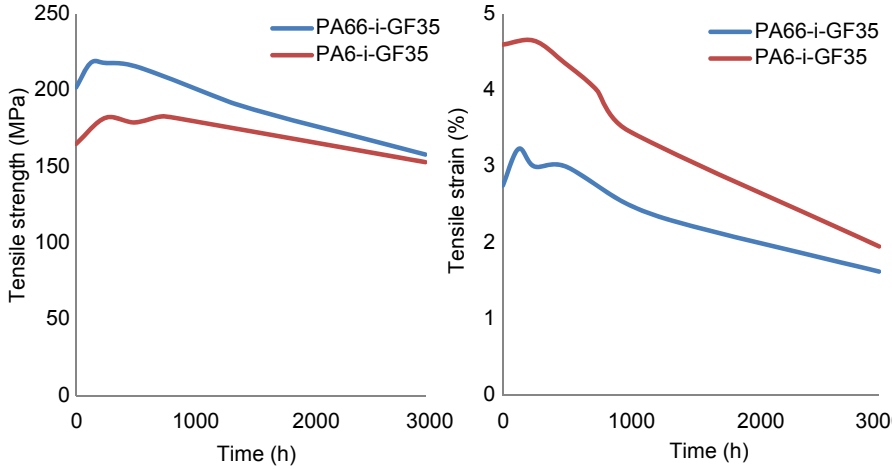

Figure 9.12 Heat ageing in air at 150°C.

9.4.4 Simulated impact response (−20, 23, 120°C)

As seen in Fig. 9.4, each material reacts differently with an increase in temperature. Fig. 9.13 illustrates the impact performance on a ribbed structure with an increase in temperature between PA66-GF35 and PA6-i-GF35 and gives the outcomes in each situation.

At −20°C, both materials are rigid and have higher strength than at 23°C, +23% for PA66-GF35 and +74% for PA6-i-GF35. However, they become essentially brittle, with their strains reduced by −14% for PA66-GF35 and −44% for PA6-i-GF35. At 120°C, both materials have their ductility considerably increased, +173% for PA66-GF35 and +204% for PA6-i-GF35 compared to 23°C. Their impact strengths on the other hand are significantly reduced, −51% for PA66-GF35 and −50% for PA6-i-GF35.

At the range of temperatures tested (−20, 23, 120°C), PA6-i-GF35 has a better impact performance at 7.5 J than PA66-GF35, thanks to its toughness that allows larger deformation. PA66-GF35 has constantly failed when impacted between the ribs especially at low temperature and at the base section of the rib. Its brittleness makes the rib crack whilst exercising pressure on the base wall because the deformation is reduced. On the other hand, PA6-i-GF35 allows more deformation at the range of temperatures tested, which spreads the impact loading undertaken by the structure.

Fig. 9.14 shows the variation of the peak load with the temperature for each material impacted at 7.5 J. An increase in temperature reduces the peak load response significantly. The rubber-modified PA grade PA6-i-GF35 exhibits a lower load level by −30% at 7.5 J compared to the non-rubber-modified material, PA66-GF35, throughout the range of −20 to 120°C. The rubber content in the modified PA makes it tougher. The brittle-to-ductile transition temperature is decreased, thus improving the impact behaviour at low temperatures. These findings agree with Borggreve et al. [20].

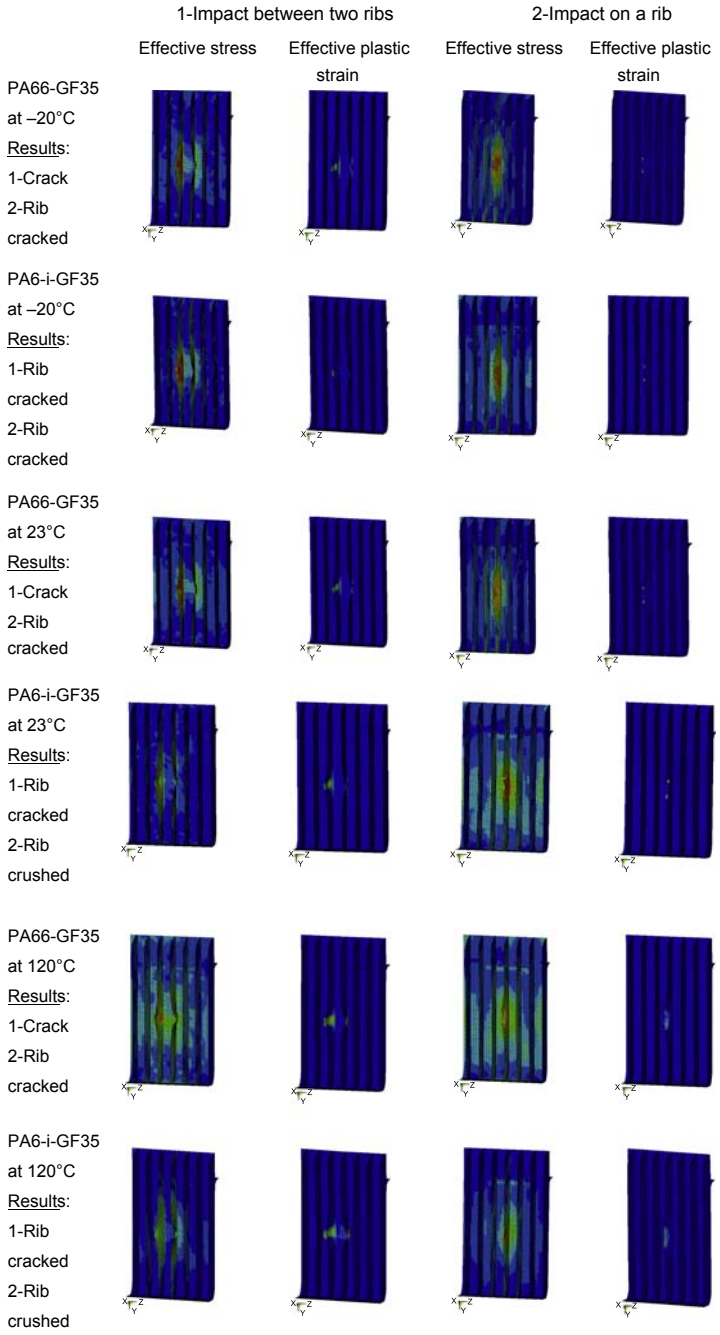

Figure 9.13 Impact performance on a ribbed structure at −20, 23, and 120°C at 7.5 J.

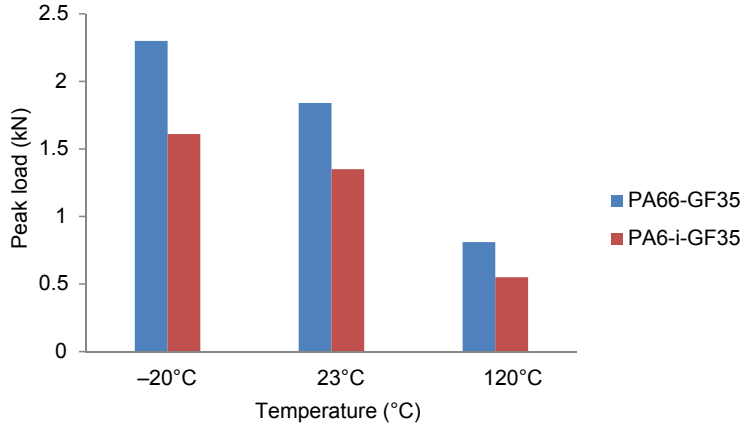

Figure 9.14 Variation of the peak load with temperature at 7.5 J.

9.5 Conclusions

DSC and TG analyses conducted on PA66-GF35, PA66-i-GF35, and PA6-i-GF35 permitted us to distinguish PA grades and the fibre glass and, more importantly, to reveal the presence of the impact modifier and its effect on the material in terms of heat exchange and temperature degradation. The polymers have their characteristic melting point temperature, which is around 260°C for PA66 and 220°C for PA6. The impact modifier interferes by lowering the consumption of heat needed for the polymer to melt. In the case of PA66-GF35 and PA66-i-GF35, this difference is 8 J/g. When subjected to heat degradation, the materials having the impact modifier lose 2% of their mass before reaching the temperature of degradation of their polymer.

Ageing effects in hot oil and in hot air revealed some disparity between PA66-i-GF35 and PA6-i-GF35. PA66-i-GF35 has a better tensile strength but a lower tensile strain than PA6-i-GF35. The oil (Shell Helix Plus SAE 5W-40) tends to slightly increase strength and strain except for the strain of PA6-i-GF35, which is regularly affected over time. The hot air, however, is the parameter that affects both materials' strength and strain very dramatically and constantly over the time.

The simulated influence of temperature on PA66-GF35 and PA6-i-GF35 ribbed structures illustrates their impact resistance and their temperature dependency. The increase in temperature softens each material, which absorbs more impact energy in deformation. The rubber-modified material PA6-i-GF35 absorbs more energy in deflection and deformation compared to PA66-GF35. The brittleness of PA66-GF35 at −20°C contributes to broken wall and ribs, whereas the toughness of PA6-i-GF35 allows progressive damage on the structure with ribs that absorb the impact energy by crushing. PA6-i-GF35 also allows a larger distribution of the impact loading, which results in a reduced peak load compared to PA66-GF35 in the range of temperature studied (−20 to 120°C).

References

[1] K. Pielichowski, J. Njuguna, Thermal Degradation of Polymeric Materials, RAPRA Technologies Limited, Shawbury, Surrey, UK, 2005.
[2] H. Bockhorn, A. Hornung, U. Hornung, J. Weichmann, Kinetic study on the non-catalysed and catalysed degradation of polyamide 6 with isothermal and dynamic methods, Thermochimica Acta 337 (1999) 97−110.
[3] P. Gijsman, R. Steenbakkers, C. Fürst, J. Kersjes, Differences in the flame retardant mechanism of melamine cyanurate in polyamide 6 and polyamide 66, Polym. Degrad. Stab. 78 (2002) 219−224.
[4] M. Vera, A. Almontassir, A. Rodríguez-Galán, J. Puiggalí, Synthesis and characterization of a new degradable poly (ester amide) derived from 6-amino-1-hexanol and glutaric acid, Macromolecules 36 (2003) 9784−9796.
[5] J. Mars, M. Wali, R. Delille, F. Dammak, Low velocity impact behavior of glass fibre-reinforced polyamide, in: Multiphysics Modelling and Simulation for Systems Design and Monitoring, Anonymous Springer, 2015, pp. 469−479.
[6] Z. Mouti, K. Westwood, D. Long, J. Njuguna, An experimental investigation into localised low-velocity impact loading on glass fibre-reinforced polyamide automotive product, Compos. Struct. 104 (2013) 43−53.
[7] Z. Mouti, K. Westwood, D. Long, J. Njuguna, Finite element analysis of localised impact loading on short glass fibre-reinforced polyamide engine oil pan subjected to low velocity impact from flying projectiles, in: 8th European LS-DYNA Users Conference, Strasbourg, 2011.
[8] Z. Mouti, K. Westwood, K. Kayvantash, J. Njuguna, Low velocity impact behavior of glass filled fiber-reinforced thermoplastic engine components, Materials 3 (2010) 2463−2473.
[9] J.L. Thomason, The influence of fibre length, diameter and concentration on the strength and strain to failure of glass fibre-reinforced polyamide 6,6, Compos. Part A Appl. Sci. Manuf. 39 (10) (2008) 1618−1624.
[10] J.L. Thomason, Structure-property relationships in glass-reinforced polyamide, part 3: effects of hydrolysis ageing on the dimensional stability and performance of short glass-fiber-reinforced polyamide 66, Polym. Compos. 28 (2007) 344−354.
[11] C. Lhymn, J.M. Schultz, Strength and toughness of fibre-reinforced thermoplastics: effect of temperature and loading rate, Composites 18 (9) (1987) 287−292.
[12] V.S. Chevali, D.R. Dean, G.M. Janowski, Effect of environmental weathering on flexural creep behavior of long fiber-reinforced thermoplastic composites, Polym. Degrad. Stab. 95 (12) (2010) 2628−2640.
[13] P. Eriksson, P. Boydell, K. Eriksson, J.-E. Månson, A. Albertsson, Effect of thermal-oxidative aging on mechanical, chemical, and thermal properties of recycled polyamide 66, J. Appl. Polym. Sci. 65 (1997) 1619−1630.
[14] S. Rudzinski, L. Häussler, C. Harnisch, E. Mäder, G. Heinrich, Glass fibre reinforced polyamide composites: thermal behaviour of sizings, Compos. Part A Appl. Sci. Manuf. 42 (2) (2011) 157−164.
[15] S.E. BASF, Processing by Injection Molding, 2011. Available at: http://www.plasticsportal.net/wa/plasticsEU ~ en_GB/portal/show/common/content/products/engineering_plastics/ultramid/processing_by_injection_molding.
[16] BASF S.E., Target Ultramid grade comparison for hot oil applications, 2009.

[17] H. Lobo, Methodology for selection of material models for plastics impact simulation, In 10th International LS-Dyna User's Conference (2006).
[18] H. Lobo, J. Hurtado, Characterization and modeling of nonlinear behavior of plastics, In ABAQUS User Conference (2006).
[19] CAMPUS, CAMPUSplastics, Available at: http://www.campusplastics.com/campus/.
[20] R.J.M. Borggreve, R.J. Gaymans, H.M. Eichenwald, Impact behaviour of nylon-rubber blends: 6. Influence of structure on voiding processes; toughening mechanism, Polymer 30 (1) (1989) 78−83.

This page intentionally left blank

The fatigue behavior of composite materials for high-temperature applications

10

N. Saad
Composite Materials Iraq, University of Babylon, College of Materials Engineering, Babylon, Iraq

10.1 Introduction

A common form of failure of materials in practical use is fatigue, in which the failure occurs from the cyclic application of stresses. These stresses are applied in various forms, such as sinusoidal (sin and cos), square, and pulsed waves. These kinds of stresses are different according to the magnitude and direction of stress, and also depending on the stress mode (system). Therefore, the failure may occur under applied stresses that are below the level required to cause yield or fracture in the case of a tension test (continuously rising stress).

The effect of such stresses is to initiate microcracks at the center of the stress concentration within the material or on the surface, and then propagation of cracks, which lead to separation of the material parts and finally to the state of sudden fracture (fatigue fracture).

10.2 Basic fatigue failure

First, some important parameters that will be useful in the subsequent discussion of fatigue, as shown in Fig. 10.1, are as follows:

Cyclic stress range: $\Delta\sigma = \sigma_{max} - \sigma_{min}$
Cyclic stress amplitude: $\sigma_a = (\sigma_{max} - \sigma_{min})/2$
Mean stress: $\sigma_m = (\sigma_{max} + \sigma_{min})/2$
Stress ratio: $R = \sigma_{min}/\sigma_{max}$
Number of fatigue cycles: N
Number of cycles to failure: N_f

In these parameters, σ_{max} and σ_{min} are the maximum and minimum stress levels, respectively [1–5].

These terms are very important for studying fatigue failure mathematically. There are empirical models that deal with various cases or conditions of fatigue and depend on the method of applied load (stress) and the conditions of the components that are subjected to these loads. There are two types of components, uncracked or cracked components, which also affects the σ_{min} and σ_{max} values with respect to yield stress of the material; therefore, we will consider fatigue under zero mean stress ($\sigma_m = 0$) and when neither σ_{max} nor $|\sigma_{min}|$ is above the yield stress, as shown in Fig. 10.2 [2].

Lightweight Composite Structures in Transport. http://dx.doi.org/10.1016/B978-1-78242-325-6.00010-4

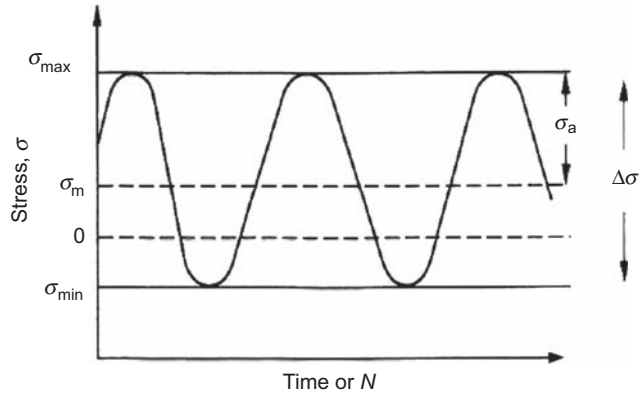

Figure 10.1 Fatigue parameters.
M.F. Ashby, D.R. Jones, Engineering Materials an Introduction to Microstructures, Processing and Design, third ed. (Butter Worth-Heinemann is an imprint of Elsevier).

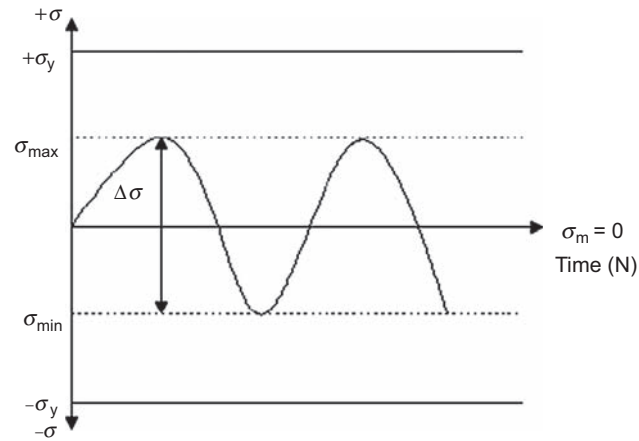

Figure 10.2 Long-cycle fatigue (based on Basquin's law).

It is found empirically that the experimental data can be fitted to Eq. [10.1] [2]:

$$\Delta\sigma N_{\mathrm{f}}^{a} = \mathrm{C}_1 \qquad [10.1]$$

This relationship is called **Basquin's law**, where a is constant between 1/8 and 1/15 for most materials and C_1 is constant also.

Eq. [10.1] deals with elastic deformation, whereas when $\sigma_{\max}$ and $|\sigma_{\min}|$ are above σ_{y} (plastic deformation) and $\sigma_{\mathrm{m}} = 0$, as shown in Fig. 10.3, the results can be fitted with a new empirical model, Eq. [10.2], which is known as the **Coffin−Manson law** [2,5]:

$$\Delta\epsilon^{\mathrm{pl}} N_{\mathrm{f}}^{b} = \mathrm{C}_2 \qquad [10.2]$$

where b (0.5−0.6) and C_2 are constants.

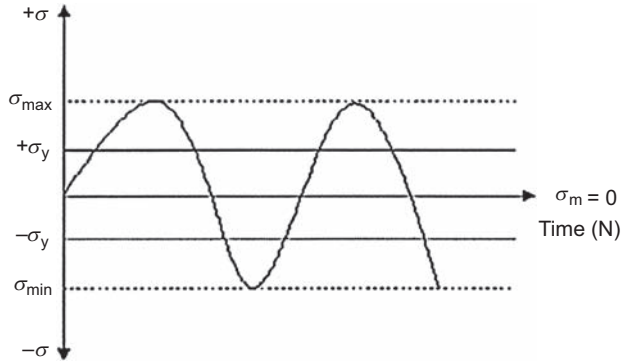

Figure 10.3 Short-cycle fatigue (based on the Coffin−Manson law).

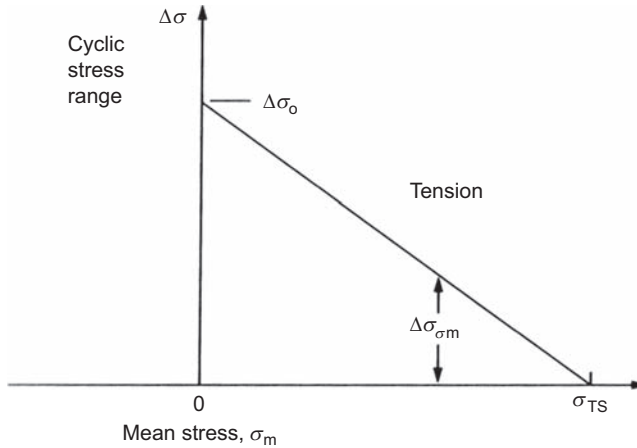

Figure 10.4 Effect of mean stress on fatigue life (Goodman's rule).
M.F. Ashby, D.R. Jones, Engineering Materials an Introduction to Microstructures, Processing and Design, third ed. (Butter Worth-Heinemann is an imprint of Elsevier).

When $\Delta\sigma$ and σ_m vary, for example, when materials are subjected to a mean tensile stress (ie, $\sigma_m > 0$), Fig. 10.4, the stress range must be decreased to preserve the same N_f according to **Goodman's rule** [1,2,5]:

$\Delta\sigma$ is the cycle stress range for failure in N_f and
$\Delta\sigma_{\sigma m}$ is the same thing for a mean stress of σ_m.

Where $\Delta\sigma$ varies during the lifetime of compound, the approach adopted is to sum the damage according to **Miner's rule of cumulative damage** (Eq. [10.3]) [2]:

$$\sum_i N_i/N_{fi} = 1 \qquad [10.3]$$

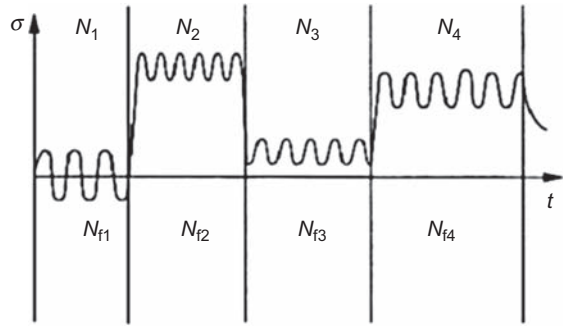

Figure 10.5 Accumulative damage.
M.F. Ashby, D.R. Jones, Engineering Materials an Introduction to Microstructures, Processing and Design, third ed. (Butter Worth-Heinemann is an imprint of Elsevier).

Here N_{fi} is the number of cycles to fracture under the stress cycle in region (i) and N_i/N_{fi} is the fraction of lifetime used up after N_i cycles in that region (Fig. 10.5) [2].

The fatigue behavior of cracked components is different from that the untracked component, which are explained. Therefore the model here is concentrated on the crack as it grows in tension and this case also deals with the cyclic stress intensity (ΔK) instead of stress range $\Delta\sigma$. It is found that the crack growth per cycle (d_C/d_N) increases with (ΔK) in the way shown in Figs. 10.6 and 10.7 [3,4,21]:

$$d_C/d_N = A(\Delta K)^m \qquad [10.4]$$

$$\Delta K = \Delta\sigma(\pi c)^{0.5}$$

$$\Delta K = K_{max} - K_{min}$$

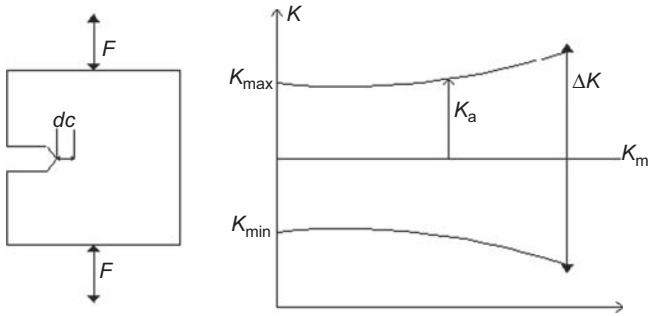

Figure 10.6 (Left) The crack length with cyclic load. (Right) ΔK increases as the crack extends. Modified from M.F. Ashby, D.R. Jones, Engineering Materials an Introduction to Microstructures, Processing and Design, third ed. (Butter Worth-Heinemann is an imprint of Elsevier).

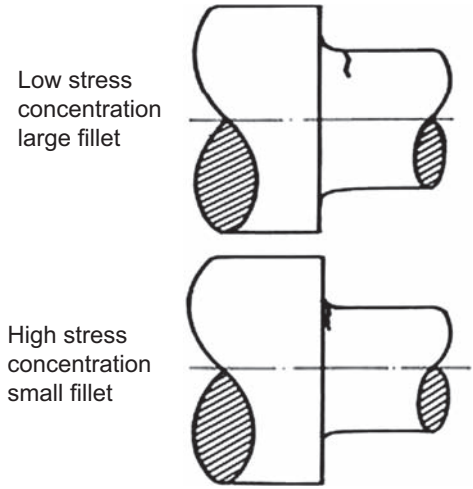

Figure 10.7 Stress concentration due to dimension change.
R.W. Hertzberg, Deformation and Fracture Mechanics of Engineering Materials, fourth ed., John Wiley & Sons, Inc.

The design of resistance to fatigue failure is achieved mainly by a depth of understanding of **the mechanisms** for this kind of failure and the important factors that affect the material resistance to this failure. Factors affecting the fatigue failure include [1,5–8]:

1. mechanical factors
2. microstructure factors
3. environmental factors

Mechanical factors include all systems of applied stresses and their values that have been touched upon in summary in the basics of fatigue failure, as well as stress increasers and their sources, for example, changes in dimensions, changes in diameter, and sharp edges, and surface conditions such as processes of finishing and smoothing and surface treatments such as coating, as shown in Fig. 10.7.

Microstructure factors include crystalline and amorphous cases for the material, the presence of second phases in the matrix materials, additives that lead to modification of the material's characteristics, and any other activities that change the material's behavior or the stability of its properties. Changes in the behavior and the characteristics, such as ultimate tensile strength, yield stress (σ_y), etc., cause changes in the fatigue strength according to the fatigue basis [1,5]. There are numerous mechanisms to increase the fatigue strength in polymers. Most of them fall into two categories [1,5,7,9]:

1. **Toughening mechanisms for the thermosetting polymers**: These mechanisms include additives of high toughening polymer, such as rubber and elastomeric materials.
2. **Strengthening mechanisms**: There are many techniques used to improve the polymer's strength, for example, using the composite principle (particle, fiber strengthening, etc.) and blending and processing techniques.

10.3 Environmental factors in fatigue and general properties of polymers

There are various environmental parameters that affect fatigue failure in polymers. These environmental factors include temperature of the service conditions, moisture, and other parameters such as ultraviolet radiation. These parameters influence the **mechanisms by which fatigue occurs**, which were described before (initiation of crack, changes in the material's behavior from ductile to brittle, and propagation of cracks) [1,5,8,10].

Plastics and polymers are some of the materials most susceptible to environmental effects that lead to initiation of cracking. Examples of such damage include the development of an extended network of crazes in a drinking glass or dish or the generation of cracks in a showerhead as shown in Fig. 10.8: These cracks were caused by exposure to temperature variations with the presence of stress, especially when the component begins under cyclic stress. The stress on these components will increase in value according to Eq. [10.5] below the glass transition temperature (T_g) [1,5,10]:

$$\sigma_{th} = E\alpha\Delta T \qquad [10.5]$$

where σ_{th} is the thermal stress, α is the linear thermal expansion, E is the modulus of elasticity, and ΔT is the temperature variation [1,2,5].

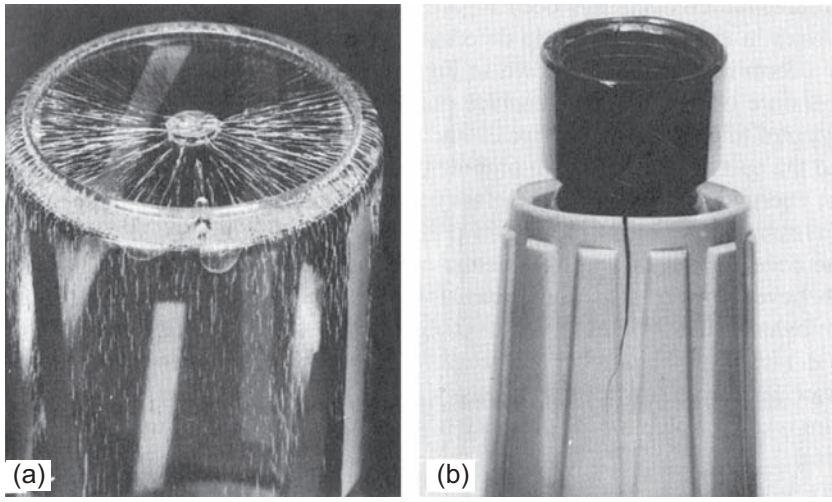

Figure 10.8 Environmental effects of crack formation in plastic components. (a) Acrylic base drinking glass. (b) Plastic showerhead.
R.W. Hertzberg, Deformation and Fracture Mechanics of Engineering Materials, fourth ed., John Wiley & Sons, Inc.

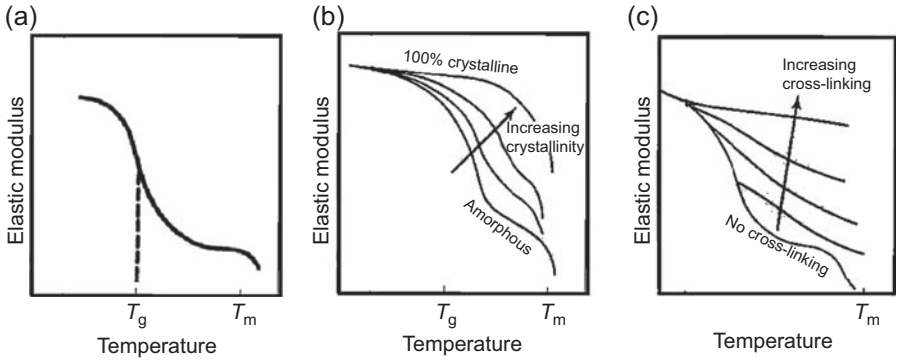

Figure 10.9 Variations in tensile modulus with temperature for three types of polymers. (a) Amorphous thermoplastic. (b) Semicrystalline thermoplastic. (c) Thermosetting.
K. Schmid, Manufacturing Process for Engineering Materials, fifth ed., Pearson Education, 2008, ISBN:0-13-227271-7.

Another example of environmental effects is the failure of gas and water transmission pipelines due to the temperature and pressure variations to which they are subjected [1].

Although deformation is accelerated as the temperature rises above T_g in thermoplastic polymers, this softening does not break the primary covalent bonds within the molecule; however, these bonds may be ruptured, of course, by any resulting change in structure that affects the properties. Excessive heat can degrade the polymer by breaking bonds. Oxidizing environments can bring about chemical change. A temperature rise in polymers, especially in a thermoplastic type, can cause a collapse in the general properties of this material, including mechanical (tensile, yield, fatigue, creep, etc.) and physical properties, above T_g, and then a viscous flow will occur, which prevents the component from carrying any load. This collapse can occur in most kinds of thermoplastic and thermosetting polymer as shown in Fig. 10.9 [1,5,10].

The properties of polymers at elevated temperatures depend on service temperature; therefore there are ranges of processing temperatures, T_g, and melting temperature (T_m), as shown in Table 10.1 [9].

Outside of these ranges, most or all of the polymer properties will decrease, as shown in Figs. 10.10 and 10.11, in which we can observe the changes in the flexural modulus and strengths with elevated temperature [7,9].

The changes in the polymers' properties with rising temperature include changes in some of thermosetting composites' properties, as shown in Table 10.2 [9].

Modulus and strength values expressed as a percentage of room temperature value and the relative properties (modulus and strength) for the high-temperature thermosetting matrices are shown in Figs. 10.12 and 10.13.

There is another factor that can reduce the polymer properties; **radiation or neutrons** can induce scission and in certain cases branching or cross-linking. Radiation by ultraviolet light can readily break a C−C bond; this process, which produces smaller molecules, is called scission. This, of course, affects properties such as strength

Table 10.1 Thermal properties of thermoplastic matrices

	Glass transition temperature, T_g (°C)	Melting temperature, T_m (°C)	Processing temperature, T_p (°C)
PP	−27	200−280	280−200
Nylon	80−100	180−27	220−310
PPYS	220	*	330
PPS	85	285	320−340
PEEK	143	334	380
PEK	162−167	360−365	400
PS	190	*	300
PEI	216	*	360
PES	230	*	350
PAI	249−288	*	400
PI	250−261	270−340	34−350

*Amorphous (therefore, there is no apparent T_m).
G. Eckold, Design and Manufacturing of Composite Structures, Wood Head publishing Limited, First Published, 1994.

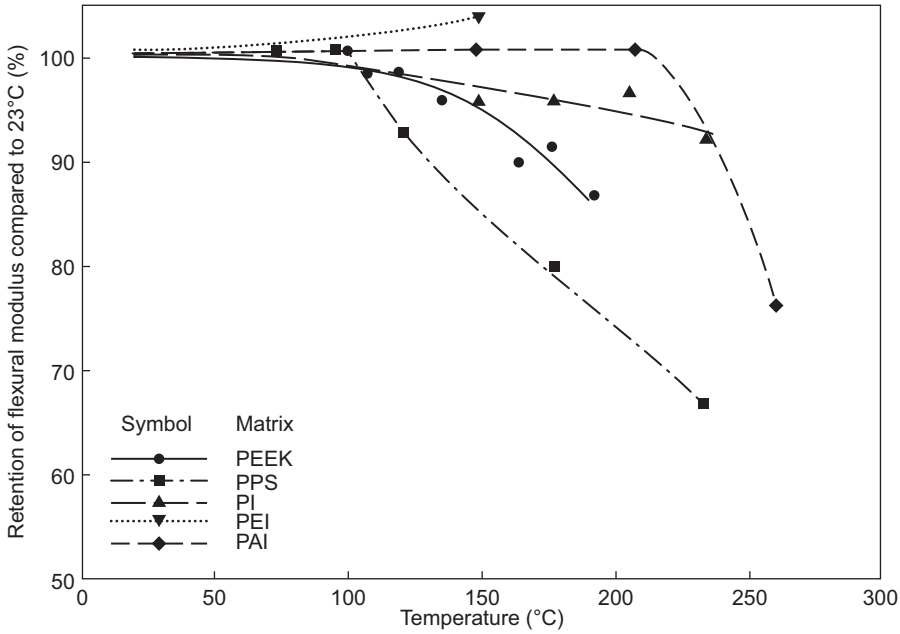

Figure 10.10 Flexural modulus of thermoplastic composites at elevated temperatures.
G. Eckold, Design and Manufacturing of Composite Structures, Wood Head publishing Limited, First Published, 1994.

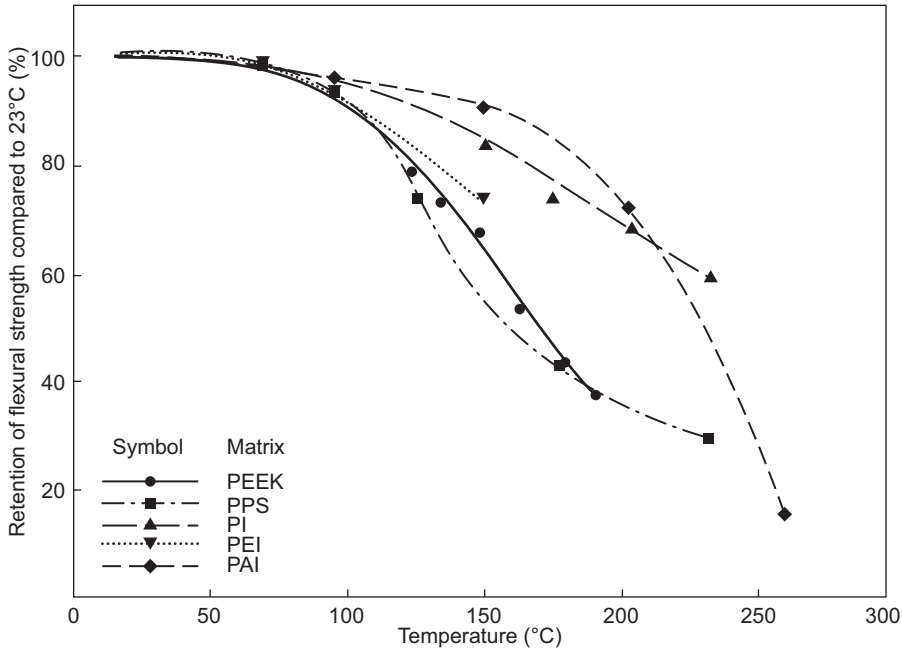

Figure 10.11 Flexural strengths of thermoplastic composites at elevated temperatures.
G. Eckold, Design and Manufacturing of Composite Structures, Wood Head publishing Limited, First Published, 1994.

Table 10.2 Properties of composites at elevated temperatures

Resin	Fiber	Modulus (%)	Strength (%)	Temperature (°C)
Epoxy	Glass	90	60	200
Phenolic	Glass	–	30	300
BMI	Carbon	79	71	250
BMI	Glass	97	80	175
PSP	Carbon	83–100	50–63	350
PSP	Glass	104	90	400
PI	Carbon	81	57	343
PPS	Glass	21	26	250
PEEK	Glass	–	58	177
PEEK	Glass	27	19	300

G. Eckold, Design and Manufacturing of Composite Structures, Wood Head publishing Limited, First Published, 1994.

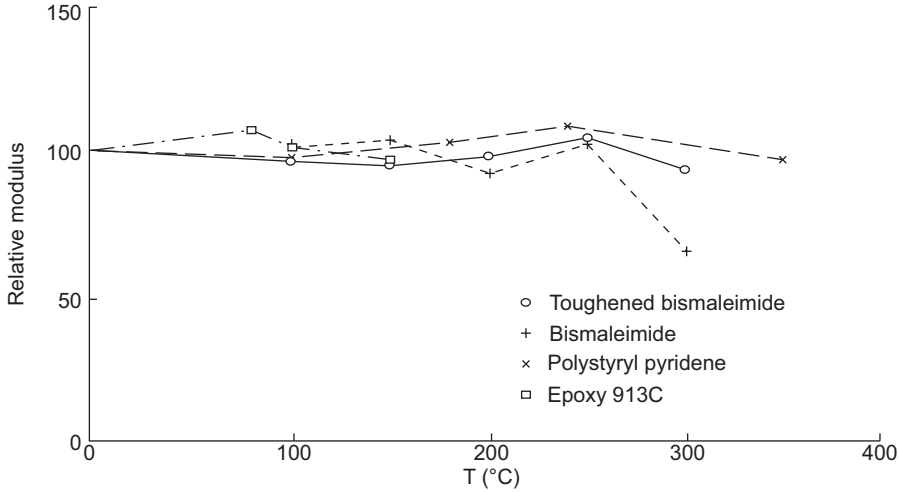

Figure 10.12 Relative modulus for high-temperature matrices.
G. Eckold, Design and Manufacturing of Composite Structures, Wood Head publishing Limited, First Published, 1994.

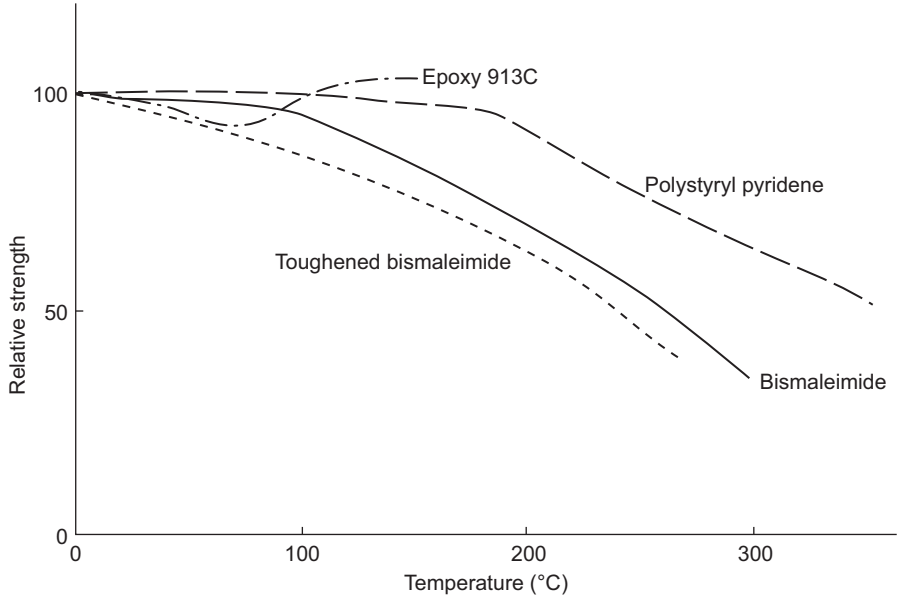

Figure 10.13 Relative strengths for high-temperature matrices.
G. Eckold, Design and Manufacturing of Composite Structures, Wood Head publishing Limited, First Published, 1994.

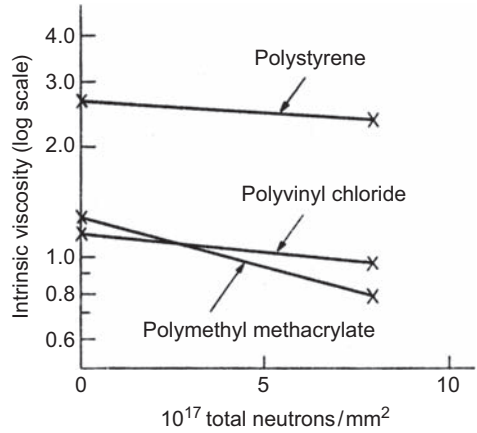

Figure 10.14 Degradation of polymers by neutron exposure.
Van Vlack, Element of Materials Science and Engineering, fourth ed., Addison-Wesley publishing company.

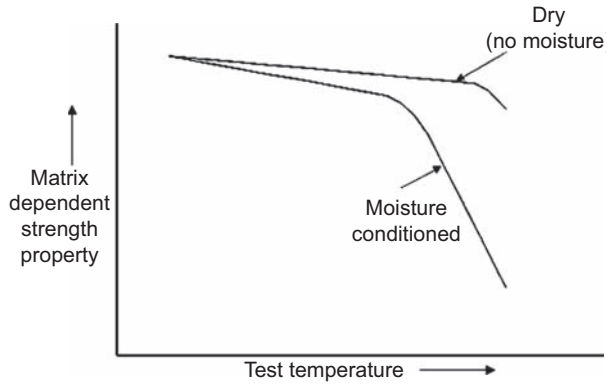

Figure 10.15 Effect of moisture absorption on hot, wet matrix-dependent mechanical properties.
F.C. Campbell, Manufacturing Processes for Advanced Composite, Elsevier Ltd, 2004.

and viscosity, etc. As shown in Fig. 10.14, most polymers lose strength through degradation and radiation damage, and that leads to reduced fatigue strength according to the basics of fatigue failure [8,10].

Also, moisture affects polymer properties and causes the degradation of these polymers at elevated temperatures. In fact almost all thermoset resins absorb moisture from the atmosphere (Fig. 10.15). This effect is well understood and can be accounted for in fatigue strength design [7].

10.4 Fatigue failure of polymers at high temperature

Early studies of fatigue in polymers concentrated on stress cycling of unnotched samples to plot the stress−life (S−N or log N_f) curve, similar to the curve plotted for metals (Wohler diagram). Wohler was the German engineer who first observed the difference in fatigue behavior of ferrous and nonferrous materials, in which one sees a fatigue limit or endurance limit (curve A in Fig. 10.16(a)), which represents a stress level below which the material does not fail and can be cycled indefinitely. Such endurance limit does not exist for nonferrous materials (curve B in Fig. 10.16(a)). The S−N curve for a variety of polymers is shown in Fig. 10.16(b) and contains three stages (I, II, III). These stages occur owing to the formation of crazes in these materials. Fig. 10.16(c) shows the S−N curves for various types of polymers [3,4].

The fatigue failure in polymers is affected by various parameters, as mentioned in the beginning of this chapter (mechanical, materials, and environmental); therefore it may be induced either by **large-scale hysteretic heating**, resulting in actual polymer melting, or by **fatigue crack initiation and propagation to final failure** (Fig. 10.17(a) and (b)). These two process have become a source of controversy among researchers [11].

The major cause of thermal failure is believed to involve the accumulation of hysteretic energy generated during each loading cycle, since this energy is dissipated largely in the form of heat associated with temperature rise, which will occur for every loading cycle when isothermal conditions are not met [1,2,12].

If we measure the surface temperature of a specimen during a cycling test (self-heating test), we can observe an increase in the average surface temperature and an oscillation around this average value (Fig. 10.18). These temperature variations are due to two different heat sources, which are the thermoelastic coupling and the intrinsic dissipation [12].

The small-amplitude oscillatory temperature variations are due to the reversible thermoelastic heating and cooling during each loading cycle. This coupling leads to an oscillation of the temperature at the same frequency as the load (Fig. 10.18). The thermoelastic stress analysis (TSA) method, which is a standard technique of stress analysis used in industry, is based on the theoretical treatment of the thermoelastic effect according to Lord Kelvin [12], who showed that the temperature change ΔT associated with adiabatic elastic deformation can be expressed in the following form:

$$\Delta T = -\mathrm{Km}T\sum_{i=1}^{3}\Delta\sigma_{ii} \qquad [10.6]$$

where Km is the thermoelastic constant and $\Delta\sigma_{ii}$ is the normal stress changes.

From the work of Berry [1], the energy dissipated in a given cycle may be described by the equation below:

$$\dot{E} = \pi f J''(f,T)\sigma^2 \qquad [10.7]$$

where f is the frequency, J'' is the loss compliance, and σ is the peak stress.

From Figs. 10.19a and 10.19b, the effect of temperature rise during fatigue testing is very clear [1].

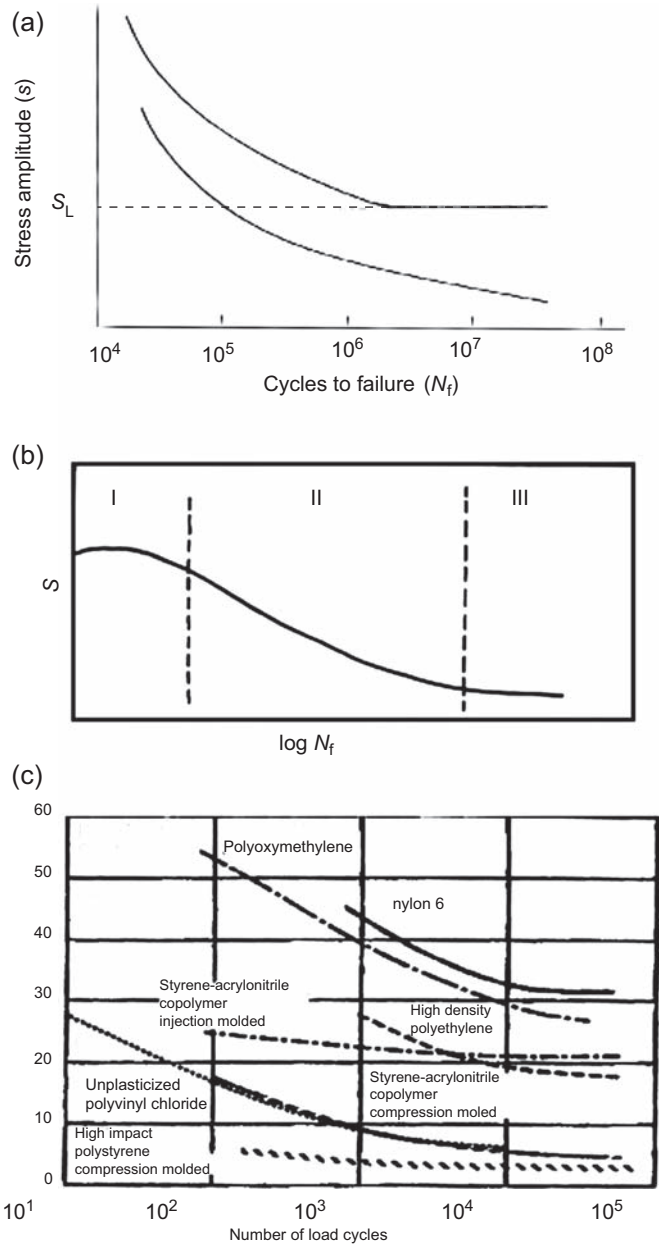

Figure 10.16 (a) S−N curves for ferrous and nonferrous metals *(M.A. Meyers, Mechanical Behavior of Materials, Prentice Hall, 1999.)*. (b) S−N curve for polymer materials *(M.A. Meyers, Mechanical Behavior of Materials, Prentice Hall, 1999.)*. (c) S−N curves for several polymers *(W.F. Hosford, Mechanical Behavior of Materials, Cambridge University Press, 2005.)*.

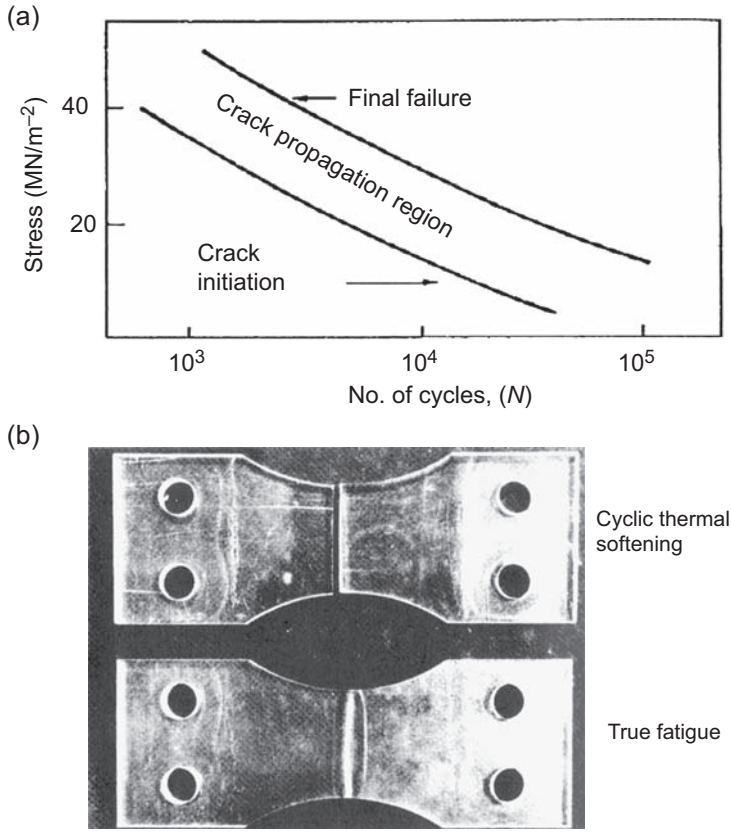

Figure 10.17 (a) Mechanisms of fatigue failure (*I.M. Ward, Mechanical Properties of Solid Polymers, second ed., John Wiley and sons Ltd, 1983.)*. (b) Typical fatigue and cyclic thermal softening of polymethyl methacrylate polymer *(R.W. Hertzberg, Deformation and Fracture Mechanics of Engineering Materials, fourth ed., John Wiley & Sons, Inc.)*.

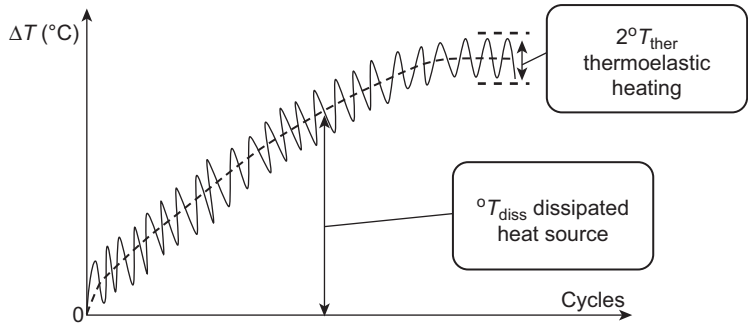

Figure 10.18 Temperature variations during cyclic test.
H. Sawadogo, S. Painier, S. Hariri, Calorimetric analysis of dissipative effects associated with the fatigue of GFRP composite "H" polymer and composite technology and mechanical engineering department, ecole des Mines de Douai,941 rue charles Bourseul, 59508 Douai, France, in: ICFC5 (fifth international conference on fatigue of composite, Nanjing, China, October16−19, 2010, pp. 165−175.

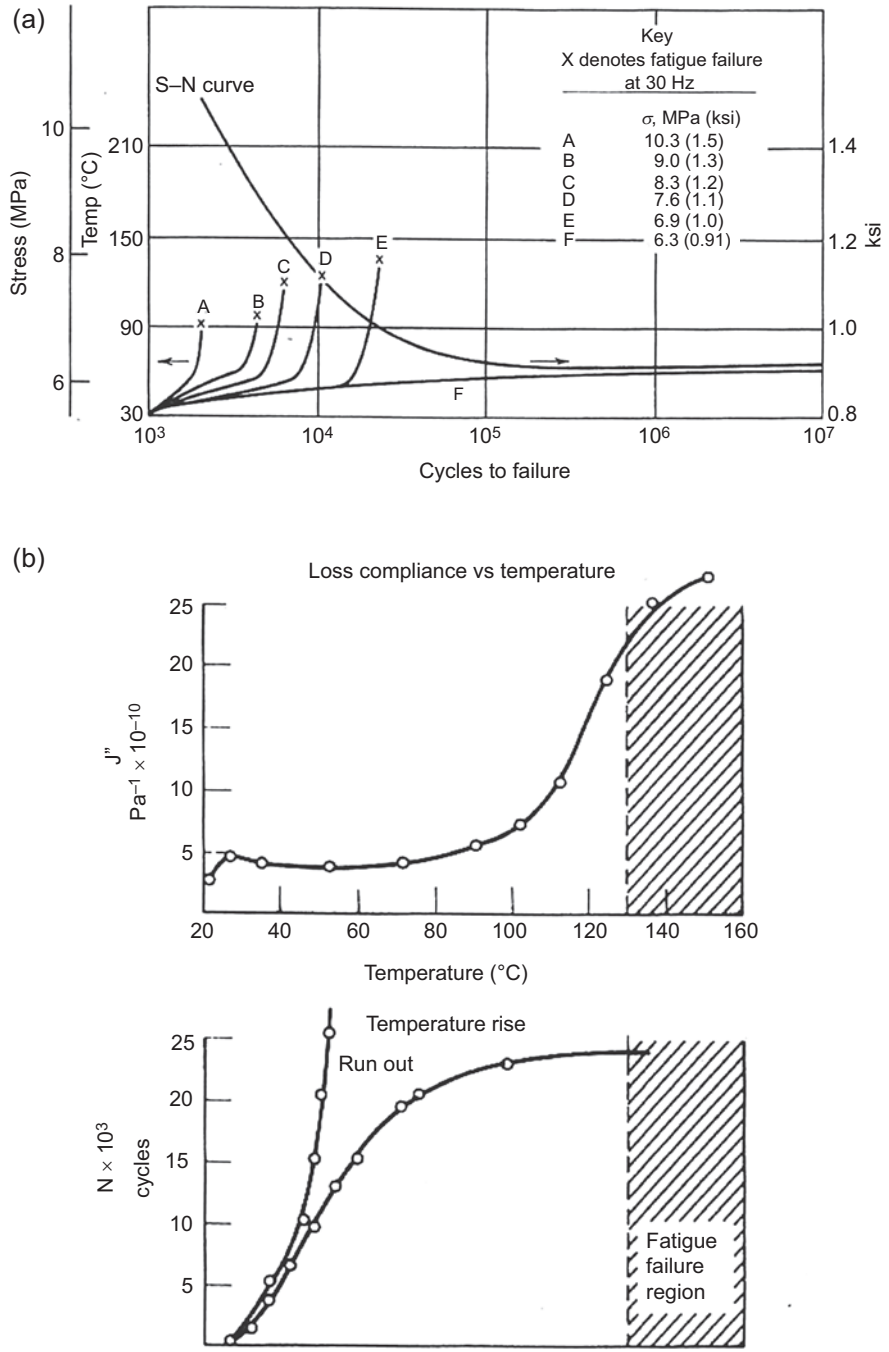

Figure 10.19 (a) Temperature rise during fatigue causes thermal failure at different stress levels (no failure is seen in curve F, in which the sample temperature stabilized). (b) Loss compliance and temperature rise.
R.W. Hertzberg, Deformation and Fracture Mechanics of Engineering Materials, fourth ed., John Wiley & Sons, Inc.

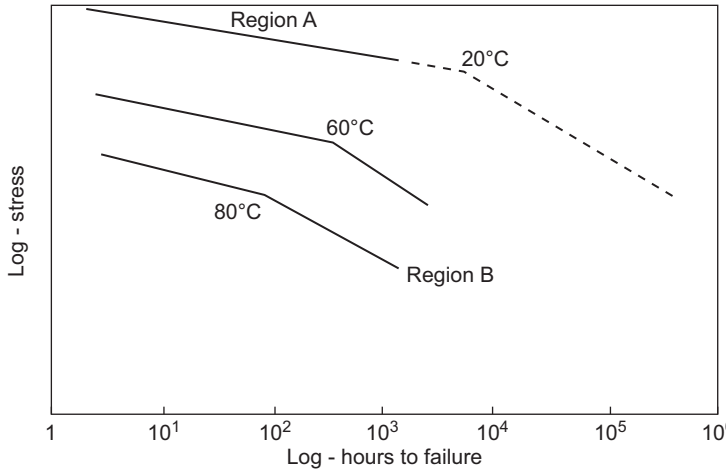

Figure 10.20 Environment-assisted cracking lifetime increases with decreasing stress and temperature.
R.W. Hertzberg, Deformation and Fracture Mechanics of Engineering Materials, fourth ed., John Wiley & Sons, Inc.

With regard to Eq. [10.7], neglecting heat losses to the surrounding environment, it may be reduced to show the temperature rise per unit time as:

$$\Delta\dot{T} = \left[\pi f J''(f,T)\sigma^2\right]/\rho c_p \qquad [10.8]$$

where $\Delta\dot{T}$ is the temperature change/unit time, ρ is the density, and c_p is the specific heat.

Numerous studies have shown that the rupture life of pipe resin increases with decreasing stress level and temperature, as shown in Fig. 10.20 [1].

10.5 Fatigue of composite polymers

There are various types of composite materials. They differ from one another according to matrix material and way of strengthening. The philosophy of matrix material selection and strengthening techniques depends on the conditions of service and the work requirements for the component that was made. According to this philosophy, manufacturing a lightweight composite material to resist fatigue at high temperatures, have high performance, and have high specific strength requires moving away from metals and ceramics as matrix materials; therefore the obvious choice of the specialists is to use polymers as a matrix material for these conditions, because they fulfill the above properties [7,9,13].

There are two groups of polymer materials used, some of them as an alternative to lightweight metal such as aluminum. These include high-temperature thermosetting polymers [9]:

Multifunctional epoxies
Polyimides
Bismaleimides
Polystyryl pyridenes
PMR (in situ polymerization with monomeric reactants)

Their properties with regard to temperature are mentioned under Section 10.3. As for the high-temperature thermoplastics based on phenylene (polyether ether ketone (PEEK), polyether sulfone (PES), polyether ketone (PEK), and polyphenylene sulfide (PPS)) [9], their properties with regard to temperature are also mentioned under Section 10.3.

- **Damage in composites**: Composite materials have specific properties in that they are inhomogeneous and anisotropic. These characteristics are not available in metals and ceramics, although metal and ceramics can be inhomogeneous and anisotropic when they are forming or in the presence of some impurities. Therefore the fatigue failure in this kind of material is different. They accumulate damage in a general rather than a localized fashion, and failure does not always occur by the propagation of a single macroscopic crack. In composites, however, damage is much more widespread and involves a number of microstructural mechanisms including fiber and matrix cracking, delaminating, and deboning, as shown in Fig. 10.21 [1,2,14].
- The damage does not always immediately reduce the strength of the composite. Such strength reductions might occur in a process described as **wear-out** as shown in Fig. 10.22, but sometimes are offset in the early of life stages by slight increases in the strength due to improved fiber alignment. It is known as **wear-in** [14].

At a later stage in life the amount of damage accumulated in some regions of the composite may be as great as the residual load-bearing capacity of the composite in that region and lead to a reduction in the maximum stress level in the fatigue cycle; of course this change will cause sudden failure according to the **Coffin–Manson law** [2].

The damage may be caused by any degradation parameters that cause dimensional change. These changes decrease the bearing capacity for the components under cyclic load. **Mechanisms of fatigue failure**, as mentioned, depend on three stages (initiation of crack, propagation of crack, and sudden fracture); therefore, when a preexisting crack is present, for any reason, in a composite it may or may not propagate under the action of cyclic load, depending upon the nature of the composite (matrix and strengthen phase). When the matrix and the strengthening phase are homogeneous and adherent, crack propagation occurs in both the strengthening phase and the matrix, but in the presence of a toughening phase, such as elastic particles or tough fibers, in front of the crack propagation movement, as shown in Fig. 10.23(a) and (b), the crack will often refuse to propagate normal to the fibers (model), but will be diverted into a splitting mode as shown in Fig. 10.23(b) [1,9].

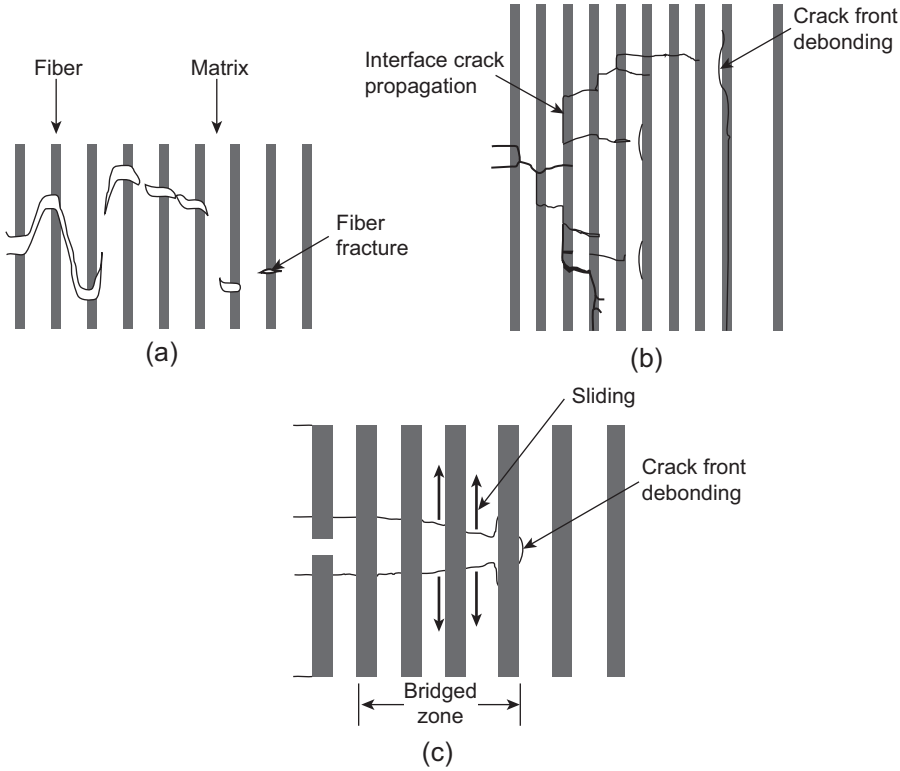

Figure 10.21 Fatigue fracture micromechanisms. (a) Strong interfaces and weak fibers. (b) Strong fibers and weak interfaces. (c) Sliding of matrix of fibers.
R.W. Hertzberg, Deformation and Fracture Mechanics of Engineering Materials, fourth ed., John Wiley & Sons, Inc.

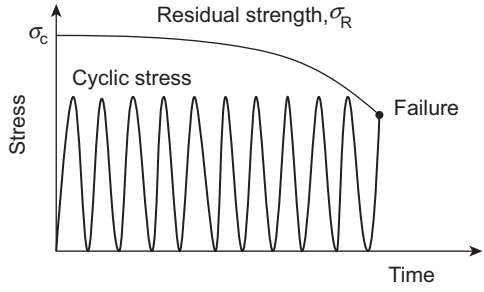

Figure 10.22 Damage in composites.
B. Harris, Engineering Composite Materials, The Institute of Materials, London, 1999.

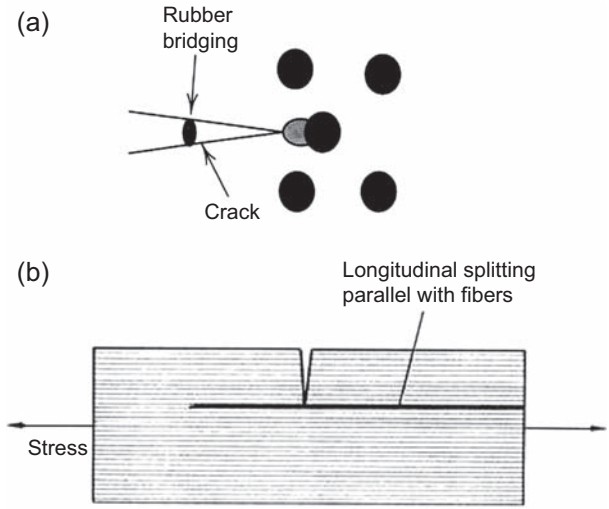

Figure 10.23 Mechanisms to stop crack propagation. (a) Tough particle (rubber bridging) (*R.W. Hertzberg, Deformation and Fracture Mechanics of Engineering Materials, fourth ed., John Wiley & Sons, Inc.).* (b) Fiber bridge *(G. Eckold, Design and Manufacturing of Composite Structures, Wood Head publishing Limited, First Published, 1994.).*

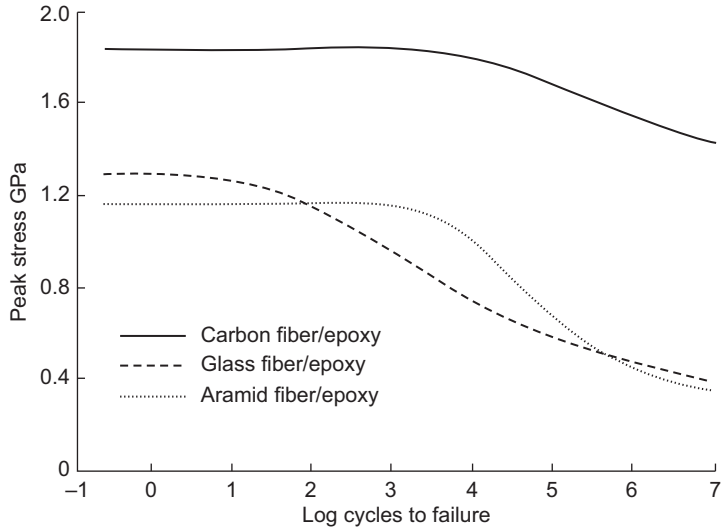

Figure 10.24 S−N curves for epoxy matrix with different kinds of fibers.
G. Eckold, Design and Manufacturing of Composite Structures, Wood Head publishing Limited, First Published, 1994.

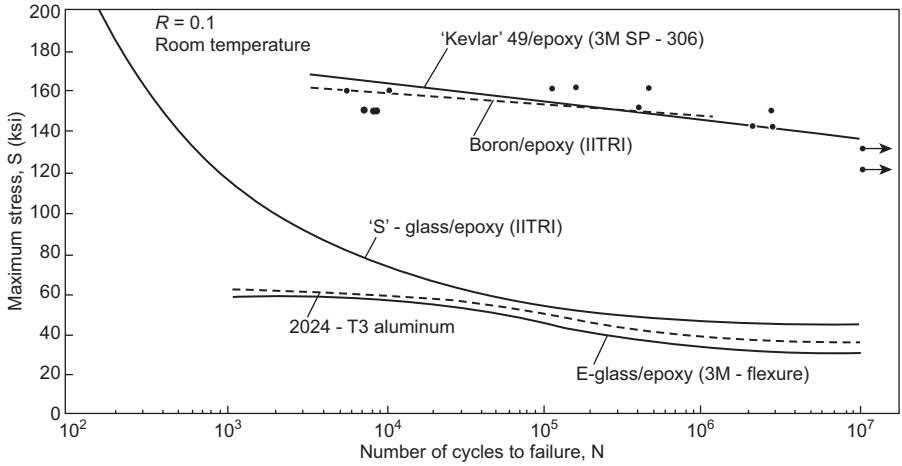

Figure 10.25 Comparison the fatigue performance of the composite materials with aluminum. G. Piatti, Advance in Composite Materials, Applied Science Publishers Ltd, London.

There are a numerous studies on fatigue in composite materials. Their results are as shown in Figs. 10.24 and 10.25. These results, which are illustrated in Fig. 10.24, show the fatigue curves for an epoxy matrix with various kinds of fiber (aramid, glass, carbon). It is very clear that the fatigue strength for the carbon fiber/epoxy composite is better than that for the glass fiber/epoxy and the aramid fiber/epoxy composite materials. Of course, these variations in fatigue behavior belong to the variations in the fibers' toughness. Fig. 10.25 shows the comparison between fatigue behavior for the composite materials and the aluminum alloy. This comparison shows that most of the composite materials have fatigue performance better than that of the aluminum alloy [13].

10.6 Fatigue of high-temperature thermoplastics (PPS and PEEK)

High-performance thermoset matrix composites, as mentioned under Section 10.5, are typically used in aircraft structures and transport applications. However, in the late 1980s, high-performance thermoplastic matrix composites were introduced. These materials had similar mechanical properties, but superior impact resistance and toughness compared to thermoset matrix composites [15–17].

There are other advantages to thermoplastic over thermoset polymers:

- good fatigue performance, damage tolerant, insensitive to moisture
- high temperature performance, very low flammability, smoke toxicity
- low residual stress in molded parts, excellent chemical resistance
- rapid processing, good re-formation, good welding, fusion bonding
- reduced cost and weight
- recyclable, less processed scrap

These characteristics explain **why thermoplastic composite polymers are an alternative to thermoset composites**.

In this section we will concentrate on the fatigue behavior of the two of the most important high-thermoplastic composites, PPS and PEEK, although of there are other kinds of high thermoplastics, because of their properties listed above.

10.6.1 Fatigue behavior of PPS

PPS is a crystalline, wholly aromatic polymer that contains sulfide (−S−) linkages as shown in Fig. 10.26. The characteristics of the polymers depend on the molecular weight of the polymers. Three types of grades are available—neat resin, glass filled, and glass/mineral filled. All PPS resins are characterized by outstanding chemical resistance and high-temperature stability, although they differ somewhat with respect to mechanical properties and processing ability. PPS resin manufacturing processes are broadly divided into partial cross-linking (branched or standard) and linear processes [6,15,18].

Branched PPS (a polymer molecule that has side chains branching out from its backbone) was introduced commercially in the 1970s, and the resulting resin is dark in color, hard, and brittle. Process refinements in the 1980s led to a linear polymer. Linear PPS polymer (a molecule essentially consisting of a long backbone) is said to offer significant cost and performance benefits over branched PPS and to overcome the weak points of branched PPS. PPS materials offer the broadest resistance to chemicals of any advanced engineering plastic [15,18].

They have no known solvents below 392°F (200°C) and offer inertness to steam, strong bases, fuels, and acids. A very low coefficient of linear thermal expansion makes PPS products ideally suitable for precise tolerance machined components. The **fatigue behavior** of high-temperature thermoplastic PPS is affected by temperature variations as well as the other properties similar to those of other types of thermoplastic, which were mentioned previously. We note some of the properties of PPS in Figs. 10.27−10.29 [16].

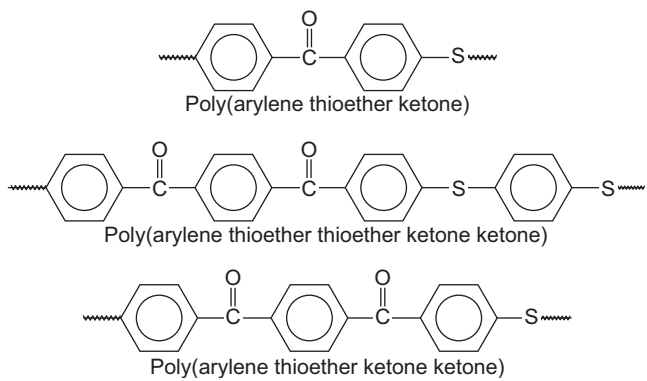

Figure 10.26 Varieties of polyphenylene sulfide.
J.K. Fink, High Performance Polymers, William Andrew Inc., USA, 2008.

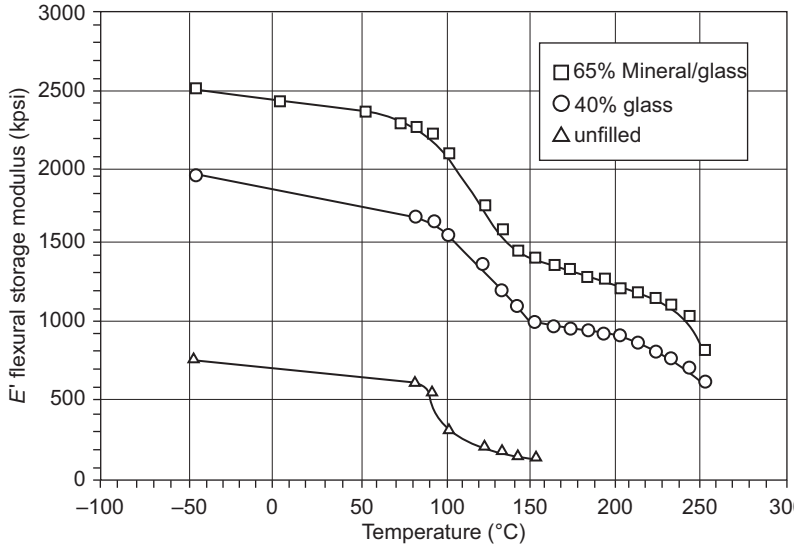

Figure 10.27 Flexural storage modulus vs temperature for Fortron® PPS.
Ticona Engineering polymers, "Designing with Fortron Polyphenylene Sulfide" design manual (FN-10). www.ticona.com.

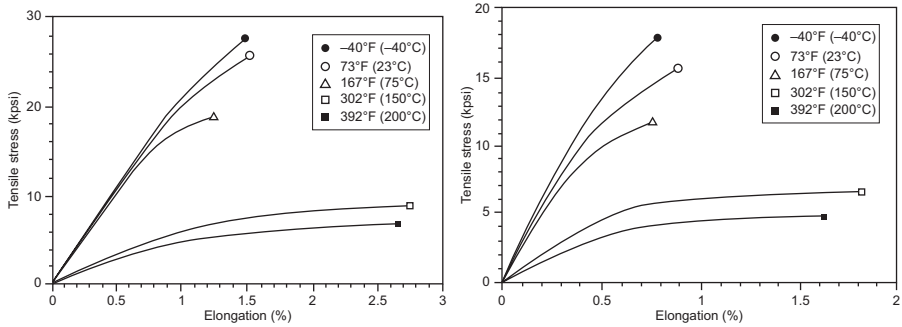

Figure 10.28 Stress−strain behavior of 40% (left) and 65% (right) glass-reinforced Fortron® PPS.
Ticona Engineering polymers, "Designing with Fortron Polyphenylene Sulfide" design manual (FN-10). www.ticona.com.

The tensile strength properties, flexural strength, modulus of elasticity, and other properties of PPS related to one another decrease with increasing temperature in general, but they depend on the volume fraction of fibers as shown in Fig. 10.27 [16].

The tensile fatigue resistance of a 40% and 65% glass/PPS composite is shown in Fig. 10.30. These data show that the fatigue strength decreases continuously with the number of cycles of load application at 23 and 160°C [19].

Mandell et al. gave S−N curves for several injection-molded thermoplastics and their glass- or carbon-filled short-fiber composites, including those of PPS. The

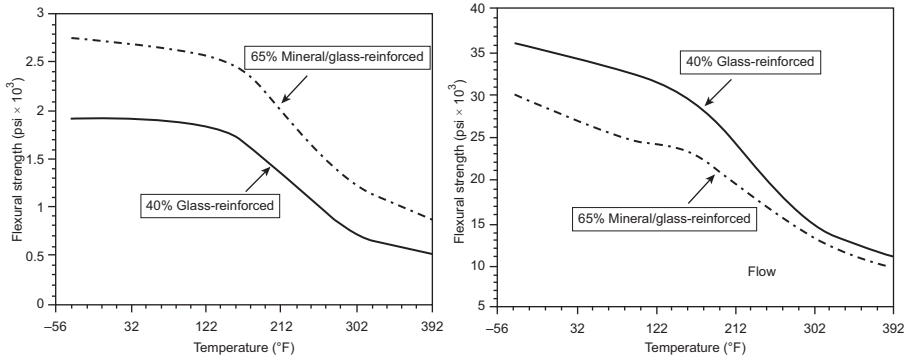

Figure 10.29 (Left) Temperature dependency of flexural strength. (Right) Temperature dependency of flexural modulus.
Ticona Engineering polymers, "Designing with Fortron Polyphenylene Sulfide" design manual (FN-10). www.ticona.com.

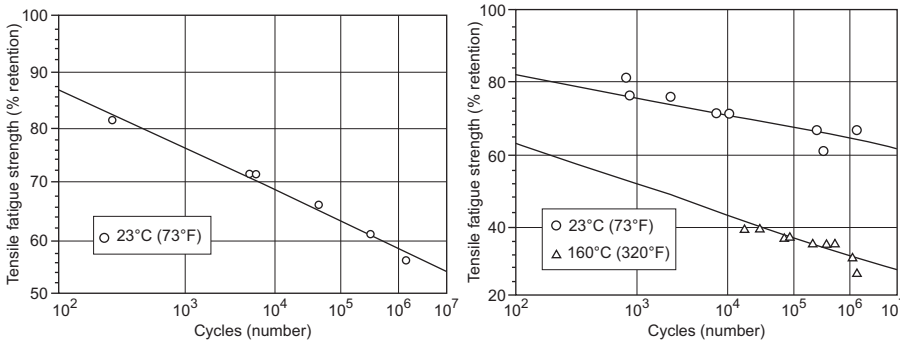

Figure 10.30 (Left) Fatigue resistance of 40% glass-reinforced Fortron® PPS. (Right) Fatigue resistance of 65% glass-reinforced Fortron® PPS.
Ticona Engineering polymers, "Designing with Fortron Polyphenylene Sulfide" design manual (FN-10). www.ticona.com.

measurements were made at room temperature in a uniaxial tension−tension mode with minimum stress/maximum stress equal to 0.1. The frequency of stress application varied, but was kept low enough to avoid appreciable heating of the samples [19].

There was no evidence of a fatigue limit for any of the thermoplastic matrix composites studied within the range of stress and number of cycles studied (up to 10^6 cycles). The S−N curves of all of the thermoplastic composites could be described by an equation of the following form [19]:

$$S = \text{UTS} - B\log(N) \qquad [10.9]$$

where UTS is the ultimate tensile strength, B is the slope of the S−N curve, and N is the number of cycles to failure [16].

10.6.2 Fatigue behavior of PEEK

PEEK is a colorless organic polymer thermoplastic in the polyaryl ether ketone (PAEK) family, used in various engineering applications. PEEK polymers are obtained by step-growth polymerization by the dialkylation of bisphenolate salts [15]. The chemical structure of PEEK is shown in Fig. 10.31.

PEEK is a semicrystalline thermoplastic with excellent mechanical and chemical resistance properties that are retained to high temperatures. The processing conditions used to mold PEEK can influence the crystallinity and hence the mechanical properties as shown in Table 10.3 [20].

Because of its robustness, PEEK is used to fabricate items used in demanding applications, bearings, piston parts, insulation, etc. It is also extensively used in the aerospace and automotive industries. The fatigue behavior of PEEK is similar to other properties affected by temperatures increasing beyond T_g. The S−N curves for PEEK with carbon fibers (CF) and other polymers, polyether ketone ketone and polyether imide, with CF and glass fibers, are shown in Fig. 10.32 [20].

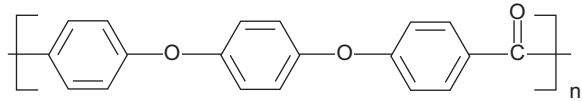

Figure 10.31 Chemical structure of PEEK.
J.K. Fink, High Performance Polymers, William Andrew Inc., USA, 2008.

Table 10.3 General properties of PEEK

General properties	PEEK
Miscellaneous properties	
• Density (g/cm^3)	1.27−1.32
• Shrinkage (%)	1.1
• Absorption of water (%)	0.1−0.5
Mechanical properties	
• Tensile strength (MPa)	100−107
• Elongation at break (%)	30−150
• Tensile modulus (GPa)	3.6−3.9
• Flexural modulus (GPa)	3.7−3.9
• Notched impact strength ASTM D256 (J/m)	80−85

Table 10.3 Continued

General properties	PEEK
Thermal properties	
• Glass transition temperature (°C)	143
• Melting temperature (°C)	334
• Thermal conductivity (W/m K)	0.25
• Specific heat(cal/g/°C)	0.32
• Coefficient of thermal expansion (10^{-5}/°C)	4−6
Electrical properties	
• Volume receptivity (Ω•cm)	10^{16}−10^{17}
• Dielectric constant	3.2
• Loss factor (10^{-4})	30
• Dielectric strength (kV/mm)	20

A. chazerain, Characterization of Resistance-welded Thermoplastic Composite Double−lap Joints (thesis), McGill university, Montreal, 2009.

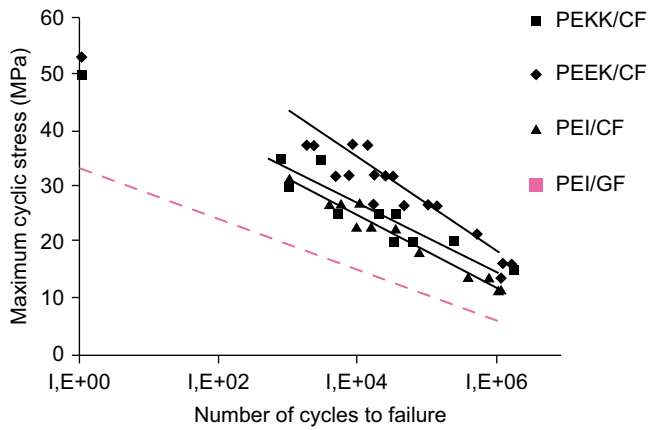

Figure 10.32 S−N curves for PEEK and another polymers.
A. chazerain, Characterization of Resistance-welded Thermoplastic Composite Double−lap Joints (thesis), McGill university, Montreal, 2009.

Abbreviations and symbols

Abbreviation	Definition
PP	Polypropylene
PPYS	Polyphenyl sulfone
PPS	Polyphenylene sulfide
PEEK	Polyether ether ketone
PAEK	Polyaryl ether ketone
PEKK	Polyether ketone ketone
PEK	Polyether ketone
PS	Polysulfone
PEI	Polyether imide
PES	Polyether sulfone
PAI	Polyamide imide
PI	Polyimide
BMI	Bismaleimide
PSP	Polystyryl pyridene
PMMA	Polymethyl methacrylate
S−N	Stress−number of cycles
CF	Carbon fiber
GF	Glass fiber
TSA	Thermoelastic stress analysis
Symbol	**Meaning**
σ	Stress
ϵ	Strain
σ_y	Yield stress (plastic deformation)
σ_a	Cyclic stress amplitude
σ_m	Mean stress
σ_R	Residual strength
σ_C	Normal composite strength
R	Stress ratio
$\Delta\sigma$	Stress range
σ_{max}	Maximum stress

Abbreviation	Definition
σ_{min}	Minimum stress
N	Number of fatigue cycles
N_f	Number of cycles to failure
$\Delta\mathcal{E}$	Plastic strain range
d_C/d_N	The crack growth per cycle
K	Stress intensity factor
ΔK	Cyclic stress intensity
KL_m	Mean stress intensity
Km	Thermoelastic constant
UTS	Ultimate tensile strength
Tg	Glass transition temperature
T_m	Melting temperature
T_p	Processing temperature
σ_{th}	Thermal stress
E	Modulus of elasticity
$\dot{E}$	Energy dissipated
f	Frequency
J'	The loss compliance
ΔT	Temperature variation or change
α	Linear thermal expansion
ρ	Density
c_p	Specific heat
c	Crack length

References

[1] R.W. Hertzberg, Deformation and Fracture Mechanics of Engineering Materials, fourth ed., John Wiley & Sons, Inc., 1996.
[2] M.F. Ashby, D.R. Jones, Engineering Materials an Introduction to Microstructures, Processing and Design, third ed. (Butter Worth-Heinemann is an imprint of Elsevier), 2006.
[3] M.A. Meyers, Mechanical Behavior of Materials, Prentice Hall, 1999.
[4] W.F. Hosford, Mechanical Behavior of Materials, Cambridge University Press, 2005.
[5] G.E. Dieter, Mechanical Metallurgy, third ed., McGraw-Hill companies, 1986.

[6] A.F. Hamzah, Investigation of Reinforced Poly Phenylene Sulfide for Air Frame Structure Application (Ph.D. thesis), University of Technology, Iraq, 2013.
[7] F.C. Campbell, Manufacturing Processes for Advanced Composite, Elsevier Ltd, 2004.
[8] N.A. Saad, M. Al−Maamori, M. Razak, A. Hashim, The effect of several service and weathering parameters on tensile properties of PVC pipe materials, Mat. Sci. Appl. 3 (11) (2012) 784−792.
[9] G. Eckold, Design and Manufacturing of Composite Structures, Wood Head publishing Limited, First Published, 1994.
[10] Van Vlack, Element of Materials Science and Engineering, fourth ed., Addison-Wesley publishing company, 1980.
[11] I.M. Ward, Mechanical Properties of Solid Polymers, second ed., John Wiley and sons Ltd, 1983.
[12] H. Sawadogo, S. Painier, S. Hariri, Calorimetric analysis of dissipative effects associated with the fatigue of GFRP composite "H" polymer and composite technology and mechanical engineering department, ecole des Mines de Douai, 941 rue charles Bourseul, 59508 Douai, France, in: ICFC5 (fifth international conference on fatigue of composite, Nanjing, China, October16−19, 2010, pp. 165−175.
[13] G. Piatti, Advance in Composite Materials, Applied Science Publishers Ltd, London, 1978.
[14] B. Harris, Engineering Composite Materials, The Institute of Materials, London, 1999.
[15] J.K. Fink, High Performance Polymers, William Andrew Inc., USA, 2008.
[16] Ticona Engineering polymers, "Designing with Fortron Polyphenylene Sulfide" design manual (FN-10). www.ticona.com, 2006.
[17] H. Bhagat, Linear Polyphenylene Sulfide (PPS) for Thermoplastic Composite, Ticona Engineering Polymers, 2008.
[18] N.A. Saad, M.S. Hamzah, A.F. Hamzah, Study of fatigue behavior of composite materials with the basis of polyphenylene sulfide (PPS) reinforced with glass fiber and carbon, Int. J. Eng. Technol. 3 (4) (April 2013).
[19] J.E. Spruiell, C.J. Janke, A Review of the Measurement and Development of Crystallinity and It's Relation to Properties in Neat Poly (Phenylene Sulfide) and Its Fiber Reinforced Composites, U.S. Department of Energy (DOE) Information Bridge, 1996.
[20] A. chazerain, Characterization of Resistance-welded Thermoplastic Composite Double−lap Joints (thesis), McGill university, Montreal, 2009.
[21] K. Schmid, Manufacturing Process for Engineering Materials, fifth ed., Pearson Education, 2008, ISBN 0-13-227271-7.

Sustainable lightweight vehicle design: a case study in eco-material selection for body-in-white

11

A.T. Mayyas
University of California-Berkeley, Berkeley, CA, United States

A.R. Mayyas
Arizona State University, Mesa, AZ, United States

M. Omar
Masdar Institute of Science & Technology, Abu Dhabi, United Arab Emirates

11.1 Introduction

Design for sustainability, eco-material selection, and green product design are used interchangeably in automotive applications to refer to the material selection process of lightweight material that has minimal environmental impact over its entire lifetime. The origin of this science is rooted back to the era of the Arab oil embargo, when a majority of the original equipment manufacturers (OEMs) started to think about more fuel-efficient vehicles, which in turn initiated the basics of vehicular lightweight design. There are a few ways to reduce fuel consumption in the vehicle, such as improved power-train efficiency, new and advanced power trains like internal combustion−diesel hybrids and fuel cell vehicles, improving aerodynamics, adoption of alternative fuels, and reduction of the vehicle's mass. Above all, mass reduction is claimed to be the most effective and least costly way, but only if the reductions are significant (such as in the range of 20−40%) (Cheah, 2010).

In fact, lightweight design pivots around two facts: First is the price of oil, which is reflected in the price of gas that consumers pay at the pump and has been increasing over the past several years. The second fact is that the public has become more conscious of environmental change and global warming (Montalbo et al., 2008), which has been reflected in government goals for fuel economy. For example, the Corporate Average Fuel Economy standards in the United States have requested OEMs to meet certain levels of fuel economy at their fleet level. Although automakers have deployed several technologies to improve the fuel economy of their vehicles, reducing weight ("lightweighting") is still one of the approaches they prefer, not only because it improves fuel economy, but also because of the emergence of advanced materials that may result in lower costs in association with good manufacturability. Lightweighting can be accomplished through

Lightweight Composite Structures in Transport. http://dx.doi.org/10.1016/B978-1-78242-325-6.00011-6

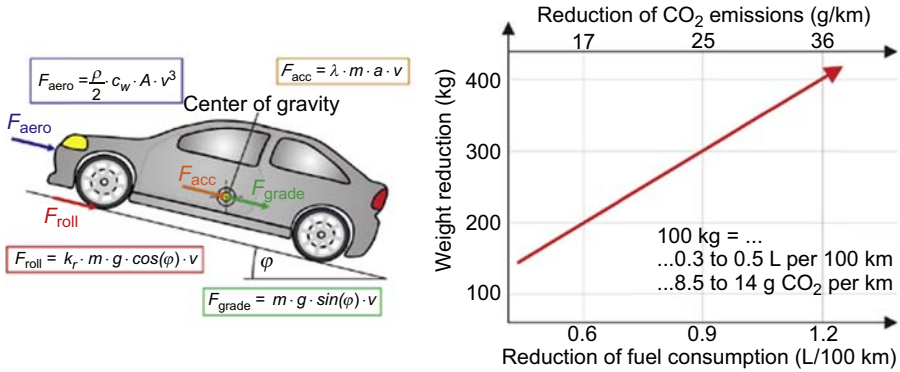

Figure 11.1 Effect of mass on the driving performance and correlation between vehicle weight, fuel consumption, and CO_2 emissions.
Adapted from: Lauter, C., Troster, T., Reuter, C., 2014. Hybrid structures consisting of sheet metal and fiber reinforced plastic structural automotive applications. In: Elmarakbi, A. (Ed.), Advanced Composite Materials for Automotive Applications. John Wiley & Sons.

downsizing, integrating parts and functions, material substitution, or a combination of these methods (Mayyas et al., 2012a). Vehicle mass is known to play a major role in lightweight design as well as in the performance of the vehicle in terms of resistance to the road and fuel economy. Reducing the mass of the vehicle not only reduces the friction force with roads by reducing rolling resistance, but also reduces acceleration resistance and climbing resistance (as shown in Fig. 11.1). Fig. 11.1 also shows the effect of reducing vehicle mass on the overall fuel economy; generally speaking, a 100-kg savings in vehicle mass will result in a fuel savings of 0.3−0.5 L per 100 km and 0.85−1.4 kg CO_2 per 100 km.

11.2 Sustainability and material selection

Early lightweight vehicle design attempted to reduce vehicle weight by substituting some of the iron and steel used in vehicles with lighter materials like magnesium or aluminum. More recently high-strength steel (HSS) and plastic composite materials have emerged as lightweight materials that are getting more acceptance due to the reducing trend in their prices and new developments in manufacturing of these materials. Other lightweight design approaches include redesigning of the vehicle and downsizing. Redesigning aims at reducing aerodynamic drag force and rolling resistance, while downsizing focuses more on reducing the dimensions of the vehicle. Although using these approaches may result in up to 40% (690 kg) vehicle weight reduction, the cost associated with manufacturing these lighter vehicles is nontrivial and could reach $3.00 to $4.00 per kilogram of total weight saved (Cheah et al., 2009; Fuchs et al., 2008). In addition, lighter materials tend to be more energy intensive compared to conventional steel grades that are widely used by OEMs nowadays.

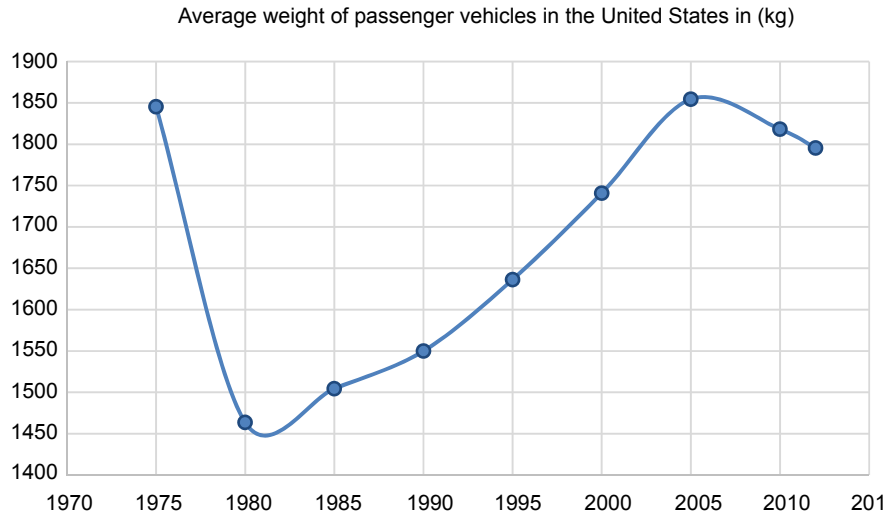

Figure 11.2 Light-duty vehicle weight trends for model years 1975–2012.
Source of data: several reports from US Environmental Protection Agency (www.epa.gov).

This fact may result in greater life-cycle energy impact for some materials—relative to steel—and hence needs to be considered in any eco-material selection process.

The average passenger vehicle weight declined from about 4000 lb (~1800 kg) in 1975 to less than 3200 lb (~1460 kg) in 1982, as the OEMs tried to use less steel in their vehicles, see Fig. 11.2. Over the same time period, the amount of plastics used in a typical US passenger vehicle increased from about 4.6% in 1980 to about 10–12% today (US EPA, 2009). However, the customer demand has shifted preference to larger and heavier vehicles (eg, sports utility vehicles) since 1995 because of their heavy-duty functions. The average vehicle weight has increased again, to where it reached about 4150 lb (~1890 kg) in 2008 (US EPA, 2009). Today, the typical US family vehicle weighs about 1400 kg (3080 lb) (Mcauley, 2003), with iron and steel accounting for the majority of this weight, as displayed in Fig. 11.3. However, the new trend in vehicle lightweighting aims at enhancing the vehicle fuel efficiency as well as improving its driving performance while lowering its emissions (Mayyas et al., 2012b). A general rule of thumb says that a 10% reduction in vehicle weight translates into a 5–7% increase in its fuel economy in terms of miles per gallon (American Plastics Council, 2014; Cheah et al., 2009; Mayyas et al., 2011).

Selection of the lighter materials was the main focus of early lightweight design in automotive applications, so the trend was focused on replacing steel parts with lightweight materials made from aluminum and magnesium and more recently plastic composite materials. However, the competition between alternative materials like HSS, aluminum, magnesium, and plastic continues to result in a rich portfolio of options to reduce vehicle mass component by component (eg, engine, body, panels, etc.). Automakers have studied the impact of replacing steel auto bodies with bodies made from aluminum, magnesium, and composite materials and found that up to a

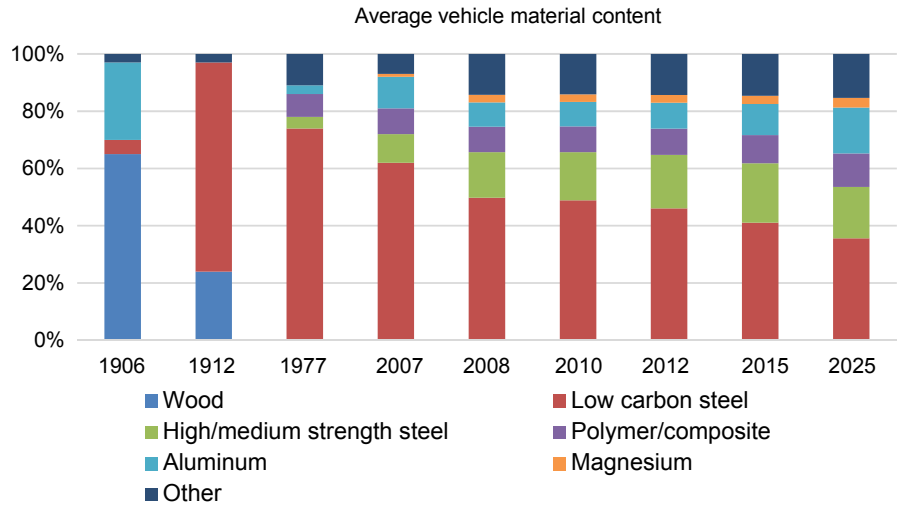

Figure 11.3 Historical trend in vehicle composition.
Source of data: Nicholas Lutsey, May 2010. Review of technical literature and trends related to automobile mass-reduction technology. UCD-ITS-RR-10-10. http://agmetalminer.com/2011/09/19/aluminum-cars-all-time-high-alcoa-novelis-taking-the-bank-part-one/.

20% reduction in the vehicle mass is achievable in the 2015−2020 time frame with minimal additional manufacturing cost due to the needs for modifying current manufacturing routes (see Table 11.1 for some of these studies) (Lutsey, 2010). Another important fact that was also found by these studies is that a 12−16% reduction in CO_2 emissions can be achieved by replacing steel parts with aluminum- and magnesium-based parts, while maintaining constant vehicle size and performance (Lutsey, 2010).

Vehicles consist of several systems and all of them are potential sources for mass savings; however, structural panels of the body-in-white (BIW) might be the first choice to consider for two reasons:

- The BIW accounts for the main part of a vehicle's curb weight; however, BIW and closures account for ∼30% of the vehicle's weight.
- The BIW has a vast potential of weight savings compared to other systems like the power train or chassis. Actually, some OEMs have already introduced lightweight BIW designs in their vehicles, such as Audi (TT, A2, and A8), Jaguar (XJ), Lotus, and Honda (NSX, Insight).

Some examples of lightweight designs made by several OEMs are summarized in Table 11.2.

The question that arises after this introduction is the following: Does lightweight material always result in better fuel economy and hence less environmental impact? If the answer is no, do we need a larger eco-material selection framework that takes into consideration all sustainability factors like cost, environmental impact, manufacturability, and environmental burden at the end of vehicle life. Although there are several partial sustainability assessment models available today for different

Table 11.1 Vehicle mass breakdown by system and components

System	Mass breakdown[a]	Major components
Body-in-white	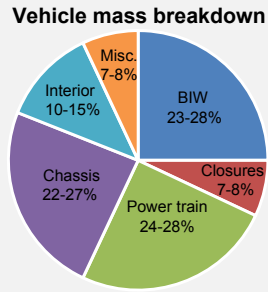	Compartment frame, fenders, cross and side bars, roof, front and end structures, floor pan, A-, B-, C-pillars
Closures		Front and rear doors, hood, and trunk lid
Power train		Engine, transmission, exhaust system, fuel tank
Chassis		Chassis, suspension, tires, wheels, steering system, brakes
Interior		Seats, instrument panel, trim, air bags, entrainment system
Miscellaneous		Electrical, lighting, air conditioning system, windows

[a]Based on Stodolsky et al. (1995), Bjelkengren (2008), and Lotus Engineering (2010); the actual system definitions and system component inclusions can vary, and percentage weight breakdown can vary substantially by vehicle. Adapted from: Lutsey, N., 2010. Review of Technical Literature and Trends Related to Automobile Mass-reduction Technology. Institute of Transportation Studies, University of California, Davis. UCD-ITS-RR-10−10.http://pubs.its.ucdavis.edu/publication_detail.php?id=1390 (last accessed on 04.11.14.).

automotive applications, none of these models have provided a holistic approach that covers all sustainability aspects. The main motivation of this chapter is to develop and discuss an eco-material selection model based on performance indices and how to utilize these proposed sustainability measures in the selection of lightweighting materials for BIW designs.

11.3 Material selection method for sustainable automobile bodies

Several sustainability models have been proposed for automotive applications. Some of these models used environmental impact as the performance measure in the eco-material selection process, while other methods chose one or several sustainability aspects (eg, energy and emissions associated with use phase, recyclability of retired product/part) in so-called sustainable material selection. This is usually carried out using a mixture of qualitative or quantitative performance measures.

Old sustainability approaches tended to be qualitative in nature and focused on using green materials that do not harm the environment; an example of qualitative sustainability measures is the rule of thumb proposed by Graedel and Allenby (1998) to "Choose abundant, nontoxic, nonregulated materials, if possible." On the other hand, quantitative approaches have been proposed, and used in the eco-material selection process, to have a ranking method that has the ability to classify materials based on their closeness to the required or target values. Some examples of quantitative approaches include a single

Table 11.2 Component weight-reduction potential

Vehicle system	Subcomponent	New material or technique[a]	Weight reduction (lb)[b]	Example automaker (model)[c]
Power train	Block	Aluminum block	100	Ford (Mustang); most vehicles
	Engine, housing, etc.	Aluminum−magnesium composite	112	BMW (R6)
	Engine	Smaller optimized molds (aluminum)	55	Toyota (Camry)
	Valve train	Titanium intake valves	0.74	GM (Z06)
	Connecting rods (8)	Titanium	3.5	GM (Z06), Honda (NSX)
	Driveshaft	Composite	7	Nissan, Mazda, Mitsubishi
	Cradle system	Aluminum	22	GM (Impala)
	Engine cradle	Magnesium	11.0−12.0	GM (Z06)
	Intake manifold	Magnesium	10	GM (V8), Chrysler
	Camshaft case	Magnesium	2	Porsche (911)
	Auxiliaries	Magnesium	11	Audi (A8)
	Oil pan	Modular composite	2	Mercedes (C-class)
	Transmission housing	Aluminum	8	BMW (730d); GM (Z06)
	Transmission housing	Magnesium	9−10	Volvo, Porsche (911), Mercedes, VW (Passat), Audi (A4, A8)

Body and closures	Unibody design	Versus truck body on frame	150–300	Honda (Ridgeline), Ford, Kia, most SUV models
	Frame	Aluminum-intensive body	200–350	Audi (TT, A2, A8), Jaguar (XJ), Lotus, Honda (NSX, Insight)
	Frame	Aluminum space frame	122	GM (Z06)
	Panel	Thinner aluminum alloy	14	Audi (A8)
	Body	Panel composite	42	BMW
	Closure doors (4)	Aluminum-intensive	5–50	Nissan (370z), BMW (7), Jaguar (XJ)
	Doors (4)	New production process	86	Porsche (Cayenne)
	Door inner (4)	Magnesium	24–47	
	Hood	Aluminum	15	Honda (MDX), Nissan (370z)
	Roof	Aluminum	15	BWW (7 series)
	Lift gate	Magnesium	5–10	
Suspension and chassis	Chassis	Aluminum	145	Porsche (Cayenne)
	Chassis	Hydroformed steel structure, tubular design	100	Ford (F150)
	Steering wheel	Magnesium	1.1	Ford (Thunderbird, Taurus), Chrysler (Plymouth), Toyota (LS430), BMW (Mini), GM (Z06)
	Steering column	Magnesium	1–2	GM (Z06)
	Chassis wheels (4)	Magnesium	26	Toyota (Supra), Porsche (911), Alfa Romeo
	Wheels (4)	Lighter weight alloy, design	13	Mercedes (C-class)

Continued

Table 11.2 Continued

Vehicle system	Subcomponent	New material or technique[a]	Weight reduction (lb)[b]	Example automaker (model)[c]
	Brake system	Heat dissipation, stainless steel pins, aluminum caps	30	Audi (A8)
	Tires	Design (low rolling resistance (RR))	4	Mercedes (C-class)
	Suspension	Control arms (2)	6	Dodge (Ram)
Interior	Seat frames (4)	Magnesium	28	Toyota (LS430), Mercedes (Roadster)
	Instrument panel	Magnesium	7-13	Chrysler (Jeep), GM, Ford (Explorer, F150), Audi (A8), Toyota (Century), GM
	Dashboard	Fiber-reinforced thermoplastic	18	VW (Golf)
	Console and shifter	Injection-molded GFRP	5	Ford (Flex)
Miscellaneous	Windows	Design, material thickness	3	Mercedes (C-class)
	Running board	GFRP	9	Ford (Escape)

SUV, sports utility vehicle; *GFRP*, glass fiber-reinforced plastic.
[a]These technologies can include a change in design, a reduction in parts, a reduction in material amount, and use of various metallic alloys; note that weight (lb) and mass (kg) variables are used in this report. 1 kg = 2.205 lb.
[b]Weight reduction estimates are approximate, based on media sources and technical reports.
[c]A number of these models are not available in the United States; some model names have been changed in recent product changes.
Adapted from: Lutsey, N., 2010. Review of Technical Literature and Trends Related to Automobile Mass-reduction Technology. Institute of Transportation Studies, University of California, Davis. UCD-ITS-RR-10−10.http://pubs.its.ucdavis.edu/publication_detail.php?id=1390 (last accessed on 04.11.14.).

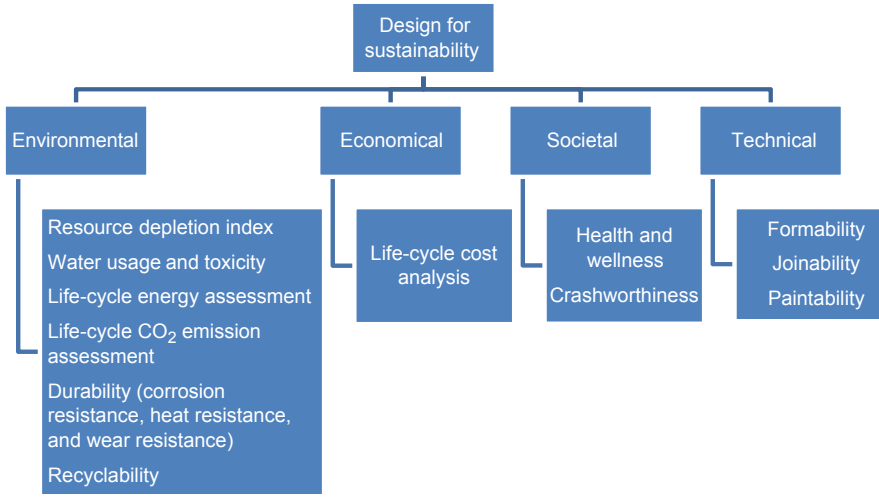

Figure 11.4 Factors of sustainable material selection for BIW.

environmental indicator suggested by Wegst and Ashby (1998) by which the developed eco-indicator is a measure of the environmental impact of the product; however, Ashby (2009) extended this eco-indicator to include an energy content indicator. Coulter et al. (1996) and Holloway (1998) worked on the same idea and they extended these eco-indicator measures to include a set of environmental indicators (eg, CO_2, SO_x, NO_x, a measure of grade of recyclability, and a resource scarcity index). Another economic indicator was proposed by Ermolaeva et al. (2004) to study environmental cost associated with the product's life-cycle stages.

Significant challenges are still facing the automotive industry when it comes to eco-material selection. Such challenges include proper material selection in association with selection of the suitable manufacturing routes; cost of the new lighter, but yet more eco-friendly materials; and expected end-of-life scenario when the vehicle retires. In fact the material selection process is a complicated numerical method that aims at selecting a set of materials from a large pool of candidate materials while taking into consideration a large number of factors. Some of these factors might be conflicting in terms of their economic and environmental impacts. Hence, the design team should precisely handle conflicting objectives (eg, cost versus light weight, functionality versus recyclability, etc.) and then establish well-defined and accepted limits for each design requirement.

Fig. 11.4 shows the proposed model for sustainable material selection for BIW, while Table 11.3 summarizes some of these factors and their importance in this model. This model pivots around material selection for sustainable lightweight design that aims not only at minimizing the weight of the vehicle, but also at ensuring that any material selection conforms to the sustainability holistic approach.

Therefore, the material selection process should cover all of the above-mentioned sustainability requirements to be considered as a sustainable or eco-material selection method.

Table 11.3 Sustainability factors and their importance

Sustainability factor	Importance
Resource depletion index (RDI)	RDI is a quantitative sustainability metric used to evaluate the scarcity level of depletion of natural resources.
Water pollution index and water usage per kilogram of virgin material	Water pollution is defined as any contamination of water with chemicals or other foreign substances that are detrimental to human, plant, or animal health. The water pollution index can be measured by the amount of water used to make a particular product and the toxicity of wastewater resulting from the production system.
Life-cycle assessment (LCA)	LCA is an environmental assessment approach used to evaluate the impact of materials/products on the local and global environments. LCA usually deals with energy usage, emissions (kg CO_2/kg of material), and materials used to make the final product.
Recyclability	Recyclability is as an indicator of the environmental friendliness of materials. Recyclability measures are ability to recycle the end-of-life product and the percentage recycle fraction (ψ).
Durability	Durability mainly addresses the performance of the given materials under typical working conditions, under which the BIW is subject to the harsh environment of salt water, wear and scratch, and hot/cold environments.
Economic impact factors	Life-cycle cost analysis (LCCA) is a numerical measure used in assessing lightweight designs by considering all life-cycle phases for material cost, manufacturing cost, use-phase cost (fuel and maintenance costs), and finally end-of-life cost. LCCA is usually expressed in monetary values per unit mass ($/kg) or per produced units ($/unit).
Societal factors	Two main measures are used in this study to express "safety" and "health and wellness." Safety is an indirect measure of material properties (ie, toughness and yield strength) and health and wellness is another indirect measure that is governed by several factors like noise−vibration−harshness performance (as controlled by dynamic stiffness of the BIW structure and damping capacity of the material) and emissions to the environment and their adverse effects such as acid rain, global warming potential, and ozone depletion.
Technical factors	Technical factors are used to evaluate the ease of manufacturing of any given part relative to the current technologies used in making a steel-based BIW. Technical factors include formability, joinability, and paintability and enhance decision-making process through a "what if" analysis: what will happen if material X is to be used instead of material Y.

11.4 Material selection indices and their role in the material selection process

In the product development process, a team of engineers from different disciplines sit together to discuss new product ideas and decide on the important design criteria, the parameters which describe operating conditions and the governing mathematical formulas, the best material (or a pool of materials to select from), and possible manufacturing routes. At this stage several design iterations will be investigated, which result in several consequences of deviation to the materials under consideration and manufacturing routes.

In this chapter we discuss the eco-material selection process for the structural auto-body panels (the so-called BIW; Fig. 11.5) of a typical passenger vehicle. In this proposed material selection strategy, the objective function for each panel is used to rank the various candidate materials based on their closeness to the best candidate that is determined numerically through derived material selection indices. The BIW is made up from several hundred parts, but contains a couple of major structural

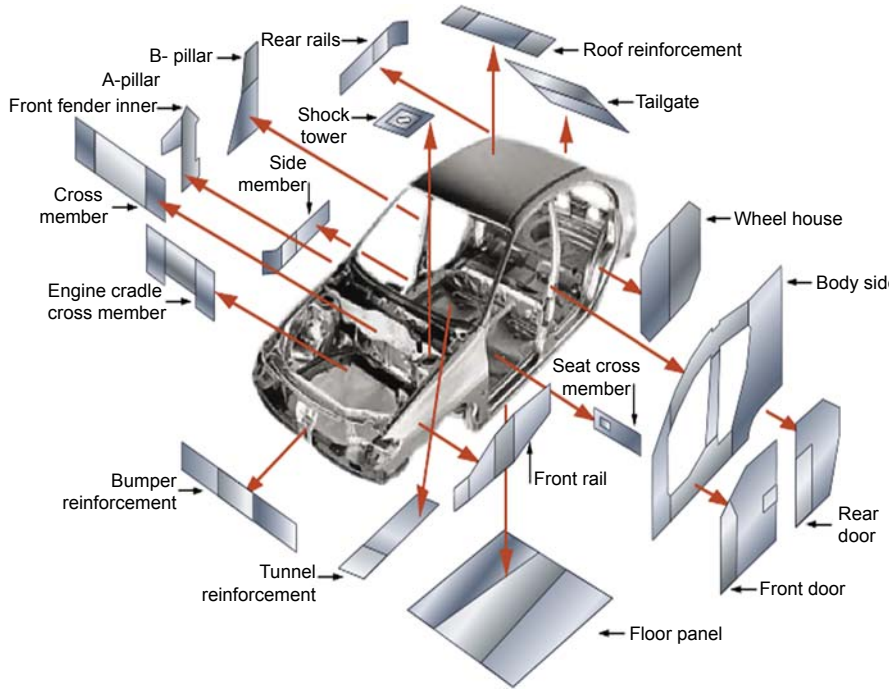

Figure 11.5 Body-in-white with closures.
Courtesy: ArcelorMittal, 2014. Multi-thickness Laser Welded Blanks: Tailored Blanks. Available online from: http://automotive.arcelormittal.com/automotive/saturnus/sheets/S3_EN.pdf (last accessed on 01.07.14.).

Table 11.4 Body-in-white major panels and their main design functions

No.	Panel name	Main design functions
1	Roof	Dent resistance, NVH, durability
2	Roof reinforcement	Bending stiffness, NVH, ease of manufacturing
3	Hood (inner)	Bending stiffness, NVH, ease of manufacturing
4	Hood (outer)	Dent resistance, NVH
5	Trunk (inner)	Bending stiffness, NVH, ease of manufacturing
6	Trunk (outer)	Dent resistance, NVH
7	Trunk pan	Strength, NVH, durability
8	Tunnel reinforcement	Strength, NVH, durability
9	Engine cradle	Crashworthiness, temperature performance, NVH, durability
10	Shock towers	Bending stiffness, NVH, durability
11	Splash/fire wall	Temperature performance, NVH, durability
12	Quarter panel	Dent resistance, NVH
13	Front fender	Dent resistance, NVH
14	Door (inner)	Bending stiffness, NVH, ease of manufacturing
15	Door (outer)	Dent resistance, NVH
16	Side members	Bending stiffness, NVH, durability
17	Wheel house	Bending stiffness, NVH, durability
18	A-, B-pillars	Bending stiffness, NVH, ease of manufacturing, durability
19	Floor pan	Strength, NVH, durability
20	Bumper	Crashworthiness, NVH, durability

NVH, noise-vibration and harshness effect.

panels that make up more than 80−90% of the final BIW weight. These major panels and their main design functions are shown in Table 11.4.

In most cases of material selection, the design objective can be expressed in terms of either maximizing or minimizing the index value. According to Ashby (2008) material selection indices are powerful tools that can be used to map all engineering materials in one chart and then isolate a subset of materials which can meet all the design objectives. However, if the design requires more than one objective function, then plotting design requirements onto selection charts and using a number of charts sequentially allows the simultaneous consideration of several design goals.

Now, let us take an example of material selection for a dent-resistant,[1] recyclable, light panel. Dent resistance has been studied extensively by automobile manufacturers and material engineers and they have proposed several formulas and simulation results for testing it. One of the most acceptable empirical formulas is that presented by (Kalpakjian and Schmid, 2003[2]) as follows:

$$R = \frac{k\sigma_y^2 t^4}{S} \quad [11.1]$$

$$S = Et^{\alpha}H \quad [11.2]$$

where R is the denting energy, k is a constant, σ_y is the material yield strength, t is the panel thickness, S is the panel stiffness, α is the power adjustment of the thickness, E is Young's modulus of elasticity, and H is the shape factor. Then, using Ashby's method in deriving the material selection index will result in the following:

Function: Material selection for a dent-resistant, low-embodied-energy, light panel.

Fixed variables: Panel width w and length L are specified.

Objectives: Minimize mass, m, and minimize embodied energy, q.

If we define energy content to be $Q = m \cdot q$, then,

$$Q = m{\cdot}q = (A\,L)(\rho){\cdot}q = (w\,t\,L)(\rho){\cdot}q \quad [11.3]$$

where m is the mass, w is the width, L is the length, ρ is the density, t is the thickness, S is the stiffness, and E is Young's modulus.

Constraint: Stiffness of the panel, S (see Kalpakjian and Schmid, 2003):

$$S = Et^{\alpha}H \quad [11.4]$$

If we set $\alpha = 2$ for the rectangular panel,[3] then the stiffness equation becomes $S = Et^2H = \frac{k\sigma_y^2 t^4}{R}$, or $t = \left(\frac{E{\cdot}H{\cdot}R}{k\sigma_y^2}\right)^{1/2}$.

Variables: Material choice and/or panel thickness, t.

Hence, if we eliminate t and rearrange the equation:

$$Q = m{\cdot}q = \left(\frac{w{\cdot}L}{\left(\frac{k}{H}\right)^{1/2}}\right) R^{1/2} \left(\frac{\rho E^{1/2}}{\sigma_y}{\cdot}q\right) \quad [11.5]$$

[1] Dent resistance is defined simply as the resistance to permanent deformation; however, there are other factors that need to be considered to have an accurate governing equation for it; such factors may include stiffness, panel shape, and thickness.

[2] See also http://www.azom.com/article.aspx?ArticleID=1629.

[3] α ranges from 1 to 2 for most panels. The H factor depends on the curvature of the panel.

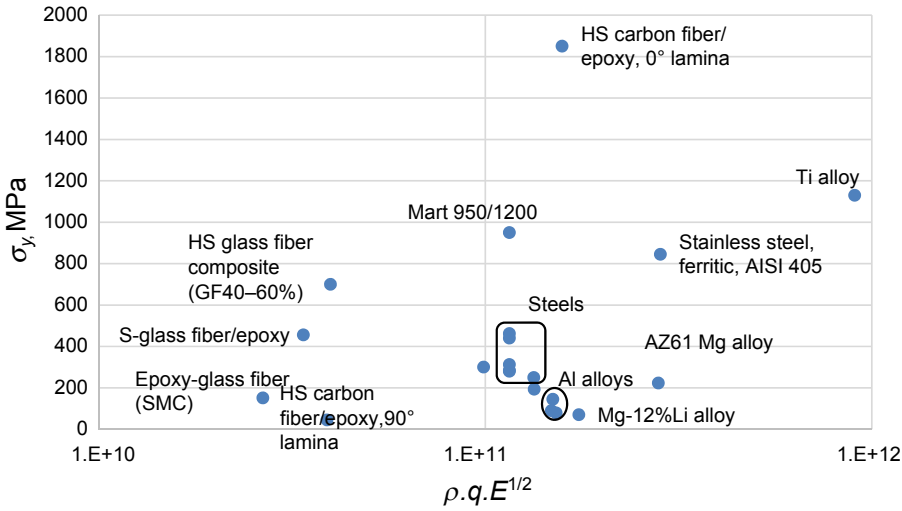

Figure 11.6 Materials for dent-resistant, lightweight, low-embodied-energy panels (eg, outer door and outer hood panels).

Choose materials with largest M:

$$M = \frac{\sigma_y}{\rho \cdot q \cdot E^{1/2}} \qquad [11.6]$$

A material selection chart for a dent-resistant, lightweight, low-embodied-energy panel is shown in Fig. 11.6.

Another example of material selection for a stiff, recyclable, lightweight panel under bending load can be derived as follows:

Fixed variables: Panel, width w and length L are specified.

Objectives: Minimize mass, m, and maximize recycle fraction, ψ.

The objective function in this case is a type of the mixed max−min function, "minimize mass, m, and maximize recycle fraction, ψ ($0 \leq \psi \leq 100\%$). Now, if we set the objective function as a minimization problem only, then:

$$m \cdot \left(\frac{1}{\psi}\right) = (A\,L)(\rho) \cdot \left(\frac{1}{\psi}\right) = (w\,t\,L)(\rho) \cdot \left(\frac{1}{\psi}\right) \qquad [11.7]$$

Constraint: Stiffness of the panel, S:

$$S = \frac{F}{\delta} \Rightarrow S = \frac{C\,E\,I}{L^3} \qquad [11.8]$$

$$I = \frac{w\,t^3}{12} \qquad [11.9]$$

where m is the mass, w is the width, L is the length, ρ is the density, t is the thickness, S is the stiffness, I is the second moment of area, and E is Young's modulus.

Variables: Material choice and panel thickness, t.

Hence, if we eliminate t and rearrange the equation:

$$\frac{m}{\psi} = \left(\frac{12\,S\,w^2}{C}\right)^{1/3} L^2 \left(\frac{\rho}{\psi \cdot E^{1/3}}\right) \qquad [11.10]$$

Choose materials with the largest M:

$$M = \frac{\Psi E^{1/3}}{\rho} \qquad [11.11]$$

So for material 2 to replace material 1, the following equation should be valid:

$$\frac{M_2}{M_1} = \frac{\left(\Psi_2 E_2^{1/3} \Big/ (\rho_2)\right)}{\left(\Psi_1 E_1^{1/3} \Big/ (\rho_1)\right)} > 1.0 \qquad [11.12]$$

A material selection chart for a stiff, lightweight, recyclable panel is shown in Fig. 11.7.

Some sustainability factors are qualitative in nature, for example, materials are classified as having high, medium, or low corrosion resistance. Similarly, fatigue resistance and wear resistance can be expressed in a qualitative fashion (an example of these scalings is shown in Fig. 11.8 for scaling strong, wear-resistant materials). Also, societal factors (ie, safety and health and wellness) should be scaled to show

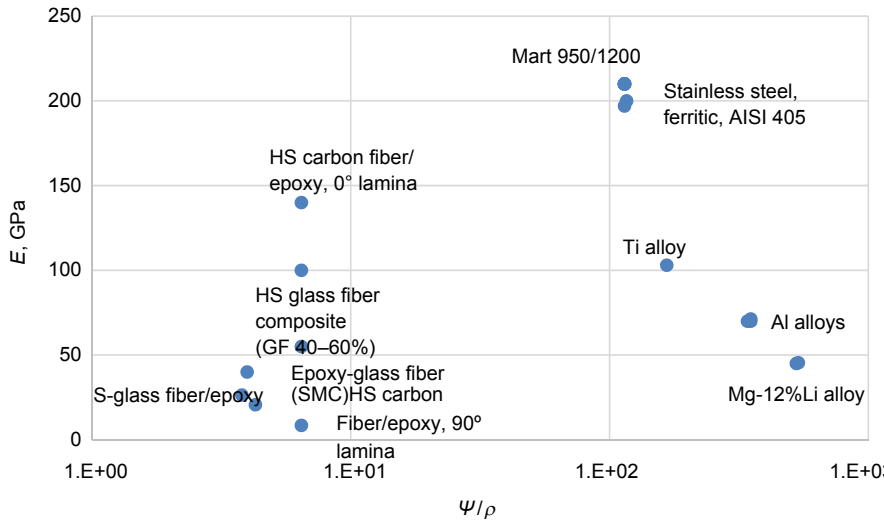

Figure 11.7 Materials for stiff, lightweight, recyclable panels (eg, inner door and inner hood panels).

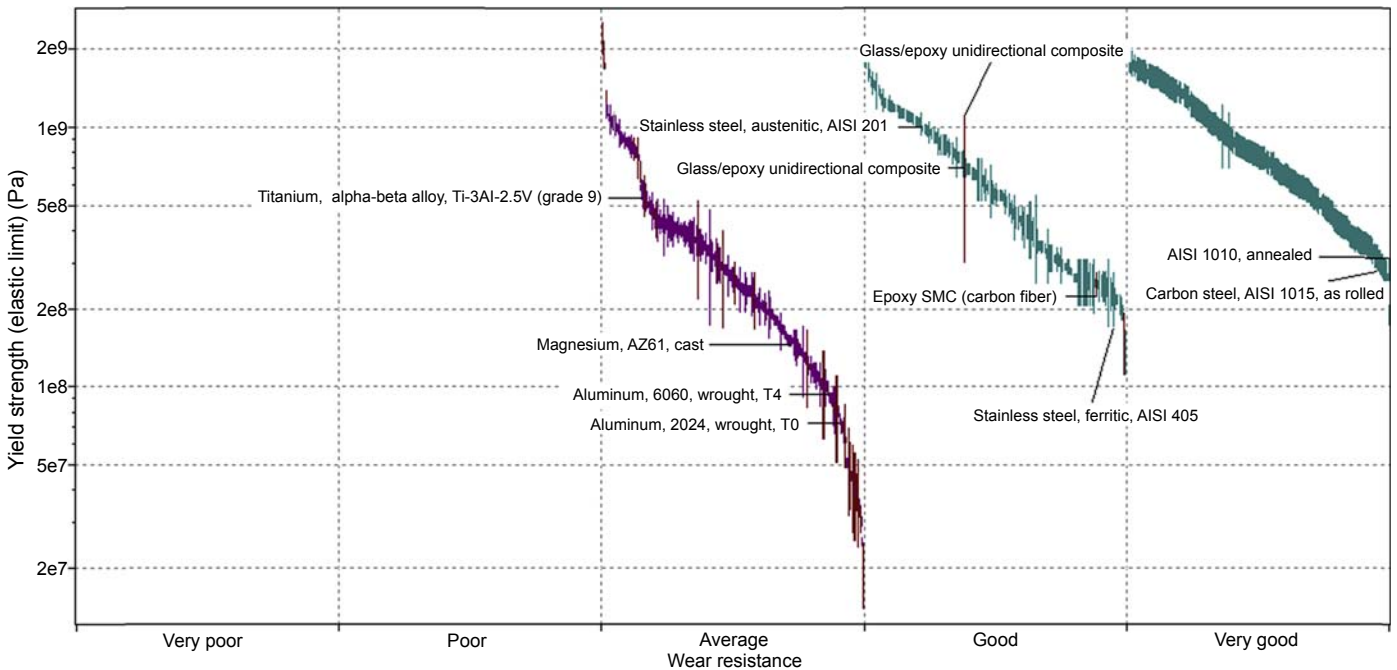

Figure 11.8 Example of scaling method for wear resistance.

the relative performance of the different materials, as there is no well-established scientific method that can quantify these factors, unless safety is assumed to be mainly controlled by the yield strength and the material toughness; however, health and wellness greatly depends on the emissions. For these reasons scaling methods are used in this study to describe some of the selection criteria (see Table 11.5). Scaling is considered to be an acceptable tool to address qualitative aspects in many engineering applications and can be very valuable in communicating results or clarifying the relative importance and significance of various factors (Saur et al., 2000). Technical factors (forming, joining, and painting) do not have well-established material selection indices, but can be rated either qualitatively (eg, good, average, and poor formability) or quantitatively (eg, 1 for poor formability and 10 for excellent formability). A scale of 1 to 10 was used to scale the following selection criteria: forming, joining, painting, health and wellness, wear and fatigue resistance, corrosion resistance, and crashworthiness. Ratings for some materials have been collected from different sources and summarized in Table 11.5, which shows some durability, societal, and technical factors based on a 1−10 scale (Mayyas et al., 2011; Davies, 2004; CES, 2008).

To summarize all derived material selection indices, all developed indices for sustainable lightweight BIW design are tabulated in Tables 11.6−11.8, for lightweight bending-resistant (stiff), dent-resistant, and strong materials, respectively.

11.5 Example: material selection for recyclable B-pillar

The goal of this example is to emphasize the method of eco-material selection using sustainability indices. The following example shows that method and the results of the eco-material selection of lightweight materials to replace conventional steel in the B-pillar panel (see Fig. 11.9). As shown in Table 11.4, the main design function is the bending stiffness followed by NVH (noise-vibration and harshness effect) and ease of manufacturing. Now, let us focus on the stiffness of the panel and expected mass reduction resulting from the replacement. Eqs. [11.11] and [11.12] show the material selection index and acceptable ratio between the new alternative materials, respectively. So, for a light, recyclable, stiff panel we should choose material that has $M = \frac{\Psi E^{1/3}}{\rho}$ equal to or greater than conventional steel (ie, dual-phase steel). The mass of the B-pillar is around 5.90 kg and it has an average thickness of 1.8 mm. The B-pillar is made from dual-phase steel with an average yield strength of 370 MPa and average ultimate tensile strength of 650 MPa. Table 11.9 summarizes material selection calculations for a set of candidate materials that includes steels, HSSs, advanced HSSs, stainless steels, magnesium alloys, aluminum alloys, and some composite materials (carbon fiber-reinforced plastics (CFRP) and glass fiber-reinforced plastics). Table 11.9 shows that aluminum alloys, magnesium alloys, some types of stainless steels, and titanium can replace dual-phase steel in the B-pillar design without problems, as all have $M_2/M_1 > 1$. However, if we consider other sustainability factors like cost and energy required to manufacture B-pillar panels, this may lead us to the selection of aluminum or magnesium as they perform better than other candidate materials from these sustainability perspectives.

Table 11.5 Scoring values for some material selection criteria

	Durability[a]			Societal		Technical[b]		
Material	**Corrosion resistance**	**Thermal performance**	**Wear resistance**	**Health and wellness (NVH[c])**	**Crashworthiness [d]**	**Forming**	**Joining**	**Painting**
AISI 1015	5	9	9	5	7	8	9	9
AISI 3140	5	9	9	5	7	8	9	9
Dual phase 280/600	5	9	9	5	8	6	8	9
High-strength low alloy steel 462/524	5	9	9	5	8	6	8	9
Martensitic steel 950/1200	5	9	9	4	9	4	7	9
Stainless steel, AISI 405	6	10	7	4	10	4	7	9
Aluminum AA2424	7	8	6	9	3	7	5	8
Aluminum AA6060	7	8	6	9	3	7	5	8
AZ61 Mg alloy	3	8	6	8	2	4	4	7
Ti/3Al/8V/6Cr/4Zr/4Mo	9	9	5	5	8	5	5	7
Isotropic high-strength carbon fiber/epoxy composite	9	5	7	3	10	8	7	8
Epoxy−glass fiber (SMC Composites)	9	5	8	3	2	8	7	8
Unidirectional high-strength glass fiber composite (GF 40−60%)	9	5	7	3	6	8	7	8

[a] CES (2008) software.
[b] Davies (2004).
[c] *NVH*, noise-vibration and harshness effect and is a function of vehicle stiffness and material damping properties.
[d] Crashworthiness is a function of yield strength and toughness of the materials used.

Table 11.6 Material selection indices for lightweight, stiff sustainable material

Environmental factor	Index	Economic factor	Index
Minimum resource depletion for lightweight bending stiffness	$\frac{E^{\alpha}}{\rho * \mathrm{RDI}}$	Minimum material cost for lightweight bending stiffness	$\frac{E^{\alpha}}{\rho * C_{\mathrm{M}}}$
Minimum water pollution for lightweight bending stiffness	$\frac{E^{\alpha}}{\rho * \mathrm{WPI}}$	Minimum manufacturing cost for lightweight bending stiffness	$\frac{E^{\alpha}}{\rho * C_{\mathrm{E}}}$
Minimum life-cycle energy for lightweight bending stiffness	$\frac{E^{\alpha}}{\rho * \mathrm{LCE}}$	Minimum fuel cost for lightweight bending stiffness	$\frac{E^{\alpha}}{\rho * C_{\mathrm{F}}}$
Minimum recycling CO_2 footprint for lightweight bending stiffness	$\frac{E^{\alpha}}{\rho * \mathrm{FP}}$	Minimum end-of-life cost for lightweight bending stiffness	$\frac{E^{\alpha}}{\rho * C_{\mathrm{EOL}}}$
Maximum recycle fraction for lightweight bending stiffness	$\frac{E^{\alpha} * \psi}{\rho}$		
Minimum recycling embodied energy for lightweight bending stiffness	$\frac{E^{\alpha}}{\rho * R_{\mathrm{E}}}$		

α depends on the shape and dimensions of the panel ($\alpha = 1/2$ for beam with specified length and shape and free sectional area; $\alpha = 1$ for beam with specified length and height and free width; $\alpha = 1/3$ for beam with specified length and width and free height; $\alpha = 1/3$ for panels and plates with specified length and width and free thickness).

Table 11.7 Material selection indices for lightweight, dent-resistant sustainable material

Environmental factor	Index	Economic factor	Index
Minimum resource depletion for lightweight dent resistance	$\frac{\left(\frac{\sigma_y^2}{E}\right)^{\beta}}{\rho \cdot \mathrm{RDI}}$	Minimum material cost (C_E) for lightweight dent resistance	$\frac{\left(\frac{\sigma_y^2}{E}\right)^{\beta}}{\rho C_{\mathrm{E}}}$
Minimum water pollution index for lightweight dent resistance	$\frac{\left(\frac{\sigma_y^2}{E}\right)^{\beta}}{\rho \cdot \mathrm{WPI}}$	Minimum manufacturing cost (C_M) for lightweight dent resistance	$\frac{\left(\frac{\sigma_y^2}{E}\right)^{\beta}}{\rho C_{\mathrm{M}}}$
Minimum life-cycle energy (LCE) for lightweight dent resistance	$\frac{\left(\frac{\sigma_y^2}{E}\right)^{\beta}}{\rho \cdot \mathrm{LCE}}$	Minimum use-phase cost (C_F) for lightweight dent resistance	$\frac{\left(\frac{\sigma_y^2}{E}\right)^{\beta}}{\rho C_{\mathrm{F}}}$
Minimum life-cycle CO_2 ($\mathrm{LCA}_{\mathrm{CO_2}}$) footprint for lightweight dent resistance	$\frac{\left(\frac{\sigma_y^2}{E}\right)^{\beta}}{\rho \cdot \mathrm{LCA}_{\mathrm{CO_2}}}$	Minimum end-of-life cost (C_{EOL}) for lightweight dent resistance	$\frac{\left(\frac{\sigma_y^2}{E}\right)^{\beta}}{\rho C_{\mathrm{EOL}}}$
Maximum recycle fraction for lightweight dent resistance	$\frac{\left(\frac{\sigma_y^2}{E}\right)^{\beta} \psi}{\rho}$		

β ranges between 1 and 2 and depends on the shape and dimensions of the panel.

Table 11.8 Material selection indices for lightweight, strong sustainable material

Environmental factor	Index	Economic factor	Index
Minimum resource depletion for lightweight strong panel	$\frac{\sigma_y^\gamma}{\rho \cdot \mathrm{RDI}}$	Minimum material cost for lightweight strong panel	$\frac{\sigma_y^\gamma}{\rho * C_\mathrm{M}}$
Minimum water pollution for lightweight strong panel	$\frac{\sigma_y^\gamma}{\rho \cdot \mathrm{WPI}}$	Minimum manufacturing cost for lightweight strong panel	$\frac{\sigma_y^\gamma}{\rho * C_\mathrm{E}}$
Minimum life-cycle energy for lightweight strong panel	$\frac{\sigma_y^\gamma}{\rho \cdot \mathrm{LCE}}$	Minimum fuel cost for lightweight strong panel	$\frac{\sigma_y^\gamma}{\rho * C_\mathrm{F}}$
Minimum recycling CO_2 footprint for lightweight strong panel	$\frac{\sigma_y^\gamma}{\rho \cdot \mathrm{LCA}_{\mathrm{CO}_2}}$	Minimum end-of-life cost for lightweight strong panel	$\frac{\sigma_y^\gamma}{\rho * C_\mathrm{EOL}}$
Minimum air pollution for lightweight strong panel	$\frac{\sigma_y^\gamma}{\rho \cdot \mathrm{API}}$		
Maximum recycle fraction for lightweight strong panel	$\frac{\sigma_y^\gamma \cdot \psi}{\rho}$		

γ depends on the shape and dimensions of the panel ($\gamma = 2/3$ for beam with specified length and shape and free sectional area; $\gamma = 1$ for beam with specified length and height and free width; $\gamma = 1/2$ for beam with specified length and width and free height; $\gamma = 1/2$ for panels and plates with specified length and width and free thickness).

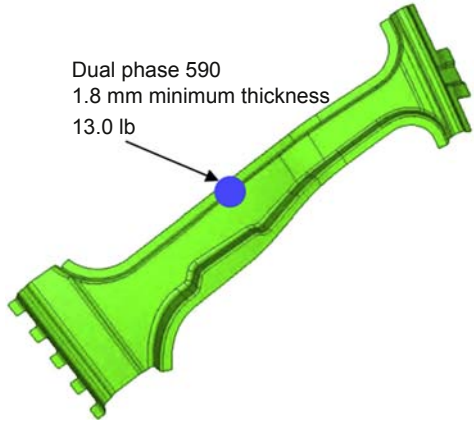

Figure 11.9 B-pillar shape and geometry.
Adapted from: http://www.autosteel.org/~/media/Files/Autosteel/Great%20Designs%20in%20Steel/GDIS%202006/15%20-%20Optimization%20Side%20Crash%20Performance%20Using%20a%20Hot-Stamped%20B-Pillar.pdf (last accessed on 11.02.14.).

Table 11.9 Mechanical properties and design parameters of some candidate materials that can replace dual-phase steel in the B-pillar

Material	Density (g/cm^3)	Modulus of elasticity (GPa)	Yield strength (MPa)	Ultimate tensile strength (MPa)	Recycle fraction (ψ) (%)	M_2/M_1	New panel mass (kg)	Thickness (mm)
Carbon steel AISI 1015 (as rolled)	7.870	210	312.5	420	90	1	5.90	1.8
Carbon steel AISI 1015 (annealed)	7.870	210	285	387.5	90	1	5.90	1.8
Carbon steel AISI 3140	7.870	210	440	700	90	1	5.90	1.8
Dual-phase steel (YS = 330 − 410 MPa; UTS = 600 − 700 MPa)	7.870	210	280	600	90	1	5.90	1.8
HSLA 462/524	7.870	210	462	524	90	1	5.90	1.8
Martensite steel 950/1200	7.870	210	950	1200	90	1	5.90	1.8
Stainless steel AISI 201; austenitic	7.870	197	845	1120	90	0.9789	6.03	1.84
Stainless steel, ferritic, AISI 405	7.720	200	223	448	90	1.0030	5.88	1.83
Aluminum alloy AA5005	2.700	71.3	145	160	95	2.1464	2.90	2.58
Aluminum alloy AA2424	2.780	70	79	185	95	2.0712	3.01	2.60
Aluminum alloy AA6060	2.700	70	90	160	95	2.1333	2.92	2.60
AZ61 magnesium alloy	1.800	45	193.5	295	95	2.7617	2.26	3.01

Continued

Table 11.9 Continued

Material	Density (g/cm^3)	Modulus of elasticity (GPa)	Yield strength (MPa)	Ultimate tensile strength (MPa)	Recycle fraction (ψ) (%)	M_2/M_1	New panel mass (kg)	Thickness (mm)
Mg−Li (12%) as cast	1.770	45.5	70	150	95	2.819	2.21	3.00
Ti/3Al/8V/6Cr/4Zr/4Mo	4.800	103	1130	1220	80	1.1494	4.56	2.28
Epoxy-carbon fiber (sheet molding compound)	1.550	100	250	300	1	0.0441	1.49	2.31
High-strength C-fiber/epoxy composite, 0° unidirectional lamina	1.550	140	1850	1850	1	0.0493	1.33	2.06
High-strength C-fiber/epoxy composite, 90° unidirectional lamina	1.550	8.5	45	32	1	0.0194	3.38	5.24
High-strength C-fiber/epoxy composite, isotropic	1.550	55	300	300	1	0.0361	1.82	2.81
Epoxy-glass fiber (sheet molding compound)	1.650	20.7	151.5	190	0.707	0.01731	2.68	3.90
High-strength glass fiber composite (GF 40−60%), unidirectional lamina	1.775	40	700	700	0.707	0.0200	2.31	3.13
S-glass fiber/epoxy composite, 0°/90° biaxial lamina (30−60% GF)	1.860	26.4	455.5	455.5	0.707	0.0167	2.78	3.59

Rows in gray represent materials that can replace dual-phase steel without sacrificing the functionality of the panel. *YS*, yield strength; *UTS*, ultimate tensile strength.

11.6 Life-cycle assessment model

Life-cycle assessment (LCA) is a method used in assessing environmental impacts associated with all the stages of a product's life, from cradle to grave (ie, from raw material extraction through materials processing, manufacture, distribution, use, repair and maintenance, and end of life, which includes disposal or recycling).

LCA models usually serve as numerical analysis tools rather than descriptive tools in sustainability and green manufacturing. The goal of comparative LCA studies is to have a numerical ranking method in the form of an eco-indicator that helps in assessing any particular product through its lifetime from material extraction to processing and manufacturing, use and maintenance, and end of life. According to Mayyas et al. (2012c), LCA can be considered as a main branch of the environmental factors that fall under the industrial ecology branch. The framework of LCA was first introduced by the International Organization for Standardization (ISO 14000, 1998) in 1998 and is structured around three main activities:

- inventory analysis, which aims at collecting relevant energy and material inputs as well as environmental impacts through material released to the environment and emissions;
- evaluating the potential impacts associated with all inputs and releases or emissions;
- interpreting the results which help designers and customers to make more eco-informed decisions.

While the ISO 14000 series acts as an accepted framework for procedures to deal with retired vehicles, other regulations in other countries tend to be stricter in this regard. A good example comes from Europe, where the European Union has established a very promising recycling and reuse initiative for retired vehicles. From 2002 onward, the European End-of-Life Vehicle Directive requires all automobile manufacturers to get back all newly registered vehicles that require disposal (Kanari et al., 2003). The European Union estimates more than 3.5 tons of waste flux per car, which results in 8−9 million tons of annual waste from retired vehicles (Ferrão and Amaral, 2006).

The European Parliament approved Directive 2000/53/EC, which deals with end-of-life vehicles (ELVs) (Kon, 2009). The goal of this directive is to reduce the potential environmental impacts from ELVs. Ferrão and Amaral (2006) summarized this directive's technical requirements for car design as well as the minimum reuse and recovery rates for retired vehicles as:

- All vehicles put on the market after January 7, 2003, must not contain lead, mercury, cadmium, or hexavalent chromium, with the exception of some cases referred in the annex of the directive.
- Starting January 1, 2006, 85%, on a mass basis, of vehicles produced in or after 1980 must be reused and recovered (recycling 80%). Reuse and recovery of 75% on a mass basis (recycling 70%) for vehicles produced before 1980 is also targeted in this directive.
- Starting January 1, 2015, vehicles must be constructed of 95% recyclable materials (with 85% recoverable through reuse or mechanical recycling and 10% through energy recovery or thermal recycling) (GHK, 2006).

However, this directive also requires that these targets should be met while ensuring that the ELV is delivered to a specialized treatment facility without any additional costs to the vehicle owner. Table 11.10 summarizes the total recycling and recovery rate of ELVs in the European Union in the period 2006−2011.

The LCA for midsize passenger vehicles is divided into five distinct phases to cover all related phases; four of these phases which have a direct impact on the environment were adopted from the classical LCA framework, namely, material extraction and production phase, manufacturing and processing phase, use and maintenance phase, and end-of-life phase; however, another indirect phase is also included in this study which accounts for fuel extraction, refining, and delivery, as they are believed to constitute a significant portion of the environmental impact and have to be considered as the fifth stage of the typical LCA framework for automotive applications (Mayyas et al., 2012c).

Most LCA studies show that the use and maintenance phase accounts for >80% of the total energy consumed and greenhouse gases (GHGs) emitted into the environment. Inventory analysis in the typical LCA framework is the most time-consuming process, which requires a lot of data collecting, making assumptions, and then analyzing data and getting the results. Conclusions can be drawn from LCA results as to whether to consider materials that have lower energy expenditure or materials that have lower emissions over the vehicle's lifetime.

As mentioned before, the LCA consists of five distinct phases. For the material and extraction phase all embodied energies and associated CO_2 emissions are obtained from engineering handbooks that discuss eco-material selection and then stored for further analysis. The second life-cycle phase, which accounts for manufacturing of the BIW, is a very detailed analysis that covers several manufacturing processes and their energy consumptions, GHG emissions, throughputs, yields, and capital costs of necessary production lines. There are three major manufacturing steps for building a metallic BIW: blanking and stamping, joining and welding, and finally painting. In the first production route of blanking and stamping, the energy consumption and CO_2 emissions are calculated based on the weight of the single large structural parts taking into account yield and rework of some defective parts. In the second production step (ie, joining and welding) the total energy consumption and CO_2 emissions are calculated based on the length of the weld lines and the number of spot welds and seam joints and then correlated to the weight of the BIW. The same idea is used for the painting process for which the total energy and CO_2 emissions are converted from units of MJ/m^2 or kg CO_2/m^2 to MJ/kg or kg CO_2/kg to be consistent with other manufacturing steps. For plastic composites, the manufacturing processes are a little different. In such case, traditional bulk molding compounds (BMCs) and sheet molding compounds (SMCs) are known to have lower production cost and higher line throughputs (Das, 2001a,b). The compounds take the form of flexible, leather-like sheets or bulky material that is easily cut, weighed, and placed in the mold for curing to the desired part configuration. Because there is no mixing or extrusion involved in preparing BMCs and SMCs, the fibers remain undamaged at their original length and quality.

Table 11.10 The recycling and recovery rate of end-of-life vehicles in the European Union in the period 2006–2011

Country	2006	2007	2008	2009	2010	2011
Belgium	87.7	87.9	88	88.4	89	88.2
Bulgaria	82.4	89.5	81	82.7	88.9	90
Czech Republic	79	79	80	80.3	80.3	80.3
Denmark	80	81	82.7	82	90.5	92.8
Germany	86.8	88.1	89.2	82.9	95.5	93.4
Estonia	82.5	82.2	92.4	87.2	77.3	76.1
Ireland	78.1	81.3	75.9	78.9	77	80.5
Greece	82.3	84.1	85.7	86.5	84.5	85.2
Spain	76	81.9	82.5	82.6	82.8	82.9
France	79.6	79.8	79.9	78.6	79	80.8
Italy	70.3	82.3	84.3	81.8	83.2	84.8
Cyprus	85.4	83.7	78.3	87.1	81.1	84
Latvia	86	88	87	85	85.7	85.4
Lithuania	88	86.4	85	86	88.1	87.2
Luxembourg	85.1	83	84	81	85	82.9
Hungary	81.2	81.6	83	84.4	82.1	84.4
Netherlands	82.5	83.1	84.4	84.1	83.3	83.1
Austria	80	80	83.7	82.9	84.2	82.8
Poland	84.7	72.8	79.5	87.1	88.8	89.5
Portugal	82.2	81.7	80.8	84.3	82.8	82.9
Romania	77.1	83.7	83.7	80.1	80.9	82.9
Slovenia	76.8	87.2	87.6	84.1	88.6	86.1
Slovakia	82.8	88	88.4	88.8	88.4	93.1
Finland	82	81	81	81	82.5	82.5
Sweden	83.4	83	83	86	84.4	84.4
United Kingdom	81	81.8	82.5	82.1	83	83.4
Liechtenstein	–	2.2	96	76	76	80
Norway	83	81.4	82.2	83	83.9	73.6

Source of data: Eurostat: http://appsso.eurostat.ec.europa.eu/nui/submitViewTableAction.do.

For the use phase, two important assumptions need to be highlighted, the distance traveled in the total lifetime, which was set to be 200,000 miles (Mayyas et al., 2012c), and type of fuel, which greatly depends on the type of power train used. However; material selection that results in a lightweight BIW design should be considered in parallel with the selection of an appropriate power train that meets the performance requirements. In this study we assumed a gasoline-based power train to be the basis for all vehicle designs under consideration, as assessing different BIW design/power train options is beyond the scope of the analysis. The most important issue to consider here is the fuel economy of the vehicle, which greatly depends on the curb weight. In this study, an empirical equation developed by Hakamada et al. (2007) was used to estimate fuel economy of the vehicle:

$$\mathrm{FE} = 6.4 \times 10^4 M^{-1.2} \qquad [11.13]$$

where FE is fuel economy expressed in km/L and M is the curb weight in kilograms.

The energy consumption and the CO_2 emissions in this stage are thus evaluated knowing that gasoline has a heating value of 34.8 MJ/L and a CO_2 footprint of 2.36 kg/L (Hakamada et al., 2007). To get the final normalized value of the energy consumption and the CO_2 emission to the environment during the use phase, the total amount of fuel consumed and the amount of CO_2 emitted over the vehicle's entire lifetime is divided by the curb weight using various BIW design options (steel-intensive BIW, HSS BIW, stainless steel BIW, aluminum-intensive BIW, magnesium-intensive BIW, and composite-intensive BIW).

For maintenance energy and CO_2 emission, it was assumed that maintenance energy accounts for 1% of the total use energy (Mayyas et al., 2012c). For fuel extraction and production, numbers were obtained from the analysis made by Argonne National Laboratory which were equivalent to 34.24 MJ/gallon of gasoline and 1.9874 kg CO_2/gallon of gasoline available at fuel station pumps for the average US market (ANL, 2011).

For end-of-life analysis we assumed that metallic-based BIWs are to be recycled and composite-based BIWs are to be landfilled/incinerated with almost zero recycle fraction. Recycle fractions for steel and stainless steel were set to 90%, compared to 95% for aluminum and magnesium and 80% for titanium. Also, it is important to mention that the end-of-life strategy may result in savings of some energy and emissions required for extracting and processing of the virgin material, if the ELVs were turned into the recycling loop.

Fig. 11.10 illustrates the life-cycle energy for the various materials represented in percentage values of the total life-cycle energy, and Fig. 11.11 shows the associated CO_2 emissions for all life stages. However, both figures indicate that Al-intensive BIWs followed by Mg-intensive BIWs are the best choices from both energy and CO_2 emission perspectives.

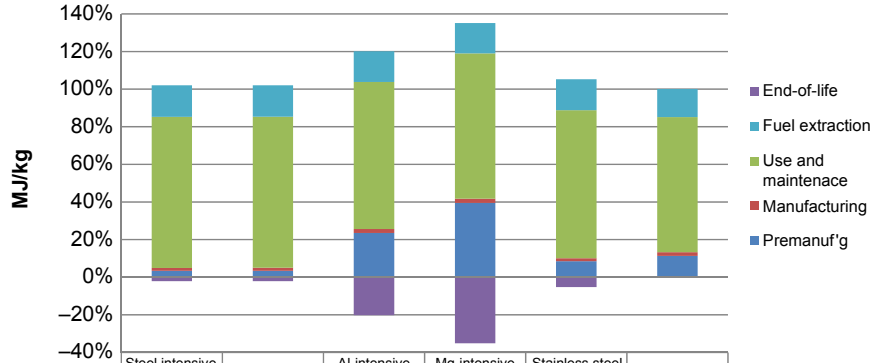

	Steel intensive BIW (945.35 MJ/kg)	AHSS BIW (937.4 MJ/kg)	Al-intensive BIW (881.78 MJ/kg)	Mg-intensive BIW (886.29 MJ/kg)	Stainless steel BIW (956.16 MJ/kg)	Composite BIW (984.1 MJ/kg)
End-of-life	–2.06%	–2.08%	–20.16%	–35.13%	–5.23%	–0.08%
Fuel extraction	16.74%	16.72%	16.29%	16.09%	16.39%	14.95%
Use and maintenace	80.38%	80.31%	78.24%	77.28%	78.73%	71.78%
Manufacturing	1.56%	1.64%	2.10%	2.20%	1.60%	1.97%
Premanuf'g	3.38%	3.41%	23.53%	39.55%	8.50%	11.38%

Figure 11.10 Life-cycle energy analysis for various BIW designs (negative numbers represent potential energy saving upon recycling end-of-life vehicle parts; total life-cycle energy = 100%). AHSS: Advanced high strength steel.

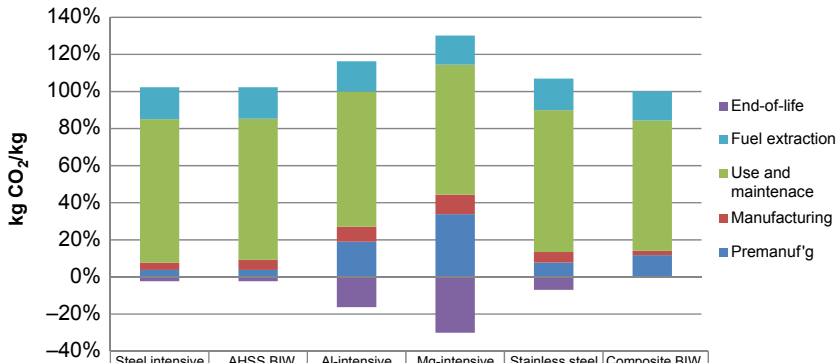

	Steel intensive BIW (65.68 kg CO_2/kg)	AHSS BIW (66.098 kg CO_2/kg)	Al-intensive BIW (63.16 kg CO_2/kg)	Mg-intensive BIW (65.27 kg CO_2/kg)	Stainless steel BIW (65.75 kg CO_2/kg)	Composite BIW (67.1 kg CO_2/kg)
End-of-life	–2.35%	–2.33%	–16.33%	–30.14%	–6.99%	–0.08%
Fuel extraction	17.28%	17.01%	16.32%	15.68%	17.10%	15.73%
Use and maintenace	77.29%	76.09%	72.97%	70.11%	76.48%	70.33%
Manufacturing	3.99%	5.47%	8.05%	10.49%	5.64%	2.32%
Premanuf'g	3.78%	3.76%	19.00%	33.86%	7.76%	11.71%

Figure 11.11 Life-cycle CO_2 emissions analysis for various BIW designs (negative numbers represent potential energy saving upon recycling end-of-life vehicle parts; total life-cycle CO_2 emissions = 100%). AHSS: Advanced high strength steel.

11.7 The cost of vehicle weight reduction

Comparing various materials used in constructing BIWs based on their material and manufacturing costs is a biased judgment and does not give an accurate performance measure; rather comparing materials in monetary value per mass saved would be more subjective. The comparison should include initial material cost and expected savings over the average vehicle lifetime. By doing so, some lightweight material will have better performance compared to heavier materials like steels. Nowadays, most researchers use technical or process-based cost modeling (Cheah, 2010). This methodology encompasses the cost implications of both material and the process variables by first identifying critical cost elements or drivers like raw material and energy, labor, capital, and tooling. Sensitivity analyses for key parameters like production volume and raw material prices are usually carried out to assess these competitive materials relative to the overall vehicle cost. Such technical cost models help decision-makers understand the cost of the lightweight vehicle parts based on the nature of the manufacturing process and how this correlates to the production volume.

Several studies concerning lightweight material cost found that cost to vary widely, from $2.00 to $14.00 per kilogram of weight savings ($/kg), depending on several factors like the type of material, the design of the vehicle component, the manufacturing process used to make this part, and the annual production volume (Cheah, 2010). In general the incremental cost per unit weight savings can be achieved by replacing conventional steel grades with HSS followed by aluminum and polymer composites. The negative cost values associated with using HSS imply cost savings that will result from using this alternative material. Automotive parts made from composite materials are still expensive given high raw material prices and long production cycle times (Cheah, 2010). This may mean that HSS and aluminum might remain the popular candidate lightweight materials to replace steel in passenger vehicles in the near term. Table 11.11 shows some lightweight projects and their corresponding manufacturing costs in terms of dollars spent per unit mass saved. While most of these case studies focused on automobile bodies, still some projects were aimed at saving some weight in other vehicle systems like the power train and interior systems.

It is important to distinguish between the costs of mass reduction of a single vehicle component or a single system like the BIW versus mass reduction of the entire vehicle. Saving several pounds from a single component will result in better fuel economy numbers over a long-term run, but saving several hundred pounds through mass reduction in the BIW will be directly reflected in the fuel economy of the vehicle as well as downsizing of the power train system, which will also result in extra mass savings. For instance, a lightweight vehicle that is optimized for minimal weight is likely to use a downsized power train and suspension as a result of this primary mass savings in the body. In this case, additional cost and weight savings in these components should be taken into account in the cost analysis to estimate final $/kg.

Currently, composite materials are gaining more attention in the automotive industry because of several advantages they have over steel. Composites are being considered to make lighter, safer, and more fuel-efficient vehicles. In addition to the lighter weight of

Table 11.11 Some lightweight projects with their corresponding cost impacts

Project	Mass reduction	Cost impact[a,b]
Porsche Engineering UltraLight Steel Auto Body advanced vehicle concept	Body: 17% (52−67 kg) Vehicle: 19−32% (200−260 kg)	The total estimated manufactured cost of the mass-optimized vehicles is about $9200 to $10,200 per vehicle. Mass-optimized vehicle designs using high-strength steels had very tiny cost increment (or even resulted in some savings). Estimated cost impact per unit mass ranges between $0.47 and $1.0/kg.
Altair SUV frame	Body: 23%	Study showed very small estimated cost impact $0.68/kg at high production volumes (220,000 vehicles per year).
Volkswagen AG	Body: 101 kg	Volkswagen estimated the incremental cost of the new mass-optimized high-strength steel body to be around $13/kg at a production volume of 1000 vehicles/day.
ThyssenKrupp new steel body	Body: 24%	The ThyssenKrupp steel body design resulted in a 24% body mass reduction, with potential for secondary mass reductions from design optimization elsewhere on the vehicle. This mass saving had increased manufacturing cost about 2%.
IBIS aluminum-intensive design	Body: 48% Vehicle: 17%	Aluminum body has a $500−$600 cost increase relative to the steel body (22% increase) with an additional cost of $100 (1% increase) over conventional baseline vehicle retail price as a direct result of power train resizing and secondary mass reductions, for a vehicle that had its mass reduced by 17% from its baseline steel-intensive vehicle.
EDAG steel-intensive Future Steel Vehicle	Body: 16−30% Vehicle: 17%	This project investigated the new mass-optimized body in association with various power trains (eg, hybrids and plug-in electric vehicles) and found that the total cost of ownership can be improved significantly as a direct result of the reductions in fuel consumption and other benefits that offset mass reduction and power train costs.

Continued

Table 11.11 Continued

Project	Mass reduction	Cost impact[a,b]
Magnesium-intensive body	Body: 49% reduced part count (−78%) along with reduced mass (−161 kg)	Increased variable cost (3%), decreased investment cost (−46%) Volkswagen-led
Super Light Car	Body: 14−39% (40−109 kg)	Project was conducted in the period 2005 to 2009 and funded by the European Commission (10.5€ million) while other companies shared another 8.7€ million. Companies involved included Volkswagen, Fiat, Daimler, Porsche, Renault, Volvo, and Opel. This consortium of companies developed and demonstrated a multimaterial concept approach, including design, materials, and manufacturing routes. A multimaterial vehicle was produced which consisted of 53% aluminum, 36% steel, 7% magnesium, 4% fiber-reinforced plastic. This study found major reductions (32−42%) in all major body-in-white components (body, front end, floor). Other designs were also investigated, like the steel-intensive vehicle, which achieved a mass reduction of 40 kg (14%) and less than 2.5€/kg; several multimaterial vehicle designs were also produced and achieved mass reductions of 62−114 kg (22−39%) with an estimated cost of 5−10€/kg.
Lotus Engineering Low Development	Body: 16% (58 kg) Vehicle: 20% (336 kg)	Lotus Engineering investigated several multimaterial designs and achieved weight saving of 21−38% in a crossover utility vehicle by using high-strength steel, aluminum, magnesium, and composites and by eliminating or consolidating some auto-body parts. For example, Lotus got a cost decrease of $60/vehicle (18%) through the use of advanced steel alloys in the body. This cost savings also resulted in another $300/vehicle (2%).

Table 11.11 Continued

Project	Mass reduction	Cost impact[a,b]
Lotus Engineering High Development	Body: 42% (162 kg) Vehicle: 33% (560 kg)	Mass-optimized body using multimaterials like high-strength steels, aluminum, magnesium, and composites throughout the vehicle in association with consolidation of some parts. Lotus is focusing now on the second phase of the project called the High Development vehicle for Model Year 2020 production, which will have a nominal estimated cost increase of 3% (with potential for cost reduction).
Composite-intensive body	Vehicle: 68−444 kg	Several mass-optimized body designs have been investigated and found that mass reductions up to 400 kg are achievable by replacing conventional steel with plastic composite materials especially in the vehicle's body. Costs associated with composite materials in the vehicles are relatively high and could increase cost by $2.20−$13.68/kg saved depending on the size, shape, material, and manufacturing processes used to make these parts.

[a] OEM cost is estimated from Toyota Venza, the baseline vehicle, retail price (MSRP) of $24,000, assuming markup of 1.4×.
[b] This estimate is the difference in raw material cost only.
Sources of data: Lutsey, N., 2010. Review of Technical Literature and Trends Related to Automobile Mass-reduction Technology. Institute of Transportation Studies, University of California, Davis, UCD-ITS-RR-10−10 http://pubs.its.ucdavis.edu/publication_detail.php?id=1390 (last accessed on 04.11.14.); Cheah, L.W., et al., 2009. The trade-off between automobile acceleration performance, weight, and fuel consumption. SAE International Journal of Fuels and Lubricants 1, 771−777; Cheah, L.W., 2010. Cars on a Diet: The Material and Energy Impacts of Passenger Vehicle Weight Reduction in the U.S. (Ph.D. dissertation). Massachusetts Institute of Technology; Altair (2003); Kelkar et al. (2001); Shaw and Roth (2002); IBIS (2008); Dieffenbach et al. (1996).

plastic composite materials, they also have the greatest specific strength and stiffness (strength-to-weight and stiffness-to-weight ratios) among other alternative light materials. They also have very good corrosion resistance, making them favorable for BIW structures, and they could significantly increase vehicle fuel economy by reducing vehicle weight by as much as 60% (Das, 2000). However, there are some challenges that need to be solved for plastic composites to be an economic alternative to steel. High material and manufacturing costs in association with limited manufacturing line throughputs are among these most important challenges. One of the well-known challenges in making CFRPs is the production of carbon fibers, which also has high material

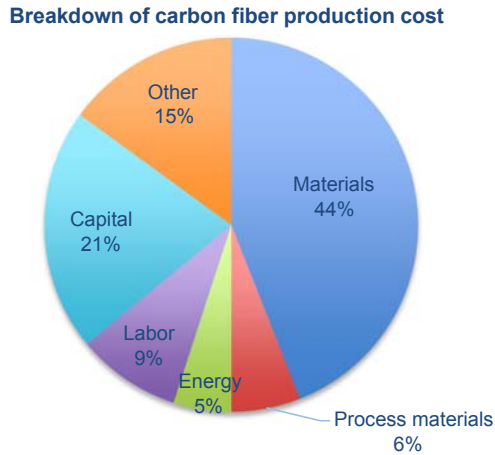

Figure 11.12 Cost breakdown of carbon fiber production process.
Based on Das, S., 2001a. The Cost of Automotive Polymer Composites: A Review and Assessment of Doe's Lightweight Materials Composites Research. Oak Ridge National Laboratory, prepared for the Office of Advanced Automotive Technology Office of Transportation Technologies U.S. Department of Energy.

costs. Carbon fiber production is slow in nature as it is still based on a semimanual production process; in addition it is capital intensive and technical, which also contributes to the high production cost of such materials. Fig. 11.12 depicts the carbon fiber production cost breakdown and shows that material is the largest contributor to the final cost, followed by capital, labor, and energy costs. As can be seen in this figure, raw material (ie, precursor) costs contribute 44% of the total. The second largest contributor is capital cost, with 21% of the total cost. Capital costs are similar to material costs when capital costs include the maintenance, insurance, and taxes on the physical plant. High processing temperature is one of the main challenges that makes carbon fiber production so capital intensive. Economies of scale for carbon fiber production can be achieved at higher production volumes of 1000 tons/year or more (Das, 2001a,b).

For composites to be cost effective for a wider range of automotive applications, large-scale production volumes are necessary. The cheapest way to get cost-competitive automotive composite parts is by speeding up the throughput, making more parts with the same equipment.

Nowadays, manufacturing of composite automotive parts is done using several technologies including SMC, BMC, reinforced reaction injection molding, and liquid composite molding processes such as structural reaction injection molding and resin transfer molding. The polymer processing routes are inherently slow, taking more than a minute for plastic parts the size of automobile body panels, compared to less than 10 s for stamped steel parts (Das, 2001a,b; Frantz et al., 2011). The cycle time greatly depends on the shape, thickness, and size of the part, as well as the resin rheology. Some intrinsic parameters of the plastic composite manufacturing processes cannot be changed, for example, the rate of chemical reactions (if too high then it would be difficult to control

the final quality of the product) or the rate of heat transfer (too rapid cooling results in brittle components) cannot be increased. In this case the only alternative left is to implement multiple machines, which will increase capital cost and administrative overhead, which in turn is reflected in incremental cost of the final components.

The choice of a specific fabrication method depends on the costs and on the technical requirements of the component to be produced. To guarantee economic production, methods with a high throughput are absolutely necessary. High throughput can be achieved by means of low clock times or by means of high integrative parts (Das, 2001a,b). Several studies have investigated possible improvements in the manufacturing of composite automotive parts, for example, the use of prepregs, which are reinforced with carbon or glass in fiber and fabric forms coated with epoxy resins, is suitable for only limited automotive applications because of lower productivity.

11.8 Summary

Sustainability in general and eco-material selection in particular are gaining more consideration by automakers, not just because they are more environment-friendly materials but also because they are likely alternative lightweight materials that can replace heavier steels in the vehicles. Design for sustainability is a branch of sustainability science that deals with eco-material selection, adoption of new vehicle designs, and using alternative fuels that have lower environmental impacts. Design for sustainability is a holistic approach that integrates all environmental, economic, and societal factors into one model to ensure selection of eco-materials that also have low cost and can be manufactured in large volumes. These last two factors are among the most important factors that automakers are considering when using new material in their vehicles. Material selection indices and material selection charts are good tools for material selection in early conceptual design stage. They act as simple and quick methods of assessing various materials and their ability to meet certain design requirements.

LCA is a quantitative tool that is used in evaluating candidate materials throughout the entire vehicle lifetime. Lighter materials like aluminum and magnesium have the lowest environmental impact because of the amount of energy and emissions they can save in the use phase, which makes up more than 80% of the total vehicle environmental impact.

Although lighter materials like aluminum, magnesium, and HSS have been used recently in the lightweight designs for auto bodies, polymer composites have very good characteristics, but also have higher costs, making them less favorable in automotive applications. The polymer composite materials in automotive applications today are used mostly in nonstructural parts of the vehicle. The cost is the key barrier for the limited application of polymer composites in automobiles today. So for these composite materials to be cost competitive in the automotive industry, several conditions need to be met, such as using low-cost, high-reliability materials; adoption of new high-speed processing techniques; and innovative structural design approaches that are tailored for fiber-reinforced polymer materials.

References

Altair Engineering, 2003. *Lightweight SUV Frame: Design Development*. May, 2003.

American Plastics Council, 2014. http://www.popsci.com/cars/article/2004-09/plastics-automotive-markets-vision-and-technology-roadmap (last accessed 30.03.14.).

Argonne National Laboratory (ANL). GREET1.7c Model. Available online at: www.arb.ca.gov/fuels/lcfs/greet1.7ca_v98.xls (last accessed 11.08.11.).

ArcelorMittal, 2014. Multi-thickness Laser Welded Blanks: Tailored Blanks. Available online from: http://automotive.arcelormittal.com/automotive/saturnus/sheets/S3_EN.pdf (last accessed on 01.07.14.).

Ashby, M., 2009. Materials and the Environment, first ed. Elsevier.

Bjelkengren, C., June 2008. The Impact of Mass Decompounding on Assessing the Value of Vehicle Lightweighting. MSc Thesis. Massachusetts Institute of Technology.

Cambridge Engineering Selector Software (CES 2008).

Cheah, L.W., 2010. Cars on a Diet: The Material and Energy Impacts of Passenger Vehicle Weight Reduction in the U.S. (Ph.D. dissertation). Massachusetts Institute of Technology.

Cheah, L.W., et al., 2009. The trade-off between automobile acceleration performance, weight, and fuel consumption. SAE International Journal of Fuels and Lubricants 1, 771–777.

Coulter, S., Bras, B., Winslow, G., Yester, S., 1996. Designing for material separation: lessons from automotive recycling. In: Proceedings of the 1996 ASME Design Engineering Technical Conferences and Computers in Engineering Conference. August 18–22, 1996, Irvine, California.

Das, S., 2000. The life-cycle impacts of aluminum body-in-white automotive material. Journal of the Minerals, Metals and Materials Society 52, 41–44.

Das, S., 2001a. Evaluation of the Benefits Attributable to Automotive Lightweight Materials Program Research and Development Projects. ORNL/TM-2001-237. Nov. 2001.

Das, S., 2001b. The Cost of Automotive Polymer Composites: A Review and Assessment of Doe's Lightweight Materials Composites Research. Technical report from Oak Ridge National lab. No. ORNL/TM-2000/283.

Davies, G., 2004. Materials for Automobile Bodies, first ed. Butterworth-Heinemann.

Dieffenbach, J.R., Palmer, P.D., Mascarin, A.E., 1996. Making the PNGV Supercar a Reality With Carbon Fiber: Pragmatic Goal, Or Pipe Dream?, in SAE International Congress & Exposition. SAE International. SAE Paper No. 960243: Detroit, MI.

Ermolaeva, N.S., Castro, M.B.G., Kandachar, P.V., 2004. Materials selection for an automotive structure by integrating structural optimization with environmental impact assessment. Materials and Design 25, 689–698.

Ferrão, P., Amaral, J., 2006. Assessing the economics of auto recycling activities in relation to European Union Directive on end of life vehicles. Technological Forecasting and Social Change 73 (3), 277–289.

Frantz, M., Lauter, C., Tröster, T., 2011. Advanced manufacturing technologies for automotive structures in multi-material design consisting of high-strength steels and CFRP. In: 56th International Scientific Colloquium. Ilmenau University of Technology, 12–16 September 2011.

Fuchs, E., Field, F., Roth, R., Kirchain, R., 2008. Strategic materials selection in the automobile body: economic opportunities for polymer composite design. Composites Science and Technology 68, 1989–2002.

Graedel, T.E., Allenby, B.R., 1998. Design for Environment. Prentice Hall.

GHK, 2006. A Study to Examine the Benefits of the End of Life Vehicles Directive and the Costs and Benefits of a Revision of the 2015 Targets for Recycling, Re-use and Recovery under the ELV Directive. Available online at: http://ec.europa.eu/environment/waste/pdf/study/final_report.pdf (last accessed on 02.07.14.).

Hakamada, M., Furuta, T., Chino, Y., Chen, Y., Kusuda, H., Mabuchi, M., 2007. Life cycle inventory study on magnesium alloy substitution in vehicles. Energy 32, 1352–1360.

Holloway, L., 1998. Materials selection for optimal environmental impact in mechanical design. Materials and Design 19, 133–143.

IBIS Associates Inc, 2008. Aluminum Vehicle Structure: Manufacturing and Lifecycle Cost Analysis–Hybrid Drive and Diesel Fuel Vehicles, in Research Report. The Aluminum Association.

International Standards Organization, 1998. ISO 14040: Environmental Management-life Cycle Assessment-principles and Framework, ISO 14041 Goal and Scope Definition and Inventory Analysis, ISO 14042. Life Cycle Impact Assessment ISO/CD 14043 Life Cycle Interpretation.

Kalpakjian, S., Schmid, S., 2003. Manufacturing Processes for Engineering Materials, fourth ed. Prentice Hall, Upper Saddle River, New Jersey, USA.

Kanari, N., Pineau, J.L., Shallari, S., August 2003. End-of-life vehicle recycling in the European Union. JOM 55 (8).

Kelkar, A., Roth, R., Clark, J., 2001. Automobile bodies: can aluminum be an economical alternative to steel? Journal of Materials 53 (8), 28–32.

Kon, R.J., 2009. The end-of-life vehicle (ELV) directive: the road to responsible disposal. Minnesota Journal of International Law 18 (2), 431–457.

Lauter, C., Troster, T., Reuter, C., 2014. Hybrid structures consisting of sheet metal and fiber reinforced plastic structural automotive applications. In: Elmarakbi, A. (Ed.), Advanced Composite Materials for Automotive Applications. John Wiley & Sons.

Lotus Engineering, Inc, 2010. An Assessment of Mass Reduction Opportunities for a 2017–2020 Model Year Vehicle Program. March 2010.

Lutsey, N., 2010. Review of Technical Literature and Trends Related to Automobile Mass-reduction Technology. Institute of Transportation Studies, University of California, Davis. UCD-ITS-RR-10–10. http://pubs.its.ucdavis.edu/publication_detail.php?id=1390 (last accessed on 04.11.14.).

Mayyas, A., Qattawi, A., Omar, M., Shan, D., 2012a. Design for sustainability in automotive industry: a comprehensive review. Renewable and Sustainable Energy Reviews 16, 1845–1862.

Mayyas, A., Qattawi, A., Omar, M., 2012b. Material selection methodology for sustainable lightweight body-in-white design. Journal of Sustainable Manufacturing 2, 317–337.

Mayyas, A.T., Qattawi, A., Mayyas, A., Omar, M., 2012c. Life cycle assessment-based selection for a sustainable lightweight body-in-white design. Energy 39, 412–425.

Mayyas, A.R., Shen, Q., Mayyas, A., abdelhamid, M., Shan, D., Qattawi, A., Omar, M., 2011. Using quality function deployment and analytical hierarchy process for material selection of body-in-white. Materials and Design 32, 2771–2782.

Mcauley, J., 2003. Global sustainability and key needs in future automotive design. Environmental Science and Technology 37, 5414–5416.

Montalbo, T., Lee, T.M., Roth, R., Kirchain, R., 2008. Modeling Costs and Fuel Economy Benefits of Light Weighting Vehicle Closure Panels. SAE paper No. 2008-01-0370.

Saur, K., Fava, J.A., Spatari, S., 2000. Life cycle engineering case study: automobile fender designs. Environmental Progress 19, 72−82.

Shaw, J.R., Roth, R., 2002. Achieving An Affordable Low Emission Steel Vehicle; An Economic Assessment of the ULSAB-AVC Program Design, in SAE World Congress & Exhibition. SAE International, SAE Paper No. 2002-01-0361: Detroit, MI.

Stodolsky, F., Vyas, A., Cuenca, R., Mar., 1995. Lightweight materials in the light-duty passenger vehicle market: Their market penetration potential and impacts. In: Proc. The Second World Car Conference, UC Riverside.

U.S. Environmental Protection Agency (U.S. EPA), 2009. Light-duty Automotive Technology and Fuel Economy Trends: 1975 through 2008. EPA420-R-08-015.

Wegst, G.K., Ashby, M.F., 1998. The development and use of a methodology for the environmentally-conscious selection of materials. In: Proceedings of the Third World Conference on Integrated Design and Process Technology (IDPT), 5, pp. 88−93.

Part Five

Case studies on lightweight composite design for transport structures

This page intentionally left blank

Composite materials for aerospace propulsion related to air and space transportation

12

A. Misra
NASA Glenn Research Center, Cleveland, OH, United States

12.1 Introduction

The use of composites in the aerospace industry has increased dramatically since the 1970s. The primary benefits that composite components can offer are reduced weight and assembly simplification. Since 2005, there has been a dramatic increase in the composite content of civil aircraft. For example, the composite content in Boeing aircraft has increased from 12 wt% in the 777 aircraft to 50% in the 787 aircraft. There is also a continuing trend toward the use of composites in space structures. Large composite structures, which can be 20−30% lighter than comparable aluminum structures, are being studied for use in elements of NASA's space exploration program, components of interest being the fairing of the launch system and composite cryotanks.

Following the trend in the use of composites in airframe and space structures, there is also growing interest in the use of composites for aerospace propulsion. The use of composites in aircraft engines is driven by increasing emphasis on reducing fuel burn and greenhouse gas emissions by the aviation industry. Reduction in fuel burn for aircraft engines can be achieved in two ways: (1) decreasing the weight of gas turbine engines and (2) increasing the thermal efficiency of the engines. Composite materials play a role in both cases. Replacing heavy metallic materials with polymer matrix composites (PMCs) in the cold section of gas turbine engines leads to a reduction in weight. The gas turbine engine thermal efficiency can be increased by increasing the turbine operating temperature, which is limited by the temperature capability of the hot section materials. As high temperature alloys used in the hot section are reaching their melting points, CMCs are the only option for increasing the operating temperature of gas turbine engines. The CMCs also offer significant weight reduction for hot components compared to superalloys.

The composite materials are also equally important for space propulsion systems. The need to increase the payload capacity of the current launchers drives rocket engine manufacturers to seek higher thrust level, specific impulse, and thrust-to-weight ratio. The use of high-temperature composite materials is an efficient way to reach these objectives by enabling high-expansion-ratio nozzle extensions and thrust chambers with higher temperature capability. High-temperature composites will enable hypersonic vehicles to be used as part of cost-effective access to space. Hypersonic engine materials and structures must operate in a stressful aerothermal environment while

Lightweight Composite Structures in Transport. http://dx.doi.org/10.1016/B978-1-78242-325-6.00012-8

being exposed to both oxidizing and reducing environments and must at the same time be capable of surviving flight vibration, handling, and launch loads. CMCs are expected to play a key role in hypersonic engines for space transportation.

The objective of this chapter is to provide an overview of the applications of composite materials in aerospace propulsion systems that are important for aviation and space transportation. The overview will include the following applications: (1) aircraft gas turbine engines, (2) rocket propulsion for space transportation, and (3) hypersonic propulsion systems for space transportation. While the application of PMCs in aerospace propulsion will be described in this chapter, the application of CMCs for aerospace propulsion will be the primary emphasis. This is due to the growing importance of CMCs for aerospace propulsion systems owing to the continuing need for increasing temperature capability and decreasing weight of hot section components.

12.2 Aircraft gas turbine engine

Fig. 12.1 shows the schematic of a gas turbine engine showing the application of various composites. In a gas turbine engine, fresh atmospheric air flows through a compressor that brings it to higher pressure. Energy is then added by spraying fuel into the air and igniting it so the combustion generates a high-temperature flow. This high-temperature high-pressure gas enters a turbine, where it expands down to the exhaust pressure, producing a shaft-work output in the process. The turbine shaft work is used to drive the compressor. Remaining high-energy gas is used for expansion across a nozzle to create the thrust. PMCs are of interest for colder sections of the engine, while CMCs are of interest for the engine hot section and the exhaust nozzle. While PMCs have been used for noncritical components (eg, ducts and piping) for a long time, there has been a steady growth in the application of PMCs for critical turbine engine components since 2005 or so, with the introduction of PMC fan blades

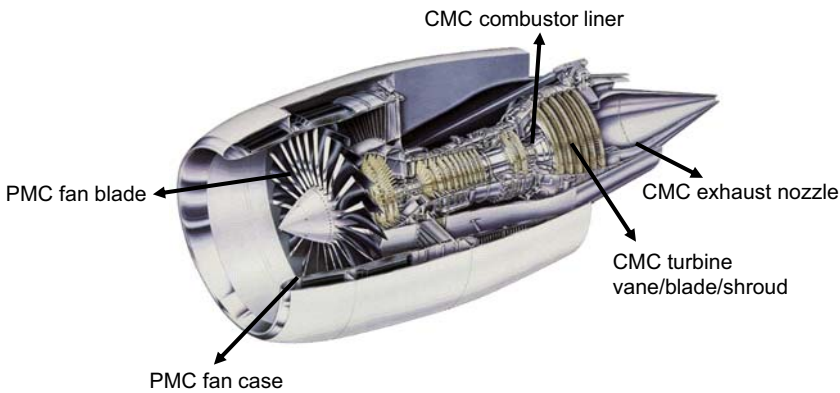

Figure 12.1 Schematic of gas turbine engine cross section showing application of composite materials. *PMC*, polymer matrix composite; *CMC*, ceramic matrix composite.

and fan containment systems. CMCs will be used for the first time in a commercial gas turbine engine in 2016 and it is expected that there will be a steady growth in the use of CMCs in commercial gas turbine engines in the coming years.

12.2.1 Polymer matrix composite fan blade

Blades on fans in current-generation turbofan engines can experience centrifugal loadings of around 100 tons—equivalent to the weight of a diesel locomotive hanging on each blade. Centrifugal loading increases with radius, with rotational speed, and with blade mass. Reduction in blade mass will reduce loadings, which is the primary reason for the introduction of PMC fan blades in turbine engines. Efficient aerodynamic shaping of the composite fan blade enables operation with fewer blades, another benefit in terms of weight savings. The composite three-dimensional (3D) aerodynamic blades can weigh 10−15% less than a hollow-core titanium blade. General Electric (GE) was the first to introduce a PMC fan blade in the GE90 engine for the Boeing 777, and has continued incorporation of PMC fan blades in the subsequent versions, eg, GEnx and GE9X [1]. Fig. 12.2 shows the fan blade used in the GE90 engine.

The PMC fan blade diameter for large turbofan engines is greater than 100 inches. The blades are made using preforms that comprise hundreds of plies of unidirectional carbon prepreg tape and fabric near the blade root, where the thickness is up to 4 in., thinning out progressively to about 0.25 in. at the tip. Plies are cut ultrasonically, each ply shape having previously been computer generated. Plies are then laid up using a laser projection system. The resulting preform is placed in a mold and resin is injected. Curing takes place

Figure 12.2 Polymer matrix composite fan blade used in the GE-90 gas turbine engine (http://www.gereports.com/post/74545209282/blast-from-the-past-edisons-discovery-powers).

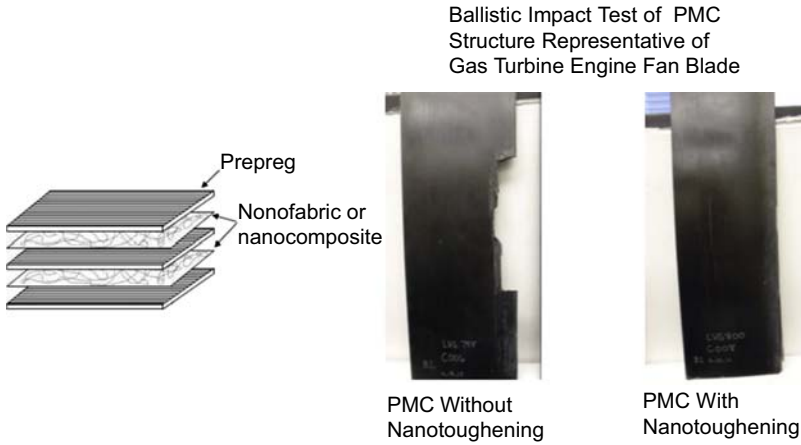

Figure 12.3 Incorporation of nanocomposite in polymer matrix composites (PMCs) to increase toughness of a PMC gas turbine engine fan blade.

in an autoclave at some 150°C, with consolidation pressure also being applied. The resulting near-net shape parts are milled to final dimensions by computerized numerical control (CNC) machining. While the simple ply layup and the prepreg approach works well for large fan blades, this may not be suitable for small fan blades typical of single-aisle aircraft, for which diameter of the fans is on the order of 60−75 in. In big engines, the long blade has the ability to flex enough in the event of a bird strike. A shorter blade with a ply design is too stiff to flex in the event of a bird strike. The approach for shorter blades is to create 3D woven blades by weaving the fibers and applying the matrix by resin transfer molding [2]. The process consists of weaving fibers into a preform, cutting the preforms into shape with a water jet, and placing the preform in a mold into which epoxy resin is injected by resin transfer molding (RTM). The 3D woven structure provides superior damage tolerance, while the RTM process allows a thinner and more curved blade, with significant aerodynamic benefits.

Current research on PMC fan blades is focused on decreasing the thickness of the fan blades (with the benefit of weight reduction) by increasing the toughness of the PMCs, which is important for providing protection from bird strikes. One promising approach to improving composite fracture toughness is interleaved toughening, a process in which toughened particles (eg, rubber, thermoplastic, etc.) or toughened layers are added to the interlinear regions to increase the microstructural resistance to fracture and delamination. An innovative approach has been developed to increase toughness of PMC fan blades [3] through incorporation of a layer of nanocomposite veil in the composite layup, shown in Fig. 12.3.

12.2.2 Polymer matrix composite fan case

The fan case is one of the biggest structures of an aircraft. The increasing trend toward high-bypass-ratio turbofan engines has resulted in larger diameter fan cases. For example, the former GE 5:3 bypass ratio fan cases CF6-80C2 accounted for about

Figure 12.4 Polymer matrix composite fan case for GEnx engine used in the Boeing 787 aircraft (http://www.geaviation.com/commercial/engines/genx/).

20% of the total engine weight, whereas the more recent 9:5 bypass ratio GEnx-1B represents a weight ratio of 33%. The use of PMCs can reduce the weight of large fan cases in modern high-bypass turbofan engines. The GEnx engine in the Boeing 787 [1] is the first jet engine with a front fan case made of composites (Fig. 12.4), with the benefit of a 350-lb weight reduction per engine. The fan case fabrication process for GEnx engine consists of using triaxial carbon fiber braid as the reinforcement, which allows for a low-cost, repeatable manufacturing process.

Other engine manufacturers than GE have embraced the composite fan case concept, as evidenced by the introduction of a PMC fan case in the Pratt & Whitney PW1500G engine dedicated to the Bombardier C series aircrafts and Williams International FJ44-4A engine now flying on the Cessna Citation CJ4 aircraft.

12.2.3 Ceramic matrix composites for hot section components

CMCs become enabling materials in the trend toward increasing the operating temperature of gas turbine engines. System analysis studies [4], shown in Table 12.1, have shown that up to 6% reduction in fuel burn can be achieved by replacing hot section metallics with CMCs having 2700°F (1482°C) temperature capability.

Two factors contribute to the reduction in fuel burn. First, the higher temperature capability of CMCs compared to metals reduces or eliminates cooling of hot section components. Second, the weight of CMCs is one-third that of high-temperature superalloys, with the weight savings multiplier effect being much more than 3:1 because everything down the chain is affected as well. For example, it is estimated that incorporating CMC turbine blades on a GE90-sized engine could reduce the overall weight by about 455 kg (1000 lb), which represents about 6% of the 7550 kg dry weight of the full-sized GE90-115 [5]. Starting with the introduction of CMC shrouds (Fig. 12.5) in

Table 12.1 Fuel burn benefits offered by ceramic matrix composites in gas turbine engine hot section components

CMC component	Specific fuel consumption (SFC) reduction	Engine weight reduction	Fuel burn reduction
High pressure turbine (HPT) vanes	−0.5%	−0.45%	−0.95%
HPT blades	−1.8%	−0.8%	−3.1%
Low pressure turbine (LPT) vanes/blades	0	−3.6%	−0.7%
Burner pressure drop (5−3%)	−0.75%	0	−1.25%
Overall reduction	**−3.0%**	**−4.85%**	**6.0%**

CMC, ceramic matrix composite.

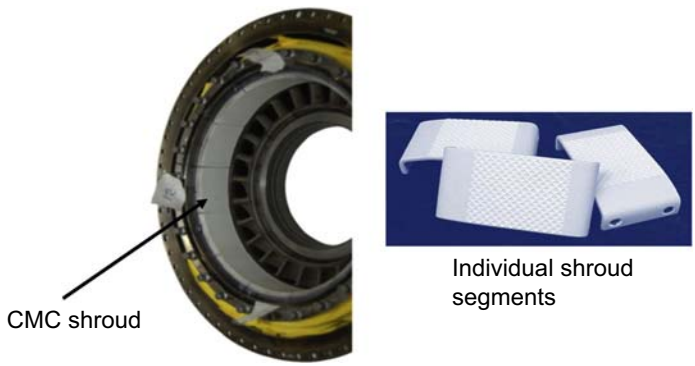

Figure 12.5 Ceramic matrix composite shrouds (the white area) replacing metallic shrouds in gas turbine engines (http://www.aviationpros.com/press_release/12022105/ge-aviation-and-turbocoating-spa-form-coating-joint-venture).

2016 in GE's LEAP engine [6], it is expected that there will be a proliferation of CMC components in the hot section of gas turbine engines as CMC technology matures.

For application in gas turbine engines, silicon carbide fiber-reinforced silicon carbide (SiC/SiC) CMC has been deemed to be the best option based on temperature capability and long-term durability [7]. Fig. 12.6 compares stress rupture properties of several high-temperature materials. Assuming 100 MPa to be a reasonable stress level for structural components, oxide/oxide CMCs are suitable for applications requiring 2100°F (1148°C). SiC/SiC CMCs provide temperature capability beyond 2400°F (1315°C). Although carbon fiber-reinforced carbon (C/C) and carbon fiber-reinforced silicon carbide (C/SiC) CMCs would have the desired stress rupture properties at higher temperatures, SiC/SiC CMCs have higher oxidative durability compared to C/C and C/SiC composites.

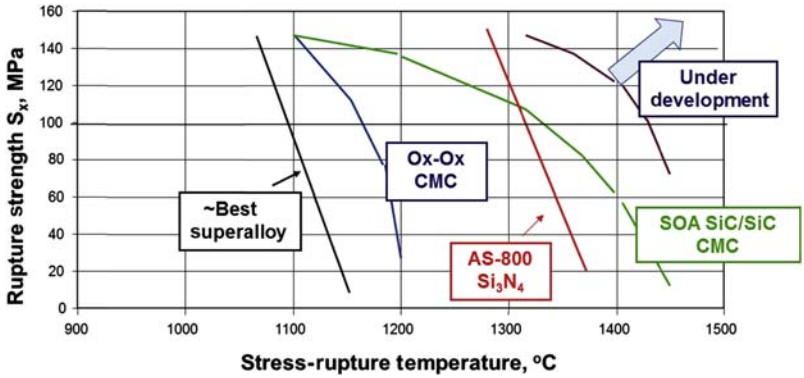

Figure 12.6 Comparison of rupture strength versus temperature for various material systems.

The first generation of SiC/SiC CMCs that are beginning to be introduced in commercial gas turbine engines have a temperature capability of 2400°F (1315°C). The composites are currently fabricated by two different processes. One is GE's prepreg and melt infiltration process [8]. In the GE process, multifiber tows of a small-diameter high-performance SiC fiber type are first spread and coated by chemical vapor deposition with a layered interfacial coating consisting of boron nitride (BN) and silicon nitride (Si_3N_4) compositions. The coated tows are then prepregged into unidirectional 2D tapes using a polymer-based binder containing SiC and carbon particulates. The tapes are then cut, oriented, and stacked into 3D preforms. To achieve the component structural and shape requirements, the 3D preforms are assembled using methods much like those used for tape layup of PMCs. In the final steps of this prepreg approach, the 3D preform is heated to high temperature to decompose the polymer and to form the final matrix composition by infiltration with molten silicon. The SiC-based matrix is formed in situ by the reaction of the silicon with the residual carbon in the preform.

The other processing route for fabricating SiC/SiC CMCs was developed under the NASA Enabling Propulsion Materials Program and was demonstrated by the production of small and large combustor liners [9]. In this process, continuous-length multifiber tows of a small-diameter high-performance SiC fiber type are woven into continuous fabric pieces, typically with a 0°/90° balanced five-harness satin fiber architecture. These 2D fabric pieces are then cut and stacked into component-shaped 3D preforms with fiber volume fractions up to 40%. Chemical vapor infiltration (CVI) is employed to first apply an interfacial coating or interphase (typically BN) on the fibers within the tows, and then to apply a thin protective SiC matrix layer over the interphase. The coating thicknesses can vary from ~0.1 to 0.5 μm depending on such factors as the fiber surface roughness and the degree of protection needed to avoid coating degradation during matrix formation and/or component service. In the final steps of matrix fabrication, SiC particulates are slurry-cast into the component preform near room temperature, followed by a finishing step in which a molten metallic silicon alloy is infiltrated near 1400°C into any open remaining matrix

porosity. The silicon bonds the SiC particulates together with little chemical reaction. This last step of this nonreactive melt infiltration route is important in that it results in a SiC-based matrix with low residual porosity, high thermal conductivity, and good environmental protection for the coated fibers.

The SiC/SiC CMCs react with the moisture in gas turbine engines [10], resulting in recession of the surface in the gas turbine engine environment (Fig. 12.7). Therefore, environmental barrier coatings (EBCs) are required to protect the SiC/SiC CMC from the gas turbine engine environment. The first generation of EBCs [11] capable of operating at 2400°F (1315°C), shown in Fig. 12.8, consists of three layers: Si bond coat, mullite (aluminosilicate) intermediate layer, and barium strontium aluminum silicate (BSAS) topcoat. The design of the EBC needs to take into consideration multiple factors, which include chemical reactivity, diffusion of oxygen, mechanical integrity, and interdiffusion between various layers.

While SiC/SiC CMCs with 2400°F (1315°C) temperature capability are beginning to be introduced in commercial gas turbine engines, there is ongoing research to increase the temperature capability to 2700°F (1482°C). The key challenges for increasing the temperature capability of SiC/SiC CMCs are (1) temperature capability of the fiber, (2) fabricating a dense composite without Si (the first generation of SiC/SiC CMCs contain free Si, which melts at 1410°C), and (3) developing an EBC with higher temperature capability.

NASA has pioneered the development of advanced SiC fibers with higher temperature capability. Starting with a commercial, lower-temperature SiC fiber, NASA has

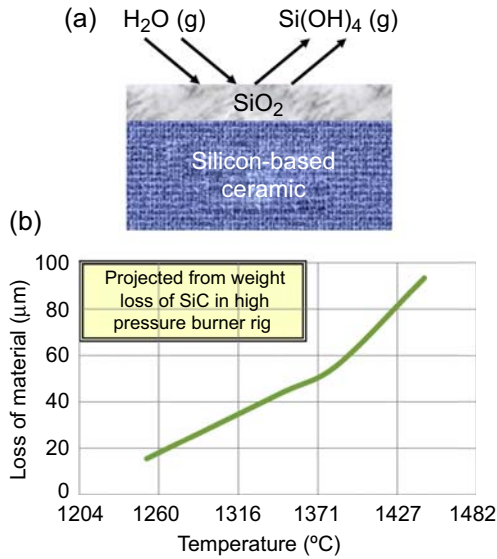

Figure 12.7 SiC experiences recession at high use temperatures. (a) Silica film formed on the SiC surface reacts with water in the combustion environment forming a gaseous product, which is swept away, only to re-form, and the cycle repeats. (b) Loss of material after 100 h as a function of temperature.

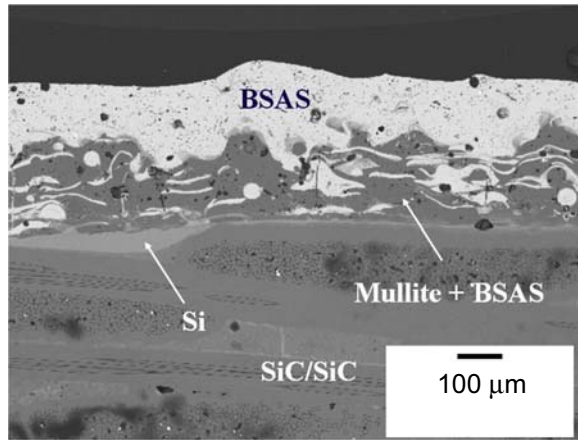

Figure 12.8 Scanning electron micrograph showing three layers for the state-of-the-art environmental barrier coating. *BSAS*, barium strontium aluminum silicate.

developed thermochemical conversion processes [12] to convert a commercial-grade SiC fiber to higher-temperature-capable SiC fibers, known as Sylramic-iBN and Supersylramic-iBN. Today, Supersylramic-iBN has the highest temperature capability among all SiC fibers (Fig. 12.9), with the capability for long-term creep resistance at 2700°F (1482°C).

Current research is focused on improving the temperature capability of SiC/SiC CMC to 2700 F (1482°C) through a combination of (1) use of Supersylramic-iBN fiber, (2) alternate fabrication processes for infiltrating SiC matrix into woven fiber architecture, and (3) engineering of fiber architecture [13]. As shown in Fig. 12.10, for any given fabrication process, increased durability and higher temperature

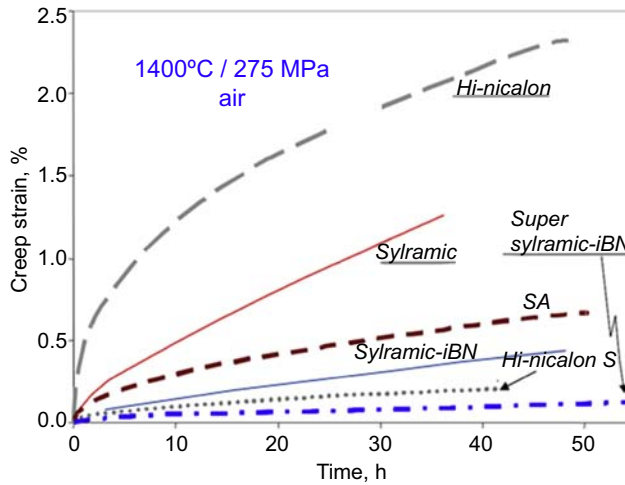

Figure 12.9 Comparison of creep properties of various SiC fibers.

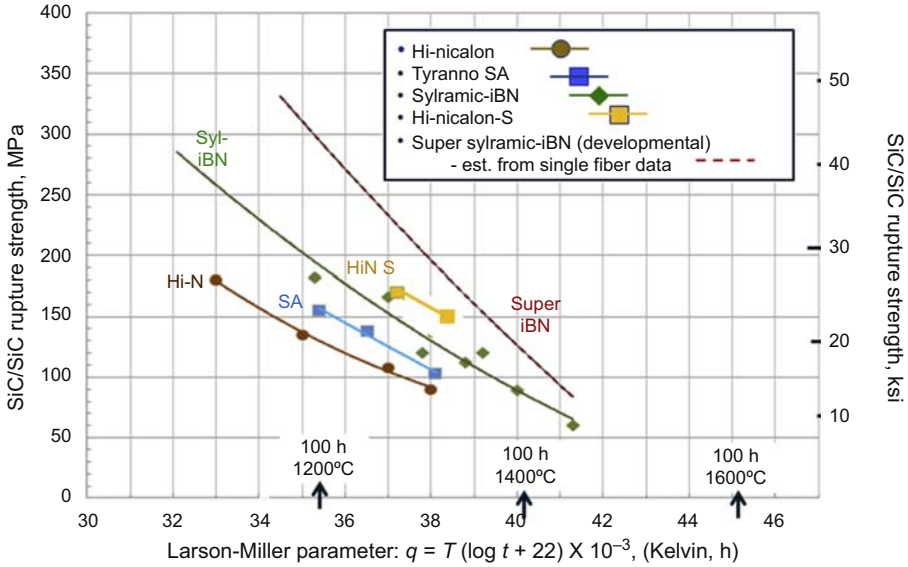

Figure 12.10 Effects of SiC fiber type on on-axis rupture strength in air for SiC/SiC ceramic matrix composite with 2D-woven 0/90-balanced fabric, on-axis fiber content of ~18%, and chemical vapor infiltration−melt infiltration matrix.

capability can be achieved by using Supersylramic-iBN fiber. The data shown in Fig. 12.10 correspond to a combination of CVI and melt infiltration processes, which results in free Si in the composite structure. Progress at NASA with alternative processes that eliminate free Si has shown the initial feasibility of achieving 2700 F (1482°C) temperature capability for SiC/SiC CMCs.

Multiple approaches are being pursued to increase the temperature capability of EBCs. New complex oxide topcoat chemistries are being developed, as shown in Fig. 12.11 [14]. Two complex coatings, Hf Re silicate (Re = rare earth element)

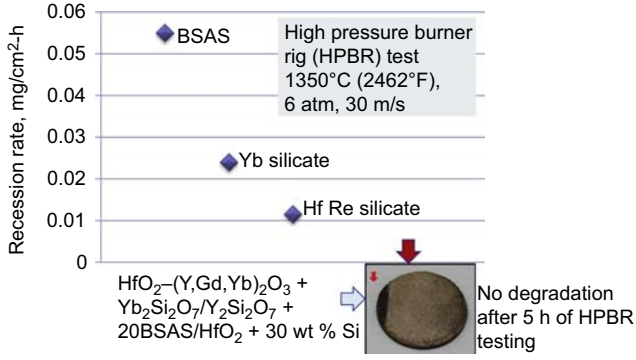

Figure 12.11 Complex silicate coatings with low recession rates compared to baseline barium strontium aluminum silicate and Yb silicate topcoat.

and HfO_2-$(Y,Gd,Yb)_2O_3$ + $Yb_2Si_2O_7/Y_2Si_2O_7$ + 20BSAS/HfO_2 + 30 wt% Si, show promise based on initial feasibility studies. A HfO_2 + Si engineered bond coat [15] has demonstrated mechanical integrity under simulated gas turbine environmental conditions and appears promising for achieving 2700°F (1482°C) temperature capability. Further advances in bond-coat technology will be critical in achieving higher temperature capability for integrated CMC/EBC systems.

12.2.4 Ceramic matrix composites for gas turbine engine exhaust nozzle

With an increase in gas turbine engine operating temperature, there is simultaneous increase in the exhaust temperature as well. As high-efficiency jet engines emit hot exhaust gases, they require materials capable of withstanding higher temperatures than titanium and superalloys, which have been the industry standard for decades. CMC nozzles offer advantages in terms of weight reduction in addition to enabling higher temperature capability. In addition, the CMC nozzles are expected to last longer compared to metallic nozzles. The exhaust nozzle temperature is lower than the hot section temperature. Therefore, oxide fiber-reinforced oxide matrix (oxide/oxide) composites are the CMCs of choice for the exhaust nozzle section. The oxide/oxide CMCs are manufactured in the same way as PMCs in the front end. The same kinds of techniques are used for forming, such as hand layup to RTM, after which the parts are cured. After this stage the polymeric precursor is converted to a ceramic by pyrolysis or sintering.

Turbofan engines utilized on both regional transport and business jets often feature an exhaust mixer, in which the bypass (cold) air is mixed with the core (hot) exhaust gases [16], before exhausting to atmospheric pressure through a common propelling nozzle (Fig. 12.12). The mixer reduces the average velocity of the exhaust. In terms of benefits of the mixer nozzle, there is a reduction in the amount of noise produced, the temperature of the exhaust plume is reduced, and a small thrust gain occurs, which improves specific fuel consumption. CMC exhaust mixer nozzles can also offer an advantage if they are able to maintain their shape during operation and avoid the performance-degrading shape distortion that metallic nozzles can exhibit. The

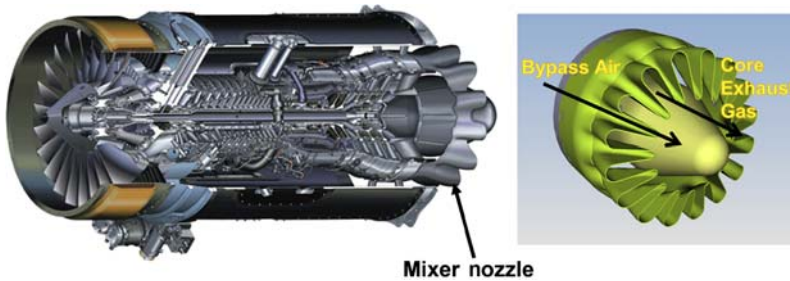

Figure 12.12 Example of aircraft turbofan engine with mixer nozzle.

fabrication and performance of a subscale oxide/oxide CMC nozzle (Fig. 12.13) has been demonstrated at NASA [17].

GE was the first to introduce an oxide/oxide CMC exhaust nozzle for a regional engine [18]. GE's Passport engine (Fig. 12.14) incorporates 15 of the oxide/oxide

Figure 12.13 Subscale oxide/oxide ceramic matrix composite turbine engine mixer exhaust nozzle demonstrated at the NASA Glenn Research Center.

Figure 12.14 Oxide/oxide ceramic matrix composite exhaust nozzle for GE's Passport regional engine (http://www.compositesworld.com/articles/aeroengine-composites-part-1-the-cmc-invasion).

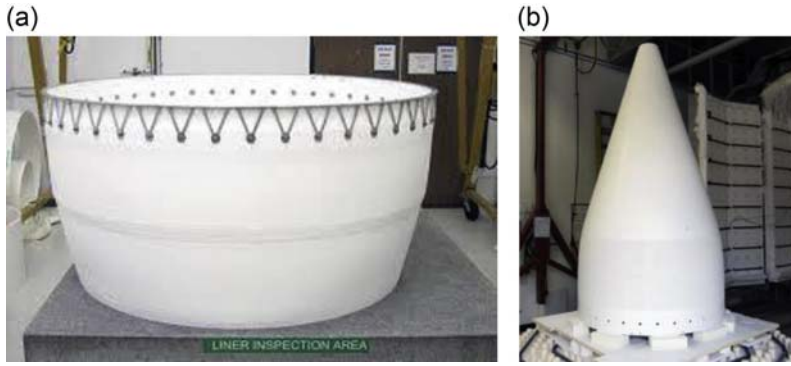

Figure 12.15 Ceramic matrix composite (CMC) exhaust nozzle for large commercial aircraft flight tested by Boeing. (a) Outer CMC ring and (b) CMC tail cone (http://www.compositesworld.com/articles/ceramic-matrix-composites-heat-up).

composite parts on three assemblies, which, combined, account for a weight savings of approximately 45 lb per engine. Among the CMC parts is the center body, a cone-shaped structure that protrudes from the back of the engine. Approximately 30 in. high with a more than 20-inch diameter on the front end, the part is surprisingly light, weighing around 9 lb. Surrounding it is the mixer, a highly complex pleated structure that takes 3 days to lay out on its form. It combines the engine's core flow with the fan flow to minimize pressure loss.

For application in large commercial aircraft, the Boeing Company has completed successful flight testing of an oxide/oxide CMC exhaust nozzle [19]. The exhaust nozzles were fabricated by ATK−COI and are the largest CMC structures made as of this writing. The outer ring, called the nozzle (Fig. 12.15(a)), measures approximately 5.25 ft (1.6 m) in diameter and is about 3 ft (1 m) long; the tail cone (Fig. 12.15(b)), which sits inside the front end of the nozzle, is approximately 7 ft (2.1 m) long.

12.3 Rocket propulsion

In a liquid-fueled rocket engine, a schematic of which is shown in Fig. 12.16, a fuel (such as hydrogen or kerosene) and an oxidizer (such as liquid oxygen) are injected into a thrust chamber where they mix and react. The fuel/oxidizer reaction products

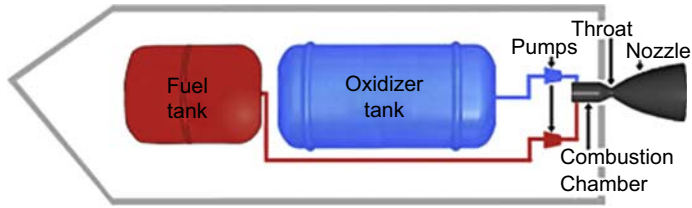

Figure 12.16 Schematic of liquid-fuel rocket propulsion system.

are high-temperature gases, which expand through a bell-shaped nozzle to produce thrust. Gas temperatures in the chamber may exceed 6000°F, while gas temperatures in the nozzle may range from 3000 to 5000°F. These temperatures are too extreme for any conventional aerospace material; therefore engines must employ some type of cooling scheme. Materials of choice for large liquid-fueled rocket engines have historically been stainless steels, nickel-based superalloys, and copper alloys. These materials are selected for their high strength and high thermal conductivity to cope with the stresses and extreme thermal environments of rocket engines. Since these alloys also have high densities (8−9 g/cm^3), widespread reliance on them has traditionally resulted in heavy engines. Designers would like to reduce the weight of rocket engines. A key performance criterion for engines is thrust-to-weight ratio. Lighter engines and launch vehicles would allow heavier payloads to be placed into orbit at a lower cost. One path to lighter weight engines is replacement of conventional high-density engine alloys with lightweight, high-specific-strength ceramic composites. Potential applications of CMCs in rocket propulsion include: (1) nozzle extension for main stage engine, (2) nozzle extension for upper stage engine, and (3) combustion chamber.

12.3.1 Rocket nozzle and nozzle extensions

CMC rocket nozzle extensions enable (1) increase in the permissible wall temperature (compared to metallic materials), (2) simplified cooling design, (3) reduction of component mass enabling high thrust-to-mass ratio, and (4) potential to increase payload capability. CMC nozzle extensions must meet the following requirements:

- high thermal shock resistance
- temperature capability up to 1700°C (nozzle-wall temperature)
- oxidation resistance
- low specific weight and high damage tolerance

Potential composite candidates for rocket propulsion application are C/C, C/SiC, and SiC/SiC composites.

The first commercial application of composite material in a rocket propulsion component is the C/C composite nozzle extension in Pratt & Whitney Rocketdyne's RL10B-2 engine, shown in Fig. 12.17. The Novoltex® C/C composite nozzle extension for RL10B-2 was developed by Snecma Propulsion Solide of the SAFRAN Group [20]. The Novoltex® preform consists of a stack of layers of raw material made of preoxidized PAN (polyacrylonitrile) carbon precursor fiber felt and fabric. As each layer is added a needling board with hundreds of hook-fitted needles passes over and punches the preoxidized PAN fiber staples, transferring them perpendicularly and through the fabric layer stack, forming the third direction of reinforcement. The 3D fiber preforms are subjected to a heat-treatment process to transform the fibers into carbon. The heat-treatment process is followed by a CVI process to deposit the carbon matrix.

The C/C nozzle extension for the RL10B-2 engine was radiation cooled. The next advancement for CMC rocket nozzles is to actively cool the nozzle. Fuel-cooled

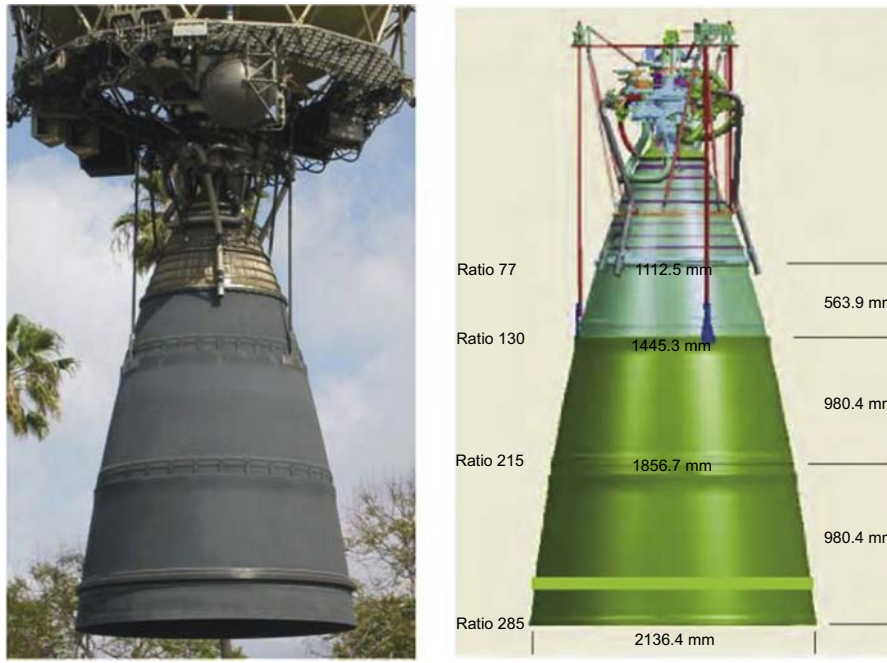

Figure 12.17 C/C composite rocket nozzle extension for Pratt & Whitney Rocketdyne's RL10B-2 engine (http://www.b14643.de/Spacerockets/Diverse/P&W_RL10_engine/index.htm).

CMC nozzles continue to be investigated for rocket nozzles [21,22]. The major design constraints are high heat flux and high internal coolant pressure. The major structural challenge for actively cooled CMC nozzles is the multiaxial state of stress, which dictates that the composite must have sufficient shear strength in as many directions as possible. The currently available 2D CMCs would have very limited lifetimes with respect to damage tolerance. To achieve the desired damage tolerance, multidirectional (3D) textile structures with a cost-effective infiltration method have been developed [21].

The feasibility of actively cooled CMC nozzle ramps has been demonstrated for a reusable launch vehicle [22,23]. Several concepts were fabricated and tested. One of the concepts consisted of a hybrid C/SiC composite panel structure with metallic tubes embedded within, through which the coolant flowed. An all-CMC cooled panel has also been demonstrated, which has greater potential for weight savings compared to the hybrid approach. One of the panels fabricated by Rockwell Scientific Company (currently Teledyne Scientific Company) and tested in the Rocket Combustion Laboratory at NASA Glenn Research Center is shown in Fig. 12.18. The panels were fabricated by a weaving process that allows the carbon fiber preform for an entire tube-wall panel to be integrally woven as a single piece, as opposed to single tubes being constructed separately and then joined together.

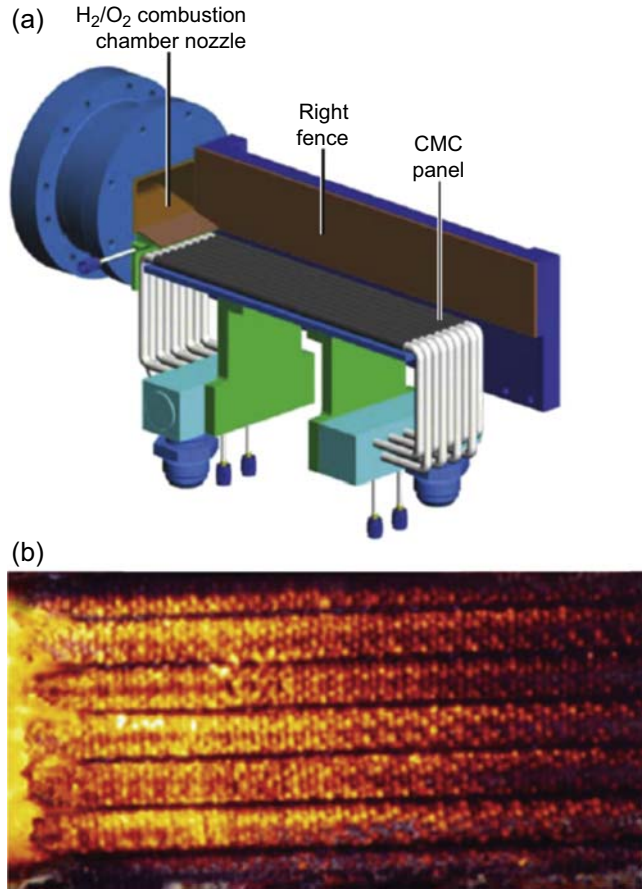

Figure 12.18 Cooled ceramic matrix composite (CMC) panels successfully tested in the Rocket Combustion Laboratory at NASA Glenn. (a) Cooled CMC rocket nozzle prototype panel in NASA test rig. (b) Optical image during the test.

12.3.2 Rocket engine thrust chamber

Cooled CMC structures have also been investigated for rocket engine thrust chambers. Regeneratively cooled CMC thrust chambers have been developed and successfully tested in the Rocket Combustion Laboratory at NASA Glenn Research Center [24]. In one of the concepts, an innovative processing approach utilized by Hypertherm, Inc., allowed woven CMC coolant containment tubes to be incorporated into the complex thruster design. In this unique design, the coolant passages had varying cross-sectional shapes but maintained a constant cross-sectional area along the length of the thruster. These thrusters, shown in Fig. 12.19, were silicon carbide matrix composites reinforced with silicon carbide fibers. An alternative and potentially more efficient way of actively cooling rocket engine thrust chambers is transpiration

Figure 12.19 Cooled ceramic matrix composite thrust chamber for rocket propulsion.

cooling [22]. A transpiration-cooled thrust chamber would eliminate the traditional cooling tubes and channels. The concept consists of three major components: a porous inner liner, an intermediate foam core, and an outer jacket for structural support and cooling. The fuel coolant is pumped into the foam layer and dispersed throughout the foam layer. The coolant would then enter the inner CMC liner, which contains millions of naturally occurring micropores. The micropores distribute the coolant uniformly over the combustion facing surface to keep it cool so that the liner can withstand the high-temperature combustion gases.

12.4 Hypersonic air-breathing propulsion

Hypersonic vehicles fly faster than five times the speed of sound and can enable a new class of flight vehicles that enable faster access to space, rapid military response at long range, and faster means of commercial air travel. Traditionally, rocket boosters have been used for hypersonic vehicles. Air-breathing engines have several advantages over rockets. Because the air-breathing hypersonic engine uses oxygen from the atmosphere, it eliminates the need to carry oxygen aboard the aircraft, thereby reducing significant vehicle weight. Furthermore, to produce the same thrust, air-breathing engines require less than one-seventh the propellant that rockets do. Air-breathing vehicles have greater maneuverability because they rely on aerodynamic forces rather than on rocket thrust, which results in higher safety, as flights can be aborted with the vehicle gliding back to Earth.

Two propulsion systems specific to hypersonic flights include ramjet and scramjet. Both concepts rely on high vehicle speed to forcefully compress the incoming air before combustion. A ramjet decelerates the air to subsonic velocities before combustion, while airflow in a scramjet is supersonic throughout the entire engine, which allows the scramjet to operate efficiently at extremely high speeds. Because neither scramjets nor ramjets can operate efficiently when they are traveling below Mach 2 or 3, a third type of propulsion (either a turbojet or a rocket) is required for takeoff. The hypersonic aircraft is a highly integrated system with a high degree of integration between the airframe and the engine, as shown in Fig. 12.20 for a scramjet-powered vehicle.

The temperatures encountered in engine components (eg, inlet, combustor, and nozzle) are significantly higher than in the other structural components [25], as shown in Fig. 12.21. These extremely high temperatures pose significant material and structural challenges. Because of the temperature limitations of all material systems, cooling of engine components is required, as shown in Fig. 12.22. The current state-of-the-art materials for the various engine components are cooled high-temperature materials, including high-conductivity copper. Cooled CMCs are attractive for hypersonic engine components because of the following benefits: (1) lighter weight than metallic designs, with potential for 50% weight reduction; (2) lower coolant flow requirements; (3) potential elimination of reentry cooling requirements; (4) allow for higher fuel injection temperatures; and (5) increased operational margin that translates to enhanced range and/or system payload. The weight reduction potential for cooled CMC engine components is shown in Fig. 12.23.

Several cooled C/SiC CMC concepts are being explored [23,26,27] and many have been successfully tested under hypersonic combustion conditions. These concepts, shown in Figs. 12.24 and 12.25, include refractory alloy tubes coprocessed with

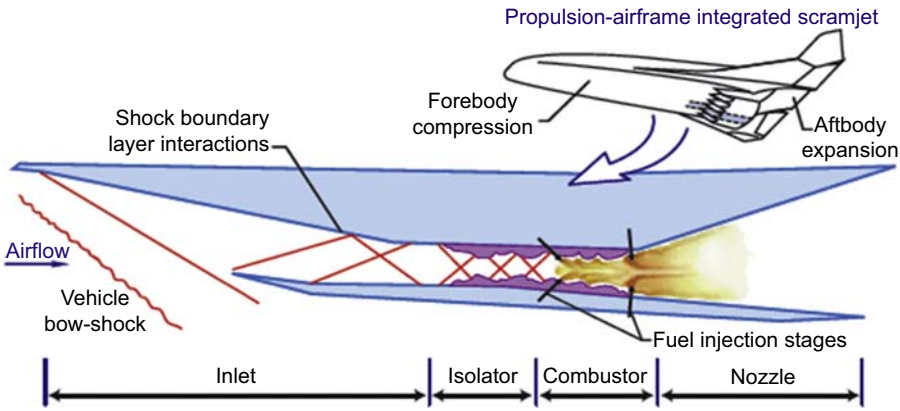

Figure 12.20 Schematic of propulsion-airframe integrated scramjet showing details of scramjet engine.

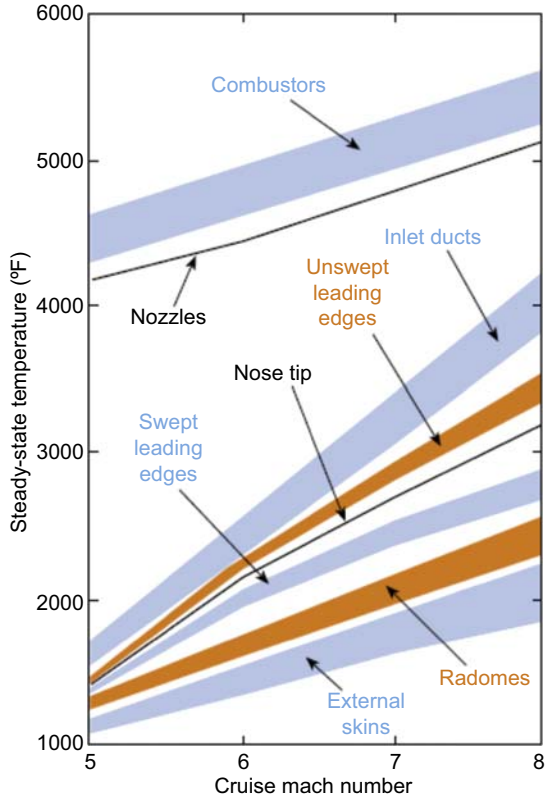

Figure 12.21 Schematic of propulsion-airframe integrated scramjet showing details of scramjet engine.
Taken from Ref. [25].

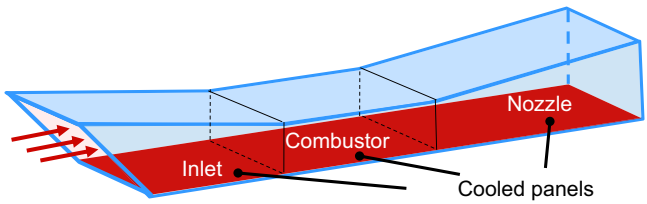

Figure 12.22 Schematic of scramjet/ramjet engine showing extensive utilization of cooled structures.

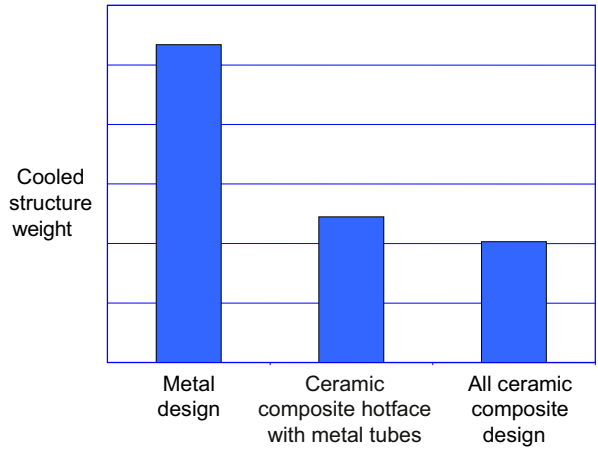

Figure 12.23 Weight benefits of cooled ceramic composite over metallic structures.

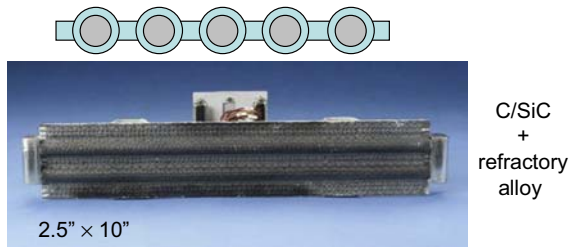

Figure 12.24 Cooled structure consisting of a refractory alloy coprocessed with a ceramic matrix composite.

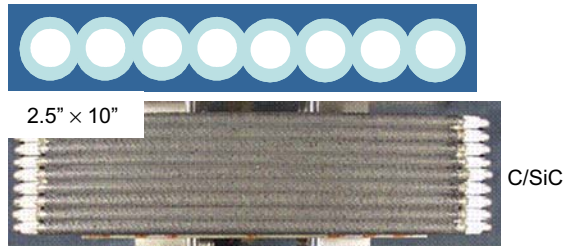

Figure 12.25 Cooled structure consisting of a woven ceramic matrix composite tube.

composite and woven CMC tubes. Astrium Space Transportation and EADS Innovation Works have developed [27] a PTAH−SOCAR (Paroi Tissee Application Hypersonique−Simple Operational Composite for Advanced Ramjet) technology based on a C/SiC composite for a dual-mode ramjet engine, as shown in Fig. 12.26.

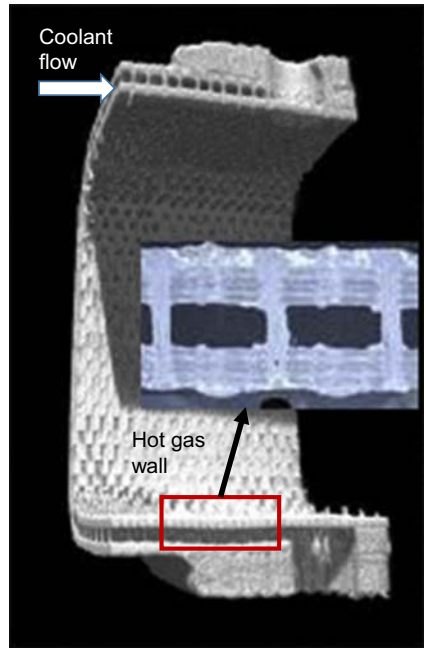

Figure 12.26 PTAH−SOCAR (Paroi Tissee Application Hypersonique−Simple Operational Composite for Advanced Ramjet) fuel-cooled structure consisting of a woven ceramic matrix composite tube.
Taken from Ref. [27].

12.5 Summary and conclusion

PMCs will find increasing applications in aerospace propulsion components owing to the increasing need for lightweight structures with significant fuel burn benefits. Future advances in PMCs for aerospace propulsion applications will require complex fiber textile architectures along with application of nanocomposites to provide location-specific engineered properties. Development of PMCs with higher temperature capability will extend the application range to hotter sections of aeropropulsion systems. For the hot sections of both aircraft and space propulsion systems, there will be increasing use of CMCs. Starting with the introduction CMC shrouds in commercial aircraft engines in 2016, the use of CMCs in gas turbine engines will increase with time as the industry gains more experience and confidence with CMCs. It is likely that the entire hot section of gas turbine engines except the disk will be made from CMC materials. The high cost of CMCs is a major challenge for their commercial introduction. The cost is expected to be lower with more usage volume and reduction of manufacturing time. Textile architectures will be required for complex CMC components such as turbine blades and cooled CMC structures for rocket propulsion and hypersonic air-breathing engines. For both PMCs and CMCs, new multiscale modeling tools will enable engineering of materials at the constituent level to provide desired properties at the component level.

References

[1] http://www.materialstoday.com/composite-industry/features/composites-get-in-deep-with-new-generation-engine/.

[2] M. Mecham, Patterned Breakthrough, Aviation Week & Space Technology, July 9, 2012, pp. 74–77.

[3] K.M. Handschuh, S.G. Miller, M.J. Sinnott, L.W. Kohlman, G.D. Roberts, J. Michael Pereira, et al., Materials, manufacturing and test development of A composite fan blade leading edge subcomponent for improved impact resistance, in: SAMPE Conference, Seattle, WA, June 2–5, 2015. Also NASA TM–2015-218340.

[4] J. Grady, CMC technology advancements for gas turbine engine application, in: Presented at 10th Pacific Rim Conference on Ceramics and Glass Technology, June 2–7, 2013. San Diego, CA.

[5] http://www.flightglobal.com/news/articles/general-electric-primes-cmc-for-turbine-blades-349834/.

[6] http://www.gereports.com/post/123737823440/up-up-and-away-ges-billion-dollar-bet-on.

[7] J.A. DiCarlo, Advances in SiC/SiC Composite for Aeropropulsion, July 2013. NASA TM–2013–217889.

[8] G.S. Corman, K.L. Luthra, Silicon melt-infiltrated ceramic composites (HiPerComp), in: N. Bansal (Ed.), Handbook of Ceramic Composites, Kluwer Academic Publishers, Boston, 2005, pp. 99–115.

[9] J.A. DiCarlo, H.M. Yun, G.N. Morscher, R.T. Bhatt, SiC/SiC composites for 1200°C and above, in: N. Bansal (Ed.), Handbook of Ceramic Composites, Kluwer Academic Publishers, Boston, 2005, pp. 77–98.

[10] J. Smialek, R.C. Robinson, E.J. Opila, D. Fox, N. Jacobson, SiC and Si_3N_4 Recession due to SiO_2 Scale Volatility Under Combustor Conditions, 1999. NASA TP 208696.

[11] K.N. Lee, D.S. Fox, N.P. Bansal, Rare earth silicate environmental barrier coatings for SiC/SiC composite and Si_3N_4, J. Eur. Ceram. Soc. 25 (10) (2005) 1705–1715.

[12] J.A. DiCarlo, G.N. Morscher, H.M. Yun, Interphase for ceramic matrix composites reinforced by non-oxide ceramic fibers, US Patent No 7,427,428 (2008).

[13] J.A. DiCarlo, Characterization and modeling of SiC/SiC composites for high temperature aerospace applications, Paper Presented at 12th International Ceramic Congress of CIMTEC 2010, Montecatini Terme, Tuscany, Italy.

[14] D. Zhu, Advanced environmental barrier coatings for Sic/Sic ceramic matrix composite: performance and directions, in: Presented at 7th International Conference on High Temperature Ceramic Matrix Composite (HT-CMC-7), Bayreuth, Germany, September 20–22, 2010.

[15] D. Zhu, Development and performance evaluation of HfO_2-Si and rare earth-Si based environmental barrier bond coat system for SiC/SiC ceramic matrix composite, in: Paper Presented at 41st International Conference on Metallurgical Coatings and Thin Films, San Diego, CA, May 2, 2014.

[16] M.C. Halbig, M.H. Jaskowiak, J.D. Kiser, D. Zhu, Evaluation of ceramic matrix composite technology for aircraft turbine engine application, AIAA 2013-0539, in: Paper Presented at the 41st AIAA Aerospace Sciences Meeting Including the New Horizon Forum and Aerospace Exposition, January 7–10, 2013.

[17] D. Kiser, N. Bansal, J. Szelagowski, J. Sokhey, T. Heffernan, J. Clegg, A. Pierluissi, J. Riedell, S. Atmur, T. Wyen, J. Ursic, Oxide/oxide ceramic matrix composite exhaust

mixer development in the NASA environmentally responsible aviation project, in: Presented at ASME Turbo Expo 2015, June 15−19, 2015. Montreal, Canada.
[18] http://cw.epubxp.com/i/546021-aug-2015/41, Composite World, August 2015, pp 38−41.
[19] Boeing Flight Tests CMC Engine Nozzle, High Performance Composites, November 2014, pp. 21−22.
[20] A. Lacombe, T. Pichon, M. Lacoste, 3D carbon-carbon composites are revolutionizing upper stage liquid rocket engine performance by allowing introduction of large nozzle extension, AIAA 2009-2678, in: Presented at 50th AIAA/ASME/ASCE/AHS/ASC Structures, Structural Dynamics, and Materials Conference, May 4−7, 2009. Palm Springs, California.
[21] O.J. Haidn, J. Riccius, D. Suslov, S. Beyer, O. Knab, Development of technologies for a CMC-based combustion chamber, Prog. Propuls. Phys. 1 (2009) 645−658.
[22] S. Steel, Ceramic materials for reusable liquid fueled rocket engine combustion devices, AMPTIAC Q. 8 (1) (2004). http://rocket-propulsion.info/resources/articles/Ceramic_Materials_For_LPRE.pdf.
[23] D.B. Marshall, B.N. Cox, Integral textile ceramic structures, Annu. Rev. Mater. Res. 38 (2008) 425−443.
[24] M.H. Jaskowiak, S.K. Elam, M.R. Effinger, Lightweight, Actively Cooled Ceramic Matrix Composite Thrustcells Successfully Tested in Rocket Combustion Lab (2005). http://ntrs.nasa.gov/archive/nasa/casi.ntrs.nasa.gov/20050199756.pdf.
[25] D.M. Van Wie, S.M. D'Alessio, M.E. white, Hypersonic airbreathing propulsion, Johns Hopkins APL Tech. Dig. 26 (4) (2005) 430−436.
[26] M.H. Jaskowiak, Advanced ceramics for NASA's current and future needs, in: Paper Presented at Association of Italian Manufacturers of Machinery and Equipment for Ceramics ACIMAC Conference, September 26, 2006. Rimini, Italy, http://ntrs.nasa.gov/search.jsp?R=20070008199.
[27] S. Beyer, S. Schmidt-Wimmer, K. Quering, C. Wilhelmi, M. Steinhilber, Technology status of fuel cooled ceramic matrix composites for dual-mode ramjet (DMR) and liquid rocket engine (LRE) applications, AIAA 2012-5877, in: Paper Presented at 18th AIAA/3AF International Space Planes and Hypersonic Systems and Technologies Conference, September 24−28, 2012. Tours, France.

This page intentionally left blank

Lightweight design and crash analysis of composites

13

S. Boria
University of Camerino — School of Science and Technology, Camerino, Italy

13.1 Introduction

In the past years, composites have been increasingly used in the automotive industry for their advantages of light weight, high strength, corrosion resistance, and easy manufacturing [1–3]. Initially, as one class of typical composites, glass fiber-reinforced plastic (GFRP) was widely adopted to reduce the weight of the vehicle structure. The replacement of conventional materials with GFRP composites into specific vehicle zones, such as roof, floor segments, body panels, frame parts, and seating systems, allowed a weight reduction from 40% to 60% and best performance [4–7]. More recently, carbon fiber-reinforced plastic (CFRP) composites have been replacing metallic components for crashworthiness applications, as attested by many numerical and experimental studies. An experimental campaign on thin-walled CFRP tubes under axial loading was conducted by Mamalis et al. [8], analyzing the influence of the geometry, laminate material properties, and compressive strain rate on the crushing response, the collapse modes, and the energy-absorbing capability. Huang et al. [9] analyzed hat-shaped section members and investigated the effects of CFRP parameters on energy absorption capability. The effect of delamination failure under the impact of hybrid box structures made by combining unidirectional with twill-weave CFRP composite materials was studied by Ghasemnejad et al. [10]. Yang et al. [11] explored square CFRP tubes under compression and showed how the composite corners play an important role in enhancing energy absorption. Last, Feraboli et al. [12] discussed the development of carbon/epoxy body panels and structural components for a high-performance vehicle, such as the Lamborghini Murcielago, while Boria [13] explored the homologation of a Formula Ford impact attenuator using CFRP composites in a sandwich structure.

In contrast to conventional structures, CFRP composites fail through a combination of several different fracture mechanisms [14–16]. These complex failure modes, which involve interlaminar failure, fiber–matrix debonding, fiber pullout, matrix deformation/cracking, and fiber breakage, together with friction effects, contribute to the overall energy absorption and give composite structures a greater specific energy absorption (SEA) than metallic ones [8,17,18]. Where the intended use is energy absorption under axial loads, such structures commonly take the form of thin-walled tubes of circular and rectangular cross section produced with fabric prepregs obtained from the combination of fibers and resins of various natures. The structural response depends also on the technology adopted for their production. The ability to predict

Lightweight Composite Structures in Transport. http://dx.doi.org/10.1016/B978-1-78242-325-6.00013-X

their behavior tends to be complicated significantly by the heterogeneity of the many structural and manufacturing variabilities. These effects make the design of composite energy-absorbing structures much more difficult than that of metals, which are extensively used for these kinds of applications. In crashworthiness design, the finite element simulations play a very important role thanks to their ability to predict behavior in the early design phases, so enabling cost reduction and shortening of the design phase. The energy dissipation by plastic deformation in ductile metallic structures is well understood and may be modeled by elastic−plastic material models in finite element analysis, reproducing good levels of predictability. The modeling of composite crushing phenomena, instead, is still developing, given the complexity and heterogeneity of the material. There are various approaches in modeling composite structures: micromechanical and macromechanical ones. In the first approach there is a high consumption of computational resources and, therefore, it cannot be applied for large automotive structures. It is therefore important to develop models that are simple enough to be employed in practical analysis situations, but at the same time capable of providing results with a suitable level of accuracy.

The goal of this work is to focus on the experimental and numerical crashworthiness design of CFRP structures under quasi-static and dynamic axial loading. The material used for this research is a prepreg obtained from high-strength carbon fibers, arranged in a canvas in a balanced manner, immersed in an epoxy resin. Initially simple geometries, such as truncated conical structures, were taken into account to evaluate the influence of several geometric parameters and loading conditions on the final deformation. Previous research has demonstrated, in fact, that cones are more suitable for impact structures than tubes since they do not require crush initiators [19]; furthermore, they more accurately reflect real-life geometry found in the automotive and motor sport arenas than simpler plate-type specimens. To understand in detail their behavior under axial load, some relevant quantities, such as peak load, average crush load, effective stroke, SEA, average crush stress, crushing efficiency, and stroke efficiency, can be calculated starting from the force−displacement curve. Afterward, a more complex geometry, equal to that adopted for the frontal impact attenuator of a Formula SAE car, was investigated. All the specimens were also tested using a numerical approach, and specific finite element models were developed using the nonlinear explicit commercial code LS-DYNA from Livermore Software Technology Corporation. For each analysis, the numerical results were compared with those obtained from real axial crushing tests. The study indicated that the deformation behavior of laminate calculated by using numerical models is in good agreement with experimental results with maximum relative errors of 10%, despite the simplification adopted.

13.2 Lightweight analysis from an energetic point of view

The lightweight and crashworthiness design of a vehicle structure is based on the research on the best geometric and material configuration to obtain a vehicle deceleration history during impact that has the desired characteristics of progression [20].

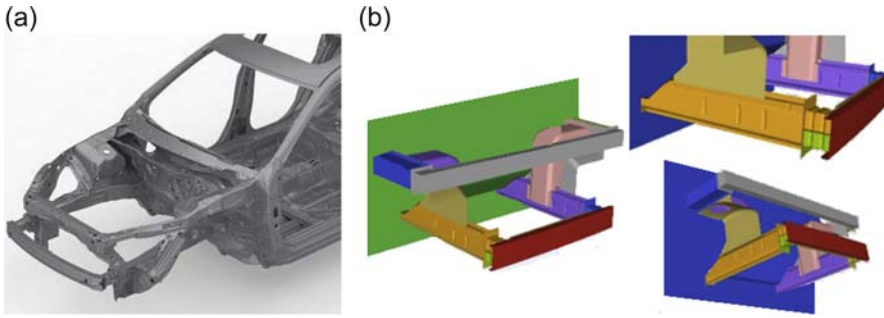

Figure 13.1 Front bumper assembly of a vehicle. (a) Real. (b) Modeled.

In the case of a passenger car the structures designed to absorb energy are in the front (Fig. 13.1), placed between the front bumper and the passenger compartment. The front structure generally consists of four longitudinal thin-walled beams, two for each side of the vehicle; two are positioned in the upper part of the engine compartment, just below the hood, and two, generally of bigger dimensions, at an intermediate height behind the bumper. In recent vehicles, at the front extremity of these two main beams, two so-called crash boxes are placed, one at each side. These crash boxes are intended to absorb energy in case of impact at low velocity, so avoiding large structural damage to the other parts of the front structure. Just behind the front bumper there is a transverse beam that has the task of positioning and supporting the bumper and it is connected at its extremities to the longitudinal main beams.

Under axial loading conditions the behavior of such structures depends heavily on the material used: while metals absorb energy by plastic deformation, the process of crushing in composites is brittle and more complex, associated with their heterogeneity. In general, simple geometries were adopted, in particular axial tubes with circular or rectangular sections. If composites are used, four different collapse modes will be observed, depending on the structural dimensions, material properties, and testing conditions [21]. An impact attenuator is designed to produce the first failure mode, which corresponds to deformation confined at the impact wall, as the structure guarantees the highest energy absorption with a progressive and controlled crushing. In contrast to conventional materials, thin-walled composite structures under axial compression do not present a sequence of plastic hinges that in terms of the force−displacement trend correspond to low and high peaks (Fig. 13.2(a)), but are characterized by the formation of a "mushrooming" failure with an almost constant crushing strength throughout the entire crushing process (Fig. 13.2(b)).

In the last curve, corresponding to composite structures, three different stages can be distinguished. In the first the compressive load reaches its maximum value, just before the formation of a main intrawall crack, which leads to a sharp drop in the force. To reduce such initial peak, very dangerous for the human body, some trigger mechanisms are often designed on the attenuator; the trigger has, moreover, the function of initiating the collapse of the structure in a well-controlled way and also in a well-defined location. The value of the peak load and the drop from it to the average

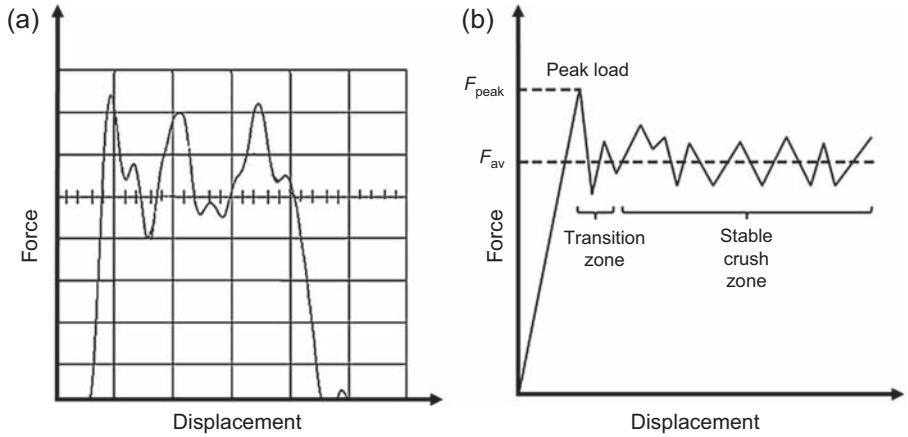

Figure 13.2 Typical force vs displacement trends for (a) metallic and (b) composite thin-walled structure under axial loading.

crushing load are strongly dependent on the trigger geometry [22]. The second crushing stage, usually very short, is the transition stage, in which the compressive load drops from its peak value and after some oscillation reaches the average crushing load. As the deformation proceeds further, the externally formed fronds curl downward with the development, along the section, of a number of axial splits followed by splaying of the material strips. The postcrushing regime is characterized by the formation of two lamina bundles bent inward and outward owing to the flexural damage; they withstand the applied load and buckle when the load or the length of the lamina bundle reaches a critical value. At this stage, a triangular debris wedge of pulverized material starts to form; its formation may be attributed to the friction between the bent bundles and the platen of the impact mass. From now on the crush zone progresses through successive cycles that are repeated in the same manner. In the last phase, in fact, the crushing proceeds through the specimen with oscillations of the force very close to the average value. It is during this phase that the major part of the energy is absorbed by the specimen.

To compare some specimens and determine which is the best in terms of energy absorption some relevant quantities can be calculated, starting from the force–displacement curve. They correspond to peak load (F_{peak}), average crushing load (F_{av}), total crushing, SEA, average crushing stress (σ_{av}), crush load efficiency (η), and stroke efficiency (S_E) [23]. The maximum crush load F_{peak} represents the first peak of the force vs displacement diagram. The average crushing force F_{av} is evaluated after the initial peak of force, during the stable crush zone; it is defined by:

$$F_{av} = \frac{1}{\delta - \delta_0} \int_{\delta_0}^{\delta} F(h)dh \qquad [13.1]$$

where δ represents the total crushing, δ_0 corresponds to the displacement after the first peak, and $F(h)$ is the instantaneous value of the load at the specific stroke h. SEA is the energy absorbed per unit of mass of the crushed structure, obtained by:

$$\mathrm{SEA} = \frac{E_{\mathrm{abs}}}{\rho \int_0^{\delta} A(h)dh} \qquad [13.2]$$

where E_{abs} is the total absorbed energy at the end of the crush, ρ is the density of the material, and $A(h)$ is the cross-sectional area at the distance h from the crushing extremity. Therefore the SEA is not an intrinsic material property; it depends not only on the material properties, but also on several other parameters, especially the specimen geometry. Two specimens made of the same material but with different geometries can collapse in very distinct ways and, as a consequence, can achieve very different values of SEA. The SEA allows comparing the energy absorption capabilities of two different materials and geometries when the weight is an important parameter of project. High values indicate lightweight crash absorbers. If the section is kept constant during the crushing, the average crushing stress σ_{av} is the average crushing force divided by the specimen cross-sectional area A, that is:

$$\sigma_{\mathrm{av}} = \frac{F_{\mathrm{av}}}{A} \qquad [13.3]$$

In general the crushing stress becomes a function of crushing if it changes with axial displacement and the average value can be calculated by:

$$\sigma_{\mathrm{av}} = \frac{1}{\delta} \int_0^{\delta} \frac{F(h)}{A(h)} dh \qquad [13.4]$$

η represents, instead, the ratio between the mean load and the maximum peak load, that is:

$$\eta = \frac{F_{\mathrm{av}}}{F_{\mathrm{peak}}} \qquad [13.5]$$

If the crushing efficiency is equal to 1 the behavior is referred to as perfect plastic, the load versus displacement diagram has a rectangular shape, and the structure is considered an ideal attenuator. With S_{E} is indicated, instead, the effective crush length divided by the total tube length L, which in terms of formulation becomes:

$$S_{\mathrm{E}} = \frac{\delta}{L} \qquad [13.6]$$

Higher values of these parameters indicate more efficient tubes. It should be noted that the absolute values of the average and peak forces are of great relevance for crashworthiness design, because they are strictly related to the accelerations transmitted to the vehicle's occupants in a real situation of crash. Not only does a certain amount of energy have to be absorbed, but also the values of the peak and average loads have to remain below a proper threshold, to pass specific homologation requirements [24].

13.3 Definition of impact attenuators

The first specimens considered for this work were manufactured using a carbon–epoxy preimpregnated fabric material. The prepreg tapes with woven carbon fibers embedded in an epoxy matrix were provided by Saati SpA and the production of the same was done by Vega Srl. In particular, the carbon fabric CF290 was used, with the high-strength carbon fiber T800 both for the warp and for the weft. While unidirectional material can be more efficient in energy absorption, fabric-reinforced materials are often preferred in impact structures because of their in-plane symmetry which favors the onset of a stable crush. For the matrix, instead, the toughened epoxy ER450 was adopted. The static mechanical properties for this material were published by Saati and are summarized in Table 13.1.

As regards the geometry, a thin-walled truncated conical tube was chosen (Fig. 13.3(a)); this kind of geometry profile is widely used by the automotive industry, especially when concerning the crashworthiness of structural components. The specimens had a length of 200 mm with inner top diameters of 25, 35, and 50 mm; wall thicknesses of 1.5, 2.5, and 4 mm; and wall inclinations of 5, 10, and 15 degrees. Later on we will refer to them by the following nomenclature: "inner top diameter_wall thickness_wall inclination" (for example, 25_1.5_5 corresponds to the specimen with 25-mm top inner diameter, 1.5-mm thickness, and 5-degree inclination).

Table 13.1 Prepreg static mechanical properties

Property	Composite CF290/ER450 carbon/epoxy fabric prepreg
Density	1.6×10^{-6} kg/mm^3
Tensile modulus	70 GPa
Tensile strength	700 MPa
Compressive modulus	60 GPa
Compressive strength	400 MPa
Flexural modulus	70 GPa
Flexural strength	700 MPa

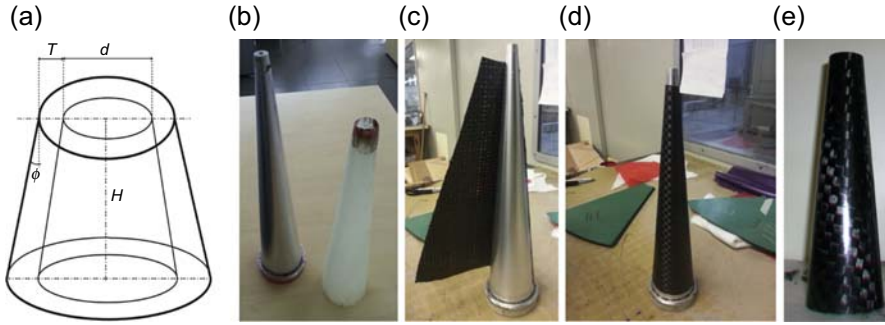

Figure 13.3 (a) Geometry of varying parameters, (b) male and female molds, (c) lamination process, (d) specimen before cutting, and (e) final specimen.

The various geometries were realized by arranging the laminae by means of a "quasi-isotropic" lamination, achieved by interleaving the orientation of the fabric from 0°/90° to +45°/−45°. The production technology used is the high-pressure autoclave curing process, commonly used by the aerospace industry for manufacturing composite material. In Fig. 13.3 are shown the male and female molds suitably realized for the purpose, a detail of the skin drawing on the conical male mold in aluminum alloy 6082 T6, and the final specimen after cutting. The counter, instead, is a glass/epoxy prepreg to ensure that under the pressure of the vacuum bag it is flexible and able to close on the mold, adhering perfectly to the laminate.

The structure to adopt as the frontal impact attenuator for a Formula SAE car was also obtained from CFRP composite material, even if different fiber and matrix were adopted [25]. As regards the geometry a truncated pyramidal structure with rounded edges and various wall inclinations was chosen (Fig. 13.4), to fit within the available volume dictated by aerodynamic and mechanical constraints and fulfill the technical regulation [26].

Three zones, corresponding to three different wall thicknesses, were implemented to ensure a stable collapse, reduce the peak load, and lighten the structure; in particular stacking sequences of 1.68, 2.16, and 2.4 mm were used. The manufacture was obtained by hand layup of preimpregnated composite layers and autoclave curing at 135°C and 7 bars applied pressure. Particular attention was paid to the lamination process; overlapping of the laminae at the corner edges was avoided to guarantee the structural stiffness and avert catastrophic failure under axial loading.

13.4 Experimental tests

To analyze the crushing behavior of CFRP truncated conical structures, static and dynamic analyses were carried out. Such tests were designed to analyze the effects of geometrical parameters and loading conditions on the energy absorption and the failure modes.

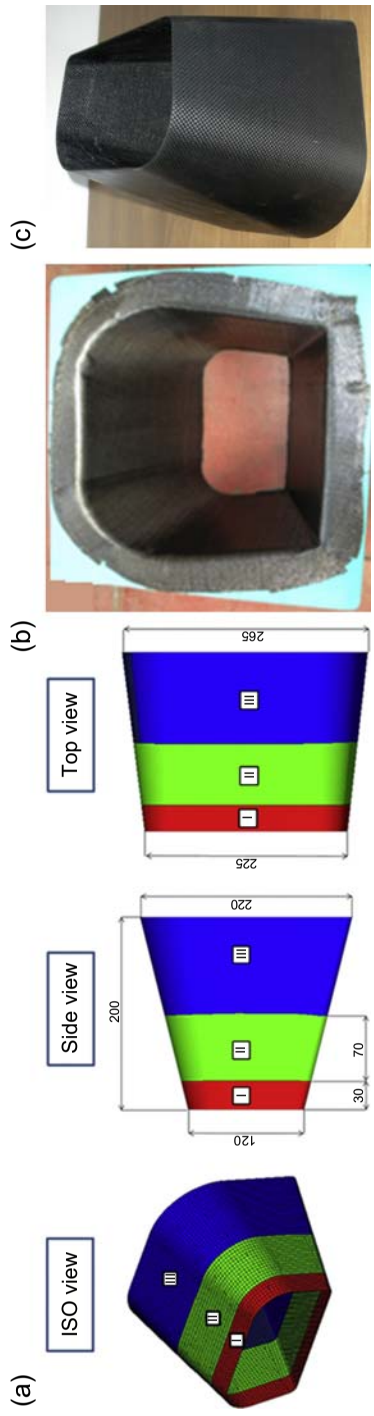

Figure 13.4 (a) Geometry, (b) mold with impact attenuator layup, and (c) final configuration.

For the front impact attenuator the same tests were conducted, even if different values of energy were used to respect homologation standards [26].

13.4.1 Quasi-static test

Initially, the truncated conical specimens were tested in quasi-static axial compression using an MTS machine with a load cell capacity of 250 kN. The tests were conducted in displacement control, with a constant forward velocity set to 5 mm/s throughout the test. The final vertical displacement was set to about 100 mm. Fig. 13.5 shows a specimen before and after the crush test.

The diagrams for load−displacement, for all the tested specimens, are shown in Fig. 13.6. All trends illustrate, up to about 5 mm of crushing, a first portion that is linearly elastic. Subsequently, the load tends to oscillate and increase during crushing, growing the inner top diameter of the truncated cone.

Table 13.2 reports some parameters characterizing the crush resistance under static loading, as just mentioned.

The impact attenuator was also tested under quasi-static axial conditions, using an electromechanical Zwick Z100 machine at a crosshead speed of 0.5 mm/s. The compression was performed with an upper moving plate and the load was measured by the load cell. The structure was tested up to a displacement of about 110 mm. Fig. 13.7 shows the impact attenuator before and after the quasi-static test.

The force vs displacement diagram obtained by the acquisition tool is represented in Fig. 13.8. After the initial peak, the second force peak is visible at the displacement of 30 mm and the third at the displacement of about 80 mm. This is due to the wall

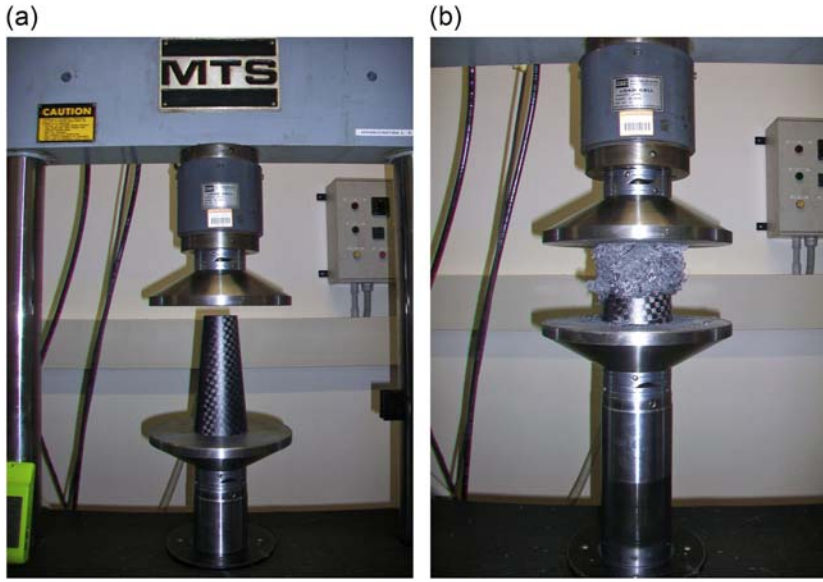

Figure 13.5 Specimen under quasi-static compression (a) before and (b) after testing.

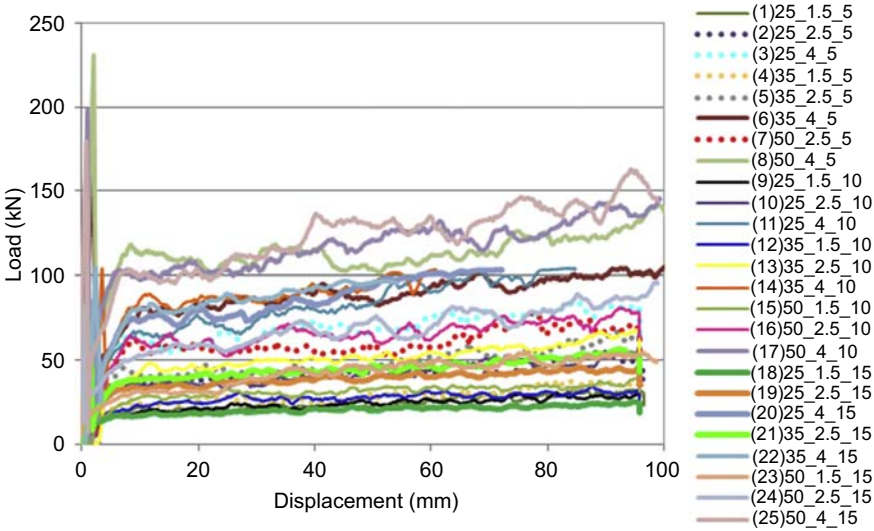

Figure 13.6 Load−displacement static diagrams.

thickness change, which becomes a very sensitive parameter; to decrease force peaks, the difference in ply thickness between impact attenuator zones should be as small as possible.

13.4.2 Dynamic test

The dynamic experimental tests, instead, were done using a drop-weight machine (Fig. 13.9(a)) at Picchio SpA. The mass and the impact velocity used for the tests on truncated conical structures were 301 kg and about 4 m/s, respectively, to subtend an impact energy of about 2400 J capable of being absorbed by all the specimens available. Impact accelerations and velocities were acquired by an FA3403 triaxial accelerometer with ±500 g full scale and an E3S-GS3E4 photocell, respectively (Figs. 13.9(b) and (c)). Moreover, a Mikrotron high-speed camera with a sampling of 1000 frames/s was used (Fig. 13.9(d)).

After the impact tests, the variations in deceleration over time for each type of specimen were analyzed and filtered with a CFC60 filter. The trend of velocity and displacement in time were obtained by integrating the acceleration signal for each geometry. Fig. 13.10 shows, therefore, the diagrams of load versus displacement for all specimens; the value of the force was obtained by multiplying decelerations, expressed in m/s^2, for impacting mass.

From the diagrams it is clear that with increasing wall thickness the trend tends to approach the axis of ordinates (increase in axial stiffness) and to achieve a higher value of the initial peak force. It should be noted that, unlike the static tests in which the value of maximum stroke was set, for these tests the value of the impact energy was fixed. The area under each curve is equal to the absorbed energy and therefore it is nearly

Table 13.2 Static results for the specimens tested

Specimen no.	Nomenclature	F_{peak} (kN)	F_{av} (kN)	δ (mm)	SEA (kJ/kg)	σ_{av} (MPa)	η (%)	S_E (%)
1	25_1.5_5	18.7	23.8	96	79.7	140	127	48
2	25_2.5_5	35.2	40.7	96	81.8	141	116	48
3	25_4_5	65.0	68.0	96	80.2	141	105	48
4	35_1.5_5	24.1	28.3	96	72.9	131	117	48
5	35_2.5_5	73.4	49.7	96	76.9	125	68	48
6	35_4_5	184.5	88.1	100	81.5	147	48	50
7	50_2.5_5	82.6	58.3	96	68.9	119	71	48
8	50_4_5	230.5	112.8	100	78.9	143	49	50
9	25_1.5_10	16.5	23.6	95	62.4	111	143	47.5
10	25_2.5_10	39.0	41.4	96	64.5	117	106	48
11	25_4_10	72.9	81.2	85	80.7	144	111	42.5
12	35_1.5_10	31.0	26.9	96	59.1	105	87	48
13	35_2.5_10	48.6	50.4	96	64.9	114	104	48
14	35_4_10	104.0	88.7	61	73.5	136	85	30.5
15	50_1.5_10	27.9	30.9	96	51.5	93	111	48

Continued

Table 13.2 Continued

Specimen no.	Nomenclature	F_{peak} (kN)	F_{av} (kN)	δ (mm)	SEA (kJ/kg)	σ_{av} (MPa)	η (%)	S_E (%)
16	50_2.5_10	76.3	64.3	96	65.8	114	84	48
17	50_4_10	198.0	115.9	99	71.9	129	58	49.5
18	25_1.5_15	15.9	20.0	96	44.2	82	126	48
19	25_2.5_15	29.9	37.8	96	51.2	89	126	48
20	25_4_15	84.9	83.9	72	75.5	131	99	36
21	35_2.5_15	47.9	43.9	96	48.9	87	92	48
22	35_4_15	104.9	90.2	55	66.7	118	86	27.5
23	50_1.5_15	47.1	41.5	99	63.5	113	88	49.5
24	50_2.5_15	81.9	67.3	99	60.6	109	82	49.5
25	50_4_15	179.0	121.0	99	66.7	120	68	49.5

SEA, specific energy absorption.

Figure 13.7 Attenuator (a) before and (b) after quasi-static test.

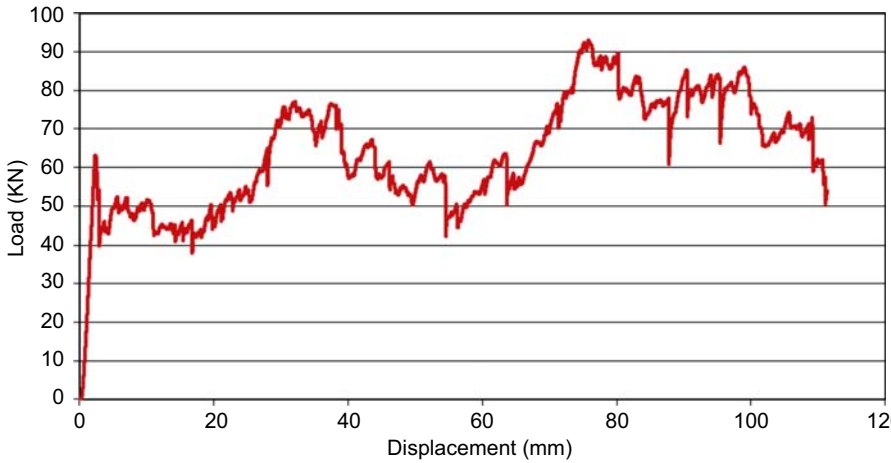

Figure 13.8 Force vs displacement diagram under static conditions.

a constant value given by the test conditions, which are almost the same for each configuration; only the impact velocity value, in fact, tends to vary slightly during each test.

The total crushing is therefore a consequence of having absorbed all the kinetic energy. Finally, some parameters characterizing the crush resistance were calculated (Table 13.3), as mentioned before.

Experimental dynamic tests were also performed on the frontal impact attenuator (Fig. 13.11). The devices were the same, but a different impact energy was adopted to respect the homologation standard [26]. In particular a falling mass of 300 kg and an impact velocity of 7 m/s were used.

The diagram in Fig. 13.12 represents the signal obtained from instrumentation as regards deceleration vs time, in both raw and filtered data. Also for such case a CFC60 filter was used, to follow the regulations and to appreciate the dynamic response more accurately. By integrating the signal one and two times it is possible

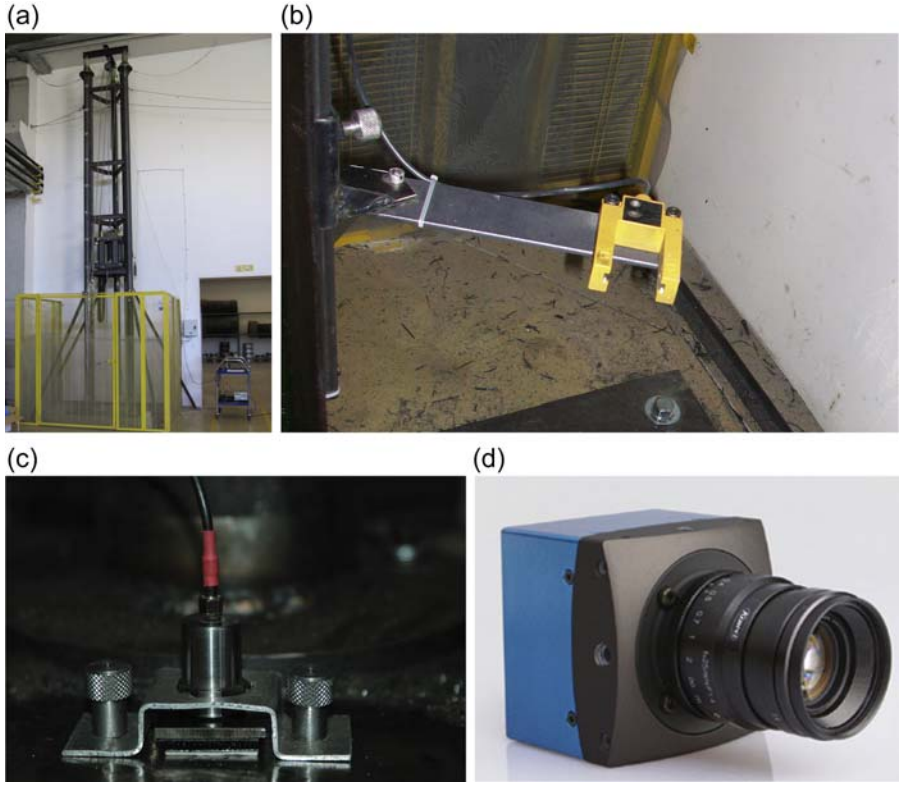

Figure 13.9 Drop tower and instrumentation: (a) drop-weight machine, (b) photocell, (c) accelerometer, (d) high-speed camera.

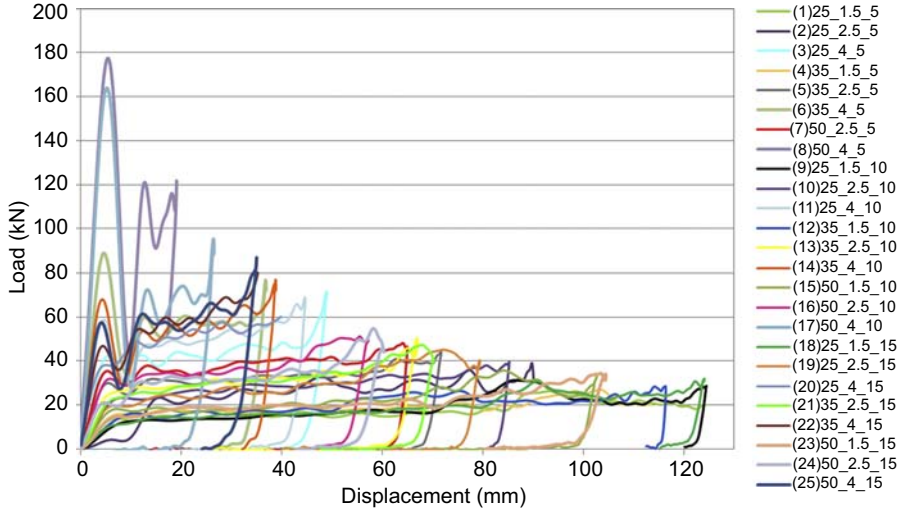

Figure 13.10 Load−displacement dynamic diagrams.

Table 13.3 Dynamic results for the specimens tested

Specimen no.	Nomenclature	Impact velocity (m/s)	F_{peak} (kN)	F_{av} (kN)	δ (mm)	SEA (kJ/kg)	σ_{av} (MPa)	η (%)	S_E (%)
1	25_1.5_5	3.85	13.9	16.9	130	52.0	97	121	65
2	25_2.5_5	3.8	4.1	24.4	90	48.7	90	595	45
3	25_4_5	3.7	42.2	42.0	50	54.8	108	99	25
4	35_1.5_5	3.8	15.7	18.9	116	47.4	84	120	58
5	35_2.5_5	3.9	29.8	32.9	70	53.1	96	110	35
6	35_4_5	3.7	88.8	60.0	35	62.3	108	68	17.5
7	50_2.5_5	4	35.4	36.9	65	44.9	84	104	32.5
8	50_4_5	3.6	177.4	100.0	19	78.7	149	56	9.5
9	25_1.5_10	3.9	13.1	18.4	125	44.2	79	140	62.5
10	25_2.5_10	4	23.3	28.2	85	46.9	84	121	42.5
11	25_4_10	3.8	58.6	48.9	45	57.7	108	83	22.5
12	35_1.5_10	3.9	16.2	20.0	115	41.1	73	123	57.5
13	35_2.5_10	3.7	25.2	30.9	68	44.1	82	123	34
14	35_4_10	3.7	67.1	60.0	35	58.1	96	89	17.5

Continued

Table 13.3 Continued

Specimen no.	Nomenclature	Impact velocity (m/s)	F_{peak} (kN)	F_{av} (kN)	δ (mm)	SEA (kJ/kg)	σ_{av} (MPa)	η (%)	S_E (%)
15	50_1.5_10	3.9	18.2	21.9	105	36.5	69	120	52.5
16	50_2.5_10	3.7	31.9	38.2	55	43.4	77	119	27.5
17	50_4_10	3.65	162.5	76.9	26	57.6	101	47	13
18	25_1.5_15	3.95	10.8	19.2	125	37.3	67	178	62.5
19	25_2.5_15	3.9	19.6	28.7	80	41.5	75	146	40
20	25_4_15	3.65	38.0	48.8	41	53.3	95	128	20.5
21	35_2.5_15	3.8	23.1	31.4	70	39.5	71	136	35
22	35_4_15	3.55	46.6	54.3	35	49.1	93	116	17.5
23	50_1.5_15	3.8	13.7	20.9	105	30.7	57	153	52.5
24	50_2.5_15	3.6	21.1	31.7	60	32.7	63	150	30
25	50_4_15	3.55	57.4	54.3	35	37.6	73	94	17.5

SEA, specific energy absorption.

Figure 13.11 Attenuator before and after dynamic test.

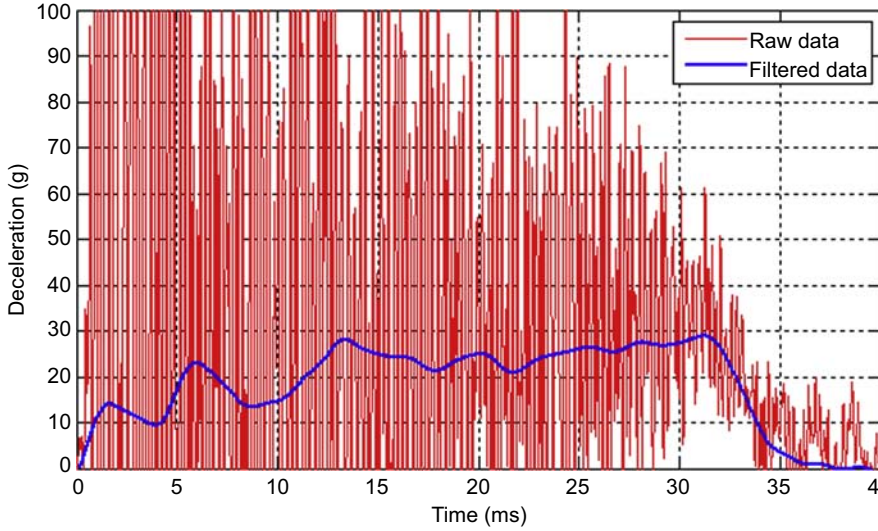

Figure 13.12 Raw data and filtered data for deceleration vs time trend.

to obtain information about the variations in velocity and crushing in time. Table 13.4 summarizes the principal crushing parameters, such as the effective initial velocity, the total impact time (T), the final stroke (δ), the average deceleration (d_{av}), the average load (F_{av}), and the absorbed energy (E_{abs}). The impact duration is the instant of time from the beginning of the crash at the moment when the velocity vanishes. The average deceleration is obtained from:

$$d_{av} = \frac{1}{T}\int_0^T d(t)dt \qquad [13.7]$$

Table 13.4 Crushing parameters for impact attenuator under dynamic load

Effective initial velocity (m/s)	Total impact time (ms)	δ (mm)	d_{av} (g)	F_{av} (kN)	E_{abs} (kJ)
6.8	32	112	21.6	63.5	6.9

where $d(t)$ is the progression of deceleration in time. The absorbed energy corresponds, instead, to the area under the load-shortening diagram.

13.5 Finite element modeling

To reproduce the crush phenomenon for all the kinds of specimens tested, specific finite element (FE) modeling was conducted. Numerical analyses were performed using the nonlinear explicit code LS-DYNA. In the literature, a variety of methodologies for modeling composite structures can be found; the following scheme (Fig. 13.13) tries to represent them [27]. The first classification is made according to the degree of mechanical detail: micro to macro [28–31]. The FE models related to the first group try to simulate the composite crushing phenomenon through a detailed modeling of its micromechanical behavior. A very fine solid mesh is required to reproduce the matrix crack propagation, involving an increase in computational efforts, often impractical for

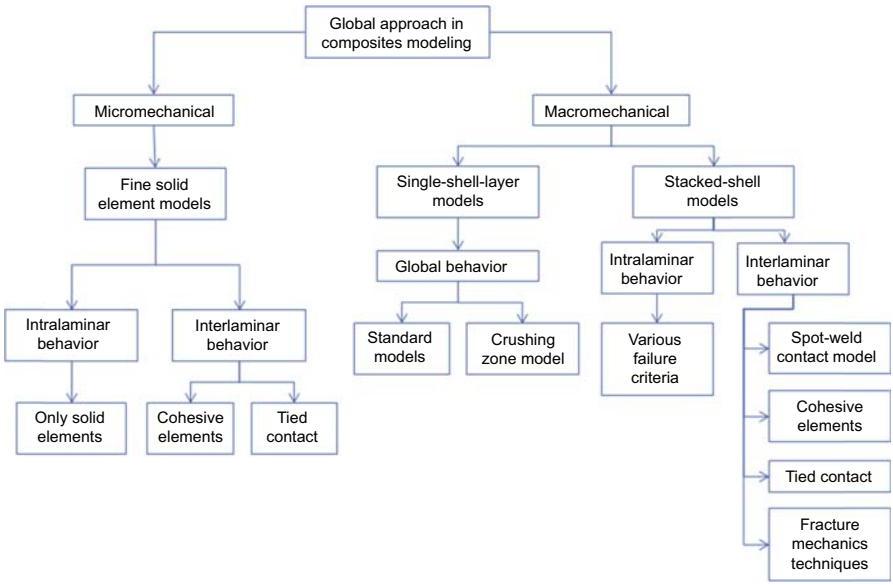

Figure 13.13 Numerical models classification.

assemblies made from many parts. This approach is used mainly to perform simulations concerning the delamination, in which the growth behavior of a single crack is studied in a very detailed way. The macromechanical group, instead, provides a general description of the material collapse [32–35]. It is much more computationally effective and, consequently, it is a suitable choice for engineering crash analysis. However, it is not capable of modeling precisely all the main failure modes that occur during a crush event. The macromechanical group, in turn, can be divided into two main types of models: the single-shell-layer models and the stacked-shell ones. The single-shell-layer models use a single layer of shell elements to model the specimen; they are not able to model the interlaminar collapse, but they are simple, with low computational cost, and are used when only load and energy level predictions are required. In such case a careful calibration of the numerous material parameters is necessary to obtain acceptable global results. In the stacked-shell models, instead, more layers of shell elements are modeled, with specific elements for joining (such as cohesive elements, tied contact, or springs). Such model allows a compromise between accuracy and efficiency depending on the number of layers used; it is capable of providing a better physical representation of the stratified composite structure but at the same time it keeps the simplicity inherent in the macromechanical approach.

The specimens considered were modeled using both micro- and macromechanical approaches. In particular the single-shell-layer model and solid element plies with a cohesive interface were implemented (Fig. 13.14).

In the first case only the middle surface of the structure was meshed with shell elements, while by using solid elements the implementation of the total geometry was done. For the truncated conical specimens the section was divided into two solid layers with the interposition of a cohesive ply. For the impact attenuator, instead, a

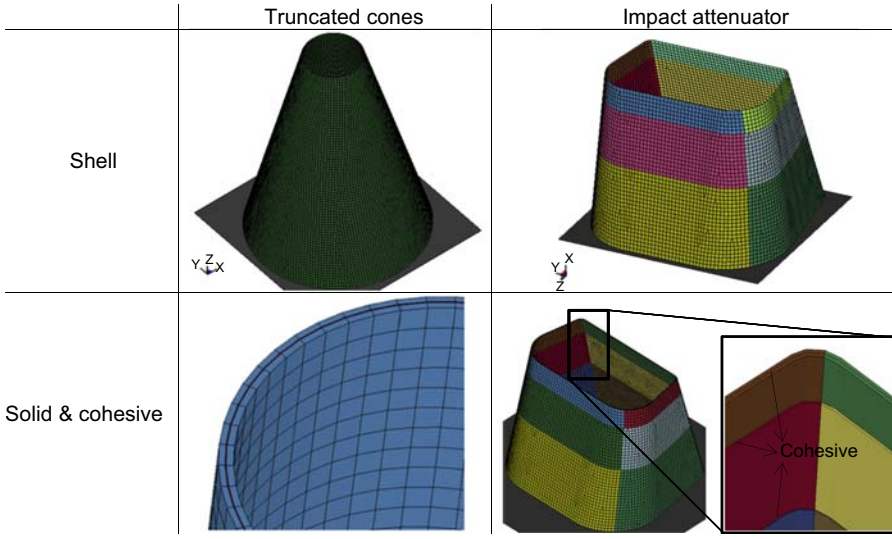

Figure 13.14 Various numerical approaches for both truncated cones and impact attenuator.

model with two, three, and four separate layers of solid elements, with cohesive elements in between, was generated for each zone, respectively, covering a certain number of different plies [36].

As regards material implementation, composite constitutive models implemented in LS-DYNA code are continuum mechanics models. Composites are modeled as orthotropic linear-elastic materials within a failure surface. The exact shape of the failure surface depends on the failure criterion adopted in the model. Beyond the failure surface, the appropriate elastic properties are degraded according to the assigned degradation laws, which can be divided into two main categories: progressive failure (MAT 22, 54/55, 59) or continuum damage (MAT 58, 161, 162). Progressive failure models have shown success [30,37] in axial crushing of composites exhibiting brittle fracture; therefore, for this study, the linear-elastic model #MAT_ENHANCED_COMPOSITE_DAMAGE was used. This material uses the Chang−Chang failure criterion [38] to determine individual ply failure. When all the layers fail the element is deleted. Elements which share nodes with the deleted element become "crash-front" elements and can have their strengths reduced by using the SOFT parameter [39] with TFAIL (time-step failure parameter set equal to 0.8 in such simulations) greater than zero.

Using a single-shell-layer approach, the laminate layup can be defined by one integration point for each ply with the respective ply thickness and fiber orientation angle. This can be done easily using the card *PART_COMPOSITE, on which the laminate has a thickness defined by the sum of each individual layer with the proper fiber orientation. Once all single layers of the shell element fail, the whole element is eroded and it simply disappears from the calculation. Underintegrated shell elements of the Belytschko-Tsai type (ELFORM = 2) with the stiffness-based hourglass control (IHQ = 4) were used for the modeling. This choice was a posteriori justified since the hourglass energy was negligible, less than 1% of the total energy. Laminate theory is also activated with the LAMSHT parameter in the *CONTROLL_SHELL card, to correct for the assumption of a uniform constant shear strain through the shell thickness.

To capture also the interlaminar failure a solid approach with cohesive elements was implemented. In particular the #MAT_COHESIVE_MIXED_MODE model was used, which includes a bilinear traction-separation law with quadratic mixed mode delamination criterion and a damage formulation.

Both for simple truncated conical tubes and for a complex impact attenuator a "rigid wall planar moving forces" card with a finite mass of 300 kg and an initial velocity of 4 m/s and 7 m/s, respectively, was adopted. Master-surface to slave-node and self-contact were defined between the impact mass and the nodes of the sacrificial structures and on the structure, respectively. As regards the boundary conditions, the same as used for the real tests were implemented on the numerical model.

13.6 Results and discussion

The characteristic modes of collapse which were observed throughout the axial compression tests correspond to those proposed in the literature. In particular, all truncated conical tubes tested absorbed impact energy through a process of gradual

crushing, with different combinations of failure mechanisms, keeping the remainder intact. Two different crushing modes were noted: splaying with axial splitting and fronds, both external and internal (Fig. 13.15(a)), and total reversal of the laminate internally to the specimen (Fig. 13.15(b)). Such configurations relate to the first stable failure mode (mode Ia and Ib [40]) of thin-walled composite structures, characterized by a better energy absorption capacity combined with a progressive and controlled crushing. In both cases the collapse initiated at the narrow end of the frustum. The externally formed fronds inverted freely outwardly with the development also of axial splits followed by splaying of the material strips. The internally formed fronds, instead, were turned inside the wall; firmly compacted hoops of material were developed, constraining the frond in this manner to fold inward. No axial tears were apparent in the internal fronds, which were more continuous than their external counterparts.

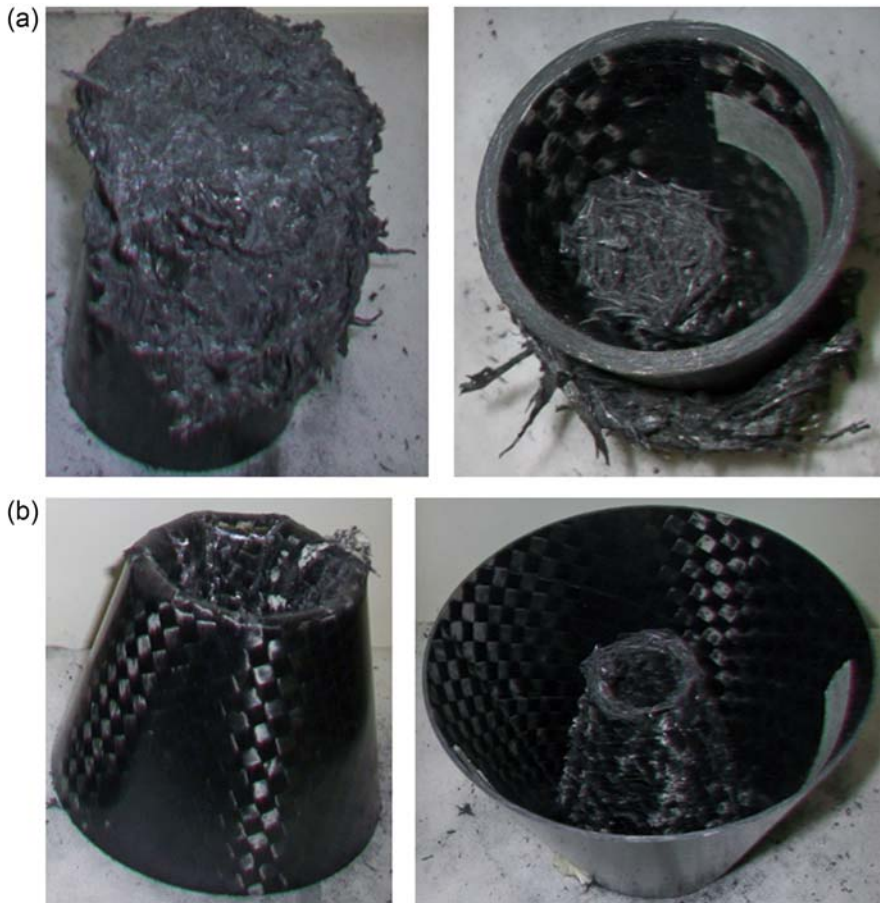

Figure 13.15 Different failure modes in the specimens tested: (a) fronds both internal and external, (b) total reversal of the laminate internally.

The major macroscopic crushing mechanisms governing the axial compression of tubes are identified as [21,41]: bending of the inward and outward fronds, hoop breakage of the outward frond, hoop compression of the inward frond, delamination, friction between the steel plate and the fronds, and friction between the fronds and the wedge.

The collapse modes on the macroscopic scale concerning the dynamically compressed specimens under progressive stable collapse seem to be similar to those obtained during the static loading of the same geometries. The delamination of the laminate with the formation of internal and external fronds is present on the specimens with inclination of 5 degrees and on those at 10 degrees with 4-mm wall thickness. In all other cases the structure wall inverts inward, bringing the material progressively fractured during crushing completely into the remaining part.

Figs. 13.16–13.18 show the variations of crushing load with shell shortening for both collapse modes, varying wall thickness, wall inclination, and top inner diameter, respectively. It is evident that average load increase with the wall thickness (Fig. 13.16). An increase in thickness of about 60% involves a congruent growth also into the load value.

Such prominent behavior is not found when varying only the wall inclination. However, the load tends to decrease with increasing inclination (Fig. 13.17).

The crushing force varies also with the top inner diameter. When increasing the diameter there is a growth into the energy absorption capacity, even if it is not remarkable (Fig. 13.18).

The crashworthiness of such CFRP composite simple structures tested in the present work under impact conditions is lower than during static loading. Comparing, in fact, the static and the dynamic results for the same type of specimen clearly shows an average reduction of about 35% of the crushing force under dynamic conditions; Fig. 13.19 is representative of specimen 5 (35_2.5_5), but the same trend is also evident for the other geometries, as is represented in Fig. 13.20.

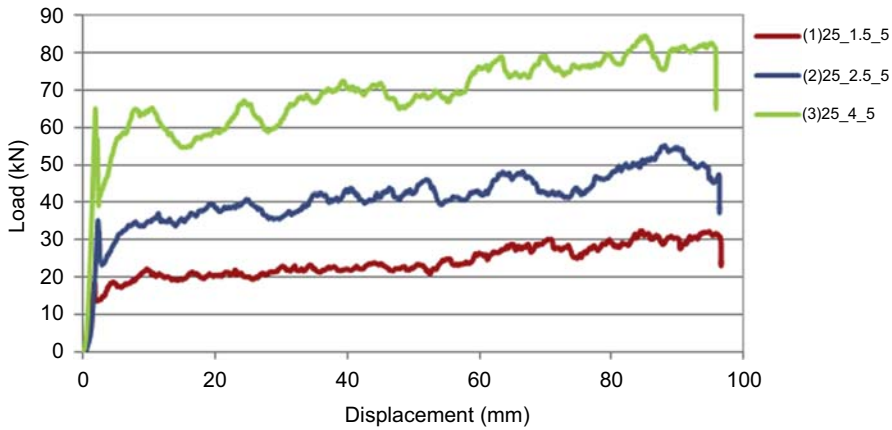

Figure 13.16 Load trend for varying wall thickness only for specimens 25 mm in diameter and 5 degrees in inclination.

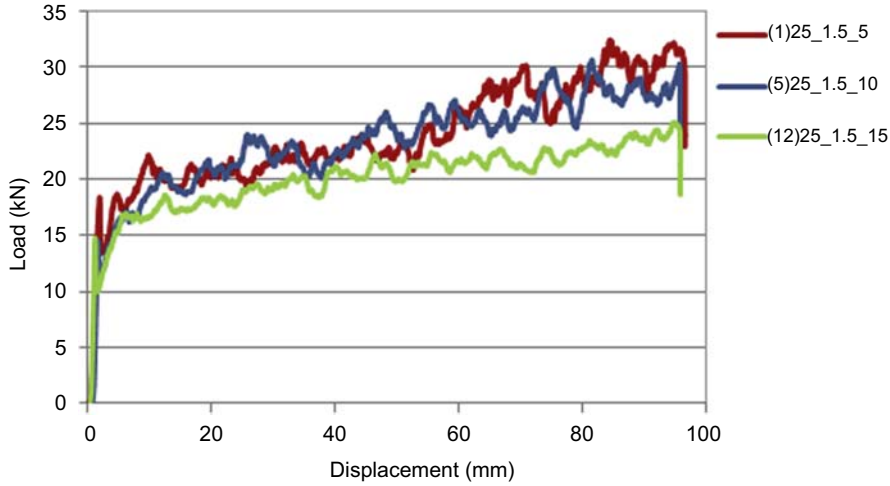

Figure 13.17 Load trend for varying inclination only for specimens 25 mm in diameter and 1.5 mm thick.

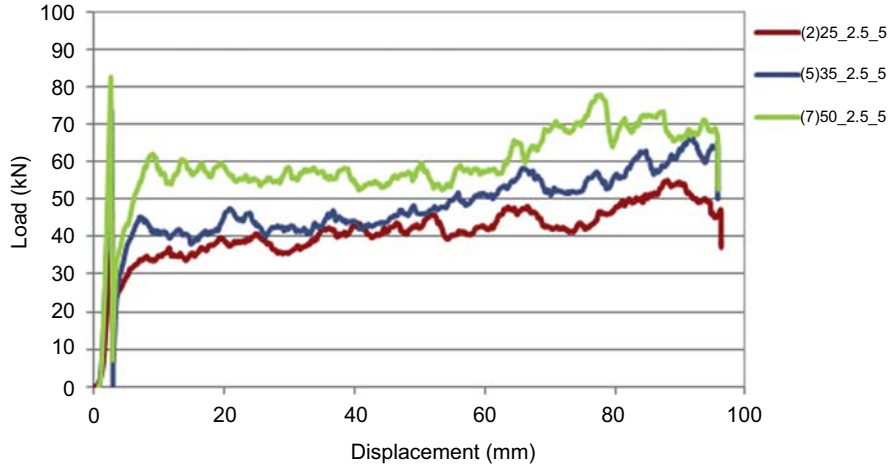

Figure 13.18 Load trend for varying top inner diameter only for specimens 2.5 mm thick and 5 degrees in inclination.

The effects of the strain rate on the specific energy and the mean load seem to be almost negligible. Static tests for the same geometries develop higher values of SEA and F_{av} than those obtained in dynamic testing (Figs. 13.21 and 13.22).

Fig. 13.21 shows how the SEA varies with the thickness/top inner diameter ratio (t:D). It is clear that by increasing the wall thickness (t) or decreasing the inside diameter (D) of the upper base the SEA increases almost linearly. The static fitted line has an inclination very similar to the one that approximates the dynamic results. The corresponding linear equations are showed directly in the diagram.

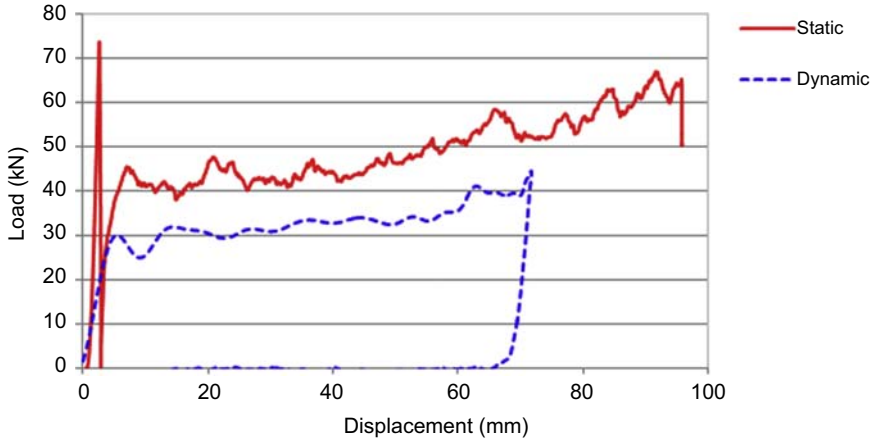

Figure 13.19 Load variation for specimen 5 under static and dynamic test.

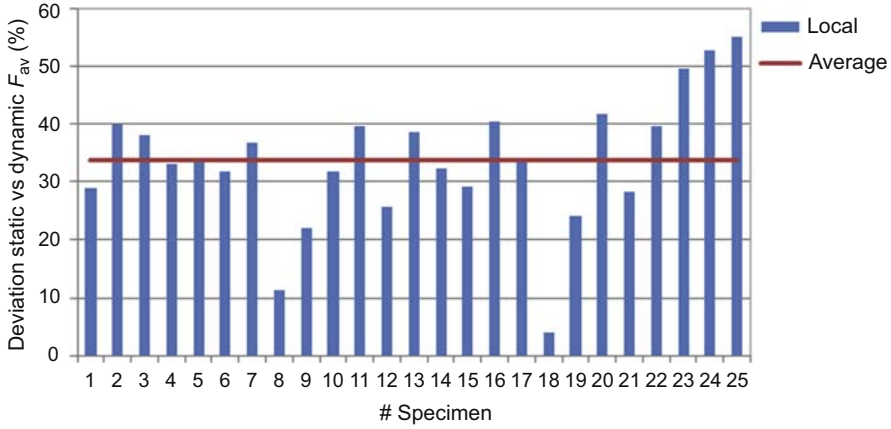

Figure 13.20 Load deviation between static and dynamic conditions for all the specimens.

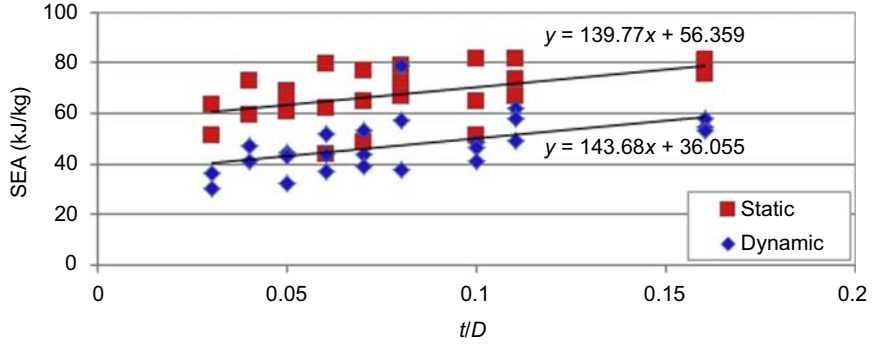

Figure 13.21 Specific energy absorption values varying thickness/diameter ratio under static and dynamic conditions.

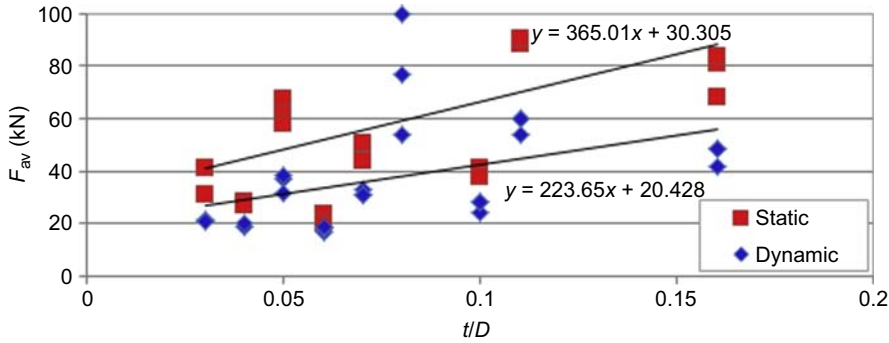

Figure 13.22 F_{av} values varying thickness/diameter ratio under static and dynamic conditions.

Fig. 13.22 shows the variation of average load with the ratio of thickness and top inner diameter. Even in such case, the experimental data obtained from static tests for the average load fit linear equations, the plots of which are almost parallel to those corresponding to impact loading. In this case the discrepancy in the angular coefficient for the two interpolating straight lines is more remarkable than that inherent to the SEA parameter; such evidence has also been noted in the literature [40].

In general, the difference between static and dynamic values can be attributed to three factors, namely the filtering of the signal (which reduces the accuracy of the data for integration), a possible strain rate dependence of the coefficient of friction, and a different friction coefficient for the crushing surfaces used in the two tests. Previous research by Hull [42], Farley [43], and Mamalis et al. [44] has shown that a great deal of energy absorption (about 50% of the total) is dissipated in friction between fronds and the crushing surface. Therefore, if the surface of the impacting sled plate is smoother than the servohydraulic machine surface or otherwise facilitates the sliding of the fronds, lower energy absorption will be measured [45].

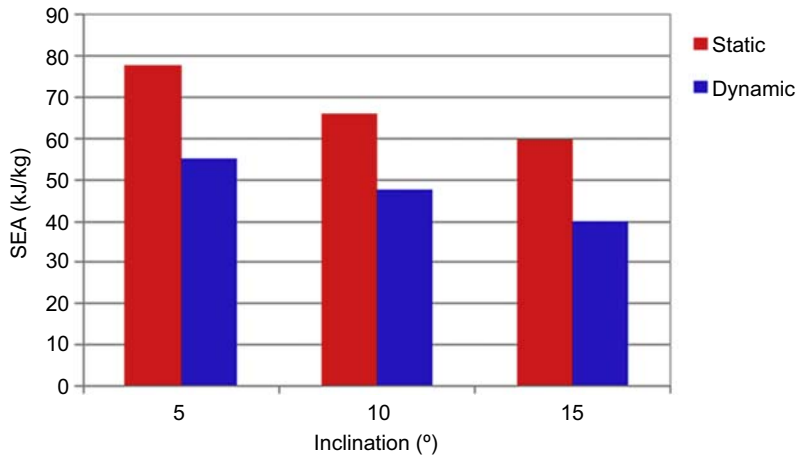

Figure 13.23 Specific energy absorption with varying wall inclination and test conditions.

From the SEA point of view of varying test conditions, it is clear that, with equal geometric parameters, specimens subjected to static loads exhibit more skill in absorption (Fig. 13.23). Furthermore, the SEA tends to decrease with the increase in the wall inclination.

Classifying the specimens from the SEA point of view, the one with 5 degrees in inclination, the smallest top diameter, and the largest wall thickness seems to be the most efficient. Therefore specimen n° 4 (25_4_5) represents the best to fill the role of impact attenuator.

The same analysis can be conducted from the average crushing stress point of view. Figs. 13.24–13.26 show how such function tends to change, varying the geometrical parameters.

Also from such results it is clear how the best impact attenuator seems to be that with the largest thickness and the smallest inclination and top diameter.

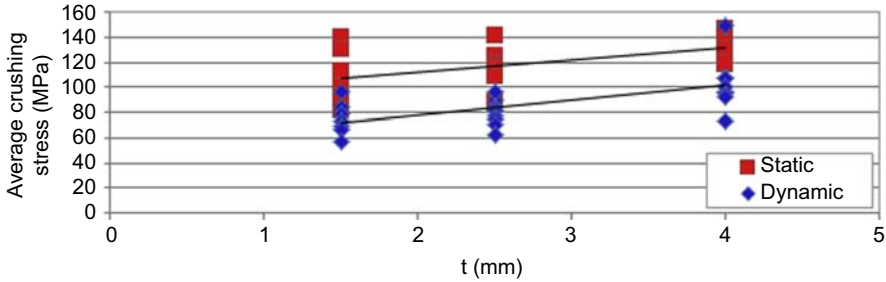

Figure 13.24 Average crushing stress varying wall thickness and test conditions.

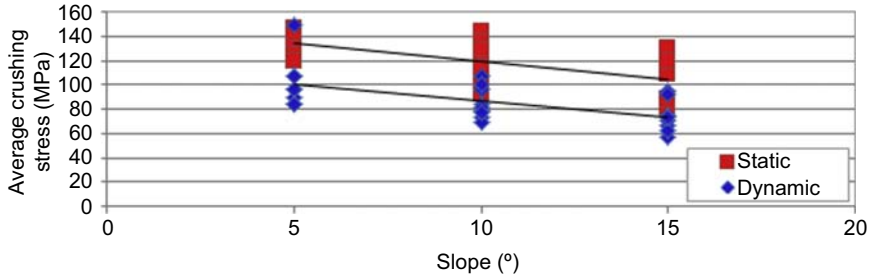

Figure 13.25 Average crushing stress varying wall inclination and test conditions.

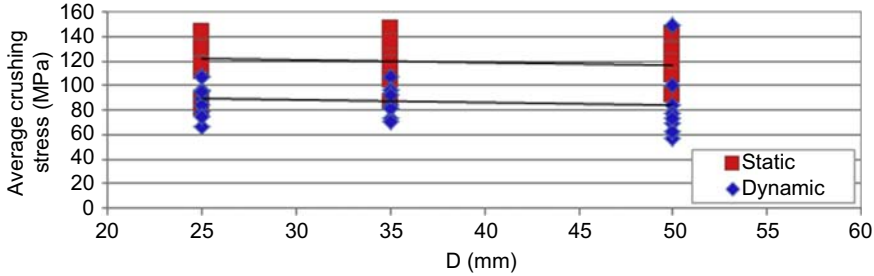

Figure 13.26 Average crushing stress varying top internal diameter and test conditions.

Table 13.5 Comparison between numerical and experimental dynamic tests

Specimen no.	Crush stroke error (%)		Mean force error (%)	
	Shell	Solid	Shell	Solid
1	3.2	5.8	2.8	6.2
2	2.7	3.5	1.9	3.8
3	3.8	4.2	3.2	3.9
4	4.1	4.9	3.9	5.2
5	2.1	2.8	2.3	3.5
6	4.9	3.9	4.4	4.8
7	5.4	5.5	5.6	4.9
8	6.8	6.1	6.9	7.7
9	1.2	2.9	1.1	3.7
10	3.6	3.1	3.9	2.9
11	7.4	9.9	7.2	8.7
12	1.9	2.6	1.8	3.1
13	2.7	1.5	2.9	2.9
14	2.3	5.8	2.1	6.8
15	4.1	2.3	3.8	2.1
16	5.2	1.4	6.2	2.8
17	8.1	6.9	8.9	5.5
18	2.9	5.4	2.2	6.9
19	3.6	9.1	3.2	8.7
20	2.2	7.2	2.8	6.2
21	3.5	2.9	3.7	3.2
22	4.2	5.9	4.1	6.7
23	3.9	4.2	3.1	5.5
24	5.8	7.2	5.8	8.1
25	8.8	8.5	8.2	5.8

The Table 13.5 reports the discrepancy between numerical (shell and solid modeling) and experimental tests under impact load as regards the final crushing and the average load. It is evident that, despite the simplification adopted, the numerical models are able to capture the main parameters with maximum relative errors of 10%.

Also, from the point of view of deformation, the numerical modeling is able to reproduce the phenomenon. Fig. 13.27 shows the final crushing under dynamic loading for specimen 25, from both real and simulated points of view. In such case the ability to reproduce the complete reversal of the laminate internally to the specimen is evident.

The observations made for truncated cones in terms of loss of absorption capacity at higher load speed can also be made for the impact attenuator. Fig. 13.28 shows, in fact, the comparison between the same structure under static and dynamic load. It is evident how there is a similar behavior in terms of force vs displacement under the two load conditions; a similar trend can be distinct in the two cases, with the presence of three peaks in succession, even if the static behavior ensures a greater capacity of energy absorption with respect to the dynamic behavior.

Even for such a structure a comparison between numerical and experimental results was conducted, using both shell and solid modeling. Fig. 13.29 reports such comparison in terms of load versus displacement curves under dynamic conditions. The trend highlights a good capability to capture the crushing process of such structure, even with the complexity and heterogeneity of the CFRP composite material used. Such correspondence is also evident in the final crushing shape. Fig. 13.30(a) shows how the use of solid

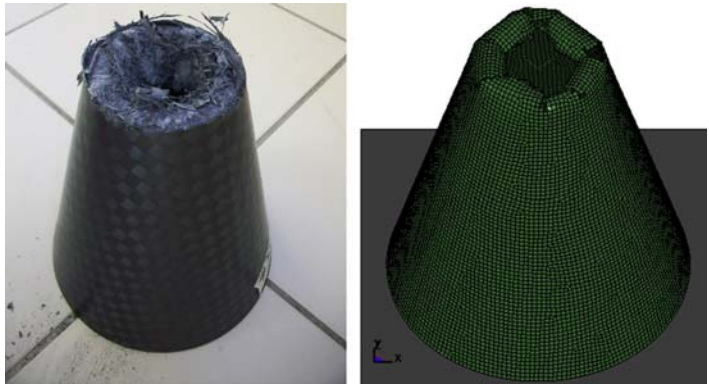

Figure 13.27 Comparison in terms of deformation for real and simulated specimens.

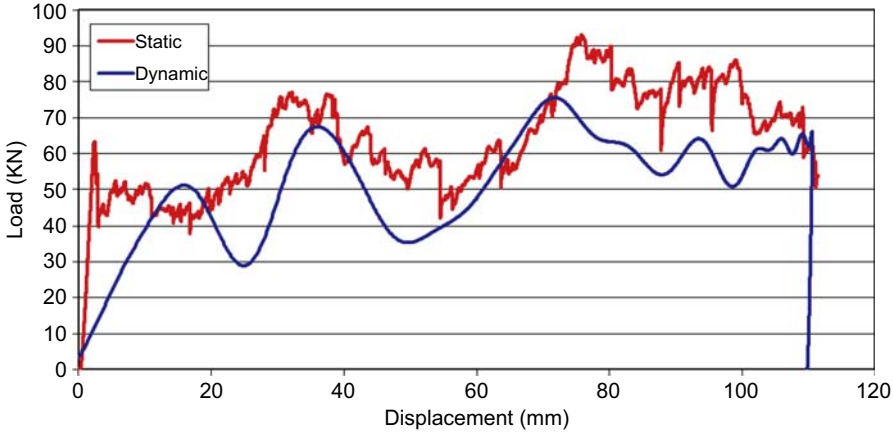

Figure 13.28 Comparison between static and dynamic load trends for the impact attenuator.

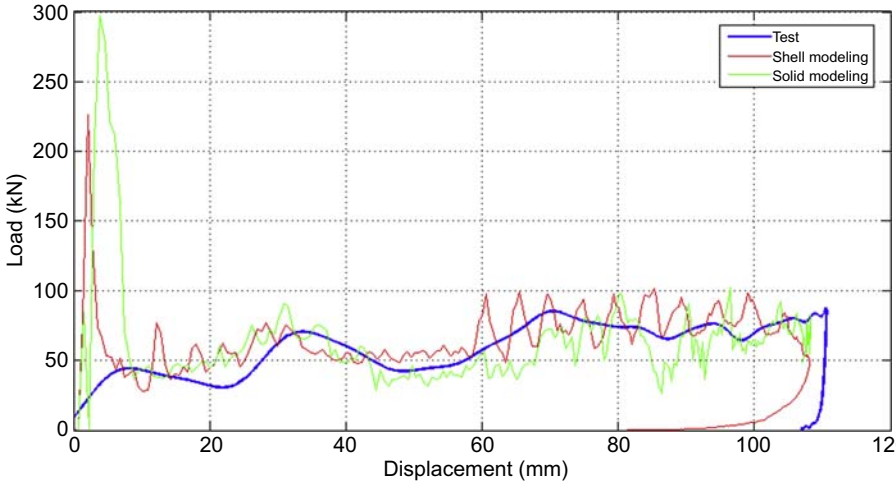

Figure 13.29 Comparison of experimental and numerical results in terms of force vs displacement under dynamic conditions.

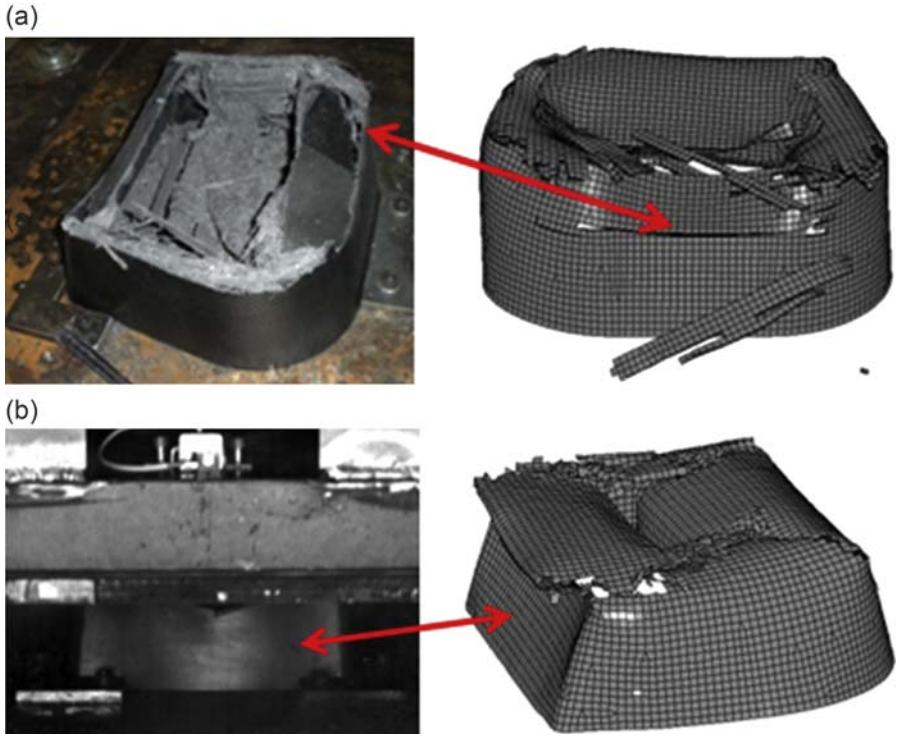

Figure 13.30 Comparison in terms of deformation for (a) solid modeling and (b) shell modeling.

modeling is able to reproduce the sharp break in the laminate in a specific zone of the impact attenuator, while Fig. 13.30(b) shows that by using shell elements it is also possible to reproduce the flexion of the straighter wall under axial compression. As mentioned before, the combination of solid and cohesive elements allows one to reproduce some interlaminar fracture phenomena that are not reproducible by using shell modeling. Unfortunately, a better crushing replication involves an increase in computing time; often it is not acceptable for large and complex assemblies.

13.7 Conclusions

This chapter describes efforts made in the lightweight design and crash analysis of specific CFRP structures. In particular, simple geometries, such as truncated cones, and a more complex one which represents the frontal impact attenuator for a Formula SAE racing car were investigated. The evaluation of the energy absorption capacity varying some geometrical parameters and test conditions was done. Specimens were subjected to static and dynamic axial loading, using well-proven testing machines. The tests carried out showed the two crushing forms typical of the first failure mode of thin-walled composite structures, characterized by the best energy absorption capacity and by a progressive and controlled deformation. No difference in deformation was observed between equal geometries subjected to static and dynamic loading. For the conical structures a remarkable loss in the energy absorption capacity, increasing the load speed, was noted; such observation cannot be said for the impact attenuator, for which a very similar behavior was observed. For all the specimens a comparison with numerical modeling was done, in terms of both micro- and macromechanical models. In both cases the FE models were able to reproduce sufficiently well the crushing phenomena, despite the complexity and heterogeneity of the CFRP material used.

Acknowledgments

The author wishes to express her appreciation to Professor Giovanni Belingardi, Ing. Alessandro Scattina, and Ing. Jovan Obradovic of Politecnico di Torino for their support and advice. Moreover, the availability of the Picchio SpA drop tower used for the experimental dynamic tests is gratefully acknowledged.

References

[1] E.R.H. Fuchs, F.R. Field, R. Roth, R.E. Kirchain, Strategic materials selection in the automobile body: economic opportunities for polymer composite design, Compos. Sci. Technol. 68 (9) (2008) 1989−2002.
[2] G.F. Smith, Design and production of composites in the automotive industry, Compos. Manuf. 1 (2) (1990) 112−116.
[3] G. Davies, Material for Automobile Bodies, Elsevier, Oxford, 2000.
[4] H. Ning, S. Pillay, U.K. Vaidya, Design and development of thermoplastic composite roof door for mass transit bus, Mater. Design 30 (4) (2009) 983−991.

[5] H. Ning, G.M. Janowski, U.K. Vaidya, G. Husman, Thermoplastic sandwich structure design and manufacturing for the body panel of mass transit vehicle, Compos. Struct. 80 (1) (2007) 82−91.
[6] H. Ning, U.K. Vaidya, G.M. Janowski, G. Husman, Design, manufacture and analysis of a thermoplastic composite frame structure for mass transit, Compos. Struct. 80 (1) (2007) 105−116.
[7] K.B. Thattaiparthasarthy, S. Pillay, H. Ning, U.K. Vaidya, Design and development of a long fiber thermoplastic bus seat, J. Thermoplast. Compos. Mater. 19 (2) (2006) 131−154.
[8] A.G. Mamalis, D.E. Manolakos, M.B. Ioannidis, D.P. Papapostolou, On the response of thin-walled CFRP composite tubular components subjected to static and dynamic axial compressive loading: experimental, Compos. Struct. 69 (4) (2005) 407−420.
[9] W.C. Huang, C.S. Cha, I.Y. Yang, Optimal crashworthiness design of CFRP hat shaped section member under axial impact, Mater. Res. Innovations 15 (s1) (2011) s324−s327.
[10] H. Ghasemnejad, H. Hadavinia, A. Aboutorabi, Effect of delamination failure in crashworthiness analysis of hybrid composite box structures, Mater. Design 31 (3) (2010) 1105−1116.
[11] Y.Q. Yang, A. Nakai, T. Uozumi, H. Hamada, Energy absorption capability of 3d braided-textile composite tubes with rectangular cross section, Key Eng. Mater. 334−335 (2007) 581−584.
[12] P. Feraboli, A. Masini, Development of carbon/epoxy structural components for a high performance vehicle, Compos. Part B Eng. 35 (4) (2004) 323−330.
[13] S. Boria, Design solutions to improve CFRP crash-box impact efficiency for racing applications, in: A. Elmarakbi (Ed.), Advanced Composite Materials for Automotive Applications, Wiley, 2013, pp. 205−226.
[14] L. Guoxing, Y. Tongxi, Energy Absorption of Structures and Materials, Woodhead Publishing, Cambridge, 2003.
[15] J.-M. Guimard, O. Allix, N. Pechnik, P. Thevenet, Energetic analysis of fragmentation mechanisms and dynamic delamination modelling in CFRP composites, Comput. Struct. 87 (15−16) (2009) 1022−1032.
[16] A. Jumahat, C. Soutis, F.R. Jones, A. Hodzic, Fracture mechanisms and failure analysis of carbon fibre/toughened epoxy composites subjected to compressive loading, Compos. Struct. 92 (2) (2010) 295−305.
[17] A.G. Mamalis, M. Robinson, D.E. Manolakos, G.A. Demosthenous, M.B. Ioannidis, J. Carruthers, Crashworthy capability of composite material structures, Compos. Struct. 37 (2) (1997) 109−134.
[18] A.G. Mamalis, D.E. Manolakos, M.B. Ioannidis, D.P. Papapostolou, On the experimental investigation of crash energy absorption in laminate splaying collapse mode of FRP tubular components, Compos. Struct. 70 (4) (2005) 413−429.
[19] J. Meredith, et al., Recycled carbon fibre for high performance energy absorption, Compos. Sci. Technol. 72 (6) (2012) 688−695.
[20] G. Belingardi, G. Chiandussi, Vehicle Crashworthiness Design − General Principles and Potentialities of Composite Material Structures, Springer, 2011.
[21] S. Boria, S. Pettinari, Mathematical design of electric vehicle impact attenuators: metallic vs composite material, Compos. Struct. 115 (2014) 51−59.
[22] D.M. Garner, D.O. Adams, Test methods for composites crashworthiness: a review, J. Adv. Mater. 40 (4) (2008) 5−26.
[23] H. Zarei, Experimental and Numerical Investigation of Crash Structures Using Aluminum Alloys, Curvillier Verlag, Göttingen, 2008.
[24] L. Morello, L. Rosti Rossini, G. Pia, A. Tonoli, The Automotive Body, vols I and II, Springer, London, 2011.

[25] J. Obradovic, S. Boria, G. Belingardi, Lightweight design and crash analysis of composite frontal impact energy absorbing structures, Compos. Struct. 92 (2) (2012) 423−430.
[26] Formula SAE Rules, 2008. students.sae.org/competitions/formulaseries/rules/rules.pdf.
[27] B.P. Bussadori, K. Schuffenhauer, A. Scattina, Modelling of CFRP crushing structures in explicit analysis, Compos. Part B Eng. 60 (2014) 725−735.
[28] M. Chatiri, T. Gull, A. Matzenmiller, An assessment of the new LS-DYNA layered solid element: basics, patch simulation and its potential for thick composite structures analysis, in: Proceedings of the 7th European LS-DYNA conference, Salzburg, May 14−15, 2009.
[29] W. Wagner, FE − modeling of fiber reinforced polymer structures, in: Proceedings of the 5th World Congress on Computational Mechanics, Vienna, July 7−12, 2002.
[30] P. Feraboli, Development of a corrugated test specimen for composite material energy absorption, J. Compos. Mater. 42 (3) (2008) 229−256.
[31] F. Greco, R. Luciano, A theoretical and numerical stability analysis for composite micro-structures by using homogenization theory, Compos. Part B Eng. 42 (3) (2011) 382−401.
[32] A. Borovkov, V. Palmov, N. Banichuk, V. Saurin, F. Barthold, E. Stein, Macro-failure criterion for the theory of laminated composite structures with free edge delaminations, Comput. Struct. 76 (2000) 195−204.
[33] A. Johnson, A. Pickett, Impact and crash modelling of composite structures: a challenge for damage mechanics, in: Proceedings of the 9th User Conference EURO-PAM, Darmstadt, October 7−8, 1999.
[34] L. Greve, F. Andrieux, Deformation and failure modelling of high strength adhesives for crash simulation, Int. J. Fract. 143 (2) (2007) 143−160.
[35] C.Y. Tang, C.P. Tsui, W. Lin, P.S. Uskokovic, Z.W. Wang, Multi-level finite element analysis for progressive damage behavior of HA/PEEK composite porous structure, Compos. Part B Eng. 55 (2013) 22−30.
[36] S. Boria, J. Obradovic, G. Belingardi, Experimental and numerical investigations of the impact behavior of composite frontal crash structures, Compos. Part B. 79 (2015) 20−27.
[37] C. Bisagni, G. Di Pietro, L. Fraschini, D. Terletti, Progressive crushing of fiber-reinforced composite structural components of a formula one racing car, Compos. Struct. 68 (2005) 491−503.
[38] F.K. Chang, K.Y. Chang, A progressive damage model for laminated composites containing stress concentration, J. Compos. Mater. 21 (1987) 834−855.
[39] S. Boria, G. Belingardi, Numerical investigation of energy absorbers in composite materials for automotive applications, Int. J. Crashworthiness 17 (4) (2012) 345−356.
[40] A.G. Mamalis, D.E. Manolakos, G.A. Demosthenous, M.B. Ioannidis, Axial collapse of thin-walled fiberglass composite tubular components at elevated strain rates, Compos. Eng. 4 (6) (1994) 653−677.
[41] A.G. Mamalis, Y.B. Yuan, G.L. Viegelahn, Collapse of thin-wall composite sections subjected to high speed axial loading, Int. J. Vehicle Design 13 (5−6) (1992) 564−579.
[42] D. Hull, A unified approach to progressive crushing of fibre-reinforce composite tubes, Compos. Sci. Technol. 40 (1991) 377−421.
[43] G.L. Farley, Relationship between Mechanical-Property and Energy-Absorption Trends for Composite Tubes, 1992. NASA TP 3284, ARL-TR-29.
[44] A.G. Mamalis, D.E. Manolakos, G.A. Demosthenous, M.B. Ioannidis, Analytical modelling of the static and dynamic axial collapse of thin-walled fiberglass composite conical shells, Int. J. Impact. Eng. 19 (5−6) (1997) 477−492.
[45] P. Feraboli, C. Norris, D. McLarty, Design and certification of a composite thin-walled structure for energy absorption, Int. J. Vehicle Design 44 (3/4) (2007) 247−267.

Flammability of composites

14

A.I. Al-Mosawi
Free Consultation, Babylon, Iraq

14.1 Introduction

The low thermal resistance of composite materials to high temperatures is considered the primary limitation to the use of these fabrics in applications that require high thermal resistance; hence an important way to increase their power to resist flame and improve the heat and thermal resistance properties of composites is to treat them with flame retardants. These additives must be easily processed with the composites, must not excessively degrade the other performance properties, and must not create environmental problems in terms of recycling or disposal. Fig. 14.1 represents the fire cycle [1–5].

Flame retardants defined as chemicals have the ability to withstand direct flame, as they work to prevent the entry of fire into the material, as well as preventing the spread of flame and even extinguishing it completely. The treatment can be during or after the fabrication of the stuffs to be protected from burning. The development of flame retardants allowed the safe use of fabrics that have a flammable nature by reducing their flammability and reducing the rate of burning. Most flame retardants consist of phosphorus, antimony, chlorine, bromine, boron, and nitrogen [6–15]. Flame retardants are commonly divided into four major groups, which are discussed next.

14.1.1 Inorganic flame retardants

A small group of inorganic compounds is suitable for use as flame retardants in plastics, and the most important are antimony trioxide containing halogen; aluminum hydroxide, which operates within the temperature range of 180–200°C; zinc sulfide; magnesium

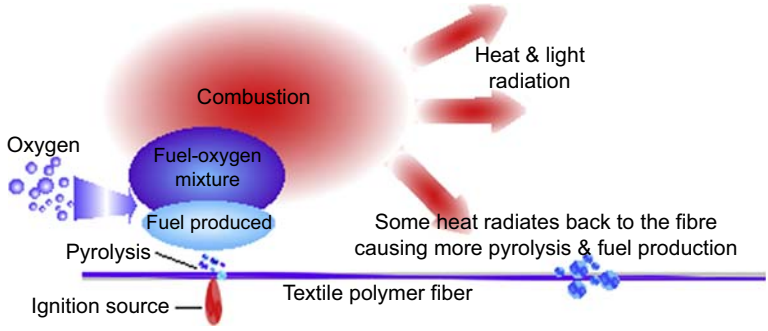

Figure 14.1 Fire cycle.

Lightweight Composite Structures in Transport. http://dx.doi.org/10.1016/B978-1-78242-325-6.00014-1

hydroxide, which has a range of 300−330°C; and zinc borate. When this kind of flame retardant is exposed to heat it does not evaporate, but disintegrates and releases water vapor and carbon dioxide into the flammable gases of the fire. The reactions of these compounds with the flammable gas are endothermic reactions. The mechanism of action is based on disintegration at high temperatures, leading to the freeing of vapors to reduce the mixture of flammable gases, and then the surface of the plastic is isolated from contact with oxygen as well as by a glass layer of protection formed on the substrate that prevents oxygen and temperature effects. This group represents more or less 50% of the worldwide output of fire-preventive materials.

14.1.2 Phosphorus-containing flame retardants

This category generally includes phosphate esters, ammonium orthophosphates, ammonium polyphosphates, and red phosphorus. These retardants are oxidized during combustion to phosphorus oxide, which turns into a phosphoric acid on its interaction with water. This acid stimulates the take-up of water out of the bottom layer of the material that has decomposed thermally, leading to char, thus increasing the carbonate waste as well as reducing the emission of combustible gases. The phosphorous compounds work in the solid state, but can also operate in a gaseous state when they contain halogenated compounds. This group represents 20% of the world flame retardant production.

14.1.3 Nitrogen-containing flame retardants

These compounds are also known as organic flame retardants. Freed gases from these retardants make the material swell, leading to the formation of the surface-insulating layer. One of the most important compounds in this group is melamine and its derivatives. The use of these retardants is constrained to a specific number of polymers.

14.1.4 Halogenated organic flame retardants

These retardants include in particular elemental bromine and chlorine. Their working principle depends on chemical intervention in the radical chain mechanism, which takes place in the gaseous state during combustion. Halogenated flame retardants work to remove the high-energy hydrogen (H) and hydroxide (OH) bond, which breaks loose during the combustion process through union with the retardant, as depicted in the following equations:

$$H^{\bullet} + O_2 \rightarrow OH^{\bullet} + O \qquad [14.1]$$

$$O + H_2 \rightarrow OH^{\bullet} + H^{\cdot} \qquad [14.2]$$

At the beginning of the process, the halogen will decompose as shown in Eq. [14.3],

$$RX \rightarrow R^{\bullet} + X^{\bullet} \qquad [14.3]$$

where X is either chlorine or bromine. Then the halogen root will react to become hydrogen halide:

$$X^{\bullet} + RH \rightarrow R^{\bullet} + HX \quad [14.4]$$

The hydrogen halide formed interferes with the radical chain mechanism as shown in Eqs. [14.5] and [14.6]:

$$HX + H^{\bullet} \rightarrow H_2 + X^{\bullet} \quad [14.5]$$

$$HX + OH \rightarrow H_2O + X^{\bullet} \quad [14.6]$$

So, the flame is poisoned by the freeing of halogen roots during combustion. Scientific experiments have identified the quantity of halogen compounds that must be added to disable a good flame and these values are 4% for bromine and 20–30% for chlorine. These retardants represent 25% of the global production.

14.2 Mode of action of flame retardants

The process of retarding flame or even stopping it depends on the nature of the flame retardant, in that it can operate chemically or physically in the solid, liquid, or gas state. The flame retardant will inhibit the combustion process at different stages of this process, in other words, during heating, decomposition, ignition, or flame spread [16–25].

14.2.1 Physical action

Physical retardation can happen in one of three ways:

1. **Cooling:** The additives generate endothermic processes, which work on cooling the bottom layer of the material to a degree lower than the degree of thermal combustion. An examples of a flame retardant that behaves so is aluminum hydroxide (see Fig. 14.2(a)).
2. **Formation of a protective layer:** The retardant forms a semiglass coating layer that works to expel the oxygen necessary for the continuation of the combustion process, leading to retardation of heat transfer. Examples of these retardants are inorganic phosphorus compounds and boron (see Fig. 14.2(b)).
3. **Dilution:** The retardant comprises a merger of inert materials (fillers) and additives that generate inert gases upon thermal decomposition, working to decrease fuel in both solid and gas states so as not to exceed the minimum limits for a flammable gas mixture. Boron and phosphorus compounds behave in this way.

14.2.2 Chemical action

Chemical retardant action takes place in two major ways:

1. **Reaction in the gas phase:** The free radical mechanism is stopped by flame retardants, leading to a block of the exothermic process and thus a cooling the system (see Fig. 14.3). They also trims down the proportion of flammable gases and even prevent their formation entirely. Flame retardants that behave this behavior are halogenated compounds.

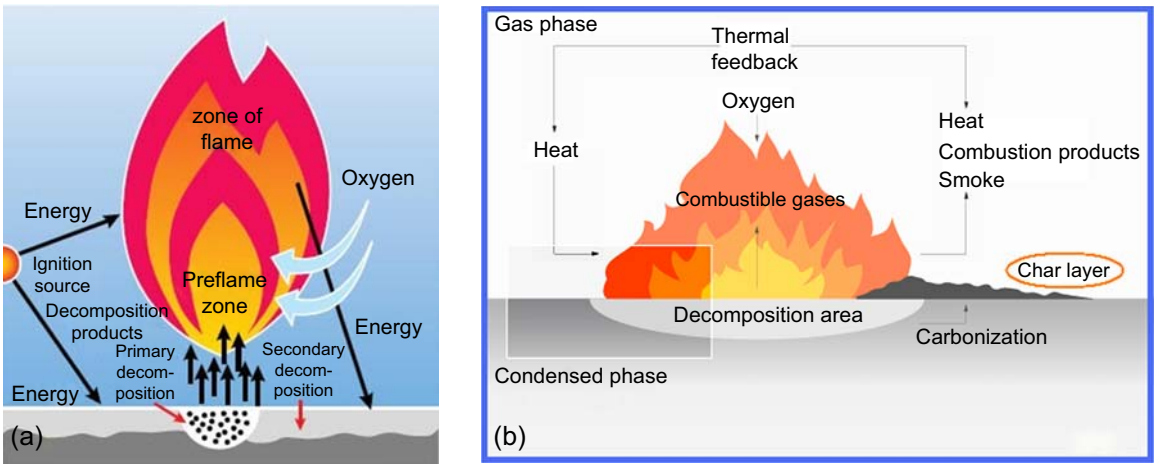

Figure 14.2 Physical action. (a) Cooling. (b) Formation of a protective layer.

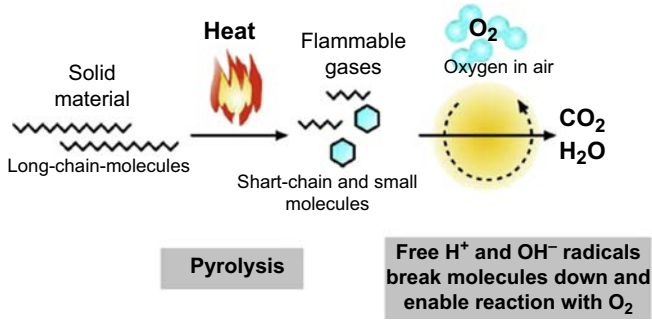

Figure 14.3 Reaction in gas phase.

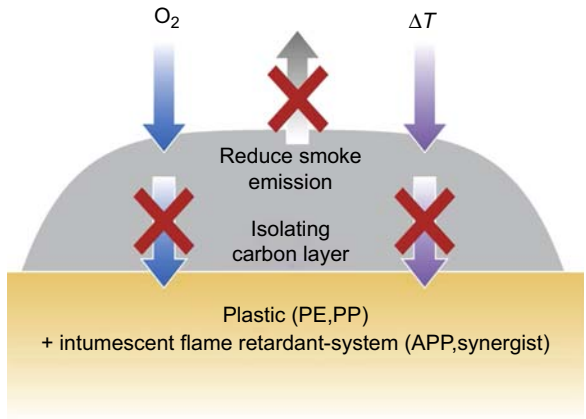

Figure 14.4 Reaction in solid phase (Polypropylene (PP), Polyethylene (PE), Ammonium polyphosphate (APP)).

2. **Reaction in the solid phase:** A carbon layer is configured on the polymer surface (see Fig. 14.4), where the flame retardant removes the water, which generates double bonds in the polymer. These double bonds form a cross-linked carbon layer. An example of such materials is phosphorescent compounds.

14.3 Classification of flame retardants

Flame retardants are classified into three groups [26–30]:

1. **Additive materials:** These materials are integrated mechanically with plastics during polymerization or before and more often than not accompany this procedure. Additive materials are used in particular with thermoplastics.
2. **Reactive materials:** These materials are chemically linked within the polymer molecule together with other manufacturing components. This binding process protects the flame retardant from exuding outside the polymer and from volatility. Reactive materials are employed in particular with thermosetting.

3. **Combinatorial materials:** Additives and reactive materials are merged or combined with one another to generate a synergistic effect to improve the flame-retarding or antagonistic force, but can reduce the flame-retarding ability in some particular applications. This integration is applied to cut down costs, in that synergistic materials are less expensive than flame retardant alone.

14.4 Future vision

It is no secret that flame retardants have developed rapidly in terms of the diversity of materials used and the way in which they work, so the author had to search for new ways to add flame retardants to the low-thermal-resistance materials that are the most important composites and polymers. One of the visual modalities of the future of how to add flame retardants to composite materials is to integrate flame retardant nanoparticles inside the polymer structure by replacing polymer atoms with flame retardant atoms, as occurs in the example of molecules of carbon and iron in steel composition (see Fig. 14.5). This mechanism could be executed by applying various schemes. Foremost, we could decorate or functionalize nanoparticles with flame retardant molecules and then mix them in by extrusion. As well, we could try to add a coupling agent to "bond" these functionalized nanoparticles with the polymer matrix. Reactive extrusion could also help with this reaction.

We would possess to check also the chemical feasibility of doing the synthesis of a copolymer (either random or block for example) composed of "retardant" monomers and "normal" monomers, and I say monomers, not atoms to be more accurate. If the "retardant" monomers are not able chemically (in terms of reactivity for example) to compose the chain, then you just can add the retardant later as in reactive extrusion or a post-grafting procedure.

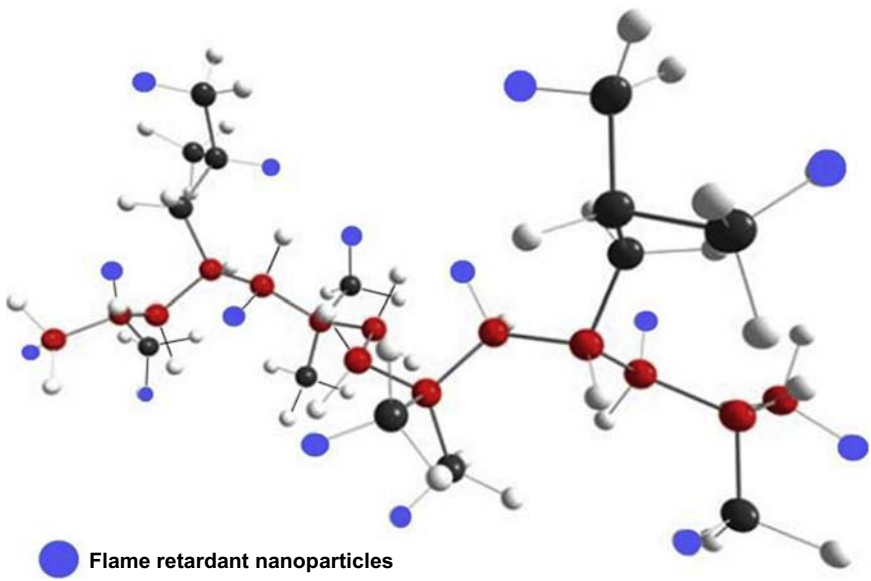

Figure 14.5 Integrated flame retardant nanoparticles inside the polymer structure.

14.5 Case study

14.5.1 Fabrics

Aluminum hydroxide (1 μm particle size) was used as a coating layer of 4 mm thickness to increase the fire retardancy of an advanced composite material consisting of polyvinyl chloride reinforced with a woven roving (45°/0°) of carbon fibers.

14.5.2 Specimen fabrication

A specimen for a thermal erosion test had a square shape, with dimensions 100 × 100 × 10 mm. These specimens consisted of two layers, a fire retardant material layer with 4 mm thickness and a composite material layer with 6 mm thickness.

14.5.3 Thermal erosion test

A butane–propane flame torch was used in this test. The system (containing fire retardant fabric and composite material) was exposed to this flame at various exposure distances (10, 15, 20 mm). Table 14.1 shows the temperature of flame used in this case study.

14.5.4 Calculated heat transition

The surface temperature method was used to calculate the amount of heat transmitted through a fire retardant material and a composite material. A transformation card (AD), named the Thermal Monitoring and Recording System (see Fig. 14.6), was used to observe and save temperatures with regard to time (in seconds).

14.5.5 Results obtained

In Fig. 14.7 curve 1 represents the thermal erosion test for the composite material with retardant surface layer at an exposure distance of 10 mm. The temperature of the surface opposite the torch begins to increase with increasing the time of exposure to the flame. Aluminum hydroxide will form a glassy char at high temperatures that prevents flame propagation. It also releases water of hydration from its chemical structure. Therefore, the substrate (composite material) will be protected and the spread of fire will decrease. The improvement in flame retardancy increases with increased exposure distance to 15 mm, as shown in Fig. 14.7, curve 2 [31–36].

Table 14.1 Temperature of flame

Gas	Symbol	Temperature, °C
Butane–propane	C_3H_8–C_4H_{10}	2000

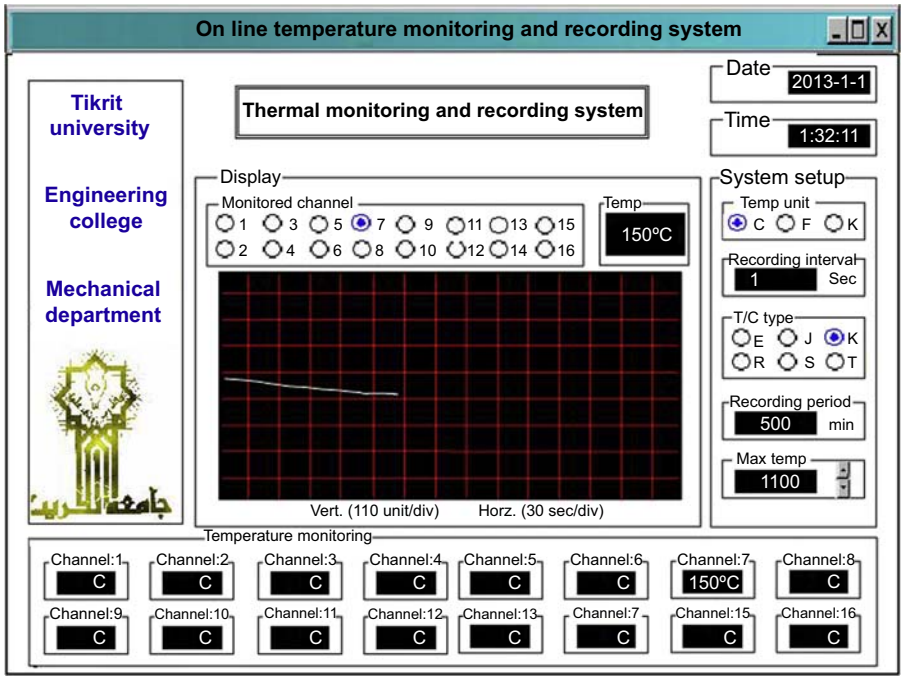

Figure 14.6 Thermal monitoring and transcription scheme.

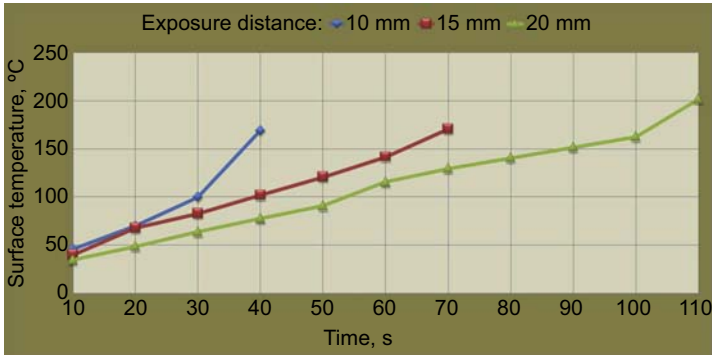

Figure 14.7 Thermal erosion test.

As a result, when the exposure distance from the flame increased to 15 mm, the time necessary to break down the fire retardant layer increased and the combustion gases were reduced, and less plastic was burned owing to the water of hydration and the protected glassy coating layer from the aluminum hydroxide.

Fig. 14.7, curve 3, represents the thermal erosion test for the composite material with retardant surface layer at an exposure distance of 20 mm, at which distance the time of breakdown for the aluminum hydroxide layer and substrate composite material

is increased. The figure shows good results obtained at the longest exposure distance (20 mm) [37−40].

14.6 Conclusions

This review on flame retardants presents the various groups of flame retardants (inorganic, organic phosphorus, nitrogen-containing, and halogenated organic) and various methods of adding these materials (additive, reactive, and combination). As well, this review shows the methods of action of flame retardants and a future vision for applying retardants to composite fabrics.

References

[1] Al-Mosawi AI. Study uses of antimony trioxide material as a flame retardant material [M.Sc. thesis]. Iraq: Materials Engineering, Engineering College, Babylon University; 2003.
[2] Al-Maamori M, Al-Mosawi A, Hashim A. Flame retardancy enhancement of hybrid composite material by using inorganic retardants. Mater Sci Appl 2011;2(8):1134−8.
[3] Troitzsch J. Plastics flammability handbook: principles, regulations, testing, and approval. 3rd ed. Hanser Verlag Publisher; 2004.
[4] Horrocks AR, Price D. Advances in fire retardant materials. Wood He Io Publishing in Materials; 2008.
[5] Al-Mosawi AI, Ahmed JK, Hussain HA. Evaluation flame retardancy of epoxy composite by using design of experiments. AMM 2012;186:156−60.
[6] Al-Mosawi AI. Hybrid fire retardants to increasing composting resistance for fibers-reinforced composites. Natl J Chem 2011;41:48−54.
[7] Velasquez K, Viani T. Capstone design project − flame retardants families. University of Oklahoma, Chemical Engineering; 2006.
[8] Levchik SV. Introduction to flame retardancy and polymer flammability. In: Morgan AB, Wilkie CA, editors. Flame retardant polymer nanocomposites. John Wiley & Sons; 2007. p. 1−29.
[9] Al-Mosawi AI, Amash HK, Al-Maamori MH, Hashim A. Increasing flammability resistance for aircraft tires by using magnesium hydroxide. Acad Res Int 2012;3(2):11−4.
[10] Matthew DW, Mark TW. Overview of flame retardants including magnesium hydroxide. Martin Marietta Magnesia Specialties LLC; 2000.
[11] Babrauskas V, Harris RH, Gann RG, Levin BC, Lee BT, Peacock RD, et al. Fire hazard comparison of fire retarded and non-fire-retarded products. July 1988. NBS Special Publication 749.
[12] Hilado CJ. Flammability handbook for plastics. 4th ed. Technomic Publishing Co; 1990.
[13] Green J. Influence of co-additives in phosphorus based flame retardant systems. Plast Compd May/June 1987;10(3):60−4.
[14] Hapuarachchi TD. Development and characterization of flame retardant nanoparticulate bio-based polymer composites [Ph.D. thesis]. School of Engineering and Materials Science, Queen Mary University of London; 2010.
[15] Kandola BK, et al. Empirical and numerical approach for optimization of fire and mechanical performance in fire-retardant glass-reinforced epoxy composites. Fire Saf J 2008; 43(1):11−23.

[16] Zhao C-S, et al. A novel halogen-free flame retardant for glass-fiber-reinforced poly (ethylene terephthalate). Polym Degrad Stab 2008;93(6):1188−93.
[17] Giu dice CA, Benitez JC. Zinc borates as flame retardant pigments in chlorine-containing coatings. Prog Org Coatings 2001;42:82−8.
[18] Al-Mosawi AI, Abbas AJ, Mushtaq TA. Experimental study of the effect of zinc borate on flame retardancy of carbon- kevlar hybrid fibers reinforced composite materials. Al-Qadisiya J Eng Sci 2008;1(1):126−32.
[19] Formicola C, De Fenzo A, Zarrelli M, France A, Giordano M, Camino G. Synergistic effects of zinc borate and aluminum trihydroxide on the flammability behavior of aerospace epoxy system. Express Polym Lett 2009;3(6):376−84.
[20] Horrocks AR, Price D. Fire retardant materials. Taylor and Francis Group, LLC; 2010.
[21] Al-Mosawi AI, Abbas SJ, Flayah Sh. Influence of retardant agent on flame spread through composite surface. Int J Innovative Res Eng Sci December 2012;6(1):13−6.
[22] Le Bras M, Wilkie CA, Bourbigot S, Duquesne S, Jama C. Fire retardancy of polymers new applications of mineral fillers. UK: The Royal Society of Chemistry; 2005.
[23] Al-Mosawi AI. Formation hybrid flame retardant and its effect on thermal resistance of polyvinyl chloride (PVC) composite. Acad Res Int 2012;3(2):66−9.
[24] Al-Mosawi AI. Performance evaluation of zinc borate to improved thermal properties of antimony trioxide at elevated temperatures. In: The Iraqi journal of mechanical and material engineering, special issue for 2nd scientific conference, engineering college. Iraq: Babylon University; 24−25 March 2010.
[25] Al-Mosawi AI. Effect of compilation between two types of inorganic flame retardants on thermal resistance for advanced composite material at elevated temperatures. In: Proceedings of 5th scientific conference, college of science. Iraq: Babylon University; 2010.
[26] Al-Mosawi AI. Effect of the antimony tetroxide on flame retardancy for advanced polymeric composite material, reinforced by hybrid fibers. In: Kerbala university journal, special issue for 6th scientific conferences. Iraq: Kerbala University; 1−2 May 2010.
[27] Al-Mosawi AI. Flame retardancy of polymers. LAP Lambert Academic Publishing; 2012. ISBN:25531 -659 -3-978.
[28] Myszak Jr EA, Sobus MT. New generation of inorganic colloids for flame retardancy and UV stabilization of polymers. Nyacol Nano Technologies, Inc.; 2000.
[29] Bromine Science and Environmental Forum. An introduction to brominated flame retardants. October 19, 2000.
[30] Bartlett J. Colloidal antimony pentoxide in flame retardant ABS. Fire Retardants Chemicals Association; 1997.
[31] Myszak EA. Use of submicro inorganic flame retardants in polymeric systemic. Nyacol Nano Technologies, Inc.; 2000.
[32] Tran HK, Johnson CE, Rasky DJ, Hui FCL. Phenolic Impregnated Carbon Ablators (PICA) as thermal protection systems for discovery missions. April 1997. NASA Technical Memorandum 110440.
[33] Brenner W, Lum D, Riley MW. High temperature plastics. Second printing. Reinhold Publishing; 1964.
[34] Al-Mosawi AI, Al-Zubadi AA, Al-Maamori MH. Increasing inhibition flame resistance for PVC composite by using $2ZnO.3B_2O_3.3.5H_2O$-Sb_2O_3 mixture. Topclass J Eng Mater Sci March 26 , 2014;1(1).
[35] Mouritz AP, Gibson AG. Fire properties of polymer composite materials. Springer; 2006.
[36] Egglestone GT, Turley DM. Flammability of GRP for use in ship superstructures. Fire Mater 1994;18.

[37] Carty P, White S. Char formation in polymer blends. Polymer 1994;35.
[38] Hornsby PR, Watson CL. A study of the mechanism of flame retardance and smoke suppression in polymers filled with magnesium hydroxide. Polym Degrad Stab 1990;30.
[39] Scudamore MJ. Fire performance studies on glass-reinforced plastic laminates. Fire Mater 1994;18.
[40] Brown SC, Herbert MJ. New developments in ATH technology and applications. In: Proceedings of flame retardants 92. London: Elsevier Applied Science; 1992.

This page intentionally left blank

Remanufacturing and whole-life costing of lightweight components

15

Y. Xu
Cranfield University, Bedfordshire, United Kingdom

J.F. Sanchez
Cranfield University, Bedfordshire, United Kingdom

J. Njuguna
Robert Gordon University, Aberdeen, United Kingdom

Lightweight components are becoming more preferred in the automotive industry owing to the benefit of lower fuel consumption they can bring. This chapter provides an introduction to remanufacturing and whole-life cost analysis for automotive components. The methods and processes adopted here can also be used for lightweight components in other industries and applications.

15.1 Product end of life

Products reaching the end-of-life (EoL) phase have several EoL options such as landfill, incineration, recycle, repair, remanufacturing, reuse or a combination of these. Traditionally EoL products have often been disposed of in landfills or sent to material recycling. However, nowadays more and more EoL products are being reused via different recovery means. Four alternative EoL options towards reuse, ie, repair, recondition, remanufacture and recycle, are illustrated in Fig. 15.1. Within the four EoL

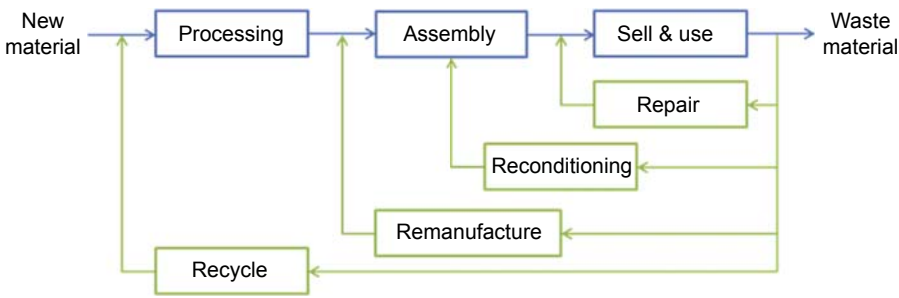

Figure 15.1 Product end-of-life options.
King AM, Burggess SC, Ijomah W, McMahon CA. Reducing waste: repair, recondition, remanufacture or recycle? Sust Dev 2006;14:257–267.

Lightweight Composite Structures in Transport. http://dx.doi.org/10.1016/B978-1-78242-325-6.00015-3

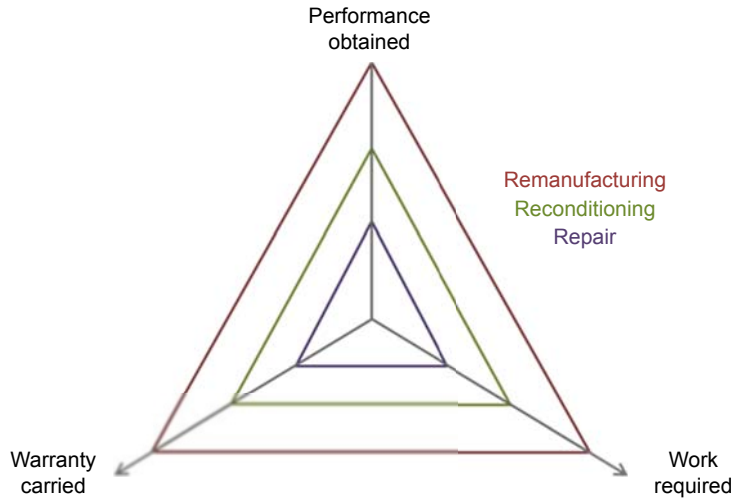

Figure 15.2 Hierarchy of product recovery options.
Adapted from Ijomah W, Childe S, McMahon C. Remanufacturing: a key strategy for sustainable development. In: Proceedings of the 3rd international conference on design and manufacture for sustainable development, 1−2 September 2004, Loughborough, UK; 2004.

options, the repair, recondition and remanufacture options represent "secondary market" processes, which differ from one another in terms of the work required, the performance obtained and the warranty carried, as depicted in Fig. 15.2. The repair option simply corrects specific faults in a product, while the recondition option usually improves the performance of the used products but does not return them to the original specifications [1]. The remanufacture option, on the other hand, improves the product performance to meet the original equipment manufacturer specifications and offers remanufactured products the same warranty as for new equivalent products.

In comparison to the above three EoL options towards reuse, the recycle option recovers value from the EoL products at the material level [3]. The original form of the product is destroyed and the materials are reprocessed (through chemical or physical reprocessing) so that the original or useful degraded materials are recovered [4]. These materials can be reused in the production of original parts if the quality of the materials is high, or reused in the production of other parts [5].

15.2 End of life of automotive components

The European Commission's ELV (end-of-life vehicle) directive encourages the reuse of components that are suitable for reuse, and encourages recycling of the materials from those components that are not suitable for reuse when environmentally viable [6].

In the automotive sector, material recycling has been the traditional EoL practice for automotive components. Other EoL options such as remanufacture account for only a small portion of vehicle recovery [7]. Original automotive manufacturers are not widely

engaged in these recovery methods owing to several obstacles: First, it is not easy to recover, as most EoL automotive components are not designed for recovery at the beginning [7]. Moreover, remanufacturers face more challenges in obtaining economic benefits from recovering and reusing components, as remanufacturing is carried out in low volumes because of the dramatically increased number of car models since 1995 [8]. In addition, the supply chain for remanufacture and reuse of components has significant inherent uncertainties in terms of the volume and condition of returned products and potential value that can be recovered [9]. Finally, recycling options are becoming economically more attractive owing to some emerging technologies used for materials recycling, such as the complex postshredder technology [10].

15.3 Remanufacturing process for end-of-life automotive components

The general remanufacturing process for EoL automotive components is shown in Fig. 15.3. The process includes disassembly of EoL products (called core), cleaning, reconditioning and replacement of components, reassembly and final testing.

The detailed remanufacturing process depends on the components. For example, for the crankshaft and thermoplastic composite oil pan as shown in Fig. 15.4,

Figure 15.3 Generic remanufacturing process.
Steinhilper R. Remanufacturing: the ultimate form of recycling, Fraunhofer IRB Verlag, Stuttgart; 1998.

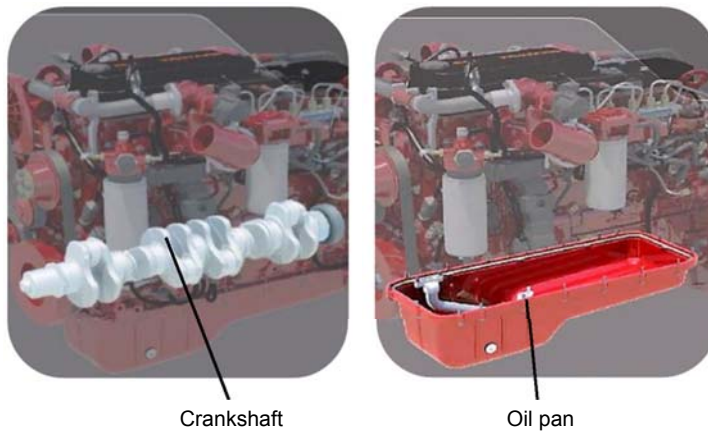

Figure 15.4 Examples of automotive components for remanufacture.
Xu Y, Sanchez JF, Njuguna J. Cost modelling to support optimised selection of End-of-Life options for automotive components. Int J Adv Manuf Technol 2014;73(1):399–407.

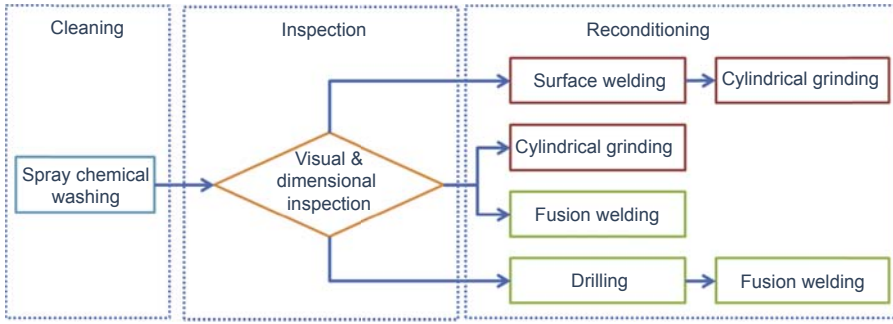

Figure 15.5 Remanufacturing process for automotive components.
Xu Y, Sanchez JF, Njuguna J. Cost modelling to support optimised selection of End-of-Life options for automotive components. Int J Adv Manuf Technol 2014;73(1):399−407.

their remanufacturing processes comprise three main phases: cleaning, inspection and reconditioning; the detailed process is shown in Fig. 15.5. Within the reconditioning phase, several remediation possibilities exist depending on the inspection results.

15.3.1 Cleaning phase

The technique for cleaning the two example components is the chemical spray technique. It involves the application of a pressurised cleaning solution (water plus detergent) to the components.

15.3.2 Inspection phase

For the crankshaft, visual inspection is used to detect superficial damage such as cracks, wear, corrosion or burns at the surface of the crankshaft journals [13]. Then, the diameter of the journals is gauged using portable measurement devices. The result of the inspection will determine the rectification solution to be adopted: (1) to rectify the damage by removing material and, therefore, reducing the size of the journal, without compromising the performance requirements, or (2) to rectify the damage by adding material to build up the desired dimension of the journal without compromising the performance requirements.

For the thermoplastic composite oil pan, its typical damage is perforation caused by low-velocity impacts [14]; visual inspection is used to detect the damage.

15.3.3 Reconditioning phase

For the crankshaft, the potential techniques for reconditioning include the following:

- Cylindrical grinding: This machining method removes damaged material from the journal using an abrasive wheel as the cutting tool.

- Surface welding: This material addition method deposits weld steel on the journal surface. In particular, the cold metal transfer (CMT) welding technique can be adopted. The main advantage of this technique is the reduced distortion resulting from significantly less heat transferred to the metals. A grinding operation is needed after the CMT welding operation to meet the surface roughness requirement.

For the oil pan, the potential reconditioning techniques include the following:

- Fusion welding: This involves heating and melting the material on the bond surfaces of the oil pan and the patch plug (additional material introduced into the damaged region) and then pressing together for solidification and consolidation. In particular, the ultrasonic welding technique, which uses high-frequency mechanical vibration to weld parts, can be adopted. A drilling operation may be required prior to the fusion welding to clear out the damage.

15.4 Whole-life cost

Cost is an important factor for business and sustainable development, especially the whole-life cost. Whole-life cost covers all the costs associated with a product, not only the product manufacturing cost, but also the cost of using and disposing of a product. The EoL cost becomes an important part of the whole-life cost. Selecting an appropriate EoL option can potentially reduce the whole-life cost. To do that, the cost–benefit needs to be analysed properly, and a reliable cost estimation methodology is needed.

15.4.1 Cost estimation process

A recommended cost estimation process is illustrated in Fig. 15.6, which was adapted from NASA Cost Estimating handbook [15]. The process comprises the following steps: understand cost estimation requirements, select cost estimation technique, develop cost breakdown structure (CBS), identify cost drivers, develop cost estimation relationships (CERs), collect data, implement cost model and validate the cost model.

15.4.2 Selecting the cost estimation technique

There are three main types of techniques for cost estimation: analogy-based costing, parametric costing, and bottom-up approach costing. Analogy-based costing basically estimates the cost of a product based on the known cost of similar products. Parametric costing is an approach to develop correlations between the cost and some attributes of the product or the process based on historical data. The bottom-up approach estimates the cost by analysing the cost constituents and causes of cost and develops the product cost based on the cost of its constituents. For the purpose of assessing the cost–benefit of the remanufacturing option versus the other EoL options for automotive components, the bottom-up approach, or more specifically the activity-based costing (ABC) technique, is recommended for the cost analysis. The ABC technique estimates the cost first by identifying the activities needed to remanufacture the components, second by identifying the resources needed for each activity and third by calculating the consumption of resources, so that the cost can be calculated.

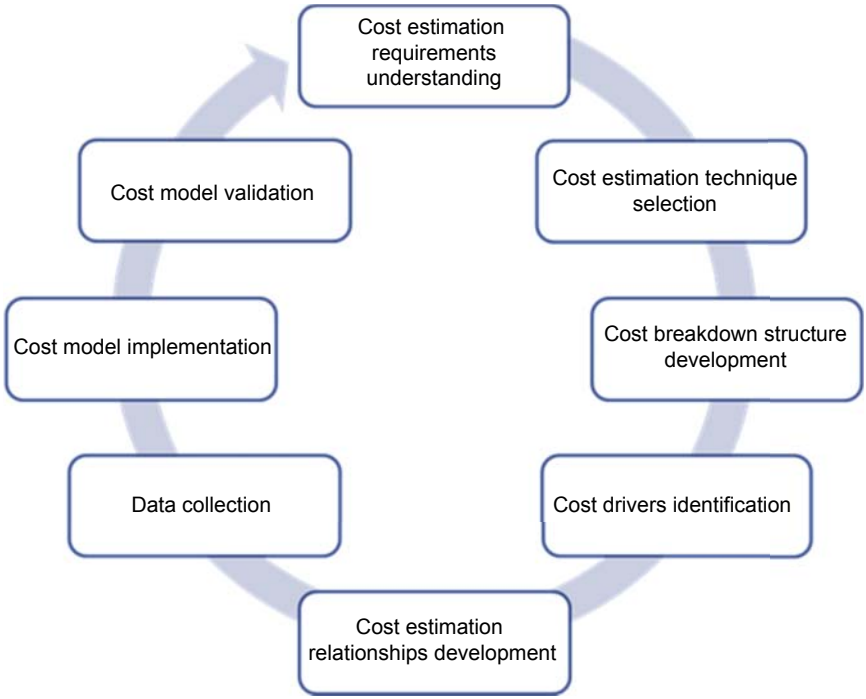

Figure 15.6 Cost estimation process.
Xu Y, Sanchez JF, Njuguna J. Cost modelling to support optimised selection of End-of-Life options for automotive components. Int J Adv Manuf Technol 2014;73(1):399–407.

15.4.3 Cost breakdown structure

Based on the remanufacturing process for the crankshaft and oil pan shown in Fig. 15.5, the main activities in the process can be identified. The main cost elements for each activity are then determined. The CBS developed for remanufacturing is shown in Fig. 15.7. As is illustrated in Fig. 15.7, for crankshaft and oil pan, the remanufacturing cost mainly includes labour cost, materials cost and machine cost (including depreciation, power and consumables cost etc.).

15.4.4 Cost drivers

Cost drivers are the main parameters/variables of activities or resources that affect the remanufacturing cost. The cost drivers can be identified based on specific knowledge from experts and open knowledge. As example, the main cost drivers for each activity and cost element in remanufacturing of the crankshaft and oil pan are given in Table 15.1.

15.4.5 Cost estimation relationships

In the CER each cost element is expressed as a function of the cost drivers. The CER can be developed for each cost element in the CBS using the identified cost drivers. For

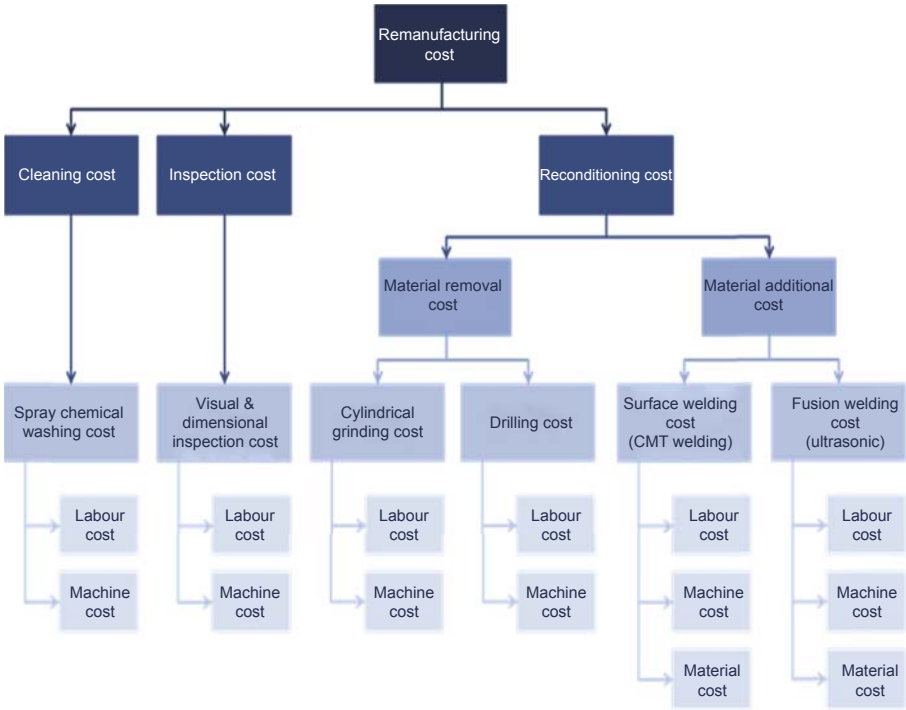

Figure 15.7 Cost breakdown structure for remanufacturing crankshaft.
Xu Y, Sanchez JF, Njuguna J. Cost modelling to support optimised selection of End-of-Life options for automotive components. Int J Adv Manuf Technol 2014;73(1):399–407.

Table 15.1 Examples of cost drivers for automotive crankshaft and oil pan

	Labour cost	Machine cost	Material cost
Cleaning	Surface area		–
Inspection	Surface area		–
Reconditioning	Initial journal diameter Final journal diameter Journal length Number of journals Oil pan thickness		

Xu Y, Sanchez JF, Njuguna J. Cost modelling to support optimised selection of End-of-Life options for automotive components. Int J Adv Manuf Technol 2014;73(1):399–407.

example, for the machine cost in crankshaft remanufacturing (adding materials by the welding technique), it can be calculated by the following process.

The direct machine cost is calculated by Eq. [15.1]:

$$C_{\mathrm{dm}} = (R_{\mathrm{power}} + R_{\mathrm{consum}}) \times t_{\mathrm{op}} \quad [15.1]$$

where C_{dm} is the direct machine cost, R_{power} is the power rate, R_{consum} is the consumables rate, and t_{op} is the operation time.

R_{power} and R_{consum} can be calculated by statistics based on the historical data; t_{op} is calculated by using Eq. [15.2]:

$$t_{\mathrm{op}} = \frac{V_{\mathrm{t}}}{R_{\mathrm{surf\_weld}}} \quad [15.2]$$

where V_{t} is the total volume to be deposited, and $R_{\mathrm{surf\_weld}}$ is the surface welding process rate.

$R_{\mathrm{surf\_weld}}$ is calculated by statistics based on the historical data, and V_{t} is calculated by Eq. [15.3]:

$$V_{\mathrm{t}} = \frac{V_{\mathrm{e}}}{E_{\mathrm{a}}} \quad [15.3]$$

where E_{a} is the material deposition efficiency (%), which measures the effectiveness of the welding deposition process; it represents the percentage of deposited material in all consumed material. V_{e} is the effective volume to be deposited and is calculated by Eq. [15.4] using the identified cost drivers final journal diameter and initial journal diameter:

$$V_{\mathrm{e}} = \frac{\pi \times l}{4} \times \left(d_{\mathrm{f}}^2 - d_{\mathrm{i}}^2\right) \quad [15.4]$$

where l is the journal length, d_{i} is the initial journal diameter, and d_{f} is the final journal diameter.

15.4.6 Cost model implementation and validation

The developed cost model can be implemented in a software platform, e.g., the MS Excel® platform, or a stand-alone software developed in other languages, e.g., C++, etc. The implemented cost model would enable a quick remanufacturing cost estimation so that the economic benefit can be analysed.

A developed cost model needs to be validated in terms of the cost estimating methodology, remanufacturing process, CBS, cost drivers and cost estimating relationships. If required data are available, the cost estimation result can be validated on different data sets. If the data are not available, face-to-face interviews with experienced experts are recommended; the confirmed data, methods and knowledge should be

documented, and improvement should be made based on the improvement feedback received from experts.

15.5 Optimising end-of-life cost

Using the developed cost estimation model, cost analysis can be done to identify the optimised EoL options for specific situations. For the purpose of comparing EoL options, data and results are normalised in the cost estimation model, and relative cost comparison between EoL options can be conducted. For example, for the crankshaft, Fig. 15.8 shows how the remanufacturing cost varies against the difference between final and initial journal diameter. Recycling cost is assumed consistent and estimated by considering only the crankshaft materials recovery. As can be seen from Fig. 15.8, the remanufacturing cost goes up as the difference between journal diameters increases; and a positive difference between the final and the initial journal diameter (material addition) leads to more costly remanufacturing than a negative difference (material removal). Also, if a positive diameter difference is greater than 4.5 mm, i.e., to add materials to more than 4.5 mm for reconditioning, recycling becomes more cost effective than remanufacturing.

For the oil pan, a cost analysis was conducted and results are presented in Fig. 15.9. Again, the recycling cost considers only the oil pan materials recovery. As can be seen in Fig. 15.9, as the oil pan thickness increases, the recycling cost increases faster than the remanufacturing cost does. In particular, when an oil pan thickness is greater than 2.5 mm, remanufacturing is more cost effective than recycling of the oil pan.

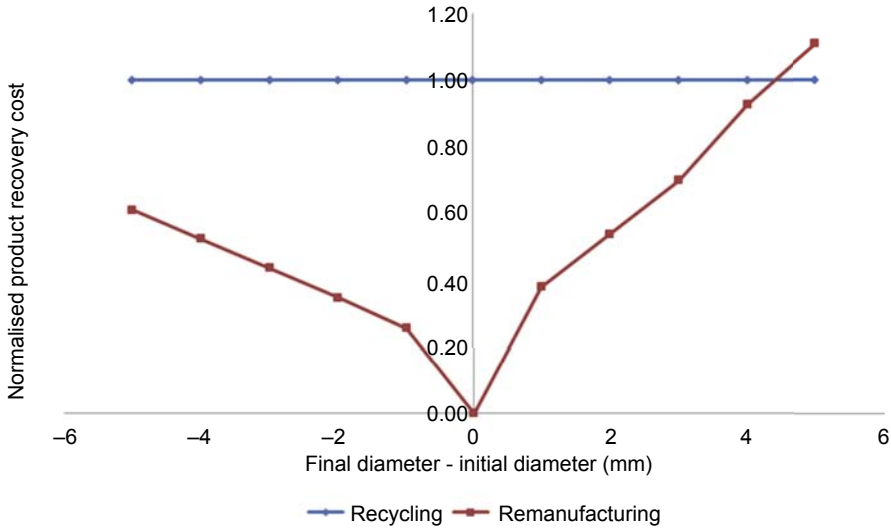

Figure 15.8 Diameter difference versus cost of EoL options.
Xu Y, Sanchez JF, Njuguna J. Cost modelling to support optimised selection of End-of-Life options for automotive components. Int J Adv Manuf Technol 2014;73(1):399–407.

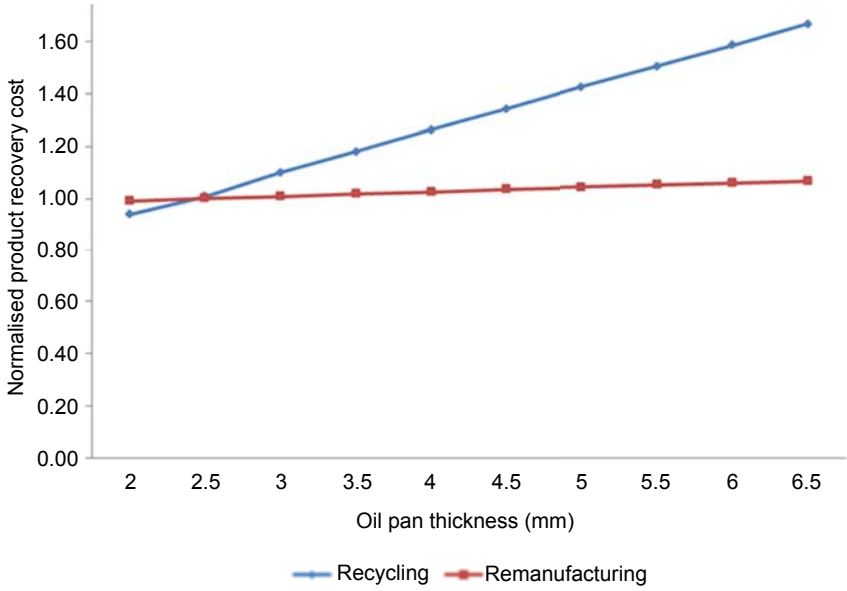

Figure 15.9 Oil pan thickness versus cost of end-of-life options.
Xu Y, Sanchez JF, Njuguna J. Cost modelling to support optimised selection of End-of-Life options for automotive components. Int J Adv Manuf Technol 2014;73(1):399−407.

15.6 Summary

Cost is an important factor for business and sustainable development, especially the whole-life cost. Whole life cost covers all the costs associated with a product, not only the product manufacturing cost, but also the cost of using and disposing of a product. The End-of-Life (EoL) cost becomes an important part of the whole-life cost, selecting an appropriate EoL option can potentially reduce the whole-life cost. Remanufacturing is an important End-of-Life option due to its potential benefit of keeping values embedded in products during manufacturing process. A typical remanufacturing process includes steps of disassembly, cleaning, reconditioning and replacement of components, reassembly and final testing. Whole life costing methodology is illustrated through an exemplar cost model assessing the cost effectiveness of various recovery alternatives for lightweight components in automotive industry. A whole-life cost model can be used to analyse the benefit of lightweight components in different applications.

References

[1] Ijomah W, Childe S, McMahon C. Remanufacturing: a key strategy for sustainable development. In: Proceedings of the 3rd international conference on design and manufacture for sustainable development, 1−2 September 2004, Loughborough, UK; 2004.
[2] King AM, Burggess SC, Ijomah W, McMahon CA. Reducing waste: repair, recondition, remanufacture or recycle? Sustain Dev 2006;14:257−67.

[3] Van Nunen J, Zuidwijk RA. E-enabled closed-loop supply chains. Calif Manag Rev 2004; 46(2):40−54.
[4] Ijomah W, Bennett JP, Pearce J. Remanufacturing: evidence of environmentally conscious business practice in the UK. In: Ecodesigń99 proceedings of the first international conference on environmentally conscious design and inverse manufacturing, 1−3 February; 1999. p. 192−6.
[5] Thierry M, Salomon M, Van Nunen J, Van Wassenhove L. Strategic issues in product recovery management. Calif Manag Rev 1995;37(2):114−35.
[6] Directive 2000/53/EC of the European parliament and of the council of 18 September 2000 on end-of life vehicles.
[7] Gerrard J, Kandlikar M. Is European end-of-life vehicle legislation living up to expectations? Assessing the impact of the ELV directive on green innovation and vehicle recovery. J Clean Prod 2007;15:17−27.
[8] Seitz MA, Peattie K. Meeting the closed-loop challenge: the case of remanufacturing. Calif Manag Rev 2004;46(2):74−89.
[9] Toffel MW. Strategic management of product recovery. Calif Manag Rev 2004;46(2): 120−41.
[10] Krikke HR, Blanc HM, van de Velde SL. Product modularity and the design of closed-loop supply chains. Calif Manag Rev 2004;46(2):23−39.
[11] Steinhilper R. Remanufacturing: the ultimate form of recycling. Stuttgart: Fraunhofer IRB Verlag; 1998.
[12] Xu Y, Sanchez JF, Njuguna J. Cost modelling to support optimised selection of End-of-Life options for automotive components. Int J Adv Manuf Technol 2014;73(1):399−407.
[13] Lam A, Sherwood M, Shu LH. FMEA-based design for remanufacture using automotive-remanufacturer data. In: SAE 2011 World Congress, March 2001, Detroit, MI, USA; 2001.
[14] Mouti Z, Westwood K, Kayvantash K, Njuguna J. Low velocity impact behavior of glass filled fiber-reinforced thermoplastic engine components. MDPI Mater 2010;3:2463−73.
[15] National Aeronautics and Space Administration (NASA). NASA cost estimating handbook. Washington DC: Cost Analysis Division, NASA Headquarters; 2002.

This page intentionally left blank

Polymer nanocomposite components: a case study on gears

16

S. Yousef
Akhbar Elyom Academy, Giza, Egypt

16.1 Polymer nanocomposites

16.1.1 Introduction

Polymer science was discovered at the end of the 17th century and at that time started a revolution in the sciences of sound recording, conductive polymers, irradiated polymers, and several other fields. Carbon, hydrogen, oxygen, and/or silicon are considered the main units of polymer structures. These units can be processed with heat and pressure into useful articles by using injection machines or presses. Currently, development in the engineering industries is moving quickly and the utilization rate of polymeric materials in many applications, such as biomedicine, automobiles, aircraft, vessels, and chemicals, is increasing. This is because polymeric materials have many advantages, such as being lighter, faster, quieter, more durable, and more cost effective than other products, and innovative designs increasingly include the use of high-performance plastics. Therefore, it has become necessary to develop these materials to keep pace with the progress in these industries through a new science, which was discovered at the end of the last century, called nanotechnology. Nanotechnology is the art, science, and technology of maneuvering matter on an atomic and molecular scale. The importance of this technology is that material properties change surprisingly at the nanometer scale (10^{-9} m) and the atoms begin to show unexpected properties that were not known before and that are not present in the parent material. This has led to minimization and reductions in the price of the devices, while providing operating power. Now this technology is ever expanding and has already covered several industrial applications like electronics, medicine, pharmaceuticals, cosmetics, food, textiles, ceramics, etc. The related field of polymer nanocomposites (PNCs) is discussed in this chapter. PNCs are defined as polymeric materials blended with nanomaterials (nanofiller materials), of which the nanofillers have at least one dimension of less than 100 nm. The nanofiller materials have a higher ratio of surface area to volume and this leads to rapid interaction and more mixing between the nanofiller and the polymeric material, thus improving the chemical and physical properties. Furthermore, several nanomaterials are used as nanofiller materials with polymers, such as carbon nanotubes (CNTs), graphene, and carbon nanofiber, to produce PNC materials that have good mechanical, thermal, electrical,

Lightweight Composite Structures in Transport. http://dx.doi.org/10.1016/B978-1-78242-325-6.00016-5

tribological, and thermal behavior. CNTs are considered one of the best nanofiller materials because of their high aspect ratio, light weight, high mechanical strength, good electrical and thermal conductivities, and excellent thermal and air stability. During the PNC synthesis process some problems have appeared, for example, how to blend nanofiller materials with polymers with uniform dispersion and also characterization procedures and measuring for PNC properties. All of these obstacles will be listed and discussed, with the optimum solutions given, in this part of this chapter.

16.1.2 Synthesis process

The PNC synthesis process consists of two phases (mixing or dispersion and compression). The mixing process is considered the critical point in the synthesis process, owing to several constraints, such as the high difference in density between polymer and nanomaterial, the fact that the raw material particles may be in powder or pellet form, and the viscosity. If the manufacturer is able to control these parameters a homogeneous PNC having a small standard division with distinctive characteristics can be produced; this can be achieved by using a variety of methods of dispersion.

16.1.2.1 Dispersion methods

Dispersion is a system in which particles of polymer and filler materials are dispersed in a continuous phase of different compositions. Sometimes facilitative materials are added during the mixing process (solvent) to decrease the viscosity of the base material and produce a uniform dispersion, but this not preferred because the solvent must be removed after the mixing process using annealing, additive materials, or other methods. The most common methods of dispersions are the following:

Mortar and pestle

A porcelain mortar and pestle set provides a simple way to crush and grind granules. Sometimes the mortar has a cover to keep the seeds in during the grinding process as shown in Fig. 16.1. For large granules is better to use a pestle that has a bigger surface area to speed up the grinding process. A mortar and pestle can be used in many places for grinding species, herbs, and medicine in the kitchen, lab, or pharmacy.

Figure 16.1 Various types of mortar and pestle.
http://www.yankodesign.com/2010/07/19/yd-store-offers-5-discount-on-the-orb-pestle-mortar-by-joseph-joseph/.

Hot plate and magnetic stir bar

A hot plate and magnetic stir bar are considered a combination unit used in heating and stirring simultaneously as shown in Fig. 16.2. The heat generated breaks the bonds between atoms and the stirring helps provide significant permeation. The hot plate has a magnetic plate, which is responsible for rotating the magnetic stir bar through the generated magnetic field. The magnetic stir bar is placed inside the required sample mix. The bar consists of two elements: an inside element manufactured from a magnetic material such as stainless steel and an outside element, usually made from Teflon as a coating material because it has a high melting temperature and can work in chemical surroundings.

Mechanical stirring

In this type of dispersion, the mixing processes depend on the twist torque and rotational speed of the spindle, as shown in Fig. 16.3. The end of the spindle is in contact with a metallic or polymer blade, which is responsible for mixing. Mechanical stirring is usually used in the preparation of paints and inks (liquid state).

Ultrasonic bath

In an ultrasonic bath, the PNC mixing process is conducted in a tank containing vibrating fluid, usually distilled water, as shown in Fig. 16.4. The source of vibration

Figure 16.2 (a) Hot plate and magnetic stir bar. (b) Stir bars in various sizes. (c) Stir bar construction.
http://reprap.org/wiki/Hot_plate_stirrer and http://www.stuart-equipment.com/product.asp?dsl=853.

Figure 16.3 Mechanical stirring components.
http://www.karkimya.com.tr/en_4_2_1_1_3_urunler_dispersiyon_laboratuvar_dissolver_dispermat_cv3.html.

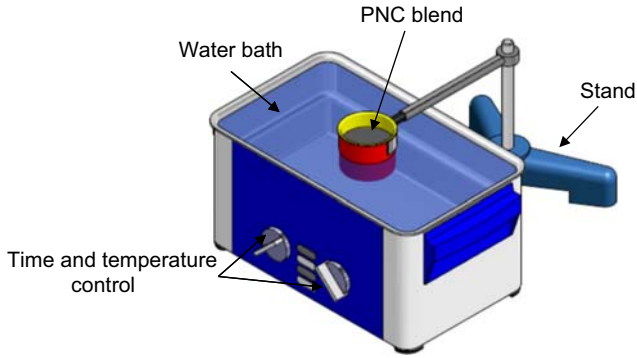

Figure 16.4 Schematic drawing of ultrasonic bath.
https://www.google.it/search?q=Mortar+and+pestle&;biw=1366&bih=659&tbm=isch&tbo=u&source=univ&sa=X&ei=AHa2VJyMJsGNaJLCgrgM&ved=0CCgQsAQ#tbm=isch&q=Ultrasonic+bath&imgdii=_&imgrc=o4DRRpkSqYFDVM%253A%3BSYaKmEVjlqYR2M%3Bhttp%253A%252F%252Fwww.keison.co.uk%252Fproducts%252Fgrantinstruments%252Fmxb.jpg%3Bhttp%253A%252F%252Fwww.keison.co.uk%252Fgrantinstruments_mxb.shtml%3B400%3B403.

is a high-frequency ultrasonic wave. Two factors contribute to the quality of dispersion: time and temperature. An ultrasonic bath can also be used for cleaning applications.

Ball milling

The ball milling process is used wherever the highest degree of fineness is required along with good mixing or dispersion. The mixing process is performed using various parameters: temperature, speed, duration, ball material (steel or zirconia), and type of working environment, such as hydrogen, argon, or vacuum atmosphere, as shown in Fig. 16.5.

Figure 16.5 (a) Ball milling apparatus and (b) balls.
http://www.azom.com/article.aspx?ArticleID=8402.

Twin-screw extrusion

Twin-screw extrusion or a MiniLab extruder now represents the best way to get PNCs with uniform dispersion under operating conditions. A MiniLab extruder can work with a small amount of raw materials and this is considered its most important feature, because most materials (polymer and nanomaterial) used are expensive. Also the rheological properties can be measured directly by it. A MiniLab extruder consists of three units: (1) a control unit to input data for the extruder (feeding time, melting temperature, rotational speed of the twin screw, and mixing time), (2) a feeding unit, and (3) a mixing apparatus, as shown in Fig. 16.6. If the polymer is in powder form, it must be ground with a nanofiller material using a mortar and pestle, and then the slurry will be suspended using a hot plate and magnetic stir bar or sonification bath for a certain time and at a certain temperature at constant rational speed to ensure the nanomaterial does not settle on the bottom. Then the slurry is placed in the hopper of the feeding unit to pass into the mixing unit and produce a PNC wire with a homogeneous dispersion. The MiniLab extruder has only one disadvantage, crystallinity of the resulting PNC after mixing slows, and this can lead to a decrease in its mechanical properties. Finally, there is another method of dispersion like the MiniLab extruder, called a blender, but it is not heavily used.

Samy Yousef (SY) dispersion technique

The use of the previously discussed methods of dispersion directly in thick PNC applications is difficult, because these methods are used to produce thin sheets, are expensive, and need a long time to prepare the final sample. Therefore it was necessary to find a new technique or a new modification to the traditional dispersion methods. Yousef [9] reported on an innovative SY dispersion technique in which a small amount of paraffin oil is added as a facilitative material to an abrasive nanomaterial with polymeric material after mixing by hand. The new method has been carried in a small extruder at Akhbar Elyom Academy, Egypt, which was designed particularly for this purpose using the materials polyoxymethylene (POM), CNTs, and paraffin oil at a melting temperature of 175°C, speed of 30 rpm, and time of 7 min, as shown in Fig. 16.7. Fig. 16.7(a) shows the transmission electron microscopy image of a CNT.

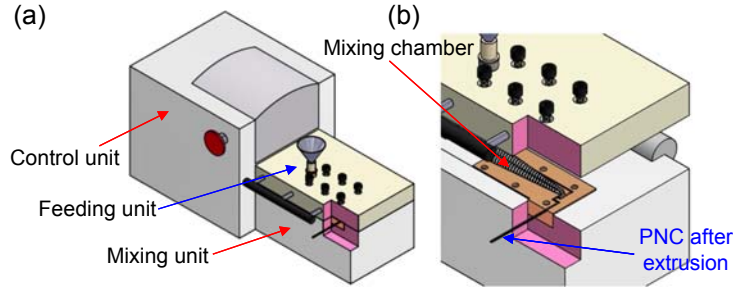

Figure 16.6 Schematic drawing of (a) MiniLab extruder and (b) mixing chamber. http://ifi.es/Productos/Thermo%20Scientific/Extrusoras/HAAKE/extrusoras_lab.html.

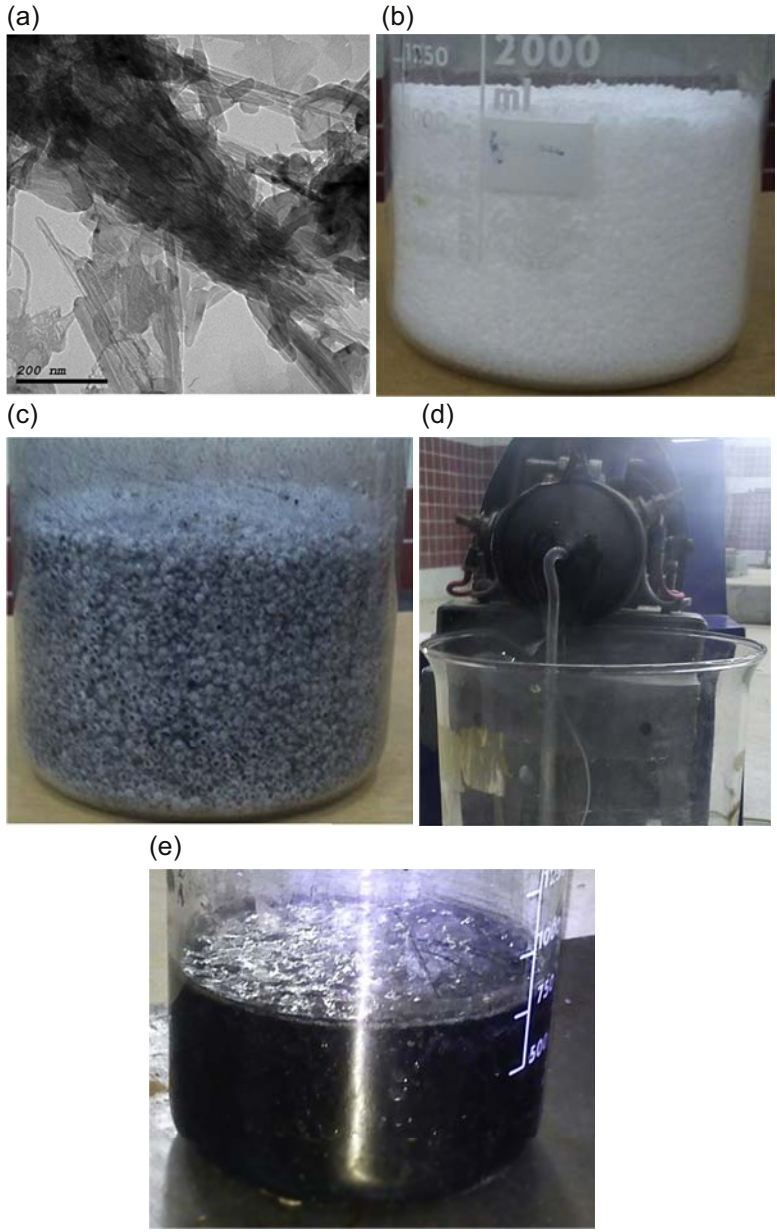

Figure 16.7 SY dispersion technique. (a) Transmission electron microscopy image of a carbon nanotube (CNT). (b) Polyoxymethylene (POM). (c) CNTs, POM, and paraffin oil after manual mix. (d) Small extruder. (e) CNT/POM nanocomposite synthesis.
S. Yousef, A. Khattab, T.A. Osman, M. Zak, Effects of increasing electrodes on CNTs yield synthesized by using arc-discharge technique, J. Nanomater. 2013 (2013) (392126) and S. Yousef, A. Khattab, M. Zak, T.A. Osman, Wear characterization of carbon nanotubes reinforced polymer gears, IEEE Trans. Nanotechnol. 12 (2013) 616−620.

The multiwall CNT type was produced by arc-discharge and its characterization is given in Section 16.2.2.1.

16.1.2.2 Compression moldes

After the slurry is prepared with homogeneous dispersion, the hot press is used to produce a thin sheet from the PNC as shown in Fig. 16.8. The quality of the resulting sheet depends on four parameters: temperature, pressure, compression time, and cooling rate. These factors change from one material to another to produce a uniform sheet thickness. This is performed only on PNC slurry that has been blended by using a mortar and pestle, hot plate and magnetic stir bar, ultrasonic bath, or ball milling. For slurry prepared by using a solvent, it is molded in a die, and the solvent must be extracted using other additives or heating depending on the reaction.

16.1.3 Characterizations

16.1.3.1 Scanning electron microscopy and high-resolution transmission electron microscopy

PNC synthesis is usually characterized using a scanning electron microscope (SEM) or high-resolution transmission electron microscope to observe the dispersion. However,

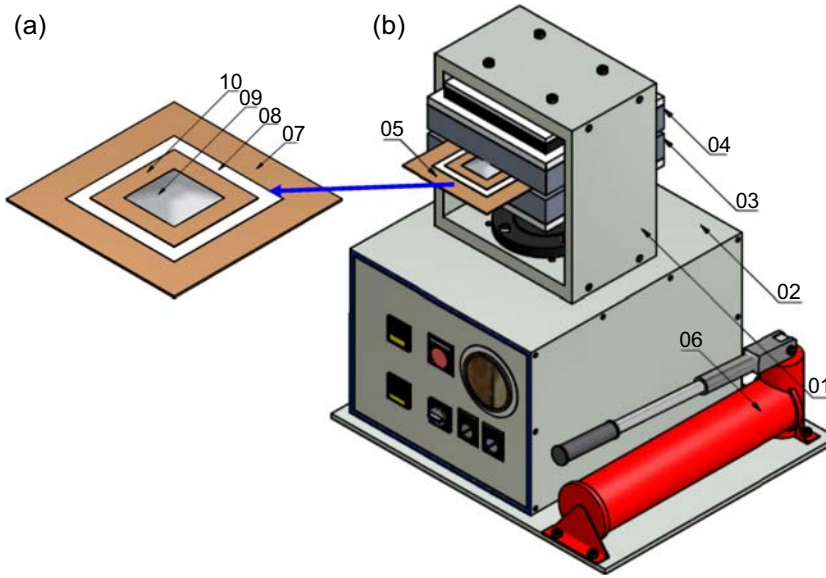

Figure 16.8 Schematic drawing of a compression mold. (1) Blended PNC base, (2) control unit, (3) upper hot plate, (4) lower hot plate, (5) die, (6) hydraulic unit, (7) die base, (8) Teflon sheet, (9) PNC blend, and (10) die cavity.
http://www.monstermarketplace.com/advanced-crystals-and-processing-equipment/25t-hydraulic-flat-hot-press-with-dual-temp-controller-up-to-250-eq-hp-88v110 and www.sufluc.com.

the SEM is preferred for some PNCs because the resulting image appears in three dimensions. The tested sample must be very thin and coated with gold, for example, because the high-resolution image magnifications need high voltage, which leads to increased temperature, which affects the surface quality of the PNC. Fig. 16.9(a) is an SEM image of multiwalled CNTs that were produced by chemical vapor deposition, with diameters in nanometers and lengths in micrometers, and the tubes look like bended pasta. Fig. 16.9(b) shows an SEM image of CNTs dispersed in polyamide (PA); the white points represent the CNTs, which have been dispersed uniformly inside the PA by using a twin-screw extruder.

16.1.3.2 Thermal analysis

A differential scanning calorimeter is used for the thermal analysis (crystallization temperature, glass transition temperature, and melting temperature) of PNC. The sample must be uniform and very thin. The tests can be conducted in a nitrogen atmosphere to prevent oxidation, with a heating rate of about 10°C per minute.

16.1.4 Nanopolymer properties

In this section, some properties of PNCs, such as tensile strength, friction and wear, rheology behavior, and impact resistance and energy absorption properties are discussed in terms of sample shape, the equipment used in the test, and test conditions.

16.1.4.1 Tensile strength

A universal testing machine is usually used to conduct tension tests on PNC standard specimens. A standard specimen is prepared according to American Society for Testing and Materials (ASTM) or any other standards using a flat (dog-bone shape) or circular shape as shown in Fig. 16.10. The minimum number of samples is five, from every percentage of nanofiller material, to calculate the standard division.

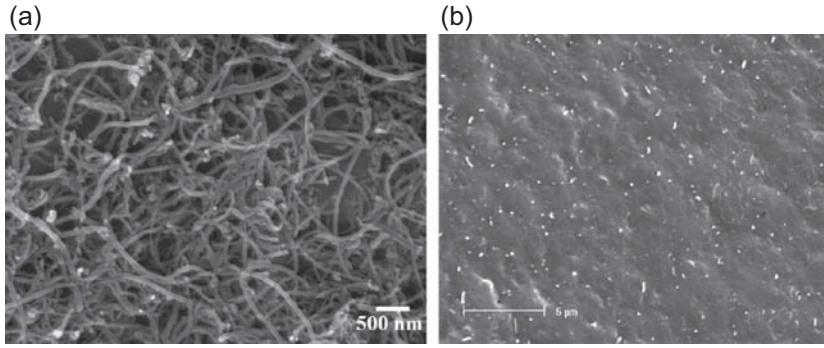

Figure 16.9 SEM images. (a) Carbon nanotubes (CNTs) and (b) polyamide/CNT composite. H. Meng, G.X. Sui, G.Y. Xie, R. Yang, Friction and wear behavior of carbon nanotubes reinforced polyamide 6 composites under dry sliding and water lubricated condition, Compos. Sci. Technol. 69 (2009) 606−611.

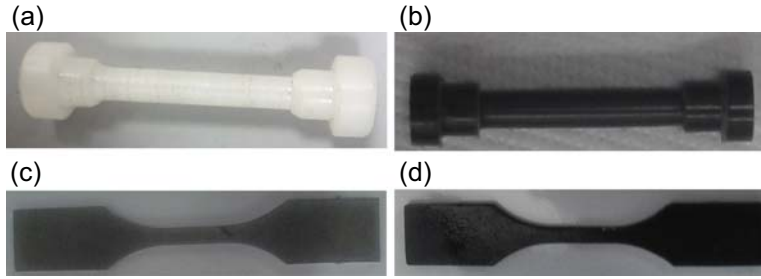

Figure 16.10 Photos of polymer nanocomposite tensile specimens. (a) Polyoxymethylene (POM) circular sample. (b) Carbon nanotube (CNT)/POM circular sample. (c,d) CNT/ultrahigh-molecular-weight polyethylene with different contents of CNT.
Samy Yousef, Annamaria Visco, Giovanna Galtieri, Davide Nocita, Improved wear resistance of UHMWPE based nanocomposites for prosthetic applications, filled with liquid paraffin and carbon nanofibers. INSTM Conference, Italy (2015). and S. Yousef, A. Khattab, M. Zak, T.A. Osman, Wear characterization of carbon nanotubes reinforced polymer gears, IEEE Trans. Nanotechnol. 12 (2013) 616–620.

Some PNCs have a greater ductility, so the test speed must be slow, about 50 mm/min, for example, while the sample length between benchmarks is 25 mm. Also the strength, Young's modulus work to break, and stiffness can be calculated directly from the machine. Generally, in ductile materials, elastic and plastic areas are clearer compared with brittle materials. Fig. 16.11 shows the stress–strain curves of CNT/ultrahigh-molecular-weight polyethylene (UHMWPE) and CNT/POM specimens. The CNT/UHMWPE specimen is more ductile so the yield strength in this case can be measured directly from the curve. But in the other case, the yield can be detected by shifting the inclined line by 0.03% at the strain axis. The point of intersection of the shifted line and the curve represents the yield strength. Also, a flexural or bending test for PNC can be carries out on a universal testing machine. Fig. 16.12 shows the flexural load–displacement curves of the CNT/POM specimens and the results show that the CNT addition improves the flexural properties of the PNC.

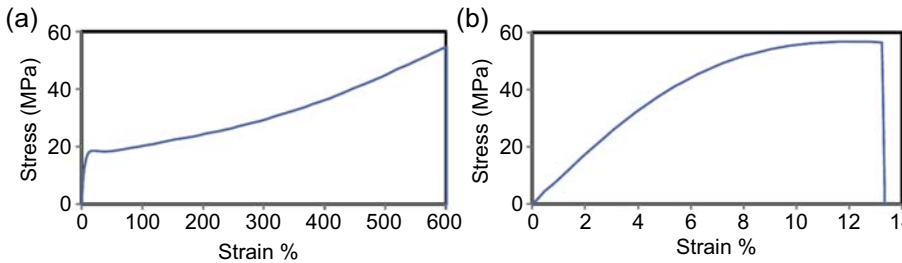

Figure 16.11 Stress–strain photos of (a) carbon nanotube (CNT)/ultrahigh-molecular-weight polyethylene and (b) CNT/polyoxymethylene.
Samy Yousef, Annamaria Visco, Giovanna Galtieri, Davide Nocita, Improved wear resistance of UHMWPE based nanocomposites for prosthetic applications, filled with liquid paraffin and carbon nanofibers. INSTM Conference, Italy (2015).

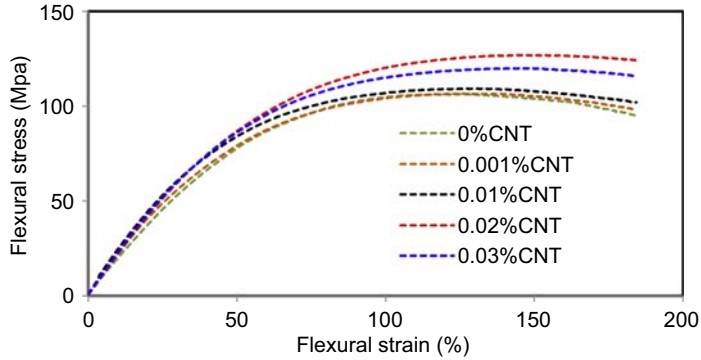

Figure 16.12 Flexural load–displacement curves of polyoxymethylene with different weights of carbon nanotube (CNT).
Samy Yousef, Annamaria Visco, Giovanna Galtieri, Davide Nocita, Improved wear resistance of UHMWPE based nanocomposites for prosthetic applications, filled with liquid paraffin and carbon nanofibers. INSTM Conference, Italy (2015).

16.1.4.2 Friction and wear behaviors

The relationship between the nanofiller material content and wear loss of PNC can be measured by pin-on-disc or ball-on-disc machines. Generally ball-on-disc is preferred in biomaterials applications (such as hip and shoulder replacements). A pin-on-disc test rig is usually used with hard polymeric materials such as PA, POM, and polyether ether ketone (PEEK). The samples' shape may be flat with small thickness or cylindrical as shown in Fig. 16.13. In the case of a flat sample, the sample is installed on the rotating disc against the stationary metallic pin, and the opposite in the case of cylindrical sample. Wear loss depends on four parameters: applied normal load, speed, test duration, and dry or wet environment. Generally the wear failure mechanism can examined by SEM and measured in three forms: (1) weight or mass loss, (2) wear rate, and (3) specific wear rate. Regarding the friction coefficient, it can be calculated from the equation $\mu = \mathrm{Fp/Ft}$, where Fp is the normal load and Ft represents the friction force that is measured directly by the machine.

16.1.4.3 Rheology behavior

This test is used to study the effects of nanofiller material type and concentration on the phase morphology and rheological properties of PNC synthesized using an advanced rheometrics system. Additionally, it measures their impact on the viscosity and storage modulus of the PNC. Fig. 16.14 shows CNT/POM disc samples with a diameter of 25 mm and a thickness of 1 mm. The samples were produced with different percentages of CNT. Frequently, the adding of materials in nano sizes or other have an effect on the linear viscoelastic results of polymer composites as shown in Fig. 16.15.

16.1.4.4 Impact resistance and energy absorption properties

A high-speed camera is used to record the impact event and study the effect of nanofiller on the impact resistance and energy absorption properties of a PNC.

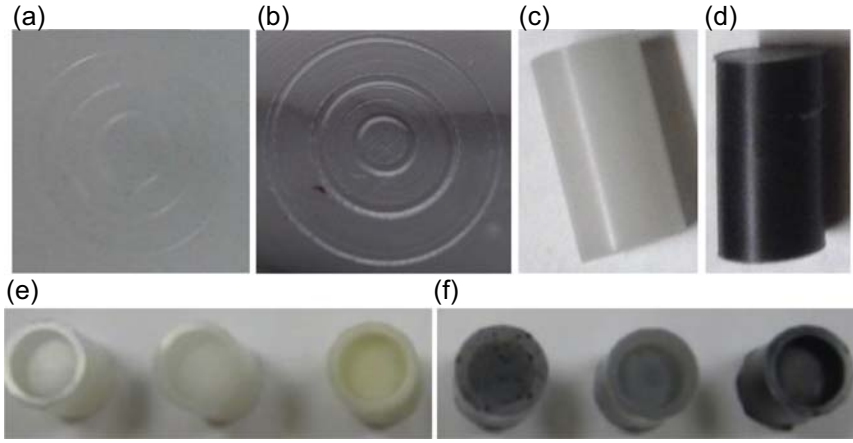

Figure 16.13 Photos of wear samples. (a) Polyoxymethylene (POM) flat sample with wear track. (b) Carbon nanotube (CNT)/POM flat sample with wear track. (c) POM bar sample. (d) CNT/POM bar sample. (e) Ultrahigh-molecular-weight polyethylene (UHMWPE) hollow cylinder sample. (f) CNT/UHMWPE hollow cylinder sample.
Samy Yousef, A. M. Visco, G. Galtieri and James Njuguna, Wear Characterizations of Polyoxymethylene (POM) reinforced with carbon nanotubes (POM/CNTs) using the paraffin oil dispersion technique. JOM-Springer 2015. http://dx.doi.org/10.1007/s11837-015-1674-3. and Y. Liu, S.K. Sinha, Wear performances and wear mechanism study of bulk UHMWPE composites with nacre and CNT fillers and PFPE overcoat, Wear 300 (2013) 44−54.

Figure 16.14 Rheology specimens prepared having 0, 0.001, 0.01, 0.02, and 0.03% wt carbon nanotube content.
Samy Yousef, Annamaria Visco, Giovanna Galtieri, Davide Nocita, Improved wear resistance of UHMWPE based nanocomposites for prosthetic applications, filled with liquid paraffin and carbon nanofibers. INSTM Conference, Italy (2015).

Also, the SEM is used to investigate the fracture surface. Crash and impact tests are conducted on a universal testing machine and a high-energy drop tower, respectively. The sample shapes may be a hollow cylinder or hollow semicone, as shown in Fig. 16.16. Some parameters must be taken in consideration during the tests, such as crosshead speed and load cell for the universal testing machine and impactor mass and velocity for the high-energy drop tower. Fig. 16.17 shows the force−displacement relationship for PA nanocomposites under a quasi-static load and dynamic conditions. PA nanocomposites were prepared using a twin-screw extruder and the results show that nanofiller (glass fiber, SiO_2, nano-clay (MMT), and glass spheres (GS)) in PA composites leads to an increase in the energy absorption capabilities of the structure.

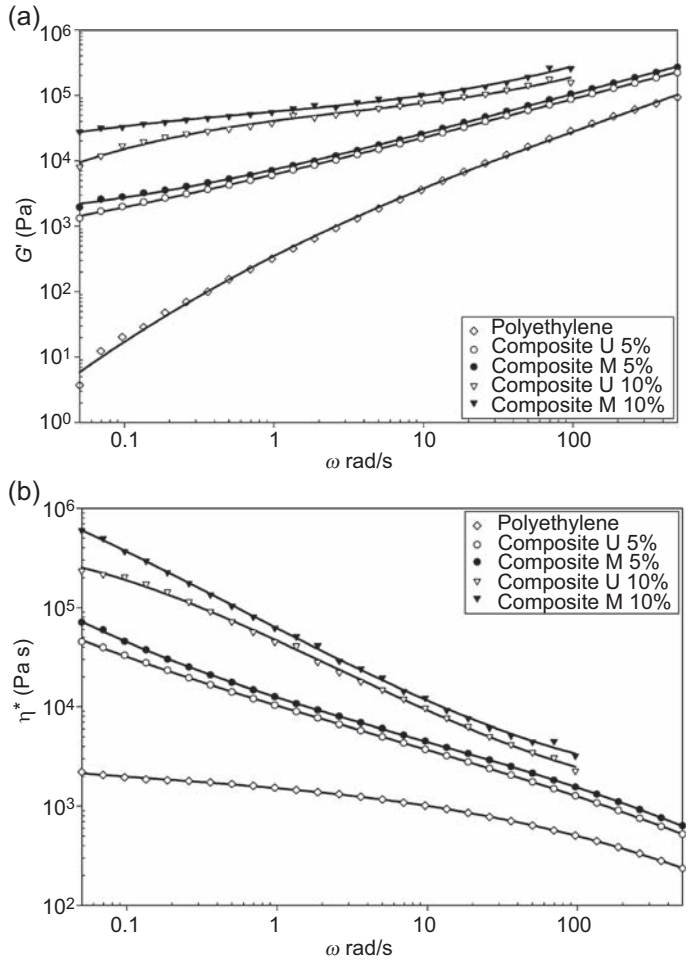

Figure 16.15 Linear viscoelastic results for polyethylene and Kevlar fiber/polyethylene composites. (a) Elastic modulus and (b) complex viscosity; U and M refer to unmodified and modified composites, respectively.
M. Rajabian, C. Dubois, M. Grmela, P.J. Carreau, Effects of polymer−fiber interactions on rheology and flow behavior of suspensions of semi-flexible fibers in polymeric liquids, Rheol. Acta 47 (2008) 701−717.

16.1.4.5 Summary

There are many methods of dispersion; ball milling and the MiniLab extruder are considered the better. Nonetheless, these two methods have some disadvantages. For ball milling these are: (1) Some nanomaterials like CNTs have a cylindrical shape with diameters in nanometers and lengths in micrometers, and during the

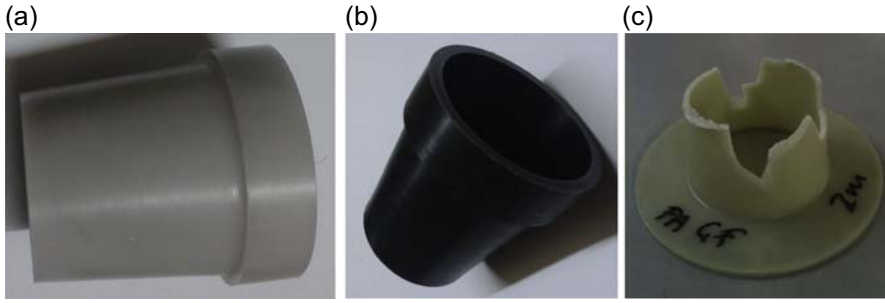

Figure 16.16 Tested samples. (a) Polyoxymethylene (POM), (b) carbon nanotube/POM, and (c) polyamide/glass fiber after testing.
F. Silva, J. Njuguna, S. Sachse, K. Pielichowski, A. Leszczynska, M. Giacomelli, The influence of multiscale fillers reinforcement into impact resistance and energy absorption properties of polyamide 6 and polypropylene nanocomposite structures, Mater. Design 50 (2013) 244−252 and S. Yousef, J. Njuguna (under research).

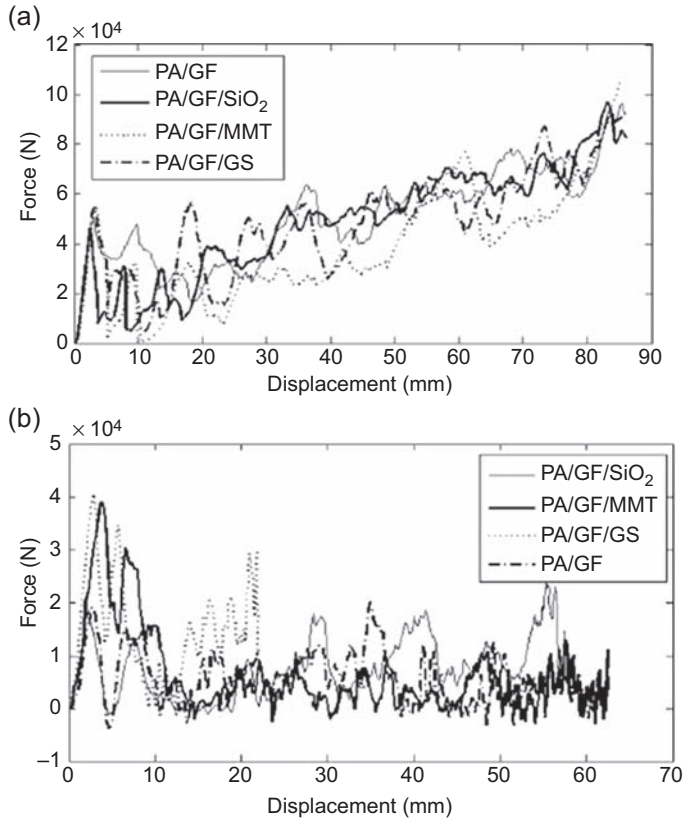

Figure 16.17 Load−displacement curves. (a) Static and (b) dynamic. *PA*, polyamide, *GF*, glass fiber.

mixing process the tubes have been broken by hard balls; furthermore the aspect ratio is decreased and some applications, such as electrical applications, need a higher aspect ratio for good electrical conductivity. (2) It takes a long time to obtain a uniform dispersion, sometimes as much as 80 h. A problem for the MiniLab extruder is that the crystallinity of PNC is decreased after the mixing process, and taking into account that the blended PNC will be compressed by the hot press to produce the final shape, the crystallinity will decrease again, thus hurting the final properties of the PNC. So it was necessary for Yousef [9] to devise the SY dispersion technique, which has the advantages of being cheap, saving time, and furthermore accomplishing the mixing and melting process in one step. So we recommend using this technique in the future.

16.2 Polymer nanocomposite carbon nanotube/polyoxymethylene gears case study

16.2.1 Introduction

The rate of fuel consumption in cars is the most important factor in determining the price. So the leading companies in the automotive industry are moving to optimize the rate of consumption by replacing metallic parts with polymeric materials, but the main problem is that polymeric materials have low strength. At the beginning of this century, many researchers tried to involve nanotechnology in polymeric materials to increase the strength so as to be able to use PNCs in mechanical engineering and automotive applications, but the desired results were not obtained, because most of the previous methods of dispersion produce thin elements and it is difficult to use these in heavy duty applications. Now this is become a realistic, since Yousef [9] developed the SY dispersion technique. This section will present a detailed explanation of some future applications in the automotive industry, in particular PNC gear production and characterization.

16.2.2 Synthesis of nanocomposite polymer gears

Polymer gears have been produced through previous research by direct injection molding, for which the shrinkage factor for polymeric materials can be calculated easily to produce a polymer gear with uniformly sectioned rims and flanges. The shrinkage factor is considered the critical point in the injection molding process for polymer gears; if it is not correct, the final involute of gear teeth will be changed and this can lead to a backlash between the meshing driver and the driven gears teeth, which will increase with time, and thus the power transition and performance of the system will decrease. In contrast, for the synthesis of PNC several properties have not been clear until now, in particular, shrinkage after the solidification process. To avoid that, Yousef [9, 20] produced PNC gears through the following steps.

16.2.2.1 Materials

The POM used in this study was from a commercial-grade powder (KOCETAL® K700) supplied by El-Slam Company, Cairo, Egypt. The CNTs were synthesized using a fully automatic machine via the arc-discharge multielectrode technique. The synthesized CNTs had an average diameter of 10 nm and an average length of 2.5 μm. The CNT contents were 1 and 0.02% wt [8,19].

16.2.2.2 Synthesis of polymer nanocomposites

Two injection-molded dies were designed and manufactured to synthesize short PNC bars with diameter of 45 mm and length of 80 mm and flanges with a diameter of 134 mm and a thickness of 29 mm after shrinkage as shown in Figs. 16.18 and 16.19. The SY dispersion technique was used to obtain a uniform distribution of CNTs inside POM. The following steps were followed for the production of the flanges and short bars;

1. The CNTs/POM pellets were poured or fed into a 400-g-capacity hopper.
2. An electric heater increased the mixing chamber temperature to 175°C.
3. When 175°C was reached, a screw thread began to rotate to push the melted granules along the heater.
4. The liquid was injected into the molded die to form the flange or short bar and then cooled to produce the final shape.

After the injection process, an SEM was used to qualitatively assess the dispersion of CNTs throughout the composite material. Fig. 16.20 shows the SEM images of CNT dispersion in the POM polymer and reveals that there was fairly excellent CNT homogeneous dispersion and strong cross-linking. It is worth mentioning, that the white areas represent the limitations of the CNTs.

16.2.2.3 Manufacturing of the gears

Hobbing and milling machines were used to fabricate the teeth of the PNC gears (spur, helical, bevel, and wheel) from the resulting PNC flanges and short bars. During the first attempt to produce PNC spur gears various defects appeared, such as the synthesis flanges had a perfect outer surface as far as quality and dispersion, but during the machining process to produce the teeth of the gears, some bubbles and unmelted pellets appeared in the PNC products. After several attempts it was found that these defects can be avoided by using injection-molding machines that contain a special feeding screw. This screw contains an air exit to eliminate the air inside the polymer pellets and the mixing chamber to prevent bubble formation. Regarding unmelted pellets, the PNC mixture was left inside the heating chamber long enough to ensure proper melting. Figs. 16.21 and 16.22 show PNC gears that were produced after several attempts. Metal sleeves were fitted in the hubs of all the gears to prevent contact between the key and the hub (metal to polymer contact), as shown in Figs. 16.21 and 16.22, which may lead to increased wear and inaccurate results.

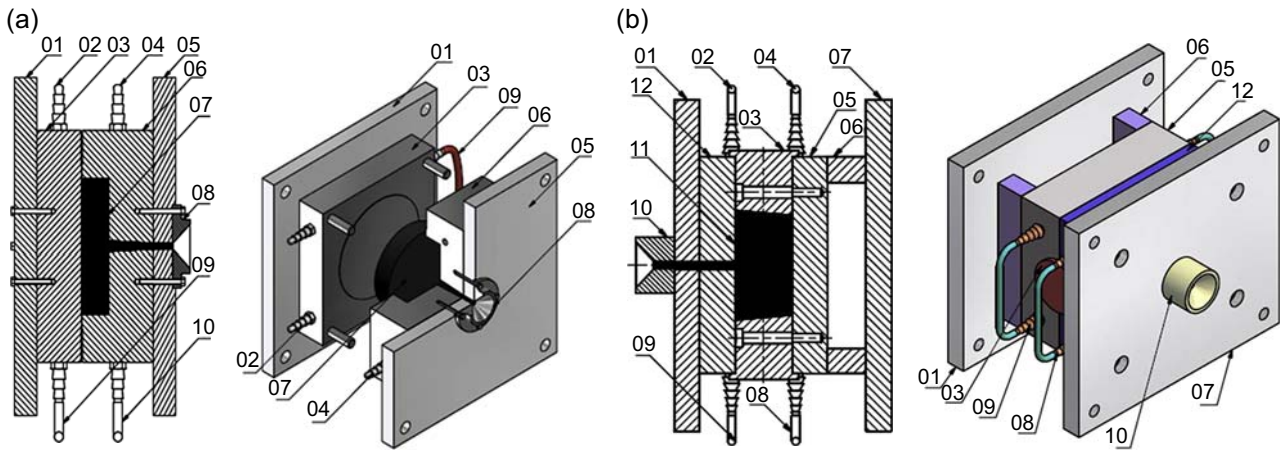

Figure 16.18 Die design. (a) Schematic drawings of the short bar injection die. (b) A final produced acetal short bar. (01) Supported movable die. (02, 04) cooling water exits and inlets. (03) Movable die. (05) Supported fixed die. (06) Fixed die. (07) Injected flange. (08) Die support with extruder head.

S. Yousef, A. Khattab, M. Zak, T.A. Osman, Wear characterization of carbon nanotubes reinforced polymer gears, IEEE Trans. Nanotechnol. 12 (2013) 616−620 and S. Yousef, T.A. Osman, A.H. Abdalla, G.A. Zohdy, Wear characterization of carbon nanotubes reinforced acetal Spur, helical, bevel and worm gears using a TS universal test rig, JOM (2014). http://dx.doi.org/10.1007/s11837-014-1268-5.

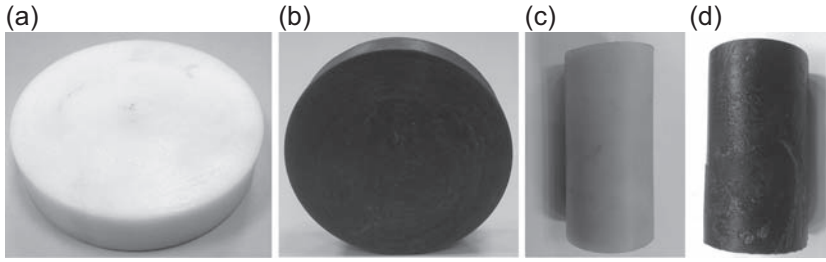

Figure 16.19 Resulting flanges and short bars. (a) Polyoxymethylene (POM) flange. (b) Carbon nanotube (CNT)/POM flange. (c) POM short bar. (d) CNT/POM short bar.
S. Yousef, A. Khattab, M. Zak, T.A. Osman, Wear characterization of carbon nanotubes reinforced polymer gears, IEEE Trans. Nanotechnol. 12 (2013) 616−620 and S. Yousef, T.A. Osman, A.H. Abdalla, G.A. Zohdy, Wear characterization of carbon nanotubes reinforced acetal Spur, helical, bevel and worm gears using a TS universal test rig, JOM (2014). http://dx.doi.org/10.1007/s11837-014-1268-5.

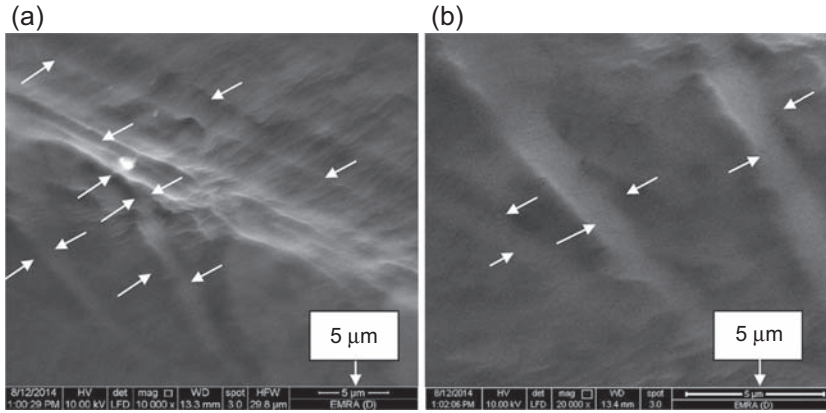

Figure 16.20 SEM images of (a) carbon nanotube (CNT)/polyoxymethylene (POM) flanges and (b) CNT/POM short bars that were produced.
S. Yousef, T.A. Osman, A.H. Abdalla, G.A. Zohdy, Wear characterization of carbon nanotubes reinforced acetal Spur, helical, bevel and worm gears using a TS universal test rig, JOM (2014). http://dx.doi.org/10.1007/s11837-014-1268-5.

16.2.3 Gear testing

In this section the test rigs that were used to investigate PNC gear characteristics are listed from their respective references. Several gear test rigs were designed and built to measure wear, friction, and thermal characteristics and additionally the noise emissions from them, starting from Mao [44] to Yousef [20]. The test rigs were classified into two types according to the material type of the tested gears: nonmetallic (polymer and composite polymer) and PNC gears.

16.2.3.1 Nonmetallic gear test rigs

The basic difference between test rigs is the loading mechanism as illustrated in the following. The Mk I test rig is considered the first polymer gear test rig, designed

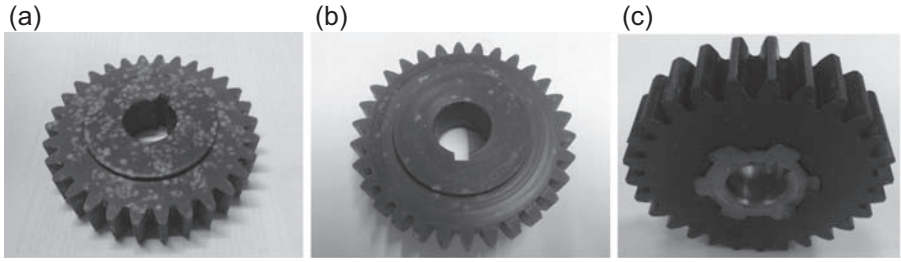

Figure 16.21 Spur gears were produced. (a) First attempt, (b) Yousef [9], and (c) Yousef [20]. S. Yousef, A. Khattab, M. Zak, T.A. Osman, Wear characterization of carbon nanotubes reinforced polymer gears, IEEE Trans. Nanotechnol. 12 (2013) 616−620 and S. Yousef, T.A. Osman, A.H. Abdalla, G.A. Zohdy, Wear characterization of carbon nanotubes reinforced acetal Spur, helical, bevel and worm gears using a TS universal test rig, JOM (2014). http://dx.doi.org/10.1007/s11837-014-1268-5.

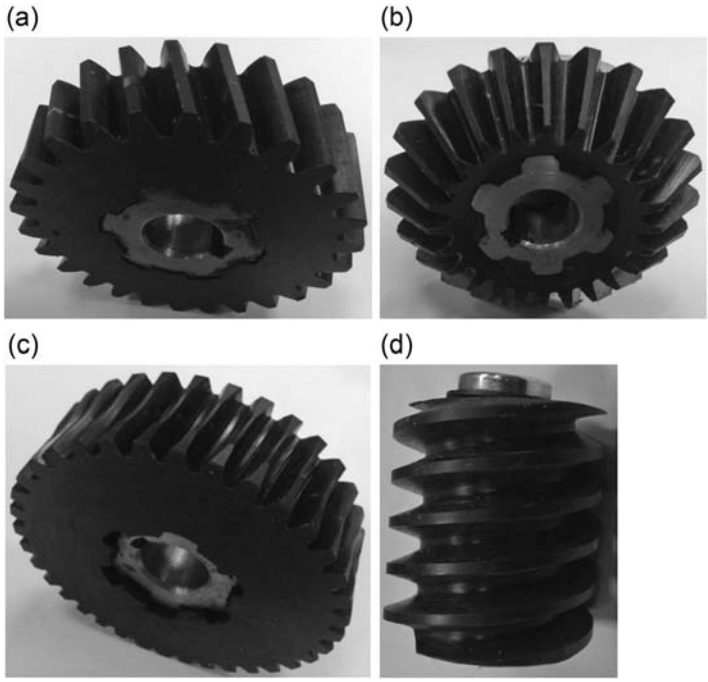

Figure 16.22 Gears were produced. (a) Carbon nanotube (CNT)/acetal helical gear, (b) CNT/acetal bevel gear, (c) CNT/acetal wheel gear, and (d) CNT/acetal worm gear.
S. Yousef, A. Khattab, M. Zak, T.A. Osman, Wear characterization of carbon nanotubes reinforced polymer gears, IEEE Trans. Nanotechnol. 12 (2013) 616−620 and S. Yousef, T.A. Osman, A.H. Abdalla, G.A. Zohdy, Wear characterization of carbon nanotubes reinforced acetal Spur, helical, bevel and worm gears using a TS universal test rig, JOM (2014). http://dx.doi.org/10.1007/s11837-014-1268-5.

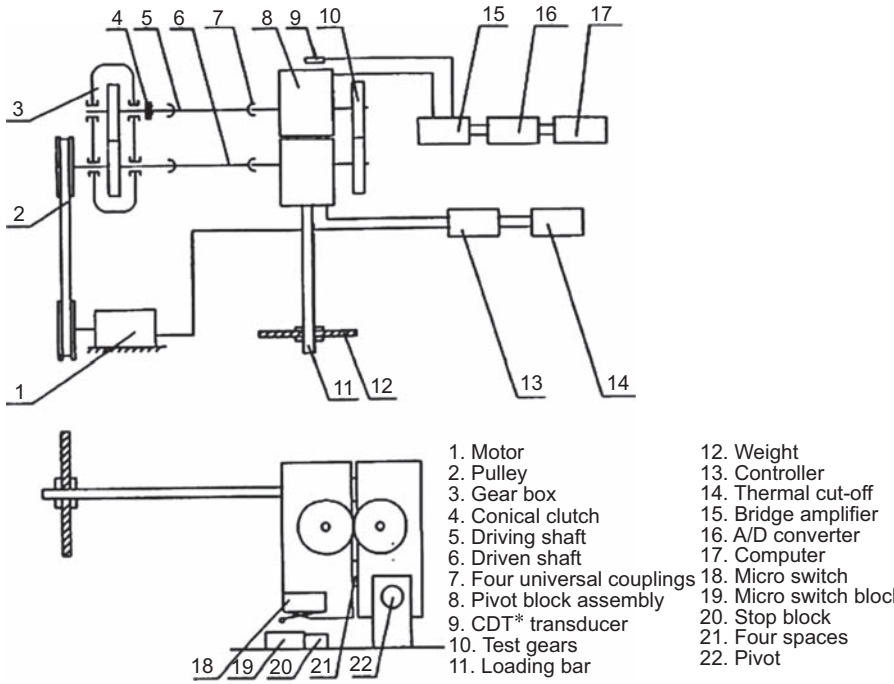

Figure 16.23 A schematic of the Mk I test rig.
A.R. Breeds, S.N. Kukurek, K. Mao, D. Waltonb, C.J. Hooke, Wear behaviour of acetal gear pairs, Wear 166 (1993) 85−91 and N.A. Wright, S.N. Kukurek, Wear testing and measurement techniques for polymer composite gears, Wear 251 (2001) 1567−1578.

by Moa [45] and housed at the University of Birmingham, to measure endurance life and wear performance of polymer gear surfaces (mm/cycle) by applying additional friction on unreinforced and reinforced polymer gear materials, as shown in Fig. 16.23. During the test, external torque generated by a dead weight hanging on a load arm (lever) is applied to test gears and can be calculated by $T = WL/2$, where W is the weight and L is the arm length.

White (1999) built the Mk II to address some of the frailties of the Mk I and to make it more flexible as shown in Fig. 16.24. The applied external torque on the test gears results from an axial force generated by a dead weight hanging from a load arm mechanism that consists of a bell crank load arm, a piston, a cap, and a housing assembly. The open-loop test rig at the Océ research facility in Venlo, The Netherlands, was built to measure the traditional behavior of polymer gears as shown in Fig. 16.25, in addition to measuring advanced characteristics such as transmission errors, gear efficiencies, vibration, acoustics, and temperature continuously. The applied external torque on test gears is controlled by an advanced DSP type system, which can be set at various speeds and loads by means of optical encoders and a torque feedback loop. Fig. 16.26 shows the gear test apparatus developed by Kurokawa et al. [24] to

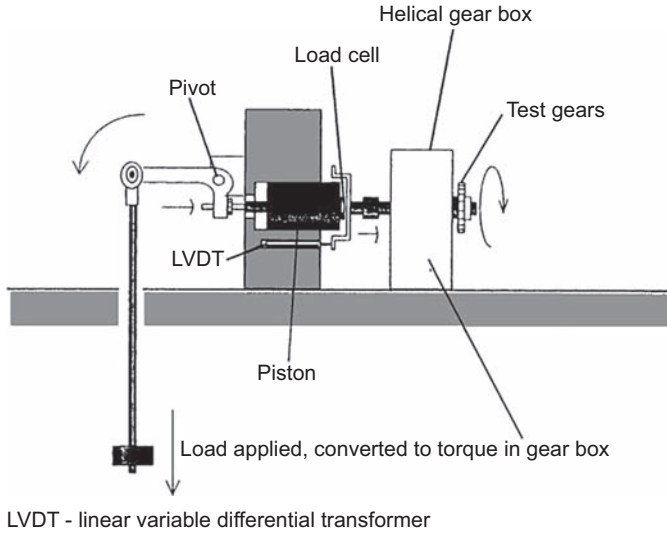

Figure 16.24 A schematic arrangement of the Mk II test rig.
N.A. Wright, S.N. Kukurek, Wear testing and measurement techniques for polymer composite gears, Wear 251 (2001) 1567−1578.

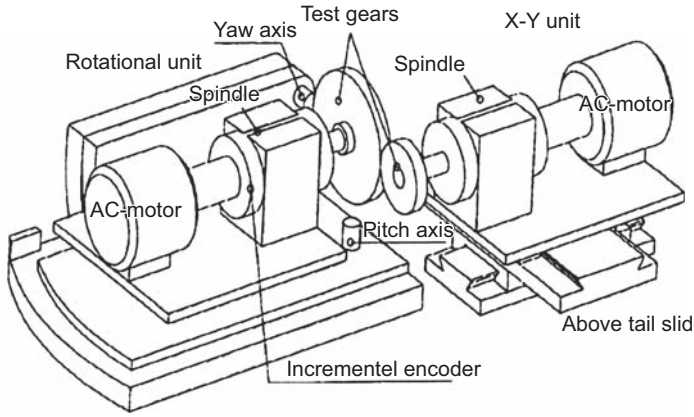

Figure 16.25 A schematic arrangement of the Océ test rig.
K.D. Dearn, An Investigation into Tribological and Performance Related Aspects of Polymeric Gearing (Ph.D. thesis), The University of Birmingham, 2008.

measure the wear performance of plastic gears. The load acting on the gear results from power absorption by means of a powder clutch/brake.

Senthilvelan et al. [25] developed a power absorption type gear test rig used for evaluating gear performance (noise and thermal performance). In this rig, the applied external torque on the test gears is established by a rheostat connected to the generator as shown in Fig. 16.27. Kim [26] at the Tribology Research Center, Korea Institute of Science and Technology, built and designed a test rig (power-circulating type) to

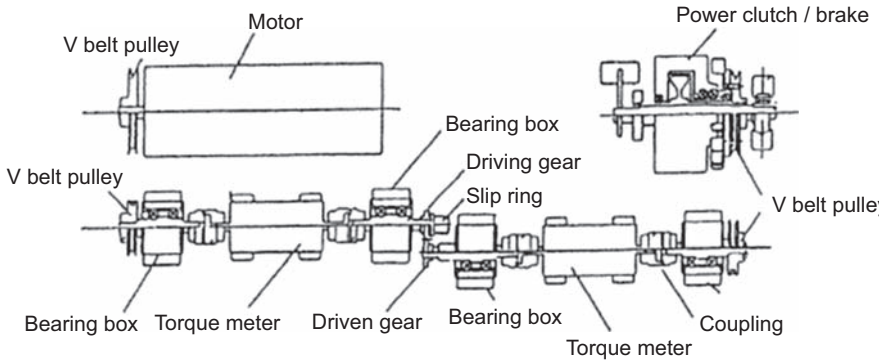

Figure 16.26 The gear test apparatus.
M. Kurokawa, Y. Uchiyama, T. Iwai, S. Nagai. Performance of plastic gear made of carbon fiber reinforced polyamide 12, Wear 254 (2003) 468−473.

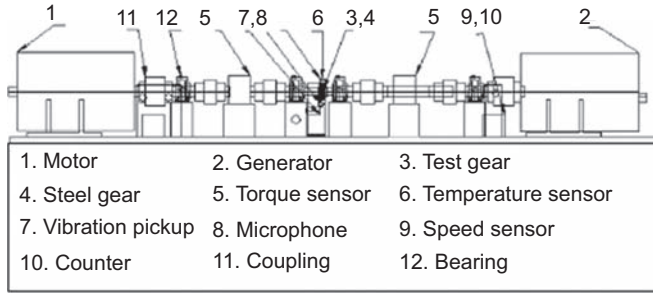

Figure 16.27 Schematic of power absorption type gear test rig.
S. Senthilvelan, R. Gnanamoorthy, Damping characteristics of unreinforced, glass and carbon fiber reinforced nylon 6/6 spur gears, Polymer Testing 25 (2006) 56−62.

inspect the characteristics of both wear and durability of polymer spur gears and to investigate power-transmission polymer spur gears, as shown in Fig. 16.28.

The Forschungsstelle fur Zahnräder und Getriebebau (FZG) test machine is commonly used for gear tests, so several researchers depend on it to investigate wear, friction, and thermal behavior. The FZG design overall is close to that of the Mk I, but the loading mechanism in this test is generated by a loading coupling as shown in Fig. 16.29. Letzelter et al. [30] developed a new test bench to study the thermal behavior of polymer gears, as shown in Fig. 16.30. The surface temperature of gears is measured using a high-performance infrared camera to provide the temperature distribution. The load acting on the gear results from a resistive brake.

Kirupasankar et al. [31] developed a test rig to study the performance of polymeric gears (transmission efficiency), as shown in Fig. 16.31, in which transmission efficiency = driven gear torque/driver gear torque. The loading application is similar to that of the loading mechanism of the power absorption gear test rig.

Kodeeswaran [32] and Mohan [33] designed and built a new bending fatigue test rig design to evaluate the bending fatigue performance of nonmetallic gears.

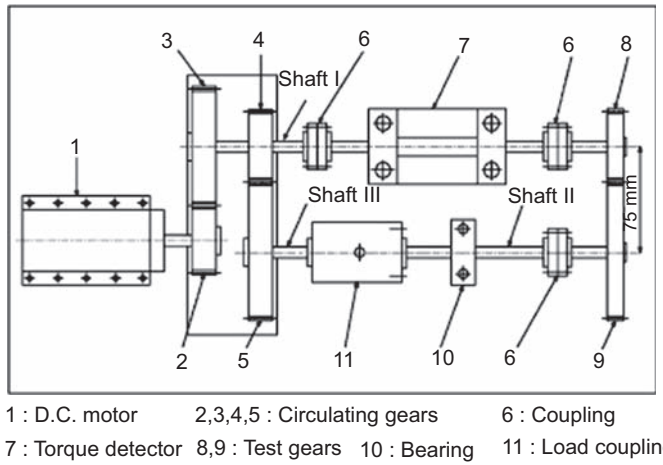

Figure 16.28 Schematic view of the gear test rig.
C. Hyun Kim, Durability improvement method for plastic spur gears, Tribol. Int. 39 (2006) 1454−1461.

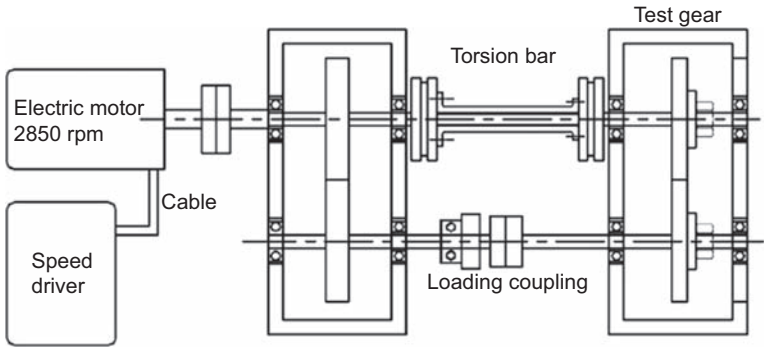

Figure 16.29 Schematic view of the FZG (Forschungsstelle für Zahnäder und Getriebebau) gear test rig.
H. Imrek, Performance improvement method for Nylon 6 spur gears, Tribol. Int. 42 (2009) 503−510; H. Duzcukoglu, Study on development of polyamide gears for improvement of load-carrying capacity, Tribol. Int. 42 (2009) 1146−1153 and H. Duzcukoglu, PA 66 spur gear durability improvement with tooth width modification, Mater. Design 30 (2009) 1060−1067.

Mohan (2013) also evaluated some characteristics of dissimilar polymer gears, as shown in Fig. 16.32. The applied external torque on test gears is produced by a servo-hydraulic testing machine to give a linear motion; this motion is converted into rotary motion using a steel driver gear.

Finally, Table 16.1 shows the experimental conditions of most published polymer gear tests, including the polymer gear materials, the type of test rig used to carry out the test, and the main results.

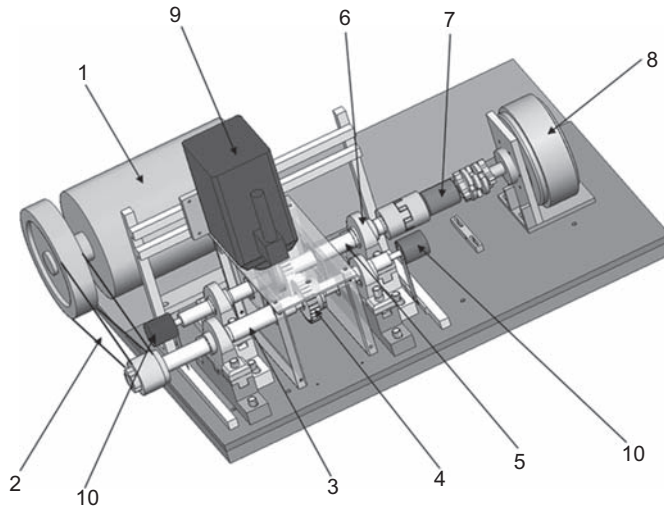

Figure 16.30 Diagram of the test bench. (1) Motor, (2) belt, (3) rotating shaft of pinion, (4) gears, (5) rotating shaft of gear, (6) bearings, (7) torquemeter, (8) brake, (9) infrared camera, (10) optical encoders.
E. Letzelter, M. Guingand, J.-P. de Vaujany, P. Schlosser, A new experimental approach for measuring thermal behavior in the case of nylon 6/6 cylindrical gears, Polymer Testing 29 (2010) 1041−1051.

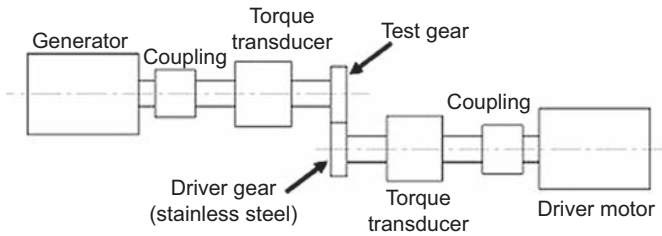

Figure 16.31 Schematic diagram of the polymer spur gear performance test rig.
S. Kirupasankar, C. Gurunathan, R. Gnanamoorthy, Transmission efficiency of polyamide nanocomposite spur gears, Mater. Design 39 (2012) 338−343.

16.2.3.2 Polymer nanocomposite gear test rigs

A limited number of test rigs have been designed and built to investigate PNC gears. The first test rig was very simple and had a loading mechanism similar to that of the Mk I as shown in Fig. 16.33. The test rig was developed by Yousef [9] to study the influence of nanofiller material on the wear behavior of polymer spur gears. The second test rig is called the TS universal test rig and considered a novel design, because all previous test rigs evaluated polymer spur gears only. It was also designed by Yousef [20]. The new design is used to measure the wear characteristics of common types of polymer gears (spur, helical, bevel, and worm).

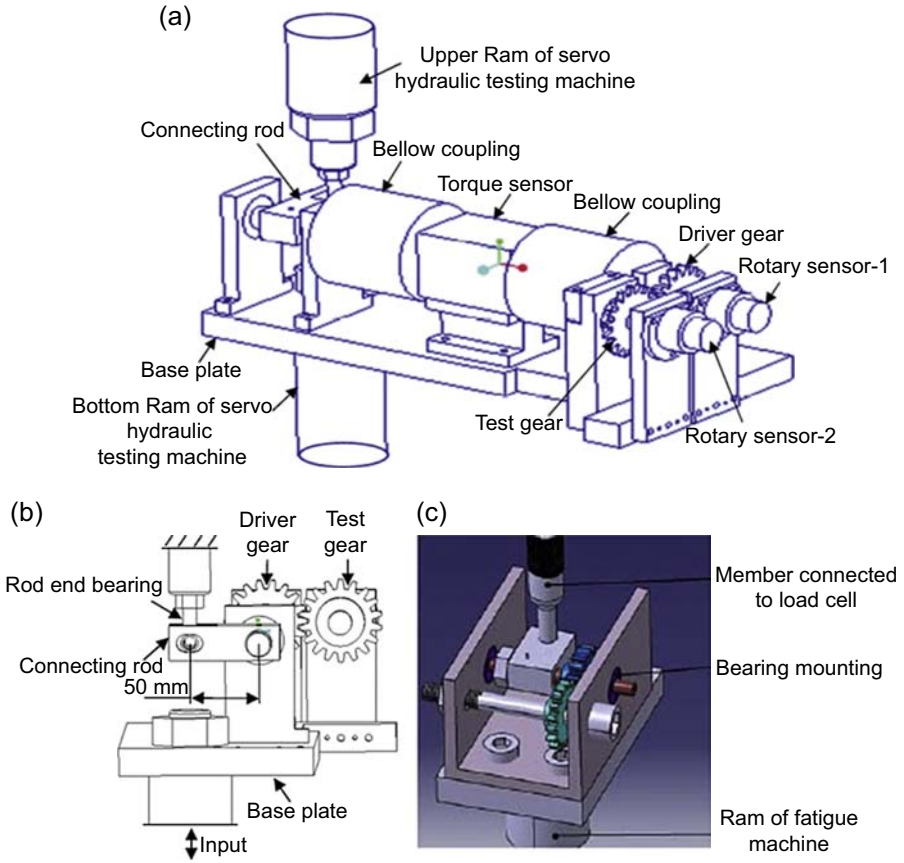

Figure 16.32 (a) Configuration of test rig. (b) Polymer gear fixation unit. (c) Mechanism layout of test rig.
M. Kodeeswaran, R. Suresh and S. Senthilvelan, Test rig design for bending fatigue performance evaluation of polymer based composite gears, in: iNaCoMM2013, 2013 and N. Anand Mohan, S. Senthilvelan, Preliminary bending fatigue performance evaluation of asymmetric composite gears, Mech. Mach. Theory 78 (2014) 92−104.

The test rig consists of three different units: the first unit is used to test bevel gears, the second unit is used to test spur or helical gears, and the third unit is used to test worm gears, as shown in Fig. 16.34. The loading mechanism was designed based on the principle of the Sierra block brake mechanism as shown in Fig. 16.34(d), and the applied external torque can be calculated from Eq. [16.1], where A is the block contact area, μ is the coefficient of friction for lining, and F is the weight. Also, two other researchers have used a power absorption test machine to inspect PNC spur gears.

$$T = \frac{Far\mu}{(C \pm \mu b)A} \qquad [16.1]$$

Table 16.1 Nonmetallic gear materials, characteristics, test parameters and conditions, and results parameters according to Refs. [21,22,24–28,30,33–38]

Refs	Gear material	Test rig	Characteristics	Test conditions	Results
[21]	Acetal and nylon	Mk I test rig	Wear (mm)	Torque 7 Nm, speed 1000 rpm, No. of cycles 16×10^4	Mk I test rig was designed and built to measure the wear rate of polymer gears.
[22]	PA 66, short glass fibers/PA, and long glass fibers/PA	Mk II test rig	Wear (weight loss)	With and without lubricant, torque 10 Nm, speed 1000 rpm, No. of cycles 5×10^6	The results showed that there is considerable variation between wear rate measured by pin-on-disc and by gear test.
[24]	PA 6, 12, 66/carbon fiber	Gear test apparatus	Wear	Lithium type grease, torque 9.8, 19.6, 29.4 Nm, speed 100–500 rpm, No. of cycles 10×10^6	The results show that PA 12/carbon fiber gear had an excellent wear resistance compared with other materials.
[34]	Nylon 66, glass and carbon-reinforced nylon 66	Power absorption type gear test rig	Damage mechanism and thermal resistance	Torque 1.5, 3 Nm, speed 1000 rpm, No. of cycles 5 million	Thermal resistance for nylon was improved by adding carbon fiber. Additionally, the composition and applied torque influence the failure mode.
[25]	Nylon, short glass/nylon, and carbon fiber/nylon 66	Power absorption type gear test rig	Noise and heat generation	Torque 0.5, 1.2, 1.8 Nm, speed 1000 rpm, No. of cycles 5 million	Nylon provides a lower noise compared to reinforced gears. Fiber/nylon provides a lower heat generation during service.

Continued

Table 16.1 Continued

Refs	Gear material	Test rig	Characteristics	Test conditions	Results
[26]	Nylon and acetal	Kim test rig	Wear vs rising temperature	Torque 9.8, 19.6, 29.4 Nm, speed 1273 rpm, No. of cycles 10×10^6	A decrease in tooth surface temperature maintains the mechanical properties for longer time and reduces wear on nylon gears.
[35]	Nylon + glass fiber and acetal + PTFE	Mk I test rig	Wear rate and surface temperature	Torque 5−35 Nm, speed 1000 rpm, No. of cycles 1.2×10^6	A new method for polymer composite gear design agreement with experimental test results.
[27]	Nylon 6	FZG	Load sharing, *F*/*b*	Torque 4.41, 6.62, 8.82 Nm, speed 1000 rpm, No. of cycles 10^7	The modification for tooth width resulted in lower tooth temperatures and increase in gear performance.
[28]	PA 6 + oil	FZG	Generated heat	Torque 6.12, 10.32, 16.53, 23.3 Nm, speed 1750 rpm, No. of cycles 4.2×10^5	The tooth surface temperature decreased after cooling holes were drilled on the tooth body; furthermore, the wear resistance was improved.
[36]	Acetal and nylon	Mk I test rig	Friction and wear	Torque 7 to 16.1 Nm, speed 1000 rpm, No. of cycles 1.2×10^7	In dissimilar gears; the optimum performance occurred when acetal was used as the driver against nylon.
[30]	Nylon 66	New test bench	Temperature distribution	Torque 5, 10 Nm, speed 300, 600 rpm, time 600 min	The meshing temperature distribution was homogeneous.

[37]	Acetal	Mk I test rig	Effect of heat on wear	Torque 7 to 16.1 Nm, speed 1000 rpm, No. of cycles 2×10^5	Acetal gear performance was entirely dependent on surface temperature.
[38]	PA, PEEK, and coated by PTFE, Molybdenum disulphide (MoS2), etc.	Mk I test rig	Friction and wear	Torque 7 Nm, speed 1500 rpm, No. of cycles 2×10^6	The coating layer worked to protect polymer gears and provided the greatest reduction in frictional forces particularly for PTFE coating. Also failure mechanisms were focused in the coating layer.
[33]	Polypropylene and glass fiber/ polypropylene	Bending fatigue test rig	Bending fatigue performance	Torque 1−20 Nm, speed 60, 90, 120 rpm, angular motion 1.7, 2.5, 3.4, 4.2, 5 degrees, deflection mode 1, 1.5, 2 Hz	The bending load carrying capacity of both symmetric and asymmetric gears was improved by adding carbon fibers.

PA, polyamide; *PTFE*, polytetrafluoroethylene; *PEEK*, polyether ether ketone; *FZG*, Forschungsstelle fur Zahnräder und Getriebebau.

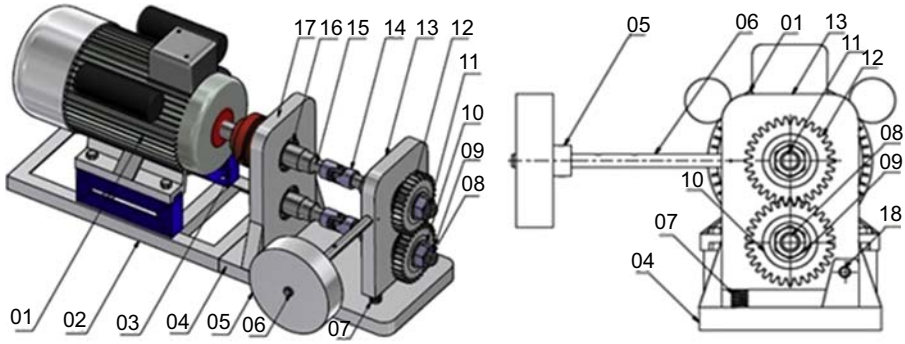

Figure 16.33 Schematic view of the experimental bench. (1) Motor, (2) motor stand, (3) coupling, (4) base, (5) weight, (6) lever, (7) spring, (8) driven shaft, (9) driven shaft, (10) washer, (11) driver shaft, (12) test gears, (13) front bearing support, (14) universal coupling, (15) driver shaft, (16) bearing, (17) back bearing support, (18) pivot.
S. Yousef, A. Khattab, M. Zak, T.A. Osman, Wear characterization of carbon nanotubes reinforced polymer gears, IEEE Trans. Nanotechnol. 12 (2013) 616–620.

Finally, Table 16.2 shows the experimental conditions of most published PNC gear tests, including the PNC gear materials, the type of test rig used to conduct the test, and the main results.

16.2.4 Wear and friction testing of polymer nanocomposites

Real wear behavior of PNC gears has been studied by Yousef [9, 20] using the TS universal test rig. Before the test was conducted, the PNC gears were cleaned using ethanol. After each completion of the test the gears were cleaned with distilled water. Wear loss was measured by weight using a high-sensitivity electronic weighing balance with accuracy to 10^{-4} g. The results showed that the wear resistance of the CNT/acetal spur, helical, bevel, and worm gears was improved by 28%, 35%, 44%, and 47%, respectively. Regarding friction, accurate measurement of the friction coefficient between meshing PNC gears is essential and additional information is required.

16.2.5 Thermal testing

In metallic gears the heat generated by cumulative meshing can be removed by two types of heat transfer: (1) convection-type transfer from gear to atmosphere and (2) conduction-type transfer through the gear material. In polymeric gears, the only type of heat transfer is convection, because conduction heat transfer depends on the thermal conductivity, and the thermal conductivity of polymeric material is very low, so all generated heat is concentrated in the contact meshing area and this causes increased wear rates. Several studies found that the thermal conductivity of polymeric material was improved by adding nanofiller materials such as CNT and graphene. Furthermore, this part presents a good configuration for testing thermal behavior, in particular tooth surface temperatures in PNC gears, using the TS universal test rig

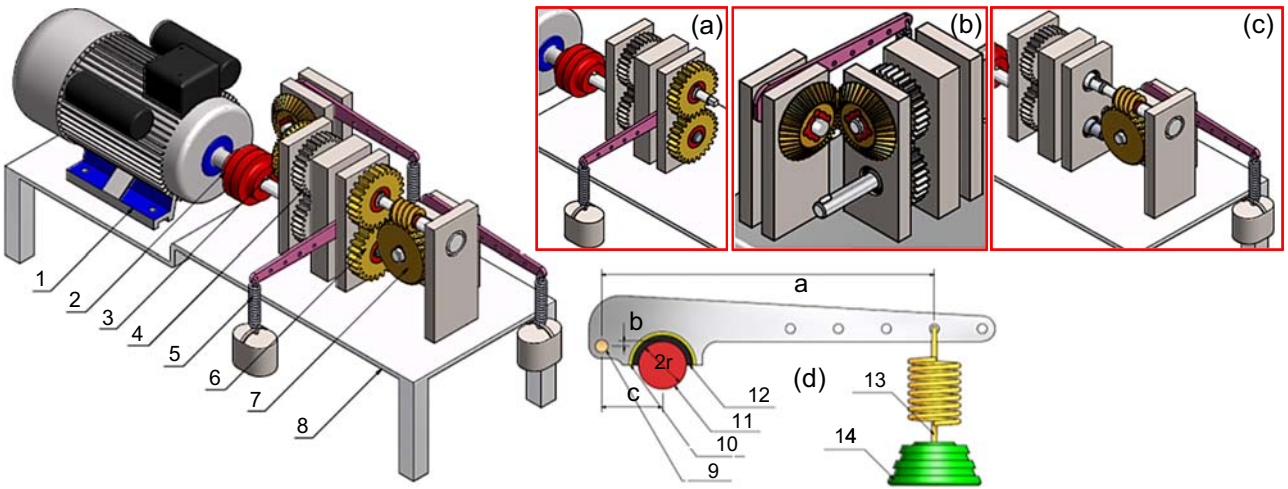

Figure 16.34 A photograph of the universal test rig. (a) Spur or helical gears testing unit design. (b) Bevel gears testing unit design. (c) Worm gears testing unit design. (d) Loading mechanism. (1) Motor, (2) coupling, (3) bevel gears testing unit, (4) metal gears, (5) loading mechanism, (6) spur and helical gears testing unit, (7) worm gears testing unit, (8) base, (9) pin, (10) lever, (11) shaft, (12) lining, (13) spring, (14) mass.
S. Yousef, T.A. Osman, A.H. Abdalla, G.A. Zohdy, Wear characterization of carbon nanotubes reinforced acetal Spur, helical, bevel and worm gears using a TS universal test rig, JOM (2014). http://dx.doi.org/10.1007/s11837-014-1268-5 and Samy Yousef, T. A. Osman, M. Khattab, Ahmed A. Bahr, Ahmed M. Youssef, A novel design of universal test rig to measure wear characterizations of polymer acetal gears (spur, helical, bevel and worm). Advances in Tribology 2015. http://dx.doi.org/10.1155/2015/926918.

Table 16.2 Gear materials, characteristics, test parameters and conditions, and tribological parameters of polymer nanocomposites according to Refs [9,20,31,40]

Refs	Gear material	Test rig	Characteristics	Test conditions	Results
[40]	Nanoclay/PA	Power absorption	Wear	Torque 1.5, 2, 2.5 Nm, speed 800 rpm, No. of cycles 9×10^3	Addition of nanoclay reduces friction and heat generation, also less wear and increased life.
[31]	Nanosize clay/PA	Power absorption type	Transmission efficiency	Torque 1.5, 2, 2.5 Nm, speed 1200 rpm, No. of cycles 10^7	Power transmission efficiency for PA nanocomposite gears better than for pristine PA.
[9]	CNT/POM	Simple test rig	Wear	Torque 4 Nm, speed 1420 rpm, No. of cycles 200×10^3	The average wear resistance of the CNT/acetal spur gear was improved by adding 15% of the weight of CNT.
[20]	CNT/POM	TS universal test rig	Wear	Torque 4 Nm, speed 1420 rpm, No. of cycles 200×10^3	The average wear resistance of the CNT/acetal spur, helical, bevel, and worm gears was improved by 28%, 35%, 44%, and 47%, respectively.

PA, polyamide, *CNT*, carbon nanotube, *POM*, polyoxymethylene.

based on Düzcükoglu (2008). Several modifications will be added to fix the infrared thermocouples on the tested unit around the meshing gears, as shown in Fig. 16.35.

16.2.6 Noise testing

Some mechanical equipment, such as generators, operates in more critical environments, such as hospitals, as well as automobiles and planes. These environments need to be quiet. Most of this equipment produces noise and this causes a lot of problems. The noise is often produced by the gearbox during operation and some other parts. Polymeric materials have a noise loss feature; furthermore, metallic materials can be replaced by polymeric materials to reduce acoustic emissions, but polymeric materials have low strength. Based on Yousef [9], the strength can be increased by adding nanomaterials. Furthermore, everything is now formatted to replace metallic gearboxes with PNCs. The TS universal test rig can be used to measure the sound power based on the development of the MI test rig, which was conducted by Drean (2009, 2011). Each unit can be enclosed in a soundproof box made of wood lined with noise-absorbing plastic foam (anechoic chamber) to minimize the noise emitted by the mechanical elements [41,42]. Fig. 16.36 shows the distribution of the microphones at each unit. Then MATLAB is used to convert the sound signal to sound pressure and analyze it. Finally, the test is conducted at different parameters (torque and speed) to find the optimum operating conditions.

16.2.7 Summary

Based on the investigations carried out on PNC gears, it has been shown that PNC gears are considered the most important step in and the nucleus for building a fully manufactured PNC gearbox. PNCs can also be used in several other applications.

The following steps should be followed in the production procedure for any type of PNC gear (spur, helical, bevel, and worm) with high performance:

1. Choose the appropriate type of polymeric material, often one of the three PA, POM, and PEEK, because these materials have good tribological and mechanical properties compared with other materials.
2. Choose the appropriate type of nanofiller material, often CNT or graphene, because these materials have good tribological and mechanical properties compared with other materials. The amount of nanofiller material should be within the limits of 0.01% up to 0.05% wt.
3. Choose the appropriate type of dispersion method. It is recommended to use the technique developed by Yousef [9], which depends on adding a small amount of paraffin oil during the injection process (SY dispersion technique).
4. The PNC should be cut in the form of standard tensile samples and other samples to find the optimum amount of nanofiller constrained by high strength, tribological performance, and thermal conductivity.
5. After the optimum amount of nanofiller material is detected, one can start to produce the PNC gears by repeating the previous steps from 1 to 3 and then injecting the slurry into an injection die to produce the gear directly, or produce a flange, and then by hooping and using a CNC milling machine one can manufacture the standard gears. But it is better to produce the gears directly without this manufacturing to avoid residual stress.

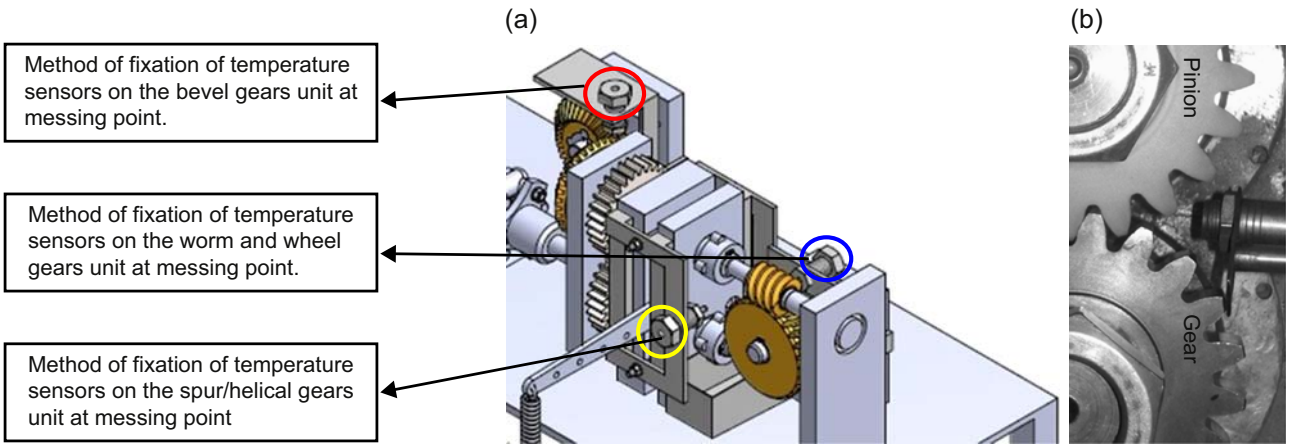

Figure 16.35 (a) Measurement of tooth surface temperature *(H. Duzcukoglu, PA 66 spur gear durability improvement with tooth width modification, Mater. Design 30 (2009) 1060–1067.)* and (b) fixation of temperature sensors on TS universal test rig.

(a)

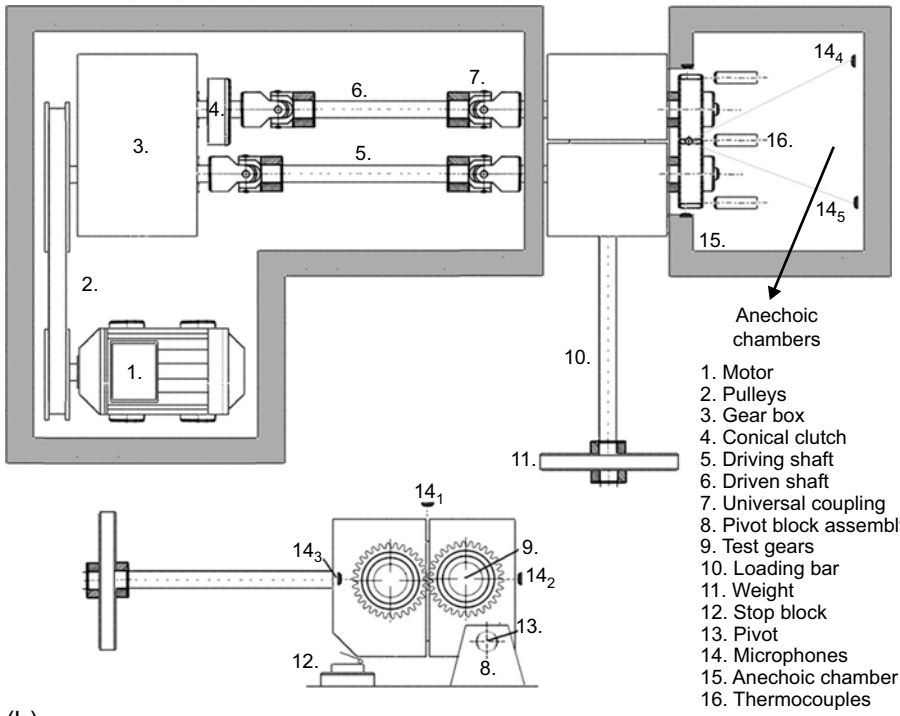

(b)

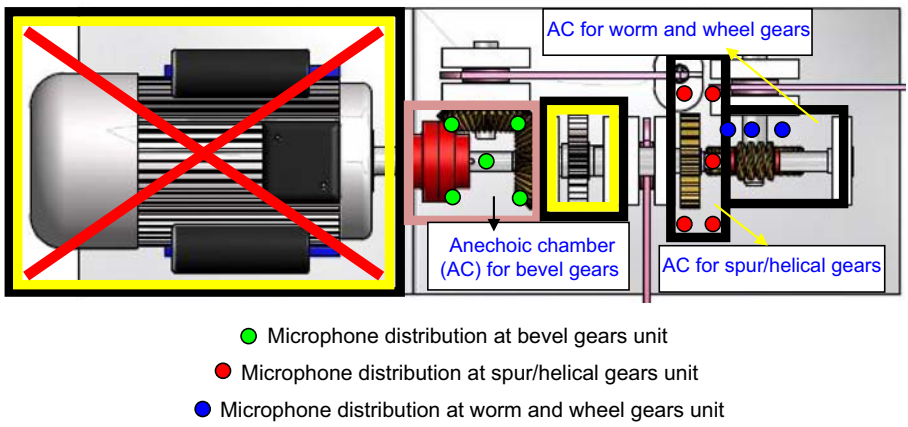

Figure 16.36 Microphone distribution in the TS universal test rig design. (a) MI test rig after development *(T.J. Hoskins, K.D. Dearn, S.N. Kukureka, D. Walton, Acoustic noise from polymer gears-A tribological investigation, Mater. Design 32 (2011) 3509–3515.)*. (b) TS universal test rig after development.

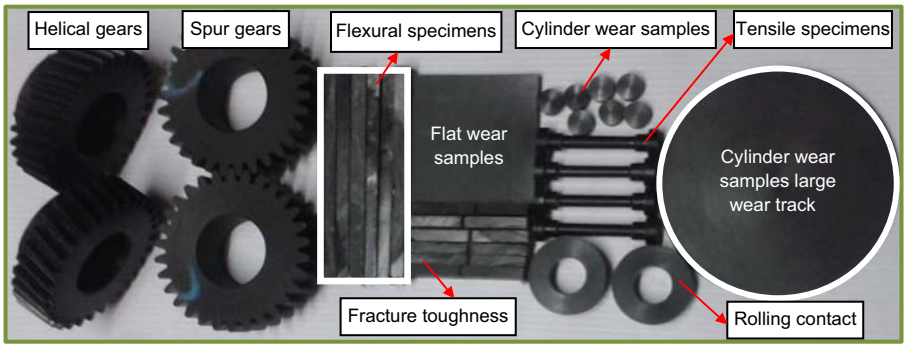

Figure 16.37 Polyamide nanocomposite samples.
S. Yousef (under research).

6. All characteristics can be evaluated by using the test rig; it is recommended to use the TS universal test rig for wear behavior and also for thermal and noise behavior after modification as shown in Figs. 16.28 and 16.29. For bending fatigue the test rig built by Mohan [33] is recommended for spurs only, but other types of gears are under research.
7. Finally, Fig. 16.37 shows a complete study for a PA nanocomposite synthesized by previus procedures and illustrates the samples most listed in this chapter.

16.2.8 Polymer nanocomposite future applications

This chapter will be very useful for the future fabrication of nanopolymer gears, in particular in automotive, robotics, and aerospace applications. Furthermore, new multifunctional nanopolymer materials will be useful for chemistry, petroleum industries, and renewable energy, in particular, wind turbine blades. Also, we have discovered a very cheap method for excellent dispersion (for polymers and any nanomaterials).

References

[1] http://www.yankodesign.com/2010/07/19/yd-store-offers-5-discount-on-the-orb-pestle-mortar-by-joseph-joseph/.
[2] http://reprap.org/wiki/Hot_plate_stirrer.
[3] http://www.stuart-equipment.com/product.asp?dsl=853.
[4] http://www.karkimya.com.tr/en_4_2_1_1_3_urunler_dispersiyon_laboratuvar_dissolver_dispermat_cv3.html.
[5] https://www.google.it/search?q=Mortar+and+pestle&;biw=1366&bih=659&tbm=isch&tbo=u&source=univ&sa=X&ei=AHa2VJyMJsGNaJLCgrgM&ved=0CCgQsAQ#tbm=isch&q=Ultrasonic+bath&imgdii=_&imgrc=o4DRRpkSqYFDVM%253A%3BSYaKmEVjlqYR2M%3Bhttp%253A%252F%252Fwww.keison.co.uk%252Fproducts%252Fgrantinstruments%252Fmxb.jpg%3Bhttp%253A%252F%252Fwww.keison.co.uk%252Fgrantinstruments_mxb.shtml%3B400%3B403.

[6] http://www.azom.com/article.aspx?ArticleID=8402.
[7] http://ifi.es/Productos/Thermo%20Scientific/Extrusoras/HAAKE/extrusoras_lab.html.
[8] S. Yousef, A. Khattab, T.A. Osman, M. Zak, Effects of increasing electrodes on CNTs yield synthesized by using arc-discharge technique, J. Nanomater. 2013 (2013), 392126.
[9] S. Yousef, A. Khattab, M. Zak, T.A. Osman, Wear characterization of carbon nanotubes reinforced polymer gears, IEEE Trans. Nanotechnol. 12 (2013) 616−620.
[10] http://www.monstermarketplace.com/advanced-crystals-and-processing-equipment/25t-hydraulic-flat-hot-press-with-dual-temp-controller-up-to-250-eq-hp-88v110.
[11] www.sufluc.com.
[12] H. Meng, G.X. Sui, G.Y. Xie, R. Yang, Friction and wear behavior of carbon nanotubes reinforced polyamide 6 composites under dry sliding and water lubricated condition, Compos. Sci. Technol. 69 (2009) 606−611.
[13] Samy Yousef, Annamaria Visco, Giovanna Galtieri, Davide Nocita, Improved wear resistance of UHMWPE based nanocomposites for prosthetic applications, filled with liquid paraffin and carbon nanofibers, INSTM Conference, Italy (2015).
[14] Samy Yousef, A.M. Visco, G. Galtieri, James Njuguna, Wear characterizations of polyoxymethylene (POM) reinforced with carbon nanotubes (POM/CNTs) using the paraffin oil dispersion technique, JOM-Springer (2015). http://dx.doi.org/10.1007/s11837-015-1674-3.
[15] Y. Liu, S.K. Sinha, Wear performances and wear mechanism study of bulk UHMWPE composites with nacre and CNT fillers and PFPE overcoat, Wear 300 (2013) 44−54.
[16] M. Rajabian, C. Dubois, M. Grmela, P.J. Carreau, Effects of polymer−fiber interactions on rheology and flow behavior of suspensions of semi-flexible fibers in polymeric liquids, Rheol. Acta 47 (2008) 701−717.
[17] F. Silva, J. Njuguna, S. Sachse, K. Pielichowski, A. Leszczynska, M. Giacomelli, The influence of multiscale fillers reinforcement into impact resistance and energy absorption properties of polyamide 6 and polypropylene nanocomposite structures, Mater. Design 50 (2013) 244−252.
[18] S. Yousef, J. Njuguna (under research).
[19] S. Yousef, A. Khattab, T.A. Osman, M. Zaki, Fully automatic system for producing carbon nanotubes (CNTs) by using arc-discharge technique multi electrodes, in: ICIES, 2012.
[20] S. Yousef, T.A. Osman, A.H. Abdalla, G.A. Zohdy, Wear characterization of carbon nanotubes reinforced acetal Spur, helical, bevel and worm gears using a TS universal test rig, JOM (2014), http://dx.doi.org/10.1007/s11837-014-1268-5.
[21] A.R. Breeds, S.N. Kukurek, K. Mao, D. Waltonb, C.J. Hooke, Wear behaviour of acetal gear pairs, Wear 166 (1993) 85−91.
[22] N.A. Wright, S.N. Kukurek, Wear testing and measurement techniques for polymer composite gears, Wear 251 (2001) 1567−1578.
[23] K.D. Dearn, An Investigation into Tribological and Performance Related Aspects of Polymeric Gearing (Ph.D. thesis), The University of Birmingham, 2008.
[24] M. Kurokawa, Y. Uchiyama, T. Iwai, S. Nagai, Performance of plastic gear made of carbon fiber reinforced polyamide 12, Wear 254 (2003) 468−473.
[25] S. Senthilvelan, R. Gnanamoorthy, Damping characteristics of unreinforced, glass and carbon fiber reinforced nylon 6/6 spur gears, Polymer Testing 25 (2006) 56−62.
[26] C. Hyun Kim, Durability improvement method for plastic spur gears, Tribol. Int. 39 (2006) 1454−1461.
[27] H. Imrek, Performance improvement method for Nylon 6 spur gears, Tribol. Int. 42 (2009) 503−510.

[28] H. Düzcükoglu, Study on development of polyamide gears for improvement of load-carrying capacity, Tribol. Int. 42 (2009) 1146−1153.
[29] H. Düzcükoglu, PA 66 spur gear durability improvement with tooth width modification, Mater. Design 30 (2009) 1060−1067.
[30] E. Letzelter, M. Guingand, J.-P. de Vaujany, P. Schlosser, A new experimental approach for measuring thermal behavior in the case of nylon 6/6 cylindrical gears, Polymer Testing 29 (2010) 1041−1051.
[31] S. Kirupasankar, C. Gurunathan, R. Gnanamoorthy, Transmission efficiency of polyamide nanocomposite spur gears, Mater. Design 39 (2012) 338−343.
[32] M. Kodeeswaran, R. Suresh, S. Senthilvelan, Test rig design for bending fatigue performance evaluation of polymer based composite gears, in: iNaCoMM2013, 2013.
[33] N. Anand Mohan, S. Senthilvelan, Preliminary bending fatigue performance evaluation of asymmetric composite gears, Mech. Mach. Theory 78 (2014) 92−104.
[34] S. Senthilvelan, R. Gnanamoorthy, Damage mechanisms in injection molded unreinforced, glass and carbon reinforced nylon 66 spur gears, Appl. Compos. Mater. 11 (2004) 377−397.
[35] K. Mao, A new approach for polymer composite gear design, Wear 262 (2007) 432−441.
[36] K. Mao, W. Li, C.J. Hooke, D. Walton, Friction and wear behavior of acetal and nylon gears, Wear 267 (2009) 639−645.
[37] K. Mao, W. Li, C.J. Hooke, D. Walton, Polymer gear surface thermal wear and its performance prediction, Tribol. Int. 43 (2010) 433−439.
[38] K.D. Dearn, T.J. Hoskins, D.G. Petrov, S.C. Reynold, R. Banks, Applications of dry film lubricants for polymer gears, Wear 298−299 (2013) 99−108.
[39] T. Samy Yousef, A. Osman, M. Khattab, A. Ahmed, M. Bahr, Ahmed, Youssef, "A novel design of universal test rig to measure wear characterizations of polymer acetal gears (spur, helical, bevel and worm)", Advances in Tribology (2015) http://dx.doi.org/10.1155/2015/926918.
[40] S. Kirupasankar, R. Gnanamoorthy, R. Velmurugan, Effect of apparent area, load, and filler content on sliding friction characteristics of polymer nanocomposites, Proc. IMechE Part J: J. Eng. Tribol. 224 (2009).
[41] K.D. Dearn, D. Walton, Acoustic Emissions from Polymeric Gears, WCE, London, U.K, July 1−3, 2009.
[42] T.J. Hoskins, K.D. Dearn, S.N. Kukureka, D. Walton, Acoustic noise from polymer gears-A tribological investigation, Mater. Design 32 (2011) 3509−3515.
[43] S. Yousef (under research).
[44] D. Walton, C.J. Hooke, K. Mao, A.R. Breeds, S.N. Kuknreka, Proc. 3rd World Congress on Gearing and Power Transmissions,CMET 92, Paris, 1992, p. 683.
[45] A.R. Breeds, S.N. Kukureka, K. Mao, D. Walton, C.J. Hooke, Wear behaviour of acetal gear pairs, Wear 166 (1993) 85−91.

Manufacture and testing of lightweight tubes for rocketry and centrifuges

17

J.C. Quagliano Amado
Institute of Scientific and Technical Research for the Defense (Citedef), Buenos Aires, Argentina

17.1 Introduction

The manufacture of lightweight tubes for sensitive applications such as rocketry and centrifuges is usually done by filament winding. Filament winding is the process of continuously wrapping individual wires or strands of glass or other filaments (usually wetted with resin) on a mandrel and then curing the resin and removing the mandrel to leave a filament-wound composite structure (Fig. 17.1).

Filament winding is the most important of the composites process in terms of the number of users and the total number of parts made. It is the oldest and most frequently considered process for machine-dominated composite structure manufacturing (Shen, 1995). A major technological breakthrough occurred in the 1950s with the development of filament-wound composite cases (Tatcher and Wetherell, 1991). However, as early as 1945, resin-impregnated fiberglass laminates were utilized in the construction of rocket motor tubes (cases) and other components (Moore, 2005). It has been an established technique for many decades (Harvey, 1963; Ravenhall, 1964; Rosato and Grove, 1974), particularly for missile applications: filament-wound reinforced plastic materials

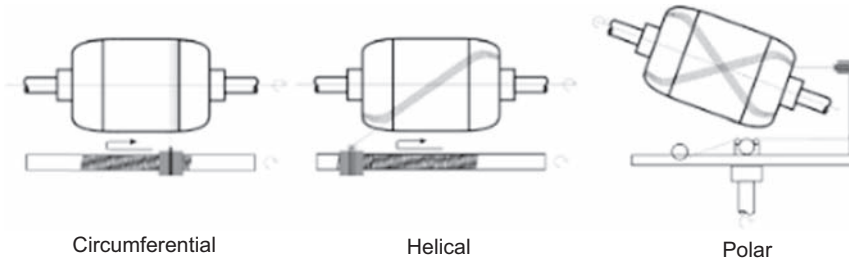

Figure 17.1 Main types of winding.
Adapted from Khennane, A., 2013. Filament winding processes in the manufacturing of advanced-fiber reinforced (FRP) polymer nanocomposites. In: Bai, J. (Ed.), Advanced Fibre-Reinforced Polymer (FRP) Composites for Structural Applications. Woodhead Publishing Series in Civil and Structural Engineering, Woodhead Publishing Ltd, Cambridge, UK, pp. 188–206 (Chapter 28).

Lightweight Composite Structures in Transport. http://dx.doi.org/10.1016/B978-1-78242-325-6.00017-7

have been used successfully for solid propellant rocket and motor cases; two of the most outstanding examples are the Polaris and Minuteman missiles (Hunson et al., 1965). In the early 1970s, the US Navy continued its emphasis on composite motor cases by developing a filament-wound C4 missile for use on the Trident I submarine. Kevlar 49 was the material of choice, and the same for Pershing and Peacekeeper missiles (Kliger and Wilson, 1990). Filament-wound structures continue to be widely used as pressure tanks, pipes, and motor cases in rockets in aerospace applications by both public and private enterprises (Coste and Gautier, 2006; Mc Connell, 2007).

The fiber spools are mounted in a rack, called a creel, and then strands from many spools are gathered together and fed through a comb or similar alignment device so that they make a band of fibers. The band then enters a resin bath in which the fibers are soaked with the resin. The resin is fully activated with an initiator or hardener so that the only requirements to cure the part are heat and time. The fibers then go through a roller or wiper system to remove the excess resin and then through a ring or some other directing device called a payoff. The payoff directs the fibers onto a mandrel (Strong, 2000).

The two general directions of fiber paths are hoop, or radial, winding and helical winding. The hoops circle the mandrel in paths that are approximately 90 degrees to the long axis of the mandrel, although there are several variations. The hoop winding is important to give radial strength. Helical winding is important to hold the hoops in place and give strength to the ends of the part. Once the mandrel is completely covered to the desired thickness, the mandrel is generally placed in an oven to solidify the resin. Once the resin has cured, the mandrel is removed, leaving the hollow final product.

Some typical parts related to rocketry and defense made by the filament winding process include the following: missile launch tubes, radomes, rocket motor cases, aircraft waste tanks, helicopter rotor shafts, and wind turbine blades. In the civil area, examples are low- and high-pressure pipes, water tanks, reverse-osmosis tubes, air tanks for firefighters, scuba tanks, industrial rollers, compressed natural gas tanks, flywheels, golf shafts, bicycle frames, and boat masts.

Filament winding combines chemistry and material science with automation and control techniques with computers, both as a full cycle and in every step of manufacturing. Although there is a huge amount of information about motor case manufacturing and testing, this is mostly disclosed through patents and the latest developments are not disclosed. Thus we attempt here to summarize the main general advances related to materials utilized in filament winding of lightweight motor cases and also damage assessment and prevention techniques used to check the integrity of cases subjected to very high pressures. The chapter is focused on reviewing advances and presenting the fundamentals of filament winding of lightweight tubes used as motor cases at the same time. Aerospace utilization of lightweight structures in the civil area are only mentioned, as there is a vast number of publications on it and it deserves special attention. We did not try as well to review the effects of filament-winding-specific conditions of operation (for example, multiangle layup configurations, mandrel rotation speed, winding direction, or tooling considerations) on the characteristic strength of tubular composite structures, except when contributing to the outline of this contribution.

17.2 Filament winding materials

A variety of fibers and resins can be utilized, depending on the cost and the level of performance needed. In general, fiberglass is the least expensive, but it has the lowest performance level; carbon fibers are the most expensive but have the highest performance level (Shen, 1995). Fibers and resins together are combined for achieving the expected results. Specific combinations of orientation of reinforcing fibers and their density and void content can increase the strength and resistance to stress (Mallick, 2007). The resin matrix should preferably bond chemically with the fiber reinforcement for maximum adhesion. It must also completely wrap the fibers to protect them from cuts and notches that would reduce their strength, and to transfer forces to the fibers. Poor transfer of energy between layers of fibers that differ from one another contributes to the improved impact resistance of hybrid composites (Strong, 2000). Resins and fibers should complement each other to achieve the desired properties for lightweight construction.

17.2.1 Resins

Filament winding is the process in which continuous strands or filaments of fiber are wound on a supporting form or mandrel, a technique that utilizes glass fibers impregnated in resin laying down fibers in the desired pattern. These operating conditions demand that resins have certain properties such as an adjustable velocity of curing (which is controlled with catalysts), good wetting, low cure temperature, sufficient long pot life to allow workability, and the right viscosity to avoid dripping during the operation. Resins have also to maintain good mechanical properties while aging.

Epoxy resin is the material of choice for standard filament winding processes. Epoxy resins are used because of their wide range of thermal and mechanical properties. However, specialty epoxy resins are available on the market. High-performance epoxy resins include phenol-novolac resin, naphthalene- and fluorene-based epoxy resins, triglycidyl-*m*-aminophenol resin, and bicyclopentadiene epoxy novolac. Otherwise, other common resins such as polyester, vinylester, polyurethane, phenolics, furans, and polyimides can be utilized.

Several mixtures were experimented with according to the application. An 80/20 blend of a diglycidyl ether of bisphenol A and a diglycidyl ether of 1,4-butanediol with a commercial mixture of methylene dianiline and *m*-phenylene diamine (Tonox 60/40) was studied at amine/epoxy ratios ranging from 1.1 to 4.4 for filament-wound composites. This system was developed for the fabrication of flight-worthy cases because of problems in trying to scale up the filament winding and cure processes from small thin-walled cylindrical missile rocket motor cases to the rather large thick-walled cases needed for the space shuttle (Golub et al., 1986).

The epoxy resin has to be formulated together with the hardener, diluent, and other additives. If viscosity is too high, warming could help to reduce it, but at the same time warming may reduce the gel time too much (Rinde et al., 1978).

The thermal limitations of epoxy resins preclude their use in applications such as tanks for aerospace. In this sense, resins capable of service in this environment include polyimides (Vaughan and Jones, 1974).

Other additives in resin systems are hardeners, flexibilizers, curing agents, and modifiers. Bismaleimides, polyimides, cyanate esters, and benzoxazines are utilized for specific applications. Imide and benzoxazine chemistries can provide exceptional mechanical, thermal, and chemical-resistant properties for some of the most demanding applications.

To reduce the weight of composites, research was initiated to develop a hydrocarbon resin derived from 1,2-polybutadiene, *t*-butylstyrene, and dicumyl peroxide, as the density of this cured thermoset is less than 1, using Kevlar 49 as fiber (Timm et al., 1994).

With respect to specialty resins for the most demanding requirements, a matrix resin evaluation and trade study was completed with commercial and NASA amorphous polyimides, on one hand, and with polyether ketone ketone mixed with polyhedral oligosilsesquioxane (POSS) nanoparticles on the other. The focus was put on resin crystallinity as without full crystallinity, the full resin modulus is never attained, and compression properties of the composite laminate suffer (Lamontia et al., 2006).

To avoid the problems associated with using liquid resins, filament winding can be done with prepregs. Decades ago it was suggested that fibers should be preimpregnated to facilitate processing (Trigg, 1969). However, pot life is still a problem. Most filament winding is done without additives. Flow control agents (mainly surfactants) that prevent resin from dripping off the part during winding and curing can be useful (Strong, 2000).

17.2.2 Fibers

Fiberglass is the most common fiber, but carbon/graphite, aramid, and ultrahigh-molecular-weight polyethylene fibers are also widely used. Chopped fibers can be sprayed onto the mandrel during conventional winding. This is used almost exclusively for inexpensive low-performance pipes and tanks.

The use of graphite fibers in an epoxy matrix as a structural material was demonstrated long ago. As a structural material in filament-wound pressure vessels, graphite fibers provide a solution to problems that are inherent to low-modulus reinforcements such as glass fibers (Hanson, 1969). The strength-to-weight ratio is an improvement of 3 for fiberglass/epoxy and today exceeds 5 for carbon fiber/epoxy compared to conventional steel (Tatcher and Wetherell, 1991). Also, carbon has several attractive features particularly relevant for rocket conditions, such as a very high sublimation point of 3450°C, capable of withstanding extreme conditions of rocket exhaust. Also, carbon/carbon composites are part of the ceramic matrix composites utilized for motor cases used in aerospace. They are composed of carbon fibers embedded in a carbon matrix (Vignoles et al., 2010; Li et al., 2011).

Carbon and aramid fibers have better mechanical and thermal properties and, for this reason, are usually selected as the reinforcement material for filament winding techniques in the aerospace and defense industry. However, both carbon and aramid fibers have the common disadvantage of high cost compared to glass fibers. Aramid fibers have high strength and low density and thus the specific strength of aramid fibers is high compared to that of other fibers. Impact resistance is also high, which gives rise

to ballistic applications of aramid fibers (Bayla, 2004). With respect to aramid fibers, several investigations have been published. Variations in resin and resin/fiber interface properties for Kevlar 49 were achieved in several ways: using various resins and using a silicone fiber releasing agent to control interfacial bond strength. It was found that for motor case applications, structural and temperature/moisture conditions must be considered carefully before selecting a high-performance matrix system for Kevlar 49 (Mumford et al., 1983). Ethylene propylene diene monomers with Kevlar, an insulating material, were inserted between the metallic boss and the composite to prevent debonding from each other and to insulate the gas or heat generated during combustion in the filament-wound motor case (Park et al., 2002). A motor case for space applications was manufactured using aramid fibers (Kevlar 49) and epoxy resin by means of wet-filament winding (Nagesh, 2003). The European MAGE (Moteur d'Apogée Géostationnaire Européen) motor cases all use filament-wound Kevlar 49, embedded in an epoxy matrix, as the case material. The case is a thin-walled pressure vessel designed to withstand about 71 MPa (Zandbergen, 2013). In other uses such as bulletproof vests, the interface between the tough fiber, which is usually aramid, and the structural fiber (such as carbon or glass fiber) further dissipates the energy, improving impact toughness. Layers of ultrahigh-molecular-weight fibers have been placed in alternating layers to achieve optimal ballistic protection.

Single natural fibers have rather high mechanical properties; especially, Young's modulus can be as high as for E-glass fibers. However, natural fibers might not have the tenacity to be pulled through the system, and the good properties of natural fibers are not exploited efficiently in existing applications. Continuous fibers are required for high-performance applications.

Flax and viscose fiber tubular composite samples were produced by filament winding and their properties were compared with the properties of E-glass fiber composites. The flax fiber yarn could be wound to produce a relatively stiff composite tube but poor adhesion between the matrix and the fibers affected the properties. The properties of the E-glass fiber composites were superior in comparison to the flax fiber composites, although they were only 25−29% of the properties of the E-glass fiber composites. Water absorption and impact strength were notably the weakest properties of the flax fiber composites. To develop the structural natural fiber composites, the adhesion and the wet-out of the fibers should be improved (Lehtiniemi et al., 2011).

In 2012, a review was published about composite materials applications and trends for the future of solid rocket motor cases. It highlighted that the motor case must be stiff and able to tolerate high pressures and be lightweight. In accordance with these kinds of requirements, the composite materials showed an adaptable efficiency, and glass, aramid, and carbon fibers were applied to order. A comparison of the motor case efficiencies of the D6AC steel alloy and the aramid and carbon fibers showed the carbon fibers to be best. Also, the capacity of the payload was increased by more than 20% by using the high-strength fibers (Lee, 2012).

In Table 17.1 we summarize the main applications of filament winding and the materials utilized.

Table 17.1 Main applications of filament winding and materials utilized (resins and fibers)

Applications	Examples	Materials
Aerospace	Rocket motor tubes, launch tubes, light antiarmor weapons, helicopter blades, plane fins	Epoxies, polyimides, polybismaleimides, carbon, Kevlar, and fiberglass
Commercial	High-pressure tanks, tubes and pipes	Epoxies and fiberglass

17.3 Filament winding in rocketry, defense, and aerospace

Filament winding techniques can be used to manufacture nanocomposite parts for various applications, including commercial aircraft structures for Boeing and Airbus, as well as many products in the industrial markets. Routine use of nanocomposites in automotive and aerospace industries is a long-term prospect as these are risk-averse sectors and extensive testing and characterization alone takes significant time (Hussain et al., 2006). Boeing Canada Technology is involved in the development and production of filament-wound composite airplane ducts and high-performance vessels (Lauder, 1995).

Filament-winding machines are used to make rocket motor cases, propellant tanks, pressure vessels, and payload shrouds. The high strength and low weight of the resulting structures make increased missile ranges and payload rates possible.

Typically, rocket motors have been built by winding resin-impregnated filament material such as carbon or aramid fibrous material about a mandrel, which is covered with insulation material until the desired shape for the rocket motor case has been achieved. The wound case is then appropriately cured and the mandrel removed, after which the solid propellant formulation is poured and thereafter cured.

Optimum filament winding angles have been determined by computer for graphite/epoxy rocket motors. The fiber has to be continuous from one end of the motor to the other to support the longitudinal stresses that try to stretch the motor when the pressure inside goes from zero to thousands of pounds per square inch in a fraction of a second. The fiber, wetted with epoxy, is wound over a mandrel and around each end and returns in barber-pole fashion, but at a relatively shallow angle. After the longitudinal winds are completed, a second process begins with a filament wound around the motor diameter in consecutive circles (hoops) to give it the strength it needs in the hoop direction. After all the windings are completed and after a curing process in an autoclave, the mandrel is removed and the case is ready for loading with propellant. This was the world's first graphite/epoxy rocket motor designed by a computer program (Woltosz, 2012).

Early motor cases were made of fiberglass/epoxy by the main contractor in the United States. Later the material of choice became Kevlar/epoxy with its higher strength and modulus qualities. As all of the filament-wound motor cases stretch under

pressurization a process was pioneered which involved curing these motors with internal pressure applied to the motor case during the propellant curing process (Chase, 2010).

For relatively low external loads representative of ballistic missile applications, a glass filament-wound resin-bonded composite resulted in the lightest motor case per enclosed volume. These authors recalled that if a greater strength (on a stress basis) is required in a given direction, either more windings can be oriented in that direction or the windings can be oriented at such a helix angle that the required directional strength characteristics can be achieved. Thus, for a motor case in which stresses due to internal pressure are critical, one can use twice as many circumferential windings as axial (Bert and Hyler, 1962).

The determination of a proper winding angle and thickness is very important to decrease manufacturing difficulties and to increase structural efficiency (Park et al., 2002).

Some of the problems associated with filament winding of cases are the need for metallic inserts, the degradation of mechanical properties at elevated temperatures, resin failure due to excessive strain concentration in filament-wound resin structures, and abrasion damage to filaments during the winding process (Bert and Hyler, 1962).

Many pressurized tanks utilized in space applications typically use a metal liner reinforced with a high-performance filamentary composite material such as carbon, graphite, aramid, and glass. If tank structural efficiency is to be maximized, it is necessary to operate at strains that may be on the order of 1%. Among the polymeric film and coating materials investigated, ethylene vinyl alcohol is a useful permeation barrier material to gases used in aerospace, such as oxygen and hydrogen (Jones and Li, 2002).

Composite lattice structures made from carbon and aramid epoxy composite materials by automated filament winding have also been utilized for interstages, intertanks, payload adapters, fairings of launch vehicles, and aircraft fuselage sections (Barynin et al., 1999).

Advanced grid stiffened composite payload shrouds have been manufactured by filament winding. Twelve thousand carbon fiber strands preimpregnated with uncured resin were wound into a bundle by the filament winder and accurately placed into grooves. Presized silicon rubber expansion inserts were then hand-installed to control lateral compaction while maintaining precise tooling tolerances and providing the desired cross-sectional geometric shape (AFRL, 2005).

In aerospace, case and nozzle designs for the boosters of an interplanetary rocket system are capable of being fabricated by filament winding a carbon/carbon composite onto a sand mandrel in one piece. Including the nozzle, the system should have a structural coefficient (dry mass to total mass ratio) of only $C = 0.06$, but be capable of withstanding bursting pressures in excess of 1 million psia (6900 MPa) (PSU, 1991). Composite overwrapped pressure vessels (COPVs) are safely used in a wide range of applications, from natural gas vehicles to military rockets. Generally, it is only in ultralightweight designs for space flight, for which there is little margin on strength, that all of the COPV failure modes are credible and must be clearly addressed in design and operation (Mc Laughlan et al., 2011).

The technology has been adopted by developing countries. Studies for rocket tube manufacturing by filament winding have been undertaken in Argentina (Fig. 17.2). Aluminum rocket tubes (30 km range) are intended to be replaced by carbon fiber/epoxy filament-wound tubes (Alinovi, 2013). In local experience, a fiber/volume ratio of 70:30 was utilized, although a 60:30 ratio was tested as well. Preliminary tests for manufacturing tubes were done utilizing carbon fiber/epoxy prepregs, which were wound horizontal to the direction of a mandrel. Then, a carbon fiber was wound vertically to strengthen the structure. Finally, the tube was sanded and the mandrel extracted. Split tests were conducted to test the resistance of the pieces in another laboratory (Gay, 2015).

This work is in progress and intended to produce vectors for civil aerospace applications in the future. Also in South America, the Brazilian space program has intensively utilized metallic cases for solid rocket motors. A complete family of sounding rockets, the Sonda rockets, was developed using this type of technology beginning in the late 1960s. The initial development of a glass fiber/epoxy motor rocket case with filament winding technology revealed that the chosen method was right (Loures da Costa, 2003). Full-scale high-resolution models of composite solid rocket motor cases were built using existing layered volume elements in a collaboration between German and Brazilian researchers. An analysis was done for the S33 composite pressure vessel used as a solid rocket motor case in the Brazilian space program. The location of the fiber breakage, leading immediately to the burst condition, was predicted in the same region as observed in the experiments. It was remarkable that the process of matrix cracking was apparently already finished when the operating pressure was reached and led to a significantly different deformation behavior (Multhoff et al., 2008). On the other side of the world, Ausroc III in Australia was being designed as a sounding rocket capable of lifting 100 kg of useful scientific

Figure 17.2 An example of a filament-wound rocket tube based on graphite fibers and epoxy resin.
www.rocketwestcomposites.com.

payload to an altitude of 500 km and then recovering it intact. The vehicle included technologies such as regenerative liquid propulsion and composite structures (Blair, 1993). In Europe, studies from Poland have shown that the main concept is to utilize sheet composite fabric instead of roving. This allows composite cases to be manufactured without expensive filament-winding machinery, while very high propellant mass fractions can be achieved (Okninski et al., 2014).

With respect to the technology for manufacturing centrifuge tubes by filament winding, we can see that this technology is old, and patents dating back to the 1960s presented the first methodologies for these purposes (Gaubatz, 1965). However, analytical models were presented early in the development of the technique. NASA researchers established the optimum shape with the minimum mass for an isotropic shell of revolution under internal pressure and axial load (Stroud, 1971), such as those that could operate inside a centrifuge tube. In another punctual development (disclosed in a patent) fibers were wound on the outer peripheral surface of a worked first drum part by a filament winding process. A plastic material was then cured on the fibers to form a second drum part, which was then worked to finish the outer peripheral surface thereof (Katodani et al., 1994). From then on this technology has continuously been protected by several patents, and few technological publications, at least for manufacturing, have been disclosed to academia. There are reasons for not disclosing information, as tubes are used for defense and in the military. Also, centrifuge tubes made by filament winding may be utilized for uranium enrichment, and this utilization is restricted by international law.

Wild and Vickers (1997) performed an analysis applied to three examples: a pressure vessel, a centrifuge rotor, and a flywheel. It was shown that the benefit of wind-angle variation was more significant for applications in which there is no axial loading to the cylindrical shell. It was also shown that, where axial loading was present, the benefits of wind-angle variation were more significant under the last-ply-failure criterion than under the first-ply-failure criterion.

Simple parts such as pipes are often wound at fiber laydown rates in the range of 300−3000 lb/h. Parts intended for high-performance markets like aerospace are often fabricated at 10−200 lb/h (Strong, 2000). As this are very exigent conditions to machinery, particularly with respect to the speed of rotating parts, new methodologies based on filament winding are continually being developed.

One of the techniques related to filament winding is tape laying. Tape-laying machines resemble filament-winding machines but are used in heavier applications that have sufficiently gradual contours or angles to allow the use of thick or wide tapes. The purpose of using a tape-laying machine instead of a filament-winding machine is to reduce the number of revolutions of the mandrel needed to wind the part produced. This speeds up production and lowers cost. Tape-laying machines are used to make reentry vehicle heat shields, exit nozzles, igniters, and other parts exposed to high temperatures. Multidirectional, multidimensional weaving machines are used to interlink fibers to make complex composite structures. Multidirectional, multidimensional weaving machines are used to make critical missile parts such as reentry vehicle nose tips and rocket nozzles that are exposed to high temperatures and stress (MCTR Handbook). The concepts of lightweight winding systems, hybrid filament

winding processes, and advanced filament winding techniques are presented in an early review (Munro, 1988).

With respect to main filament operational winding parameters, the fiber/volume ratio is important for vessel design. It is the ratio between the volume of fibers and the volume of the composite. A computer program was developed based on the thermokinetics of the resin and processing conditions is used to calculate the fiber/volume fraction distribution in the filament-wound vessel. The strand's strength-versus-fiber volume data together with the computer program were used to predict composite vessel burst pressure (Cohen et al., 2001). Faria et al. (2009), using the Abaqus-FEA software, modeled filament winding implementing a modular methodology, allowing a decoupled description and calculation of the several physical variables of the process. In Table 17.2 we summarize the main parameters and reference values that they chose for filament winding of cylindrical bodies.

Avinash et al. (2014) give a detailed set of properties for materials for composite motor casing parts, including compressive parameters and modulus across and along fibers, among others, in modeling composite casing shells.

Table 17.2 Main parameter data input for an epoxy/carbon fiber system for filament winding

Parameters	Reference value
Density of fibers (kg/m^3)	1760
Diameter of fibers (m)	7×10^{-6}
Modulus of fibers (Pa)	231×10^9
Density in cured state (kg/m^3)	1267
Modulus of resin in cured state (Pa)	26×10^9
Specific heat of fibers (J/kg × K)	889
Thermal expansion of resin (1/K)	3.2×10^{-5}
Wound section geometry	
Radius of the mandrel (m)	0.15
Total number of wounds	18
Processing conditions	
Initial fiber volume fraction (%)	63
Winding angle (°)	±40
Winding force (N)	300

Adapted from Faria, H., Rocha, A., Miranda, H., Pires, F., Marquez, A., (2009). Numerical modelling of the filament winding process. International Committee on Composite Materials, ICCM17, Edinburgh, July 27–31.

With respect to the operating conditions in a standard filament-winding machine, the range of the winding angle, or the fiber orientation angle, starts from 20 to 90 degrees, depending on the mandrel diameter used. Mandrel speed is kept constant at 13.6 rpm, while the speed of screw of the delivery unit varies from 0 rpm to a maximum of 250 rpm. In the filament winding process used, a single glass roving was drawn through a bath of precatalyzed resin, which was mounted on the lead screw by the rotating mandrel. It provided a capability for producing pipe specimens with an internal diameter up to 100 mm and lengths up to 1000 mm (Abdalla et al., 2007).

In a commercial filament winding modeling software, inputs are divided into material properties, load cases, and geometry parameters. The program provides in graphical mode the relationship between modulus properties (axial, transverse, and shear modules) and winding angle (www.cadfill.com).

17.4 Damage assessment and prevention

Possible types of defect or damage in composite rocket motor cases include matrix cracking, fiber breakage, delamination between plies, and debonding between liner and composite overwrap. Monitoring the structural integrity of filament-wound composite structures such as solid rocket motor cases can help prevent catastrophic failures and prolong their service life. It is vital to be able to establish appropriate confidence in its reliability and safety.

As previously mentioned, a COPV may, in the event of composite failure, experience a catastrophic explosive release of energy due to the high pressure of the stored gas. Although the possibility of failure is remote, the potential consequences of such a failure, especially in a human space flight application, mandate a high level of design reliability (McLaughlan et al., 2011).

Increasing use of these structural parts has given rise to the need for tests to identify characteristics of their fatigue behavior (Kaynak and Mat, 2001). The initial method of assessing impact damage is to visually inspect the damaged part. However, there could be considerable matrix cracking and fiber breakage below the surface. Nondestructive testing (NDT) should be used to assist in further assessment. Modern damage assessment and prevention systems are often complex systems including a built-in sensor network, supporting diagnostic hardware, and data processing/analysis software (Qing et al., 2006).

X-ray, infrared, and ultrasonic techniques were early reported NDT techniques for filament-wound glass fiber/resin rocket motor cases (Harvey, 1963). Hill and Lewis (1985) performed an acoustic emission test on a full-scale filament-wound composite rocket motor case during hydroproofing. An X-ray test was also conducted to find the areas in which there was an absence of fibers or resin richness or starvation.

Important NDT methods for rocket motor cases are noncontacting methods that allow inspection from one side. Among these are vibrothermography and pulse-echo methods based on acoustic−ultrasonic methods. High-resolution techniques such as X-ray computed tomography appear to have merit for accurate geometrical characterization of local damage to support development of analytical models of

micromechanics (Paris, 1994). Fiber Bragg grating (FBG) optical sensor arrays were embedded in filament-wound composite rocket motor cases. In a series of experiments, these filament-wound motor cases were subjected to internal pressures while embedded FBG sensor arrays measured the internal strain. It was concluded that FBG optical sensor arrays were useful devices to measure internal strains within a composite structure (Rea et al., 2002). A prototype of a filament-wound composite bottle with an embedded sensor network has been fabricated and preliminary data analysis tools have been developed (Lin et al., 2005). Vibration-based damage-detection methods have the potential to be employed to monitor the health status of the structures based on the fact that damage occurring in a structure would result in changes in its structural dynamic characteristics (Wu et al., 2010).

An impact study has been undertaken on filament-wound graphite/epoxy casings, such as those proposed for NASA's space shuttle solid-fuel rocket boosters. In thick composite materials, low-velocity impact damage may not be visually evident, depending on the impactor shape; yet the damage may compromise the composite's ultimate strength (Madaras et al., 1987). Rocket propellant tanks are often constructed of wound carbon fiber. The fuel and oxidizer tanks are usually of very lightweight construction, as they operate at low pressures. On the other side, propulsion systems, in particular tanks, are exposed to extremely reactive and aggressive fluids, such as fuels, oxidizers, and cleaning agents, that can promote stress corrosion cracks (Lee and Hwang, 2011). Safe life-cycle fatigue and static loading stress levels are selected for both the metal liner and the overwrap based on specified service-life requirements. These levels are used to establish required material thicknesses and the resulting pressure-vessel burst strength (Shen, 1995).

As stated before, in rockets, internal pressure is the primary constraint. Sun et al. (1999) performed a nonlinear finite element analysis to calculate the stress and final bursting pressure of rocket motor cases. Maximum stress failure criteria and a stiffness-degradation model were introduced into the failure analysis. The location and burst pressure predicted showed good agreement with experimental results. Cohen (1997) showed that the composite vessel strength was affected by the manufacturing and design variables. In general, he found that composite strength was significantly affected by the laminate stacking sequence, winding tension, winding-tension gradient, winding time, and interaction between winding-tension gradient and winding time. The mechanism that increased composite strength was related to the strong correlation between fiber volume in the composite and vessel strength. Franz and Nurick (2002) found that the laminate stacking sequence had an effect on the ability of the motor case to dissipate kinetic projectile energy.

With the increasing use of filament-wound structures, analysis of wind structure and winding patterns has drawn more and more attention (Park et al., 2002; Morozov, 2006). The type of braiding influences the type of damage. In an experiment in which both biaxial and triaxial braided fiber preforms were used, the failure modes of tubes made from these two braiding architectures were different. For biaxially reinforced tubes, the initial cracks are aligned along the direction of the fiber tows, while for triaxially reinforced tubes the initial cracks along the longitudinal direction appear first

(Tsai et al., 1998). The optimal design of a fiber-reinforced composite cylindrical rocket case subjected to a buckling strength constraint and an overstressing strength constraint under aerodynamic torque and axial thrust was examined. The present optimal design problem is involved in determining the best laminate configuration to minimize the weight of the cylindrical skirt (Liang and Chen, 2003).

The property degradation of the transverse direction rarely increases the fiber directional stress, but affects the solution stability when matrix and delamination failures are accumulated. The predicted bursting pressure is somewhat high compared with experimental results, but the location where the final burst occurs is well predicted in the progressive failure analysis (Park et al., 2002).

Kaynak and Mat (2001) found that the following stages were observed in uniaxial fatigue studies of filament-wound glass fiber/epoxy composite tubes: first craze initiation in the matrix, then craze propagation and densification along the fiber winding direction, and finally breakage in the fibers leading to disintegration. Fatigue lives of the specimens decreased with an increase in the stress level, while they were generally increased by increasing the frequency.

17.5 Conclusions

In this chapter we have reviewed advances in the manufacturing of lightweight motor cases, while giving a short account of how filament winding has evolved. The reason for developing lightweight tubes has been the need for the reduction in weight of motor cases and consequently increasing range and rocket payload. From our literature review, we have noticed that many efforts have been devoted to perfecting the conditions of filament winding, such as angle layup configurations, mandrel rotation speed, winding direction, or other tooling considerations. Also, a wide area of research that was identified is damage assessment and failure prevention, as rocket motor cases operate at high temperatures and pressures, which can lead to catastrophic failure.

With respect to materials utilized for lightweight motor case manufacturing, carbon fiber provides the highest performance, lightest weight fabrication material for vessels operating at high pressures and temperatures. However, aramid fibers are also utilized, particularly for aerospace missions. Although epoxy resins have some limitations, they are widely used as resin for lightweight motor cases for rocketry and aerospace because of their lower cost. Damage assessment is not done anymore only by visual inspection, as there could be considerable matrix cracking and fiber breakage below the surface. NDT methods are normally utilized, from the most common X-ray, infrared, and ultrasonic techniques to more sophisticated and modern techniques such as vibrothermography, pulse-echo, FBG, and vibration-based damage detection methods. Finally, emerging from our study, impact studies and their modeling seem to be an area of growing interest, considering the importance of tube integrity to the successful operation of rocket systems and other related systems.

References

Abdalla, F., S.A., Mutasher, S., Khalid, Y., Sapuan, S., Hamouda, A., Sahari, B., Hamdan, M., 2007. Design and fabrication of low cost filament winding machine. Materials and Design 28, 234−239.

AFRL, 2005. "Breakthrough" Technologies Developed by the Air Force Research Laboratory and Its Predecessors. Air Force Research Laboratory History Program, US.

Alinovi, M., 2013. Winding Materials. Tec2 Magazine of the Argentine Institute of Scientific and Technical Research for the Defense (Citedef), pp. 13−15.

Avinash, G., Rama Krishna, S., Shrivastava, S., 2014. Design and analysis of composite rocket motor casing. International Journal of Emerging Technology and Advanced Engineering 6 (4), 231−236.

Balya, B., 2004. Design and Analysis of Filament Wound Composite Tubes. The Graduate School of Natural and Applied Sciences, Middle East Technical University.

Barynin, V., Bunakov, V., Rasin, Vasiliev, V., 1999. Aerospace composite lattice structures. In: ICCM12 Conference, Paper 679, Paris, France.

Bert, C., Hyler, W., 1962. Design Considerations in Selecting Materials for Large Solid-Propellant Rocket-Motor Cases. Defense Metals Information Center (DMIC), Columbus, OH, US. Report 180.

Blair, M., 1993. Ausroc III: the development of an Australian launch vehicle capability. In: Eighth National Space Engineering Symposium 1993: Proceedings. Institution of Engineers, University of Queensland, Barton, ACT, pp. 146−160. Australia.

Cadfil Filament Wound Tube Stress Analysis. www.cadfill.com.

Chase, C., 2010. Pioneers in propulsion—A history of CSD, Pratt & Whitney's solid rocket company. In: 46th AIAA/ASME/SAE/ASEE Joint Propulsion Conference & Exhibit 25−28 July, Nashville, TN, US.

Cohen, D., 1997. Influence of filament winding parameters on composite vessel quality and strength. Composites Port A 28A, 1035−1037.

Cohen, D., Mantell, S., Zhao, L., 2001. The effect of fiber volume fraction on filament wound composite pressure vessel strength. Composites Part B: Engineering 32 (5), 413−429.

Coste, Y., Gautier, J., 2006. Strategic missile solid rocket motor cases qualification. In: 42nd AIAA/ASME/SAE/ASEE Joint Propulsion Conference & Exhibit, 9−12 July, Sacramento, California.

Faria, H., Rocha, A., Miranda, H., Pires, F., Marquez, A., 2009. Numerical modelling of the filament winding process. In: International Committee on Composite Materials, ICCM17, Edinburgh, July 27−31.

Franz, M., Nurick, G., 2002. The effect of laminate stacking sequence of CFRP filament wound tubes subjected to projectile impact. Composite Structures 58 (2), 259−270.

Gaubatz, A., 1965. Filament winding of rocket cases. US Patent 3,174,388.

Gay, E., 2015. Personal Communication.

Golub, M., Lerner, N., Hsu, M., 1986. Kinetic study of polymerization/curing of filament-wound composite epoxy resin systems with aromatic diamines. Journal of Applied Polymer Science 32 (5), 5215−5229.

Hanson, A., 1969. Tensile and Cyclic Fatigue Properties of Graphite Filament-wound Pressure Vessels at Ambient and Cryogenic Temperatures. NASA Technical Note D-5354.

Harvey, D., 1963. Nondestructive test techniques for filament-wound glass fiber resin rocket motor cases. In: Criscuolo, E., Wenk, S. (Eds.), Symposium on Recent Developments in Nondestructive Testing of Missiles and Rockets. American Society for Testing and Materials.

Hill, E., Lewis, T., 1985. Acoustic emission monitoring of a filament wound composite rocket case during hydroproof pressure testing. Materials Evaluation 43, 859−863.

Hunson, M., Richards, T., Hickel, R., 1965. Preliminary Investigation of Plastics and Liners for Cryogenic Pressure Vessels Filament-wound Glass-reinforced. NASA Technical Note TN-D2741, US.

Hussain, F., Hojjati, M., Okamoto, M., Gorga, R., 2006. Polymer-matrix nanocomposites, processing, manufacturing, and application: an overview. Journal of Composite Materials 40 (17), 1511−1575.

Jones, B., Li, M., 2002. Liner-less tanks for space application-design and manufacturing considerations. In: Proceedings of the 5th Conference on Aerospace Materials, Processes, and Environmental Technology, NASA/CP-212931, September 16−18, Huntsville-Alabama, USA.

Katodani, K., 1994. High-speed rotation drum for use with a centrifugal separator for gaseous mixture. US Patent 3797737 A.

Kaynak, C., Mat, O., 2001. Uniaxial fatigue behavior of filament-wound glass-fiber/epoxy composite tubes. Composites Science and Technology 61, 1833−1840.

Khennane, A., 2013. Filament winding processes in the manufacturing of advanced-fiber reinforced (FRP) polymer nanocomposites. In: Bai, J. (Ed.), Advanced Fibre-Reinforced Polymer (FRP) Composites for Structural Applications. Woodhead Publishing Series in Civil and Structural Engineering, Woodhead Publishing, Ltd, Cambridge, UK, pp. 188−206 (Chapter 28).

Kliger, H., Wilson, B., 1990. Continuous fiber molding processes, A. Filament winding. In: Mallick, P., Newman, S. (Eds.), Composite Materials Technology Process and Properties. Oxford University Press.

Lamontia, M., Jensen, B., Gruber, B., 2006. Optimal composite material for low cost fabrication of large composite aerospace structures using NASA resins or POSS nanoparticle modifications. In: SAMPE Europe, 27th International Conference and Forums, 27−29 March, Paris, France.

Lauder, A., 1995. Manufacture of rocket motor cases using advanced filament winding processes. Material and Manufacturing Process 10 (1), 75−87.

Lee, S., Hwang, S., 2011. Impact response and damage analysis of composite overwraped presure vesels. In: 52nd AIAA/ASME/ASCE/AHS/ASC Structures, Structural Dynamics and Materials Conference 19th, 4−7 April, Denver, Colorado, US.

Lee, T., 2012. Review of the composite materials application to the solid rocket motor cases. Composites Research 25 (3), 82−89.

Lehtiniemi, P., Dufva, K., Berg, T., Skrifvars, M., Järvelä, P., 2011. Natural fiber-based reinforcements in epoxy composites processed by filament winding. Journal of Reinforced Plastics and Composites 30 (23), 1947−1955.

Li, K., Shen, X., Li, H., Zhang, S., Feng, T., Zhang, L., 2011. Ablation of the carbon/carbon composite nozzle-throats in a small solid rocket motor. Carbon 49, 1208−1215.

Liang, C.C., Chen, H., 2003. Optimum design of fiber-reinforced composite cylindrical skirts for solid rocket cases subjected to buckling and overstressing constraints. Composites Part B: Engineering 34 (3), 273−284.

Lin, M., Kumar, A., Qing, X., Beard, S., Russell, S., Walker, J., Delay, T., 2005. Monitoring the Integrity of Filament Wound Structures Using Built-in Sensor Networks. Missile Defense Agency, Arlington,VA, US.

Loures da Costa, L., 2003. The composite option for solid rocket motor cases in Brazil. In: 54th International Astronautical Congress of the International Astronautical Federation, the

International Academy of Astronautics, and the International Institute of Space Law, IAC-03-S.2.06.

Mc Connell, J., 2007. Demand grows for automation and turnkey systems. Reinforced Plastics 20–26.

McLaughlan, S., Forth, C., Grimes-Ledesma, R., 2011. Composite Overwrapped Pressure Vessels. A Primer. NASA/SP–2011–573. Johnson Space Center, US.

Madaras, E., Poe, C., Illg, W., Heyman, J., 1987. Estimating residual strength in filament wound casings from nondestructive evaluation of impact damage. Review of Progress in Quantitative Nondestructive Evaluation 6A, 1221–1230.

Mallick, P., 2007. Fiber-Reinforced Composites: Materials, Manufacturing, and Design. CRC Press, Boca Raton, FL, US.

MCTR Handbook, 2009. Item 6. Composite Production. Available in: http://fas.org/nuke/control/mtcr/text/mtcr_handbook_item6.pdf.

Moore, T., 2005. The space motors of Allegany Ballistics Laboratory. In: 41st AIAA/ASME/SAE/ASEE Joint Propulsion Conference & Exhibit, AIAA 2005-3808, 10–13 July 2005, Tucson, Arizona, US.

Morozov, E., 2006. The effect of filament-winding mosaic patterns on the strength of thin-walled composite shells. Composite structures 76, 123–129.

Munro, M., 1988. Review of manufacturing of fiber composite components by filament winding. Polymer Composites 9 (5), 352–359.

Multhoff, J., Loures da Costa, L., Krieger, J., Betten, J., 2008. Numerical simulation of damage and failure of composite pressure vessels. In: Proceedings of COBEM 2003-17th International Congress on Mechanical Engineering, November 10–14, Sao Paulo, Brazil.

Mumford, M., Hopkins, P., Lloyd, B., 1983. Matrix/fiber interface effects on Kevlar 49® pressure vessel performance. Engineering Notes 20 (4), 399–400.

Nagesh, 2003. Finite-element analysis of composite pressure vessels with progressive degradation. Defence Science Journal 53 (1), 75–86.

Okninski, A., Marciniak, B., Bartkowiak, B., Kaniewski, D., Matyszewski, J., Kindracki, J., Wolanski, P., 2014. Development of the Polish Small Sounding Rocket Program. Acta Austronautica, IAC-13-D2.6.9, 13 pp.

Paris, H., 1994. Assessment of Impact Damage of Composite Rocket Motor Cases. Final Report, 1 November–28 February. Electro-Optics, Environment and Materials. Georgia Institute of Technology, Atlanta, US.

Park, S., Kim, Ch, Kang, H., Hong, Ch, Kim, C., 2002. Structural analysis and strain monitoring of the filament wound motor case. Journal of Composite Materials 36 (20), 2373–2388.

PSU, 1991. Mars Sample Return Mission: Two Alternate Scenarios. Final Report (NASA-CR-19970). Pennsylvania State University, 510 pages.

Qing, X., Shawn, J., Beard, J., Kumar, A., Chan, H., Ikegami, R., 2006. Advances in the development of built-in diagnostic system for filament wound composite structures. Composites Science and Technology 66, 1694–1702.

Ravenhall, R., 1964. Stiffness and buckling in filament-wound motors. Journal of Spacecraft and Rockets 1 (3), 260–263.

Rea, D., Flis, W., Foedinger, R., Vandiver, T., 2002. Analytical model prediction of strain measured by fiber optic sensors embedded in composites. In: Loud, S. (Ed.), Bridging the Centuries With SAMPE's Materials and Processes, Book 1. DE Technologies Publication, PA, US, pp. 1255–1266.

Rinde, J., Mones, E., Newey, H., 1978. Filament Winding Epoxy Resins for Elevated Temperature Service. Lawrence Livermore Laboratories, University of California.

Rosato, D., Grove, C., 1964. Filament Winding: Its Development, Manufacture, Application, and Design. John Wiley & Sons, New York, US.

Shen, F., 1995. A filament-wound structure technology overview. Materials Chemistry and Physics 42, 96−100.

Strong, A., 2000. Fundamentals on Composites Manufacturing: Materials, Methods, and Applications, second ed. Society of Manufacturing Engineers (SME), Dearborn, Michigan, US.

Stroud, W., 1971. Minimum-Mass Isotropic Shells of Revolution Subjected to Uniform Pressure and Axial Load. NASA Technical Note D-6121, US.

Sun, X., Du, S., Wang, G., 1999. Bursting problem of filament wound composite pressure vessels. International Journal of Pressure Vessels and Piping 76, 55−59.

Tatcher, J., Wetherell, R., June 24−26, 1991. Solid rocket history at Hercules. In: AIAA/SAE/ASME/ASEE 27th Joint Propulsion Conference, Sacramento, CA, US.

Timm, D., Ayorinde, A., Lee, C., Steele, F., Plass, N., 1994. Kevlar 49 composite performance: dependence on thermoset resin microstructure. Polymer Engineering and Science 24 (11), 930−935.

Trigg, C., 1969. Carbon Fiber Composites in Solid Motor System. Bristol Aerojet Ltd N69−33893, England.

Tsai, H., 1994. Model superposition method for dynamic analysis of structures excited by proscribed support displacements. Computers Structres 66 (5), 675−683.

Vaughan, R., Jones, R., 1974. Filament Winding S-Glass/Polyimide Resin Composite Processing Studies. NASA Lewis Research Center, Cleveland, Ohio, US.

Vignoles, G., Arpa, Y., Quintard, M., 2010. Modelling of carbon−carbon composite ablation in rocket nozzles. Composites Science and Technology 70 (2010), 1303−1311.

Wild, P., Vickers, G., 1997. Analysis of filament-wound cylindrical shells under combined centrifugal, pressure and axial loading. Composites Part A Applied Science and Manufacturing 28 (1), 47−55. https://www.researchgate.net/journal/1359-835X_Composites_Part_A_Applied_Science_and_Manufacturing.

Woltosz, W., 2012. If we designed airplanes like we design drugs. Journal of Computer Aided Molecular Design 26 (1), 159−163.

Wu, Z., Zhou, W., Li, H., 2010. Modal analysis for filament wound pressure vessels filled with fluid. Composite Structures 92, 1994−1998.

Zandbergen, I., 2013. Some typical solid propellant rocket motors. Memorandum M-712 (Version 2.0). Delft University of Technology, The Netherlands.

This page intentionally left blank

Index

Note: Page numbers followed by "f" indicate figures, "t" indicate tables.

This page intentionally left blank

WOODHEAD PUBLISHING SERIES IN COMPOSITES SCIENCE AND ENGINEERING

Specialising in cutting-edge developments within the various lightweight materials and structures used in transport, *Lightweight Composite Structures in Transport* provides readers with a detailed review of composite materials and structures, and their use in the transport industry's vehicular applications with a particular look at surface and air transport. Chapters in Parts 1 and 2 of the book consider the lightweight philosophy and current developments in manufacturing techniques for lightweight composite structures in the transport industry. Subsequent chapters in Parts 3–5 discuss structural optimisation and analysis, properties and performance of lightweight composite structures, durability, damage tolerance and structural integrity. Part 6, the closing chapters of the book, presents case studies on lightweight composite design for transport structures.

This book covers a range of different material classes, with emphasis on advanced material, for the benefit of those working in the aerospace, motorsport, defence and automotive engineering industries; R&D managers, designers and materials engineers are particularly catered for here. An invaluable reference, this book consists of segments on material selection, the properties and performance of materials and structures, design solutions and manufacturing techniques.

Dr James Njuguna is a Reader in Composite Materials and Structures at Robert Gordon University, whose research interests include composite materials and nanomaterials for structural applications, primarily focusing on transport lightweight structures.

ISBN 978-1-78242-325-6

9 781782 423256

WP
WOODHEAD PUBLISHING
An imprint of Elsevier • store.elsevier.com

ELSEVIER